The Analyst

An international analytical science journal

Information for Authors

Full details of how to submit material for publication in *The Analyst* are given in the Instructions to Authors in the January issue. Separate copies are available on request.

The Analyst publishes original research papers, critical reviews, tutorial reviews, perspectives, news articles, book reviews and a conference diary.

Original research papers. The Analyst publishes full papers on all aspects of the theory and practice of analytical chemistry, fundamental and applied, inorganic and organic, including chemical, physical, biochemical, clinical, pharmaceutical, biological, environmental, automatic and computer-based methods. Papers on new approaches to existing methods, new techniques and instrumentation, detectors and sensors, and new areas of application with due attention to overcoming limitations and to underlying principles are all equally welcome.

Full critical reviews. These must be a critical evaluation of the existing state of knowledge on a particular facet of analytical chemistry.

Tutorial reviews. These should be informally written although they should still be a critical evaluation of a *specific* topic area. Some history and possible future developments should be given. Potential authors should contact the Editor before writing reviews.

Perspectives. These articles should provide either a personal view or a philosophical look at a topic relevant to analytical science. Alternatively, they may be relevant historical articles. Perspectives are included at the discretion of the Editor.

Particular attention should be paid to the use of standard methods of literature citation, including the journal abbreviations defined in Chemical Abstracts Service Source Index. Wherever possible, the nomenclature employed should follow IUPAC recommendations, and units and symbols should be those associated with SI.

Every paper will be submitted to at least two referees, by whose advice the Editorial Board of *The Analyst* will be guided as to its acceptance or rejection. Papers that are accepted must not be published elsewhere except by permission. Submission of a manuscript will be regarded as an undertaking that the same material is not being considered for publication by another journal.

Regional Advisory Editors. For the benefit of potential contributors outside the UK and N. America, a Group of Regional Advisory Editors exists. Requests for help or advice on matters related to the preparation of papers and their submission for publication in *The Analyst* can be sent to the nearest member of the Group. Currently serving Regional Advisory Editors are listed in each issue of *The Analyst.*

Manuscripts (four copies typed in double spacing) should be addressed to:
H. S. Minhas, Editor, or
J. F. Tyson, US Associate Editor

All queries relating to the presentation and submission of papers, and any correspondence regarding accepted papers and proofs, should be directed either to the Editor, or Associate Editor, *The Analyst.* Members of the Analytical Editorial Board (who may be contacted directly or *via* the Editorial Office) would welcome comments, suggestions and advice on general policy matters concerning *The Analyst.*
There is no page charge.

Fifty reprints are supplied free of charge.

Routine Analytical Fourier Transform Raman Spectroscopy

Part 2.* An Updated Review

Patrick J. Hendra, Heather M. M. Wilson, Peter J. Wallen, Ian J. Wesley, Philip A. Bentley, Morella Arruebarrena-Baez, James A. Haigh, Paul A. Evans, Christopher D. Dyer, Ralph Lehnert and Martin V. Pellow-Jarman

Department of Chemistry, University of Southampton, Highfield, Southampton, UK SO17 1BJ

This paper provides an update on an earlier paper published in 1989 and summarizes the contemporary value of Fourier transform (FT) Raman spectroscopy as an analytical tool. In particular the value of sample heating and cooling, the uses of the technique in the fields of polymer characterization, pharmaceutical analysis and biochemical identification are highlighted. Fourier transform Raman studies on surfaces, gases and in inorganic systems are also discussed. The review concludes with a critical consideration of the use of alternative wavelengths to 1064 nm (that of the neodymium yttrium aluminium garnet laser) in the future development of the field.

Keywords: Fourier transform Raman spectroscopy; near-infrared; design; sampling; application; review

Introduction

In 1986 Chase and Hirschfeld[1] demonstrated the feasibility of using a near-infrared laser as a source for Raman spectroscopy by collecting the scattered radiation and analysing it using a modified Fourier transform infrared (FTIR) spectrometer. Since the original paper appeared a considerable body of literature has developed describing instrumental developments, the production of combined IR–Raman spectrometric systems and a bewildering range of applications of the technique to chemistry, physics, materials and biological sciences. Progress has been summarized in a recent book[2] whilst an annual update is provided in the spectroscopic journal, *Spectrochimica Acta*.[3,4,5,6] In 1989 we prepared a short review paper for the Analyst showing how the near-infrared (NIR)–FT technique had successfully lifted Raman methods from the research environment into the routine analytical laboratory.[7] The burthen of the message was that:

(*i*) Raman scattering, the 'other half' of vibrational spectroscopy to IR, is now easy to use, rapid, versatile and works in the vast majority of cases providing new qualitative and quantitative analytical opportunities.

(*ii*) The combination of speed, ease of sampling and feasibility makes the cost per analysis highly competitive, and further, as the sample areas are interlocked with the laser source, the instruments operate in complete safety.

(*iii*) A range of applications including the determination of unsaturation in natural oils, studies on natural rubber and its vulcanization and the identification of forensic drugs were surveyed to demonstrate the new found versatility. In this paper, we offer an 'update' in which we elaborate on the improvements in the already highly developed versatility of

the methods that have appeared recently and survey some of the latest applications to be announced.

Experimental

All the leading manufacturers of FTIR instruments now offer 'Raman accessories' enabling users to record both the IR and the Raman spectrum on the same instrument and to present both on the visual display unit and hard copy output. As a result, comparisons of both spectra are simple and analytical deductions can be made as appropriate. An example of the approach is given in Fig. 1.

The instruments used at Southampton to record the spectra given in this paper are a peculiar 'hotch potch' of a rather old prototype based on a model 1720 combined FTIR–Raman (modified to operate in the NIR), a commercial Model 1760 FTIR instrument and a Model 2000 FTIR–Raman instrument, all manufactured by Perkin-Elmer (Norwalk, CT, USA). A very wide range of accessories have been developed at Southampton enabling spectra to be recorded at both low and high temperatures of liquids, solids and gases, of electrochemical systems studied *in situ*, of catalysts, films and of fibres. In all instances the cells can be rapidly inserted into the sample areas of any of the spectrometers and used with the sample area lids closed and hence in complete safety. All our spectrometers carry 2 in × 3 in IR style holders in the sample areas and cells are built on metal cards and slotted into the instrument. Although far from precise, location is perfectly
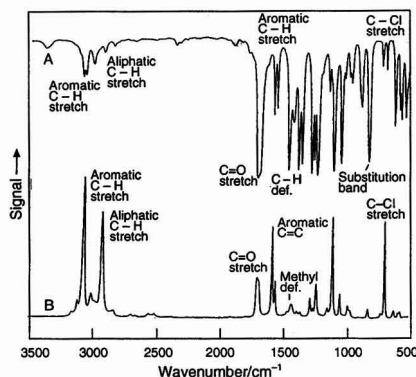

Fig. 1 A, Infrared and B, Raman spectra of 2,5-dichloroacetophenone.

adequate and no alignment between sample changes is required. Several of the cells are described below as we outline a range of applications of FT Raman spectroscopy to analytical chemistry.

Polymers

One of the most rapidly growing areas of analysis and research where vibrational spectroscopy has a major role is in the polymer industry. Although in classical organic chemistry infrared has 'lost out' to nuclear magnetic resonance (NMR), the versatility of IR has kept it in a prime analytical position. Fourier transform Raman is as versatile and has the further advantage that sampling is much less demanding. Thus, it is routine to record spectra of lumps or fibres, films or coatings, melts or solutions provided a sufficient depth of sample is available. If the material is oriented, then depending on the nature of the orientation (cylindrical or three dimensional) Raman methods can be used to measure the degree of orientation. Clearly, there is not room here to describe in detail all the applications that have appeared, but readers may wish to consult a brief review on synthetic polymer characterization[8] and another on the analysis of elastomers.[9] Recently a book has appeared in this field.[10] Four applications have been selected here, to illustrate significant points.

Polymerization and Crosslinking

Polymerization reactions and their inverse, degradation of materials in service, have been described but the field considered here in detail is the vulcanization of natural and synthetic rubbers. Rubber is vulcanized almost exclusively with sulfur and the reaction, accelerated with the appropriate additives, is normally carried out at approximately 150 °C. It is simple to devise a heated Raman cell suitable for us in an NIR excited FT machine. The cell is very simple in design, as shown in Fig. 2. The main body consists of an aluminium block that is mounted centrally on the standard 2 in × 3 in IR card. A small heating element is incorporated into the end of the block and a thermocouple is mounted in the top just behind the sample position. The samples for analysis can either be placed in a standard test-tube if they are powders or liquids, or in a metal inset fitted into the sample hole if they are in solid form. The temperature and heating rate are controlled using a CAL 9000 thermostatic unit. Using this cell, temperatures of over 200 °C can be achieved, but it must be noted that at these temperatures the region of the spectrum above 2000 cm^{-1} is obscured by the intense blackbody background.

Although the temperature range is restricted, it has been possible to follow the complex reactions that occur during the sulfur accelerated vulcanization of unsaturated rubbers *in situ*. This is particularly advantageous because some of the species thought to form during the process are unstable and would no longer be present if the sample was allowed to cool to room

temperature prior to analysis. In the first series of experiments reported, the interaction between the vulcanization agents sulfur, zinc oxide and the accelerator mercaptobenzothiazole (MBT) was explored in an inert medium. The Raman spectrum of a ZnO–MBT–S mixture (5 + 2 + 4 m/m/m) in liquid paraffin heated to the vulcanization temperature of 150 °C is shown in Fig. 3, B. A number of changes in the spectrum are apparent when it is compared with that recorded at room temperature (Fig. 3, A). Two separate processes were identified.

(*i*) When crystalline sulfur is melted, the normally intense bands near 470 and 220 cm^{-1} are reduced in intensity. Using their presence or absence as evidence, the solubility of sulfur *versus* temperature in both natural rubber and ethylene propylene diene monomer (EPDM) has been assessed.

(*ii*) Formation of a Zn–MBT complex by a solid–liquid phase acid–base reaction accounting for the changes in the region 1600–600 cm^{-1}, at temperatures around 60 °C. On cooling back to room temperature and re-recording the spectrum the reaction was predictably found to be non-reversible.

The hot cell was also used to investigate the reactions occurring when heating a mixture of MBT–S (1 + 4). These results showed some interesting changes that occur to the thiazole as shown in Fig. 4. MBT is known to exist as two tautomers, the thione and the thiol. At room temperature the thione form is preferred, whereas at higher temperatures MBT adopts the thiol form. From the spectra recorded at elevated temperatures it is clear that there is partial, but by no means complete, conversion to the thiol form. At present it is not clear if these changes are caused by the action of heat alone or the solution of MBT in molten sulfur or a combination of both processes. However, on cooling back to room temperature and re-recording the spectrum, the sample found to be identical to the initial one, indicating a reversible process.

Clearly, the reactions described above, although relevant to rubber chemistry are really inorganic in nature. When mixed

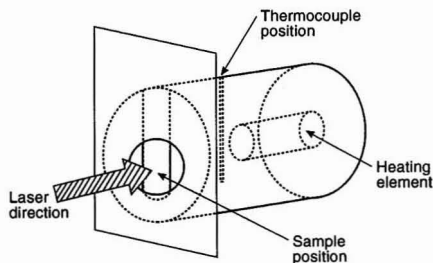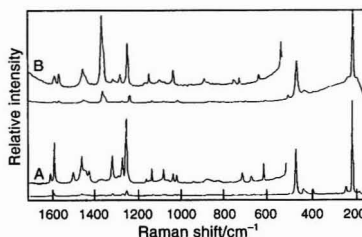**Fig. 3** Raman spectra of a ZnO–MBT–S mixture in liquid paraffin at A, room temperature and B, 150 °C.

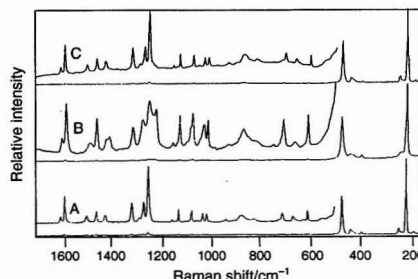**Fig. 2** Diagram of a hot cell.

Fig. 4 Raman spectra of an MBT–S mixture at A, room temperature, B, 150 °C and C, as in B but cooled back to room temperature.

with the rubber and heated the bands near 1680 cm^{-1} owing to $\nu_{C=C}$ in *cis*-polyisoprene develop lower frequency shoulders; unquestionably due to re-isomerization, ring formation and other perturbations of the crosslinking process. Further, as the reaction proceeds bands owing to the sulfur disappear. This field is being investigated using FT methods and extended to synthetic rubbers such as polybutadiene or ethylene propylene diene tercopolymers. In all instances, FT Raman is of unique value because, unlike its visible relative, NIR method is free from fluorescence.

As mentioned above, there is a severe restriction in the temperature to which samples may be heated before the black body emissions 'swamp' the Raman bands. This is a serious problem because so many polymers melt or undergo phase changes or reactions above 200 °C. There are, however, ways of reducing the nuisance of blackbody backgrounds.

The vibrational spectrum of a polymer melt usually differs markedly from those of the crystalline or partially crystalline materials. This is owing to the larger number of molecular conformations present in the molten state and also a break-down of the crystal and molecular symmetry. The spectroscopic selection rules can then cause 'crystalline' bands to disappear, new bands to appear and also existing bands to widen and become diffuse. An example of a polymer that shows different behaviour is shown in Fig. 5 where the Raman spectrum of poly(tetrafluoroethylene) (PTFE) at 36 °C is compared with that recorded at 380 °C.

It has been noted above that using the conventional laser for FT Raman spectroscopy [neodymium yttrium aluminium garnet (Nd: YAG) operating c.w. at 1064 µm] it is impossible to record adequate spectra at temperatures much above 20 °C due to blackbody emission. The spectrum of PTFE recorded at 380 °C was obtained using two spectroscopic ruses.

(*i*) The laser source wavelength was reduced to 780 nm moving the whole spectrum towards the visible and hence reducing the nuisance of blackbody emission.

(*ii*) A cut-off filter was incorporated after the sample to reduce the emission still further.

The laser filter used in this experiment was of modest quality, hence radiation was detectable only above $\Delta\nu = 500$ cm^{-1}, but it did serve to allow us to explore some of the differences that occur when a high melting polymer is fused. In the frequency range that could be investigated none of the bands present in the spectrum of the crystalline material disappeared in Fig. 5, the only major change in the spectrum

Fig. 5   Raman spectra of PTFE at (*a*) 36 and (*b*) 380 °C.

being a slight softening of the frequencies and a marked band broadening.

The vibrational behaviour of PTFE is that of a helix of severity 6 turns in a chain of 13 CF$_2$s or 7 in 15 depending on temperature. The vibrational modes of a non-helical rando-mized chain of CF$_2$s would be very different and give rise to broad, diffuse IR or Raman spectra. Exactly this behaviour is found in polyethylene, which on melting randomizes from a planar zig-zag structure. The minor changes in the PTFE spectrum on melting requires that the helical structure persists over lengths of several rotations (probably $\approx C_{20}$). Citations to this reasoning based on studies on oligomers of PTFE are given in refs. 11 and 12

The use of Raman methods to measure the degree of crystallinity in solid PTFE specimens and to do so rapidly and reliably has been reported very recently.[13]

Effect of Stress

Stretching polymer specimens can have two profound effects: crystalline materials may reorganize themselves into oriented fibrillar morphologies and do so in an isothermally irreversible manner (*e.g.*, the production of high tenacity fibre and film). Rubbers kept well above their 'glass transition' temperatures undergo orientation and even crystallization when stretched and the relaxation and melting processes are partially revers-ible. Several accounts are now available describing stress-induced (and thermally-induced) crystallization in natural rubber. It seems that the Raman evidence conforms to what is already known; that on straining to >400% oriented crystal-lites form with a morphology identical to those found when rubber is kept at around -10 °C for long periods.[13,14] Natural rubber is not the only elastomer to behave in this way.

Recently we have investigated the stress-induced crystalli-zation in cross-linked poly(isobutylene) (PIB) using FT Raman methods. Rubber-like polymers can be stressed to yield oriented, or in some instances, even oriented crystallized materials, above their glass transition temperatures. PIB is a common example of an elastomer that is known to show such behaviour when stretched. Vibrational spectroscopy has already been used to investigate stress-induced crystallization in this polymer, but most work has been carried out using IR, the information presented here was obtained using FT Raman spectroscopy.

The spectra shown in Fig. 6 are of butyl rubber (unstretched and stretched $\approx \times 10$). The huge differences between the spectra are surprising, the bands at 725 and 810 cm^{-1} being caused by stress-induced crystallization. It is, however, worth mentioning that natural rubber also changes its Raman characteristics markedly when it crystallizes.

As carried out in an FT Raman accessory, all measurements contain an anisotropic element because the laser is polarized. If the sample is isotropic and no polarization analyser is incorporated into the optical train, the spectrum collected can be assumed to contain no anisotropic information. If an analyser is incorporated, two spectra are available, one where the analyser and laser sector are parallel ‖, the other where they are perpendicular ⊥. The intensity $I_\perp/I_\parallel$ can be highly informative in assigning bands to fundamental modes and all textbooks cover this subject.[2] If the sample is anisotropic further series of spectra become possible. Thus in the presented example of stretched rubbers the laser can be polarized ‖ and ⊥ to the stretch direction and again the scattered light can be analysed. In crystals six experiments are possible. The details of the analysis of these spectra in polymers and/or their use in defining degrees of orientation are given in in ref. 9. In Fig. 6 the polarization of the laser and sample orientation are indicated.
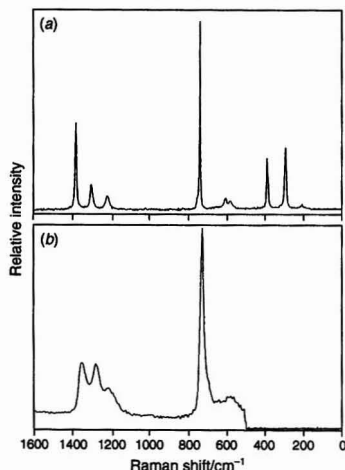
Use of Low Temperature Sampling

One of the restrictions involved in FT Raman spectroscopy is that the NIR laser radiation is absorbed to some extent and the sample heats. In the vast majority of situations the temperature rise is small (*e.g.*, < 20 °C) and the problem non-existent. In others, the temperature rise can be significant. In these instances the use of a low temperature cell is highly desirable and such a cell has been devised that is compact enough to fit inside the closed sample area of the spectrometer. It is of the transfer gas type and made entirely of glass. The Dewar vessel is sealed and no external connection is required. Temperature can be monitored with a thermocouple passed down central sample supporting tube to the aluminium sample holder.

Apart from the avoidance of destructive sample heating, cooling a sample can be very beneficial as the bands narrow and hence increase in height. However, a word of caution: if the morphology changes as the sample cools, spectral changes are to be expected. To demonstrate the point about the spectral quality, Fig. 7 shows a spectrum of semicrystalline polystyrene recorded at room temperature and at −130 °C. There are dramatic differences between these spectra, particularly noticeable is the splitting of the band at 1000 cm⁻¹. The band profile is related to the degree of crystallinity of the polystyrene and a report on the subject has recently been published.[15]

Gases

No one interested in gas analysis and deciding upon Raman methods would use an FT Raman instrument from choice. The ability to identify quantitatively homopolar diatomics is attractive but conventional Raman spectroscopy with its inherent simplicity and sensitivity is perfectly feasible in these situations. Fourier transform Raman methods are an 'overkill': fluorescence is not a problem here. However, analysts equipped with FT instruments are likely to be asked to do their best with what they have. We have devised a special gas cell and recently demonstrated its value.[16] The cell consists of a long tube of glass (1.4 mm id) and gold-coated down the bore. The tube is mounted into the spectrometer in the normal sample position with the laser projected down its centre. Raman radiation is multiply reflected back along the tube and into the collection lens. An example of the spectra that can be obtained is shown in Fig. 8.

Surfaces

Fourier transform Raman methods have already found a place in surface science. Several accounts have appeared where
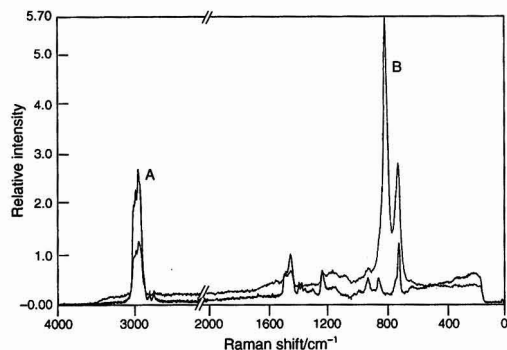
Fig. 6 Raman spectra of butyl rubber: (*a*) unstretched and (*b*) stretched ×10. Extension direction horizontal, laser polarization vertical.

pyridine has been sorbed onto zeolite and other oxide surfaces, the Raman spectra being used to characterize the surface acidic sites, *i.e.*, to quantify the proportion of Brönsted, Lewis and H-bonded sites.[17,18] It is also feasible to examine and characterize changes that occur in oxides as they are treated with a variety of reagents. One such change concerns the hydration of gamma alumina, a project involving cooperation between ourselves and the University of Luleå in Northern Sweden. The remarkable ease with which the hydrated surface may be characterized as bayeritic $Al(OH)_3$ using near-infrared FT Raman is noteworthy[19]; the latest results[20] show that the adsorption of phenylphosphate anion onto the gamma alumina surface prior to hydration blocks the reaction almost completely. Only the harshest hydration conditions produce a little bayerite. The two spectra shown in Fig. 9 demonstrate the blocking effect on the surface layer transformation.

Surface Enhanced Raman Scattering

Fourier transform Raman methods have also been applied to electrochemical cells *in situ*. It has been known for many years that illumination of copper, silver and gold surfaces electrochemically roughened in a cell produces a great enhancement of the Raman spectrum of species adsorbed and/or coordinated to the metal surface, *i.e.*, the spectrum observed originates in a monolayer in the electrical double layer.[21] It is
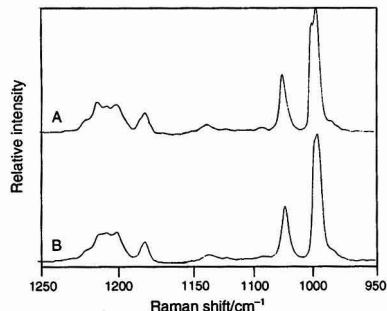
Fig. 7 Raman spectra of semicrystalline polystyrene at A, −130 °C and B, room temperature.
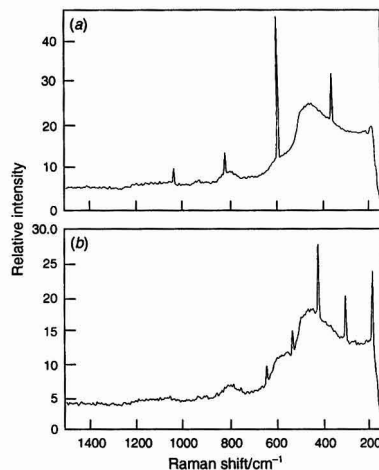
Fig. 8 Raman spectra of (*a*) H_2 and (*b*) D_2 at 1 atm.

now clear that this type of spectroscopy [the technique is called surface enhanced Raman scattering (SERS)] can be carried out using NIR excitation, and, with remarkable speed and convenience, using the FT approach,[22] thus providing the potential for rapid ultra-sensitive analysis.

Confining SERS activity to Cu, Ag and Au is obviously a severe limitation. One of several available techniques to extend the scope of the method is to coat the non-active metal surface with colloidal silver and then to lay the adsorbate onto the 'sandwich'. Fig. 10 shows the spectrum of the corrosion inhibitor MBT adsorbed onto smooth, and hence inactive, copper foil using 780 nm excitation. The SERS enhancement is provided by concentrated silver colloid deposited onto the smooth metal substrate. The term 'smooth' is used to indicate an unroughened metal surface which showed no sign of SERS enhancement without the addition of the silver colloid. Details of the preparation of the colloid and foil are given in a published account.[23] By using this technique it should be possible to identify the presence of trace organics on other non-SERS active substrates. However, it is important to note that the MBT is not a free uncomplexed state on the copper surface making this kind of technique especially valuable in corrosion studies.

Inorganic Compounds

In some respects NIR FT Raman methods have been disappointing in inorganic chemistry because in many instances absorption occurs or fluorescence is excited by the
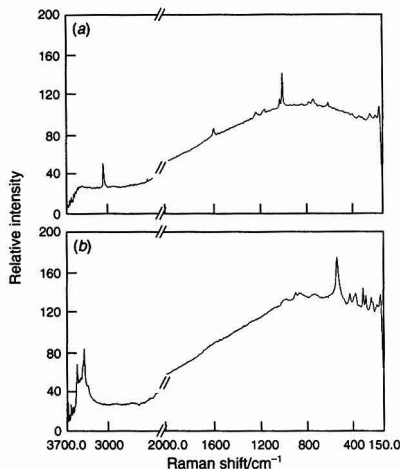
Fig. 9 Raman spectra of gamma Al_2O_3 (*a*) hydrated with phenylphosphate and (*b*) hydrated without phenylphosphate.
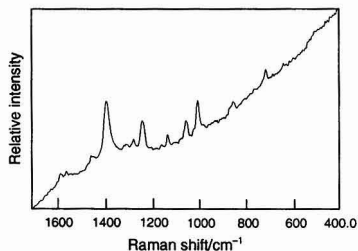
Fig. 10 Raman spectrum of copper foil treated with MBT and silver colloid.

Nd:YAG laser. The situation has been reviewed.[24] In some instances the NIR laser is particularly appropriate, *e.g.*, in situations where photosensitivity is a problem, such as in photographic chemistry. One such application is the study of fixing solution species used in photography. In solution, the reaction occurs between thiosulfate, often the ammonium salt, and the silver halide on the photographic film, which is usually composed of a mix of bromide and iodide. The principle products are silver thiosulfate complexes but other species do occur such as the thionates. It has been possible to produce Raman spectra from the thiosulfate reactants[25] and minor products such as the polythionates. (Fig. 11).

All the advantages of FT Raman spectroscopy apply in the inorganic field; freedom from sampling convenience and lack of skill but fluorescence can be a particularly annoying problem. This situation occurs in the study of fixing solutions; spectra are obtained, but over a persistent background. To avoid these and absorption problems it is essential to have available sources other than 1064 nm; this point is addressed below.

Biosamples

A considerable literature is developing where biochemists are examining a wide range of species using NIR methods. These range from bones[26] and eyes[27] to deposits inside arteries.[28] Similarly, we are just beginning to see results from systematic investigations of molecular systems, *e.g.*, edible fats where the degree of unsaturation can be rapidly quantified[29] carbohydrate characterization,[30] pharmaceutical analyses (there are several of these)[31,32] and peptides.[33,34]

To demonstrate just one application, NIR FT Raman spectroscopy has been shown to be very effective in the differentiation of hard and soft woods.[35] The major difference in the spectra is due to the type of lignin found in the sample. Lignin is a random polymer with a complex three dimensional structure. The lignin found in hardwoods is classified as Type GS (guaiacyl-syringyl) and is believed to be formed by the free-radically initiated polymerization of the precursors *trans*-coniferyl and *trans*-sinapyl alcohols (Fig. 12). Softwood lignin is classified as type G (guaiacyl) and is based almost entirely on *trans*-coniferyl alcohol. The spectra of beech, a typical hardwood, and spruce, a typical softwood, are shown in Fig. 13 and the spectra of their respective milled wood lignins (MWLs) are shown in Fig. 14. The spruce MWL consists of 99 mol% *trans*-coniferyl alcohol whilst the beech MWL consists of 33 mol% *trans*-coniferyl alcohol and 67 mol% *trans*-sinapyl alcohol. The bands which differentiate between the two whole woods are also clearly observable in the MWL spectra.
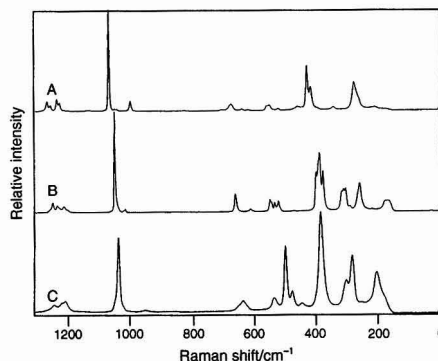
Fig. 11 Raman spectra of A, sodium trithionate, B, potassium tetrathionate and C, potassium pentathionate.

Further information on the assignments of bands in the Raman spectra are discussed in greater detail in another article.[30] It is likely that Raman spectroscopy will become a useful method in several areas of bioscience particularly if sources in the 'deep red' are available.

Use of 'Deep Red' Sources for FT Raman Spectroscopy

An alternative approach to Raman spectroscopy that has become popular recently is to use a spectrograph and a position sensitive detector. By far the best of the latter is the charge-coupled device (CCD). This combination can offer very high sensitivity because the detector has a very high quantum efficiency and the spectrograph exploits the multiplex* advantage. Previously, the shorter wavelength required by CCDs meant that these devices were used with blue–green sources and hence the fluorescence problem was large. However, CCDs are now available operating efficiently into the 'far red' (down to ~830 nm) and hence the use of 'deep red' laser sources with these new detectors has proliferated recently[37,38] and offer now perhaps best practice in current Raman technique.
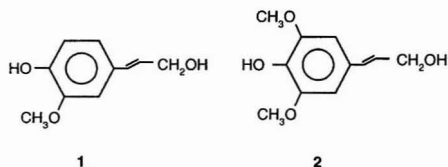
Fig. 12 Structures of the lignin precursors **1**, *trans*-coniferyl alcohol and **2**, *trans*-sinapyl alcohol.
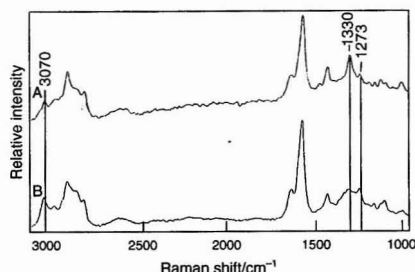
Fig. 13 Raman spectra of A, beech wood and B, spruce wood.
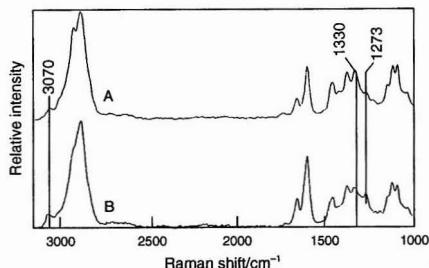
Fig. 14 Raman spectra of milled wood lignin of A, beech and B, spruce.

---

* Unlike a scanning spectrometer, a spectrograph views the whole spectrum for the duration of the experiment.

The most popular approach is to couple the spectrograph to a microscope and to carry out the Raman experiment on the microscope stage. This in turn makes microscopic Raman spectroscopy versatile and a powerful analytical method but greater skill is, of course, needed in its use than is typical of the FT methods where speed, convenience and the routine nature of sampling are the strong points.

The advantages and disadvantages that might arise from using sources shorter in wavelength than 1064 nm have been mentioned above and discussed elsewhere.[39] Briefly these might be listed:

Advantages—

(*i*) Removal of water absorption leading to the possibility that dilute aqueous solutions might become accessible.

(*ii*) An increase in value in inorganic chemistry.

(*iii*) The use of cheaper detectors lowering the cost of instruments.

Disadvantages—

(*i*) An inevitable increase in fluorescence in organic analytical samples.

(*ii*) Possible increases in the incidence of laser absorption and hence sample heating and destruction.

To assay these conflicting considerations we have set up an instrument to operate at 780, 835, 920 and 1064 nm and a wide range of samples are being studied to quantify the advantages *versus* the disadvantages.

On comparing the spectra of poly(phenylene sulfide) (PPS) and MBT excited at four wavelengths (see Figs. 15 and 16), the trends are apparent. Although the samples fluoresce using 780 and 835 nm sources moving to 920 nm yields a significant improvement. It is too early to judge the value of sources in the very near IR but preliminary results indicate that across a wide range of samples it will be inappropriate to reduce the wavelength much below 900 nm. This in turn means that low cost silicon detectors cannot be used and hence moving from the established Nd:YAG sources seems unlikely. These comments do not apply to inorganic compounds where the availability of several sources is highly desirable.

Conclusions

Fourier transform Raman methods have made significant strides in the analytical field since our earlier report
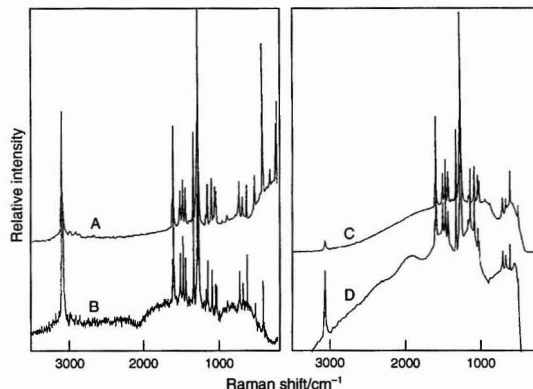
Fig. 15 Raman spectra of PPS obtained using A, 1064; B, 920; C, 835; and D, 780 nm.
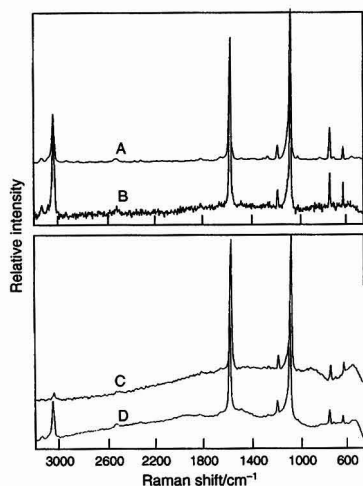
Fig. 16 Raman spectra of MBT obtained using A, 1064; B, 920; C, 835; and D, 780 nm.

appeared.[7] Instruments have improved applications are proliferating and the machines are being installed worldwide at a rapid rate. Several sources of information exist and are to be recommended including a chapter in an encyclopedia of analytical chemistry[41] and as already mentioned above, an annual series of special editions of a learned journal dedicated to the technique.

References

1. Chase, B., and Hirschfeld, T. B., *Appl. Spectrosc.*, 1986, **40**, 133.
2. Hendra, P. J., Jones, C. H., and Warnes, G. M., *Fourier Transform Raman Spectroscopy*, Ellis Horwood, Chichester, 1991.
3. *Spectrochim. Acta, Part A*, 1990, **46** (2), 121.
4. *Spectrochim. Acta, Part A*, 1991, **47** (9/10), 1133.
5. *Spectrochim. Acta, Part A*, 1993, **49** (5/6), 609.
6. *Spectrochim. Acta, Part A*, 1994, **50** (11), 1811.
7. Ellis, G., Hendra, P. J., Hodges, C. M., Jawhari, T., Jones, C. H., le Barazer, P., Passingham, C., Royaud, I. A. M., Sánchez Blásquez, A., and Warnes, G. M., *Analyst*, 1989, **114**, 1061.
8. Edwards, H. G. M., Johnson, A. F., and Lewis, I. R., *J. Raman Spectrosc.*, 1993, **24**, 475.
9. Maddams, W., *Spectrochim. Acta, Part A*, 1994, **50**, 1967.
10. Bower, D. I., and Maddams, W. F., *The Vibrational Spectroscopy of Polymers*, Cambridge University Press, Cambridge, 1989.
11. Lyerla, J. R., and Vanderhort, D. L., *J. Am. Chem. Soc.*, 1976, **98**, 1697.
12. Rabolt, J. F., and Fanconi, B., *Polymer*, 1977, **18**, 1258.
13. Lehnert, R., and Hendra, P. J., *Polymer*, submitted for publication.
14. Jackson, K. D. O., and Hendra, P. J., *Spectrochim. Acta, Part A*, 1994, **50**, 1987.
15. Wesley, I. J., and Hendra, P. J., *Spectrochim. Acta, Part A*, 1994, **50**, 1959.
16. Dyer, C. D., and Hendra, P. J., *Analyst*, 1992, **117**, 1393.
17. Ferwerda, R., van der Maas, J. J., and Hendra, P. J., *J. Phys. Chem.*, 1993, **97**, 7331.
18. Ferwerda, R., van der Maas, J. H., and Hendra, P. J., *Vib. Spectrosc.*, 1944, **1**, 37.
19. Dyer, C. D., Hendra, P. J., and Forsling, W., *Spectrochim. Acta, Part A*, 1993, **49**, 715.
20. Dyer, C. D., Hendra, P. J., Forsling, W., and Ranhcimer, M., *Spectrochim. Acta, Part A*, 1993, **49**, 691.
21. *Review, Surface Enhanced Raman Scattering*, ed. Chang, R. K., and Furtak, T. E., Plenum Press, New York, 1982.
22. Angel, S. M., Katz, L. F., Archibald, D. D., Lin, L. T., and Honigs, D. E., *Appl. Spectrosc.*, 1988, **42**, 1327.
23. Wilson, H. M. M., *Vib. Spectrosc.*, 1994, **7**, 287.
24. Almond, M. J., Yates, C. A., Horrin, R., and Rice, D. A., *Spectrochim. Acta, Part A*, 1990, **46**, 177.
25. Day, T. N., Hendra, P. J., Rest, A. J., and Rowlands, A. J., *Spectrochim. Acta, Part A*, 1991, **47**, 1251.
26. Haigh, J. A., Hendra, P. J., Rowlands, A. J., Degen, I. A., and Newman, G. A., *Spectrochim. Acta, Part A*, 1993, **49**, 723.
27. Nie, S., Bergbauer, K. L., Ruck, J. F. R., and Yu, N. T., *Spectroscopy*, 1990, **5**, 24.
28. Nie, S., Bergbauer, K. L., Kuck, J. F. R., and Yu, N. T., *Exp. Eye Res.*, 1990, **51**, 619.
29. Rava, R. P., Baraga, J. J., and Feld, M. S., *Spectrochim. Acta, Part A*, 1991, **47**, 509.
30. Sadeghi-Jorabchi, H., Hendra, P. J., Wilson, R. H., and Belton, P. S., *J. Am. Oil Chem. Soc.*, 1990, **67**, 483.
31. Góral, J., and Zichy, V., *Spectrochim. Acta, Part A*, 1990, **46**, 253.
32. Davis, M. C., Binns, J. S., and Melia, C. D., *Spectrochim. Acta, Part A*, 1990, **46**, 277.
33. Cutmore, E. A., and Skett, P. W., *Spectrochim. Acta, Part A*, 1993, **49**, 809.
34. Gani, D., Hendra, P. J., Maddams, W. F., Passingham, C., Royaud, I. A. M., Willis, H. A., and Zachy, V., *Analyst*, 1990, **115**, 1313.
35. Hallmark, V., and Rabolt, J. F., *Macromolecules*, 1989, **22**, 500.
36. Evans, P. A., *Spectrochim. Acta, Part A*, 1991, **47**, 1441.
37. Wienstock, I. A., Atalla, R. H., Agarwal, U. P., Minor, J. L., and Petty, C. J., *Spectrochim. Acta, Part A*, 1993, **49**, 819.
38. Schulte, A., *Appl. Spectrosc.*, 1992, **46**, 891.
39. Wang, Y., and McCreery, R., *Anal. Chem.*, 1989, **61**, 2647.
40. Hendra, P. J., Pellow-Jarman, M., and Bennett, R., *Vib. Spectrosc.*, 1993, **5**, 311.
41. Hendra, P. J., *Encyclopedia of Analytical Chemistry*, ed. Townsend, A., Academic Press, London 1995, 4399–4497.

Qualitative and Semi-quantitative Trace Analysis of Acidic Monoazo Dyes by Surface Enhanced Resonance Raman Scattering

C. H. Munro, W. E. Smith and P. C. White*

Department of Pure and Applied Chemistry, University of Strathclyde, Glasgow, G1 1XL UK

Resonance Raman (RR) and surface enhanced resonance Raman scattering (SERRS) procedures are described for the analysis of acidic monoazo dyes. By the comparison of the RR spectra, discrimination is achieved between 20 acidic monoazo dyes, including structural isomers. However, difficulties are experienced due to fluorescence, to the narrow concentration range over which scattering is observed (10^{-3}–10^{-4} mol l^{-1}) and to the relatively high detection limit (approximately 3–5 µg). These difficulties were overcome by the development of a robust, sensitive and selective SERRS procedure. Controlled aggregation of a citrate-reduced silver colloid and strong SERRS of the adsorbed dyes can be obtained if a 0.01% aqueous solution of poly(L-lysine) is added to an aliquot of colloid followed by aqueous solutions of the dye and ascorbic acid. The enhancement in scattering intensity compared to solution resonance is approximately 10^5–10^6 and strong SERRS is observed for sub-nanogram amounts of dye. In addition, the fluorescence background is quenched and a wide concentration range can be examined. Models are proposed for the bonding of poly(L-lysine) with *o*-hydroxy-, *p*-hydroxy- and *o*-dihydroxyarylazo dyes and a single model of interaction is proposed for the adsorption of the full set of dyes on the silver surface in the presence of ascorbic acid. The results of a blind trial confirm the usefulness of SERRS for qualitative analysis and highlight the importance of sample purity. Linearity in a plot of concentration *versus* scattering intensity was observed at low solution concentrations ($<3 \times 10^{-6}$ mol l^{-1}), supporting the application of SERRS for both qualitative and semi-quantitative analysis of trace amounts ($\geqslant$300–500 pg) of acidic monoazo dyes.

Keywords: Surface-enhanced resonance Raman scattering; monoazo dyes

Introduction

Acidic dyes are used to colour a large number of materials, including food, drink, water-based paints, cosmetics, inks, leather and a range of fibres (wool, nylon, silk and modified acrylic). The discrimination of these dyes in low-concentration mixtures is an important analytical problem. For example, it is often necessary within forensic science to examine materials that have been coloured using these dyes. Simple qualitative methods such as thin-layer chromatography are generally employed to compare control and suspect dye samples.

However, the ability to characterize the molecular structure of small amounts of dyes (typically 10 ng or less) would be highly advantageous. A high-performance liquid chromatographic (HPLC) technique that utilizes multivariate analysis of data generated from a polystyrene–divinylbenzene (PSDVB)-packed column combined with a multi-wavelength detection system is capable of providing structural information.[1] However, some difficulties are still experienced in their characterization. In particular, the discrimination between structural isomers is limited.

Surface enhanced resonance Raman scattering (SERRS) has emerged as a potentially useful analytical technique for the examination, under electronic resonant conditions, of trace amounts of Raman-active compounds adsorbed on silver.[2–9] The SERRS process is extremely efficient, allowing detection levels in the region of 10^{-9}–10^{-11} mol l^{-1} to be achieved.[3–5] In addition, fluorescence from adsorbed species is often quenched by radiationless energy transfer to the metal surface, and this has enabled Raman spectra to be obtained for compounds for which this would normally be hindered by the presence of a strong fluorescent background.[10,11]

In a recent study, a SERRS procedure was described for the analysis of acidic mono-azo dyes.[12] SERRS of these compounds was obtained if a 0.01% solution of poly(L-lysine) was added to a citrate-reduced silver sol. Further enhancement of the SERRS intensities was obtained by the addition of ascorbic acid. Significant differences in the recorded SERR spectra were reported between dyes of different structural type, indicating that SERRS may have unique advantages for the selective determination of specific dyes at low concentrations in mixtures. To assess the applicability of the technique to the analysis of acidic monoazo dyes, a primary test set of 20 of these dyes was examined. This set included three main subsets of dyes; *o*-hydroxy-, *p*-hydroxy- and *o,o*-dihydroxyarylazo dyes. The dyes examined correspond to those examined by a current HPLC method.[1] An additional set of six unknown dyes was examined in a blind trial.

Experimental

Sodium citrate, silver nitrate (Johnson Matthey), ascorbic acid (Aldrich) and poly(L-lysine) hydrobromide, M_r 4000–15 000 (Sigma) were of analytical-reagent grade. The dyes used were Acid Brown 102 (CI 14615), Acid Orange 8 (CI 15575), Acid Red 88 (CI 15620), Mordant Violet 5 (CI 15670), Mordant Black 15 (CI 15690), Mordant Black 17 (CI 15705), Acid Orange 12 (CI 15970), Food Orange 2 (CI 15980), Food Yellow 3 (CI 15985), Acid Orange 16 (CI 16011), Food Red 17 (CI 16035), Acid Red 13 (CI 16045), Acid Orange 14 (CI 16100), Mordant Red 9 (CI 16105), Acid Red 26 (CI 16150), Food Red 6 (CI 16155), Acid Red 27 (CI 16185), Acid Orange

---

* To whom correspondence should be addressed.

10 (CI 16230), Acid Red 44 (CI 16250) and Acid Red 18 (CI 16255). Dye samples were provided from the reference dye collection in the Forensic Science Unit, University of Strathclyde.

Purified dye samples were obtained by preparative thin-layer chromatography (TLC). Preparative TLC plates were prepared by applying a 50% m/v aqueous slurry of Merck silica gel 60G to 100 × 200 mm glass plates at a thickness of 0.5 mm using a spreader. The plates were dried for 1 h at 110 °C prior to use. The TLC solvent system used was butanol–acetone–water–ammonia (5 + 5 + 1 + 2 v/v). Each dye was applied individually as a line 15 mm from the long edge of the preparative plates. The plates were then developed over a distance of 75 mm in a sealed, saturated TLC tank. After development, the major coloured band was scraped from the plate, extracted with methanol and filtered. The filtrate was evaporated to dryness and the purified dye dissolved in distilled water.

Silver sols were prepared according to a modified Lee and Meisel method.[2] All glassware was rigorously cleaned before use by treatment with *aqua regia* [HNO_3–HCl (1 + 3 v/v)] followed by gentle scrubbing in a soap solution. A sample of silver nitrate (90 mg) was suspended in distilled water (500 ml) and heated rapidly to 100 °C. A 1% solution of sodium citrate (10 ml) was added under vigorous stirring and the solution was kept boiling for 80 min with continuous stirring. A 50% v/v solution of the resultant silver colloid was prepared in distilled water prior to SERRS analyses.

For determinations by resonance Raman spectrometry, individual solutions containing concentrations of 10^{-3}–10^{-4} mol l^{-1} of each dye were prepared in distilled water. For SERRS, individual solutions containing concentrations of approximately 10^{-5}–10^{-8} mol l^{-1} of each dye were prepared in distilled water. To promote adsorption of the dye and controlled aggregation of the silver colloid a 0.01% aqueous solution of poly(L-lysine) (150 µl) was added to an aliquot of the silver sol (2 ml), followed by an aqueous solution of the purified dye (10^{-5}–10^{-8} mol l^{-1}; 100 µl) and ascorbic acid (1 mol l^{-1}; 150 µl).

Visible absorption spectra in distilled water were recorded with a Unicam 8700 Series spectrophotometer using 10 mm quartz cuvettes. Resonance Raman spectra were recorded using a Spectra-Physics Model 2020 argon ion laser (100 mW) as the excitation source (457.9 nm), with conventional 90° geometry. The spectra were dispersed by an Anaspec-modified Cary 81 scanning monochromator with a spectral resolution of 4 cm^{-1}. A cooled Thorn EMI 9658R photomultiplier tube was used for detection, with photon-counting electronics for data acquisition. A micro-positionable quadrant cell holder was used for accurate and precise positioning of a 10 mm cuvette. Each spectrum took approximately 12 min to acquire.

Results and Discussion

The structures of the 20 test dyes in this study are shown together with their generic names and Colour Index (CI) numbers in Fig. 1. The visible absorption spectra (400–700 nm) of the dyes were recorded in universal buffer at pH 3, 6 and 12. The spectrum for each dye recorded in distilled water (pH 6) matched that recorded in universal buffer at pH 6. Comparison of the absorption spectra confirmed that, under the present conditions, the hydrazone form (**I**) is predominantly adopted by these dyes. The spectra recorded at pH 6 are virtually identical with those recorded at pH 3 for all but one of the dyes [Mordant Black 15 (CI 15690)]. The absorption spectrum for this dye at pH 6 undergoes a bathochromic shift in comparison with that for pH 3. However, it was virtually identical with the absorption

spectrum recorded at pH 12, thereby indicating that the azo form (**II**) is predominant in this case.
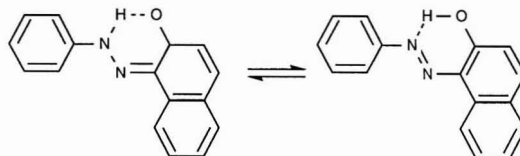
I Hydrazone form   **II Azo form**

On examination of the remaining absorption spectra recorded at pH 12, strong hypsochromic shifts are observed for the sixteen *o*-hydroxyarylazo dyes, consistent with a tautomeric shift to the azo form ($\Delta\lambda_{max} \approx 40$ nm). However, the other dyes examined do not fit this model, and bathochromic shifts were observed at pH 12. These dyes are the *p*-hydroxyarylazo dye Acid Brown 102 (CI 14615) and the *o,o*-dihyroxyarylazo dyes Mordant Violet 5 (CI 15670), Mordant Black 15 (CI 15690) and Mordant Black 17 (CI 15705). The bathochromic shift observed at pH 12 for Acid
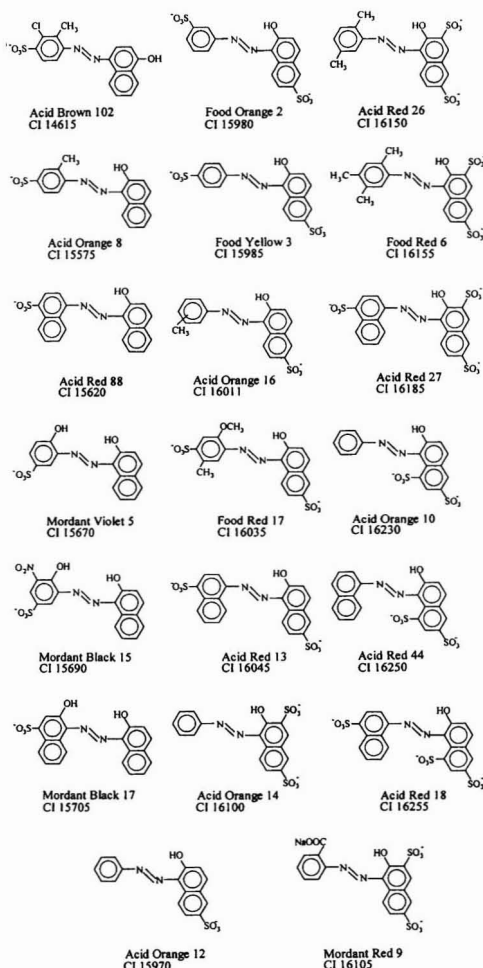
Fig. 1 Chemical structures of the 20 test dyes together with the generic name and colour index (CI) numbers.

Brown 102 (CI 14615) is consistent with the reported sensitivity of the tautomeric equilibrium of the 4-phenylazo-1-naphthol system to solvent and pH effects.[13] These dyes are readily ionized, even by weak bases, to form a red mesomeric anion. An analogous ionization may provide an explanation for the similar behaviour of the *o,o*-dihydroxyarylazo dyes. At pH 9, strong bathochromic shifts are reported for the resultant anionic species in both the azo and hydrazone tautomeric forms, and on further ionization at pH 13 an additional bathochromic shift is observed. The fully ionized species can only exist in the azo form.[14]

At pH 6, the visible absorption spectra have maxima in the range 455–510 nm for all the dyes except Mordant Black 15 (CI 15690) (544 nm). The frequency of the argon ion laser line at 457.9 nm lies in the range covered by the adsorption band of the majority of the dyes in the set and was selected as the excitation source for the Raman examinations under electronic resonant conditions. Mordant Black technically is pre-resonant with the incident radiation at 457.9 nm rather than resonant, but significant resonance enhancement may be expected. Maximum resonant scattering may be achieved for some dyes owing to a coincidence of the absorbance maxima with the excitation frequency (457.9 nm) and tunable lasers could be used to maximize resonance enhancement for each dye. However, the greater frequency stability of a fixed line gives a better reference point which can be reproduced more simply and readily in other laboratories, hence a fixed excitation frequency was preferred.

Resonance Raman Examination of Acidic Monoazo Dyes

Resonance Raman (RR) spectra were recorded for each of the 20 dye samples in the test set. Examples of RR spectra for two structural isomers are illustrated in Fig. 2. As a result of the selective enhancement of certain bands due to resonance, the observed spectra were relatively simple and well resolved at a spectrometer slit width of 4 cm^{-1}. Strong fluorescence was seen to obscure partially the spectra of ten of the dyes (CI 14615, CI 15670, CI 15590, CI 15705, CI 15980, CI 15985, CI 16035, CI 16105, CI 16155 and CI 16230). In particular, the spectra for CI 14615, CI 15705 and CI 16155 were almost

Fig. 2 Resonance Raman spectra of structural isomers. Dyes: (*a*) Food Orange 2 (CI 15980) and (*b*) Food Yellow 3 (CI 15985).

entirely obscured by the underlying fluorescence. Similarities were observed in the RR spectra across the set of dyes and many of the strong resonance Raman bands appear to be common within the set of monoazo dyes ($\approx$1600, $\approx$1550, $\approx$1480, $\approx$1340, $\approx$1235 cm^{-1}). The strongest resonance Raman bands were observed in the region of the spectra between 1100 and 1700 cm^{-1}. These bands correspond to vibrations with significant in-plane skeletal nuclear displacements which vibronically couple the ground and excited electronic states (π, π^*). The majority of these bands are assigned to vibrations with atomic displacements predominantly on the phenyl or naphthyl moieties, but the bands at $\approx$1235 and $\approx$1340 cm^{-1} are assigned to vibrations with atomic displacements predominantly on the bridging atoms ($>$C–NH–N=C$<$).[15] The less intense bands that are observed between 200 and 1100 cm^{-1} correspond to out-of-plane skeletal deformations and C–H stretches and deformations. A notable feature was that, although similar, no two resonance Raman spectra were identical. Therefore, discrimination between all of the dyes in the test set, including structural isomers that differ only in the position of one or more substituents, is possible by Raman spectrometry.

For most of the dyes examined, the substituents (predominantly sulfonic acid) are auxochromes and are not themseleves chromophoric. Mordant Black 15 (CI 15690) does contain a nitro group. However, this group will act principally as a strong electron-withdrawing group, resulting in both the stabilization of the azo tautomer at pH 6, which was observed only for this dye and the bathochromic shift of the azo form relative to the hydrazone. The vibrations with nuclear displacements predominantly on the substituent groups are not observed in the resonance Raman spectra and the strong similarities observed in the spectra are therefore expected for dyes that share the same chromophore. The differences that are observed are due to the effect of the substituent on specific normal vibrational modes of the chromophore, resulting in shifts in the vibrational frequencies. In addition, the influence of the auxochromes on the electronic structure of the chromophore will alter the Franck–Condon overlap and result in variations in resonance enhancement for some of the bands. Therefore, the relative intensity of each band is as useful as its vibrational frequency for the discrimination of the dyes in the test set examined, particularly for those bands common to this set.

RR scattering was observed only within a narrow concentration range of the aqueous dye solutions (10^{-4}–10^{-3} mol l^{-1}). At concentrations greater than 10^{-3} mol l^{-1} the radiation was effectively absorbed by the dye and no appreciable scattering was observed. At concentrations less than 10^{-4} mol l^{-1} the scattering was weak and the signal-to-noise ratio was low. The lower limit corresponds to a total dye quantity of approximately 3–5 µg (based on 100 µl of 10^{-4} mol l^{-1} dye solution).

SERR Scattering Examination of Acidic Monoazo Dyes

The ultraviolet–visible (UV/VIS) absorption spectrum of the silver sols showed maxima at approximately 404 nm, which can be associated with the dipolar surface plasmon for silver spheres with small radii ($\leqslant$20 nm) compared with the illumination wavelength. Addition of an aqueous solution of each dye to the silver sol produced no aggregation or SERRS. Further, on acid aggregation (1% HNO$_3$; 35 µl) only non-anionic dyes gave good SERRS. This was attributed to poor adsorption of the anionic dye molecules to the sol particles owing to the negatively charged organic layer at the surface of the silver.[16] To overcome this difficulty and to provide a more general method, poly(L-lysine) was added along with the dye. Poly(L-lysine) is a polycationic molecule for which the ability to promote cell adhesion to solid substrates has been
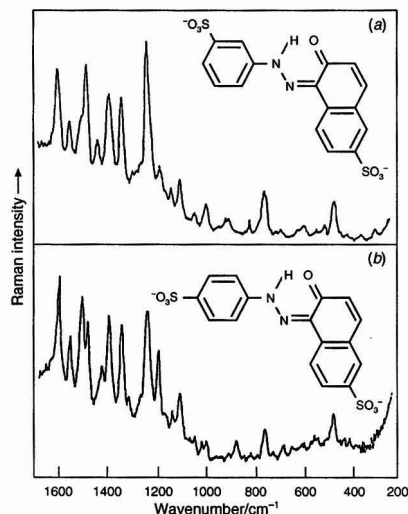
reported.[17] On addition of poly(L-lysine) solution (0.01%; 150 µl) to the silver sol immediately prior to the addition of the dyes, aggregation and intense SERRS were observed. Subsequent addition of ascorbic acid (1 mol l⁻¹; 150 µl) to the colloidal suspension resulted in an over-all increase in the observed SERRS intensity for the 16 *o*-hydroxyarylazo dyes and both an increase in scattering and strong shifts in the vibrational frequencies observed for the *p*-hydroxyarylazo dye, Acid Brown 102 (CI 14615), and also for the *o,o*-dihydroxyarylazo dyes, Mordant Violet 5 (CI 15670), Mordant Black 15 (CI 15690) and Mordant Black 17 (CI 15705). The SERR spectra of the acidic monoazo dyes are illustrated in Figs. 3–9 and the corresponding vibrational frequencies are listed in Table 1. The most intense bands are listed in decreasing order in parentheses.

On examination of the SERRS spectra, three effects were observed. First, the fluorescence background that had partially obscured many of the resonance Raman spectra was no longer observed. Second, there was an over-all enhancement in scattering intensity compared with solution resonance of approximately 10⁵–10⁶-fold. Finally, the vibrational frequencies of the strongest SERR bands observed in the presence of both poly(L-lysine) and ascorbic acid coincide approximately with the strongest resonance enhanced bands for most of the dyes examined. However, close comparison of the RR and SERR data indicates a slight change in the relative intensities for many of the observed bands.

Mordant Black 15 (CI 15690) was found earlier to predominate in the azo form at pH 6. Therefore, the differences in the vibrational frequencies observed in the SERRS before and after the addition of ascorbic acid are rationalized by a switching of tautomeric form of the dye molecule from the azo to the hydrazone consistent with that expected for a decrease in pH. The other *o,o*-dihydroxylated dyes, Mordant Violet 5 (CI 15670) and Mordant Black 17 (CI 15705), were previously found to predominate in the hydrazone tautomeric form under the current pH conditions. However, the differences in the vibrational frequencies observed are also consistent with a switch from the azo form in the presence of poly(L-lysine) to the hydrazone form on the subsequent addition of ascorbic acid. Therefore, poly(L-lysine) appears to alter the tautomeric equilibrium in favour of the azo tautomer. The differences observed in the SERRS for the *p*-hydroxyarylazo dye Acid Brown 102 (CI 14615) before and after the addition of ascorbic acid are less marked than those observed for the *o,o*-dihydroxyarylazo dyes, but are significant enough to indicate that the addition of ascorbic acid does in some way affect the interaction of poly(L-lysine) and the dye.

Effects of Poly(L-lysine) and the Subsequent Addition of Ascorbic Acid

To provide a basis for understanding the action of poly(L-lysine), its interactions with the dye solutions were studied by visible absorption spectrometry and SERRS. Following this, the interaction between the poly(L-lysine)–dye complexes and the silver surface was investigated and a model for their adsorption proposed.
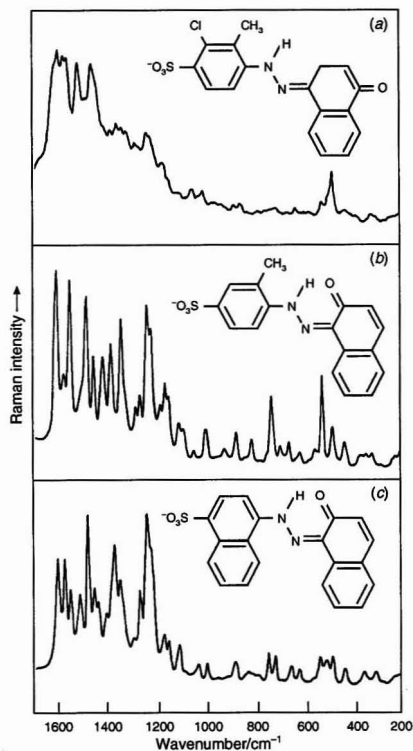
Fig. 3 SERR spectra of poly(L-lysine)–dye complexes in the presence of ascorbic acid. Dyes: (*a*) Acid Brown 102 (CI 14615), (*b*) Acid Orange 8 (CI 15575) and (*c*) Acid Red 88 (CI 15620).
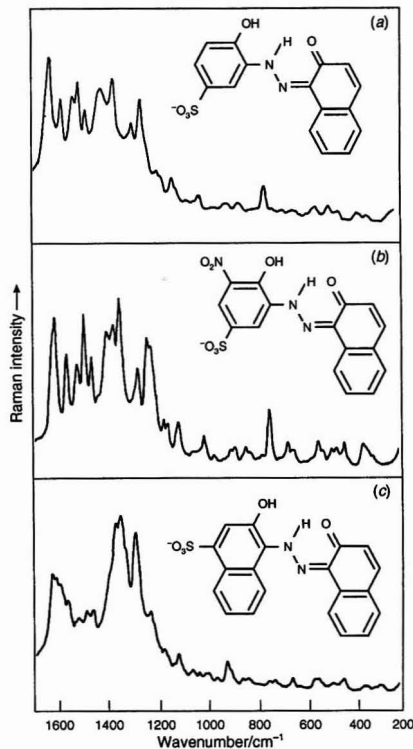
Fig. 4 SERR spectra of poly(L-lysine)–dye complexes in the presence of ascorbic acid. Dyes: (*a*) Mordant Violet 5 (CI 15670), (*b*) Mordant Black 15 (CI 15690) and (*c*) Mordant Black 17 (CI 15705).
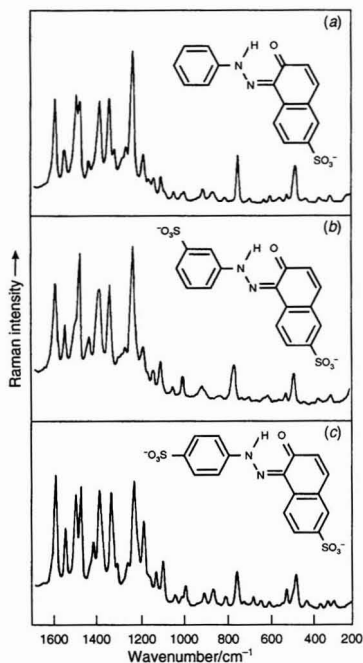
Fig. 5 SERR spectra of poly(L-lysine)–dye complexes in the presence of ascorbic acid. Dyes: (*a*) Acid Orange 12 (CI 15970), (*b*) Food Orange 2 (CI 15980) and (*c*) Food Yellow 3 (CI 15985).
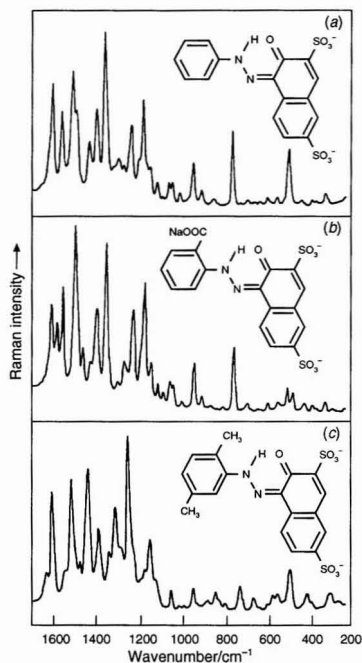
Fig. 7 SERR spectra of poly(L-lysine)–dye complexes in the presence of ascorbic acid. Dyes: (*a*) Acid Orange 14 (CI 16100), (*b*) Mordant Red 9 (CI 16105) and (*c*) Acid Red 26 (CI 16150).
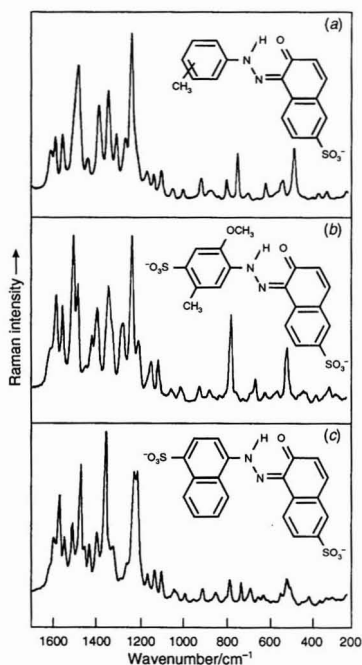
Fig. 6 SERR spectra of poly(L-lysine)–dye complexes in the presence of ascorbic acid. Dyes: (*a*) Acid Orange 16 (CI 16011), (*b*) Food Red 17 (CI 16035) and (*c*) Acid Red 13 (CI 16045).
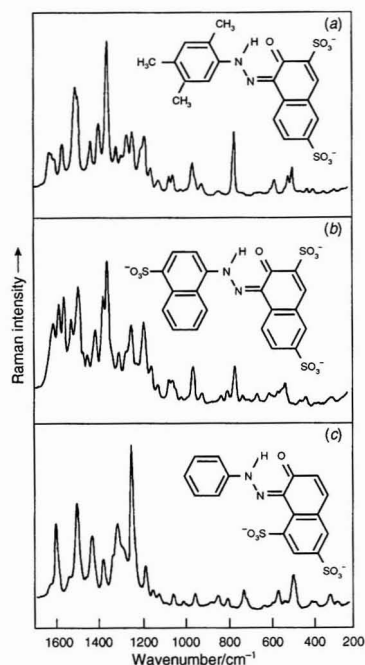
Fig. 8 SERR spectra of poly(L-lysine)–dye complexes in the presence of ascorbic acid. Dyes: (*a*) Food Red 6 (CI 16155), (*b*) Acid Red 27 (CI 16185) and (*c*) Acid Orange 10 (CI 16230).

The UV/VIS absorption spectra of the dyes in the test set (10^{-5} mol l^{-1}; 2 ml) were recorded after the addition of poly(L-lysine) solution (0.01%; 500 µl), and again after the addition of ascorbic acid (1 mol l^{-1}; 150 µl) and compared with those obtained for the dye solutions prior to the addition of the poly(L-lysine) and the ascorbic acid. The addition of poly(L-lysine) to the dye solutions at pH 6 resulted in changes in the absorption spectra. Hypsochromic shifts were observed for the *o*-hydroxyarylazo dyes and bathochromic shifts were

Fig. 9 SERR spectra of poly(L-lysine)–dye complexes in the presence of ascorbic acid. Dyes: (*a*) Acid Red 44 (CI 16250) and (*b*) Acid Red 18 (CI 16255).

observed for the *p*-hydroxyaryl azo and the *o,o*-dihydroxyarylazo dyes. On the subsequent addition of ascorbic acid the hypsochromically shifted *o*-hydroxylarylazo dyes showed little change in the recorded spectra; a number showed a further slight hypsochromic shift. However, a hypsochromic shift was observed for the bathochromically shifted *p*-hydroxyarylazo dye and the *o,o*-dihydroxyarylazo dyes.

The effects of poly(L-lysine) and the ascorbic acid on the *o*-hydroxyarylazo dyes indicate interaction between the dye molecules and poly(L-lysine) via the anionic sulfonic acid substituent. In each instance, the hypsochromic shift observed on the addition of poly(L-lysine) to the dye solutions at pH 6 was not as strong as that recorded when the pH was changed to 12, and clearly from the SERR data was not due to switching from the hydrazone to the azo tautomeric form. Instead, the hypsochromic shift may result from an increase in the electron-withdrawing nature of the sulfonic acid substituents as a result of their interaction with the protonated amino groups of the lysine residues. The further slight hypsochromic shift observed on the subsequent addition of ascorbic acid is also consistent with this model and is due to the promotion of protonation of the amino groups, enhancing the over-all process. The proposed model of interaction between poly(L-lysine) and the *o*-hydroxyarylazo dyes in the presence of ascorbic acid is illustrated in Fig. 10.

The observations for the *p*-hydroxyarylazo and the *o,o*-dihydroxyarylazo dyes cannot be explained by the same proposed model of interaction of poly(L-lysine) and ascorbic acid. The bathochromic shift observed for Acid Brown 102 (CI 14615) on addition of poly(L-lysine) is very similar to that observed at pH 12 and therefore is possibly due to the ionization of the molecule, followed by binding of the poly(L-lysine) at the new anionic site on the dye molecule in competition with binding at the sulfonic acid substituent. On the addition of ascorbic acid ionization would be hindered, favouring binding at the sulfonic acid group and resulting in a hypsochromic shift as observed. There is no obvious explana-

Fig. 10 Proposed model of interaction of poly(L-lysine) and ascorbic acid with an *o*-hydroxyarylazo dye [Acid Orange 12 (CI 15970)].

Table 1 SERRS frequencies (cm⁻¹)* of poly(L-lysine)–dye complexes in the presence of ascorbic acid

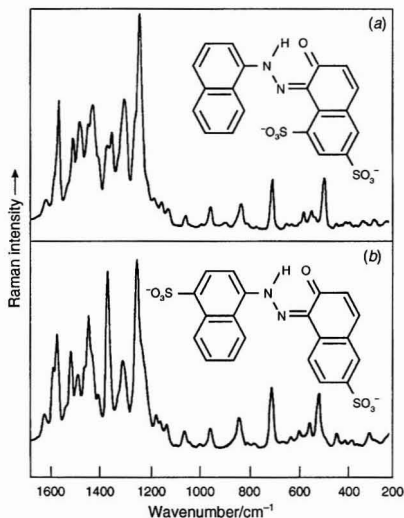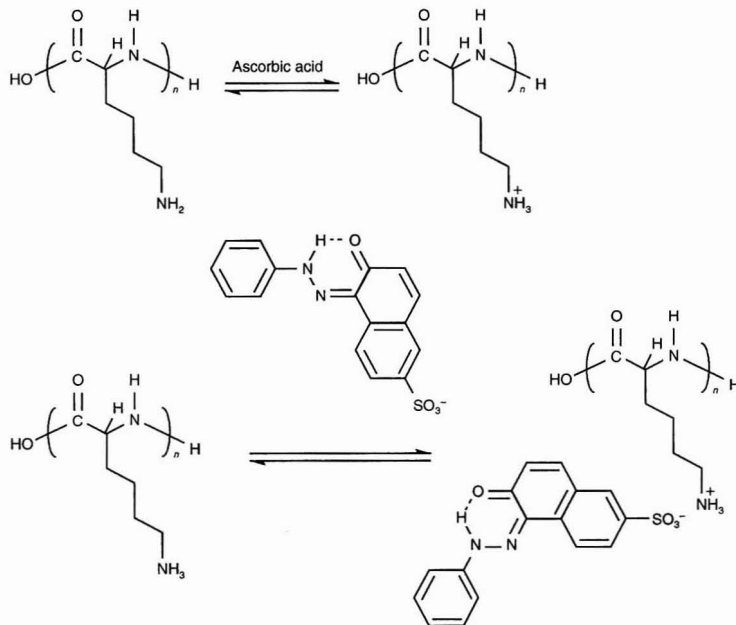| C14615	C15575	C15620	C15670	C15690	C15705	C15970	C15980	C15985	C16011	C16035	C16045	C16100	C16105	C16150	C16155	C16185	C16230	C16250	C16255
1662 m	1603 vs (1)	1603 vs (5)	1599 vs (1)	1599 s (2)	1618 s (4)	1594 vs (3)	1598 s (5)	1596 vs (1)	1603 m	1603 m	1602 m	1597 vs (3)	1608 s (5)	1623 m	1607 m	1600 s (7)	1620 w	1624 w	1630 m
1592 vs (2)	1577 m	1575 vs (6)	1502 vs (6)	1550 s (8)	1603 s (5)	1492 vs (2)	1551 m	1548 s (8)	1582 m	1582 s (5)	1574 s (5)	1498 vs (2)	1552 s (4)	1594 s (4)	1587 m	1573 vs (5)	1590 s (5)	1588 m	1593 m
1572 vs (4)	1550 vs (2)	1551 s (7)	1480 vs (3)	1510 s (10)	1585 s (6)	1478 vs (4)	1482 vs (2)	1499 vs (6)	1548 m	1550 s (6)	1550 m	1480 vs (6)	1490 vs (1)	1533 m	1547 m	1550 vs (4)	1532 w	1572 s (2)	1576 s (4)
1552 vs (3)	1482 vs (3)	1517 s (9)	1450 s (8)	1480 vs (3)	1555 s (7)	1433 m	1433 m	1475 s (4)	1477 vs (2)	1480 s (3)	1516 m	1419 m	1453 m	1499 vs (3)	1488 vs (2)	1517 s (6)	1491 s (2)	1530 w	1538 m
1510 vs (1)	1451 s (9)	1480 s (1)	1385 vs (4)	1450 s (9)	1518 m	1385 vs (5)	1388 vs (4)	1417 s (9)	1433 m	1437 w	1479 vs (2)	1384 s (5)	1388 s (7)	1463 m	1480 s (3)	1482 vs (2)	1455 w	1513 m	1518 s (5)
1480 s (6)	1410 s (8)	1453 s (8)	1337 vs (2)	1385 vs (6)	1507 m	1340 vs (6)	1337 vs (3)	1387 vs (3)	1383 s (4)	1387 s (7)	1460 m	1347 vs (1)	1348 vs (2)	1423 vs (2)	1416 m (1)	1462 m	1424 m	1484 m	1490 m
1450 s (5)	1376 vs (7)	1402 m	1261 s (9)	1350 vs (4)	1480 m	1315 m	1290 m	1333 vs (5)	1340 s (3)	1334 s (4)	1438 m	1286 m	1289 m	1378 m	1378 m	1437 m	1376 m	1450 m	1460 m
1400 s (7)	1334 vs (5)	1363 vs (3)	1227 vs (7)	1335 vs (1)	1453 m	1275 m	1260 m	1307 m	1304 m	1270 m	1403 m	1261 m	1261 m	1330 m	1342 vs	1401 s (10)	1328 m	1432 s (3)	1443 vs (3)
1372 s (11)	1274 m	1341 s (10)	1158	1260 s (11)	1357 vs (2)	1258 m	1230 vs (1)	1257 m	1262 m	1262 m	1365 vs (1)	1227 m	1222 s (6)	1299 s (5)	1299 m	1363 vs (3)	1302 s (4)	1408 m	1403 m
1350 s (9)	1257 m	1288 m	1143	1221 s (5)	1334 vs (1)	1231 vs (1)	1178 m	1228 vs (2)	1232 vs (1)	1224 vs (2)	1328 m	1188 m	1169 vs (3)	1277 m	1273 m	1343 vs (1)	1280 m	1372 m	1363 vs (2)
1329 s (8)	1227 vs (4)	1260 s (11)	1100 m	1210 s (7)	1275 vs (3)	1176 m	1131 m	1180 s (7)	1160 m	1191 m	1290 m	1172 s (4)	1142 m	1261 m	1249 m	1287 m	1234 vs (1)	1351 m	1318 m
1302 s (10)	1211 vs (6)	1231 vs (2)	1085 m	1158	1215 m	1151 w	1097 m	1157 m	1130 w	1131 m	1260 m	1141 m	1111 w	1237 vs (1)	1223 m	1252 m	1178 m	1303 s (4)	1302 m
1274 m	1173 m	1213 vs (4)	1040 m	1140	1161 m	1131 w	1040 w	1127 m	1092 w	1096 m	1231 vs (4)	1108 w	1086 w	1167 m	1180 m	1229 s (9)	1144 w	1252 m	1238 vs (1)
1224 m	1152 m	1161 m	990 m	1098 m	1148 m	1097 w	992 w	1093 m	1040 w	1073 vw	1218 vs (3)	1080 vw	1054 w	1141 m	1168 m	1207 m	1117 w	1238 vs (1)	1219 s (6)
1195 m	1140 m	1141 m	940 w	1040 w	1103 m	1078 w	904 w	1037 w	989 w	1038 w	1164 m	1056 w	1040 w	1118 w	1138 m	1172 s (8)	1081 vw	1208 m	1167 w
1163 w	1098 m	1100 m	880 w	1015 w	1049 w	1037 w	822 vw	1006 w	903 w	994 m	1113 m	1039 w	1000 vw	1045 w	1102 w	1138 m	1048 w	1178 w	1150 w
1140 m	1082 w	1026 w	828 w	995 w	1020 w	988 w	756 m	985 w	862 w	904 w	1100 m	1003 w	940 m	1007 vw	1052 w	1108 w	1002 vw	1146 w	1126 w
1137 m	1040 w	988 w	770 m	955 vw	994 w	968 w	718 vw	920 vw	820 vw	856 w	1040 w	939 m	904 w	985 vw	1033 w	1054 w	982 w	1122 w	1051 w
1090 vw	989 w	945 vw	730 m	890 w	980 w	928 w	687 vw	900 w	783 w	834 vw	1026 w	900 w	858 vw	941 w	998 vw	1039 w	943 w	1090 vw	1030 vw
1042 w	914 w	900 vw	695 w	872 w	950 w	903 w	658 w	860 w	731 m	807 vw	987 w	842 vw	801 vw	921 vw	939 m	994 w	867 vw	1048 w	987 w
998 m	869 w	872 w	665 w	811 w	908 w	854 w	617 vw	802 w	683 vw	756 s	945 vw	749 m	750 m	869 w	896 w	895 w	835 w	982 w	946 w
950 vw	806 w	819 w	610 w	780 vw	848 w	800 vw	598 w	747 m	603 w	729 w	904 w	715 vw	686 vw	832 w	819 vw	806 w	790 w	945 w	860 vw
925 vw	722 w	786 w	540 w	767 w	821 w	739 w	550 vw	717 vw	570 vw	698 vw	843 w	678 vw	628 vw	813 w	743 m	778 w	714 w	884 w	829 w
873 w	689 w	740 w	525 w	732 m	788 w	688 w	513 w	673 w	550 w	663 vw	796 vw	645 vw	587 w	787 vw	717 vw	741 m	700 vw	824 w	795 vw
849 w	652 w	711 w	473 w	662 w	718 w	665 w	474 w	638 w	530 w	641 w	775 w	619 vw	541 w	713 w	703 vw	702 w	620 vw	794 vw	767 vw
827 vw	610 w	688 w	430 w	638 w	660 w	619 w	450 w	600 vw	520 w	597 w	722 w	586 vw	496 w	652 w	630 vw	678 vw	574 vw	758 vw	697 m
780 vw	570 w	646 m	335 vw	590 vw	647 w	590 w	424 vw	550 vw	469 w	537 w	678 w	538 w	468 w	624 w	575 vw	637 w	550 w	745 vw	648 vw
750 vw	550 w	617 w	320 w	562 vw	559 w	545 w	385 vw	533 vw	426 vw	494 m	644 w	480 m	416 m	580 vw	559 w	618 vw	517 vw	696 m	620 w
725 vw	518 w	595 vw	—	538 w	547 w	510 w	360 w	513 w	358 w	440 m	618 w	422 w	373 w	556 vw	492 w	582 w	474 w	636 w	585 w
702 vw	474 w	532 w	—	520 w	484 vw	472 w	300 w	470 m	319 w	420 m	597 vw	372 vw	358 vw	535 w	472 w	565 w	410 vw	580 w	542 w
624 vw	428 w	500 w	—	484 w	438 w	420 w	240 w	421 vw	272 vw	406 w	568 vw	355 vw	314 vw	473 w	435 vw	543 w	392 vw	567 w	502 w
575 vw	360 w	480 w	—	465 w	390 w	390 vw	227 w	357 vw	227 w	360 m	536 w	310 w	279 vw	420 w	404 vw	520 w	372 w	532 w	475 vw
520 w	340 w	428 w	—	433 w	354 vw	360 vw	—	320 w	—	318 vw	507 w	255 vw	210 vw	394 w	376 vw	504 w	325 vw	517 w	429 w
475 m	317 w	347 w	—	354 w	340 w	304 w	—	290 w	—	298 w	491 w	—	—	368 vw	327 vw	470 vw	304 vw	481 vw	393 vw
426 vw	280 vw	300 w	—	320 w	318 vw	225 w	—	—	—	278 vw	437 vw	—	—	327 vw	278 vw	433 vw	270 w	427 vw	367 vw
380 vw	223 w	275 w	—	295 vw	292 vw	—	—	—	—	240 w	425 vw	—	—	286 w	225 w	404 w	—	390 vw	338 vw
350 w	—	—	—	—	—	—	—	—	—	—	405 w	—	—	242 w	—	365 vw	—	372 vw	293 w
320 w	—	—	—	—	—	—	—	—	—	—	357 vw	—	—	—	—	350 w	—	347 vw	268 vw
250 w	—	—	—	—	—	—	—	—	—	—	326 vw	—	—	—	—	286 w	—	317 vw	—
—	—	—	—	—	—	—	—	—	—	—	293 vw	—	—	—	—	—	—	271 w	—
—	—	—	—	—	—	—	—	—	—	—	271 vw	—	—	—	—	—	—	222 w	—

* vs = Very strong; s = strong; m = medium; w = weak; vw = very weak; — = no band.

tion for the effect of poly(L-lysine) and ascorbic acid on the *o,o*-dihydroxyarylazo dyes from these observations alone.

The effect on the *o,o*-dihydroxyarylazo dye Mordant Violet 5 (CI 15670) was examined at a series of concentrations (1×10^{-5}–2×10^{-4} mol l^{-1}). To reproduce better the effect of poly(L-lysine) at various dye concentrations, the concentration of the poly(L-lysine) was increased accordingly (0.01% to 0.2% m/v) to maintain the ratio of lysine residues to dye molecules. On the addition of poly(L-lysine) to the highest concentration Mordant Violet 5 solution (2×10^{-4} mol l^{-1}) no bathochromic shift was observed in the UV/VIS spectrum. However, on dilution of the mixture with distilled water a bathochromic shift was observed. Further investigations confirmed that at a fixed ratio of lysine residues to dye molecules the effect of the poly(L-lysine) is dependent on the concentration of the dye and also on time. At concentrations below 5×10^{-5} mol l^{-1} strong bathochromic shifts are observed. At higher concentrations the initial shifts observed were considerably smaller, but increase when the poly(L-lysine)–dye mixtures were left for several days. A plot of absorption (500 nm) *versus* the concentration of aqueous solutions of Mordant Violet 5 (Fig. 11) indicates a deviation from Beer's law above 5×10^{-5} mol l^{-1}, consistent with the aggregation of dye molecules and the formation of dimers that is typically observed in the concentration range 10^{-4}–10^{-6} mol l^{-1}.[17-19]

It has been reported that an equilibrium exists between the dye monomer and dimer species in solution.[17-19] From the results of this study it has been observed that the number of

free monomer units is decreased on the formation of poly(L-lysine)–dye complexes, and therefore, in order to maintain equilibrium, a number of the dimer species will split to form dye monomers. The interaction of the poly(L-lysine) with the released monomers will continue to upset the equilibrium, repeating the process and resulting in the increase in bathochromic shift with time observed at concentrations above 5×10^{-5} mol l^{-1}.

These observations indicate that the effect of poly(L-lysine) is greatly hindered by the formation of dimers at high concentrations in aqueous solution, suggesting that the sites of poly(L-lysine) interaction on the dye molecules are involved in dimerization. The literature suggests that parallel plane dimers are formed, with interaction of the resonance circuits of aliphatic or cyclic systems of double bonds, *i.e.*, the two-ring systems and the azo group.[18-20] Aggregation does not involve the sulfonic acid groups, which would in fact promote solvation of the molecule, thus hindering dimerization. This would suggest that the site of poly(L-lysine) interaction that induces the bathochromic shift is not the anionic sulfonic acid substituent of the dye molecule.

In the presence of chromium(III), cobalt(III) and copper(II) ions, the mordant dyes act as tridentate ligands, forming complexes with the metals *via* the two *o*-hydroxy groups and the azo group.[13] Correct conformation of the dyes in the azo tautomer is essential for complex formation of this type and both *o*-hydroxy groups are required to be on one side of the plane of the azo group before bonding with the metal centre can occur. On the formation of parallel plane dimers, the monomer dye units will be held in a fixed confirmation with the two *o*-hydroxy groups oriented on opposite sides of the plane of the azo group. Thus, the formation of dye–metal complexes is largely prevented by dimerization and high dye concentrations. It is proposed that the protonated amino groups of the lysine residues are complexed with the dye in a similar fashion. At low concentrations ($<5 \times 10^{-5}$ mol l^{-1}), this interaction will affect the azo–hydrazone tautomeric equilibrium in favour of the azo form. This is consistent with the bathochromic shift observed in the visible absorption spectra and the observation that the SERR spectra are in the azo tautomeric form. On addition of ascorbic acid, the hydrazone form would be stabilized, preventing complex formation of this type. In this case the poly(L-lysine)–dye interaction would occur *via* the sulfonic acid group. This is consistent with the hypsochromic shift observed in the visible
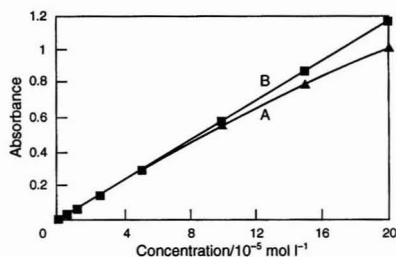

Fig. 11 Graph of absorbance (500 nm) *versus* concentration of Mordant Violet 5 (CI 15670). A, absorbance measured and B, absorbance calculated.
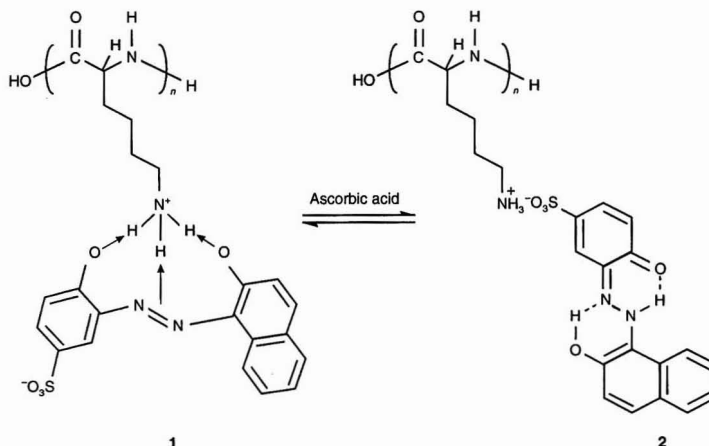

Fig. 12 Proposed model of interaction of poly(L-lysine) with **1**, an *o,o*-dihydroxyarylazo dye (Mordant Violet 5) and **2**, the result of ascorbic acid being present.

absorption spectra and the SERRS of the hydrazone tautomeric forms on the addition of ascorbic acid. The proposed model of interaction between the poly(L-lysine) and the *o,o*-dihydroxyarylazo dyes with and without the presence of ascorbic acid is illustrated in Fig. 12. Mordant Red 9 (CI 16105) also acts as a tridentate ligand, but chelation is notably weaker via the carboxylate group of this dye type than *via* a hydroxy group and hence it acts in a similar fashion to the other *o*-hydroxyarylazo dyes.

In the presence of ascorbic acid, the bonding of all the acidic monoazo dyes to the poly(L-lysine) is proposed to be analogous to the action of these dyes in the colouring of wool fibres. The lysine residues of the wool α-keratin are the primary sites of attachment of the anionic dye molecules. Under the correct conditions for dyeing, the amino groups of the residues will become protonated, attracting the negatively charged dye molecules. In a similar fashion, the ionic interactions between the poly(L-lysine) and the sulfonic acid groups of the dye molecules lead to the formation of poly(L-lysine)–dye complexes. The proposed model of interaction between poly(L-lysine) and the full set of acidic monoazo dyes individually in the presence of ascorbic acid is the same as that for *o*-hydroxyarylazo dyes (Fig. 10).

Role of poly(L-lysine) and Ascorbic Acid in the SERRS Procedure

The protonated amino groups of the unbound lysine residues of the poly(L-lysine)–dye complexes are attracted to and readily adsorbed onto the negatively charged organic layer at the surface of the sol particles, leading to controlled aggregation of the particles and an intense SERRS effect. The amount of ascorbic acid used will promote the protonation of the lysine residues and will also hinder the ionization of the *p*-hydroxylated and the *o,o*-dihydroxylated dyes. It does not directly promote aggregation and thus provides a more stable aggregate than that obtained on the addition of a mineral acid, *e.g.*, nitric acid or hydrochloric acid. Ascorbic acid is a mild reducing agent capable of cleaving monoazo species at the N=N bond to form two colourless primary amines. However, reduction of these dyes was found to be negligible under the present conditions. From the absorbance spectra recorded at a concentration where linearity is observed for Beer's law, a maximum of 7.5% of azo dye was found to be reduced over 100 h.

Poly(L-lysine) is commonly used for the determination of the secondary structure content of proteins by Raman spectrometry.[21,22] As such, the Raman spectra of the α-helical, β-sheet and random coil conformations are well characterized. Under the conditions used in this study, the literature would support a preference for the random coil conformation.[23] For random coiled poly(L-lysine) in solution, the amide I and III frequencies are reported to be at 1665 and 1243–1248 cm^{-1}, respectively. However, these bands are absent in the SERR spectra of the poly(L-lysine)–dye complexes indicating that poly(L-lysine) makes no observable contribution to the spectra. Comparison of the SERRS spectra with the RR spectra of the individual dyes confirmed that the Raman bands observed can be attributed in full to the dye molecule. This observation is attributed to the magnitude and selectivity of SERRS enhancement. The excitation wavelength (457.9 nm lies directly under the principle absorbance bands of the dyes examined. However, poly(L-lysine) does not absorb in the visible region. The principle absorption band is in the vacuum ultraviolet region (approximately 218 nm). Although the poly(L-lysine)–dye complex may form an extended chromogen, only the bands corresponding to certain vibrations with atomic displacements within the resonant chromophore, *i.e.*, the parent dye structure, will be enhanced. Therefore, Raman scattering due

to the vibrations of the poly(L-lysine) are not observed in the SER spectra as the intensity of these bands is very small relative to the SERR bands of the parent dye structure.

Reproducibility of the SERRS Procedure

Surface enhancement is greatest when aggregation is induced in the silver colloids as the electromagnetic field is strongest in the interstices of the aggregates. Therefore, the stability and reproducibility of the aggregation procedure are vital to ensure a consistent surface enhancement of the Raman-active species. This is of particular importance when scanning instrumentation is employed to ensure that the degree of surface enhancement is maintained throughout the duration of a single scan. Otherwise the relative intensities of bands will be falsely represented. Precise sample alignment is also very important for all Raman spectrometry and small variations can greatly affect the scattering intensity observed, thereby increasing the between-run error.

The SERR spectrum (1000–1700 cm^{-1}) for a single colloidal mixture aggregated by the above procedure was recorded six times at 20 min intervals with the sample cell being removed and replaced between each scan. The relative standard deviations (s_r) in scattering intensity (counts s^{-1}) for four individual Raman bands were all found to be approximately 4.8%. This was found to be consistent across the set of dyes. This was repeated for a sample of pure ethanol. The s_r in scattering intensity for the principle Raman band of ethanol (885 cm^{-1}) was found to be 1.9%. This corresponds to the random error associated with minor fluctuations in excitation intensity, the precision of photon counting and the precision of sample alignment. Therefore, the within-run error resulting from instability of the aggregates with time should be no greater than 3%.

The SERR spectra of the 20 dyes were recorded at various undetermined intervals over an 8-week period. The same instrumentation was used for all analyses but three separately prepared silver colloids and six separate poly(L-lysine) solutions (three each from two batches) were used. In addition, ascorbic acid solutions were freshly prepared before each analysis. The between-run error varied between individual dyes. The s_r for the principle band of each ranged between 5.7% for CI 15690 and 25.0% for CI 16035 (mean s_r = 13.0%). A notable feature was that low between-run errors were observed for the *p*-hydroxy- and *o,o*-dihydroxyarylazo dyes. However, no other relationship between dye structure and between-run error provided an explanation for the large variation observed.

The deviation observed in vibrational frequency was negligible (<3 cm^{-1}) and could be attributed to operator error.

Concentration Dependence and Detection Limits

The SERRS for Acid Orange 10 (CI 16230) was recorded at a number of initial dye concentrations <10^{-5} mol l^{-1}. Plots of initial dye concentrations of 0–3 × 10^{-6} mol l^{-1} and 0–10^{-5} mol l^{-1} *versus* scattering intensity (1234 cm^{-1}) are illustrated in Fig. 13. Over the concentration range 0–3 × 10^{-6} mol l^{-1}, the plot is linear, but the deviation from linearity is outwith the expected within-run error at concentrations above 3 × 10^{-6} mol l^{-1}. At higher concentrations (3 × 10^{-6}–1 × 10^{-5} mol l^{-1}), increased absorption of the radiation by the dye results in a reduction in scattering intensity from that expected. The linearity at concentrations <3 × 10^{-6} mol l^{-1} supports the application of this SERRS procedure for both qualitative and semi-quantitative analyses of trace amounts of dyes.

The final concentration examined corresponded to a total amount of dye of approximately 300–500 pg. However, this is not the true detection level as only a small portion of the 2.5 ml of colloidal suspension is irradiated. A fraction of the bulk sample size may be examined easily by Raman microscopy, improving sensitivity, and charge-coupled device (CCD) detection is expected to further this improvement.

Fingerprint Analysis

Resonance enhancement plays a major role in the SERRS of the acidic monoazo dyes and, as with the resonance Raman spectra, strong similarities in the vibrational frequencies were expected for dyes that share the same chromophore. The differences observed in the SERR spectra are due to the effect of the auxochromes on specific normal vibrational modes of the chromophore, resulting in shifts in the vibrational frequencies, and are also due to the influence of the auxochromes on the electronic structure and therefore the relative intensities of each band. The differences in relative intensity are more significant than the shifts in vibrational frequency and greatly aid discrimination between the dyes.

Discrimination between all the dyes was possible on the basis of their five principal bands compared in order of relative
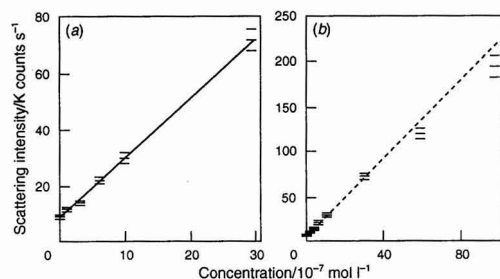
Fig. 13 Graph of SERRS intensity (1234 cm^{-1}) *versus* initial dye concentration (Acid Orange 10 (CI 16230). Initial dye concentration ranges: (*a*) 0–3 × 10^{-6} mol l^{-1} and (*b*) 0–10^{-5} mol l^{-1}.

Table 2 Five principal bands in order of relative intensity of the test set of 20 acidic monoazo dyes. Principal bands required for discrimination of individual bands are in bold type

Dye		Principal SERRS band/cm^{-1}				
Generic name	Colour Index No.	1	2	3	4	5
Acid Orange 12	CI 15970	**1231**	**1492**	**1594**	**1478**	1385
Acid Orange 10	CI 16230	**1234**	**1491**	**1590**	**1302**	1424
Food Orange 2	CI 15980	**1230**	**1482**	1337	1388	**1598**
Acid Orange 16	CI 16011	**1232**	**1477**	**1340**	**1383**	**1548**
Acid Red 26	CI 16150	**1237**	**1423**	1499	1594	1299
Acid Red 44	CI 16250	**1238**	**1572**	1432	1303	1484
Acid Red 18	CI 16255	**1238**	**1363**	1443	1576	1518
Mordant Black 15	CI 15690	**1335**	**1599**	1480	1350	1221
Mordant Black 17	CI 15705	**1334**	**1357**	1275	1618	1603
Acid Orange 14	CI 16100	**1347**	**1498**	1597	1172	1384
Food Red 6	CI 16155	**1342**	**1488**	**1480**	1378	1223
Acid Red 27	CI 16185	**1343**	**1488**	**1363**	1550	1573
Acid Red 13	CI 16045	**1365**	**1479**	1218	1231	1574
Acid Red 88	CI 15620	**1480**	**1231**	1363	1213	1603
Mordant Red 9	CI 16105	**1490**	**1348**	1169	1552	1608
Acid Brown 102	CI 14615	**1510**	**1592**	1552	1572	1450
Food Red 17	CI 16035	**1501**	**1224**	1480	1334	1582
Acid Orange 8	CI 15575	**1603**	**1550**	1482	1227	1334
Mordant Violet 5	CI 15670	**1599**	**1337**	1480	1385	1550
Food Yellow 3	CI 15985	**1596**	**1228**	1387	1475	1333

intensity. The five principal bands of the acidic monoazo dyes are reported in Table 2. The identification of one of the 20 dyes is possible on the basis of the first principal band, 13 dyes require two bands, two dyes require three bands, two require four bands and the final two dyes require all five principal bands to ensure complete discrimination.

Blind Trials

Six unknown samples (A–F) were examined as a blind trial to assess the above SERRS procedure. Initial SERRS examinations were carried out for each sample without purification of the dye mixture. The vibrational frequencies and the relative intensities of the five principle bands for each sample were compared with those recorded for the 20 dyes in the test set. The vibrational frequencies of the principle bands in order of intensity for each sample are listed in Table 3. From the initial examination, samples C, D and F were correctly identified as each containing single dye components, Food Red 17 (CI 16035), Acid Red 27 (CI 16185) and Food Orange 2 (CI 15980), respectively. Sample B was correctly identified as containing two dye components, Acid Red 44 (CI 16250) and Acid Red 18 (CI 16255). The recorded spectrum for this mixture was dominated by Acid Red 44, although the actual mixture was 1 + 1. TLC indicated more clearly that the sample mixture was approximately 1 + 1 and enabled the SERR spectra to be recorded for the individual components of sample B [Acid Red 44 (CI 16250) and Acid Red 18 (CI 16255)] extracted from the TLC plate.

Samples A and E were identified as both being phenylazonaphthol dyes, but were not believed to correspond to any of the dyes in the test set. This was confirmed for sample E, which was revealed to be the acidic bis-azo dye Biebrich Scarlet (CI 26905). However, the initial examination had failed to identify sample A from the dye test set. TLC of sample A indicated the presence of a second minor dye component ($R_F = 0.39$) in the sample mixture in addition to the principle dye component ($R_F = 0.57$). From the subsequent SERRS examination of the predominant component extracted from the TLC plate, sample A was found to have new principle bands at 1237, 1425, 1501, 1595 and 1300 cm^{-1}, and was correctly identified as containing Acid Red 26 (CI 16150). Although Acid Red 26 was the predominant component of sample A, the absorbance maximum of the unknown minor dye component was approximately 480 nm compared with approximately 505 nm for Acid Red 26. Therefore, with excitation at 457.9 nm the resonance enhancement will be greater for the minor component.

Conclusions

The initial resonance Raman studies indicate that Raman scattering can be applied to the characterization of acidic monoazo dyes. By the comparison of the RR spectra discrimination between the 20 dyes examined, including

Table 3 Five principal bands in order of relative intensity of the unknown dye samples

Blind trial sample	Principal band/cm^{-1}				
	1	2	3	4	5
A	1419	1235	1593	1497	1381
B	1237	1431	1572	1298	1358
C	1498	1222	1478	1332	1580
D	1345	1480	1365	1550	1573
E	1480	1392	1602	1450	1332
F	1228	1480	1335	1388	1598

structural isomers, was achieved. However, some difficulties were still experienced owing to the underlying fluorescence background, the narrow concentration range over which scattering is observed (10^{-4}–10^{-3} mol l^{-1}) and the relatively high detection limit. Therefore, although highly selective, RR spectrometry does not provide the sensitivity required.

Addition of an aqueous solution of each dye to the silver sol produces no aggregation or SERRS. This is attributed to poor adsorption of the anionic dye molecules to the sol particles due to the negatively charged citrate layer on the surface of the silver. However, the addition of the poly(L-lysine) solution, prior to that of the dye solution, produces aggregation and intense SERRS for the poly(L-lysine)–dye complexes. In addition to an enhancement of approximately 10^5–10^6-fold in scattering intensity compared with solution resonance, the fluorescence background that partially obscures the RR spectra for many of the dyes is quenched by radiationless energy transfer to the metal surface.

The bonding of the poly(L-lysine) with the acidic monoazo dyes is dependent on the subset to which the individual dye belongs. For the *o*-hydroxyarylazo dyes the effect of poly(L-lysine) of the UV/VIS spectra suggests the interaction of the protonated amino group of the lysine residues with the sulfonic acid sites on these dyes. The presence of ascorbic acid promotes the protonation of the amino groups and increases the efficiency of the process. On the addition of poly(L-lysine) to the *p*-hydroxyarylazo dyes ionization occurs and subsequent binding at the new anionic sites is in competition with binding at the sulfonic acid substituent. The addition of ascorbic acid hinders ionization and favours binding at the sulfonic acid group. For the *o,o*-dihydroxyarylazo dyes the addition of poly(L-lysine) results in the ionization of the two hydroxy groups. The ionized dyes act as tridentate ligands, forming complexes with the protonated amino groups of the poly(L-lysine) *via* the two *o*-hydroxy groups and the π-electrons of the azo group. The addition of ascorbic acid prevents ionization and favours binding at the sulfonic acid groups of the dyes. For the last two subsets of dyes the interaction of poly(L-lysine), in the presence of ascorbic acid, appears to revert to that observed for the former. This is reflected in the observed SERR spectra. Therefore, a single model can be used to describe the action of poly(L-lysine) with the set of acidic monoazo dyes collectively.

The between-run error varied greatly between individual dyes. However, the within-run error was both consistent and low across the set ($s_r \leqslant 5\%$), indicating the possibility of quantitative dye analysis. Linearity of concentration *versus* scattering intensity was observed at low concentrations ($< 3 \times 10^{-6}$ mol l^{-1}). This supports the application of this SERRS procedure for both qualitative and semi-quantitative analysis of trace amounts of acidic monoazo dyes.

The findings of the blind trials confirm the usefulness of SERRS for qualitative analysis. However, the importance of sample purity is also demonstrated, indicating that the technique may be of greatest use in forensic science following an initial TLC examination of unknown dye samples.

References

1 White, P. C., and Harbin, A.-M., *Analyst*, 1989, **114**, 877.
2 Lee, P. C., and Meisel, D., *J. Phys. Chem.*, 1982, **86**, 3391.
3 Hildebrandt, P., and Stockburger, M., *J. Phys. Chem.*, 1984, **88**, 5935.
4 Xu, Y., and Zheng, Y., *Anal. Chim. Acta*, 1989, **225**, 227.
5 Sheng, R.-S., Zhu, L., and Morris, M. D., *Anal. Chem.*, 1986, **58**, 1116.
6 Xi, K., Sharma, S. K., and Muenow, D. W., *J. Raman Spectrosc.*, 1992, **23**, 621.
7 Xi, K., Sharma, S. K., Taylor, G. T., and Muenow, D. W., *Appl. Spectrosc.*, 1992, **46**, 819.
8 Tran, C. D., *Anal. Chem.*, 1984, **56**, 824.
9 Kneipp, K., Hinzmann, G., and Fassler, D., *Chem. Phys. Lett.*, 1983, **99**, 503.
10 Ohshima, S., Kajiwara, T., Hiramoto, K., and Sakata, T., *J. Phys. Chem.*, 1986, **90**, 4474.
11 Pineda, A. C., and Ronis, D. J., *J. Chem. Phys.*, 1985, **83**, 5330.
12 Munro, C. H., Smith, W. E., and White, P. C., *Analyst*, 1993, **118**, 731.
13 Gordon, P. F., and Gregory, P., *Organic Chemistry in Colour*, Springer, Berlin, 1983.
14 Sagaster, H.-R., Schadlich, H., and Robisch, G., *Z. Chem.*, 1987, **27**, 298.
15 Munro, C. H., Smith, W. E., Armstrong, D. R., and White, P. C., *J. Phys. Chem.*, 1995, **99**, 879.
16 Jolivet, J. P., Gzara, M., Marieres, J., and Lefebvre, J., *J. Colloid Interface Sci.*, 1985, **107**, 429.
17 Jacobson, B. S., and Branton, D., *Science*, 1977, **195**, 302.
18 Monahan, A. R., and Blossey, D. F., *J. Phys. Chem.*, 1970, **74**, 4014.
19 Monahan, A. R., Germano, N. J., and Blossey, D. F., *J. Phys. Chem.*, 1971, **75**, 1227.
20 Sheppard, S. E., and Geddes, A. I., *J. Am. Chem. Soc.*, 1944, **66**, 1995.
21 Chen, M. C., and Lord, R. C., *J. Am. Chem. Soc.*, 1974, **96**, 4750.
22 Lippert, J. L., Tyminski, D., and Desmeules, P. J., *J. Am. Chem. Soc.*, 1976, **98**, 7075.
23 Yu, T.-J., Lippert, J. L., and Peticolis, W. L., *Biopolymers*, 1973, **12**, 2161.

Near-infrared Reflectance Spectrometry in the Determination of the Physical State of Primary Materials in Pharmaceutical Production

Elena Dreassi, Giuseppe Ceramelli and Piero Corti

Dipartimento Farmaco Chimico Tecnologico, Via Banchi di Sotto 55, 53100 Siena, Italy

Silvano Lonardi

Glaxo SpA, Via Fleming 2, 37100 Verona, Italy

Piero Luigi Perruccio

Stabilimento Chimico Farmaceutico Militare, Via R. Giuliani 201, 50144 Florence, Italy

Near-infrared reflectance spectrometry was used to determine various physical characteristics of primary materials currently used in the pharmaceutical industry. It was possible to distinguish substances with different grain sizes, crystalline states and densities.

Keywords: Near-infared reflectance spectrometry; qualitative analysis; physical state; pharmaceuticals

Introduction

In recent years there has been a revival of interest in the near-infrared spectral region (1100–2500 nm) for the analytical determination of chemical parameters in multiple matrices and industrial products. This has been due to the specific characteristics of this spectral region, the availability of modern instrumentation and the development of advanced chemometric approaches.[1]

This study is part of a research programme into the applications of near-infrared reflectance spectrometry (NIRS) in the analysis and control of pharmaceuticals.[2-11] The capacity of NIRS to distinguish different substances and to provide quickly precise and accurate determinations of pharmaceutical substances contained in solid matrices is well known. In order to justify further its use in the pharmaceutical sector, we considered it of interest to investigate its use for characterizing pharmaceuticals on the basis of their physical properties. Information on the crystalline state, grain size and density of a powder is very important in the stages of formulation and control of the activity of an active ingredient. The products studied and their physical properties are listed in Table 1.

Experimental

NIRS Analysis

NIRS analysis was performed with an InfraAlyzer 500 spectrophotometer (Bran + Luebbe) operating in the 1100–2500 nm band. The powders were placed in polyethylene cells and covered with a microscope slide. Each sample was read in triplicate, refilling the cells with powder for each reading.

Processing of Spectral Data

Linear discriminant analysis was used to process the raw absorbance data. The software used for the analysis was Idas-pc v. 1.41 (Bran + Luebbe). The normalized distances of unknown samples were used as the discriminating parameter: when these distances were less than 3 from one of the reference groups, the sample was assigned to that group; when the distance was greater than 3 the sample was not assigned to any group. For each product a single calibration map was plotted, and each was verified using samples taken as unknowns. For each product we used, for the single form, six samples obtained from different production cycles.

Reference Analysis

The physical properties of the various samples were determined before NIRS with appropriate traditional methods (microscopy, differential thermal analysis, density measurement).

Results and Discussion

The capacity of NIRS to differentiate compounds with substantially similar structures has already been demonstrated by other workers.[12,13] In our laboratory, we have obtained

Table 1 Products investigated and their properties

Compound	Systematic name	Properties
Nitrofurantoin	1-(5-Nitro-2-furanyl)-methyleneamino-2,4-imidazolidinedione	Macro- and micro-crystalline
Paracetamol	*N*-(4-Hydroxyphenyl)-acetamide	Two forms of different density
Gemfibrozil	5-(2,5-Dimethylphenoxy)-2,2-dimethylpentanoic acid	Crystallized from different solvents
Chenodeoxycholic acid	(3α,5β,7α)-3,7-Dihy-droxycholan-24-oic acid	Four polymorphs
Ibuprofen	α-Methyl-4-(2-methyl-propyl)benzeneacetic acid	High and low density
Levamisole–tetramisole	2,3,5,6-Tetrahydro-6-phenylimidazo(2,1-*b*)-thiazole	Levo form and racemic mixture

good results in identifying structurally similar primary materials[9-11] and pharmaceuticals prepared by different methods.[6,10]

Nitrofurantoin

Micro- and macrocrystalline nitrofurantoin were investigated. Their differential identification is of interest because of their different bioavailabilities. The NIR spectra of the two forms are reported in Fig. 1. The Mahalanobis distance obtained in the calibration map between the two groups was 12.7. Table 2, A shows the results obtained for several samples taken as unknowns. None of the samples were erroneously assigned: their distances were always less than 3 with respect to their group and more than 3 with respect to the other group.

In order to verify the operating capacity of the method, physical mixtures of different percentages of the two forms were prepared. In this instance the distances obtained were much greater than 10 normalized distances (range 10.70–21.92) from the reference groups. The different crystallinities of the mixtures gave absorptions directly correlated with the nature of the sample analysed.

Paracetamol

Fig. 2 shows the spectra of two forms of paracetamol having different apparent densities. The Mahalanobis distance obtained during analysis was 64.4. Although the spectral distances were less evident than for nitrofurantoin, the testing of samples taken as unknowns gave even better results. Table 2, B shows the results obtained with the test samples; in no instances were the normalized distances less than 3 with respect to the reference group and they were always more than 13 with respect to the other group. This again confirms the good capacity of the method.

A sample rejected by traditional reference methods was not assigned, as it had normalized distances greater than 3 with respect to both reference groups.

Gemfibrozil

In this instance there were three groups of samples to be distinguished on the basis of the solvent from which the drug was crystallized (hexane, methanol–water and acid–based treatment). After keeping the compounds in a vacuum oven until constant mass was obtained, the solvent residues in the three forms were below 0.5% in all instances. Despite the sensitivity of NIRS for solid-state systems, these levels did not influence differentiation between the three groups.

The spectra of the three species are shown in Fig. 3. Table 3, A shows the Mahalanobis distances between the three groups. Discrimination between the three species was good. Testing with samples taken as unknowns confirmed the
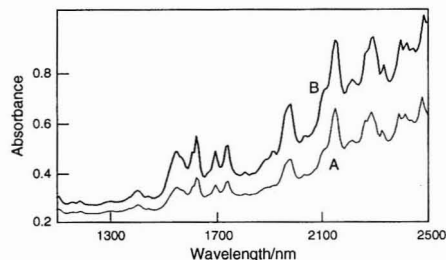
Fig. 1   NIR spectra of A, micro- and B, macro-crystalline nitrofurantoin.

Table 2 A, Range of variation of normalized distances obtained for 20 samples of both forms of nitrofurantoin taken as unknowns and B, range of variation of normalized distances obtained for 18 samples of both forms of paracetamol taken as unknowns

System	Form	Normalized distances from	
		Micro form	Macro form
A	Micro-crystallized nitrofurantoin	0.2–2.5	10.3–16.4
	Macro-crystallized nitrofurantoin	9.6–12.4	0.9–2.0

System	Form	Normalized distances from	
		Paracet-amol A	Paracet-amol B
B	Paracetamol A	0.1–1.0	16.7–17.5
	Paracetamol B	14.0–14.5	0.4–1.1
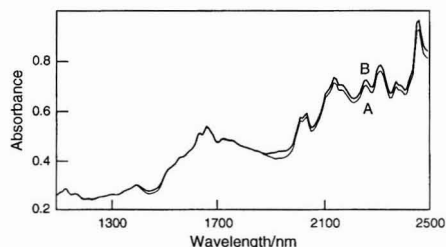
Fig. 2   NIR spectra of paracetamol forms A and B.
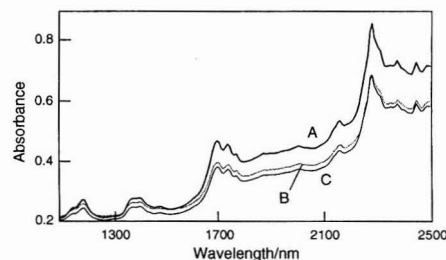
Fig. 3   NIR spectra of gemfibrozil samples crystallized from A, hexane; B, methanol–water; and C, acid–base treatment.

Table 3 A, Mahalanobis distances for gemfibrozil crystallized from hexane, methanol–water and acid–base treatment and B, Mahalanobis distances for four polymorphs (Pm) of chenodeoxycholic acid

System	Crystallized from	Mahalanobis distances from		
		Hexane	Methanol–water	Acid–base
A	Hexane	—		
	Methanol–water	102.7	—	
	Acid–base	98.3	26.8	—

System	Form	Mahalanobis distances from			
		Pm 1	Pm 2	Pm 3	Amor-phous
B	Pm 1	—			
	Pm 2	173.3	—		
	Pm 3	85.3	93.5	—	
	Amorphous	258.7	85.4	177.3	—

Table 4 A, Range of variation of normalized distances obtained for 15 samples of the three forms of gemfibrozil taken as unknowns and B, range of variation of normalized distances obtained for 16 samples of each polymorph (Pm) of chenodeoxycholic acid taken as unknowns

System	Crystallized from	Normalized distances from		
		Hexane	Methanol–water	Acid–base
A	Hexane	1.2–2.8	82.7–84.1	26.3–32.8
	Methanol–water	58.6–59.8	1.1–2.7	48.4–49.6
	Acid–base	72.8–74.0	24.0–26.4	0.5–2.4

System	Form	Normalized distances from			
		Pm 1	Pm 2	Pm 3	Amorphous
B	Pm 1	0.8–1.6	82.8–83.5	57.3–58.6	161.5–164.3
	Pm 2	108.6–109.2	1.1–1.6	62.8–64.8	53.1–54.6
	Pm 3	54.7–55.8	43.4–45.8	1.4–2.3	110.5–112.9
	Amorphous	161.7–164.8	40.5–42.3	117.9–124.6	1.4–2.7
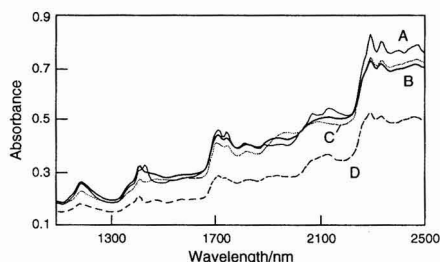
Fig. 4 NIR spectra of four polymorphs of chenodeoxycholic: A, Pm 1; B, Pm 2; C, Pm 3; and D, amorphous.
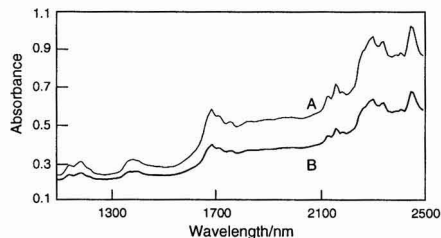
Fig. 5 NIR spectra of A, high- and B, low-density ibuprofen.

Table 5 A, Range of variation of normalized distances obtained for 22 samples of both forms of ibuprofen taken as unknowns and B, range of variation of normalized distances obtained for 16 samples of levo form (levamisole) and 21 samples of racemic mixture (tetramisole) taken as unknowns

System	Form	Normalized distances from	
		High density ibuprofen	Low density ibuprofen
A	High-density ibuprofen	1.1–2.4	49.6–51.2
	Low-density ibuprofen	56.5–62.3	1.5–2.5

System	Form	Normalized distances from	
		Levamisole	Tetramisole
B	Levamisole	1.1–2.6	49.7–51.8
	Tetramisole	60.4–61.6	0.9–2.0

differentiating capacity of the method (Table 4, A): no sample was erroneously assigned and the normalized distances with respect to other groups were always greater than 10.

Chenodeoxycholic Acid

Four polymorphs of chenodeoxycholic acid were investigated: three forms differed in crystallinity and the other was amorphous (melting points 168, 138, 119 and 107 °C, respectively). Fig. 4 shows the NIRS spectra of the four polymorphs. Table 3, B gives the Mahalanobis distances obtained during plotting of the calibration map. Again, the distances obtained guaranteed good discrimination. Table 4, B shows that the assignments of samples taken as unknowns were always correct and never borderline. It is interesting that Giuseppetti and Paciotti[14] had difficulty in obtaining meaningful results with mid-IR spectral resolution.

Ibuprofen

High- and low-density ibuprofen samples were tested. Fig. 5 shows the spectra of the two species. The distance obtained for the calibration system was 102.7. The large distance between the two groups guarantees the discriminating capacity of the method. Table 5, A shows the distances for test samples taken as unknowns. There were no erroneous or dubious assignments and normalized distances with respect to the other group were always greater than 47.

Levamisole and Tetramisole

The method was even capable of distinguishing the *levo* form (levamisole) from the racemic mixture (tetramisole). The two samples differed in crystallinity. Fig. 6 shows the spectra of the *levo* form and the racemic mixture. The Mahalanobis distance obtained for the two systems was 48.3. When the map was tested with samples taken as unknowns, no wrong assignments occurred (Table 5, B).

Conclusions

The results obtained are interesting because they confirm the capacity of NIRS as a fast and simple analytical system for checking the physical parameters of pharmaceutical substances. The complexity of the calibration required is considerable, for both quantitative and qualitative analysis, but the extreme simplicity of their subsequent use for testing unknown samples fully justifies the attention that NIRS has attracted, especially in pharmaceutical control.

The results of this study confirm that the method provides a reliable over-all verification of primary materials or a pharmaceutical in the course of production. The method is very rapid and is non-destructive and non-invasive of the samples.
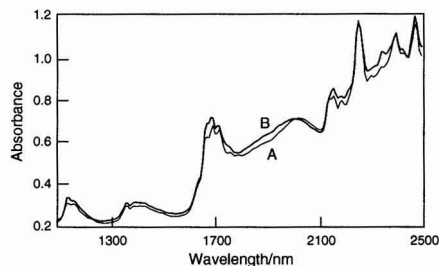
Fig. 6 NIR spectra of A, levamisole and B, tetramisole.

Our results confirm various investigations by Ciurczak and co-workers[15–17] on NIR spectra and the physical properties of powders. The possibility of correlating NIR spectra with the crystallinity (nitrofurantoin, chenodeoxycholic acid, gemfibrozil, levamisole–tetramisole) and apparent density (ibuprofen) of the species tested is of particular interest.

Once the calibration maps have been plotted, it is possible to obtain quickly and simply an over-all view (qualitative or quantitative) of the substances used in the formula, thus guaranteeing the quality of the product.

References

1 Corti, P., Dreassi, E., and Lonardi, S., *Farmaco*, 1993, **48**, 1.
2 Lonardi, S., Viviani, R., Mosconi, L., Bernuzzi, M., Corti, P., Dreassi, E., Murratzu, C., and Corbini, G., *J. Pharm. Biomed. Anal.*, 1989, **7**, 303.
3 Corti, P., Dreassi, E., Murratzu, C., Corbini, G., Ballerini, L., and Gravina, S., *Pharm. Acta Helv.*, 1989, **64**, 140.
4 Corti, P., Dreassi, E., Corbini, G., Ballerini, L., and Gravina, S., *Pharm. Acta Helv.*, 1990, **65**, 189.
5 Corti, P., Dreassi, E., Corbini, G., Lonardi, S., and Gravina, S., *Analusis*, 1990, **18**, 112.
6 Corti, P., Dreassi, E., Corbini, G., Montecchi, L., and Paggi, J., *Analusis*, 1990, **18**, 117.
7 Corti, P., Dreassi, E., Corbini, G., Lonardi, S., Viviani, R., Mosconi, L., and Bernuzzi, M., *Pharm. Acta Helv.*, 1990, **65**, 28.
8 Corti, P., Dreassi, E., Franchi, G. G., Corbini, G., Moggi, A., and Gravina, S., *Int. J. Crude Drug Res.*, 1990, **28**, 185.
9 Corti, P., Dreassi, E., Ceramelli, G., Lonardi, S., Viviani, R., and Gravina, S., *Analusis*, 1991, **19**, 198.
10 Corti, P., Dreassi, E., Savini, L., Petriconi, S., Genga, R., Montecchi, L., and Lonardi, S., *Proc. Control Qual.*, 1992, **2**, 131.
11 Corti, P., Savini, L., Dreassi, E., Ceramelli, G., Montecchi, L., and Lonardi, S., *Pharm. Acta Helv.*, 1992, **67**, 57.
12 Ciurczak, E. W., and Maldacker, T. A., *Spectroscopy*, 1986, **1**, 36.
13 Rostaing, B., Delaguis, P., Guy, D., and Roche, J., *Soc. Fr. Sci. Techn. Pharmaceut.*, 1988, **4**, 509.
14 Giuseppetti, G., and Paciotti, M., *Farmaco*, 1978, **33**, 644.
15 Ciurczak, E. W., paper presented at the 8th Annual Symposium on NIRA, Technicon, Tarrytown, NY, 1985.
16 Buchanan, B. R., Ciurczak, E. W., Grunke and A. Q., Honigs, D. E., *Spectroscopy*, 1988, **3**, 54.
17 Kradjel, C., and Ciurczak, E. W., paper presented at the 1st Pan American Chemistry Conference, San Juan, Puerto Rico, 1986.

Data Processing for Amperometric Signals

Jo Simons, Martinus Bos and Willem E. van der Linden*

Mesa Research Institute, Laboratory of Chemical Analysis, Department of Chemical Technology, University of Twente, P.O. Box 217, 7500 AE Enschede, The Netherlands

Multicomponent analysis with arrays of individually modified electrodes is under investigation. This paper is concerned with a preliminary study of data processing of the signals of such an array. Voltammetric measurements of solution mixtures consisting of two nitrophenols were made with two disc electrodes (gold and rhodium, diameter 2.8 mm) in well stirred solutions. Linear scan voltammograms were used to test a data reduction and filtering method, and two multivariate calibration techniques, *i.e.*, a linear and a non-linear model, were evaluated. The non-linear model gave better results, indicating that non-linear effects occur with amperometric measurements of multicomponent solutions.

Keywords: Neural network; multivariate calibration; amperometric sensor; modified electrode; multicomponent analysis

Introduction

This study forms a part of a more extensive programme on the development and use of arrays of microelectrodes which, because of their specific properties,[1] have several advantages over macroelectrodes when used in voltammetry and amperometry, such as (1) high current densities caused by high rates of mass transfer as a result of non-linear diffusion contributions, (2) low ohmic drop, which allows measurements in highly resistive media, (3) better signal-to-noise ratio and (4) rapid attainment of steady-state currents, which makes it suitable for measurements in flowing fluids.

An attractive perspective for multicomponent analysis appears when the advantages of microelectrodes can be combined with modification of the electrode surface. An array consisting of a number of electrodes, each modified in a different manner, may be used as an integrated sensor for the selective detection of separate compounds in a multicomponent sample.

At the present stage of the project, the possibility of using differently modified electrodes for multicomponent analysis in combination with various data evaluation methods was evaluated. To avoid in this stage the specific problems accompanying the use of microelectrodes, it was preferred to employ a set of macroelectrodes.

Modification of the surfaces can consist of plating with various metals, immobilization of enzymes, deposition of electropolymerizable polymers, in combination with electrocatalysts or enzymes, etc.[2-6] The modification procedures should allow in a later stage the deposition of a certain material on an individual microelectrode, of which the typical size is <100 μm. This means that only electrodeposition or microlithographic techniques can be considered for modifying these surfaces. By successively modifying the individual electrodes within an array, it may be possible to introduce a certain selectivity towards analytes in complex mixtures. It

should be noted, however, that it is not the goal, nor is it necessary, to introduce absolute selectivity by modification of the various electrodes. A signal measured in a multicomponent solution will, in general, contain information about several components in solution, but it will be difficult, or even impossible, to extract all information about all components from a single signal. However, by combining the signals of several electrodes within an array there will be more information available and also some redundancy. Multivariate calibration techniques will then be able to extract information about the concentrations of different components in the mixture.

The response of one electrode can depend on the composition of the solution in a complex and non-linear way especially when the measured current is the result of more then one electrode reaction. Some processes that may cause non-linear behaviour include (1) blocking of the electrode surface by reactant or product, (2) changes in the reaction mechanisms through changes in the neighbourhood of the electrode surface (*e.g.*, pH) and (3) reactant or product acting as an intermediate for other redox reactions.[7]

The purpose of the preliminary experiments described in this paper was to establish whether a linear model is capable of solving the relationships between measured current and concentrations or whether a non-linear model should be chosen, and if addition of the signal of a second, modified electrode improves the analytical results.

Experiments were performed with macroelectrodes because of the availability and easier control of the measurement parameters (modification, electrode surfaces, higher currents, *etc.*). In order to establish conditions that simulate the behaviour of microelectrodes, the solutions were intensively stirred and the measurements were performed at low scan rates (10 mV s^{-1}).

In order to attain substantial data reduction and noise filtering, the data obtained were fitted with orthonormal Legendre polynomials. Although this procedure is called fitting, it merely is a tool for finding a more workable representation of the data points. With the coefficients of these polynomials, two multivariate calibration methods were tested, one using a linear model, which was solved with singular value decomposition (SVD), and the other using artificial neural networks (ANN) as a non-linear calibration model.

Experimental

Reagents

Rhodium trichloride (RhCl$_3$·xH$_2$O) (Drijfhout, The Netherlands) was used as received. Acetic acid, sodium acetate and methanol were of analytical-reagent grade (Merck). Dimethyl sulfoxide (DMSO) (Merck) was distilled under reduced pressure and stored under nitrogen. Tetraethylammoniumacetate (TEA) (Janssen) was recrystallized twice from methanol and subsequently dried in a desiccator. 3-Nitrophenol (*m*-NP) (Merck) and 2-nitrophenol (*o*-NP) (Janssen 99+%) were used as received.

---

* To whom correspondence should be addressed

Equipment

The electrochemical experiments were carried out using an Eco-Chemie Autolab potentiostat (Model PSTAT10) controlled by a G2 personal computer with an 80286 processor and 80287 coprocessor. The potentiostat was equipped with a multiplexing module (modified SCNR8 module from Eco-Chemie), allowing currents of up to eight electrodes to be measured during one scan.

The experiments were all carried out in a three-electrode configuration in a conventional electrochemical cell of 50 cm³. Solutions were de-aerated by bubbling with polarographic-grade nitrogen. Potentials were measured with respect to an aqueous Ag/AgCl (3 mol dm⁻³ KCl) reference electrode connected to the cell through a salt bridge containing 0.1 mol dm⁻³ tetraethylammonium chloride in DMSO. The counter electrode was a glassy carbon rod electrode (Metrohm 6.1247.000; about 65 mm long and with a diameter of 2 mm).

The measurements were performed with two gold disc electrodes of diameter 2.8 mm (Metrohm), one of which was electrochemically plated with a rhodium layer. The plating bath contained 0.6 g dm⁻³ of RhCl₃·xH₂O in a solution of 0.1 mol dm⁻³ acetic acid and 0.1 mol dm⁻³ sodium acetate. Plating was performed by 20 cyclic scans between 0.1 and −0.6 V (versus Ag/AgCl), with a scan rate of 100 mV s⁻¹. The electrodes were polished and electrochemically conditioned by potential cycling in 0.1 mol dm⁻³ H₂SO₄. All solutions of nitrophenols were prepared in DMSO containing 0.1 mol dm⁻³ tetraethylammonium acetate and 0.1 mol dm⁻³ acetic acid.

Measurements were made on 117 solutions with concentrations of o-NP varying from 2.1 x 10⁻⁴ to 2.12 x 10⁻³ mol dm⁻³ and concentrations of m-NP varying from to 1.9 x 10⁻⁴ to 2.1 x 10⁻³ mol dm⁻³. The concentrations are evenly distributed over the concentration ranges indicated with the understanding that no concentrations were used that were below the limit of detection apart from solutions in which one component was absent and one solution in which both components were omitted (blank).

Linear scans from −0.5 to −1.5 V, with a scan rate of 10 mV s⁻¹, were performed in these solutions under intensive stirring with a propeller (1000 rpm). Programs for the Legendre fitting procedure and the singular value decomposition (SVD) were written in the laboratory according to ref. 8 The program for artificial neural network (ANN) calculations was developed in the laboratory.[9] Calculations were mainly performed on a personal computer with an 80486 50 MHz processor.

Results and Discussion

First we checked whether the signal measured in solutions with two components can be described as the sum of the signals measured for the separate components [see Fig. 1(a) and 1(b)]. All signals were corrected for the blank signal. Some small non-linear effects can be observed in Fig. 1(e), where the noise-filtered real voltammogram of the mixture is presented together with the voltammogram constructed from the voltammograms of the individual components. The measured data sets consisted of several hundred points per electrode per voltammogram and contained considerable noise. Because noise filtering was one of the aspects to be investigated the source of the noise was not investigated. In order to diminish the noise and to decrease the amount of data, a fitting procedure was applied on each separate signal in order to obtain a more useful data representation. For this purpose fitting with a set of Legendre polynomials was chosen.[10]

The Legendre polynomials are orthonormal and for data sets with equally spaced points and uncertainties with a common standard deviation, the expansion of the fit with a higher order polynomial does not affect the already calculated coefficients of the lower order polynomials. This property is very useful for computation: when the first polynomial of the set is fitted, the second is calculated by fitting to the rest function, and so on. An example of a representation of a voltammogram by the first 12 Legendre polynomials is given in Fig. 1(c). We tried fitting by 12, 24, 36 and 48 polynomials, for each measured signal. The coefficients of these fitted curves were used in the further calculations in both the linear and non-linear models. In order to optimize for the number of Legendre polynomials to be used for fitting the data, the signals of both electrodes were fitted and combined to one input for the final calculations. For the different fittings (24,48,72 and 96 polynomials) SVD calculations were performed for various numbers of singular values.

This results in $m \times n$ data matrices D_i ($m = 117$ measurements and $n = 24$, 48, 72 or 96 polynomial coefficients) and vectors c_1 and c_2 (117 concentrations) for o-NP and m-NP, respectively. With the linear model, the aim of the calculations is to solve the equations

$$D \cdot w_1 = c_1$$
$$D \cdot w_2 = c_2$$
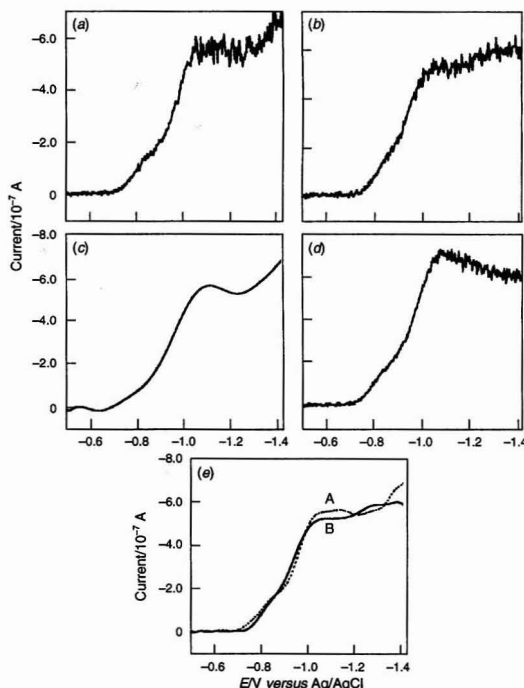
Fig. 1 (a) Measured signal of a rhodium-plated gold electrode corrected for blank signal (composition: 8.64 mol dm⁻³ 2-nitrophenol, 7.84 mol dm⁻³ 3-nitrophenol in standard solution). (b) Signal constructed from signals of the separate components. [Simulated composition same as (a)]. (c) Curve fitted to (a) composed from the first 12 Legendre polynomials. (d) Signal as in (a) at a bare gold electrode. (e) Curve fitted to (a) (A), and (b) (B) from the first 24 Legendre polynomials.

Singular value decomposition produces solutions for model vectors w_1 and w_2 that are the best approximations in the least squares sense.[8]

The calculations were performed in a 'leave one out' method. One row of the data matrix **D** was left out (the ith), which means leaving out one measurement. With the remaining 116 rows model the vectors w_1 and w_2 were computed. Through:

$$c_1[i] = d_i \cdot w_1$$

$$c_2[i] = d_i \cdot w_2$$

the concentrations of the left out measurement were calculated. This procedure was repeated for all 117 measurements.

The error used to evaluate the procedure was the 'relative mean error' defined by $\Sigma |(C - C_{cal})|\Sigma C$, where C is the real concentration and C_{cal} the concentration calculated as above. The results are summarized in Table 1. and show that modelling with more than 48 polynomials (24 per signal) does not improve the results, because a higher order polynomial fit will include not only the general features of the voltammogram but also the noise.

As expected, for small numbers of singular values the results for the modelled curves do not show a large variation with change in the number of Legendre polynomials used. In each instance the first Legendre polynomials determine the main body of the fit and therefore the first singular values determined for the models with various numbers of polynomials will be similar. An improvement of the result can be obtained by using more singular values. The optimum in our calculations was with a 48 Legendre polynomial fit and a singular value decomposition to 34 singular values. This resulted in a 'relative mean error' of 5.99%.

The second objective of this study was to determine whether the use of a second, different, electrode and therefore the use of two signals would enhance the quantitative analytical results. In Fig. 1(d) the Legendre polynomial fits for the signals of a bare gold and a rhodium-plated electrode measured in the same solution are shown. There is a small difference between the shapes of the curves. The results of the linear model calculations for the separate electrode signals (24 polynomial fit) and for the combined signals (48 polynomials) are given in Table 2; for these calculations the maximum number of singular values (24 resp. 48) were used.

The third objective was to test if an artificial neural network (ANN) would give better calculation results than the linear model. ANNs are capable of dealing with non-linear behaviour and therefore should improve the results of the analytical calculations in comparison with the linear model. An ANN is trained to map inputs to a solution space.

A trained network is capable of interpolating (and sometimes extrapolating) in this solution space. Symbolically the calculation could be written for the training stage as:

$$D \rightarrow ANN \leftarrow C$$

and for the evaluation as:

$$D \rightarrow ANN = C$$

in which **D** is the data matrix, **ANN** the neural network and **C** the concentration matrix (combination of vectors c_1 and c_2).

For these calculations we used a scaled conjugated gradient network[9] with the number of inputs equal to the coefficients of the polynomial fit, 13 hidden neurons and two output neurons (all sigmoid). All networks were trained for 10 000 epochs. Also in this instance the calculations were performed using the 'leave one out' method. The network was trained with 116 inputs and for the ith input the concentrations were calculated according to:

$$d_i \rightarrow ANN = c_1[i], c_2[i]$$

For the neural network calculations, as for the linear model, it was found that the optimum number of Legendre polynomials used for fitting the data sets was around 24.

The results of calibrations with the neural network for the separate electrode signals (24 polynomial fit) and for the combined signals (48 polynomials) are also given in Table 2.

The analytical results for the bare gold electrode are better than those for the rhodium-plated electrode, which may be due to the fact that the data sets used in the calibrations were not corrected for the blank signal. The rhodium plated electrode shows a less negative reduction potential for the reduction of H^+ and the contribution of the background signal to the total signal is therefore larger for this electrode, and this may hinder the calculations.

In all three instances the 'relative mean error' is smaller for the neural network than for the linear model. These two approaches to data evaluation for each electrode are based on the same set of signals. Hence, the observed differences must be attributed to the data processing method.

Table 1 'Relative mean error' as a function of number of Legendre polynomials used in the fit and the number of singular values used in the linear model.

| Singular values | Polynomials | | | |
	24	48	72	96
4	9.93	9.66	9.64	9.60
8	8.38	8.38	8.63	9.84
16	8.40	7.70	8.20	8.69
32	—	6.25	7.43	9.18
48	—	6.82	6.57	8.09
64	—	—	7.10	7.41
72	—	—	7.38	7.58
80	—	—	—	7.74
96	—	—	—	12.3

Table 2 'Relative mean error' of artificial neural network and linear model

	Rhodium-plated electrode	Gold electrode	Combined signals
Linear model	8.93	8.17	7.45
Neural network	6.81	5.26	4.13

Conclusions

The combination of two signals improves the analytical results for the linear model and for the neural network. The largest improvement is obtained with the ANN calculations, the decrease in the 'relative mean error' being about 25%. When more components have to be determined and electrodes with greater selectivity are used, the additional signals can have an even larger effect.

The results of the calibration models with the neural network are better in all instances, as can be seen form the significantly smaller 'relative mean errors.' It seems to be justified to conclude that for complex mixtures and more electrode signals the linear model will not be suitable for obtaining accurate analytical results and that neural networks or another non-linear modelling technique will be needed to produce useful analytical results.

References

1   Montenegro, M. I., Queiros, M. A., and Dasbach, J. L., *Microelectrodes: Theory and Applications, NATO ASI Series E*, vol.197, Kluwer, Dordrecht, 1991.
2   Murray R. W., Ewing, A. G., and Durst, R. A., *Anal. Chem.*, 1987, **59**, 379A.
3   Wang, J., *Anal. Chim. Acta*, 1990, **234**, 41.
4   *Molecular Design of Electrode Surfaces, Techniques of Chemistry*, vol. XXII, ed. Murray, R. W., Wiley, New York, 1991.
5   *Biosensors and Chemical Sensors*, ACS Symposium Series, No. 487, ed. Edelman, P., and Wang, J., American Chemical Society, Washington, DC, 1992.
6   Glass, R. S., Perone, S. P., and Ciarlo, D. R., *Anal. Chem.*, 1990, **62**, 1914.
7   Conway, B. E., *Theory and Principles of Electrode Processes*, Ronald Press, New York, 1965.
8   Press, W. H., Flannery, B. P., Teukolsky, S. A., and Vetterling, W. T., *Numerical Recipes C*, Cambridge University Press, Cambridge, 1988.
9   Bos, A., *PhD Thesis*, Enschede, 1993.
10 Bevington, P. R., *Data Reduction and Error Analysis for the Physical Sciences*, McGraw-Hill, New York, 1969.

Response Kinetics of Chemically-modified Quartz Piezoelectric Crystals During Odorant Stimulation

Bruce W. Saunders, David V. Thiel and Alan Mackay-Sim*

Faculty of Science and Technology, Griffith University, Nathan, QLD 4111, Australia

When chemically-modified piezoelectric quartz crystals are used to detect odorous compounds in air the maximum frequency changes induced by odorants vary both within and between sensors. This variability is reduced when stimulation variables, such as flow rate, odorant concentration and duration, are closely controlled. Precise control of the stimulus allows time-dependent frequency responses to be observed as odorants interact with the sensor surface. The aim of the present experiments was to examine in detail the time-dependent frequency responses of sensors (functionalized with one of six different surface coatings) when exposed to one of 18 odorants. The results demonstrate that these time-dependent responses (termed 'kinetic signatures') were characteristic of each odorant–surface interaction. They were repeatable for each sensor and reproducible among sensors with inter-crystal variability reduced virtually to zero. Kinetic signatures were independent of the maximum frequency change induced by odorants and they appear to be useful as a new method of analysing odorant–surface interactions; an application for odorant discrimination using a six-sensor array and artificial neural network analysis is demonstrated.

Keywords: Gas sensor; odorant; artificial neural network; quartz piezoelectric crystal; response kinetics

Introduction

The use of chemically-modified piezoelectric quartz crystals as sensors for the selective detection of gases and odorants is well documented.[1–4] When substances adsorb onto the crystal surface, there is a change in the resonant frequency of the crystal. This change in resonant frequency depends partly on the additional mass added to the surface,[5] and partly on the change in viscosity of the surface, even in crystals oscillating in air.[6,7] Chemical modification of the crystal surface, by deposition or by covalent bonding of a substrate, produces sensors which vary in their specificity for different gaseous analytes. Thus different analytes can be discriminated from each other by the relative amplitudes of the responses they induce in sensors whose surfaces are coated with different compounds.

Piezoelectric odorant sensors are conceptually simple but of limited utility, because sensor responses can be highly variable.[1,8] This inconsistency can arise from variability in chemically modifying the crystal surface (spraying, dropping or smearing the substrate onto the surface). Inter-crystal variability is still a problem after covalent modification of the surface and even uncoated crystals show substantial variability, indicating that it may prove difficult to eliminate during the sensor fabrication process.[9] Sensor responses are also

subject to change because the coating may 'creep' or 'bleed' from the surface.[1] Temperature and water vapour provide potential sources of interference in most applications.[1,10] In practice, the impact of sensor variability can be reduced to some extent by using an array of sensors, each coated with a different substrate. Odorant identification then depends on the relative responses of all the sensors in the array. Multi-sensor systems have been described which use the maximum change in frequency induced by different analytes as input either to statistical techniques,[11–13] or to artificial neural networks[14–17] to provide identification of the gaseous analyte.

Although inter-sensor variability remains a problem, within-sensor variability can be reduced when the physical parameters of the stimulus are controlled. Odorant concentration and flow rate can be controlled by an equilibrated, flow-through delivery system and the timing of the stimuli can be regulated by computer-controlled solenoid valves.[9] Under these conditions, reproducible, time-dependent sensor responses can be observed. Preliminary observations revealed that the shapes of these time-dependent responses were less variable than the maximum frequency changes induced by odorants and they appeared to be characteristic of specific odorant– and surface–substrate interactions. The aims of the present study were to investigate further these odorant-induced, time-dependent responses of piezoelectric sensors, to compare the relative variability between time-dependent responses and maximum frequencies, the latter being the most common measure of sensor function and to investigate the utility of kinetic signatures for odorant identification using an artificial neural network array.

Experimental

Apparatus

Quartz crystals (10 MHz, AT-cut) with silver electrodes (Hy-Q International, Clayton, Victoria, Australia) were used in an oscillator circuit of our design, powered by a 5.5 V dc regulated power source.

The crystal was housed in a flow chamber into which flowed odorant or air, which was delivered under computer control as described previously.[9] This apparatus minimizes cross-contamination and allows single or multiple odorants to be delivered to the crystal at standardized concentrations, flow rates and durations. Briefly, air and odorant flows are controlled by three-way solenoid valves which direct either dried, purified air or odorants (diluted in dried, purified air) to the crystal flow chamber. Odorant-saturated air was divided into equal 100 ml min^{-1} flows which were directed perpendicularly to the centres of each face of the crystal. The radius of the odorant outlet tubes was 2 mm and they were located 1–2 mm from the surface, thus, it is estimated that the odorant reached the sensor surface in about 10 ms after odorant onset.

The volume of the crystal flow chamber was 6 ml. This was replaced about every 2 s at the flow rate used (200 ml min⁻¹) but odorant was replenished at the sensor surface many times per second. The dried, purified air flushed the chamber from one end at 200 ml min⁻¹, reaching the sensor about 0.6 s after the odorant was switched off (the volume of the 'dead' space in front of the crystal was 2 ml). This delivery system therefore provides the necessary rates of odorant delivery and removal to allow examination of second-by-second kinetics of odorant–surface interactions.

Sensor Coatings

Prior to coating, all crystals were cleaned by refluxing over acetone (Aldrich, Milwaukee, WI, USA) for 20 min, and air dried. Crystals were coated with one of five coatings: pyridoxine hydrochloride (Sigma, St. Louis, MO, USA), Antarox CO-880 (GAF Chemicals, Wayne, NJ, USA), pyridoxine hydrochloride–Antarox CO-880, ascorbic acid (Sigma) and OV-17 (Supelco, Bellefonte, PA, USA). Pyridoxine hydrochloride has been reported as a reversible adsorbent for the detection of ammonia and Antarox CO-880 as a support matrix to extend its working life.[18] Ascorbic acid was used for detecting ammonia in the atmosphere,[19] and OV-17 for the detection of camphor.[20]

All sensor coatings were applied to the crystal surface by applying a 5 µl drop of the appropriate solutions to both sides of the crystal face. Solutions of pyridoxine hydrochloride, Antarox CO-880 and ascorbic acid were prepared by dissolving 100 mg of the substrate in 50 ml of an ethanol–water solution (1 + 1, v/v). The pyridoxine hydrochloride–Antarox CO-880 solution was prepared by mixing the single substrate solutions (1 + 1, v/v). The OV-17 solution was prepared by dilution in acetone (1 + 79, v/v). The crystals were dried overnight in a desiccator, and used the following day.

Odorants

Commercial, analytical-reagent grade chemicals served as odorants. They were a group of related amines (diethyl, triethyl, isopropyl, diisopropyl, diisopropylethyl, dicyclohexyl), a group of related acetates (methyl, ethyl, propyl, amyl, hexyl, heptyl and octyl) and several others (piperidine, *n*-methylpiperidine, camphor, napthalene, citronellol). All the experiments were carried out at 21 °C, the temperature of the air-conditioned room.

Experimental Procedures

Each sensor was tested for its response to stimulation by each of the odorants. Each odorant stimulation was of 200 s duration. Between odorant stimulations the sensor was flushed with a flow of dried, de-odorized air for a period of 700 s. All odorants were delivered as saturated vapour in dry, purified air.

The frequency response of each sensor was measured, at 1 s intervals, for 900 s, 200 s before odorant stimulation (to establish a baseline), during the 200 s odorant stimulation and for 500 s following the odorant stimulation. Of particular interest were the 200 s period during odorant stimulation ('odorant on') and the 200 s period immediately after odorant stimulation ('odorant off'). The resonant frequencies of the crystals were measured with a Hewlett-Packard universal counter (Hewlett-Packard, North Ryde, New South Wales, Australia; Model 5334b). Resonant frequency was displayed in real time on the computer screen and stored on disk for later analysis.

In the initial experiments six crystals were used; five were coated with one of the surface substrates described above and

one was left uncoated. Each crystal was stimulated three times with each of the 18 odorants. This provided data for 324 trials, (3 repeats × 18 odorants × 6 crystals), each of which was represented by resonant frequency measurements for 400 s, (200 s after odorant on and 200 s after odorant off). The data after odorant on were used to train an artificial neural network to discriminate between the different odorants (described below).

The reproducibility of the time-dependent responses was examined. Two different pairs of odorant–surface coating interactions were chosen. One pair (camphor–OV17) had the simplest form of time-dependent response. The other pair (ethyl acetate–OV17) had a time-dependent responses with several inflections. For each odorant–surface pair, three crystals were coated with the substrate and stimulated 25 times consecutively. The time-dependent responses and maximum frequency responses were recorded in order to compare the relative variability of these two measures of sensor function.

Computation of 'Kinetic Signature'

The time-dependent response of a sensor to an odorant is shown in Fig. 1(a). These responses were divided into two parts: the 200 s after the odorant was switched on and the 200 s after the odorant was switched off. Each part of the response was normalized with respect to the baseline frequency, f_b, and maximum, odorant-induced frequency response, Δf_{max}. The equation for the normalized frequency response, $S(t)$, is defined as:

$$S(t) = [f(t) - f_b]/\Delta f_{max} \tag{1}$$

where $f(t)$ is the frequency response of the crystal measured as a function of exposure time, t. We refer to these normalized responses of the odorant–sensor interaction as 'kinetic signatures', an example of which is shown in Fig. 1(b).

Analysis by Artificial Neural Networks

Artificial neutral networks (ANNs) provide a method for discriminating among odorants presented to a multi-sensor

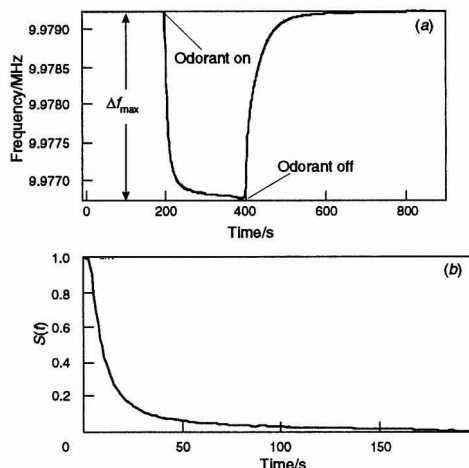**Fig. 1** Calculation of the kinetic signature. (a) Frequency response of a piezoelectric quartz crystal sensor when stimulated with a controlled flow of odorant. Odorant flow was switched on at 200 s and off at 400 s. The maximum frequency change (Δf_{max}) is shown. (b) The kinetic signature of the response shown in (a). The response during odorant stimulation is expressed relative to Δf_{max}.

array.[14–16] This method has several advantages over computational methods such as statistical analysis,[12,21] namely, the comparative speeds of operation and the ease with which they can be implemented in electronic instruments. There are several types of ANNs; those used here are 'pattern-classifying' ANNs. These are computational devices which can be 'trained' to match a pattern at the input (*e.g.*, the responses of an array of sensors to an odorant) with some identifier at the output (*e.g.*, the name of the odorant). Training consists of repeated presentations of the input data and the internal state of the ANN is adjusted according to a 'learning' algorithm until it reliably matches the identifier with the sensor input. ANNs consist of a number of 'processing elements' which are organized into separate 'layers' and linked together using connections whose weighted values change as a consequence of training. When an ANN is fully 'trained' it ascribes a probability of correct identification to any new odorant presented to the sensor array.

In the analysis used here, the input layer for each sensor consisted of 50 processing elements representing the kinetic signature (not all 200 data points in each kinetic signature were used; only every fourth point, 50 in all), the hidden layer consisted of 30 processing elements and the output layer consisted of 18 processing elements (each representing an odorant category). The input and output processing elements are separated by a 'hidden' layer of processing elements. Hidden layers describe the connectivity between the input and output processing elements. The number of processing elements in the hidden layer can vary and is optimized for the specific analytical task.[22] Six separate networks, one for each sensor, were organized to produce a single output matrix [Fig. 2(*a*)] which presented the cumulative responses of the ANN for all sensors to each odorant [Fig. 2(*b*)]. Training was performed by repeated presentations (*n* = 5000; hidden layer momentum term = 0.30; output layer momentum term = 0.15) of each separate array of sensor responses to each odorant. Correct association of odorants was performed using the back propagation learning algorithm.[22,23]

Results and Discussion

Kinetic Signatures

Kinetic signatures represent a new method of observing time-dependent interactions between a gaseous odorant and an adsorbent surface. Frequency changes were recorded for each of six sensors which were stimulated three times with each of 18 odorants. Kinetic signatures were calculated for responses at both odorant on and odorant off. This provided a data set of 324 kinetic signatures, 36 of which are illustrated in Fig. 3. There are several features of these kinetic signatures of particular interest:

(1) The forms of the kinetic signatures were characteristic of each odorant–sensor interaction: compare the same odorant on different surface coatings [*e.g.*, Fig. 3(*b*) and (*e*)] or the same coating with different odorants [*e.g.*, Fig. 3(*c*) and (*e*)].

(2) Kinetic signatures for odorant on were usually different from those at odorant off; though in most cases the number of inflections in the response curves were the same.

(3) Kinetic signatures were quite reproducible, although in some cases the initial response differed somewhat from subsequent responses (indicated by the traces labelled '1' in Fig. 3).

(4) Not all odorant–sensor interactions caused pronounced frequency changes. Approximately 17% of interactions gave maximum frequency responses of less than 10 Hz. Noisy kinetic signatures were discernible for most of these.

Taken together these results demonstrate that kinetic signatures represent different modes of interaction between

the odorants and the sensor surfaces. Each odorant–surface interaction was represented by a characteristic kinetic signature which differed markedly in form. The difference between kinetic signatures was often dramatic [*e.g.*, Fig. 3(*a*) and (*c*)] but some differences were more subtle, with kinetic signatures showing similar inflections but at different times after odorant on or off [*e.g.*, Fig. 3(*c*) and (*d*)]. Relatively few of the interactions resulted in simple single exponential kinetics [*e.g.*, Fig. 3(*a*)], most involved at least one inflection in the kinetic signature. This leads us to conclude that the forms of the kinetic signatures represent time-dependent combinations of different adsorption processes such as combinations of physisorption and chemisorption. As well as odorant–surface interactions, there are probably interactions between incident odorant molecules and those adsorbed onto the surface. In one case the odorant caused a repeatable increase in resonant frequency of the sensor rather than a decrease, as expected.[5] We believe that this could arise when adsorption of the odorant onto the sensor surface decreases the surface viscosity, thus allowing the crystal to oscillate more freely.[7,8] This conclusion is supported by the observation that the increase in oscillation frequency was always preceded by a period during which the frequency decreased, *i.e.*, during which mass was added to the surface.

Kinetic signatures were characteristic of each odorant–surface interaction, although their general form was not unique to each interaction. That is, odorant–surface interactions fell into broad classes defined by the shapes of the kinetic signatures. The most similar were the kinetic signatures with a form similar to a single exponential as illustrated in Fig. 3(*a*). Many other interactions could be classed as having an obvious inflection in the kinetic signature but the inflections occurred

(*a*)

(*b*)
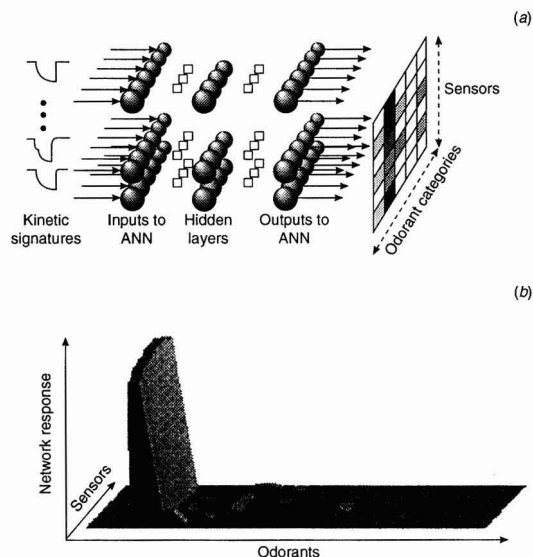
Fig. 2 A representation of the artificial neural network and its response. (*a*) The artificial neural network is represented as six tiers, each representing the processing elements (shown as balls) concerned with each sensor. Within each tier the processing elements were interconnected. The outputs of each tier were brought together in a single output matrix shown on the right which represents 18 odorants and 6 sensors. (*b*) The output of the artificial neural network can be represented as a three-dimensional map of network responses distributed across the output matrix. Response to the odorant, isopropylamine is illustrated.

at different times after odorant on. Differences were also evident in the occurrences of the inflections after odorant off.

Repeatability of Kinetic Signatures

For individual sensors the kinetic signature proved to be very consistent across repeated trials. This is illustrated in Fig 4. The form of the kinetic signature remained constant over 25 trials even though there was considerable drift in the baseline frequency and a gradual increase in the maximum frequency change. The most variable kinetic signatures were those recorded after the initial odorant presentation to each sensor (Fig. 4), although this variability was not observed for all odorant–sensor interactions (see Fig. 3).

Kinetic signatures proved to be very consistent between sensors. When kinetic signatures for three sensors are overlaid, the majority of the 75 kinetic signatures for each odorant–surface interaction fell within very narrow limits of each other despite considerable variability in baseline frequencies (Fig. 4) and in maximum frequency changes (Fig. 5). The greatest variation observed in the kinetic signatures was between the first and subsequent responses. This suggests that during the initial exposure, the odorant modifies the surface in some way and that all subsequent odorant interactions take place with this modified surface. In support of this observation is the fact that the most variable maximum frequency changes were observed also after the initial odorant presentation. The maximum frequency changes recorded after the first and twenty-fifth odorant exposure for the three sensors exposed to camphor were 22 916 and 18 433 Hz, 15 171 and 16 204 Hz, and 25 035 and 23 770 Hz. Similar variability was observed between the first and twenty-fifth presentations of ethyl

acetate to three other sensors: 641 and 5862 Hz, 5841 and 6688 Hz and 5683 and 7102 Hz. Because of this variability the initial responses were omitted from Fig. 5 but even without these initial responses the maximum frequencies varied greatly among the sensors and with repeated odorant exposures (Fig. 5).
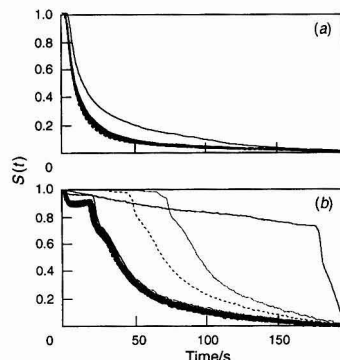
Fig. 4 Different sensors produced similar kinetic signatures which varied little with repeated odorant presentations. In each panel are overlaid kinetic signatures recorded from three sensors in response to 25 successive odorant stimulations on each sensor. The responses of three sensors are given as solid, dashed and dotted lines. The most variable responses were those to the initial odorant presentation on each sensor [most obvious in (*b*)]. Each panel shows responses of three different sensors coated, with OV-17, to odorants: (*a*) camphor and (*b*) ethyl acetate.
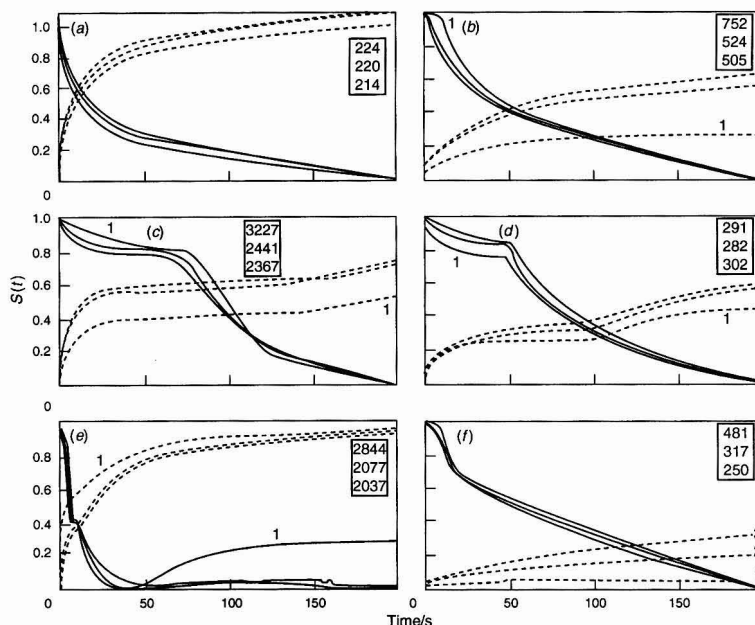
Fig. 3 Examples of kinetic signatures. The solid lines show kinetic signatures for responses after the odorant is switched on and the dashed lines show kinetic signatures for responses when the odorant is switched off. Each panel shows kinetic signatures for three consecutive odorant presentations: lines indicated by '1' were recorded from the first exposure of the odorant to the sensor surface. The insets show the maximum frequencies (Hz) recorded for each of the three responses. Each panel shows the kinetic signatures for a different odorant–sensor combination: (*a*) dicyclohexylamine on pyridoxine HCl + Antarox CO-880; (*b*) diisopropylethylamine on ascorbic acid; (*c*) piperidine on pyridoxine HCl; (*d*) *n*-methyl piperidine on ascorbic acid; (*e*) diisopropylethylamine on pyridoxine HCl; and (*f*) naphthalene on ascorbic acid.

Collectively these results indicate that kinetic signatures provide a reliable measure of the interfacial kinetics of odorant–surface interactions. As such they may be useful as analytical tools to model the molecular events occurring during these interactions. Kinetic signatures will also be much more useful in electronic odorant detection than the maximum frequency response, which is the measure of response commonly used in piezoelectric sensor systems. Firstly, kinetic signatures are less variable than the maximum frequency response. The maximum frequency response varied within and between sensors, whereas the kinetic signature varied little within or between sensors for all odorant stimulations (except, in some cases, the initial stimulation). Secondly, for a given sensor surface, kinetic signatures contain information about the identity of the odorant since the time-dependent response is characteristic for each odorant–surface interaction. Therefore, although the kinetic signature for an odorant may not be unique to each surface, only a few sensors would be required to generate a set of kinetic
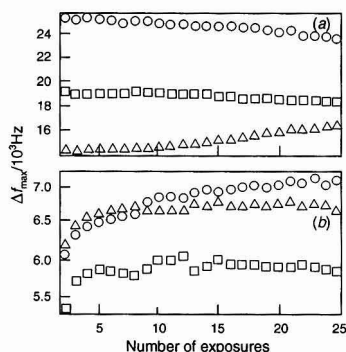
Fig. 5 Maximum frequency responses varied between sensors and with repeated odorant presentations. The maximum frequency responses were recorded in response to 25 successive odorant stimulations on each sensor, from the same sensors the kinetic signatures of which are shown in Fig. 4. The responses of three sensors are given as circles, squares and triangles. The responses to the initial odorant presentation on each sensor were not included on these graphs because of their variability. Responses are shown to the odorants (*a*) camphor and (*b*) ethyl acetate.

signatures which would be unique to each odorant. In contrast, the maximum frequency response is a one-dimensional measure which varies between sensors and which compounds odorant identity with odorant concentration.[10]

Artificial Neural Network Analysis

The artificial neural network achieved a high degree of discrimination among the odorants. For each set of input data (that is, six sensor responses to one presentation of an odorant), the ANN assigns a value from 0 to 100% to each of the output nodes (that is, odorant names). Values closer to 100% indicate that the ANN is 'more certain' of its identification of that odorant. Conversely, values closer to 0 indicate that the ANN is 'less certain' of its choice. In the present experiment, the ability of the trained network to identify the odorants was examined by presenting it with the original training data. Thus for each odorant the certainties of identification across all output nodes were averaged across the three presentations for each odorant. These results are presented in Table 1. For all odorants the ANN ascribed the highest certainty to the correct odorants. In other words it learned to discriminate the input data with a high degree of certainty. Overall the average certainty for the correct odorants was 93.5%, the average certainty for the next most certain odorants was only 1.5%. Even for the two odorants which the ANN found most difficult to discriminate, amyl acetate and octyl acetate, the certainty for the correct odorant was 65%, well above the certainty of the next best choice, 1.3% in each case.

The poorer performance of the ANN in correctly identifying amyl acetate and octyl acetate was due to the lack of responsiveness of the sensors to these odorants. Only two of the six sensors responded to amyl acetate with a frequency shift greater than 10 Hz. For these two sensors the average maximum frequency shifts for the three odorant exposures were 34 and 32 Hz, respectively. Similarly, only two sensors responded to octyl acetate, average 78 and 24 Hz, respectively. By comparison, most of the other odorants elicited significant responses from most of the sensors and average maximum frequency shifts of over 100 Hz were common. The obvious conclusion is that, even with kinetic signatures as input, reliable performance of the ANN depends upon reliable and robust responses from more than two of the six sensors.

Table 1 Certainty of the responses of the trained ANN

Correct odorant	Certainty (%)	Incorrect odorant	Certainty (%)
Diethylamine	96.5	Piperidine	0.9
Triethylamine	96.0	Propyl Acetate	1.6
Isopropylamine	96.6	Propyl Acetate	1.4
Diisopropylamine	96.5	Methyl Acetate	2.0
Diisopropylethylamine	97.9	Camphor	1.4
Dicyclohexylamine	96.9	Ethyl Acetate	1.4
Piperidine	97.3	Diethylamine	2.0
n-Methyl Piperidine	97.9	Isopropylamine	1.3
Methyl Acetate	96.8	Triethylamine	2.0
Ethyl Acetate	97.7	Dicyclohexylamine	1.1
Propyl Acetate	96.1	Dicyclohexylamine	1.8
n-Amyl Acetate	65.2	*n*-Hexyl Acetate	1.3
n-Hexyl Acetate	96.7	Citronellol	1.3
n-Heptyl Acetate	97.2	Isopropylamine	1.7
n-Octyl Acetate	64.7	Isopropylamine	1.3
Citronellol	96.9	*n*-Hexyl Acetate	1.9
Camphor	97.9	Diisopropylethylamine	1.8
Napthalene	97.3	Propyl Acetate	2.1

References

1 Alder, J. F., and McCallum, J. J., *Analyst*, 1983, **108**, 1169.
2 McCallum, J. J., *Analyst*, 1989, **114**, 1173.
3 Gardner, J. W., Hines, E. L., and Wilkinson, M., *Meas. Sci. Technol.*, 1990, **1**, 446.
4 Ward, M. D., and Buttry, D. A., *Science (Washington, D.C., 1883–)*, 1990, **249**, 1000.
5 Sauerbrey, G. Z., *Physik*, 1959, **155**, 206.
6 Hauptmann, P., Lucklum, R., Hartmann, J., Auge, J., and Alder, B., *Sens. Actuators, A*, 1993, **37**, 309.
7 James, D., Thiel, D. V., Bushell, G. R., Busfield, K. W., and Mackay-Sim, A., *Analyst*, 1994, **119**, 2005.
8 Boufenar, R., Boudjerda, T., Benmakroha, F., Djerboua, F., and McCallum, J. J., *Anal. Chim. Acta*, 1992, **264**, 31.
9 Mackay-Sim, A., Kennedy, T. R., Bushell, G., and Thiel, D., *Analyst*, 1993, **118**, 1393.
10 Fraser, S. M., Edmonds, T. E., and West, T. T., *Analyst*, 1986, **111**, 1183.
11 Carey, W. P., and Kowalski, B. R., *Anal. Chem.*, 1986, **58**, 3077.
12 Carey, W. P., Beeb, K. R., and Kowalski, B. R., *Anal. Chem.*, 1987, **59**, 1529.

13 Carey, W. P., and Kowalski, B. R., *Anal. Chem.*, 1988, **60**, 541.
14 Ema, K., Yokoyama, M., Nakamoto, T., and Moriizumi, T., *Sens. Actuators*, 1989, **18**, 291.
15 Nakamoto, T., Fukuda, A., and Moriizumi, T., *Sens. Actuators B*, 1991, **3**, 221.
16 Chang, S.-M., Iwasaki, Y., Suzuki, M., Tamiya, E., Karube, I., and Muramatsu, H., *Anal. Chim. Acta*, 1991, **249**, 323.
17 Moriizumi, T., Nakamoto, T., and Sakaruba, Y., in *Sensors and Sensory Systems for an Electronic Nose*, ed. Gardner, J. W., and Bartlett, P. N., NATO ASI Series, London, 1992, pp. 217–237.
18 Lai, C. S. I., Moody, G. J., and Thomas, J. D. R., *Analyst*, 1986, **111**, 511.
19 Webber, L. M., and Guibault, G. G., *Anal. Chem.*, 1976, **48**, 2244.
20 Deveza, R., Russell, A., Thiel, D. V., and Mackay-Sim, A., *Int. J. Robotics Res.*, 1993, **13**, 232.
21 Carey, W. P., Beebe, K. R., Kowalski, B. R., Illman, D. L., and Hirschfeld, T., *Anal. Chem.*, 1986, **58**, 149.
22 Simpson, P. K., *Artificial Neural Systems: Foundations, Paradigms, Applications, and Implementations*, Pergamon Press, New York, 1989.
23 Rummelhart, D. E., Hinton, G. E., and Williams, R. J., *Nature (London)*, 1986, **323**, 533.

Applications of Conducting Polymers in Potentiometric Sensors*

Mira Josowicz

Materials and Chemical Sciences Center, Pacific Northwest Laboratory, Richland, Washington 99352, USA

Conducting polymers may be used as sensitive layers in chemical microsensors leading to new applications. They offer the potential for developing material properties that are critical to the sensitivity, selectivity and fabrication of chemical sensors. The advantages and limitations of the use of thin-polymer layers in potentiometric sensors are discussed.

Keywords: Conducting polymer; electrochemical sensor; sensitive layer

Introduction

Microsensors, for analyses of gases and liquids, are often seen as tools for monitoring pollution problems, for reasons of size, speed or cost. The essential strategy for the development of chemical sensors[1,2] is to synthesize a layer which, due to its chemical interaction with a target analyte, generates the primary recognition signal.[3]

Much work has been devoted to the study of charge transport through polymeric materials containing extended π-conjugated backbones, such as poly(pyrrole) (PP),[4] poly-(thiophene) (PT)[5] and poly(aniline) (PANI).[6] These materials may be prepared electrochemically, typically by oxidation of their monomer, *e.g.*, pyrrole, thiophene, or aniline, in the presence of an electrolyte in aqueous or organic solutions.[7] The *in situ* polymerization process of the conducting polymers (CPs) on conducting substrates has led to their application in electrochemical sensors.[8] In this type of sensor, the transfer of electric charge occurs from the polymer modified electrode to the liquid through the bulk or surface of the polymer or *vice versa* from the gas analyte to the electrode through the surface and in the bulk of the polymer. Therefore, the molecular design and properties of the surface and bulk of the polymer are the most important factors that govern the sensitivity of the layers. Moreover, the electrochemical-synthesis route opens an easy way for fabrication of an array of sensors which, in combination with chemometrics, can lead to an enhancement of sensor selectivity.

It is known that in electrochemical sensors, the charge transfer can be captured through the relative change of the intrinsic properties of the polymer, such as electrochemical potential, current density, conductivity,[9] or the modulation of the work function of the polymer.[10] Combined measurements of mass and specific resistance have proved to be suitable for mechanistic studies of interactions between conducting polymers and organic vapours.[11,12] The study of the sorption process during the vapour/polymer interaction under steady state[13,12] and transient conditions[14] provides useful information about the origin of the primary recognition signal in potentiometric vapour sensors.

The aim of the work described in this paper is to demonstrate the versatility of the application of thin-polymer layers such as PP, PT, PANI, *etc.*, in potentiometric sensors and to discuss the necessity to 'tailor' their molecular structure and properties such as permeability, ion selectivity, and redox activity through a rational physico–chemical design.

Selectivity and Sensitivity Approaches

The considerable interest in the application of CPs for potentiometric sensors is governed by the electronic and ionic charge transport processes taking place within the polymer and the metal/polymer and polymer/solution or polymer/gas interfaces.[15] The ionic-charge transport is controlled by the partitioning process that occurs, more or less selectively at the sensitive layer between the indicator electrode and the liquid medium of the sample. The electronic charge transport is controlled by the charge-density rearrangement of delocalized π electrons. The extent of their delocalization is modulated by polarization effects occurring during the electrochemical deposition process. The charge transport properties of these materials may be varied over a relatively broad range:

(*i*) by altering the method and conditions of preparation, *e.g.*, by the level of doping or by the deposition potential,[16–19] or by changing the monomer concentration[20,21] as well as the concentration of the counter ion and the solvent used for polymerization;[16,22]

(*ii*) by selecting size and nature of counter ions;[17,18,23–26]

(*iii*) by using monomers with different hetero-atoms, *e.g.*, PP, PT,[27] or substituted monomers;[28] and

(*iv*) by insertion of a metal cluster into the CP matrix.[29]

The size, nature and location of the anion in the polymerized structure of CP determine the redox activity of the film.[30,31] It has been shown by X-ray photon spectroscopy (XPS) studies on CP,[32] that the ring-anion geometric arrangement determines whether the charge is extracted from a specific ring site (favoured by an ordered arrangement). This result offers the opportunity for manipulation of redox, conductivity, partitioning and permeation properties. Furthermore, precise control of surface and bulk micro-structures[33] and preparation of size selective micro-structures[34] may also be demonstrated.

After the electrodeposition, the CPs re-organize themselves according to the inter- and intra-molecular forces that exist in the polymer matrix. During the relaxation period, the polymer chains readily accept transport and transfer electrons in the same manner as a solid-state material. The conduction band electrons become less strongly bound and the matrix becomes a strong reducing agent. This phenomenon has been studied in detail for PT,[35] poly(N-vinylcarbazole),[33] and PANI.[29] In order to enhance the stability of the electro-synthesized films, an immediate equilibration in the background electrolyte containing the same salt from which the polymerization was carried out, is necessary. The modified

---

electrode is equilibrated until the electrode potential remains stable.[36-38]

In principle, by incorporating a catalyst into the CP, an enhancement of the sensor response can be acheived. If a catalytic process is taking place, the analyte will migrate to the electrode surface and be oxidized or reduced by the electrocatalyst. Following the charge exchange at the surface, the charge must be transported from the substrate to the modified boundary either, *via* a charge-hopping process (self-exchange reactions), or a limited diffusion procedure.

The most studied CP for use in potentiometric sensors is PP, which appears to be a very promising ion-exchange material, due to its fast ionic diffusion and small temperature dependence of the ionic diffusion coefficient.[39,40] The diffusion of mass transport of ions in partially oxidized PP studied by a radioactive ClO_4^- self-exchange technique shows that the exchange kinetic can be described by a finite planar Fickian diffusion, which implies that ion transport is independent of the polymer thickness and solution-ion concentration.[41] The relatively high stability of the CP in air is of interest to gas (vapour) sensor applications. The sorption processes are the driving force of the weak interactions between the vapour and the CP film. The sorption follows the Langmuir-type isotherm and the mass transport follows the one-dimensional Fickian diffusion. The response of the CP also depends on the kind of solvent used as the analyte, because polymer swelling is a major consideration.[41,42] This also explains why, in aqueous solutions, a faster ion exchange is observed than in organic solutions.

Potentiometric Sensors for Liquids

For the detection of ions in solution, the ion-exchange properties of the CP are essential. The anions, A, introduced into the CP during electropolymerization can be reversibly exchanged for anions, B, of a smaller or comparable size in solution without any loss of electroactivity of the polymer[41,43] according to the following equation:

$$(PA_y)_x + xyB^- = (PB_y)_x + xyA^- \qquad (1)$$
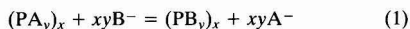
The ion exchange equilibrium constant can be calculated from the mole ratio of B^- to A^-. In principle, the size-exclusion selectivity of the CP can be controlled by changing the electropolymerization conditions of the CP, *i.e.*, polymerization time, current density, monomer concentration,[44] or by selecting different counter ions of different size.[38] Reversible anion-exchange behaviour was observed, *e.g.*, when poly(pyrrole hydroxide) film was treated with nitric acid[45] or poly(pyrrole halide) was exposed to HSO_4^- in an H_2SO_4,[46] or when poly(pyrrole chloride) or poly(pyrrole fluoride) was exposed to perchlorate.[47] Poly(3-methyl thiophene) based on Cr-oxyanions has been described as an anion-selective membrane.[48]

The anion exchange occurs spontaneously and does not affect the electronic structure of the conducting polymer.[49] The effect of the ionic strength on the ion exchange was found to be similar to that observed for ion-exchange resins; the greater the ionic strength the greater the rate of ion exchange.[50] For example, within 1 h BF_4^-, I^-, Cl^-, SO_4^{2-} or $S_2O_8^{2}$ can be exchanged for ClO_4^-, and incorporated into a 2500 Å thick PP film in an aqueous solution of 0.1 mol dm^{-3} solute.[51] However, anions such as F^-, or PO_4^{3-}, did not replace ClO_4^-, even after prolonged soaking of up to two hours.[51] Similar anion-exchange tests of the PP (PF_6^-) film have been performed.[52] It was reported that the exchange of the counter-anion, PF_6^-, with the halogens at room temperature was unsuccessful.[53] In a basic solution, the NO_3^-, ClO_4^-, Cl^- counter ions of PP were exchanged with OH^- from NaOH solution.[54] It has been reported that very fast responses

(within 1 min) of PP (A^-)/Pt electrode to A^- anions in neutral aqueous solution can be achieved if the electrode, after the polymerization, is immersed in a solution containing the salt of the ions which were used for the electropolymerization of the film.[38]

The PP modified electrode satisfies the Nernst response to anions like NO_3^-,[49] Br^-, Cl^-[55] and ClO_4^-[56] within the concentration range of 10^{-1} to 10^{-4} mol dm^{-3}. The interference effects on the selectivity of the film can be related to the ionic radius and charge of the anion.[55] Better response slopes were observed for smaller anions than for the bigger ones which means that the insertion of smaller anions is due to their intercalation into the polymer. In general, in spite of the high anion sensitivity, the PP film shows poor anion selectivity.[56,57]

Some films, such as poly(thiophene) (PT), poly(2,2'-bithiophene) (PBT), poly(3-methylthiophene) (PMT), poly(3-octylthiophene) (POT) and poly(4,4'-dioctyl-2,2'-bithiophene) (POTd), have been investigated for their use in potentiometric measurements in aqueous solutions.[28] These films were polymerized from a 0.1 mol dm^{-3} $LiBF_4^-$ propylene carbonate solution containing the corresponding monomer or dimer. Interestingly, all the PT films were found to give a cationic response to monovalent cations and also showed some sensitivity to divalent cations (Table 1).

The responses were in general always fast and the cation selectivity was poor. For PT films the slopes are a function of the hydrated cationic radii. When BF_4^- was used as an anion, the slopes observed for POT were only 20.5 and 14.3 mV decade^{-1} for Na^+ and Li^+, respectively. This clearly demonstrates that the counter ion of the PP backbone influences the potentiometric response to cations and may contribute to the sub-Nernstian response. This behaviour is assumed to be governed by the interaction between the cations and the polythiophene backbone which is easily influenced by the level of oxidation of the polymer.

The ion-exchange properties can be improved, at least in theory, by incorporation of ionic substituents into the polymer backbone. An attempt has been made to explore this idea by polymerization of the 3-methylpyrrole-carboxylic acid (MPC) monomer in acetonitrile solution containing 0.1 mol dm^{-3} Et_4NClO_4.[58] The study showed a strong pH dependence of the polymer and a high affinity to binding big organic molecules.

The rate of ion exchange is affected by the pH of the solution since it provides a reversible protonation or deprotonation of the polymer backbone. During the deprotonation in alkaline solution the –NH– bond in the pyrrole unit is disrupted[45] [Fig. 1(a)]. This effect is reversed in acidic solution, where the protons are again re-attached [Fig. 1(b)]. During the deprotonation, the counter ion also leaves the polymer matrix, ensuring the charge neutrality. During the protonation, the anions move into the polymer to balance the charge.

This deprotonation–protonation affects the electronic structure of the polymer by varying the electron hopping distance and leads to decreasing–increasing conductivity.[59] This increase–decrease in conductivity apparently also results in a change of the potential of PP modified electrode. In neutral

Table 1 Slopes in mV per decade of the potentiometric response curves for some PT films deposited on Pt in a 0.1 mol dm^{-3} Cl^- solution of different cations (reprinted from ref. 28).

Polymer	H^+	Li^+	Na^+	K^+	NH_4^+	Mg^{2+}	Ca^{2+}
PT	48.2	39.4	41.8	42.4	44.9	13.6	13.7
BPT	10.6	29.6	34.9	38.5	40.8	5.3	6.0
PMT	22.3	30.7	37.4	38.1	38.8	-2.0	3.5
POT	44.4	46.6	46.2	47.4	45.0	17.5	11.7
POTd	42.8	35.5	39.1	43.5	46.2	12.3	12.6

solutions of pH 7, the potential decays only very little into more negative values with time until a stable potential value is reached. In acidic or basic solutions the potential-decay curves consist of two parts, an initial decay (basic solutions) or an initial increase (acidic solutions) of the electrode potential is observed, which follows levelling until a stable potential value is reached. A slope of around -45 mV per pH unit for thin PP film has been obtained by several groups. The time at which the potential of the PP/Pt electrode approaches an equilibrium, the value increases with the thickness of the PP film (150 min for 0.8 μm and 10 h for 8 μm PP film).[59] Consequently, slower changes of the electrode potential are observed.

The electrode potential changes only slightly over a range of pH 4–8. In strongly acidic and basic solutions the values are much smaller than the 50 mV decade^{-1}, as shown in Table 2 for the NO_3^- doped PP film.

The ion movement at the polymer/solution interface is compensated for by electron transfer at the electrode–polymer interface in order to satisfy the conditions of electroneutrality. In strongly basic solutions the anion is not involved, therefore, the redox reaction for PP is as follows:

$$PP + H_2O + e^- \rightarrow PP\text{–}H + OH^- \qquad (2)$$
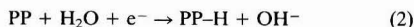
In strongly acidic solution the PP, as deposited, in its oxidized state, $(PP)^{y+}(yX^-)$ will first be reduced by losing the anion and then protonated to a certain extent depending on how strong the acid is. The redox reaction is

$$(PP)^{y+}(yX^-) + ye^- \rightarrow PP\text{–}H + yX^- \qquad (3)$$

The fast response of the electrode potential to anion-concentration change in solution, mirrors changes in the redox states of the polymer which results from the mass transport of anions and cations through that polymer.[22] Therefore, when a formed CP is placed in the electrolyte solution containing both redox and non-redox species a mixed potential, E_{mix}, is established at the interface.[24] Its value depends on the relative magnitudes of the contributions of the electron and ion-exchange processes, *i.e.*, on the sum of partial exchange current densities i^o_e and i^o_i flowing through that interface. An

Fig. 1 Deprotonation mechanism of a PPN(BF₄) film (reprinted from ref. 45).

Table 2 Slopes of the electrode potential–log [NO₃⁻] (slopes mV/log *c*) of 8 μm thick PP(NO₃⁻)/Pt electrode in solutions of different pH prepared from NaNO₃ or NaOH (non-buffered) (reproduced from ref. 49)

Solution pH	Slopes mV/log C
1.3	−16.1
2.5	−36.4
6.5	−56.3
8.7	−41.0
9.2	−36.0
10.5	−20.3
12.1	−18.4

equation describing the simple case of an electron and one ion transfer in which $i^o_e \gg i^o_i$ was derived:[60]

$$E_{mix} = E_{o,i} - \frac{RT}{z_iF}\frac{i^o_e}{i^o_i}\exp\left\{\frac{(\alpha z\eta)_e F}{RT}\right\} + \frac{RT}{z_iF}\ln a_i \qquad (4)$$

where z_i is the charge of the ion, $E_{o,i}$ is the standard potential due to the ion transfer, α_e, and η_e are the electron transfer coefficient, and the overpotential of the electron transfer, respectively, and the a_i is the activity of the ion in the solution. Another, logical but more explicit expression for E_{mix} is analogous to the Nikolskij–Eisenman equation:

$$E_{mix} = S \ln\{a_i + K_{redox}(a_R/a_O) + \Sigma_j(k_{ij},a_j)\} \qquad (5)$$

where a_i, and a_j denote the activity of the analyte and of the interferent ions, respectively, and k_{ij} is the potentiometric selectivity coefficient which reflects the ability of the sensor to discriminate against the interfering ion. A modified version of the Nikolskij–Eisenmann equation was produced by Buck.[61]

It has been shown[36] that in the case of PT the electron transfer rate is at least two orders of magnitude faster than that of the ion-transfer rate and that E_{mix} is dominated by the redox process. It was mentioned[28] that the PT films are possibly less redox-sensitive than poly(pyrrole) layers and that the electron transfer between the redox couple in solution is faster for PP than it is for PT films. This can be related to the difference in the oxidation potential between the two polymers.

There is no redox term in eqn. 5 for conventional ion-selective electrodes based on ionically conducting organic polymers such as Nafion (for cation) or Tosflex (for anion) membranes. It has been demonstrated that at electrodes coated with ion-exchange polymeric films, the charge and concentration of the electroactive species are unable to affect the electrode potential shift, provided that the quantities of the redox couples incorporated in the ion-exchange coating represent less than 5% of the film capacity.[62] These type of membranes, therefore, have a great advantage over CPs. The price that has to be paid for this advantage is that the coupling of a conventional ionically conducting ion-selective layer to the electronically conducting physical part of a macroscopic sensor is usually more difficult. The possibility of constructing miniaturized cation-selective electrodes by doping the cation exchangers into electrochemically grown PP films has been investigated.[63] By this route, it is possible to, at least partially, suppress the redox activity of the PP film and to manipulate the density of the sulfonic acid groups in the film. Another approach was driven through a preparation of electrically-neutral films. It was demonstrated that PP, electrodeposited by constant potential electrolysis at 1.5 V *versus* Ag/AgCl or cyclic voltammetry from 0.01 mol dm^{-3} NaOH aqueous solution containing 0.25 mol dm^{-3} pyrrole remains electro-inactive and, therefore, is also not redox sensitive.[64] The electro-inactive PP film coated on the Pt electrode shows a near Nernstian response (-50 mV per pH unit) with pH of the solution within the range of 2 to 10 without interference from other co-existing ions in the buffer solution.

The pH and the ionic strength effects are of the same origin as those observed on conventional anion exchangers, *i.e.*, with higher pH or lower ionic strength, the ion exchange is more difficult.[65] The effects of pH and ionic strength are of the same character for the polymer as is the effect of applied electrical potential to the modified electrode. Naturally, if the redox species are absent from the solution, the interfacial potential is determined entirely by the ion exchange at the polymer/solution interface. It has been shown that redox behaviour appears in solution having pH values higher than 2. In solutions of lower pH, hydrogen evolution becomes predominant, resulting in shadowing of the redox behaviour.[16]
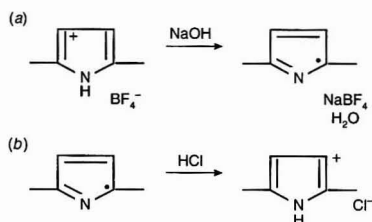
Gas Potentiometric Sensors

The response of CP to gas or vapour in potentiometric sensors is driven by modulation of the work function (WF).[3,66] The measurement of the WF requires that the CP is capacitively coupled to the rest of the sensor at one interface. This requirement is satisfied in the Kelvin Probe (vibrating plate capacitor),[67] and in all solid-state devices utilizing the field-effect *e.g.*, chemically sensitive diodes or in suspended-gate field-effect transistors (SGFETs).[68,69] The WF measurement responds to electron affinity changes and surface dipole changes between two electrodes. Assuming that one of the electrodes is not sensitive to the analyte and, therefore, can be seen as a reference, information about the changes in the WF of the other can be used for the detection of gases or vapours. If the electron affinity of the matrix is low, electrons are transferred to the guest molecule. In other words, the matrix behaves as a reducing agent with respect to the guest molecule. However, if the value of the WF is high, electrons move from the guest molecule to the matrix: *i.e.*, the molecule becomes partially oxidized. During the interaction of the neutral molecule with the polymer matrix a fractional integral value of a charge is exchanged between the molecule and the energy bands of the polymer matrix. It has been shown experimentally[70] that the number δ of molecules participate in the charge exchange process reflects in the charge transfer coefficient. As shown Fig. 2, for the same guest molecule the slope of the measured WF difference, $\Delta\Phi$, between the organic semiconductor and a reference plate, varies linearly with the magnitude of the initial work function, WF_{init}, of the polymer.

The WF_{init} mirrors the electron affinity of the synthesized polymer film. Furthermore, it can be seen that for certain values of WF_{init}, $\Delta\Phi$ is zero; *i.e.*, the molecule does not form a charge-transfer complex. At higher values of WF_{init} the molecule behaves as an electron donor, while at values below the zero-crossing point the molecule becomes an electron acceptor. The fact that these zero crossing points lie at different values of WF_{init} indicates that, in principle, the 'reference material' could be obtained by adjusting the WF_{init}, accordingly. The gas-solid equilibrium, K_G, leads to a ln P_G dependence which can be formulated as

$$K_G = [e]^{2\delta}/\alpha P_G \qquad (6)$$

where δ represents the partial charge transfer, α represents the partition coefficient of the gas molecule and P_G the partial pressure of the gas.[10]

It has been observed that the relative change of WF for the same guest molecule depends on WF_{init} of the synthesized polymer.[71,72] For a mixture of gases, each species will

exchange partial charge, δ. For a matrix of a different value of WF_{init}, δ will also be different. It is possible, in a formal analogy with the Eisenman–Nikolskij equation, to formulate the response of the WF sensor in a mixture. The magnitude of the contribution of the interfering species to the overall signal can be manipulated by the adjustment of WF_{init} of the selective layer, proposed earlier. This greatly increases the range of the species that can be quantified by this transduction principle.

The fact that the response to methanol was stronger when the electrodeposition of PP was carried out from methanol rather than from acetonitrile, indicates that solvation during polymerization may have left the final polymer with 'solvent footprints' which made it an entropically more favourable binder for the organic substrate of similar shape. This may be termed a solvent-induced template effect, similar to one proposed for example by Shea and Dougherty.[73] It has been experimentally confirmed that by changing the solution composition of the background electrolyte, the degree of cross-linking, the doping level and the morphology of the polymer vary simultaneously.[74] It was found that metal clusters, *e.g.*, Hg, Ag, Pd which are formed by changes of the redox potential of the PANI matrix, as discussed above, enhance sensitivity of the polymer matrix towards specific analytes; *i.e.*, HCN gas[29,75] or H_2 gas.[76] A step response of the PANI film with incorporated Pd clusters to H_2 in air are shown in Fig. 3. The PANI-Pd film was prepared by immersing the PANI film immediately after polymerization (final potential −0.1 V) into a solution of 2×10^{-3} mol dm^{-3} PdSO$_4$ in 1.0 mol dm^{-3} H$_2$SO$_4$ for 3 d.[76]

Conclusion

Analytical application of CPs for use in chemical sensors was reviewed in the context of existing and future trends in electroanalysis. The need for enhancement of the information-acquisition process by modern statistical data evaluation techniques; *i.e.*, chemometrics, neural nets, *etc.* can be supported by grouping individual sensors into multichannel probes. Recognizing the ease of preparation of CPs, the fabrication of multichannel sensing probes is not so far away.

The electrochemcial deposition mode of CPs guarantees a good adhesion of the polymer film to the substrate, fine control of anodic growth of the films (even in a small and a geometrically complex area of a substrate), accurate control of the final polymer thickness and also provides an easy way to automate the sensor fabrication process.

The limited selectivity of the CP to various ions represents a doubtful prospect for the ion-sensing application. Furthermore, when a CP is placed in the solution of electrolyte

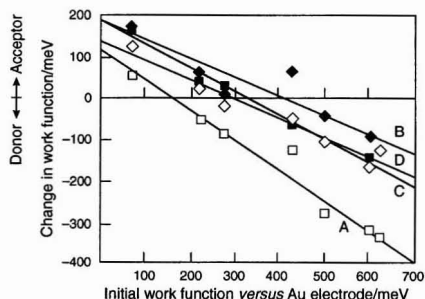**Fig. 2** Dependence of the vapour-induced shift in the poly(pyrrole) films work function on its original value. Values are quoted *versus* the work function of the Au reference grid electrode. A, MeOH; B, CHCl$_3$; C, iPrOH; and D, CH$_2$Cl$_2$.
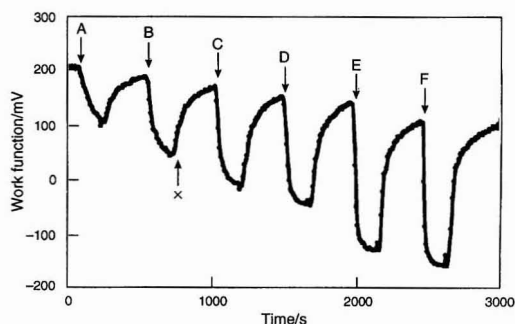

Fig. 3 Response of PANI–Pd film to hydrogen at room temperature. A, 100; B, 200; C, 500; D, 1000; E, 5000; F, 10 000; and X, 9.17 ppm of hydrogen in air.

containing both redox and non-redox species, a mixed potential, E_{mix}, is established at the interface. Its value depends on the relative magnitudes of the contributions of the electron and ion-exchange processes.

The issue of selectivity is governed by the solubility of the gas in the polymer phase and in the donor–acceptor relationship between the guest molecule and the condensed phase. If the gas is not soluble in the polymer layer, it is not expected to modulate the bulk properties of that material. However, it is obvious that a molecule that cannot partition to the condensed phase can still adsorb at its surface and, thus, modulate the surface properties. As there is not physical restriction on the surface, or bulk interactions, a broad range of non-specific interferences is expected to occur. The structure and morphology of the polymer coatings determine the permeability of sorbent coatings and the diffusion rate of the analyte in the polymer. More rational structural design of the polymers and structural control in the synthesis of the materials should result in broader application of these materials in chemical gas sensors.

References

1 Göpel, W., *Sens. Actuators, B*, 1994, **18–19**, 1.
2 Schierbaum, K. D., *Sens. Actuators, B*, 1994, **18–19**, 71.
3 Janata, J., in *Principles of Chemical Sensors*, Plenum, New York, 1989, pp. 1–14.
4 Diaz, A. F., Castillo, J. L., Logan, J. A., and Lee, W.-Y., *J. Electroanal. Chem.*, 1981, **129**, 115.
5 Waltman, R. J., Diaz, A. F., and Bargon, J., *J. Electrochem. Soc.*, 1984, **131**, 1452.
6 Genies, E. M., Boyle, A., Lapkowski, M., and Tsintavis, C. P., *Synth. Met.*, 1990, **36**, 139.
7 Skotheim, T. A., in *Handbook of Conducting Polymers*, Marcel Dekker, New York, 1986, pp. 81–132.
8 Josowicz, M., and Janata, J., in *Applications of Electroactive Polymers*, ed. Scrosatti, B., Chapman and Hall, London, 1993, pp. 310–343.
9 Bidan, G., *Sens. Actuators, B*, 1992, **6**, 45.
10 Janata, J., *Anal. Chem.*, 1991, **63**, 2546.
11 Charlesworth, J. M., Partridge, A. C., and Neil, G., *J. Phys. Chem.*, 1993, **97**, 20.
12 Slater, J. M., Watt, E. J., Freeman, N. J., May, I. P., and Weir, D. J., *Analyst*, 1992, **117**, 1265.
13 Topart, P., and Josowicz, M., *J. Phys. Chem.*, 1992, **96**, 7824.
14 Topart, P., and Josowicz, M., *J. Phys. Chem.*, 1992, **96**, 8662.
15 Fletcher, S., *J. Chem. Soc., Faraday Trans. II*, 1993, **89**, 311.
16 Kuwabata, S., Okamoto, K., and Yoneyama, H., *J. Chem. Soc., Faraday Trans. I*, 1988, **84**, 2317.
17 Salmon, M., Diaz, A. F., Logan, A. J., Krounbi, M., and Bargon, X., *Mol. Cryst. Liq. Cryst.*, 1982, **83**, 265.
18 Tourillon, G., and Garnier, F., *J. Polym. Sci., Polym. Phys. Ed.*, 1984, **22**, 33.
19 Bloor, D., Hercliffe, R. D., Galiotis, C. G., and Young, R. J., in *Electronic Properties of Polymers and Related Compounds*, ed. Kuzmany, H., Metring, M., and Roth, S., *Springer Series in Solid-State Sciences*, Springer-Verlag, Berlin, 1984, pp. 179–182.
20 Moss, B. K., Burferal, R. P., and Skylas-Kazacos, M., *Mater. Forum*, 1989, **13**, 35.
21 Krische, B., and Zagorska, M., *Synth. Met.*, 1989, **33**, 257.
22 Smyrl, W., and Lien, M., in *Applications of Electroactive Polymers*, ed. Scrosatti, B., Chapmann and Hall, London, 1993, ch. 2, p. 29.
23 Shen, Y., Qiu, J., and Qian, R., *Makromol. Chem.*, 1987, **188**, 2041.
24 Curtin, L. S., Komplin, G. C., and Pietro, W. J., *J. Phys. Chem.*, 1988, **92**, 12.
25 Shinohara, H., Aizawa, M., and Shirakawa, H., *J. Chem. Soc., Chem. Commun.*, 1986, 87.
26 Naoi, K., Lien, M., and Smyrl, W. H., *J. Electrochem. Soc.*, 1991, **138**, 440.
27 Beer, P. D., in *Chemical Sensors*, ed. Edmonds, T. E., Blackie, New York, 1988, p. 17.
28 Bobacka, J., Lewenstam, A., and Ivaska, A., *Talanta*, 1993, **40**, 1437.
29 Langmaier, J., and Janata, J., *Anal. Chem.*, 1992, **64**, 523.
30 Walton, D. J., Hall, C. E., and Chyla, A., *Analyst*, 1992, **117**, 1305.
31 Shimidzu, T., Ohtani, T., and Honda, K., *J. Electroanal. Chem.*, 1987, **224**, 123.
32 Atanasoska, L., Naoi, K., and Smyrl, W. H., *Chem. Mater.*, 1992, **4**, 988.
33 Papez, V., and Josowicz, M., *J. Electroanal. Chem.*, 1994, **365**, 139.
34 Wang, J., Chen, S.-P., and Lin, M. S., *J. Electroanal. Chem.*, 1989, **273**, 23.
35 Gratzl, M., Duan-Fu Hsu, Riley, A. M., and Janata, J., *J. Phys. Chem.*, 1990, **94**, 5973.
36 Duan-Fu Hsu, Gratzl, M., Riley, A. M., and Janata, J., *J. Phys. Chem.*, 1990, **94**, 5982.
37 Warren, L. F., Walker, J. A., Anderson, D. P., and Rhodes, C. G., *J. Electrochem. Soc.*, 1989, **136**, 2286.
38 Dong, S., Sun, Z., and Lu, Z., *J. Chem. Soc., Chem. Commun.*, 1988, 993.
39 Herberg, B., and Pohl, J. P., *Ber. Bunsen-Ges. Phys. Chem.*, 1988, **92**, 1275.
40 Mirebeau, P., *Journal de Phys.*, 1983, **44**, C3–57.
41 Schlenoff, J. B., and Chien, J. C., *J. Am. Chem. Soc.*, 1987, **109**, 6269.
42 Josowicz, M., and Topart, P., in *Sensors and Sensory Systems for an Electronic Nose*, ed. Gardner, W., and Bartlett, P. N., *NATO ASI Series Serie E: Applied Sciences*, Kluver, Netherlands, 1992, ch. 8, p. 122.
43 Otero, T. F., Tejda, R., and Elola, A. S., *Polymer*, 1987, **28**, 651.
44 Wang, J., Chen, S.-P., and Lin, M. S., *J. Electroanal. Chem.*, 1989, **273**, 231.
45 Inganas, O., Erlandsson, R., Nylander, C., and Lundstrom, I., *J. Phys. Chem. Solids*, 1984, **54**, 427.
46 Munstedt, H., *Polymer*, 1986, **27**, 899.
47 Chao, T. H., and March, J., *J. Polym. Sci., Part A: Polym. Chem.*, 1988, **26**, 743.
48 Teasdale, P. R., Spencer, M. J., and Wallace, G. G., *Electroanalysis (N.Y.)*, 1989, **1**, 541.
49 Oei, Q., and Quian, R., *Electrochim. Acta*, 1992, **37**, 1075.
50 Ge, H., and Wallace, G. G., *React. Polym.*, 1992, **18**, 133.
51 Curtin, L. S., Komplin, G. C., and Pietro, W. J., *J. Phys. Chem.*, 1988, **92**, 12.
52 Yamaura, M., Sato, K., Hagiwara, T., and Iwata, K., *Synth. Met.*, 1992, **48**, 337.
53 Yamaura, M., Sato, K., and Hagiwara, T., *Synth. Met.*, 1990, **39**, 43.
54 Li, Y., and Qian, R., *Synth. Met.*, 1989, **28**, C127.
55 Dong, S., Sun, Z., and Lu, Z., *Analyst*, 1988, **113**, 1525.
56 Lu, Z., Sun, Z., and Dong, S., *Electroanalysis*, 1989, **1**, 271.
57 Cadogan, A., Lewenstam, A., and Ivaska, A., *Talanta*, 1992, **39**, 617.
58 Pickup, P., *J. Electroanal. Chem.*, 1987, **225**, 273.
59 Pei, Q., and Qian, R., *Synth. Met.*, 1991, **45**, 35.
60 Cammann, K., in *Topics in Current Chemistry*, Springer-Verlag, Berlin, 1985, vol. 128, p. 219.
61 Buck, R., and Stover, F., *Anal. Chim. Acta*, 1978, **101**, 231.
62 Toniolo, R., Comisso, N., Bontempelli, G., and Schiavon, G., *Talanta*, 1994, **41**, 473.
63 Okada, T., Hiratani, K., Sugihara, H., and Koshizaki, N., *Anal. Chim. Acta.*, 1992, **266**, 89.
64 Osaka, T., Fukuda, T., Kanagawa, H., and Momma, T., *Sens. Actuators, B*, 1993, **13–14**, 205.
65 Krasko, V. V., Yakovleva, A. A., *Elektrokhimiya*, 1989, **25**, 1016.
66 Janata, J., in *Sensors and Sensory Systems for an Electronic Nose*, ed. Gardner, W., and Bartlett, P. N., *NATO ASI Series Serie E: Applied Sciences*, Kluver, Netherlands, 1992, ch. 7, p. 103.

67 Phillips, G. J., *Sci. Instrum.*, 1951, **28**, 342.
68 Josowicz, M., and Janata, J., in *Chemical Sensor Technology*, ed. Seiyama, T., Elsevier, New York, 1988, vol. 1, pp. 153–177.
69 Zhang, T.-H., Petelenz, D., and Janata, J., *Sens. Actuators*, 1993, **12**, 175.
70 Blackwood, D., and Josowicz, M., *J. Phys. Chem.*, 1991, **95**, 493.
71 Josowicz, M., and Janata, J., *Anal. Chem.*, 1986, **58**, 514.
72 Josowicz, M., Janata, J., Ashley, K., and Pons, S., *Anal. Chem.*, 1987, **59**, 253.
73 Shea, K. J., and Dougherty, T. K., *J. Am. Chem. Soc.*, 1986, **108**, 1091.

74 Topart, P., and Josowicz, M., *Talanta*, 1994, **41**, 909.
75 Li, J., Petelenz, D., and Janata, J., *Electroanalysis*, 1993, **5**, 791.
76 Li, H.-S., Josowicz, M., Baer, D., Englehard, M., and Janata, J., *J. Electrochem. Soc.*, 1995, **142**, 798.

Impregnation of a pH-Sensitive Dye Into Sol–Gels for Fibre Optic Chemical Sensors

G. E. Badini, K. T. V. Grattan* and A. C. C. Tseung

Department of Electrical, Electronic and Information Engineering, City University, Northampton Square, London, UK EC1V 0HB

The sol–gel method was used to investigate the preparation of gels which were subsequently impregnated with a pH-sensitive fluorescent dye, fluorescein isothiocyanate (FITC). The work enabled the examination of several aspects of the system, including the leaching of the dye from the gel, a problem which has more severe consequences for fluorescence-based than absorption-based systems, where the use of a silylating agent was found to improve the immobilization of the dye to the substrate. The effect of the loss of dye was investigated in terms of the fluorescent response of the prepared gels, and this was cross-compared with that of the dye in solution, as a function of pH. This showed good agreement. The response time of the gel to pH changes was also observed. Further, aspects of the drying of the gels were investigated in terms of their physical appearance and the characteristics of the substrates thus produced for chemical sensing purposes. Various observations of failure characteristics of these gels under re-immersion in water were considered in light of their potential use, in chemical sensor probes, of sol–gel based systems.

Keywords: Sol–gel; fibre optic; sensor; probe

Introduction

Sol–gel techniques have been extensively used in various aspects of physical chemistry and discussed in their application to chemical sensing by a number of authors.[1–4] However, in spite of the considerable interest in the use of sol–gels as substrates to contain chemically-sensitive agents for fibre optic sensors,[4] there is a considerable amount of work which still needs to be performed to produce high-quality, impregnated sol–gels with the right characteristics for sensor purposes. The achievement of this is not easy, and is the goal of a number of groups worldwide.[4] For the limited investigation reported here, several important characteristics, such as the stability of the gel acting as the substrate for the chemically-sensitive agent and its tendency to allow the impregnated dye to leach out into the environment, *viz.* its structural integrity on re-wetting, for example when immersed in a liquid on which the measurement is to be made, are considered.

As would be expected, simple investigations[5] showed that if aged and partially-dried gels were simply transferred into aqueous solutions of a pH-sensitive dye, such as fluorescein isothiocyanate (FITC), after two to three days the dye would be completely impregnated into the gel which would then adopt the characteristic green colour of the dye itself, and a characteristic fluorescence response could be observed from such a sample. However, if such a gel, prepared in this simple way, were either placed in an aqueous solution for a period of several days or under running water, it was found that almost

all of the dye would leach from the gel, with such a rapid loss of indicator that made it unacceptable for fibre optic chemical sensing. One of the major limitations of fluorescence-based sensors is the stability of the dye in its binding to the substrate, as this affects the calibration of such an intensity-based sensor scheme. This is less of a problem, particularly in terms of calibration, for fluorescence-based systems relying upon decay–time changes as a measure of the parameter under consideration or absorption-based sensors, when using a two-wavelength isosbestic point method. The contamination of the sample, particularly for *in vivo* applications, is critically affected by the leaching of the dye, regardless of the measurement method and, thus, this is a most important consideration in producing and evaluating such systems. The contamination of the species to be investigated could range from being either inconvenient to highly dangerous, for example, in most biomedical applications. With the aim of producing a more stable dye–substrate arrangement, whether for fluorescent or absorbing dyes, an attractive method of preparation of the dye-impregnated system was investigated, *i.e.*, a two-step reaction. It was believed that this method would yield an over-all more stable product, and advance knowledge in the preparation of satisfactory pH-sensitive substrates for fibre optic chemical sensors.

Experimental Procedure

The experimental procedure is shown schematically in Fig. 1, where the reactants used (in the ratios shown) were transferred to polythene vials which were sealed and placed in an oven at 80 °C to gel and age. This temperature was chosen as a representative temperature at which to carry out the study, based on our previous experience. It was also a reasonably stable temperature to achieve using apparatus available in the laboratory. Clearly, in more extensive studies, the effects of a wider range of temperature could be considered, as well as the overall ageing time which would be expected to increase as temperature decreased. However, the above represents a compromise between an adequate speed of preparation and a drying speed that was not too rapid which could lead to fragmentation. After 3 d the seals on the first pair of samples were removed and replaced by aluminium foil which was pierced to promote drying. The same procedure was used for the remaining three pairs of samples on consecutive days so that at the beginning of the fifth day the samples had undergone between four and one days drying. The gels were removed, immersed in anhydrous *N,N′*-dimethylformamide (DMF), covered with a molecular sieve and left to stand for 2 d with occasional gentle agitation, in order to dehydrate the gels. One gel of each pair was then transferred into a fresh 1% solution of 3-aminopropyltriethoxysilane (3APTS) in anhydrous DMF and after 2 d the gels were removed and placed in an aqueous solution of FITC. They were allowed to stand for another 2 d so the dye could fully impregnate this structure.

Finally, the gels were washed under running water for about 18 h in order to observe the effects of this procedure.

In previous work,[6] it has been observed that the use of 3APTS improved the uptake of dye into the sol–gel. A detailed discussion of the process by which this happens is beyond the scope of the paper, but the technique is the same as that used by Matlin *et al.*[7] who performed an investigation of the preparation of sol–gels for non-sensor purposes. In this previous work, 3APTS was observed to show excellent affinity for glass silanols and appears to provide a means of bonding between the (organic) indicator and the (inorganic) substrate. In order to investigate the uptake of the dye, the fluorescence induced from one pair of gels was obtained using laser excitation at 488 nm and the emission centred at about 530 nm was recorded *versus* pH. A satisfactory fluorescent response, being similar in character to that of the dye in solution, as discussed in detail later, indicated the satisfactory uptake of the fluorescent dye into the substrate medium. The main criterion here is the achievement of a variation in the fluorescence characteristic, changing as a function of pH (in this case), as determined by spectroscopic observations which then could be transferable to a pH-sensitive optical fibre probe. The influence of the extent of drying of a gel after it had been impregnated with FITC was not investigated in detail, as the changes produced by the drying process were believed to be the main factors in determining the initial stability of the dyes in the substrate. It is, of course, recognized that longer term changes can occur (usually more slowly) and these can have an effect upon the dye-impregnated substrates. A more detailed study of dye-impregnated substrates, subjected to ageing over a period of years, is reported elsewhere.[6,8]

Results and Discussion

Gelation and Drying Stages

The mixture discussed was gelled overnight to give the characteristic two distinct phases observed visually, with the gel clearly seperated from the sides of the container. During the ageing period, the gels underwent a significant reduction in volume and mass loss due to solvent evaporation, as illustrated quantitatively in Fig. 2. The DMF solutions containing 3APTS developed a white precipitate during the time that the gels were immersed in them, probably owing to polymerization reactions involving the silylating agent and traces of remaining water or water which was produced as a result of continued sol-to-gel transformation. The gels were observed as the dye was allowed to impregnate the pores of the polymeric network and a strong green colour due to the

FITC was observed. In a related experiment, gels which had been prepared in the same manner were tested for uniformity of dye penetration and cut by pressing a scalpel onto their cylindrical side. It was clear, by observation of the cut sample, that the FITC had penetrated mostly uniformly through the entire structure. This contrasted with gels which had been prepared using the silylating agent which appeared slightly darker at the edges, thus showing a less uniform penetration of the dye into the gel formed in this way.

Effect of Drying Prior to Impregnation of FITC Into the Gel

The extent to which the gels were dried pior to impregnation with the dye was found to affect them greatly, resulting in noticeably different appearances and properties of the gel. Those which had undergone very little drying were soft and easily cut; by contrast those which had been allowed to dry for a number of days became denser and harder and when the scalpel was pressed into their side a flaw would form which would propagate across the axis of the gel. If the gels were allowed to become very dry then they would turn opaque and be difficult to cut without cracking in all directions. These results suggested that, as the gel becomes drier, the three-dimensional polysiloxane network becomes stronger, as might be expected. Visual observation of a series of gels prepared in this way confirms this result. In one example of a similar preparation, a sample had been left to dry at 65 °C for 6 d. It was found to be heterogeneous in appearance, possessing a lower opaque region and an upper clearer region, as illustrated schematically in Fig. 3, C. It was observed that when immersed in DMF it cracked immediately along the line dividing the opaque region from the clearer region and after about 10 min this opaque region had become clear. This suggested that the lower area was dry and porous and that the DMF was able to . impregnate the porous network. The presence of such an opaque zone below a clear region can be explained by assuming that it was formed as the solvent in the gel evaporated towards the network in an upward direction, suggesting that the porous network was largely continuous in the sample.

Leaching of FITC From the Gels

When the gels were kept under running water, it was found that the FITC had a tendency to wash out much more quickly and to a greater degree from those samples that had not been treated with the silylating agent. This seemed to indicate that FITC can be bound irreversibly to a gel by a method similar to that used for its immobilization on to conventional silica.[7] Fluorescence spectra obtained showed the expected peak at 530 nm, with approximately four-fold greater fluorescence intensity than from those prepared without 3APTS, as shown
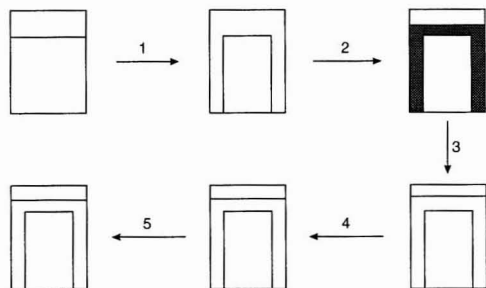
Fig. 1 Process used for the impregnation of FITC into a pre-formed gel. Reactants: TEOS–H_2O–ethanol–DMF–HCl $(1 + 10 + 2 + 1.5 + 0.1)$. Procedures: 1, Mix, seal, gel and age at 80 °C; 2, immerse in anhydrous DMF, dry with molecular sieve; 3, add DMF or 1% solution of 3APTS in DMF; 4, after 12 h, replace DMF with aqueous FITC; and 5, gradually impregnate gel with FITC solution.
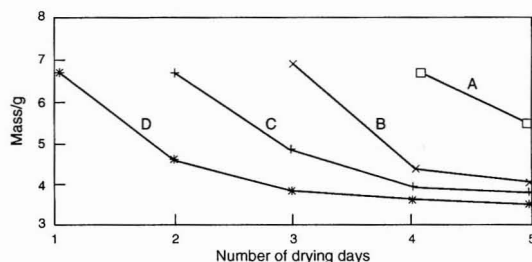
Fig. 2 Graph of mass changes in samples as a function of drying days prior to impregnation by FITC, for four different samples dried for A, 1; B, 2; C, 3; and D, 4 d.

in Fig. 4. Similarly, this effect was found when samples were reduced to powder and rinsed thoroughly with distilled water. The influence of the extent of drying prior to dye impregnation on the fluorescent response and the rate of leaching of the dye was not studied in great detail. The absolute intensity of the fluorescence response will, of course, depend on the concentration of FITC used to impregnate the gel, and in the present work, the fluorescence intensity was within the order of that observed for derivatized porous glass[8] which itself is an alternative substrate for FITC, or other dye, for chemical sensor purposes.

Fluorescent Response to Varying pH

The fluorescent response of an impregnated gel under conditions of varying pH is shown in Fig. 5, essentially paralleling its intended use in a chemical sensor. The curve is similar to that which would be expected for FITC in solution and, in order to obtain this graph, the gel had been washed under running water for at least 3 h prior to analysis. Excitation at 488 nm was used and the fluorescence intensity was observed for pH 6–8. When a step change in pH was applied, it was observed that the maximum response was reached after approximately 20–30 s for the range of samples studied, prepared by the methods described. This was comparable to some of the best results achieved with microporous glass impregnated by similar types of dyes, and reported in the literature to be about 20–35 s,[9] using a single sphere of derivatized porous glass. Our comparable experiments with porous glasses (whose porosity was not measured quantitatively) have shown even longer response times, in the region of several minutes.[8]

Effect of Drying Gels After Impregnation With FITC

A series of such impregnated gels was investigated and it was found that on exposure to air, the gels would dry and crack in the space of a few hours. Even if the samples had previously
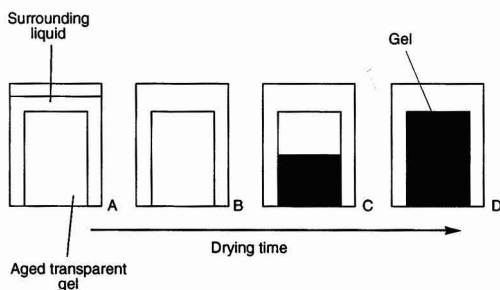
Fig. 3 Schematic representation of drying of gel. A, B, C, and D represent the sample at various stages during the drying time.
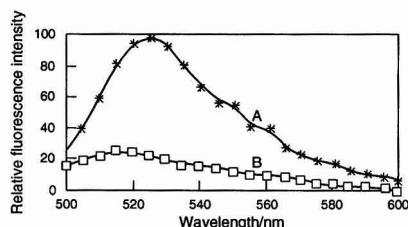
possessed some glass-like qualities prior to immersion in DMF solution, after impregnation with the dye, subsequent further drying led to a loss of these properties. On the contrary, the gels would be opaque and quite friable and if re-immersed in water they would fragment and in some cases, especially for wet, soft gels, they would be reduced to powder. On the other hand, if the gels were stored in a saturated environment, such as being kept in a sealed vial, they were found to retain their coherent structures for a very long time. A number of samples were stored over a period of years and one gel kept in this manner was found to have retained its characteristics over a period of storage of four years. However, notwithstanding this example, the inability of some gels to survive changes of environment highlights a problem with the specific approach in their use in fibre optic chemical sensors. It is quite clear that a preparation process which leads to samples which do not show the desired stability characteristics on immersion is not satisfactory. The work has shown the problem in achieving the right conditions for preparation, impregnation and storage and the difficulties which can occur with certain types of wet, soft gel which do not survive the process. It is clear that a balance must be struck in the preparation to ensure that the gel is not over-dry, which leads to cracking and fracture or over-wet which causes powdering and instability. In addition, in any practical use of such systems, a long term storage is likely to be essential to enable batch production and so samples must be stable over the long term. Some samples did show this stability over long periods, even of years.

Conclusion

For the samples prepared and considered, the use of a silylating agent was found to improve the immobilization of a dye onto a substrate and significantly to reduce the amount of dye which leaches from the gel when compared with a sample prepared without the use of the agent. A satisfactory fluorescent intensity response was observed for the samples considered and a temporal step response to an optical impulse of 20–30 s was observed. However, with the use of a silylating agent the uniformity of penetration of the dye was seen to be more of a problem for the samples considered. For thin films, such as those used for sensors, this would be less of a difficulty and the stability to leaching outweighs this, in an intensity-based optical measurement system. As the gels under test became drier prior to impregnation with FITC, they became harder and more glass-like and if they were allowed to dry after impregnation with the dye they would crack, become friable and lose their glass-like qualities and then on re-immersion would fragment and break down completely. For the samples prepared, this represents a limitation in their use in fibre optic chemical sensors and care must be taken to use preparation means which do not result in either over-dry or over-wet samples, which would be unsuitable for exposure to normal sensor conditions.

Fig. 4 Emission spectra of gels prepared A, with and B, without 3APTS.
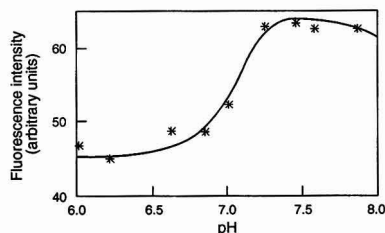
Fig. 5 Fluorescence intensity of sol–gel *versus* pH.

References

1 Kirkbright, G. F., Narayanaswamy, R., and Welti, N. A., *Analyst*, 1984, **109**, 1025.
2 Badini, G. E., Grattan, K. T. V., Palmer, A. W., and Tseung, A. C. C., *Proceedings of the Conference on Lasers and Electro-optics (CLEO 89)*, Institute of Electrical and Electronics Engineers, New York, 1989, p. 106.7.
3 MacCraith, B. D., McDonagh, C. M., O'Keeffe, G., Keyes, E. T., Vos, J. G., O'Kelly, B., and McGilp, J. F., *Analyst*, 1993, **118**, 385.
4 Klein, L., *Sol Gel Optics: Processing and Applications*, Kluwer Academic Press, Boston, MA, USA, 1994.
5 Badini, G. E., PhD Thesis, City University, London, 1994.
6 Badini, G. E., Grattan, K. T. V., and Tseung, A. C. C., *Rev. Sci. Instrum.*, submitted for publication.
7 Matlin, S. A., Tinler, J. S., Lloret, A. T., Lough, W. J., Chan, C., and Bugan, D., *Proc. Anal. Div. Chem. Soc.*, 1979, **16**, 354.
8 Badini, G. E., Grattan, K. T. V., and Tseung, A. C. C., *Sens. Actuators B*, submitted for publication.
9 Fuh, M.-R. S., Burgess, L. W., Hirchfeld, T., Christian, G. D., and Wang, F., *Analyst*, 1987, **112**, 1159.

Sensing With Chemically and Biologically Modified Carbon Electrodes

A Review

Markas A. T. Gilmartin and John P. Hart

*Faculty of Applied Sciences, Biosensors/Electrochemical Sensors Group,
University of the West of England, Coldharbour Lane, Frenchay Campus, Bristol,
UK BS16 1QY*

Summary of Contents

Background

In voltammetry and amperometry, the potential applied to a working electrode governs the oxidation state of a particular species at its surface, with the resulting charge-transfer process transducing quantitative data into a measurable current signal. As these methods monitor the current flowing through an electrode following a voltage perturbation, the working electrode may be considered to be the heart of the experiment. Consequently, much effort has been devoted to electrode fabrication and maintenance. The noble metals, *e.g.*, platinum,[1,2] nickel[3] and gold,[4] have been commonly employed in electroanalysis, the first finding the widest application, owing to its inertness and useful potential window.

In recent years, considerable attention has been focused on the production of carbon-based electroanalytical sensors, as carbon is a versatile and inexpensive electrode material. Such devices are amenable to chemical and biological 'engineering' with modifying agents such as polymeric membranes, enzymes and redox mediators, to impart the requisite selectivity for analyses in complex matrices.

This review is by no means exhaustive, but serves to illustrate the desirable characteristics and versatility of carbon as an electrode material for the fabrication of electrochemical sensors. The readers will also be introduced to the diverse range of selectivity-enhancing techniques that may permit analyses in 'real' samples. The emphasis of such modification techniques will be on biologically tailoring sensory interfaces, although broader aspects, such as aprotic solution electrochemistry, biosensor evolution and their impact on the clinical market, are also discussed.

Carbon as an Electrode Substrate: Properties, Manufacture and Modification

Carbon, in many respects, is an ideal electrode substrate. Its attractive features include access to a wide anodic potential range, low electrical resistance and residual currents and a reproducible surface structure. It is morphologically diverse, existing in a variety of forms suitable for electrochemical applications, *e.g.*, carbon fibres,[5] glassy (vitreous) carbon,[6] graphite pastes[7] and composites[8] and carbon films.[9] Examples of the analytical utility of the last four electrode substrates are detailed in this review.

Graphite

Graphite has been used extensively in electroanalytical studies.[9–12] Although it occurs naturally in the Earth's crust (Sri Lanka and the Malagasy Republic possessing the largest deposits), the high ash content (5–20%) of this material limits its electrochemical utility. Instead, the use of a purer, artificial graphite is commonplace in electroanalytical experiments. This chemically cleaned graphite is generally prepared using a procedure developed by Acheson in 1896,[9] whereby petroleum coke is heated to remove volatiles, mixed with coal-tar pitch, consolidated into the desired form and then subjected to a two-step heat-treatment process. A temperature of 1000 °C is used in a non-oxidizing environment, to expel unwanted volatile constituents from the pitch. The resulting amorphous carbon is transformed into graphite by further heating between 2500 and 3000 °C. Pyrolytic graphite is another synthetic structure, formed by the thermal decomposition of carbonaceous gases, such as methane, at temperatures in excess of 1200 °C.[9]

Crystallographically, graphite consists of layers of carbon atoms arranged in hexagonal rings, stacked in a repeating anisotropic ABAB pattern; this is termed hexagonal graphite. A less common form is rhombohedral graphite, which consists of ABCABC repeating patterns. The lowest resistance of graphite (approximately 10^{-4} Ω cm) is in the direction parallel to the hexagonal carbon planes and electrical conduction through this plane confers its metal-like properties.[9]

Glassy (Vitreous) Carbon

Glassy carbon electrodes (GCEs) have been widely employed in voltammetric studies,[13–18] for electrochemical detection

following liquid chromatographic separations[13,19,20] and in flow injection (FI).[21-23] Glassy carbon is a solid isotropic material composed of thin convoluting microfibrils that interlock to form strong interfibrillar bonds. It is produced by the thermal degradation (approximately 1800 °C) of selected organic polymers.[9]

The most striking feature of glassy carbon is its extremely low gas permeability compared with that of synthetic graphites, which arises from an extensive closed void network (as opposed to the open spaces present in its artificial graphite counterparts), allowing only discontinuous gas permeation of the material. The peculiarities of its surface structure permit analyses in extreme environments, such as organic solvents. This is important in the area of organic-phase electrochemistry, which offers the possibility of detecting hitherto inaccessible analytes, for example those that are insoluble or partially soluble in aqueous media.[24] Other inherent benefits are that polar interferents are poorly soluble and that the absence of water may facilitate the fabrication and enhance the longevity of sensors.[25]

This exciting field of research continued to grow apace in the study of non-aqueous enzymology.[24-30] Although the observation that enzymes retain their catalytic activity in aprotic media was made in 1913,[31] there have until recently been few reports exploiting this finding. This is surprising, as workers have demonstrated accelerated electron kinetics between the active centre of enzymes and the electrode surface in the organic phase.[29] As most biocatalysts are encapsulated in a carbohydrate sheath, electron 'tunnelling' to the active site is tortuous.[32] It is postulated that organic solvents disrupt these polysaccharide moieties, improving access to the catalytic site.[33]

It is critical, however, that an appropriate solvent is used to maintain the integrity of the hydrated shell, which also engulfs enzymes and is fundamental to catalytic activity. The longevity of this essential water layer is dependent on the solvent system used. The selection of an appropriate solvent is based on the logarithmic partition coefficient (log P) of the test medium in an octanol–water two-phase system.[34] Solvents with log $P < 4$ are generally not suitable as they induce distortion of the enzyme–water interaction. Solvents with a log $P > 4$ are normally biocompatible, that is, their active site configuration is retained. There are some anomalies to this model but, despite these, this remains the best current guide to predicting biocatalytic activity in a given solvent system.

It transpires that hydrophobic water-immiscible solvents best suit these applications, and there are many to choose from. In contrast, water-miscible solvents tend to desorb the critical water layer, although this may be overcome by adding small amounts of water to satisfy the solvent's 'thirst'. Sakurai et al.[35] have shown that some enzymic reactions are characterized by a release of enzyme-bound water accompanying substrate complexation. Hydrophilic solvents are thought to render these transfer processes more energetically favourable, by enhancing water transfer from the prosthetic group to the solvent medium concurrently with enzyme–substrate binding.

Carbon-based Electrochemical Sensors

Carbon electrodes may be modified in a number of ways to improve their response characteristics to permit determinations in complex fluids, such as biological fluids. There are four principle enhancement techniques for voltammetric and amperometric electrodes, namely selective preconcentration, permselectivity, selective recognition and electrocatalysis.[36-40] The merits of these modification procedures and a selection of their applications are described in the following section.

Selective Preconcentration

The accumulation of electroactive analytes into or onto an electrode through partitioning, ion-exchange, complexation or simple adsorption processes has been the subject of several studies.[41-46] Selective preconcentration may be induced *via* the deliberate addition of modifying agents such as organic acids,[43] magnesium silicates,[44] zeolites[45] and organisms, e.g., mosses.[46] Alternatively, accumulation may occur as a serendipitous consequence of electrode design, e.g., the extractive properties of the mulling liquids used in carbon paste electrodes (CPEs).[43] In any event, these techniques allow sensitive determinations typically at the sub-micromolar level, e.g., Ag^I, Cu^{II},[41] Au^{III}[42] and the anti-tumour drug daunorubicin.[43] Here, CPEs provide a suitable substrate such as organic adsorption of the four-ring hydronaphthacene nucleus of daunorubicin. Optimum conditions for analyses comprised an accumulation time (T_{acc}) of 2 min, an accumulation potential (E_{acc}) of -0.3 V and an acetate buffer adjusted to pH 4.4. The cathodic peak at -0.6 V, ascribed to the electroreduction of the quinone group to the hydroquinone moiety, was used for analytical purposes. The interfacial preconcentration and its subsequent measurement following medium exchange afforded a rapid and sensitive [limit of detection (LOD) approximately 10^{-8} mol dm^{-3}] method for determining this anti-cancer agent in urine-spiked samples.

Silver- and linuron-sensitive devices have also been developed based on the respective accumulating propensities of zeolite- and sepiolite-containing CPEs.[44,45] Zeolite-modified electrodes possess cation selectivities, whereas clay-containing CPEs possess adsorptive capacities towards certain organic compounds. The surface-attached silver or linuron was stripped into solution using the differential-pulse (DP) waveform and the resulting reduction peak at $+0.22$ and oxidation peak at $+1.2$ V were used for quantitative purposes.

A variety of prokaryotic and eukaryotic organisms are also known to accumulate metals selectively and the analytical utility of this behaviour has been investigated. Moss-modified CPEs provide a good example of this occurrence. Ramos et al.[46] used a CPE containing a *Sphagnum* species to preconcentrate Pb^{2+} selectively into the graphite matrix. DPV was used to strip the divalent cation into solution and the reduction peak at -0.65 V was used for lead determinations in natural and fresh waters.

Permselectivity

Modification of electrode surfaces with permselective membranes has proved to be an important consideration when designing biosensors. These membranes are polymeric in nature and may be deposited or laid down over electrodes, creating mesh-type, cross-linked or continuous-phase interfaces. They are used for a number of reasons, including restricting substrate access to the active site of enzymes, isolating the electrode from potential interferences and preventing surface fouling by macromolecules. The most commonly used are permselective films which function as anti-interference barriers on the basis of size- or charge-exclusion phenomenon. In principle, such physical modification prevents unwanted species interacting with the electrode while retaining its heterogeneous electron-transfer characteristics. Polyelectrolyte coatings, in contrast, selectively exclude certain compounds on the basis of charge. Perfluorosulfonate ionomers, such as Nafion, are typical examples. Nafion is a strongly acidic cation-exchange polymer and hence has a tendency to repel anionic species whilst allowing the passage of cations (in particular divalent hydrophobic cations) to the electrode surface. Consequently, the literature is replete with reports detailing its usefulness as an anti-interference barrier in electroanalysis.

Nitric oxide (NO) is an important bioregulatory molecule responsible for endothelium-derived relaxing factor (EDRF).[47] EDRF abnormalities have been incriminated in conditions such as atherosclerosis. At present, the technology does not exist to distinguish between NO and nitrite, so the release, distribution and reactivity of endogeneous NO cannot be assessed. A microsensor has been constructed from carbon fibres and chemically modified with a p-type semiconducting polymeric porphyrin and Nafion.[48] Operating in the amperometric mode, a linear response up to 300 µmol dm^{-3} and a detection limit of 10 nmol dm^{-3} were achieved. The principle of the assay is that Nafion is highly permeable to NO, whereas the unwanted diffusion of anions such as NO_2^- is prevented, so selectivity is attained on the basis of charge repulsion.

On a similar theme, miniaturized Nafion-based glucose sensors have been fabricated for *in vitro* and *in vivo* evaluation of sugar metabolism in dogs.[49] Again, potential interferents, such as ascorbic and uric acids, are negatively charged at physiological pHs and thus electrostatically repelled from the electrode surface.

Nafion has also been modified with sequestering agents to improve the response characteristics of electrodes. An elegant technique developed by Gao *et al.*[50] exploits the selective cobalt–2,2-bipyridyl-accumulating ability of a Nafion membrane. The water-soluble modifier 2,2-bipyridyl selectively binds to Co^{2+}, forming a cationic complex, which preferentially traverses the Nafion film. DPV yielded an anodic wave at +0.1 V, which was used for quantification.

The juxtaposition of size-exclusion membrane on electrodes has been the centre of much effort in the quest for enhanced selectivity. Cellulose acetate (CA) has been studied extensively for this purpose and has been shown to be one of the most promising permselective membranes.[51–54] The application of such a membranes formed the basis of the Yellow Springs Instrument sensor, which was the first commercial biosensor for the measurement of glucose in blood.[51] Selectivity was attained through a CA–glucose oxidase (GOD)-active membrane placed over a platinum H_2O_2-sensing anode, only the small H_2O_2 molecules liberated *via* the specific enzyme-substrate reaction can reach the electrode surface and elicit a signal. This configuration is widely regarded as being the reference method for the selective determination of glucose.

Extending this theme, Colton *et al.*[52] have investigated the possibility of altering the retardation profiles of a variety of cellulosic membranes. They examined the true diffusive permeabilities of commercial, modified commercial and laboratory-cast cellulose-based membranes using 15 solutes as probe species. The distinct pattern of solute transport through the films led them to believe that they could be adopted for electrochemical studies, *i.e.*, to tailor the response of the electrode to a particular analyte of interest.

More recently, Amine *et al.*[53] have described the casting of CA membranes directly over a GOD-harbouring platinum anode. The H_2O_2 liberated from the immobilized GOD layer was detected amperometrically at +1.1 V *versus* SCE. In the absence of the CA membrane, large contributory currents were obtained for ascorbic and uric acids and the dynamic range of the sensor was limited. A CA membrane deposited over the sensor assembly served to remove positive interference from the organic acids and to extend the linear range of the sensor. The exclusion of ascorbate at the sensory interface also prevented the vitamin from scavenging dioxygen, thus sustaining biocatalytic capability.

Concurrent with the shift in the diagnostic market's emphasis from 'non-distributed' to 'distributed' or 'decentralized' clinical testing, disposable sensors are becoming the centre of much attention. Screen-printing methods appear to be the most economical and reliable means of producing 'single-shot' devices and those based on carbon as an electrode substrate are generally considered to be the most successful.[54–60] To date, printed sensor strips have been developed for many metabolites and drugs including paracetamol,[54] cholesterol,[55] glucose[56] and salicylic acid.[57] In particular, such an approach has facilitated the translation of biosensor technology to near-patient glucose testing. The device, invented by MediSense, is known as the ExacTech and is the first commercially available hand-held instrument that can convert chemical information, *i.e.*, the concentration of glucose, into a digital readout.[56] A carbon-based working electrode, containing GOD and a ferrocene derivative, is printed alongside an Ag–AgCl pseudo-reference electrode. The ferrocene molecules serve to mediate the flow of electrons from glucose, to the enzyme's active site, to the electrode. The whole cascade is initiated by the application of a drop of blood in the latest instruments and is completed in around 20 s.

Our group have used screen-printing technology to fabricate base sensors on a large-scale basis, the dimensions and configuration of which are depicted in Fig. 1. The squared-ended working area (A) is subject to chemical and biological tailoring while the connecting strip (B) provides a means of linking the devices to a potentiostat. An insulating layer (C) enables the user to define the geometry of the working area and prevents solution 'creeping'.

The method of creating CA membranes in close association with the base transducer has been applied to screen-printed carbon electrodes (SPCEs) manufactured in our laboratory. Indeed, the combination of screen-printing and permselective technologies by our group has led to the development of a disposable, solid-phase sensor for the determination of paracetamol.[54] SPCEs were drop-coated with a CA solution of the correct composition to allow the specific measurement of paracetamol whilst screening out interference from a wide range of physiological biomolecules. Rapid ($t_{95} \leqslant 60$ s) and reproducible ($s_r = 6\%$, $n = 3$) responses were obtained over a wide functional range. Good correlation ($r = 0.995$) was obtained with a hospital enzyme–colorimetric assay kit purchased from Cambridge Life Sciences (CLS). Particularly propitious were the storage properties of the surface-modified strips as no biological recognition components were included in the sensor design. These screen-printed sensors provided a novel format for the rapid detection of this drug that would be clearly advantageous in a hospital emergency room.

We have used CA membranes in the fabrication of a screen-printed biosensor for cholesterol.[55] The membrane was used in this instance to entrap physically surface-adsorbed cholesterol oxidase at the base transducer. The polymeric matrix did not appear to induce any conformational changes in the enzyme's structure and, consequently, the biosensor's analytical efficiency was maintained.
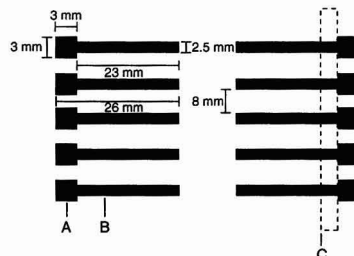

Fig. 1 Diagrammatic representation of the electrode arrangement following the screen-printing process. The carbon ink is forced through a stainless-steel screen, leaving the desired ink pattern deposited on an inert, PVC support. Points to note are the working area (A), connecting strip (B) and insulating layer (C).

Sternberg *et al.*[61] have introduced another dimension to the applications of CA membranes. They used CA as an immobilization support for GOD owing to its facile casting and permselective properties and biocompatability for an *in vivo* glucose sensor. The stability of CA over collagen membranes at 37 °C is a particularly attractive feature for the development of implantable sensors. Ordinarily there is a low accessibility of OH groups on CA, so bovine serium albumin (BSA) was used to increase the number of potential enzyme-linking sites. GOD was activated with *p*-benzoquinone and subsequently coupled to the activated CA–BSA membrane. The immobilization procedure was fairly reproducible and produced thin (5–20 μm) enzyme membranes exhibiting high surface activities (1–3 U cm^{-2}) that were stable over 1–3 months.

This approach has been simplified in our work directed towards the development of an amperometric sensor for uric acid.[62] The use of coupling agents (see above) has been precluded by the exploitation of simple, surface-adsorption processes. Uricase has been attached to an H_2O_2-selective, solvent-cast CA membrane and mounted over a cobalt phthalocyanine (CoPC) SPCE. The electrode-permselective membrane ensemble is depicted in Fig. 2. The sensor's dependable operation was pivotal on detecting the H_2O_2, enzymically generated from uric acid by the specific action of uricase, at a CoPC SPCE. H_2O_2, being a small solute, readily traverses a CA membrane, whereas larger molecules, including uric acid, are prevented from participating in the electrode reactions.

Films may also be deposited using electropolymerization.[63,64] This technique permits 'all-chemical' *in situ* membrane synthesis, and is therefore applicable to coating complex surfaces that are also in close proximity with one another. These criteria are essential for the development of miniaturized and multi-analyte sensors. The membranes are generally 'grown' from the oxidation of monomers (*e.g.*, diaminobenzene and pyrrole) and may be insoluble, conducting or insulating in nature. Such modification shows tremendous promise for the preparation of enzyme electrodes, as the catalyst may be simply entrapped in the deposited membrane. In particular, immobilization of enzymes within conducting polymers formed during the oxidation of the monomer is especially advantageous, facilitating the control of enzyme deposition and its spatial distribution, whilst maintaining low instrumentation costs. Additionally, electropolymerized films have been produced with permselective and anti-fouling properties, while minimizing the problems associated with long diffusion pathways.

Heider *et al.*[63] have reported on the permselective properties of a poly(1,2-diaminobenzene) (DAB) electropolymerized insulating film. A reticulous vitreous carbon electrode was electrochemically platinized to catalyse the oxidation of H_2O_2, liberated from GOD entrapped in a DAB film. The DAB polymer coating provided a meshwork to immobilize the GOD, improving the enzyme's thermal stability, whilst functioning as a barrier to physiological interferents. When subjected to FI, no fouling was observed for 60 repetitive injections of serum.

GOD has also been immobilized on a GCE in an electropolymerized conducting polypyrrole film with a poly-metallophthalocyanine (cobalt tetraaminophthalocyanine, CoTAPC) redox mediator.[64] In essence, GOD-generated H_2O_2 chemically reduces CoTAPC, which is then electrochemically re-oxidized at the GCE, permitting the application of a lower operating potential.

Selective Recognition

Enzymes

A prerequisite of analyses in biological fluids is a high degree of selectivity. This mandate may be achieved by modifying electrodes with molecular recognition elements, such as enzymes, antibodies, protein receptors or nucleic acids. (There is extensive published work on the use of enzymes and electrocatalysts in bioanalysis; as these applications are particularly germane to the authors' studies, some novel and exciting examples are expanded upon later in the paper.)

Enzyme electrodes have become a prominent area of research as a result of the pioneering work of Clark and Lyons[65] in 1962. Since the inception of this first-generation biosensor, a myriad of configurations have ensured and these generally confirm to the same basic principles allowing determinations by a number of routes:

(*a*) The current may be monitored following the enzymic degradation of the analyte, *e.g.*, Wring *et al.*[66] used *tert*-butyl hydroperoxide for the selective removal of glutathione. This technique allowed quantifications in suitably prepared biological samples.

(*b*) The enzymic liberation of a product (invariably H_2O_2)[67,68] or the disappearance of an electron acceptor, such as O_2,[69] may be followed.

(*c*) By converting an ordinarily electroinactive substance into an electrochemically detectable species, a new range of analytes may be investigated. Frew and Green[70] used salicylate hydroxylase to convert salicylate into catechol, which was electrooxidized at the expense of oxygen and NAD(P)H.

(*d*) The enzymic elimination of potentially interfering species present in biological matrices enhances the selectivity of the method, *e.g.*, ascorbic acid may be removed using L-ascorbic acid oxidase.[71,72]

Antibodies

Antibodies may be labelled with enzymes and the rate of product formation or substrate loss determined.[73] Alternatively, an antigen may be labelled with a group that renders it electroactive with the resulting complex undergoing redox processes in a potential range over which the unlabelled antigen is electroinactive.

A novel biosensor based on a competitive immunoassay and the reversible deactivation of an enzyme has been described. This is the subject of World Patent Application PCT 91/16630, assigned to Optical Systems Development Partners, California, USA.[74] One version of the sensor involves the specific
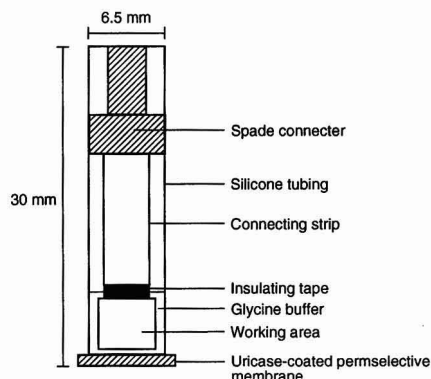

Fig. 2 Diagrammatic representation of the electrode–permselective membrane configuration used to isolate the electrode from potential interferents.

Labels in figure:
6.5 mm
30 mm
Spade connecter
Silicone tubing
Connecting strip
Insulating tape
Glycine buffer
Working area
Uricase-coated permselective membrane

binding of the target species (x) to an immobilized enzyme (y). A second molecule (z), labelled with an enzyme-reactivating agent (*e.g.*, an apoenzyme prosthetic group), competes with x to bind to y. On addition of a sample containing x, x binds to y and z is thus free to diffuse to the enzyme, which is then reactivated, producing an electrical signal. In samples devoid of x, z binds to y and is unable to diffuse, and cannot replenish enzyme activity. This biosensor obviates the need for the extensive sample manipulation associated with conventional homogeneous and heterogeneous immunoassays.

Protein receptors

The notion that the dynamic, specific and sensitive responses of organisms could be incorporated into biosensor design was first proposed by Rechnitz[75] in 1975. Neurotransmitter proteins (*e.g.*, the nicotinic acetylcholine receptor) have been attached to electrode surfaces to measure certain neurostimulants.[76] There has been limited success owing to the complexity of the structures involved, their labile nature at room temperature and difficulties in extracting significant amounts for biosensor studies. These drawbacks have been largely circumvented by the implementation of entire chemosensing structures. The first 'receptrode' was constructed from the antennule of the blue crab *Callinectes sapidus* by Belli and Rechnitz[77] in 1986. The antennule served as a specific and sensitive recognition element and a biological transducer in an environment optimized by evolution. The prototype sensor was based on nerve signals from olfactory chemoreceptors at the sensory apex of the antennule. This arrangement allowed rapid detection (10^{-3} s) of amino acid solutions below 1.0×10^{-6} mol dm^{-3} and was linearly related to concentration over three orders of magnitude.

Electrocatalysis

Before one can comprehend the fundamentals of electrocatalysis, it is useful to introduce the concept of overpotential, particularly as the elimination of overpotential effects is a near-universal goal in the design and development of electrochemical sensors and biosensors.
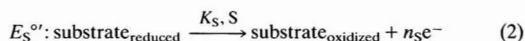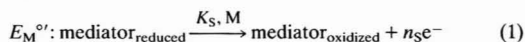
For a perfectly reversible redox system, $E_{\frac{1}{2}} = E°$. Any deviation from this ideal behaviour will result in a certain overpotential (η), where $\eta = E_{\frac{1}{2}} - E°$; there will therefore be, an overpotential ($\eta_{effective}$) for a given voltage, which may arise from a combination of four sources that have been discussed elsewhere.[78] In brief, these consist of mass transport effects ($\eta_{mass\,transfer}$), reaction overpotentials ($\eta_{reaction}$), resistance effects (η_{ohmic}) and activation overpotentials ($\eta_{activation}$). In the studies described in this review, the last form of overpotential predominates as protic electrolytes and comparatively low-resistance working electrodes are used.

Most clinically important compounds evince sluggish and irreversible electron kinetics at traditional electrodes owing to the overpotential phenomena outlined above. Such slow exchange of electrons between the target species and the electrode surface may be accelerated by incorporating redox mediators (electrocatalysts), either by chemisorption or admixing with the electrode constituents, into the base sensor.[78]

Redox mediators are small, electroactive compounds that effectively shuttle electrons between the enzyme and the electrode. Fig. 3(*a*) shows a schematic diagram of the electrocatalytic charge-transfer process for a soluble molecule undergoing chemical oxidation by a mediator that is subsequently re-oxidized at the electrode surface. This mechanism is summarized as a chemical–electrochemical (CE) process; alternatively, the mediator itself may be electrochemically oxidized prior to its reaction with the substance [*e.g.*, ferrocene,[79] Fig. 3(*b*)], which is known as an electrochemical–chemical (EC) process.

For all mediated reactions, the driving force is dependent on the $E°'$ values of the substrate ($E_s°'$) and electrocatalyst ($E_M°'$) and for an EC sequence this is described by the equations:

$$E_M°': \text{mediator}_{reduced} \xrightarrow{K_S, M} \text{mediator}_{oxidized} + n_S e^- \quad (1)$$

$$E_S°': \text{substrate}_{reduced} \xrightarrow{K_S, S} \text{substrate}_{oxidized} + n_S e^- \quad (2)$$

A common feature of EC and CE processes is the catalytic regeneration mechanisms that allow mediator replenishment, thus affording further interactions with the substrate. The rate constants (K_S) for the mediator and substrate dictate the ease of their respective oxidations and are therefore also important in this context. As most electrocatalysts are used in tandem with enzymes, these will be expanded upon later in the review.

Much of our research has been directed along these lines. The effectiveness of cobalt phthalocyanine (CoPC) as a redox mediator for many compounds has sustained its incorporation into our SPCEs. Much research[80-85] has shown that the central metal exhibits favourable catalytic activity towards various thiol-containing substances. Using this methodology, disposable, amperometric sensors for thiocholine[81,83] and glutathione[80,82] have been produced. Thiocholine sensing is used for the indirect measurement of organophosphorus pesticides (OPs) in the aqueous environment. The detection system is based on the following rationale. Acetylcholineesterase (ACE) catalyses the deacetylation of acetylthiocholine iodide to generate thiocholine stoichiometrically (see Fig. 4), which is monitored amperometrically at a CoPC SPCE. The thiocholine is electrocatalytically oxidized according to the sequence of homogeneous and heterogeneous charge-transfer events displayed in Fig. 5. In brief, the enzymically liberated thiocholine chemically reduces Co^{2+} to Co$^+$, which is electrochemically re-oxidized at $+0.1$ V (*versus* SCE). This facilitates the determination of the thiol at a substantially lower operating potential, which enhances the response and operational characteristics of the sensor. Organophosphorous pesticides irreversibly phosphorylate the serine residues of ACE's catalytic site, reducing their activity, with a parallel attenuation in the anodic current for the electrocatalytic oxidation of thiocholine. Using the disposable sensors, pesticides such as paraoxon and dichlorvos may be detected at levels down to 10^{-8} mol dm^{-3}.

Carbon-based Biosensors

Biosensor technology is an expanding field in the quest for innovative approaches to bioanalysis.[86-88] A biosensor is an
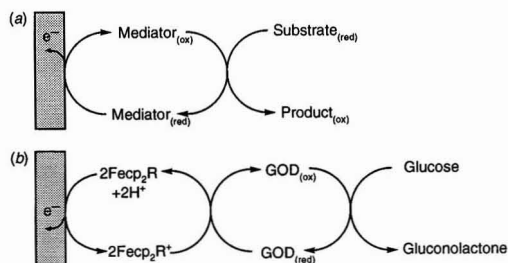

Fig. 3 (*a*) Course of electron-transfer events from a reduced biomolecule to an oxidized mediator. (*b*) Schematic diagram of the ferrocene-mediated oxidation of reduced GOD used for the amperometric determination of glucose.

analytical device based on the union of a biological component and an appropriate physico-chemical transducer (Fig. 6). The biocomponent is immobilized, generally in intimate physical contact or integrated with the transducing element, and may catalyse chemical reactions (purified enzymes, microbes, organelles and tissue slices) or bind specifically to the analyte (antibodies or receptors).[86] The various sources of biological material used in biosensor construction, and how they are categorized, *e.g.*, metabolic, catalytic or affinity, are depicted in Fig. 7.

Although only small amounts of the biorecognition element are generally required, they have to satisfy several analytical requirements. They must exhibit a high degree of specificity, be stable under different temperature, pH, ionic strength and operating conditions, retain their biological activity in the immobilized state and produce no undesirable sample contamination effects.

Biosensors rely on conformational biomolecule changes and/or physical changes in the immobilization medium, *e.g.*, charge, thickness, temperature or optical parameters (colour or fluorescence), induced by analyte–bioligand interactions.[86,88] The most widely applied are those relying on the measurement of current following the application of a fixed voltage, *i.e.*, amperometry. The transduced signal can be viewed as a secondary one, in that it follows the unique recognition event between the bioactive and target species. The utilization of this indirect assay means that chemically similar compounds can be measured by their biospecific reaction with the immobilized biosensing element. Other biosensor attractions lie in their low cost, simple operation and amenability to miniaturization. These characteristics are typically realized by the implementation of enzymes, which allow the determination of an extensive range of analytes. Enzymes that catalyse redox reactions are eminent candidates as electrode-modifying agents, as intrinsic features of their activity are their reusability, a high degree of specificity and electron-transfer events. Consequently, such enzymic reactions can be harnessed to engender a device with highly desirable properties. The plethora of functional groups present on the surface of carbon electrodes[9] and the facile incorporation of modifying agents into the carbon matrix[54–60] predicate the usefulness of this material in this regard.

Without doubt, the major impetus for the advancement in sensor technology stems from health care requirements, which demand instant, in-house tests for a gamut of metabolites and pharmaceutical compounds. Such rapid, on-site assays would be clearly beneficial, providing a biochemical snapshot of the local metabolic state.[59] A recent report by Cave[89] has highlighted the merits of decentralized pathology tests. A pilot study, involving 170 patients over a 6 week period, showed that a practice-based service provided easier and more convenient management of routine assays, immediate results (particularly useful with acute conditions), fewer follow-up consultations, less telephone calls and more convincing patient reassurance. Clearly, if analyses can be performed by untrained staff, in a rapid, economic and reproducible manner, then the routine introduction of biosensors into the hospital and commercial environment cannot be too distant.

Enzyme-coupled Mediation

A variety of electron mediators have been used in conjunction with enzymes for biosensor construction. Arguably the most
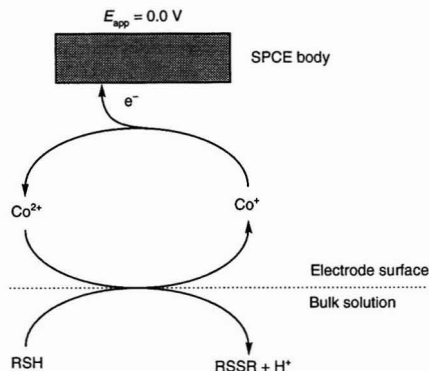
Fig. 4 Sequence of events involved in the electrocatalytic oxidation of thiocholine (RSH) at CoPC SPCEs: the basis of the disposable, amperometric biosensor.
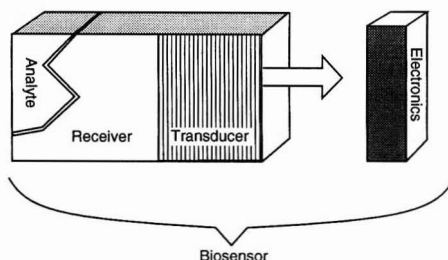
Fig. 6 Schematic diagram of the integral components of a typical biosensor. (Adapted from Scheller *et al.*[86])

Fig. 5 Cyclic voltammograms recorded at CoPC SPCEs for concentrations: A, 2.9×10^{-3}; B, 1.5×10^{-3}; C, 1.0×10^{-3}; D, 5.2×10^{-4}; and E, 2.3×10^{-3} mol dm^{-3} thiocholine in 0.05 mol dm^{-3} phosphate buffer (pH 8.0).
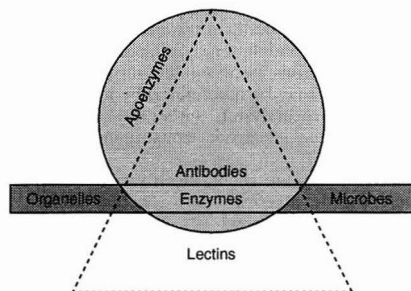
Fig. 7 Sources of biological elements used in biosensor design and their mode of action. The rectangle represents metabolic/enzymic, the circle catalytic and the triangle binding-based sensing systems.

successful biosensors are those based on oxidase or dehydrogenase-mediated reactions and, accordingly, the final section of this review focuses upon such systems.

Oxidases

Cass et al.[79] have shown the utility of the ferrocene–ferricinium ion couple as an effective mediator between GOD and a graphite electrode, marking the inception of enzyme-coupled mediation. A graphite foil base electrode was surface modified with 1,1'-dimethylferrocene (DMFc) dissolved in toluene. The sensor was further modified by attaching GOD to the oxidized graphite surface with a carbodiimide covalent linkage. The amperometric enzyme electrode functioned at 160 mV *versus* SCE at pH 7.0 and 25 °C according to the following scheme (where cp_2 represents a cyclopentadienyl ring):

$$glucose_{(red)} + GOD_{(ox)} \rightarrow \delta\text{-gluconolactone} + GOD_{(red)} \quad (3)$$

$$GOD_{(red)} + 2Fecp_2R^+ \rightarrow GOD_{(ox)} + 2Fecp_2R + 2H^+ \quad (4)$$

$$2Fecp_2R \xrightleftharpoons[]{+\ 160\ mV\ versus\ SCE} 2Fecp_2R^+ + 2e^- \quad (5)$$

On the whole, the low operating potential (60 mV more positive than $E^{\circ\prime}$ for DMFc) used to reoxidize the reduced form of the mediator obviated the need for a permselective membrane to enhance selectivity, although a response was obtained for physiological levels of ascorbate. The system exhibited minimal O_2 dependence and functioned in a rapid and reproducible manner. Problems associated with the greater solubility of the ferricinium ion induced workers to seek alternative mediators that could be incorporated into electrode designs, forming a more stable arrangement.

Heiduschka and Scheller[90] have created a sensor surface with a high density of binding sites for the attachment of GOD. In brief, the procedure involved coating a GCE with platinum microparticles by a single linear sweep to −3.0 V. A poly(nitrophenol) film was formed by cyclic sweeps between 0.1 and 1.1 V. The resulting NO_2 groups were then electrochemically reduced to amino species *via* two linear sweeps form −0.5 to −1.4 V and subsequently treated with a 2.5% solution of glutaraldehyde. GOD was covalently linked to the abundant aldehyde moieties, producing a biosensor that allowed rapid glucose analyses over a clinically acceptable range.

Tsionsky et al.[91] have described a novel class of composite electrodes for biosensing applications made of sol–gel-derived carbon–silica materials, which are robust, porous and have a renewable external surface. As they are modifiable and may be produced in a variety of dimensions and geometric configurations, they are particularly suitable for biosensor construction. Recent studies have shown them to be extremely conductive and electrochemically well behaved. By incorporating GOD into the sol–gel matrix, it was shown that the biocatalytic catalytic activity is still maintained. The biosensor evinced a response to the GOD-generated H_2O_2 that was linearly related to glucose concentrations in excess of 10 mmol dm^{-3}.

Beh et al.[92] have also produced stable sensors by modifying the substrate binding material. They used a cellulose acetate to bind ferrocene-doped CPEs and a GOD-active nylon membrane positioned over the CPE to complete the assembly. FI was used to determine glucose *via* the H_2O_2 enzymolysis, amperometrically at 160 mV (*versus* Ag–AgCl). Sensor features of note were their pronounced stability (24 months), minimal susceptibility to ascorbate interference and wide linear range (0.01–70×10^{-3} mol dm^{-3}).

Marcinkeviciene and Kulys[93] have developed an amperometric screen-printed biosensor for glucose based on GOD, peroxidase and hexacyanoferrate(II) entrapped in a hydroxy-

ethylcellulose–graphite matrix. Enzymically generated H_2O_2 oxidizes hexacyanoferrate(II) to hexacyanoferrate(III), which is subsequently electrochemically reduced at 0.0 V. The reaction scheme is described by the equations

$$glucose + O_2 \xrightarrow{\text{GOD}} \delta\text{-gluconolactone} + H_2O_2 \quad (6)$$

$$H_2O_2 + 2Fe(CN)_6^{4-} + 2H^+ \xrightarrow[\text{peroxidase}]{\text{horseradish}} 2H_2O + 2Fe(CN)_6^{3-} \quad (7)$$

$$2Fe(CN)_6^{3-} + e^- \xrightarrow{0.0\ V\ versus\ Ag\text{–}AgCl} 2Fe(CN)_6^{4-} \quad (8)$$

The biosensor's response was linear up to a 25×10^{-3} mol dm^{-3} concentration of glucose, yielded 90% of the steady-state cathodic current between 50 and 60 s and was insensitive to ascorbate at 40×10^{-6} mol dm^{-3} final concentrations.
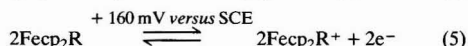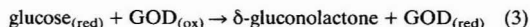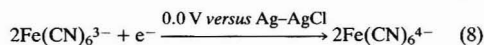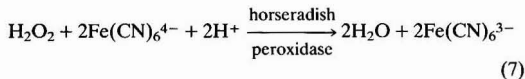
Moore et al.[94] presented the first report of an electrocatalytic reaction between several flavoprotein oxidases (glucose, lactose and sarcosine oxidases) and the oxidized form of paracetamol. This phenomenon was exploited to permit the chemical amplification of the electrooxidation of the drug with a concomitant improvement in biosensor efficiency. Paracetamol is electrolytically oxidized in a heterogeneous $2e^-$, $2H^+$ step to N-acetyl-p-aminoquinoneimine (NPAQI), which is fairly labile and hydrolyses to benzoquinoneimine.[95,96] In the presence of a reduced flavin enzyme and its primary substrate, however, NPAQI serves as an alternative electron acceptor to O_2 at a substantially greater rate than it hydrolyses. Paracetamol is thus chemically regenerated and available for a second heterogeneous electrochemical oxidation. If the substrate is in excess it maintains the initial concentration of reduced oxidase and a kinetically pseudo-first-order redox cycle exists between enzyme, mediator and transducer.[97] Electron flow in the catalytic loop is controlled by paracetamol's redox state. A further benefit is that the response increases without an accompanying co-amplification of the background signal.

Substituting various groups on the cyclopentadienyl rings of ferrocene has proved to be an effective route to circumvent mediator leaching.[98-101] One of the earliest examples was reported by Hale et al.,[98] who used a ferrocene-modified siloxane polymer to 'anchor' the mediator in a CPE matrix. The flexible structure of the polymer afforded an effective electron acceptor for flavoprotein enzymes. Another strategy for preventing mediator dissolution involves modifying GOD with covalently linked ferrocenyl derivatives.[102]

Recently, Zhao and Luong[103] have advanced a technique for extending the operational life of a biosensor by minimizing mediator leakage. Tetrathiafulvalene (TTF) was dissolved in silicone oil (methylphenyl polysiloxane) and embedded in a graphite disc electrode. The porous nature of the graphite afforded an ideal environment for the successful incorporation of the mediator into the electrode. Next, the electrodes were coated with flavoprotein enzymes, followed by a layer of glutaraldehyde (glut)–bovine serum albumin (BSA). The electrode–enzyme–glut–BSA ensemble was finally covered with a dialysis membrane. The biosensor was used to determine phenylalanine (L-amino acid oxidase), hypoxanthine (hypoxanthine oxidase) and glucose (glucose oxidase), according to which particular flavoenzyme was immobilized on the electrode surface. Selectivity was attained by the ability of TTF to re-oxidize the reduced prosthetic group of each enzyme at +150 mV (*versus* Ag–AgCl). When operated in the amperometric mode, rapid, reproducible and linear responses were obtained for each of the oxidase substrates studied. A typical glucose biosensor was shown to be stable for 2 months when stored at 4 °C, enabling more than 500 reliable assays to be undertaken.

A host of electrocatalysts have also been used in conjunction with oxidases to reduce the overvoltage of H_2O_2 oxidations, (*e.g.*, CoPC,[54,55,104] platinization procedures[105] and metal oxide films[106]) and to render certain electrodes insensitive to variations in partial pressures of dioxygen.[107,108]

We have developed a reagentless, disposable, screen-printed biosensor for uric acid based on this principle.[109] The system represented a further 'fine-tuning' of a previously designed sensor for measuring this clinically significant purine.[57] By producing a CA film in intimate association with the CoPC SPCE surface and subsequently coating it with uricase, the enzymically liberated H_2O_2 was detected amperometrically. The biosensor's response was rapid, reliable and linearly related to urate concentration over a wide dynamic range. A typical amperometric calibration recorded with a single biosensor strip is depicted in Fig. 8. A summary of the homogeneous and heterogeneous electron-transfer events is displayed in Fig. 9. Briefly, uricase liberates H_2O_2 concurrent with the enzyme-catalysed oxidation of uric acid. H_2O_2, being a small solute, readily traverses the CA membrane and chemically reduces Co^{2+} to Co^+, which is then replenished at the SPCE surface by electrochemical re-oxidation. We have elucidated the mechanisms involved in the homogeneous and heterogeneous electron-transfer processes by voltammetric and X-ray photoelectron spectroscopic techniques.[110]

Second-generation biosensors possess certain drawbacks, such as mediator-leaching and dependence on oxygen concentration, that may limit their analytical utility. An approach to circumvent such drawbacks involves the synthesis of novel sensory interfaces adept at exchanging electrons directly with the prosthetic groups of enzymes.[11,36,111-115]

This is by no means an easy feat, as through evolution enzymes have been bestowed with protective mechanisms that inhibit indiscriminate electron transfer with surrounding redox macromolecules. Many enzymes are typically enshrouded in a glycoprotein sheath and their catalytic centres are buried deep within the macromolecular structure, both of which prevent electron tunnelling. Workers have attached various ferrocene derivatives, including ferrocenemonocarboxylic acid[111] and ferroceneacetic acid,[112] onto GOD and TTF onto LOD.[113] In all instances, electron 'hot-wiring' was observed in rapidly responding and acceptably stable biosensors.

Maidan and Heller[116] have reported on an exciting expansion of this thesis. They combined an electrically wired glucose-sensing carbon electrode and an interferent-eliminating layer with a highly propitious outcome. GOD was connected to a vitreous carbon electrode *via* an osmium–polyvinylpyridine backbone with part of the pyridine quaternized with ethylamine. H_2O_2 liberated from the glucose–GOD interaction was detected at $+0.4$ V *versus* SCE (pH 7.2). Contributing currents from the osmium-catalysed reduction of peroxide were averted by using an operating voltage of $+0.5$ V (thus maintaining the osmium in the non-catalytic trivalent state), for less complex fluids, and an electrically insulated barrier was created over the biolayer, for analyses in biological fluids.

The basis of the super-selective biosensor was that potentially interfering compounds such as paracetamol, ascorbate and urate were removed by an immobilized layer of horseradish peroxidase (HRP) and lactate oxidase (LOX) over the glucose-detecting zone. LOX produced H_2O_2 from lactate, present in the sample, which in the presence of HRP effected the pre-oxidation of interferents according to

$$H_2O_2 + interferent_{reduced} \xrightarrow{\text{HRP}} 2H_2O + interferent_{oxidized} \quad (9)$$
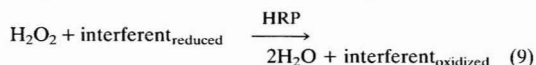
Peroxidases are classical catalysts for the oxidation of hydrogen-donating species (interferent$_{reduced}$), thus problem substances, such as ascorbate, are removed of their reducing propensity as they pass on their electrons to HRP. Conversely, glucose and lactate are not oxidized in this way and thus participate in this novel scheme as described above.

Apart from improving electron kinetics, these highly evolved biosensors should prove to be powerful tools in understanding the redox chemistry of enzymes, *e.g.*, permitting the direct electrochemical interrogation of the cytochrome-based, respiratory electron-transport chain. Such third-generation biosensors also have implications in neurochemical studies. A vinyl polymer, containing nitroaromatic groups, has been produced to which dopamine has been covalently attached *via* an amide linkage. This polymer was subsequently coated onto an electrode and the whole assembly was immersed in solution. The nitroaromatic centres are readily reduced, yielding an increased negative charge which effects the electrochemical dissolution of the amide bond, thus releasing the neurotransmitter into solution. Such a translation of electrical information into a highly specific chemical signal resembles the firing of a neurone, *i.e.*, effectively mimics the propagation of a nerve impulse.[36]

Dehydrogenases

Dehydrogenases are a class of oxido-reductase enzymes dependent on the cofactors β-nicotinamide adenine dinucleotide (NAD^+) or β-nicotinamide adenine dinucleotide phosphate ($NADP^+$). Phenoxazines, phenathiazines and quinones are reputedly the most efficient mediators for re-oxidizing the reduced forms of these cofactors. However, a diverse range of alternatives have been studied, including conducting salts[117] and ferrocenes.[118] Ordinarily, analyses based on the NAD^+–NADH-dependent dehydrogenases are hampered by side and abortive reactions[119] and overpotential effects.[120-122] Elegant electrode designs have, however, been developed to solve
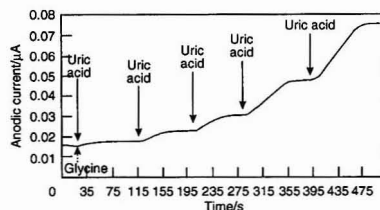
Fig. 8 Amperometric uric acid calibrations performed using a disposable, screen-printed, carbon-based biosensor. The arrows indicate the incremental additions of uric acid over the range 1.3×10^{-6}–4.87×10^{-4} mol dm^{-3}. Applied voltage, $+0.4$ V; supporting electrolyte, 0.1 mol dm^{-3} glycine buffer (pH 9.2); temperature, 31 °C; and time base, 0.2 mm s^{-1}.
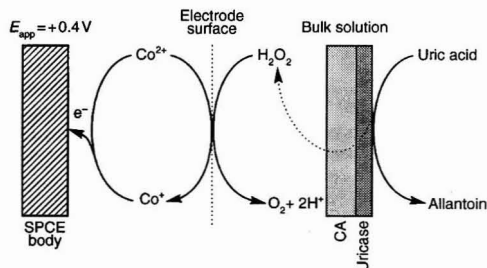
Fig. 9 Sequence of intra- and extra-membrane events involved in the determination of uric acid using the screen-printed biosensor.

these problems, creating novel ways to exploit these enzymes. A typical reaction scheme for a typical dehydrogenase-catalysed process is

$$\text{substrate} + \text{NAD}^+ \underset{\text{dehydrogenase}}{\overset{K_{\text{eq}}}{\rightleftharpoons}} \text{product} + \text{NADH} + \text{H}^+$$

(10)

As the formal potential for the NAD^+–NADH pair (-560 mV *versus* SCE, pH 7, 25 °C) and the equilibrium constant (K_{eq}) for the enzyme-catalysed reaction are low, the forward chemical reaction is suppressed, causing non-rectilinear calibrations.[121]

A number of strategies have been proposed to address these drawbacks,[123,124] the simplest and arguably the most effective of which employ redox mediators. These bridge the catalytic exchange of electrons between the NAD^+–NADH couple and the electrode surface, so the reaction is dictated by the $E^{\circ\prime}$ of the mediator. Other alternatives include trapping an excess amount of NAD^+ at the electrode surface,[123] enzyme amplification[124] and electrooxidizing NADH as soon as it is formed.[120]

Dominguez and co-workers[125,126] have devised a reagent-less amperometric biosensor for ethanol by co-immobilizing alcohol dehydrogenase (ADH) and NAD^+ in a polyaromatic phenathiazine mediator-modified CPE. Toluidine Blue O (TBO) was dissolved in dimethylformide (DMF) and yielded a characteristic $E^{\circ\prime}$ of -285 mV (pH 7.0 *versus* SCE) when adsorbed on graphite particles, too low to evoke a high reaction rate with NADH. By reacting the primary amine functionality in position 3 of TBO with naphthoyl chloride, the $E^{\circ\prime}$ shifted to -165 mV with a concomitant enhancement in the efficacy of NADH mediation. The components were maintained in close physical proximity by dissolving ADH and NAD^+ in polyethylenimine (PEI), which was mixed vigorously with the TBO–graphite powder. When dry, paraffin oil was added and mulled until a uniform paste was obtained.

Dominuguez *et al.*[126] postulated that predominately electrostatic interactions between the polycationic PEI and the anionic cofactor, enzyme and graphite residues stabilized the modifying agents, thus preventing their leakage. This configuration explains the improved stability of the biosensor, characterized by a 90% retention of the activity for ethanol over a day's continual usage.

A reagentless, disposable, amperometric screen-printed biosensor for lactic acid has been fabricated using dehydrogenase enzyme technology.[127,128] The device exploits the size-exclusion properties of CA membranes, the selectivity of lactic acid dehydrogenase (LDH) and the electrocatalytic propensity of Meldola's Blue (MB) towards NADH.[128] The hydrodynamic voltammogram in Fig. 10 clearly shows that the oxidation of NADH is more favourable at an SPCE chemically modified with MB than at its unmodified counterpart. Indeed, the MB SPCE permits the oxidation of NADH at 0.0 V, a potential at which electroactive interferents are unlikely to impinge upon analyses. By judicious selection of the CA composition, CA may be used to contain LDH and NAD at the MB-doped SPCE surface. Thus, any leaching of the essential immobilized surface components is minimized. The CA film also serves to eliminate macromolecular electrode fouling species. Although the passage of interfering biomolecules such as uric acid and paracetamol (acetaminophen) is merely retarded in the CA matrix, as they are not electrooxidizable at 0.0 V (*versus* SCE), they do not contribute to the current obtained. The principle of the lactate biosensor is shown in Fig. 11.

The longevity of the mediator is an essential consideration in biosensor design, as it is mediator leaching that generally limits their reusability and operational lifetime. Athey *et al.*[129]

have recently described an electrode modification technique that not only allows analyses to be carried out using low working potentials, but also produces robust and highly stable sensors. Platinized activated carbon electrodes (PACEs) are fabricated by adsorbing colloidal platinum on carbon of high surface area at a concentration of 10% m/m. The platinized carbon is then mixed with an equal m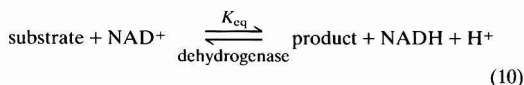ass of colloidal poly(tetrafluoroethylene) (PTFE) and bonded to conductive carbon paper by sintering at 330 °C. The PACEs allowed reproducible and precise oxidations of NADH at $+150$ mV (*versus* Ag–AgCl), with a typical linear range from 2×10^{-6} to 10×10^{-3} mol dm^{-3}. The system was based on a homogeneous amperometric immunoassay and applied to the determination of the bronchiodilator theophylline in whole blood.

Persson *et al.*[130] have briefly reviewed the various formats available for the measurement of dehydrogenase substrates. The sensors were operated in the region of 0 mV *versus* SCE, and enabled the typically unfavourable equilibrium of a dehydrogenase-catalysed reaction to bias the product side. These sensors are reagentless in that NAD^+ need not be added to the sample. Minimization of component loss and enhanced interferent rejection were provided by poly(ester sulfonic acid) cation-exchange membranes (Eastman AQ 29D).[130]

A more complicated strategy, devised by Vreeke *et al.*,[131] involves the electrical connection of HRP redox sites to
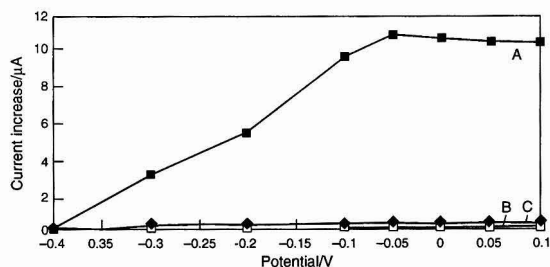
Fig. 10 Hydrodynamic voltammograms recorded using SPCEs. A, Catalytic oxidation of 0.64×10^{-3} mol dm^{-3} NADH at a 5% MB-containing sensor, B and C, response in plain 0.05 mol dm^{-3} phosphate buffer (pH 7.0) at MB-doped and unmodified electrodes, respectively.
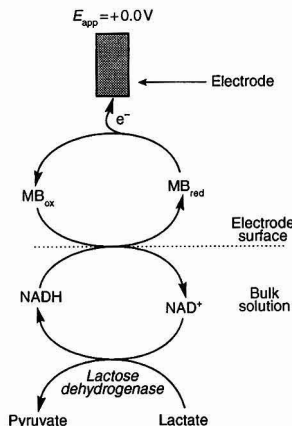
Fig. 11 Principle of lactate measurements at a chemically modified, screen-printed biosensor.

carbon electrodes through a three-dimensional electron relaying network. Briefly, NAD(P)H transfers $2e^-$ and $2H^+$ to a dissolved quinoid, which subsequently transfers $2e^-$ and $2H^+$ to molecular O_2. This reduction quantitatively produces H_2O_2 and the oxidized form of the quinoid. The H_2O_2 then oxidizes HRP, which serves as an electron acceptor for an Os^{2+} polymer, converting it to Os^{3+}, which is then electrochemically reduced. Given the low applied potential required to drive the reaction, this system should be highly selective. Such novel electrical wiring provides a versatile approach to bioanalysis and highlights the multifarious aspects of sensory interface modification.

Conclusions

The objective of this review has been to illustrate the benefits of sensing with carbon electrodes. We have also set out to provide an insight into the diverse modification techniques available for tailoring the performance of sensors for analyses in more complex matrices. At present there are no universal modification strategies, although this is gradually changing with ever-increasingly sophisticated surface-altering methodologies. Consequently, the future holds promise for 'generic' sensors, for example those based on oxidase systems, detecting H_2O_2, or on dehydrogenase enzymes, monitoring the reduced cofactor. These should permit considerable advances

Table 1 Beneficial instant assays in patient diagnosis

Analyte	Alternative methods	Clinical disorder	Notes	Ref.
Glucose	Aldehyde group of β-D-glucose is oxidized by GOD to give gluconic acid and H_2O_2, the latter compound is then broken down to H_2O and O_2 by HRP and if an oxygen acceptor is present, is converted into a coloured species. Trinder's reagents (phosphotungstate containing phenol and *p*-aminophenazone) are considered to be the most effective	Diabetes mellitus	Ascorbate and drug interference	132
	Spectrofluorimetric and chemiluminescence methods also available to detect GOD-liberated H_2O_2		Very sensitive, continuous-flow measurement over a wide dynamic range	
	YSI is the reference method for hospital glucose determinations		Paracetamol interference	51
			All unsuitable for bedside monitoring	
Cholesterol	Old methods based on the ability of cholesterol to be converted into coloured substances in strong acid solvents possessing dehydrolysing, oxidizing and sulfonating properties. Liebermann–Burchard and Salkowski reactions produce green and red compounds, respectively	Myocardial infarction Artheriosclerosis Hypertension	Lengthy analyses Specificity problems	133
	Enzymic assays developed by Richmond used *Nocardia erythropolis* cholesterol oxidase to produce cholest-4-en-3-one and H_2O_2. The ketone was extracted in 2-propanol and read at 240 nm spectrophotometrically. Alternatively, H_2O_2 may be detected using Trinder's reagents		Enhanced selectivity Only measures free cholesterol	134
	Hydrolysis of ester cholesterol by ethanolic KOH or cholesterol esterase permits the determination of total cholesterol. Again, H_2O_2 is the target species		Total cholesterol but still selectivity problems	135
Lactic acid	NAD^+-dependent LDH converts lactate into pyruvate under alkaline conditions and the NADH formed is detected spectrophotometrically at 340 nm	Hypoxia	Simple and specific but needs cumbersome instrumentation; incongruous in an emergency room	133, 136, 137
Paracetamol	Weiner has reviewed methods for paracetamol detection. Spectrophotometric and colorometric techniques detect dye or nitrous acid generated *p*-aminophenol	Hepatotoxicity	An antidote has to be administered within 12 h to be effective, so speed is a mandate. Thus salicylate interference and pre-treatment steps compromise the analytical utility of these approaches	138
	GLC and HPLC methods with cation- or anion-exchange or reversed-phase chromatography have also been reported			
	Immunological assays		Address selectivity difficulties but require long incubation times	139, 140
	Price *et al.* have evaluated a rapid enzymic kit (available from CLS). Aryl acylamidase specifically cleaves the amide bond of acylated aromatic amines yielding acetate and *p*-aminophenol, which reacts with *o*-cresol in the presence of ammonia to give a blue indophenol dye		Shortens analysis times to 30 min	141
Uric acid	Exploit reducing properties or adsorption at 293 nm separation steps serve to remove potential interferents: (*i*) precipitation as the copper, silver or magnesium salts, (*ii*) ion-exchange chromatography and (*iii*) tests on a protein-free filtrate	Gouty arthritis	Poor specificity Complicated and long analyses	142 143–145

Table 1—*continued*

Analyte	Alternative methods	Clinical disorder	Notes	Ref.
Creatinine	Typically based on the Jaffé reaction, whereby a red compound is formed in alkaline picrate solutions. The chromogen is detected spectrophotometrically at 490 nm	Renal dysfunction	Severe pH and temperature dependence Up to 20% of non-creatinine chromogens in blood and 5% in urine are also detected	133
	A *Pseudomonas*-derived creatinine amidohydrolase is used in conjunction with the Jaffé reaction in a differential spectrophotometric mode		Improved selectivity	146, 147
	Reversed-phase HPLC with 'on-line' Jaffé reaction on the column effluent has also been reported		Good performance but inconvenient for bedside tests	
	Lim *et al.* attempted to produce a definitive creatinine assay. HPLC was followed by conversion of *o*-triflu oroacetylcreatinine and its quantification by GC–MS		Unsuitable for near-patient tests	148
Urea	Urease-generated ammonia is detected colorimetrically by the formation of a blue indophenol compound in hypochlorite and phenol solutions (Berthelot reaction)	Renal failure	Obeys Beer's law but susceptible to atmospheric ammonia	149
	Urease coated on a poly(propylene) or Teflon membrane covering an ammonium potentiometric electrode has also been used		Easily contaminated and too expensive to be produced in the requisite single-shot format for clinical testing	150
	Azostix (Ames) uses a urease-and bromothymol-impregnated paper strip for the analysis of urea. A drop of blood is applied to the test area (protected from macromolecular fouling by a semi-permeable membrane), urea diffuses into the urease domain where it is converted into ammonia producing a concomitant colour change. Yellow, green or green–blue colours develop depending on the concentration of the analyte		Suitable for decentralized analysis but requires some pre-treatment (fluoro and ammonium salts need to be removed)	133
Salicylic acid	Trinder's colorimetric test is the most popular in the UK. Fe^{3+} ions complex with the phenolic group of the drug, producing a purple compound	Hepatotoxicity	Poor sensitivity and cross-reactivity	151
	Chromatographic and spectrofluorimetric detection systems are also available		Do not conform to requirements: rapid, accurate portable testing regimes	152–155
3-Hydroxy-butyrate	Rothera's test, based on the production of a red compound with salicylaldehyde	Diabetes mellitus causes increased fat metabolism, thus ketones accumulate in the blood	Semi-quantitative and unspecific. Ketone ratios are 3-hydroxybutyrate 78%, acetoacetate 20%, acetone 2%. Permits differentiation between diabetic and non-diabetic coma. Not amenable to near-patient testing	133
	Gallows and Watkins devised a spectrofluorimetric enzymic assay using D-3-hydroxydehydrogenase to catalyse the interconversion of the two acids. Hydrazine was included to remove acetoacetate as it was formed. UV/VIS spectrophotometry was used to measure the decrease in absorbance at 340 nm due to the accompanying oxidation of NADH to NAD^+			156 157, 158
Oxalic acid	Titrimetric, olorimetric, chromatographic, isotachophoretic and enzymic methods have been described. Those using oxalate decarboxylase or oxalate oxidase are the most successful. The two systems are geared to detect enzymically generated formate (for the decarboxylase) or H_2O_2 (for the oxidase). The latter, when linked to a peroxidase–chromophore reaction, is potentially more sensitive. Ascorbate removal by acidifying the sample or treating with L-ascorbate oxidase is advantageous	Increased colonic oxalate absorption is associated with various gastrointestinal disorders, particularly fat malabsorption producing hyperoxaluria and thus urinary calculi	Ascorbate competitively inhibits oxalate enzymes and is also converted into oxalate in alkaline urine Relatively long analyses, which are also hampered by other excipient species, such as nitrate	56, 159 160
Aspartate amino transferase (AST)	2-Oxoglutarate is converted by AST into oxaloacetate, which is then converted into malate by malate dehydrogenase at the expense of NADH. The decrease in absorbance is monitored spectrophotometrically at 340 nm	AST increases 3–4 h after myocardial infarction and is also an indicator of parenchymal liver damage and muscular dystrophy	AST transfers an amino group from an α-amino acid to an α-oxo acid using pyridoxal-5′-phosphate as a cofactor. Although plentiful in most cells, it is present in low levels in red cells. Thus, AST's increased activity is related to an increased level of cofactor, which in turn is related to cellular damage. A rapid, disposable detection system is required	133 161

Table 1—*continued*

Analyte	Alternative methods	Clinical disorder	Notes	Ref.
Creatinine kinase (CK)	CK catalyses the phosphorylation of creatinine by adenosine triphosphate (ATP) in muscle cells and brain tissues. The rate of formation of ATP is measured using the increase in absorbance at 340 nm according to:	Acute myocardial infarction and skeletal disorders	Single-shot and speedy assay suitable for an emergency room. Would be particularly useful when ECG findings are equivocal	133

$$\text{creatine phosphate} + \text{ADP} \xrightarrow{\text{CK}} \text{ATP} + \text{creatine}$$

$$\text{ATP} + \text{glucose} \xrightarrow{\text{hexokinase}} \text{ADP} + \text{glucose-6-phosphate (G6P)}$$

$$\text{G6P} + \text{NADP}^+ \xrightarrow{\text{G6P dehydrogenase}} \text{6-phosphogluconate} + \text{NADP}^+ + \text{H}^+$$

Analyte	Alternative methods	Clinical disorder	Notes	Ref.
	A peroxidase–Trinder coupled method is also available		Inconvenient in an emergency	162
α-Amylase	Amylase and glucosidase produce *p*-nitrophenol, which is detected spectrophotometrically at 405 nm.	Acute and chronic pancreatitis	Slow and susceptible to interference	59
	Amylase effects the disintegration of starch to smaller, soluble oligosaccharides and dextrins with much reduced light-scattering properties		Semiquantitative	133

Table 2 Predicted and emerging instant diagnostic tests

Parameter	Comments	Requirement	Ref.
pH	During open-heart surgery and transplantation, the heart is stopped and frequently cooled to 7 °C with an attendant drop in pH. If this falls too great it is difficult to revive the cardiac system	A miniature, biocompatible disposable sensor for remote sensing of the myocardium. Conventional pH probes are prohibitively expensive for disposable purposes, fragile and susceptible to macromolecular fouling (*e.g.*, proteinaceous materials such as with fibrin)	163
Leutinizing hormone (LH)	Women with difficulties in conceiving need to monitor their reproductive cycles, more specifically their ovulation times. Ovulation is signalled by a surge in LH, which can be detected in the blood or urine	Disposable test strip that is not prone to cross-reactions	164
High- and low-density lipoproteins (HDL, LDL)	Provide a clearer and more readily interpretable means of assessing the state of lipid metabolism. More accurate measure of susceptibility to heart and related diseases	Convenient and speedy test that may be undertaken at the practitioner's desk	165
Nitrogen oxide (NO)	A vital signalling compound involved in a myriad of bioregulatory processes. Abnormal levels of NO have been linked to various diseases, including artherosclerosis	Ultramicroelectrode for *in situ* monitoring of NO. Also needs to be interference free and to function over a wide dynamic range	47, 48
Thyroxine (T4)	Elucidation of the biosynthesis, secretion and transport of T4 is important in control of the hypothalamic–pituitary–thyroid axis. The introduction of specific antibodies to T4 in the early 1970s improved measurement regimes markedly, but there is room for improvement	Typical methods are still slow, require long incubation periods and complicated multi-step procedures. A solid-phase, one-shot strip for the rapid determination of T4 would be eminently desirable	166, 177
Thyroid-stimulating hormone (TSH)	Production of thyroid hormones is controlled mainly by the glycoprotein hormone TSH, which is secreted by thyrotrophs located in the anterior pituitary gland. Thus measurement of TSH confirms congenital hypothyroidism after an initial screening test detects low T4 levels	Simple, rapid and reliable single-shot assay	163
Glycosylated 'fast-fraction' haemoglobin	Normal adults have 90% of haemoglobin as haemoglobin A (HbA). Glucose combines reversibly with the α-amino groups of HbA's valine residues at the *N*-terminus of the β-globin chains to form an aldimine (Schiff base) intermediate. Such glycosylation proceeds slowly during the 120 d lifespan of an erythrocyte and thus is a measure of blood glucose concentration over the preceding weeks. HbA evinces altered electrophoretic mobility and ion-exchange chromatography uniquely due to the glycosylation at the *N*-terminus of the β-globin chain	Disposable biosensor for more effective diabetic control	166, 168

Table 3 Possible and current applications of carbon-based sensors in clinical analysis

Parameter	Principle	Benefits	Notes	Ref.
Glucose	Carbon paste–GOD electrodes containing rhodinized microparticles to catalyse the reduction of GOD-evolved H_2O_2 from glucose which is measured amperometrically at -0.1 V (*versus* Ag–AgCl)	Super-selective, owing to low working voltage, facile and reliable fabrication ($s_r = 5\%$), with rapid ($t_{95} = 15$ s) and linear responses	Unsuitable for mass production; needs to be translated to a disposable device, *i.e.*, screen-printing or micromachining methods	169
	First report of a CoPC SPCE and Ag–AgCl two-electrode disposable strip. The metallophthalocyanine-containing working electrode is tailored to the amperometric detection of glucose (at $+0.4$ V) through a CA–GOD bilayer produced contiguously over the sensor assembly	Single-use, generic biosensor that can be fabricated at low cost and on a large-scale basis	Response characteristics require further tuning	170
	MediSense's ExacTech sensor based on a carbon ink modified with GOD and a ferrocene derivative. Fe^{3+} ions mediate the flow of electrons exchanged during the substrate–enzyme interaction. The device is operated in the chronamperometric mode at $+0.3$ V (*versus* Ag–AgCl)	Throw-away strips incorporated into a hand-held instrument. Excellent analytical performance; results are obtained in 30 s	Not generic, geared for a narrow analyte range (substrates for flavoenzymes). Fe^{2+} ions are more soluble and thus tend to leach from the electrode surface	56*
	The Japanese company Kyoto Dai-ichi Kagaku (KDK) have also produced a disposable device for diabetalogical purposes. In this instance hexacyanoferrate(III) ions serve to regenerate GOD's reduced prosthetic group	Suitable for in-house pathology testing	Methodology is not translatable to all of the required systems	171*
Lactic acid	TTF and LOX are absorbed on a disposable carbon foil. The conducting salt regenerates the active site of the oxidase, which becomes reduced during its interaction with lactate, and is subsequently amperometrically re-oxidized at 160 mV *versus* SCE	Good selectivity and amenability to mass production. Lack of O_2 dependence. Extremely fast responses at low lactate levels	Restricted analyte range. Narrow linear range limits application as lactate concentrations may reach 20 mmol dm^{-3} during physical exertion	113
	A modification of the glucocard designed by KDK incorporates LOX and hexacyanoferrate(III). The Fe^{3+} ions receive an electron from reduced LOX, producing Fe^{2+} ions, which are chronoamperometrically oxidized at $+0.5$ V	Rapid and convenient method permitting point-of-care assays	Excessive overvoltage compromises the selectivity of the method. Also not a universal system	172*
Uric acid	SPCEs doped with CoPC and coated with CA and uricase. Oxidase-generated H_2O_2 preferentially traversed the permselective membrane, whereupon it was electrocatalytically oxidized by CoPC at $+0.4$ V *versus* SCE	Simple and convenient test that may be adopted to measure many other oxidase substrates	Paracetamol interference may be reduced by modifying the casting conditions for CA	109
	A glassy carbon–bienzyme configuration has also been proposed. HRP was immobilized onto a GCE by a glutaraldehyde–bovine serum albumin cross-linking method. Hexacyanoferrate(II) was included to mediate the reaction between HRP and uricase-liberated H_2O_2. The hexacyanoferrate(III) ions formed were electroreduced at 0 V (*versus* Ag–AgCl)	Low interference	Complicated reaction scheme but does lend itself to the construction of generic biosensors	173
Cholesterol	Graphite electrodes modified with tetrathiafulvalene, HRP and ChOX. Oxidase-evolved H_2O_2 chemically oxidizes the conducting salt, in the presence of HRP, and is then electrolysed at 0.02 V *versus* Ag–AgCl	Good selectivity	Complex fabrication and reaction sequence. Free cholesterol only	174
	Cholesterol esterase liberates cholesterol from lipoprotein complexes. This rationale is combined with ChOX, HRP and ferrocene to produce a biosensor for total cholesterol. Ferrocene interacts with oxidized HRP, which is reduced by ChOX-generated H_2O_2 with the concomitant production of the ferricinium ion, which is electrochemically reduced	Total sterol detected with favourable performance characteristics	Suitable for point-of-care testing	175*
3-Hydroxy-butyrate	3-Hydroxybutyrate dehydrogenase, NAD^+ and 4-methyl-*o*-quinone (4-MQ) were incorporated into a disposable carbon electrode with a view to monitoring this important ketone body. The dehydrogenase-catalysed reaction generated acetoacetate and NADH. The reduced cofactor was then catalytically oxidized by 4-MQ, regenerating NAD^+ and *o*-benzoquinone, which was chronocoulometrically determined at $+0.3$ V (*versus* Ag–AgCl)	Simple, rapid and inexpensive test for diabetologists	Susceptible to interference from readily oxidizable species such as ascorbic and uric acids and paracetamol. Further sensory tailoring is under way to address this drawback	176†

Table 3—*continued*

Parameter	Principle	Benefits	Notes	Ref.
Paracetamol	CA-modified SPCEs have been used for the direct electrochemical oxidation of the drug at +0.4 V *versus* SCE. Potential interferents were excluded on the basis of size. The amperometric method was in reasonable agreement ($r = 0.995$) with a CLS colorimetric enzymic assay	Simple, rapid quantifications on a single-use strip. Good stability as no biorecognition agent was employed	Design may be improved by coating aryl acyl amidase on to the outside of the CA film and detecting *p*-aminophenol, which is oxidized more readily than the parent compound	54
	Aryl acyl amidase in solution was used to convert paracetamol into *p*-aminophenol, which was monitored chronoamperometrically, after 30 s, at +0.4 V (*versus* SCE) using a GCE	Improved selectivity. Measures free plasma paracetamol (the portion that actually imparts its hepatological effect)	Studies are under way to replace the solid, renewable GCE with a carbon strip and to render the devices reagentless	177 178[†]
	The amidohydrolase enzyme has also been used by Bramwell *et al.* to generate *p*-aminophenol from paracetamol, which is monitored amperometrically at +0.25 V (*versus* Ag–AgCl) using a disposable carbon-based electrode. A glutathione-impregnated paper strip was placed over the sensor assembly to eliminate interference from thiols, *i.e.*, antidotes are based on thiols such as *N*-acetylcysteine.	Available in a single-shot format. Simple, reagentless and convenient	Some interference from excipient substances (such as ascorbate)	175[†]
Salicylic acid	Salicylic acid hydroxylase converts the electroinactive analgesic into an electroactive catechol in oxygenic solutions. Catechol formation was directly proportional to the concentration of salicylate in the sample and was followed chronocoulometrically at +0.3 V using carbon working and Ag–AgCl reference electrodes printed alongside one another	Dry test strips do not require the addition of further reagents. A drop of blood effected the reconstitution of dry agents	Analytical utility was limited by a narrow dynamic range. This was addressed by using an analogue of the drug, benzoate, which uncoupled hydroxylase activity from cofactor oxidation, thus modifying its affinity for salicylate	179[†]
Creatinine kinase (CK)	CK catalyses the dephosphorylation of creatine phosphate at the expense of adenosine diphosphate (ADP) to produce creatinine and adenosine triphosphate (ATP). When coupled to hexokinase, an enzyme that converts glucose and ATP into G6P and ADP, a glucose biosensor in conjunction with the CK–hexokinase scheme monitors the decrease in current arising from ferrocene reoxidizing $FADH_2$ molecules. The rate of decrease is related to the rate of formation of G6P, which in turn is directly proportional to CK activity	Wide accessible analyte range	Facilitates the detection of a range of metabolites and enzymes. The sequence uses several labile biomolecules, thus complicating fabrication procedures	59
α-Amylase	The enzyme α-glucosidase is used as a coupling enzyme for α-amylase in the enzymic generation of *p*-nitrophenol from *p*-nitrophenyl oligosaccharides. The analytical signal is derived from the electrochemical oxidation of *p*-nitrophenol	Amperometric detection of a hitherto inaccessible enzyme	System requires further tuning to permit quantifications in physiological fluids	176
Oxalic acid	Glazier and Rechnitz have modified a CPE with an oxidase-rich beet stem tissue and the H_2O_2 liberated was detected amperometrically at +0.9 V *versus* SCE in succinic acid–EDTA buffer (pH 4)	Low-cost, sensitive and rapidly responding biosensor. Shows concept for oxalate test	Reproducibility and selectivity problems can be addressed by using isolated enzymes. Ascorbate interferes directly and through enzyme inhibition	180

* Commercially available sensors.
† Near-commercially available sensors.

in biosensor development, forging paths to multi-parameter testing.

The health care market is, however, averse to change and for biosensors to become established they must displace existing methods of analysis. Compounds that are currently believed to be good indicators of disease and routine methods for their determination are shown in Table 1. Generally, the analysis times are extended by long incubation/reaction periods, sample pre-treatment or column conditioning and require expensive and dedicated laboratory equipment. The need to add extra reagents at the time of use is also a disadvantage for bedside monitoring, especially in acute cases such as drug intoxication and myocardial infarction where fast tests are a mandate.

Table 2 shows additional substances that clinicians perceive to require instant tests if the technology were available. In the development of new methods, factors such as minimal operator expertise and sample manipulation must be considered. Solid-phase, single-use sensors address many of these issues. Table 3 shows various analytes accessible with sensors from published works, the number of commercial or near-commercial devices on the market and the principle of their operation. Whereas the number of potential analytes is large (and constantly adjusting to meet the challenges laid down by diagnostic companies), the actual number of commercial products is comparatively small. No doubt the fabrication optimization, lengthly analytical trials and financial investment (MediSense's glucose meter cost around US$50 million

to develop) hinder such progress. However, when these barriers are surmounted the realization of disposable biosensors will be brought to fruition. Given the decentralized nature of the testing regime, they are destined to have a pronounced impact on the diagnostic market, and carbon as an electrode substrate is likely to be a strong contender in this context.[181]

References

1 Håkanson, H., Kyrölainen, M., and Mattiason, M., *Biosens. Bioelectron.*, 1993, **8**, 213.
2 Blaedel, W. J., and Engstrom, R. C., *Anal. Chem.*, 1980, **52**, 1691.
3 Willner, I., and Riklin, A., *Anal. Chem.*, 1994, **66**, 1535.
4 Silber, A., Bräuche, C., and Hampp, N., *Sens. Actuators*, 1994, **18–19**, 235.
5 Csöregi, E., Gorton, L., and Marko-Varga, G., *Anal. Chim. Acta*, 1993, **273**, 59.
6 Ruiz, B. L., Dempsey, E., Hua, C., Smyth, M. R., and Wang, J., *Anal. Chim. Acta*, 1993, **273**, 425.
7 Adams, R. N., *Anal. Chem.*, 1958, **30**, 1576.
8 Céspedes, F., Fàbregas, M. J., Bartrolí, J., and Alegrats, S., *Anal. Chim. Acta*, 1993, **273**, 409.
9 Kinoshita, K., *Carbon—Electrochemical and Physiochemical Properties*, Wiley-Interscience, New York, 1988.
10 Ikeda, T., Miki, K., Fushimi, F., and Senda, M., *Agric. Biol. Chem.*, 1987, **51**, 747.
11 Koopal, C. G., Bos, A. A., and Nolte, R. J., *Sens. Actuators*, 1994, **18–19**, 166.
12 Martorell, D., Céspedes, F., Martinez-Fàbregas, E., and Alegret, E., *Anal. Chim. Acta*, 1994, **290**, 343.
13 Zhou, Z. X., and Wang, E. K., *Electroanalysis*, 1994, **6**, 29.
14 Kronkvist, K., Wallentin, M., and Johansson, G., *Anal. Chim. Acta*, 1994, **290**, 335.
15 Jin, L. T., Ye, J. S., Tong, W., and Fang, Y. Z., *Mikrochim. Acta*, 1993, **112**, 71.
16 Sagar, K. A., Smyth, M. R., and Munden, R., *J. Pharm. Biomed. Anal.*, 1993, **11**, 533.
17 Shiraishi, H., and Takahashi, R., *Anal. Sci.*, 1994, **10**, 133.
18 Wang, J., Dempsey, E., Eremenko, A., and Smyth, M. R., *Anal. Chim. Acta*, 1993, **279**, 203.
19 Martinez, C. R., Gonzalo, R. E., Garcia, G. F., and Méndez, H. J., *J. Chromatogr.*, 1993, **644**, 49.
20 Goicolea, M. A., Debalugea, Z. G., Portela, M. J., and Barrio, R., *Analyst*, 1994, **119**, 269.
21 Ikeda, S., and Satake, H., *Bunseki Kagaku*, 1994, **43**, 247.
22 Chi, Q. J., and Dong, S. J., *Anal. Chim. Acta*, 1993, **278**, 17.
23 Fernandez, C., Chico, E., Yanezsedeno, P., Pingarron, J. M., and Polo, L. M., *Analyst*, 1992, **117**, 1919.
24 Deetz, J. S., and Rozzel, J. D., in *Biocatalysts for Industry*, ed. Dordick, J. S., Plenum Press, New York, 1991, ch. 9. pp. 181–191.
25 Wang, J., Dempsey, E., Eremenko, A., and Smyth, M. R., *Anal. Chim. Acta*, 1993, **279**, 203.
26 Burke, P. A., Smith, S. O., Bachovchin, W. W., and Kilbanov, A. M., *J. Am. Chem. Soc.*, 1989, **111**, 8290.
27 Saini, S., and Turner, A. P. F., *Biochem. Soc. Trans.*, 1991, **19**, 28.
28 Adeyoju, O., Iwuoha, E. I., and Smyth, M. R., *Talanta*, 1994, **41**, 1603.
29 Iwuoha, E. I., and Smyth, M. R., *Analyst*, 1994, **119**, 265.
30 Mionetto, N., Marty, J. L., and Karube, I., *Biosens. Bioelectron.*, 1994, **9**, 463.
31 Bouquelot, E., and Bridel, M., *Ann. Chim. Phys.*, 1913, **29**, 145.
32 Degani, Y., and Heller, A., *J. Am. Chem. Soc.*, 1988, **110**, 2615.
33 Dics, J. M., Cardosi, M. F., Turner, A. P. F., and Karube, I., *Electroanalysis*, 1993, **5**, 1.
34 Laane, C., Boeren, S., Vos, K., and Veeger, C., *Biotechnol. Bioeng.*, 1987, **30**, 81.
35 Sakurai, J. Margolin, A. L., Russell, A. J., and Kilbanov, A. M., *J. Am. Chem. Soc.*, 1988, **110**, 7236.
36 Faulkner, L. R., *Chem. Eng. News*, 1984, 28.
37 Murray, R. W., *Acc. Chem. Res.*, 1990, **23**, 128.
38 Xie, B., Khayyami, M., Nwosu, T., Larsson, P. O., and Danielson, B., *Analyst*, 1993, **118**, 845.
39 Wilson, R., and Turner, A. P. F., *Biosens. Bioelectron.*, 1992, **7**, 165.
40 Heller, A., *Acc. Chem. Res.*, 1990, **23**, 128.
41 Rivas, G. A., and Ortiz, P. I., *Anal. Lett.*, 1994, **27**, 751.
42 Turyan, I., and Mandler, D., *Anal. Chem.*, 1993, **65**, 2089.
43 Wang, J., *Analyst*, 1987, **112**, 1303.
44 Hernandez, P., Vicente, J., Gonzalez, M., and Hernandez, L., *Talanta*, 1990, **37**, 789.
45 Rolinson, D. R., Nowak, R. J., Welsh, T. A., and Murray, C. G., *Talanta*, 1991, **38**, 27.
46 Ramos, J. A., Bermejo, E., Zapardiel, A., and Perez, J. A., *Anal. Chim. Acta*, 1993, **273**, 219.
47 Malinski, T., and Taha, Z., *Nature (London)*, 1992, **358**, 676.
48 Moussy, F., Harrison, D. J., and Rajotte, R. V., *Int. J. Artif. Organs*, 1994, **2**, 88.
49 Wang, J., Tuzhi, P., and Golden, T., *Anal. Chim. Acta*, 1987, **194**, 129.
50 Gao, Z., Wang, G., Li, P., and Zhao, Z., *Anal. Chem.*, 1991, **63**, 953.
51 Dray, D. N., Keyes, M. H., and Watson, B., *Anal. Chem.*, 1977, **49**, 1067A.
52 Colton, C. K., Smith, K. A., Merril, E. W., and Farrell, P. C., *J. Biomed. Mater. Res.*, 1971, **5**, 459.
53 Amine, A., Kauffmann, J. M., Patriarche, G. J., and Christian, G. D., *Talanta*, 1993, **40**, 1157.
54 Gilmartin, M. A. T., and Hart, J. P., *Analyst*, 1994, **119**, 2431.
55 Gilmartin, M. A. T., and Hart, J. P., *Analyst*, 1994, **119**, 2331.
56 Matthews, D. R., Brown, E., Watson, A., Holman, R. R., Steemson, J., Hughs, S., and Scott, D., *Lancet*, 1987, **1**, 778.
57 Batchelor, M. J., Green, M. J., and Sketch, C. L., *Anal. Chim. Acta*, 1989, **221**, 289.
58 Cardosi, M. F., and Birch, S. W., *Anal. Chim. Acta*, 1993, **276**, 69.
59 Hall, E. A. H., *Biosensors*, Open University Press, Milton Keynes, 1990.
60 Wring, S. A., and Hart, J. P., *Electroanalysis*, 1994, **6**, 617.
61 Sternberg, R., Bindra, D. S., Wilson, G. S., and Thévenot, D. R., *Anal. Chem.*, 1988, **60**, 2781.
62 Gilmartin, M. A. T., Hart, J. P., and Birch, B. J., *Analyst*, 1994, **119**, 247.
63 Heider, G. H., Sasso, S. V., Huang, K.-M., Yacynych, A. M., and Wieck, H. J., *Anal. Chem.*, 1990, **62**, 1106.
64 Sun, Z., and Tachikawa, H., *Anal. Chem.*, 1992, **64**, 1112.
65 Clark, L. C., and Lyons, C., *Ann. N.Y. Acad. Sci.*, 1962, **102**, 29.
66 Wring, S. A., Hart, J. P., Bracey, L., and Birch, B. J., *Anal. Chim. Acta*, 1990, **231**, 203.
67 Guilbault, G. G., and Lubrano, G. J., *Anal. Chim. Acta*, 1973, **64**, 439.
68 Trevenot, D. R., Sternberg, R., Coulet, P. R., Laurent, J., and Gautheron, C. D., *Anal. Chem.*, 1979, **51**, 96.
69 Durand, P., David, A., and Thomas, D., *Biochim. Biophys. Acta*, 1978, **527**, 277.
70 Frew, J. E., and Green, M. J., *Anal. Proc.*, 1988, **25**, 276.
71 Gilmartin, M. A. T., Hart, J. P., and Birch, B. J., *Analyst*, 1992, **117**, 1299.
72 Rennerberg, R., Scheller, F., Riedel, K., Litschko, E., and Richter, M., *Anal. Lett.*, 1983, **16** (B12), 877.
73 Frew, J. E., and Hill, H. A. O., *Anal. Chem.*, 1987, **59**, 933A.
74 Terpstra, M., *Biosens. Bioelectron.*, 1992, **7**, 157.
75 Rechnitz, G. A., *Chem. Eng. News*, 1975, **53**, 29.
76 Wijesuriya, D. C., and Rechnitz, G. A., *Biosens. Bioelectron.*, 1993, **8**, 155.
77 Belli, S. L., and Rechnitz, G. A., *Anal. Lett.*, 1986, **19**, 403.
78 Wring, S. A., and Hart, J. P., *Analyst*, 1992, **117**, 1281.
79 Cass, A. E. G., Davis, G., Francis, G. D., Hill, H. A. O., Aston, W. J., Higgins, E. J., Scott, L. D. L., and Turner, A. P. F., *Anal. Chem.*, 1984, **56**, 667.

80   Wring, S. A., Hart, J. P., and Birch, B. J., *Analyst*, 1991, **116**, 123.
81   Hart, J. P., and Hatley, I., *Analyst*, 1994, **119**, 259.
82   Wring, S. A., and Hart, J. P., *Analyst*, 1992, **117**, 1283.
83   Hartley, I. C., and Hart, J. P., *Anal. Proc.*, 1994, **31**, 333.
84   Halbert, M. K., and Baldwin, R. P., *Anal. Chem.*, 1985, **57**, 591.
85   Zagal, J., Fierro, C., and Rozas, R., *J. Electroanal. Chem.*, 1981, **119**, 403.
86   Scheller, F., Schubert, F., Pfeiffer, D., Hintsche, R., Dransfeld, I., Renneberg, R., Wollenberger, U., Riedal, K., Pavlova, M., Kühn, M., Müller, H.-G., Tan, P.-M., Hoffman, W., and Moritz, W., *Analyst*, 1989, **114**, 653.
87   Gibson, T. D., Hulbert, J. N., Parker, S. M., Woodward, J. R., and Higgins, I., *Biosens. Bioelectron.*, 1992, **7**, 701.
88   Icaza, M.-A., and Bilitewski, U., *Anal. Chem.*, 1993, **65**, 525A.
89   Cave, S., *Fundholding*, 1994, 14.
90   Heiduschka, P., and Scheller, F. W., *Biosens. Bioelectron.*, 1994, **9**, 7.
91   Tsionsky, M., Gun, G., Glezer, V., and Lev, O., *Anal. Chem.*, 1994, **66**, 1747.
92   Beh, S. K., Moody, G. J., and Thomas, J. D. R., *Analyst*, 1991, **116**, 459.
93   Marcinkeviciene, J., and Kulys, J., *Biosens. Bioelectron.*, 1993, **8**, 209.
94   Moore, T. J., Nam, G. G., Pipes, L. C., and Coury, L. A., Jr., *Anal. Chem.*, 1994, **66**, 3158.
95   Van Benschoten, J. J., Lewis, J. Y., and Heineman, W. R., *J. Chem. Educ.*, 1983, **60**, 772.
96   Miner, D. J., Rice, J. R., Riggin, R. M., and Kissinger, P. T., *Anal. Chem.*, 1981, **53**, 2258.
97   Coury, L. A., Oliver, B. N., Egekeze, J. O., Sosnoff, C. S., Brumfield, J. C., Buck, R. P., and Murray, R. W., *Anal. Chem.*, 1990, **62**, 452.
98   Hale, P. D., Inagaki, T., Karan, H. I., Okamoto, Y., and Skotheim, T. A., *J. Am. Chem. Soc.*, 1989, **111**, 3482.
99   Ikeda, S., and Oyama, N., *Anal. Chem.*, 1993, **65**, 1910.
100   Schuhmann, W., *Biosens. Bioelectron.*, 1993, **8**, 191.
101   Razumas, V., Kulys, J., Knichel, M., Wiemhöfer, H.-D., and Göpel, W., *Electroanalysis*, 1993, **5**, 399.
102   Heller, A., *Acc. Chem. Res.*, 1990, **23**, 128.
103   Zhao, S., and Luong, J. H. T., *Biosens. Bioelectron.*, 1993, **8**, 438.
104   Wang, J., Wu, L.-H., Li, R., and Sanchez, J., *Anal. Chim. Acta*, 1990, **228**, 251.
105   Gorton, L., *Anal. Chim. Acta*, 1985, **178**, 247.
106   Taha, Z., and Wang, J., *Electroanalysis*, 1991, **3**, 215.
107   Wang, D. L., and Heller, A., *Anal. Chem.*, 1993, **65**, 1069.
108   Staskeviciene, S. L., Cenas, N. K., and Kulys, J. J., *Anal. Chim. Acta*, 1991, **243**, 167.
109   Gilmartin, M. A. T., and Hart, J. P., *Analyst*, 1994, **119**, 853.
110   Gilmartin, M. A. T., Ewen, R., Hart, J. P., and Honeyborne, C. L., *Electroanalysis*, in the press.
111   Heller, A., *Acc. Chem. Res.*, 1990, **23**, 128.
112   Bartlett, P. N., Whitaker, R. G., Green, M. J., and Frew, J., *J. Chem. Soc., Chem. Commun.*, 1987, 1603.
113   Palleschi, G., and Turner, A. P. F., *Anal. Chim. Acta*, 1990, **243**, 459.
114   Ikeda, T., Matsushita, F., and Senda, M., *Biosens. Bioelectron.*, 1991, **6**, 299.
115   Todoriki, S., Ikeda, T., Senda, M., and Wilson, G. S., *Agric. Biol. Chem.*, 1989, **53**, 3055.
116   Maidan, R., and Heller, A., *Anal. Chem.*, 1992, **64**, 2889.
117   Chang, H.-C., Ueno, A., Yamada, H., Matsue, T., and Uchida, I., *Analyst*, 1991, **116**, 793.
118   Jaegfeldt, H., Kuwana, T., and Johansson, G., *J. Am. Chem. Soc.*, 1983, **105**, 1805.
119   Chenault, H. K., and Whitesides, G. M., *Appl. Biochem. Biotechnol.*, 1987, **14**, 147.
120   Wring, S. A., and Hart, J. P., *Analyst*, 1992, **117**, 1215.
121   Gorton, L., Persson, B., Hale, P. D., Boguslavsky, L. I., Karan, H. I., Lee, H. S., Skotheim, T., Lan, H. I., and Okamoto, Y., in *Biosensors and Chemical Sensors*, ed., Edelman, P. J., and Wang, J., ACS Symposium Series, No. 487, 1992, ch. 6, pp. 56–83.
122   Bernt, E., and Gutman, I., in *Methods in Enzymatic Analysis*, ed. Bergmeyer, H. U., Verlag Chemie, Weinheim, and Academic Press, New York, 2nd edn., 1974, pp. 1499–1502.
123   Dominguez, E., Marko-Varga, G., Lan, H. L., Okamoto, Y., Hale, P. D., Skotheim, T. A., Hahn-Hägerda, B., and Gorton, L., *Ann. N.Y. Acad. Sci.*, 1992, **672**, 230.
124   Olsson, B., Marko-Varga, G., Gorton, L., Applequist, R., and Johansson, G., *Anal. Chim. Acta*, 1988, **206**, 49.
125   Dominguez, E., Lan, H. L., Okamoto, Y., Hale, P. D., Skotheim, T. A., Gorton, L., and Hahn-Hägerda, B., *Biosens. Bioelectron.*, 1993, **8**, 229.
126   Dominguez, E., Lan, H. L., Okamoto, Y., Hale, P. D., Skotheim, T. A., and Gorton, L., *Biosens. Bioelectron.*, 1993, **8**, 167.
127   Sprules, S. D., Hart, J. P., Pittson, R., and Wring, S. A., *Analyst*, 1994, **119**, 253.
128   Sprules, S. D., Hart, J. P., Pittson, R., and Wring, S. A., *Anal. Chim. Acta*, in the press.
129   Athey, D., McNeil, C. J., Bailey, W. R., Hager, H. J., Mullen, W. H., and Russell, L. J., *Biosens. Bioelectron.*, 1993, **8**, 415.
130   Persson, B., Lan, H. L., Gorton, L., Okamoto, Y., Hale, P. D., Boguslavsky, L. I., and Skotheim, T., *Biosens. Bioelectron*, 1993, **8**, 81.
131   Vreeke, M., Maidan, R., and Heller, A., *Anal. Chem.*, 1992, **64**, 3084.
132   Giorgio, D., in *Clinical Chemistry Principles and Practice*, ed. Henry, R. J., Cannon, D. C., and Winkleman, J. W., Harper and Row, New York, 2nd edn., 1974, p. 504.
133   Gowenlock, A. H., *Varley's Clinical Biochemistry*, Heinemann Medical Books, London, 6th edn., 1988.
134   Zeatris, A., and Zak, B., *Anal. Chem.*, 1969, **29**, 143.
135   Allain, C. C., *Clin. Chem. (Winston-Salem, N.C.)*, 1974, **20**, 470.
136   Barker, J. B., and Summerson, W. H., *J. Biol. Chem.*, 1941, **138**, 535.
137   Stern, H. J., *Ann. Clin. Biochem.*, 1994, **31**, 410.
138   Weiner, K., *Ann. Clin. Biochem.*, 1978, **15**, 187.
139   Campbell, R. S., and Price, C. P., *J. Clin. Chem. Biochem.*, 1986, **24**, 155.
140   Hammond, P. M., Scawen, M. D., Atkinson, T., Campbell, R. S., and Price, C. P., *Anal. Biochem.*, 1984, **143**, 157.
141   Price, C. P., Hammond, P. M., and Scawen, M. D., *Clin. Chem. (Winston-Salem, N.C.)*, 1983, **29**, 358.
142   Folin, O., and Denis, W. A., *J. Biol. Chem.*, 1912–13, **13**, 469.
143   Bittner, D., Halls, S., and McCleary, M., *Am. J. Clin. Pathol.*, 1963, **40**, 423.
144   Folin, O., *J. Biol. Chem.*, 1930, **86**, 179.
145   Carrol, J. J., Coburn, H., and Douglas, R., *Clin. Chem. (Winston-Salem, N.C.)*, 1971, **17**, 158.
146   Miller, B. F., and Dubos, R., *J. Biol. Chem.*, 1937, **121**, 457.
147   Masson, P., Ohlsson, P., and Björkhem, I., *Clin. Chem. (Winston-Salem, N.C.)*, 1981, **27**, 18.
148   Lim, C. K., Richmond, W., Robinson, D. P., and Brown, S. S., *J. Chromatogr.*, 1978, **145**, 41.
149   Chaney, A. L., and Marbach, E. P., *Clin. Chem. (Winston-Salem, N.C.)*, 1962, **8**, 130.
150   Guilbault, G. G., and Mascini, M., *Anal. Chem.*, 1977, **49**, 795.
151   Trinder, P., *Biochem. J.*, 1954, **57**, 301.
152   Walter, L. J., Briggs, D. F., and Coutts, R. T., *J. Pharm. Sci.*, 1974, **63**, 1755.
153   Caterson, R. R., Duggin, G. C., Horrath, J. S., and Tiller, D. J., *Aust. J. Pharm. Sci.*, 1978, **7**, 111.
154   Bjerre, S., and Porter, C. J., *Clin. Chem. (Winston-Salem, N.C.)*, 1965, **11**, 137.
155   Schater, D., and Manis, J. G., *J. Clin. Invest.*, 1958, **37**, 800.
156   Gallows, S., and Watkins, P. J., *Clin. Chim. Acta*, 1968, **19**, 511.
157   Laker, M. F., *Adv. Clin. Chem.*, 1983, **23**, 259.
158   Rofe, A. M., Pholenz, S. M., Bais, R., and Conyers, R. A. J., *Clin. Chem. (Winston-Salem, N.C.)*, 1985, **31**, 1574.
159   Mazzani, B. C., Teubner, J. I. C., and Ryall, R. L., *Clin. Chem. (Winston-Salem, N.C.)*, 1984, **30**, 1339.
160   Chalmers, A. H., Cowley, D. M., and McWhinney, B. C., *Clin. Chem. (Winston-Salem, N.C.)*, 1985, **31**, 1703.
161   Karman, A., *J. Clin. Invest.*, 1955, **33**, 131.
162   Wimmer, M. C., Artiss, J. D., and Zak, B., *Clin. Chem. (Winston-Salem, N.C.)*, 1985, **31**, 1616.
163   Owen, V. M., *Biosens. Bioelectron.*, 1994, **9**, 29.
164   Howles, C. M., and Macnamee, M. C., *Br. Med. Bull.*, 1990, **49**, 616.

165   Albers, J. J., Marcovina, S. M., and Kennedy, H., *Clin. Chem.* *(Winston-Salem, N.C.)*, 1992, **58**, 658.

166   Hilton, S., *Br. J. Gen. Pract.*, 1990, **40**, 32.

167   Chopra, I. J., Nelson, J. C., Solomon, D. H., and Beall, G. N., *J. Clin. Endocrinol. Metab.*, 1971, **32**, 299.

168   Broods, A. P., Nairn, I. M., and Baird, J. D., *Br. Med. J.*, 1980, **281**, 702.

169   Wang, J., Liu, J., Cheng, L., and Lu, F., *Anal. Chem.*, 1994, **66**, 3600.

170   Gilmartin, M. A. T., Patton, D. T., and Hart, J. P., *Analyst*, in the press.

171   Davis, B. D., *Clin. Chem. (Winston-Salem, N.C.)*, 1992, **38**, 2093.

172   Shimojo, N., Naka, K., Uenoyama, H., Hamamoto, K., Yoshioka, K., and Okuda, K., *Clin. Chem. (Winston-Salem, N.C.)*, 1993, **37**, 2312.

173   Kulys, J., and Schmid, R. D., *Biosens. Bioelectron.*, 1991, **6**, 43.

174   Ball, M. R., Frew, J. E., Green, M. J., and Hill, H. A. O., *Proc. Electrochem. Soc.*, 1986, **86**, 7.

175   Bramwell, H., Cass, A. E. G., Gibbs, P. N. B., and Green, M. S., *Analyst*, 1990, **115**, 185.

176   Batchelor, M. J., Williams, S. C., and Green, M. J., *J. Electroanal. Chem.*, 1988, **246**, 307.

177   Vaughan, P. A., Scott, L. D. L., and McAleer, J. R., *Anal. Chim. Acta*, 1991, **248**, 361.

178   Jones, A. F., McAleer, J. F., Braithwaite, R. A., Scott, L. D., Brown, S. S., and Vale, S. A., *Lancet*, 1990, **335**, 793.

179   Frew, J. E., Bayliff, S. W., Gibbs, P. N. B., and Green, M. J., *Anal. Chim. Acta*, 1989, **224**, 39.

180   Glazier, S. A., and Rechnitz, G. A., *Anal. Lett.*, 1989, **22**, 2929.

181   Gilmartin, M. A. T., *PhD Thesis*, University of the West of England, Bristol, 1994.

Determination of Trace Thallium After Accumulation of Thallium(III) at a 8-Hydroxyquinoline-Modified Carbon Paste Electrode

Qiantao Cai and Soo Beng Khoo*

Department of Chemistry, National University of Singapore, Kent Ridge, 0511, Singapore

Thallium(III) was selectively accumulated, in an open circuit, from a stirred Britton–Robinson buffer solution (pH 4.56) onto a carbon paste electrode incorporating 8-hydroxyquinoline. The ensuing measurement was carried out by differential pulse anodic stripping voltammetry after reducing the thallium(III) to metallic thallium in ammonia–ammonium chloride buffer (pH 10.00). Factors affecting the accumulation, reduction and stripping steps were investigated and an optimized procedure was developed. Under optimized conditions, a calibration plot for thallium(III) concentration in the range 5.00×10^{-10}–1.60×10^{-5} mol l^{-1} gave two linear regions arising from different controlling factors during the accumulation step. A detection limit of 2.30×10^{-10} mol l^{-1} (0.047 ppb) (S/N = 3) was found for a 2 min accumulation. For 10 successive determinations of 1.00×10^{-6} mol l^{-1} and 1.00×10^{-7} mol l^{-1} Tl^{III}, relative standard deviations, s_r, of 2.8 and 4.8% were obtained, respectively. Interferences from other ions and organic substances were examined. The developed method was applied to thallium determinations in sea-water and human urine samples.

Keywords: Thallium(III) accumulation; 8-hydroxyquinoline; modified carbon paste electrode; differential pulse anodic stripping voltammetry; sea-water; human urine

Introduction

Thallium is usually found in sulfur-containing ores and potassium minerals.[1] The determination of low levels of thallium is important because of its toxicity. The maximum allowable concentration of thallium in air is reported to be 0.1 mg m^{-3}.[2] Increasing anthropogenic activities such as combustion, operations of mines and cement plants, etc.,[3] promote the spread of thallium, thereby posing a latent environmental pollution problem.[4]

In view of its high toxicity, the development of highly sensitive and selective methods to monitor thallium levels in various samples is of considerable importance. Numerous techniques have been used for thallium analysis.[2] After appropriate sample pre-treatment, thallium determination has been performed using spectrophotometry,[5] atomic absorption spectrometry,[6] emission spectrophotometry,[7] and stripping voltammetry.[6,8] Anodic stripping voltammetry (ASV) at the mercury electrode is a well-established technique for the determination of low levels of metal ions. However, its usage in real samples is complicated by interferences from co-existing metal ions and organic compounds

present in the sample matrices.[2,9] In thallium analysis, interfering metal ions include lead,[8,9] cadmium,[9] copper,[10] bismuth,[11] indium,[12] titanium[13] and iron.[14] In some of these cases, the interferences can be eliminated by addition of complexing agents, *e.g.*, ethylenediaminetetraacetic acid (EDTA) and/or surfactants.[10–14]

One approach to eliminate the problem of interferences is to employ chemically modified electrodes (CME)[15–19] together with medium exchange. Here, the electrode is modified with an agent (chosen for its special affinity for the target analyte) to preconcentrate the analyte, after which analysis (usually electrochemical stripping) is performed in a pure electrolyte solution. The preconcentration step imparts high sensitivity to this technique, whereas the exchange of medium to a pure electrolyte solution removes interferences from the sample background. One form of this class of electrodes is the carbon paste electrode (CPE) modified by incorporation of a sparingly soluble complexing agent. The use of this type of electrode in analysis is gaining popularity because of its high selectivity and sensitivity. Amongst its advantages are that the modifier concentration is readily adjustable, a fresh and reproducible surface is easily and rapidly generated, and the electrode response is stable.[16–19]

Recently, we reported a procedure for the speciation and analysis of thallium based on the open circuit accumulation of Tl^I at the 8-hydroxyquinoline-modifed carbon paste electrode (HOx-MCPE).[20] In that procedure, the accumulated Tl^I was reduced to metallic thallium at the electrode surface, which was then stripped anodically by differential pulse voltammetry. Speciation was achieved by first masking Tl^{III} with EDTA while determining Tl^I. Thallium^{III} was converted to Tl^I by chemical reduction with hydroxylamine hydrochloride, so that the total thallium content could be obtained. Using this procedure, a detection limit of 4.90×10^{-9} mol l^{-1} was obtained. The precision for a 1.00×10^{-7} mol l^{-1} solution was found to be 3.20%.

However, further experiments subsequently showed that, based on the same principle and using the same modified electrode, the accumulation of Tl^{III} followed by differential pulse stripping voltammetry under optimized conditions provided a better than ten-fold improvement in the detection limit (2.30×10^{-10} mol l^{-1}) for thallium determination, compared with the procedure employing Tl^I accumulation, with no degradation in precision. Therefore, we report here the results of the systematic investigation of the factors affecting the accumulation of Tl^{III} at the HOx-MCPE. A method was then developed, under optimized conditions, for the determination of total thallium. This method was applied to the determination of thallium in human urine and sea-water matrices.

---

* To whom correspondence should be addressed.

Experimental

Reagents

Chemicals used were all of analytical-reagent grade, or better. Polyethylene bottles for storing stock solutions were soaked in 1.4 mol l^{-1} nitric acid overnight and rinsed with Millipore water (Millipore Alpha–Q purification system, Bedford, MA, USA).

Thallium(III) stock solution (5.00×10^{-3} mol l^{-1}) was prepared by dissolving thallic oxide (Tl_2O_3, Hopkin and Williams, Essex, UK) in 25 ml of 1.0 mol l^{-1} HCl, and diluting to 250 ml with water. Working solutions were diluted from this stock with 0.10 mol l^{-1} HCl as required. Thallium(I) stock solution (5.00×10^{-3} mol l^{-1}) was prepared by dissolving thallium(I) sulfate (Riedel de Haen, Seelze, Germany) in 0.010 mol l^{-1} nitric acid. Working solutions were diluted from this stock with 0.010 mol l^{-1} HNO_3. Both thallium stock solutions were protected from light by wrapping aluminium foil around the polyethylene bottles in which they were stored. Britton–Robinson (B–R) buffer solution (pH 4.56) was prepared by adding 30 ml of aqueous NaOH (0.20 mol l^{-1}) into 100 ml of an aqueous solution containing 0.040 mol l^{-1} acetic acid, 0.040 mol l^{-1} perchloric acid and 0.040 mol l^{-1} boric acid (B–R acid mixture). Ammonia–ammonium chloride buffer (pH 10.00) was obtained by mixing 0.20 mol l^{-1} ammonia solution and 0.20 mol l^{-1} ammonium chloride solution (17.0 + 3.0, v/v). All other solutions were prepared by dissolving appropriate amounts of the respective chemicals in water.

Graphite powder (Ultra F grade, Johnson Matthey, Royston, Cambridgeshire, UK), liquid paraffin (Merck, Darmstadt, Germany; boiling range at 1000 hPa, 300–400 °C, dynamic viscosity at 20 °C was 25–80 mPa s) and 8-hydroxyquinoline (GR, Merck) were used for preparation of the carbon paste and HOx-MCPE.

Fabrication of the CPE and HOx-MCPE

Details of the procedure for preparing the carbon paste and the 8-hydroxyquinoline (HOx)-impregnated carbon paste are given in an earlier work.[20] Briefly, a solution containing the required amount of HOx in ethanol was placed in a beaker and magnetically stirred. An amount of 3.0 g of graphite powder was also introduced into the beaker. Stirring was continued at room temperature, until all the ethanol evaporated. The graphite powder–HOx mixture was allowed to dry in air for another 24 h to ensure the complete removal of ethanol. The dried mixture was thoroughly mixed with 1.6 g of liquid paraffin in a mortar. A series of pastes with percentages of HOx, ranging from 0.010% to 5.0% (m/m) were prepared. For the blank carbon paste without HOx, the HOx-coating step was omitted. In the fabrication of the CPE or HOx-MCPE, the paste was packed into the end of a glass tube (3 mm i.d.) and a copper rod (⩽3 mm diameter) with a pointed tip inserted through the opposite end to establish electrical contact. The carbon paste surface was polished on a piece of stiff, white paper until it had a shiny appearance. A fresh electrode surface can be easily obtained by extruding a small amount of paste from the tip of the electrode with the copper rod, scraping off the excess and smoothing on the paper as before.

Apparatus

Electrochemical experiments were performed with a microprocessor-controlled Princeton Applied Research Model 384B polarographic analyser (EG & G, PARC, Princeton, NJ, USA). Voltammograms were recorded using a Houston DMP-40 series digital plotter (Houston Instrument, Austin,

Texas, USA). A home-made three-electrode glass cell, with a capacity of about 5 ml, was used for all electrochemical measurements. The working electrode was the CPE or HOx-MCPE, while the counter electrode was a platinum coil. The reference electrode was Ag/AgCl (saturated KCl) placed in a compartment containing the supporting electrolyte and separated from the working electrode compartment by a 4 mm diameter Vycor frit. All pH measurements were made with a Hanna Instruments Model HI 8417 microprocessor-controlled pH-meter (Hanna Instruments, Woonsocket, RI, USA). All experiments were performed at an ambient temperature of 25 ± 1 °C.

Procedure

Before the start of every experiment, a fresh surface was generated for the electrode (CPE or HOx-MCPE), using the procedure described earlier. Each measurement cycle consisted of three steps—accumulation, reduction and stripping.

Accumulation step

The HOx-MCPE was immersed in 25 ml of a magnetically stirred solution containing Tl^{III} in B–R buffer (diluted 5 times from the stock solution) at pH 4.56. Accumulation of the Tl^{III} was allowed to proceed for a given time, t_a, at open circuit. After this, the electrode was removed, washed thoroughly with water, and dried with absorbent paper.

Reduction step

The electrode was transferred into the electrochemical cell containing blank supporting electrolyte (ammonia–ammonium chloride buffer at pH 10.00). Here, the accumulated Tl^{III} was reduced to metallic thallium at a potential, E_d, for a period of time, t_d, in still solution.

Stripping step

After the reduction step, the potential was scanned anodically in the differential pulse mode from −1.20 V to −0.72 V [The final potential may vary slightly depending on the concentration of Tl^{III}] at a scan rate of 10 mV s^{-1} and using a pulse height of 50 mV. The differential pulse anodic stripping voltammogram (DPASV) thus obtained, was stored in software by the Model 384B polarographic analyser. The stored voltammogram can be output to the plotter together with values of the peak potential and peak current. At the end of each analysis cycle, the blank supporting electrolyte in the working electrode compartment was changed to prevent contamination.

Sample Treatment

For the purpose of method testing, the US Environmental Protection Agency (USEPA) water quality control sample (WP 386) was used. Since this sample did not contain any thallium, it was spiked with known amounts of Tl^I and Tl^{III}. Sample preparation was carried out by introducing 0.25 ml of the USEPA WP 386 water sample, together with 5 ml of water, 0.050 ml of 1.0 mol l^{-1} HCl and aliquots of the standard solutions of Tl^I and Tl^{III} into a 25 ml beaker. A volume of 0.50 ml of saturated bromine water was then added. The mixture was heated to near boiling. Heating was discontinued when the colour of the bromine had disappeared. After cooling, the solution was transferred into a 25 ml calibrated flask. A volume of 5.0 ml of B–R buffer solution (pH 4.56) and 0.0625 ml of 0.20 mol l^{-1} sodium diethyldithiocarbamate (DDTC) were also added before making up to the mark with water. With this treatment, all Tl^I was oxidized to Tl^{III}.[5]

Human urine and sea-water samples were collected in high-density polyethylene bottles and acidified immediately to pH 1.0 with concentrated nitric acid (14.4 mol l^{-1}). Digestion, prior to analysis, was performed by transferring 25 ml of the sea-water or human urine samples into a 100 ml Kjedahl flask, together with 12.5 ml of concentrated nitric acid (14.4 mol l^{-1}) and 2.5 ml of concentrated perchloric acid (9.1 mol l^{-1}). After covering with a watch-glass, the flask was heated gently on a hot-plate with frequent swirling until the solution started to boil. Gentle boiling was allowed to continue until the solution was reduced in volume to about 5 ml, and had turned almost colourless. After cooling, 0.50 ml of saturated bromine water was added and the solution was re-heated to near boiling until the colour due to the bromine had disappeared. The sample solution was allowed to cool and the pH was adjusted to 4–5 with 2.5 mol l^{-1} NaOH before transferring into a 25 ml calibrated flask. A volume of 5 ml of B–R buffer (pH 4.56) was added before making up to the mark with water. Using this procedure, complete digestion of organic materials could be effected[21] and all the thallium converted to Tl^{III}.[2,5]

Results and Discussion

Accumulation and Electrochemical Behaviour of Tl(III) at CPE and HOx-MCPE

Figs. 1(a) and (b) show the cyclic voltammograms for the CPE and HOx-MCPE [0.10% HOx (m/m) was used unless otherwise stated], respectively, in ammonia–ammonium chloride buffer (pH 10.00). Prior to the cyclic voltammetric scan, the electrodes had been exposed to the stirred blank B–R buffer (pH 4.56) for 3 min. Both electrodes gave a reduction wave, starting at about −0.50 V, with an elongated plateau. This wave was persistent, even after vigorous de-aeration with purified nitrogen. It was attributed to the reduction of oxygen dissolved in the carbon paste or adsorbed on the surface of the graphite particles.[22] For the HOx-MCPE, the irreversible oxidation wave of 8-hydroxyquinoline at a peak potential of

about +0.35 V [Fig. 1(b)] can be clearly seen.[23] No corresponding oxidation was observed in the case of CPE [see Fig. 1(a)] as HOx was absent. However, when the HOx-MCPE was immersed for 3 min in the stirred B–R buffer containing 1.00 × 10^{-4} mol l^{-1} Tl^{III}, then washed thoroughly with water, its cyclic voltammogram in ammonia–ammonium chloride buffer [Fig. 1(d)] showed two additonal peaks; a new reduction peak at +0.14 V due to the reduction of Tl^{III} to Tl^{I}[24] and on reversal the oxidation peak for metallic thallium to Tl^{I} with a peak potential of −0.57 V. The reduction of Tl^{I} to metallic thallium at the electrode surface could not be observed because it was hidden by the reduction wave of oxygen. Identical treatment for the CPE did not give rise to these two additional peaks [Fig. 1(c)].

Fig. 2(a) shows the differential pulse voltammogram at the HOx-MCPE in ammonia–ammonium chloride buffer after 90 s open circuit accumulation in the stirred blank B–R buffer. As can be observed, a low, stable residual current was obtained over the major portion of the potential range scanned, from −1.20 V to −0.72 V. In the presence of 1.00 × 10^{-5} mol l^{-1} Tl^{III} in the B–R buffer solution, a sharp anodic stripping peak with a peak potential at −0.89 V appeared [Fig. 2(b)]. The height of this peak increased with increasing accumulation time, and Tl^{III} concentration in the B–R buffer. These experimentals confirmed that Tl^{III} could be accumulated at the HOx-MCPE at open circuit. Comparing Figs. 2(b) and 1(d), the oxidation of the deposited thallium to Tl(I) for the differential pulse experiment occurred at a more negative potential (peak potential −0.89 V) than for the cyclic voltammetric experiment (peak potential −0.57 V). We have shown earlier that for accumulation of Tl(I) followed by reduction and then stripping, the peak potential for the differential pulse stripping voltammogram shifted negatively with decreasing concentration of the Tl^{I}. In the present case, the Tl^{III} concentration for the differential pulse experiment was 1.00 × 10^{-5} mol l^{-1} while that for cyclic voltammetry was 1.00 × 10^{-4} mol l^{-1}. In addition, this concentration-difference effect was further enhanced by the fact that only 90 s accumulation time was employed for the differential pulse experiment, while in the cyclic voltammetric experiment, 3
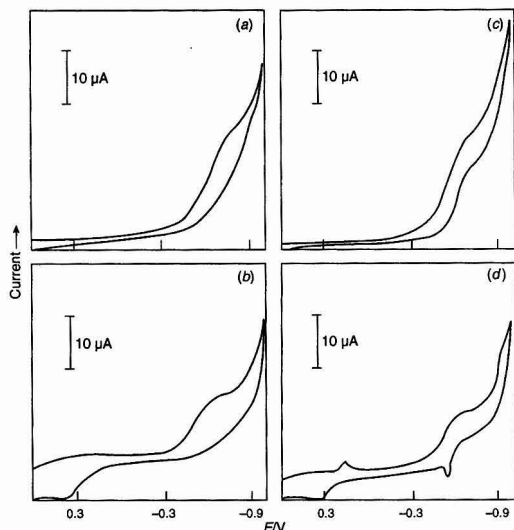
Fig. 1 Cyclic voltammograms at: (a) CPE and (b) HOx-MCPE in ammonia–ammonium chloride buffer pH 10.00, immersed in stirred blank B–R buffer solution for 3 min; (c) CPE and (d) HOx-MCPE; in ammonia–ammonium chloride buffer, pH 10.00, immersed in stirred B–R buffer containing 1.00 × 10^{-4} mol l^{-1} Tl^{III} for 3 min. All at scan rate of 100 mV s^{-1}.
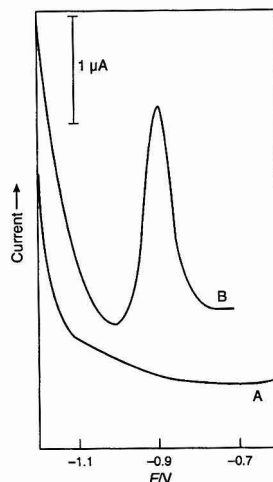
Fig. 2 Differential pulse voltammograms at HOx-MCPE. A, Accumulation in stirred B–R buffer for 90 s and B, accumulation in stirred B–R buffer containing 1.00 × 10^{-5} mol l^{-1} Tl^{III} for 90 s. Stripping in ammonia–ammonium chloride buffer (pH 10.00). Scan rate = 10 mV s^{-1}, pulse height = 50 mV, t_d = 10 s, E_d = −1.20 V.

min was allowed for accumulation. Therefore, a negative shift in peak potential for the differential pulse voltammogram over the cyclic voltammogram for thallium oxidation could be expected. Another factor which might contribute to the difference in the stripping peak potentials could be in the different nature of the two techniques, also bearing in mind that redox processes involved in the plating and stripping of thallium at the graphite electrode are likely to be kinetically slow. No significant peak was observed when performing differential pulse stripping voltammetry and cyclic voltammetry at the CPE, showing that the presence of HOx facilitated the accumulation of Tl^{III} under the experimental conditions. It is known that Tl^{III} complexes with 8-hydroxyquinoline resulting in the formation of the complex $Tl(C_9H_6N)_3$.[25] Therefore, the whole process from the accumulation step to the stripping step at the HOx-MCPE could be described as follows:

(i)   Accumulation in B–R buffer solution (pH 4.56) containing $Tl(III)$

$$3HOx_{(s)} + Tl^{III} = Tl(Ox)_{3(s)} + 3H^+ \qquad (1)$$
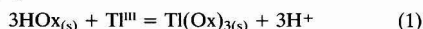
(ii) Reduction in NH_3–NH_4Cl buffer solution (pH 10.00)

$$Tl(Ox)_{3(s)} + 3e^- = Tl^0_{(s)} + 3Ox^-_{(s)} \qquad (2)$$

(iii) Stripping in NH_3–NH_4Cl buffer solution (pH 10.00)

$$Tl^0_{(s)} + HOx_{(s)} = Tl(Ox)_{(s)} + H^+ + e^- \qquad (3)$$

where subscript (s) denotes the electrode surface.

Optimization of Conditions for Thallium Determination

Effect of HOx loading in HOx-MCPE

The effect of HOx loading in the carbon paste for the determination of Tl^{III} was investigated for HO_x in the loading range from 0.010 to 5.0%. The results (Fig. 3) showed that the stripping peak for 1.00×10^{-5} mol l^{-1} Tl^{III} increased to a maximum of up to an HOx loading of 0.10% after which it decreased slightly with HOx loading. The decrease in peak height at higher HOx loading was probably due to increase in resistance of the paste. This trend was similar to that found for Tl^I accumulation.[20] For all subsequent work, a HOx loading of 0.10% was used.

Choice of accumulation medium

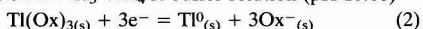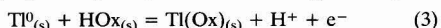Of the three media, namely B–R buffer (pH 4.56), acetic acid–sodium acetate buffer (pH 4.60) and ammonium chloride (0.20 mol l^{-1}, pH 5.12) tested for Tl^{III} accumulation, the B–R and acetate buffer gave essentially similar results in terms of peak shape and height. However, the peak height obtained for the ammonium chloride medium was much reduced as compared with the other two, probably because of complexa-

tion of Tl^{III} by the chloride ion to form $TlCl_x{}^{-(x-3)}$. The B–R buffer was chosen for use over the acetate buffer because of its wider buffering pH range.

The influence of the pH of the chosen B–R buffer on the accumulation of Tl^{III} was examined. For this purpose, B–R buffers of different pH were prepared by taking 2.5 ml of the B–R acid mixture, titrating to the desired pH with 0.20 mol l^{-1} NaOH and making up to volume in a 25 ml calibrated flask. Fig. 4 shows that from pH 2.00 to 3.60, the differential pulse anodic stripping peak for thallium increased and reached a maximum value at pH 3.60, and then remained approximately constant in the pH range of 3.60–5.00. Beyond pH 5.00, the peak decreased. The accumulation of $Tl(III)$ would be expected to be dependent on the distribution of Tl^{III} species in solution and HOx species at the electrode surface. This expectation is borne out by the data of Fig. 4. The diminished stripping peak at a pH greater than about 5.0 was due to the hydrolysis of Tl^{3+} which is known to hydrolyse in relatively acidic solutions,[26] thus, leaving less Tl^{III} available for complexation with HOx. At the lower pH region, increasing protonation of HOx to form H_2Ox^+ with decreasing pH, reduced the effectiveness of complexation of Tl^{III} by the surface hydroxyquinoline groups. Therefore, a narrow pH region between 3.60 and 5.00 appears to be the most favourable for Tl^{III} accumulation at the HOx-MCPE. This behaviour is in contrast to that for the accumulation of Tl^I at the HOx-MCPE where the stripping peak current increased from a low value at about pH 4.1, and reached a maximum constant value at pH 7.5 and beyond.[20] This difference could possibly be exploited for the purpose of discrimination between the two. For further experiments, the pH of the B–R buffer was fixed at 4.56.

The effect of the ionic strength of the accumulation medium on the stripping peak was studied by diluting the original B–R buffer stock to varying degrees, ranging from 25 times dilution to no dilution, and using these for accumulation of 1.00×10^{-5} mol l^{-1} Tl^{III}. In all cases, the stripping peak height remained unchanged. The constancy of the peak height over such a large variation in ionic strength of the B–R buffer gave an indication of the high stability of the $Tl(Ox)_3$ complex.[22] A 5 times dilution was finally chosen for subsequent work.

Effect of accumulation time, t_a

The effect of accumulation time was studied for three Tl^{III} concentrations at 10.00 nmol l^{-1}, 2.00 μmol l^{-1} and 10.00 μmol l^{-1}. The data given in Fig. 5 shows that the rate of Tl^{III} uptake was faster at the higher Tl^{III} concentration, as evidenced by the steeper initial slope of the plots. After the initial rise, the peak current started to level off for all three cases. At the plateau (for each Tl^{III} concentration) equilibrium was established, as opposed to the rising portion where the height of the stripping peak was still governed by the kinetics of Tl^{III} accumulation.

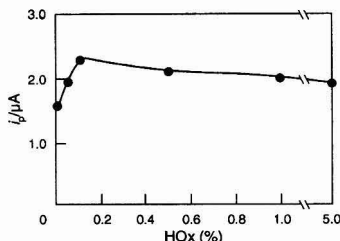**Fig. 3**   Differential pulse stripping peak current dependence on HOx loading in HOx-MCPE. $c_{Tl^{III}} = 1.00 \times 10^{-5}$ mol l^{-1}, $E_d = -1.20$ V, $t_d = 10$ s, $t_a = 60$ s; scan rate = 10 mV s^{-1}; pulse height = 50 mV.
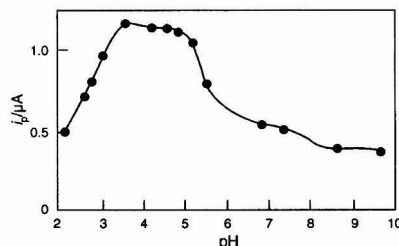

Fig. 4   Differential pulse stripping peak current as a function of pH of accumulation medium. $c_{Tl^{III}} = 1.00 \times 10^{-5}$ mol l^{-1}. Other parameters as in Fig. 3.

Choice of stripping medium

The buffer systems (sodium acetate–acetic acid, ammonia–ammonium chloride and Britton–Robinson at various pH values) were tested for the anodic stripping of thallium. The NH_3–NH_4Cl buffer at pH 10.00 gave the best results in terms of peak shape and sensitivity and was chosen for further use. Studies of the effect of the dilution of the prepared stock solution of NH_3–NH_4Cl buffer indicated that excessive dilution (more than 10 times) led to smaller and broader stripping peaks due to increase in solution resistance. The stock buffer without dilution was eventually chosen as it gave the sharpest peaks.

In general the stripping characteristics after accumulation of Tl^{III} in this work were found to be very similar to those of Tl^I.[20] This was expected because after the reduction step in both cases, the stripping process was identical, *i.e.*, the oxidation of metallic thallium to Tl^I at the electrode surface.

Effect of the reduction potential, E_d, and the reduction time, t_d

It can be seen from Fig. 6 that the differential pulse anodic stripping peak current for thallium increased from zero at -0.95 V and reached a plateau starting at about -1.15 V as the reduction potential became more negative. This plateau continued up to the most negative E_d studied at -1.40 V. Therefore, for the most efficient conversion of the accumulated Tl^{III} to metallic thallium, E_d should be -1.15 V or more negative. An E_d of -1.20 V was chosen as most appropriate.
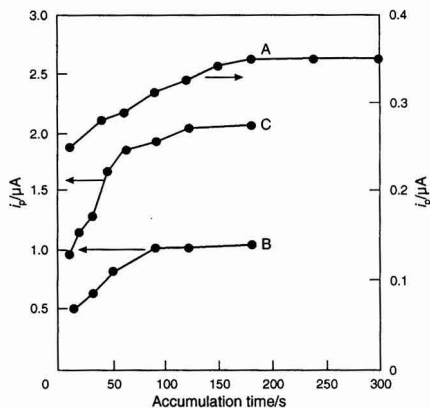

Fig. 5 Effect of accumulation time (t_a) on the differential pulse stripping peak current. A, 1.00×10^{-8} mol l^{-1} Tl^{III}, B, 2.00×10^{-6} mol l^{-1} Tl^{III} and C, 1.00×10^{-5} mol l^{-1} Tl^{III}. Conditions as in Fig. 3.
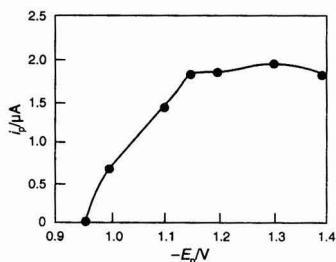

Fig. 6 Effect of reduction potential, E_d, on the differential pulse stripping peak current. $c_{Tl^{III}} = 1.00 \times 10^{-5}$ mol l^{-1}. Conditions as in Fig. 3.

At potentials more negative than this value, the reduction of HOx may interfere.[20] Further investigations showed that, for the highest concentration of 1.00×10^{-5} mol l^{-1} used here, the total reduction of the accumulated Tl^{III} was accomplished even if no reduction time period, t_d, was enforced. However, to ensure complete reduction, a t_d of 10 s was allowed for in all experiments.

Effect of Tl^{III} concentration

The variation of the differential pulse anodic stripping peak current with Tl^{III} concentration was studied for concentrations ranging from 5.00×10^{-10} to 1.60×10^{-5} mol l^{-1}. For the concentration region of 5.00×10^{-10}–1.00×10^{-8} mol l^{-1}, a linear plot was observed for a 2 min accumulation. Linear regression analysis gave an equation,

$$i_p \,(\mu A) = 0.0536 + 0.0147c \,(nmol \, l^{-1})$$

and a correlation coefficient of 0.995. For the concentration region 1.00×10^{-8}–8.00×10^{-8} mol l^{-1}, a curved plot was obtained with negative deviation from the above straight line (not shown). Between 8.00×10^{-8} and 1.00×10^{-5} mol l^{-1} Tl^{III}, another linear region with regression equation

$$i_p \,(\mu A) = 0.244 + 0.171c \,(\mu mol \, l^{-1})$$

and correlation coefficient of 0.994 was obtained. Beyond 1.00×10^{-5} and up to 1.60×10^{-5} mol l^{-1} Tl^{III}, a curved plot with negative deviation was again observed.

The above observations for the calibration plot can be explained, as follows. Two linear regions arose because of the different factors governing accumulation. At the lower concentration region for 2 min accumulation, the uptake of Tl^{III} of the HOx-MCPE surface was still kinetically controlled. This is supported by the data of Fig. 5(a) which shows that for a Tl^{III} concentration of 1.00×10^{-8} mol l^{-1} and 2 min accumulation, the peak current was still in the rising portion of the plot, indicating kinetic control. However, for the linear portion at higher concentrations, equilibrium was reached after a 2 min accumulation (see Fig. 5). In between these two regions, curvature was due to mixed control of the Tl^{III} accumulation. Above a Tl^{III} concentration of 1.00×10^{-5} mol l^{-1}, saturation of the surface HOx-complexing sites was probably the reason for flattening of the calibration plot. Except for the higher sensitivity for Tl^{III} accumulation, these observations were similar to those for Tl^I accumulation, found previously,[20] for the same reasons.

For a 2 min accumulation, the detection limit was estimated to be 2.30×10^{-10} mol l^{-1} (0.047 ppb) Tl^{III} based on $3s$ of the blank. The precisions obtained for 10 replicate determinations of 1.00×10^{-6} and 1.00×10^{-7} mol l^{-1} Tl^{III} were 2.8 and 4.8% (s_r), respectively.

Interferences

Under the developed set of optimized conditions, the method was used for the determination of 1.00×10^{-6} mol l^{-1} Tl^{III}, with 1 min accumulation, in the presence of selected metal ions. No interferences were observed from the additions of 1.00×10^{-3} mol l^{-1} K$^+$, Na$^+$, 1.00×10^{-5} mol l^{-1} Al^{III}, Ag^I, Be^{II}, Ca^{II}, Cd^{II}, Cr^{III}, Fe^{III}, Hg^{II}, Mn^{II}, Ni^{II}, Pb^{II}, Sb^{II}, Zn^{II}, Mg^{II}, 2.00×10^{-6} mol l^{-1} Cu^{II} and Bi^{III}. However, the presence of 1.00×10^{-5} mol l^{-1} of Cu^{II} and Bi^{III} in the Tl^{III} solution resulted in 53 and 84% depressions of the stripping peak, respectively. Even though Bi^{III} interfered at this concentration, no stripping peak for Bi^{III} was observed. In contrast, copper gave an anodic stripping peak with peak potential at -0.76 V.

Organic and other inorganic materials were also examined for possible interferences. For the determination of 1.00×10^{-6} mol l^{-1} Tl^{III} with 1 min accumulation, no interference was

found after addition of 1.00×10^{-3} mol l^{-1} KBr, NH$_4$Cl, (NH$_4$)$_2$C$_2$O$_4$, (NH$_2$)$_2$CO, ammonium tartrate, sodium citrate, diethyldithiocarbamate and 5.00×10^{-4} mol l^{-1} NH$_4$SCN. It was also found that 5.00×10^{-4} mol l^{-1} NH$_2$OH·HCl completely reduced Tl^{III} to Tl^I under the experimental conditions. Furthermore, the presence of 4.00×10^{-5} mol l^{-1} EDTA (disodium salt) completely masked Tl^{III} from forming Tl(Ox)$_3$ with the surface HOx-groups and caused the complete disappearance of the stripping peak. The addition of 6.00×10^{-5} mol l^{-1} 1,10-phenanthroline (phen) and 1.00×10^{-3} mol l^{-1} NH$_4$SCN were found to suppress the stripping peak by 40 and 60%, respectively, due to competitive complexation between SCN$^-$, phen and surface HOx groups with Tl^{II}.

Interferences from reducing agents were overcome by digesting samples with *aqua regia* or saturated bromine water. Interferences from Cu^{II} and Bi^{III} can be eliminated by masking with ammonium tartrate, sodium citrate or DDTC. For example, in the determination of 1.00×10^{-6} mol l^{-1} Tl^{III}, the

Table 1 Determination of thallium added to the USEPA water quality control sample WP 386*

Tl^I added/μg	Tl^{III} added/μg	Total Tl found/μg†	s_r (%)	Recovery of Tl added (%)
0.383	0.383	0.743	3.54	97.0
0.894	0.894	1.742	2.05	97.4
1.277	1.277	2.580	1.70	101.0

* This water sample contains the following elements in μg l^{-1}: Al, 500; As, 100; Be, 100; Cd, 25; Co, 100; Cr, 100; Cu, 100; Fe, 100; Hg, 5.0; Mn, 100; Ni, 100; Pb, 100; Se, 25; V, 250; and Zn, 100.
† Mean value of five determinations.

Table 2 Comparison of peak current, i_p(μA), in different matrices at various Tl^{III} concentrations* The values in the parentheses represent the percentage of peak current reduction compared with the peak current obtained in Millipore water.

	Differential pulse stripping peak current/μA				
Amount of Tl^{III}/μg spiked Matrix	0.35	0.60	1.00	1.60	2.40
Millipore water	0.12	0.21	0.34	0.50	0.81
Digested sea-water†	0.11	0.13	0.20	0.28	0.39
	(8.3%)	(38%)	(41%)	(44%)	(52%)
Undigested sea-water‡	—	0.086	0.13	0.18	0.22
		(59%)	(62%)	(64%)	(73%)

* t_a = 2 min, t_d = 10 s.
† Digestion following procedure given in Experimental section.
‡ 20 ml sea-water plus 5 ml B–R buffer (pH = 4.56) (final pH was adjusted to 4.56 with 2.5 mol l^{-1} NaOH).

Table 3 Determination of thallium in spiked samples. ND = Not detected.

Sample	Tl^I added/μg	Tl^{III} added/μg	Total Tl found/μg*	s_r (%)	Recovery (%)
Sea-water	0	0	ND	—	—
	0.383	0.383	0.741	6.24	96.7
	0.894	0.894	1.921	6.06	107.4
	1.533	1.533	2.856	6.04	93.2
Human urine	0	0	ND	—	—
	0.894	0.894	1.752	5.14	98.0
	1.533	1.533	3.209	4.90	104.7
	2.555	2.555	5.355	4.00	104.8

* Average of four determinations.

interference caused by 1.00×10^{-5} mol l^{-1} Cu^{II} was removed by adding 1.00×10^{-3} mol l^{-1} DDTC. Furthermore, addition of 1.00×10^{-3} mol l^{-1} sodium citrate or ammonium tartrate masked 1.00×10^{-5} mol l^{-1} Bi^{III} without affecting the Tl^{III} response.

Practical Applications

The recommended procedure was employed for the determination of total thallium in a USEPA water quality control sample (WP 386) after oxidizing the Tl^I to Tl^{III}.[5] This sample did not contain any thallium so it was spiked with appropriate amounts of Tl^I and Tl^{III}. After treatment, the total thallium was determined in replicate using the linear regression equation obtained from a series of standard solutions. From Table 1, it can be observed that results were good, with good recoveries and precisions.

The proposed method was also applied to the determination of thallium in sea-water and human urine samples. Our preliminary studies indicated that thallium was not detected in both samples. Therefore, for the purpose of method testing, both the digested sea-water and urine samples were spiked with appropriate amounts of Tl^I and Tl^{III}. For accurate determinations, calibration plots were prepared using backgrounds as similar as possible to the actual samples. The importance of the matrix effect was demonstrated by the data in Table 2. The data showed differential pulse stripping peak currents for Millipore water, digested and undigested sea-water, containing various spiked amounts of Tl^{III}. It can be seen that, in all cases, peak currents decreased in the order of Millipore water > digested sea-water > undigested sea-water. The current reductions in sea-water compared with Millipore water could arise from two sources. The presence of organic compounds and complexing species in sea-water could bind some Tl^{III} and reduce its accumulation by HOx. Also, some of the HOx sites on the electrode surface may be occupied by substances present in sea-water, and, thus, may not be available for binding Tl^{III}. Digestion of the sea-water destroyed most of the organic compounds, which explained the smaller current reduction (referred to Millipore water) in digested sea-water compared to undigested sea-water.

Therefore, for the determination of the spiked sea-water and urine samples, calibration plots were obtained using standards prepared in digested sea-water and urine as backgrounds. The results, for various amounts of spiked Tl^I and Tl^{III}, are summarized in Table 3. It can be observed that good recoveries and precisions were obtained.

Conclusion

A simple, selective and sensitive method was developed for the determination of thallium. The detection limit was 2.3×10^{-10} mol l^{-1} (0.047 ppb) (S/N = 3) for a 2 min accumulation. This detection limit is comparable to some[9,28] and better than most[2,6,29,30] other methods reported. However, even this low value achieved was not good enough for direct analysis of unpolluted sea-water and urine. For these samples, a prior concentration step, by extraction or ion exchange, is usually employed.[8,31]

References

1 Merian, E., in *Metals and Their Compounds in the Environment*, VCH, Weinheim, 1991, p. 1227.
2 Griepink, B., Sager, M., and Tölg, G., *Pure Appl. Chem.*, 1988, **60**, 1425.

3 Smith, I. C., and Carson, B. L., in *Trace Metals in the Environment, Thallium*, Ann Arbor Science Publishers, Ann Arbor, MI, 1977, vol. 1.

4 Zitko, V., *Sci. Total Environ.*, 1985, **4**, 185.

5 Onishi, H., in *Photometric Determination of Traces of Metals, Part IIB: Individual Metals, Magnesium to Zirconium*, John Willey & Sons, New York, 4th edn., 1989, pp. 419–448.

6 Liem, I., Kaiser, G., Sager, M., and Tölg, G., *Anal. Chim. Acta*, 1984, **158**, 179.

7 Elson, C. M., and Albuquerque, C. A. R., *Anal. Chim. Acta*, 1982, **134**, 393.

8 Batley, G. E., and Florence, T. M., *J. Electroanal. Chem.*, 1975, **61**, 205.

9 Bonelli, J. E., Taylor, H. E., and Skogerboe, R. K., *Anal. Chim. Acta*, 1980, **118**, 243.

10 Ciszewski, A., and Lukaszewski, Z., *Talanta*, 1985, **32**, 1101.

11 Ciszewski, A., *Talanta*, 1985, **32**, 1051.

12 Wikiel, K., and Kublik, Z., *J. Electroanal. Chem.*, 1985, **165**, 71.

13 Ciszewski, A., and Lukaszewski, Z., *Talanta*, 1988, **35**, 191.

14 Lukaszewski, Z., Ciszewski, A., Lukaszewski, Z., and Szymanski, A., *Chem. Anal. (Warsaw)*, 1987, **32**, 903.

15 Baldwin, R. P., Christensen, J. K., and Kryger, L., *Anal. Chem.*, 1986, **58**, 1790.

16 Kalcher, K., *Electroanalysis (N.Y.)*, 1990, **2**, 419.

17 Murray, R. W., in *Electroanalytical Chemistry*, ed. Bard, A. J., Marcel Dekker, New York, vol. 13, 1984, pp. 191–368.

18 Wang, J., Greene, B., and Morgan, C., *Anal. Chim. Acta*, 1984, **158**, 15.

19 Prabhu, S. V., and Baldwin, R. P., *Anal. Chem.*, 1987, **59**, 1074.

20 Cai, Q., and Khoo, S. B., *Electroanalysis (N.Y.)*, in the press.

21 Analytical Methods Committee, *Analyst*, 1960, **85**, 643.

22 Adams, Ralph N., in *Electrochemistry at Solid Electrodes*, Marcel Dekker, New York, 1969, pp. 26, 121.

23 Cai, Q., and Khoo, S. B., *Anal. Chim. Acta*, 1993, **276**, 99.

24 Vydra, F., Stulik, K., and Julakova, E., in *Electrochemical Stripping Analysis*, Translated by Tyson, J., Ellis Horwood, Chichester, 1976, p. 203.

25 Hollingshead, R. G. W., *Oxine and Its Derivatives*, Butterworths, London, 1954, vol. 2, p. 461.

26 Baes, C. F., and Mesmer, R. E., in *The Hydrolysis of Cations*, Wiley, New York, 1976, p. 328.

27 Gao, Z., Wang, G., Li, P., and Zhao, Z., *Anal. Chem.*, 1991, **63**, 953.

28 Wang, J., and Lu, J., *Anal. Chim. Acta*, 1993, **282**, 329.

29 Barisci, J. N., and Wallace, G. G., *Electroanalysis (N.Y.)*, 1992, **4**, 139.

30 Diewald, W., Kalcher, K., Neuhold, C., Svancara, I., and Cai, X., *Analyst*, 1994, **119**, 299.

31 Calderoni, G., and Ferri, T., *Talanta*, 1982, **29**, 371.

Ion-selective Electrodes Based on Calix[4]arene Tetraester in the Determination of Formaldehyde *via In Situ* Generation of Ionic Lipophilic Hydrazone

Wing Hong Chan and Ruo Yuan

Department of Chemistry, Hong Kong Baptist University, 224 Waterloo Road, Kowloon, Hong Kong

A formaldehyde-selective electrode was designed based on the host–guest interaction between *p-tert*-butylcalix[4]arene tetraester and lipophilic hydrazone generated *in situ* from formaldehyde and a modified Girard's reagent G2. The poly(vinyl chloride) membrane electrode contains 4.5% m/m of a tetraester derivative of calix[4]arene as the neutral carrier and dioctyl phthalate as the plasticizer. At pH 5.4, the electrode exhibits a dicationic Nernstian response in the range 4×10^{-5}–0.1 mol l^{-1} formaldehyde with a slope of 32.4 mV per decade. In contrast, at pH 9.2, the electrode shows a near Nernstian response with a slope of 50.3 mV per decade in a narrower working concentration range. The electrode has a fast response time and a long working lifetime. The viability of using the electrode for the micro-determination of formaldehyde was also demonstrated.

Keywords: Formaldehyde determination; modified Girard's reagent; ion-selective electrode; calixarene ionophore; host–guest interaction

Introduction

Formaldehyde has been identified as a combustion product from many sources, including fuel combustion in automobiles, and is a constituent of cigarette smoke. Because of its potential toxic effect, it is regarded as a principal indoor pollutant. Therefore, the development of simple and sensitive methods of determining trace amounts of formaldehyde has been continued to be a topic of active investigation.[1,2] Various spectrophotometric[3-5], HPLC[6-8] and voltammetric[9] methods have been established for the determination of formaldehyde.

Calixarenes, which are cyclic oligomers of phenol–formaldehyde condensates, have attracted considerable attention in host–guest chemistry. A wide range of analytical methods employing the calixarene derivatives as active sensing materials have emerged.[10] Recently, we have designed a novel type of aldehyde-selective electrode based on the host–guest interaction between *p-tert*-butylcalix[4]arene ionophore and hydrazone generated *in situ* from a long-chain aldehyde exemplified by heptanal and Girard's reagent P.[11] However, this method is inapplicable to the determination of low relative molecular mass aldehydes, including formaldehyde, presumably owing to the weak interaction between the analyte and the calixarene host. This paper describes our efforts to extend the use of calix[4]arene ionophores as electrochemical sensors in formaldehyde determination.

Experimental

Apparatus

Potentiometric measurements were made with an Orion Model SA720 digital ionanalyser. Calix[4]arene tetraester–poly(vinyl chloride) (PVC) matrix membrane electrodes (see below) in conjunction with an internal Ag–AgCl reference electrode and 1×10^{-3} mol l^{-1} formaldehyde–Girard's reagent G2 adduct (FGA2) at pH 5.4 as the reference solution were used. An Orion saturated calomel electrode (SCE) (Model 9006) served as the external electrode. All measurements were made at a constant temperature in the range 22–25 °C. The pH of the solution was measured with an Orion Model 231 combined pH meter. ^{1}H NMR spectra were recorded on a Jeol JMN-EX 270 NMR spectrometer. Elemental analyses were performed at the Shanghai Institute of Organic Chemistry, Chinese Academy of Science.

Reagents

All reagents were of analytical-reagent grade. Doubly distilled water was used throughout for the preparation of all solutions. High relative molecular mass PVC and ethyl bromoacetate were purchased from Aldrich (Milwaukee, WI, USA) and 36.5% formaldehyde solution from Riedel-de Haën (Seelze, Germany). Hydrazine hydrate, bis(2-ethylhexyl) phthalate, *p-tert*-butylcalix[4]arene, *p-tert*-butylpyridine and 3- and 4-methylpyridine were obtained from Fluka (Buchs, Switzerland). The ethoxycarbonyl methyl derivatives were synthesized according to the literature.[12]

Electrode Fabrication

The general procedure for casting the electrode membranes and fabrication of the electrode were described in detail elsewhere.[11] The membrane used consisted of PVC (140 mg, 35.2% by mass), bis(2-ethylhexyl) phthalate (240 mg, 60.3% by mass) and *p-tert*-butylcalix[4]arene tetraester (18 mg, 4.5% by mass). The PVC membrane electrodes were preconditioned by soaking in 1×10^{-3} mol l^{-1} FGA2 solution for several hours before use.

Calibration

A representative electrochemical cell for emf measurements is

Ag–AgCl FGA2 solution (10⁻³ mol l⁻¹)	PVC–calixarene membrane electrode	sample or standard solution	saturated calomel reference electrode

For calibration, 0.1 mol l^{-1} FGA solutions were prepared separately by reaction of the corresponding Girard's reagents (*i.e.*, G1–G4) with formaldehyde. Subsequently, after appropriate dilution with ammonium acetate solution, a series of standard solutions containing 0.01 mol l^{-1} ammonium acetate and a concentration range of 0.1–4 × 10^{-5} mol l^{-1} FGAs were obtained. Aliquots of 50 ml of these standard solutions were used for ion-selective electrode measurements. The steady cell emf readings (mV) were recorded. Calibration graphs were constructed by plotting the potential readings against the logarithm of the concentration of the adduct solution.

Micro-determination of Formaldehyde

For the micro-determination of formaldehyde, standard solutions of formaldehyde in the range 1 × 10^{-2}–1 × 10^{-4} mol l^{-1} were prepared. To 10 ml of the standard formaldehyde solution in a 25 ml beaker with a magnetic stirrer bar, Girard's reagent G2 (approximately 2–5 equiv. or 5 mg for concentrations of formaldehyde below 10^{-3} mol l^{-1}) was added and the mixture was stirred for 1 h. Subsequently, a sufficient amount of solid ammonium acetate was introduced to adjust the pH of the solution to 5.4. The solutions were then ready for potentiometric measurement.

Results and Discussion

Derivatization Agents

Our previously described electrode system based on a calix[4]arene tetraester derivative (Calix) worked extremely well for long-chain aldehydes as exemplified by heptanal. However, the electrode responded fairly poorly with the hydrazone generated *in situ* from formaldehyde and Girard's reagent P (G1). Not only did the slope of the calibration graph deviate substantially from the Nernst equation, but also the working concentration range was restricted to 1 × 10^{-3}–0.1 mol l^{-1} formaldehyde solution [Fig. 1(C)]. The poor performance of the Calix electrode with low relative molecular mass aldehydes is attributable to the following two reasons. First,

the high water solubility of the adduct (FGA1) from Girard's reagent P (G1) and formaldehyde leads to unfavourable partitioning between the PVC matrix and water, which would adversely affect the detection limit of the method. Second, it is conceivable that the sensitive response of the Calix electrode to the heptanal adduct is due to the favourable host–guest interaction of the *endo* complex [Fig. 2(A)]. In this complex form, the long alkyl chain of the aldehyde interacts favourably with the hydrophobic wall of the calixarene molecule whereas the hydrophilic interaction between the pyridinium nitrogen and carbonyl group reinforces the host–guest interaction. By shortening the alkyl chain the aldehyde adduct, the host–guest interaction is greatly reduced regardless of whether *exo* or *endo* complexes can be formed [Fig. 2(B) and (C)]. If this is the reason for the inapplicability of the electrode to detect formaldehyde effectively, the host–guest interaction between the Calix host and FGA in the *exo* complex could be enhanced by incorporating a hydrophobic carbon moiety on the pyridinium ring [Fig. 2(D)].

With this scenario in mind, we developed a synthetic route for the preparation of three new Girard's type reagents, G2–G4, starting from commercially available substituted pyridine (Scheme 1).[13] The derivatization agents G2–G4 were adequately characterized by high-field ^{1}H NMR spectrometry and elemental analysis. G2: m.p. 168–174 °C (found, C 45.95, H 6.23, N 14.60; calculated for C$_{11}$H$_{18}$N$_3$OBr, C 45.84, H 6.29, N 14.58%). G3: m.p. 159–162 °C (found, C 39.59, H 4.83, N 17.16; calculated for C$_8$H$_{12}$N$_3$OBr, C 39.04, H 4.91, N

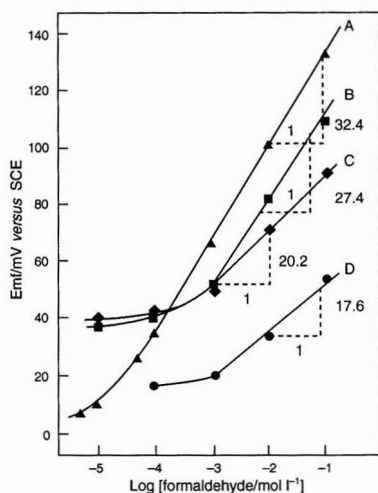**Fig. 1** Potential response of the Calix electrode to different Girard's adducts of formaldehyde: A, FGA2; B, FGA3; C, FGA1; and D, FGA4.
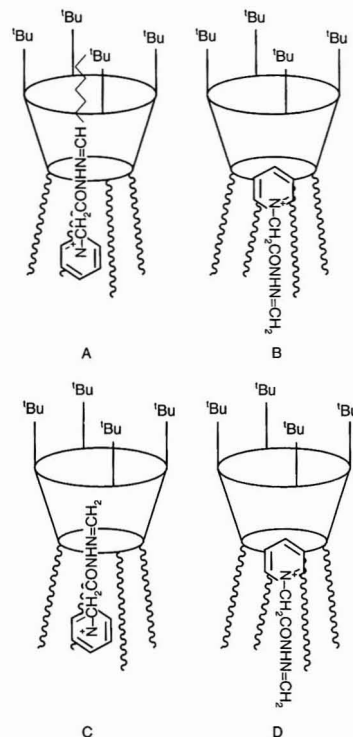

Fig. 2 Structures of Calix–Girard's adduct complexes: A, *endo* complex of Calix–Girard's adduct of heptanal; B, *exo* complex of Calix–FGA1; C, *endo* complex of Calix–FGA1; and D, *exo* complex of Calix–FGA2 (attached chains = –CH$_2$COOEt).

17.07%). G4: m.p. 169–173 °C (found, C 38.45, H 4.89, N 17.68; calculated for $C_8H_{12}N_3OBr$, C 39.04, H 4.91, N 17.07%).

Response of the Calix Electrode to FGA1–FGA4

Both the lipophilicity of FGAs and the stability of host–guest complexes derived from the Calix host and Girard's reagents G1–G4 are the crucial factors that affected the response of the electrode to the respective hydrazone of formaldehyde. Calibration graphs for the Calix electrode with the four Girard's adducts FGA1–FGA4 were constructed and are depicted in Fig. 1. Several interesting features of the graphs are worthy of comment. First, the calibration graph for FGA2 derived from derivatization agent G2, which contained a *p-tert*-butyl group on the pyridinium ring, exhibited the broadest linear range of formaldehyde concentration, from 4 × 10^{-5} to 0.1 mol l^{-1}. As mentioned above, both the lipophilicity of the adduct and the stability of the host–guest complex (presumably *via* the *exo* complex) benefit from the incorporation of a *p-tert*-butyl moiety on the aromatic ring of the derivatization agent, and this would consequently result in a better response of the electrode. In comparison, incorporating a *p*-methyl group on the pyridinium ring of the Girard's reagent improved the response of the electrode only marginally. Second, the poor response of the electrode to FGA4 was conceivably due to the non-bonding repulsion between the sterically stretching *m*-methyl group of the pyridinium ring and the relatively narrow Calix sheath. Finally, it is surprising that even for the best response calibration graph [*i.e.*, Fig. 1(A)], the slope was far below the Nernst value. This observation was inconsistent with our previous observations.[11] Further, the slope of 32.4 mV per decade observed is indicative of a dicationic character of the detected species (see below).

Effect of pH

In order to maximize the hydrophobic interaction between the Calix and FGA2, the host–guest complex should adopt an *exo* in preference to an *endo* orientation. Under such a circumstance, the basic nitrogen of the hydrazone moiety of the adduct that is exposed outside the Calix sheath will be susceptible to protonation at low pH. When the electrodes were calibrated with FGA2 at different pH values, very different calibration graphs resulted (Fig. 3). Under strongly acidic conditions (pH 2.5), the adduct would be hydrolysed rapidly, especially with dilute solutions. On the other hand, when calibration was carried out at pH 9.2, a nearly Nernstian calibration graph resulted, except that the linearity was inferior to that at pH 5.4. At pH 9.2, the active species in the solution should be the unprotonated hydrazone, and a Nernstian response of the electrode with a slope of 50.3 mV per decade provided evidence for the presence of such a monocationic species. Owing to the ready accessibility of the basic nitrogen of the hydrazone, protonation of the adduct was

apparent at pH 5.4 [Fig. 2(D)]. The slope of the calibration graph of 32.4 mV per decade was consistent with the formation of dicationic species. In contrast to our previous work,[11] for long-chain aldehydes, the corresponding hydrazone would adopt an *endo* orientation with the alkyl chain concealed within the Calix sheath, in which the hydrophobic interaction would be maximized. Under such conditions, the basic nitrogen of the hydrazone group, being completely shielded inside the Calix cavity, does not undergo protonation. Hence the electrode exhibits a perfect Nernstian response over a wide pH range, as reported previously. In the present study, to optimize the sensitivity of the method, all subsequent measurements were made at pH 5.4.

Characteristics of the Calix Electrode With Respect to FGA2

It became obvious that the determination of formaldehyde with the Calix electrode can be realized *via* the *in situ* derivatization of formaldehyde by the tailor-made lipophilic derivatization agent G2. At pH 5.4, the electrode exhibits a Nernstian response in the range 4 × 10^{-5}–0.1 mol l^{-1} with a detection limit of 1.2 × 10^{-5} mol l^{-1}. The electrode has a fast response time. Even for dilute solutions, the electrode exhibited a constant and stable potential within 1 min (Fig. 4).

For a stability study, the electrode was immersed in 1 × 10^{-2} mol l^{-1} solution for 2 h at pH 5.4 and its potential reading was recorded repeatedly at 10 min intervals. The
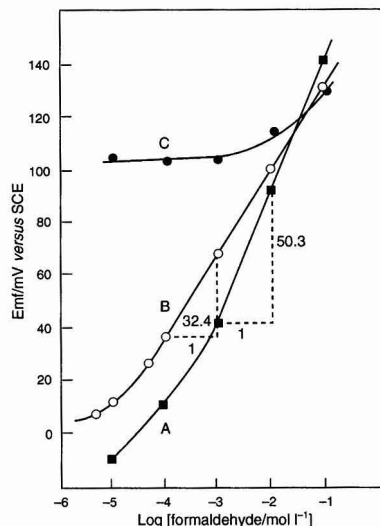
Fig. 3 Effect of pH on the response of the Calix electrode to FGA2: A, 0.01 mol l^{-1} TRIS-HCl buffered solution at pH 9.2; B, 0.01 mol l^{-1} $CH_3CO_2NH_4$ buffered solution at pH 5.4; and C, 0.01 mol l^{-1} H_3PO_4 buffered solution at pH 2.5.

G1 and FGA1 : R^1 = H, R^2 = H   G3 and FGA3 : R^1 = H, R^2 = CH$_3$

G2 and FGA2 : R^1 = H, R^2 = C(CH$_3$)$_3$ G4 and FGA4 : R^1 = CH$_3$, R^2 = H
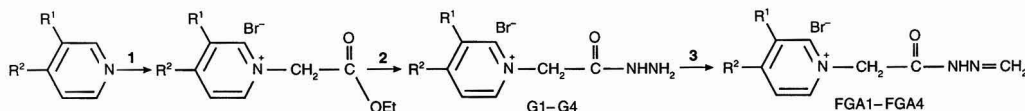
Scheme 1 Reagents: **1**, BrCH$_2$COOEt–EtOH; **2**, NH$_2$NH$_2$·H$_2$O; and **3**, HCHO.

over-all fluctuation was confined to 0.97 mV (standard deviation, $n = 24$). On the other hand, when the electrode was consecutively immersed in 1×10^{-2} and 1×10^{-3} mol l^{-1} FGA2 solution alternatively six times, reproducibly steady readings were obtained throughout (Table 1).
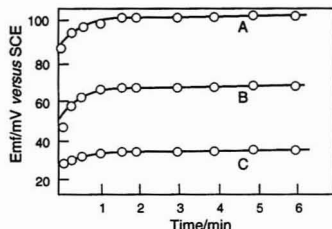
Fig. 4 Response time of the Calix electrode A to different concentrations of FGA2 solutions at pH 5.4: A, 1×10^{-2}; B, 1×10^{-3}; and C, 1×10^{-4} mol l^{-1}.

Table 1 Response of the electrode to standard adduct solutions (FGA2) at two different concentrations by alternative measurements over 2 h

Measurement No.	Emf/mV	
	1×10^{-2} mol l^{-1}	1×10^{-3} mol l^{-1}
1	108.7	66.4
2	107.8	66.5
3	107.5	65.9
4	108.3	66.7
5	108.4	67.1
6	108.1	65.8

Table 2 Selectivity characteristics of the Calix electrode in the determination of formaldehyde

Interfering species	Concentration of interfering species/mol l^{-1}	$K_{i,j}^{Pot}$
CH$_3$CH$_2$OH	1×10^{-1}	2.7×10^{-4}
CH$_3$CH$_2$CH$_2$CH$_2$NH$_2$	1×10^{-3}	8.7×10^{-2}
CH$_3$CH$_2$CH$_2$CHO	1×10^{-3}	6.8
NH$_4^+$ (CH$_3$CO$_2$NH$_4$)	1×10^{-1}	3.4×10^{-4}
K$^+$ (KCl)	1×10^{-2}	2.6×10^{-3}
Na$^+$ (NaCl)	5×10^{-5}	8.5

| | 1×10^{-3} | 2.4×10^{-2} |

Table 3 Determination of formaldehyde with the Calix electrode

Taken	Formaldehyde concentration/mol l^{-1} Found	Error (%)
1×10^{-4}	1.05×10^{-4}	+5.0
3×10^{-4}	3.13×10^{-4}	+4.3
5×10^{-4}	4.80×10^{-4}	−4.0
7×10^{-4}	7.11×10^{-4}	+1.6
1×10^{-3}	0.98×10^{-3}	−2.0
3×10^{-3}	3.14×10^{-3}	+4.7
5×10^{-3}	4.77×10^{-3}	−4.6
8×10^{-3}	7.91×10^{-3}	−1.1
1×10^{-2}	1.05×10^{-2}	+5.0

The electrode proved to have a long lifetime. After being used repeatedly for a period of 2 months, its response to the analyte was almost identical with that of a new electrode in terms of response slope and working range.

To define the scope of this electrode method for formaldehyde determination, the characteristics of electrodes towards common organic and inorganic species were studie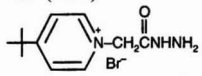d using the fixed interference method. The corresponding selectivity coefficients ($K_{i,j}^{Pot}$) for foreign species were calculated and are given in Table 2. Primary amines and the derivatizing agent G2 interfered only slightly with the determination. Hence in the micro-determination of formaldehyde, a slight excess of the derivatizing agent will not affect the accuracy of the method. As expected, and in agreement with our previous findings, the electrode exhibited a preference towards high molecular mass aldehydes. With regard to the interference of inorganic species, sodium ion matched the hydrophilic cavity of the Calix host molecule well and interfered significantly with the determination. In contrast, the interference effects of potassium and ammonium ions were not important; therefore, ammonium acetate solution was used to adjust the ionic strength and control the pH of the solution.

Mico-determination of Formaldehyde

Under simple and specific conditions, different concentrations of formaldehyde solutions were derivatized to the hydrazone with G2 prior to potential measurements. By employing the calibration graph established, the concentrations of formaldehyde solutions were determined. Table 3 demonstrates the feasibility of using the Calix electrode and the lipophilic derivatization agent G2 in the micro-determination of formaldehyde. The results show that the minimum detectable concentration of formaldehyde is 1×10^{-4} mol l^{-1} or as little as 30 µg of formaldehyde can be determined accurately by the method. The errors of all determinations are well within ±5%.

References

1 Clement, R. E., Koester, C. J., and Eiceman, G. A., *Anal. Chem.*, 1993, **65**, 85R.
2 Fox, D. L., *Anal. Chem.*, 1993, **65**, 156R.
3 Dickinson, R. G., and Jacobsen, N. W., *J. Chem. Soc., Chem. Commun.*, 1970, 1719.
4 Nair, J., and Gupta, V. K., *Talanta*, 1979, **26**, 962.
5 Matsuhisa, K., and Ohzeki, K., *Analyst*, 1986, **111**, 175.
6 Magin, D. F., *J. Chromatogr.*, 1980, **202**, 255.
7 Dahlgran, J. R., and Jameson, M. N., *J. Assoc. Off. Anal. Chem.*, 1988, **71**, 560.
8 Sesana, G., Nano, G., Baj, A., and Balestreri, S., *Fresenius' Z. Anal. Chem.*, 1991, **339**, 485.
9 Cai, X., and Kalcher, K., *Electroanalysis*, 1994, **6**, 397.
10 Chan, W. H., Lee, A. W. M., and Wang, K., *Analyst*, 1994, **119**, 2809 and references cited therein.
11 Chan, W. H., Cai, P. X., and Gu, X. H., *Analyst*, 1994, **119**, 1853.
12 Mckervey, M. A., Seward, E. M., Ferguson, G., Ruhl, B., and Harris, S. J., *J. Chem. Soc., Chem. Commun.*, 1985, 388.
13 Furniss, B. S., Hannaford, A. J., Smith, W. G., and Tatchell, A. R., *Vogel's Textbook of Practical Organic Chemistry*, Longman, Harlow, 5th edn., 1989, p. 434.

Voltammetric Behaviour of Vitamin B₁ (Thiamine) at a Glassy Carbon Electrode and Its Determination in Multivitamin Tablets Using Anion-exchange Liquid Chromatography With Amperometric Detection Under Basic Conditions

John P. Hart, Michael D. Norman and Stephen Tsang

Faculty of Applied Sciences, University of the West of England, Coldharbour Lane, Frenchay, Bristol, UK BS16 1QY

Vitamin B₁ (thiamine) was found to give one anodic peak and three anodic peaks by cyclic voltammetry at a planar glassy carbon electrode, when treated with 0.1 mol dm⁻³ sodium hydroxide for 5 and 30 min, respectively. The reverse cyclic voltammograms did not show any cathodic peaks. The electro-active form of thiamine was subjected to cyclic voltammetric studies under a variety of solution conditions. The effect of pH was investigated over the range pH 7.0 to 12.5. The magnitudes of the αn_a values suggested that the initial oxidation reaction of thiamine involved the loss of one electron and the product of this reaction is likely to be a disulfide. The electrode reaction was found to be adsorption-controlled when only phosphate buffer was used. However, when acetonitrile was added to this supporting electrolyte at concentrations of 17.5 and 20% v/v the peak current became diffusion-controlled. A convenient and rapid method of analysis for two different multivitamin tablet formulations was developed. After a simple pre-treatment procedure, extracts were analysed using HPLC with a wall-jet amperometric detector. The results of the analyses suggest that the proposed method has promise for the routine determination of vitamin B₁ in the products examined.

Keywords: Vitamin B₁; cyclic voltammetry; liquid chromatography; amperometric detection; glassy carbon electrode

Introduction

Vitamin B₁, thiamine (A), is a water-soluble vitamin. A deficiency of this substance in the diet results in the disease known as *Beri Beri*.[1]
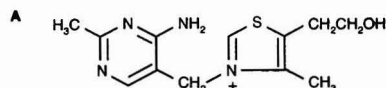
A plethora of pharmaceutical products contain thiamine. These range in complexity from single vitamin to multivitamin formulations. In the latter case, analytical methods for determination of the vitamin need to be both selective and sensitive owing to the presence of potential interferences and to the low concentrations present. Hart and co-workers[2-7] have focussed attention on the trace measurement of a variety of vitamins using liquid chromatography with electrochemical detection (LCEC). This is now recognized as a powerful technique for trace determinations in complex matrices. A method employing a coulometric detector was developed for the measurement of both normal and sub-normal circulating levels of vitamin K₁ in human plasma;[2,3] the possibility of measuring vitamin B₆ in plasma with a coulometric detector was also reported.[4] A wall-jet amperometric detector was employed for the determination of vitamin A₁ in human serum.[5] It was also shown that the method could be adapted to measure this vitamin in a pharmaceutical product.[6] The same type of detection system was exploited for the measurement of vitamins D₂ and D₃ in multivitamin tablets.[7] In all of these applications the columns contained reversed-phase packing materials.

One of the aims of the present study was to investigate the possibility of using an anion-exchange column, together with a wall-jet amperometric detector, for vitamin B₁ determinations in multivitamin tablets. This approach seemed feasible as previous reports[8-10] had indicated that the vitamin was electro-active under alkaline conditions where, an anionic species predominates.[11,12] Electrochemical studies on thiamine have been carried out with a dropping mercury electrode[8,9] and a carbon paste electrode.[10] Glassy carbon has been used to electrochemically generate a fluorescent thiamine derivative in a flow-injection system where the intensity of fluorescence was used for the quantification of the vitamin.[13] However, there have been no reports on the electrochemical detection of thiamine at a glassy carbon electrode following liquid chromatography.

In previous reports[2-6] we have shown that cyclic voltammetry could be readily utilized to obtain the optimum solution conditions for electrochemical detection. It was revealed that the pH and ionic strength of buffer, as well as organic solvent strength, can exert considerable influence on the electrode reaction at glassy carbon electrodes. Therefore, cyclic voltammetry was employed in the first part of the present investigation both for optimization purposes and also to obtain information on the nature of the oxidation process. The results of these studies were then used in the development of an LCEC assay for vitamin B₁ in multivitamin preparations. This paper describes the results of our studies.

Experimental

Chemicals and Reagents

All chemicals were of analytical-reagent grade unless stated otherwise. Vitamin B₁ was purchased from Sigma, Poole, Dorset, UK.

The supporting electrolytes used for the cyclic voltammetric studies were prepared by mixing stock solutions of 0.2 mol dm⁻³ trisodium orthophosphate with 0.2 mol dm⁻³

disodium orthophosphate, or 0.2 mol dm^{-3} sodium dihydrogen orthophosphate with 0.2 mol dm^{-3} disodium orthophosphate to give pH values between 7.0 and 11.0. Sodium hydroxide (0.1 mol dm^{-3}) was used to extend the pH range of the study. These solutions were then used to prepare standard solutions containing 5×10^{-4} mol dm^{-3} vitamin B$_1$ at the appropriate pH, ionic strength and acetonitrile concentration.

Benerva vitamin B compound tablets were manufactured by Roche (Welwyn Garden City, UK) and contained vitamin B$_1$ (1 mg), vitamin B$_2$ (1 mg), vitamin B$_3$ (15 mg), lactose, starch, talc, sucrose, and magnesium stearate.

'One-a-day' multivitamin tablets with iron were obtained from 'Superdrug' (Croydon, UK) and contained vitamin A (750 µg), vitamin B$_1$ (2 mg), vitamin B$_2$ (2 mg), vitamin B$_3$ (20 mg), vitamin C (30 mg), vitamin D$_3$ (2.5 µg), vitamin E (2 mg), iron (12 mg), folic acid (300 µg), dicalcium phosphate (282 mg), sucrose, talc, yeast, and starch.

Apparatus

Cyclic voltammograms were recorded with an Eco-Chemie Autolab (Utrecht, The Netherlands) electrochemical analyser in conjunction with a Viglen SL1 PC (London, UK) and on Epson LX-400 dot-matrix printer (Nagano, Japan). A three-electrode cell was employed incorporating a glassy carbon working electrode (area 0.283 cm^2) unless stated otherwise, a Ag/AgCl reference electrode and a platinum wire counter electrode.

Studies involving liquid chromatography with amperometric detection were carried out with a Metrohm 641 VA-Detector together with a wall-jet cell (Metrohm 656 electrochemical detector) (Herisau, Switzerland) containing a glassy carbon working electrode, a gold counter electrode and a Ag/AgCl reference electrode. Sample injections were made through a syringe loading Rheodyne valve (Cotati, CA, USA). Separations were carried out with a polymeric reverse phase anion exchange column (250 × 4.6 mm, particle diameter 5 µm; Jones Chromatography, Hengoed, UK). Chromatograms were recorded on a Servogor 120, BBC Goerz Metrawatt recorder. A Pye Unicam LC-XPD pump (Cambridge, UK) was used to propel the mobile phase through the chromatographic system.

Voltammetric Procedures

A preliminary investigation was carried out to study the effect of time on the cyclic voltammetric behaviour of thiamine in 0.1 mol dm^{-3} sodium hydroxide. A stock solution containing 5×10^{-2} mol dm^{-3} thiamine in de-ionized water was diluted with sodium hydroxide (0.1 mol dm^{-3}) to produce a solution containing 5×10^{-4} mol dm^{-3} of the vitamin. This was then subjected to cyclic voltammetry at selected intervals over a 2 h period (in all studies solutions containing thiamine were protected from light by covering flasks with aluminium foil). The voltammetric conditions were as follows: scan rate, 50 mV s^{-1}; initial potential, 0 V; final potential, +1.2 V. Between successive runs, the working electrode was cleaned by washing with distilled water, polishing the surface with aluminium oxide powder (0.3 µm), rinsing again with distilled water and finally drying with tissue paper. These conditions were used throughout (unless otherwise stated).

The effect of pH on electrochemical behaviour was studied by cyclic voltammetry using solutions containing 5×10^{-4} mol dm^{-3} thiamine. Phosphate buffers in the pH range 7.0–11.0 and 0.1 mol dm^{-3} NaOH were employed for this purpose. The final pH of the solutions was recorded after cyclic voltammetry.

The effect of the strength of phosphate buffer (pH 11.0) was studied in the concentration range 0.02 to 0.1 mol dm^{-3}.

The presence of any adsorption processes was investigated by varying the scan rate over the range 20 to 200 mV s^{-1} for solutions containing 5×10^{-4} mol dm^{-3} thiamine dissolved in 0.02 mol dm^{-3} phosphate (pH 11.0). This was also performed on thiamine solutions containing 10–20% v/v acetonitrile–0.02 mol dm^{-3} phosphate buffer (pH 11.0).

Hydrodynamic voltammetry was performed by injecting 100 ng quantities of the vitamin, dissolved in 20% v/v acetonitrile–0.02 mol dm^{-3} phosphate buffer (pH 11.0), onto the column and varying the potential between 0 and +1.2 V *versus* Ag/AgCl. The mobile phase flow rate was 2 cm^3 min^{-1}.

Determination of Vitamin B$_1$ in Multivitamin Tablets

Benerva vitamin B compound tablets were weighed, then ground to a fine powder with a pestle and mortar. Portions of the powder (about 0.2 g) were treated with 10 cm^3 of 0.1 mol dm^{-3} sodium hydroxide in a glass quickfit tube and shaken for 15 min on a mechanical shaker. After centrifugation for 15 min at 750g, a 0.5 cm^3 aliquot of the supernatant solution was transferred into a 10 cm^3 calibrated flask and made up to the mark with the mobile phase. Aliquots of this final solution were then injected onto the anion-exchange column using a syringe loading Rheodyne valve and a 20 µl loop.

The 'Superdrug' multivitamin with iron tablets were treated as above, except that about 0.4 g of powdered tablet was taken for analysis.

Calibration Graph and Linear Range for LCEC

A series of external vitamin B$_1$ standards was prepared by first dissolving the vitamin in 0.1 mol dm^{-3} sodium hydroxide to give about 1000 µg cm^{-3} and leaving it to react for 30 min. This was subsequently diluted with the mobile phase, 20% v/v acetonitrile–0.02 mol dm^{-3} phosphate buffer (pH 11.0), to produce the required standards. From these a calibration graph of peak current *versus* mass of vitamin B$_1$ injected was constructed over the range 20–250 ng. In this study, the detector was set at an operating potential of +0.7 V *versus* Ag/AgCl, the mobile phase flow rate was 2.0 cm^3 min^{-1}.

Results and Discussion

Cyclic Voltammetric Behaviour of Thiamine at a Glassy Carbon Electrode and Optimization of Conditions

We began our studies by investigating the cyclic voltammetric behaviour of thiamine, dissolved in 0.1 mol dm^{-3} sodium hydroxide, over a 2 h period. Fig. 1(*a*) and (*b*) show cyclic voltammograms of the vitamin, recorded for 5 and 30 min, respectively, after the addition to the sodium hydroxide. When the voltammogram shown in Fig. 1(*a*) was recorded the solution was yellow and clearly only one oxidation peak [Fig. 1(*a*)] was observed. The yellow colour had disappeared by 10 min and all subsequent voltammograms exhibited the three anodic peaks shown in Fig. 1(*b*). The magnitudes of these peaks had reached a maximum by 30 min and were constant for at least 2 h. The reverse scan, obtained by switching the potential after peak C had appeared [Fig. 1(*b*)], did not exhibit any cathodic peaks over the voltage range investigated; this indicated that the overall oxidation process was irreversible. In addition, the potential was switched after peak A [Fig. 1(*b*)] but before the appearance of peak B [Fig. 1(*b*)] and again no peaks were observed on the reverse scan. This procedure was repeated after the appearance of peak B [Fig. 1(*b*)], but before peak C [Fig. 1(*b*)] appeared and no cathodic peaks were observed. This behaviour indicates that all three oxidation processes are irreversible.

B

C
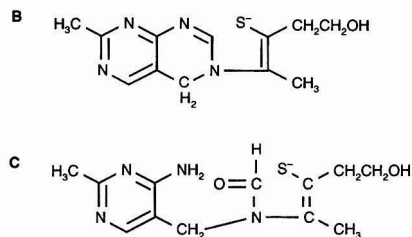
It has been reported[14] that when thiamine is added to media at pH 11 or higher, it is converted to a yellow form (**B**). This species then undergoes hydrolysis to produce the colourless thiol (**C**).

Bearing in mind our initial studies discussed above, it would appear that species (**B**) gave rise to peak A shown in Fig. 1(*a*) and that species (**C**) was responsible for the three peak pattern shown in Fig. 1(*b*). In all of the remaining studies a reaction time of 30 min or greater was used, therefore, species (**C**) should have been present in all of these subsequent investigations.

In order to gain a better understanding of the nature of the electrochemical oxidation of (**C**) at a glassy carbon electrode, and to optimize the conditions for LCEC, detailed cyclic voltammetric studies were performed under a variety of solution conditions.

The effect of pH was studied using a constant concentration of 5.0×10^{-4} mol dm^{-3} with respect to the original thiamine concentration. Fig. 2 shows the plot of peak current for peak A [Fig. 1(*b*)] *versus* pH. Clearly, the magnitude of the peak current increased with increasing pH, but appeared to be reaching a plateau around pH 13. The peak potential of peak
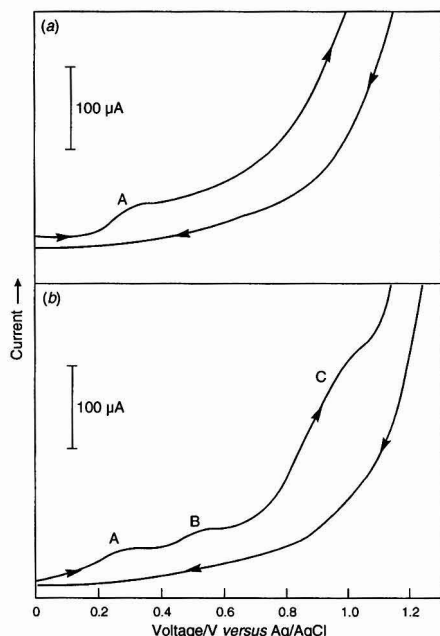

Fig. 1 Cyclic voltammograms of 5×10^{-4} mol dm^{-3} thiamine in 0.1 mol dm^{-3} sodium hydroxide using a glassy carbon electrode: (*a*) after 5 min and (*b*) after 30 min reaction time. Initial potential 0 V *versus* Ag/AgCl; scan rate, 50 mV s^{-1}.

A [Fig. 1(*b*)] did not show any pH dependence. The mean E_P value for the pH range 9.0–13.0 was found to be $+0.330 \pm 0.01$ V *versus* Ag/AgCl. The lack of pH dependence indicates that protons do not participate in the rate determining step of the electrochemical oxidation reaction. This strongly suggests that the species giving rise to peak A [Fig. 1(*b*)] is an anion; this concurs with the earlier report[14] that anionic species (**C**) is formed at high pH values after an appropriate time period.

Cyclic voltammetry was also used to obtain αn_a values[5] (where α is the electron transfer coefficient and n_a is the number of electrons involved in the rate determining step) shown in Table 1. The magnitudes of the αn_a values[5] suggest that one electron is involved in the rate determining step of the oxidation process. Therefore, it may be postulated that species (**C**) initially undergoes a one-electron oxidation at the glassy carbon electrode to produce a free radical [eqn. (1)] which may then be followed by a dimerization reaction to give a disulfide species (**D**) [eqn. (2)].

$$RS^- \rightarrow RS^\cdot + e^- \quad (1)$$

$$2RS^\cdot \rightarrow RSSR \quad (2)$$

D
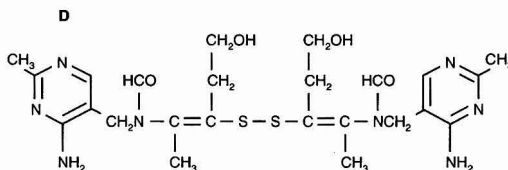
This mechanism seems feasible as it has been reported that mild chemical oxidation of thiamine under alkaline conditions gives rise to species (**D**).[15] However, it has also been found that in alkaline solutions, containing a high methanol content, thiamine (**A**) initially undergoes oxidation at a glassy carbon electrode to produce thiochrome (**E**).[13] If this occurred during the present study, a cyclic voltammogram of (**E**) in 0.1 mol dm^{-3} sodium hydroxide might be expected to exhibit the two peaks B and C shown in Fig. 1(*b*). We examined this possibility but, as shown in Fig. 3, thiochrome showed only one anodic peak and its E_p value did not coincide with either of the peak potentials obtained earlier [Fig. 1(*b*)]. Therefore, it is probable that under the conditions used in the present investigation, the initial electrochemical oxidation of (**C**) produces (**D**). This latter species is then considered to give rise to peak B [Fig. 1(*b*)]. The resulting oxidation product of (**D**) would then be responsible for peak C [Fig. 1(*b*)].

E
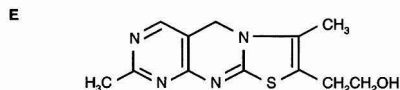
It is clear from Fig. 2 that higher pH values result in larger currents for peak A [Fig. 1(*b*)]. As we required a sensitive and reliable LCEC method it seemed appropriate to choose a supporting electrolyte with high pH and good buffer capacity; phosphate buffer (pH 11.0) was considered suitable as this satisfied both criteria. In addition, this solution was expected to possess the desired properties for the anion-exchange separation step prior to electrochemical detection.

The effect of phosphate ion concentration (at pH 11.0) on peak current was investigated over the range 0.02 to 0.1 mol dm^{-3}. Fig. 4 shows that the largest peak current was to be expected with 0.02 mol dm^{-3} phosphate buffer (pH 11.0), therefore, this medium was used in all further studies.

In order to determine whether or not the initial oxidation process was accompanied by adsorption phenomena, plots of

$i_P/cV^{\frac{1}{2}}$ *versus* $V^{\frac{1}{2}}$ (where i_P = peak current, c = concentration and V = scan rate) were plotted for peak A [Fig. 1(b)] in Fig. 5 A. The positive slope does indeed indicate that species (C) undergoes adsorption at the glassy carbon electrode. As we intended adding acetonitrile to the phosphate buffer for LCEC studies, it was considered necessary to ascertain the effect of this solvent on the voltammetric behaviour of (C). Fig. 5,B shows a plot of $i_P/cV^{\frac{1}{2}}$ *versus* $V^{\frac{1}{2}}$ for the thiamine derivative in 0.02 mol dm^{-3} phosphate buffer (pH 11.0) containing 20% v/v acetonitrile. Clearly, this plot does not exhibit a positive slope and the reaction appears to be diffusion controlled. Actually, the process giving rise to peak A [Fig. 1(b)] was also found to be diffusion controlled in buffer solutions of the same pH and ionic strength, but containing 17.5% v/v acetonitrile. However, when the organic solvent strength decreased to 15% v/v and below, the reaction became adsorption controlled (not shown). As adsorption phenomena can cause passivation of the glassy carbon electrode surface[7] we decided to begin the studies involving LCEC with a mobile phase containing 20% acetonitrile–0.02 mol dm^{-3} phosphate buffer (pH 11.0).

Optimization of LCEC Conditions, Calibration and Linear Range

In order to determine the optimum applied potential for amperometric detection, following liquid chromatography, a hydrodynamic voltammogram was constructed for thiamine (C). Fig. 6 shows two waves in the voltage range studied corresponding to cyclic voltammetric peaks A and B [Fig. 1(b)]. When the applied voltage was increased to more positive values than shown, the background current increased considerably and the baseline equilibration time also increased. Both of these effects were considered undesirable. In addition, the higher the applied potential, the greater the possibility that some interfering species may be oxidized and interfere with the measurement of interest. Therefore, for all further studies we decided to set the potential at +0.7 V *versus* Ag/AgCl which corresponds to the plateau of the second voltammetric wave (Fig. 6).

The effect of acetonitrile concentration on the chromatographic peaks of thiamine as species (C) was studied next. When the solvent strength decreased from 20 to 10%, the retention time increased from 2 to 7.3 min. This was also accompanied by a decrease in peak height and an increase in

Fig. 2 Effect of pH on peak current for peak A. The original concentration of thiamine was 5.0×10^{-4} mol dm^{-3} and the concentrations of the supporting electrolytes were 0.1 mol dm^{-3}.

Table 1 Values of αn_a for peak I_a (cyclic voltammetry) at each pH value

pH	αn_a
9.0	0.74
10.0	0.64
11.0	0.54
12.5	0.47
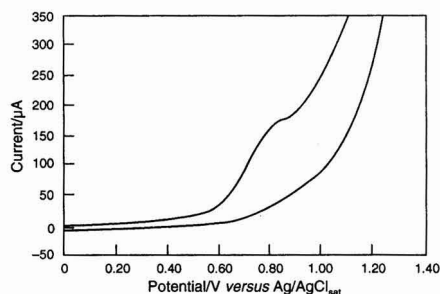
Fig. 3 Cyclic voltammogram of thiochrome in 0.1 mol dm^{-3} sodium hydroxide.

Fig. 4 Effect of buffer strength on peak current for peak A using phosphate buffer pH 11.0 as the supporting electrolyte.
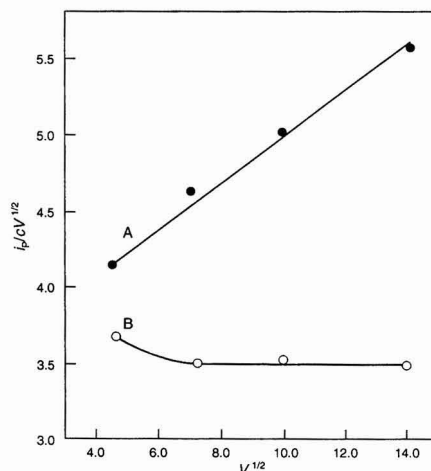
Fig. 5 Current function *versus* $V^{\frac{1}{2}}$ for 5×10^{-4} mol dm^{-3} in (a) 0.02 mol dm^{-3} phosphate buffer pH 11.0 and (b) 20% v/v acetonitrile–0.02 mol dm^{-3} phosphate buffer pH 11.0.
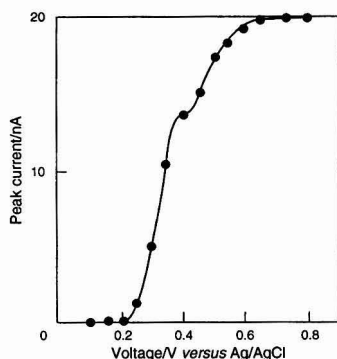
Fig. 6 Hydrodynamic voltammogram for thiamine obtained by injecting 100 ng amounts and increasing the potential in 50 mV increments; mobile phase, 20% v/v acetonitrile–0.02 mol dm^{-3} phosphate pH 11.0.
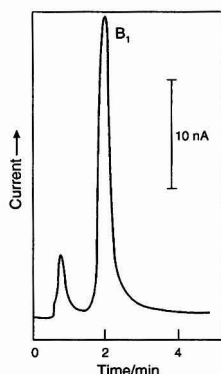
Fig. 7 LCEC chromatogram of the extract from Benerva tablets.
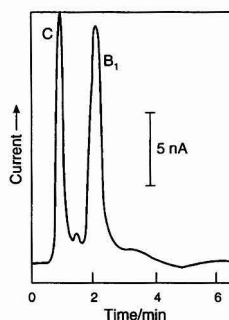
Fig. 8 LCEC chromatogram of the extract from Superdrug with iron tablets.

peak width. This behaviour strongly suggests that the anionic derivative of thiamine undergoes some hydrophobic interaction with the anion-exchange resin. In order to reduce this effect, so that a well defined peak appeared at a short retention time (see Figs. 7 and 8), all further LCEC studies were performed with the mobile phase containing 20% v/v acetonitrile.

The calibration graph of peak current *versus* mass of thiamine injected was found to be linear over the range 20–250 ng. This calibration range was considered to be a suitable for the determination of the vitamin in the multivitamin tablets to be analysed (see later).

Determination of Vitamin B_1 in Multivitamin Tablets by LCEC

The LCEC chromatograms obtained on extracts from the Benerva multivitamin tablets showed a well defined chromatographic peak for vitamin B_1 in its derivatized form, at a retention time of 2 min (Fig. 7). T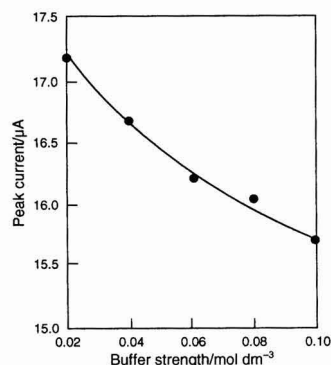he overall method was evaluated by carrying out six replicate determinations on individual portions (about 0.2 g) of the powdered tablets. Each injection of the solution extract, and standards, was performed in duplicate and the mean values were used in subsequent calculations. The results of the determinations are given in Table 2. The thiamine content obtained by our method was slightly higher than that specified; however, this could be explained by the fact that some manufacturers add a slight excess of some vitamins to allow for degradation on storage.[7] The other possible explanation for this observation is that an interfering peak from one, or both, of the other vitamins (B_2 and B_3) may have been unresolved from the thiamine derivative peak. However, this was found not to be the case as neither of these vitamins exhibited a peak with a retention time of 2 min. The s_r was found to be 3.8% ($n = 6$), therefore, these results indicate that the present method shows promise for thiamine determinations in Benerva tablets.

The LCEC chromatograms obtained on extracts from the 'Superdrug' multivitamin tablets with iron also exhibited a well defined peak for the thiamine derivative (Fig. 8). The only other constituent of these tablets, which gave a significant response, was vitamin C but this peak was well resolved from the peak of interest (Fig. 8). This observation was very encouraging as, in addition to thiamine and vitamin C, this particular formulation contained other electro-active water-soluble vitamins (B_2, B_3 and folic acid) as well as electro-active fat-soluble vitamins (A, D and E),[16] and the potentially oxidizable ferrous ions. It should also be mentioned that our LCEC system was operated over a period of at least 8 h. No late eluting peaks were observed on the chromatograms. Table 2 shows the data obtained for six replicate determinations on individual portions (about 0.4 g) of the powdered tablets. The thiamine recoveries for these tablets are lower than obtained for the Benerva product which may be the result of the more complex matrix, e.g., there may be some loss through interaction of the thiamine derivative with the fat-soluble vitamins present in the sample. It is considered unlikely that loss occurs owing to decomposition of species (C)

Table 2 Vitamin B_1 content of multivitamin tablets obtained by proposed LCEC method

| | Sample number | | | | | | | |
	1	2	3	4	5	6	Mean	s_r (%)
Benerva tablets*/mg tablet	1.11	1.14	1.19	1.08	1.17	1.18	1.15	3.8
Superdrug tablets†/mg tablets^{-1}	1.49	1.45	1.50	1.40	1.51	1.49	1.47	2.8

* Manufacturers specification 1 mg per 0.2 g tablet.
† Manufacturers specification 2 mg per 0.8 g tablet.

as this was found to be stable over at least 2 h (see earlier discussion). Further studies to elucidate this problem could include an initial solvent extraction step, prior to the hydrolysis reaction, to remove the fat-soluble vitamins. However, the s_r of 2.8% shows that the method holds promise, particularly as the LCEC step requires only 2 min.

Conclusion

The present study has demonstrated that vitamin B_1 can be converted to an electro-active derivative that undergoes oxidation at a glassy carbon electrode. This electro-active species is considered to exist in anionic form (**C**) under the basic conditions investigated. The initial product of oxidation is considered to be a disulfide species (**D**) which then undergoes further oxidation. The product of this reaction is then oxidized at more positive potentials. It was found that the oxidation processes giving rise to peaks A and B [Fig. 1(*b*)] could be exploited for the amperometric detection of the vitamin following separation on an anion-exchange column. Using this system multivitamin tablets could be analysed after only a simple sample pre-treatment procedure. There was no need to carry out elaborate solvent extraction or solid phase extraction procedures prior to injection onto the column. The precision data obtained for the overall method of analysis, on both tablets formulations, were very encouraging. However, it should be possible to incorporate an internal standard into the method which might be expected to further improve the overall precision. Bearing in mind that one of the tablets contained a wide range of vitamins and excipients, it should be possible to apply our LCEC method to other multivitamin preparations.

The electrochemical methods previously reported for thiamine determinations[8–10] are considered to be less suitable than the proposed method as they are more time consuming, less convenient and also less sensitive. In addition, mercury, as the working electrode, is often regarded as being undesirable owing to its toxic properties. It has been reported that reversed-phase liquid chromatographic methods can be employed for thiamine determinations in mixtures of vitamins, including vitamin B_2, using an ultraviolet[17] or spectrofluorimetric[18] detector; vitamin B_2 gave peaks with both detectors at retention times of 14 min and 18 min, respectively. In our method this vitamin does not give a chromatographic peak and the retention time of thiamine (derivative) is only 2 min. In conclusion, the proposed method offers an alternative approach to the determination of thiamine in multivitamin products which has certain advantages over previously published methods.

References

1 Dyke, S. F., *The Chemistry of the Vitamins*, Interscience Publishers, London, 1965, pp. 4–30.
2 Hart, J. P., Shearer, M. J., McCarthy, P. T., and Rahim, S., *Analyst*, 1984, **109**, 477.
3 Hart, J. P., Shearer, M. J., and McCarthy, P. T., *Analyst*, 1985, **110**, 1181.
4 Hart, J. P., and Hayler, P. S., *Anal. Proc.*, 1986, **23**, 439.
5 Wring, S. A., Hart, J. P., and Knight, D. W., *Analyst*, 1988, **113**, 1785.
6 Hart, J. P., and Jordon, P. H., *Analyst*, 1989, **114**, 1633.
7 Hart, J. P., Norman, M. D., and Lacey, C. J., *Analyst*, 1992, **117**, 1441.
8 Vergara, T., Marin, D., and Vera, J., *Anal. Chim. Acta*, 1980, **120**, 347.
9 Sanz Pedrero, P., and Lopez Fonseca, J. M., *Analyst*, 1972, **97**, 81.
10 Soderhjelm, P., and Lindquist, J., *Acta Pharm. Suec.*, 1976, **13**, 201.
11 Maier, G. D., and Metzler, D. E., *J. Am. Chem. Soc.*, 1957, **79**, 4386.
12 Matsukawa, T., Hirana, H., and Yurugi, S., in *Methods in Enzymology*, ed., McCormick, D. B., and Wright, L. D., vol. 18, Academic Press, New York, 1970, p. 155.
13 Kusube, K., Abe, K., Hiroshima, O., Ishiguro, Y., Ishikawa, S., and Hoshida, H., *Chem. Pharm. Bull.*, 1983, **31**, 3594.
14 Gudbjarnason, S., in *Methods in Enzymology*, ed., McCormick, D. B., and Wright, L. D., vol. 18, Academic Press, New York, 1970, p. 96.
15 Utsumi, I., Harada, K., Kohno, K., and Tsukamoto, G., in *Methods in Enzymology*, ed. McCormick, D. B., and Wright, L. D., vol. 18, Academic Press, New York, 1970, p. 168.
16 Hart, J. P., *Electroanalysis of Compounds of Biological Importance*, Ellis Horwood, Chichester, 1990, pp. 137–191.
17 Lam, F.-L., Holcomb, I. J., and Fusari, S. A., *J. Assoc. Off. Anal. Chem.*, 1984, **67**, 1007.
18 Augustin, J., *J. Assoc. Off. Anal. Chem.*, 1984, **67**, 1012.

Adsorptive Stripping Voltammetric Determination of Uranium With Cephradine

Azza M. M. Ali and M. A. Ghandour

Chemistry Department, Faculty of Science, Assiut University, Assiut, Egypt

Mahmoud Khodari

Chemistry Department, Faculty of Science, Assiut University, Qena Branch, Qena, Egypt

Uranium adsorbed with cephradine is reduced on a hanging mercury drop electrode. This property was exploited in developing a highly sensitive stripping voltammetric procedure for the determination of uranium. A detection limit 2×10^{-9} mol l^{-1} (0.5 µg l^{-1}) of uranium ion is obtained with an 180 s accumulation time. Cyclic voltammetry was used to characterize the interfacial and redox behaviour. The effects of various parameters are discussed. Experimental conditions include the use of 5×10^{-6} mol l^{-1} cephradine in 0.05 mol l^{-1} sodium perchlorate (pH $\approx$ 6.5), an accumulation potential of 0.0 V *versus* SCE and a direct current stripping technique. The response is linear up to 5×10^{-6} mol l^{-1} uranium and the relative standard deviation at 1×10^{-7} mol l^{-1} UO_2^{2+} is 4.4%. The effect of other metal ions was investigated.

Keywords: *Uranium determination; cyclic voltammetry; direct current adsorptive stripping voltammetry; cephradine*

Introduction

Cephalosporins are a series of antibiotics containing a β-lactam ring fused with a six-membered dihydrothiazine ring and having an acetoxymethyl group at position 3. Sterile cephradine (**1**), as a member of the first generation of the cephalosporin group, has been widely used in medicine in the treatment of some diseases.[1]

1
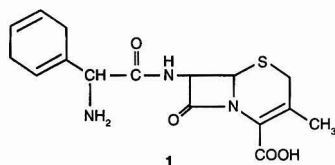
Sterile cephradine has been investigated in voltammetric studies[2] using the adsorptive cathodic stripping technique. It is assumed that this compound can act as a ligand, hence it is possible to accumulate the metal ion complex on the mercury electrode surface. A simple, rapid and highly sensitive method was used in this work as the basis for cathodic stripping adsorptive voltammetric measurements.

Several methods have been used for the determination of uranium, *e.g.*, atomic absorption spectrometry,[3] neutron activation analysis,[4] X-ray fluorescence spectrometry[5], complex metric titration[6] and gas chromatography[7]. These methods often gave insufficient sensitivity and various difficulties not least of which was expensive instrumentation. The adsorption of uranyl ion on an electrode surface with various single-ligand systems has been described; lower levels of uranium can be measured by using cathodic stripping voltam-

metry[8,9] based on the interfacial accumulation of a uranium–catechol complex on a hanging mercury drop. The adsorption of uranium has been studied in a medium composed of perchloric acid and tartrate.[10] Uranium has been determined in the presence of different ligands, *e.g.*, 8-hydroxyquinoline,[11] 4-(2-pyridylazoresorcinol,[12] Mordant Blue 9[13] and others.[14–16] Also, the determination of low concentrations of uranium has been studied using strongly adsorbed mixed complexes with 2-thenoyltrifluoroacetone and tributyl phosphate.[17] Uranium has also been determined using solid electrodes coated with trioctylphosphine oxide.[18,19]

Experimental

Materials and Reagents

A 1 mmol l^{-1} stock standard solution of Velosef (sterile cephradine; Squibb, New York, USA) was prepared by dissolving the appropriate mass in doubly distilled water. A 1 mmol l^{-1} stock standard solution of U^{VI} was prepared by diluting an appropriate uranyl perchlorate solution. Solutions of 1 mmol l^{-1} calcium, copper, iron(III), lead, nickel and zinc nitrate (Merck) and potassium dichromate (Merck) were prepared and used in interference studies.

Supporting electrolytes

Solutions of 0.1 mol l^{-1} perchloric, phosphoric and nitric acids and 0.1 mol l^{-1} acetic acid–sodium acetate buffer were used as supporting electrolytes. Sodium hydroxide solution (0.1 mol l^{-1}) was used to adjust the pH of the supporting electrolytes using an Orion 601 A Precision Research Ion-analyzer digital pH meter.

The instrumentation used was an EG&G Princeton Applied Research (PAR, Princeton, NJ, USA) Model 264 A stripping analyser, coupled with a PAR 303A mercury drop electrode (SMDE) (drop size, medium; area of the drop, 0.014 cm²). The polarographic cell (PAR Model K 0060) was fitted with an Ag/AgCl (saturated NaCl) reference electrode and a platinum wire counter electrode. A PAR 305 stirrer was connected to the PAR 303A SMDE. The SMDE and the stirrer were controlled by the instrument. A PAR RE 0089 *X–Y* recorder was used for the collection of experimental data.

Procedure

Transfer 10 ml of 0.05 mol l^{-1} sodium perchlorate solution (pH $\approx$ 6.5) as supporting electrolyte into the cell and de-aerate by passing nitrogen through for 10–16 min. Use an accumulation potential of 0.0 V and a scan rate of 100 mV s^{-1}. After the accumulation step and a further 15 s (equilibrium time), record the voltammogram (quiescent solution) and

terminate the potential at -1.1 V. Introduce the uranium sample and the ligand using an automatic pipetter (Volac 10–100 µl). Stir while purging with nitrogen, then proceed through the deposition and stripping step as before.

All the results in this paper were obtained at room temperature (25 $\pm$ 1 °C) with a nitrogen atmosphere maintained over the solution surface.

Results and Discussion

The optimum conditions for studying the formation of the cephradine–uranium complex were investigated. The influence of different supporting electrolytes, *i.e.*, phosphoric, nitric and perchloric acids and sodium acetate–acetic acid buffer, was studied in order to obtain a reproducible current for the uranium–cephradine peak. The highest signal was obtained in the presence of sodium perchlorate medium. The effect of pH (1, 3, 4.5, 6.5, 8, 10 and 12) on the peak height were tested in sodium perchlorate medium by the addition of carbonate-free sodium hydroxide to obtain the required pH. The optimum pH for studying the uranium–cephradine chelate is about 6.5 (Table 1). Also, the effect of sodium perchlorate concentration at constant pH ($\approx$6.5) was examined (Table 2). The sodium perchlorate concentration giving the highest signal is 0.05 mol l^{-1}. The influence of deposition potential on the peak height was tested using the direct current stripping voltammetric technique where the uranium–cephradine chelate exhibits strong adsorption at 0 V. The peak height decreased as the initial potential increased in the negative direction (-0.1 to -0.35 V). Therefore, a potential of 0 V was used as the accumulation potential for all the experimental measurements. Hence, the optimum conditions for studying the adsorptive stripping voltammetry of uranium with cephradine in this work was 0.05 mol l^{-1} sodium perchlorate at pH $\approx$ 6.5 with an initial potential of 0 V.

The dependence of the uranium–cephradine chelate peak on the antibiotic concentration was studied in the presence of 1×10^{-7} mol l^{-1} uranium and 0.05 mol l^{-1} sodium perchlorate at pH $\approx$ 6.5 with an accumulation time of 60 s. The peak height increases with increasing cephradine concentration up to 4×10^{-6} mol l^{-1}, after which it starts to level off, as shown in Fig. 1. Therefore, in subsequent experiments the concentration of the antibiotic was fixed at 5×10^{-6} mol l^{-1}.

Table 1 Effect of pH on the peak height (i_p) of 1×10^{-6} mol l^{-1} uranium–5×10^{-6} mol l^{-1} cephradine chelate in the presence of 0.1 mol l^{-1} sodium perchlorate with a scan rate of 100 mV s^{-1}

pH	i_p/nA	E_p/V
1.0	10.0	-0.58
3.0	35.0	-0.63
4.5	98.5	-0.72
6.5	185.0	-0.76
8.0	110.5	-0.79
10.0	40.0	-0.84
12.0	15.5	-0.87

Table 2 Effect of sodium perchlorate concentration on the peak height of 1×10^{-6} mol l^{-1} uranium–5×10^{-6} mol l^{-1} cephradine at constant pH ($\approx$6.5) with a scan rate of 100 mV s^{-1}

Sodium perchlorate concentration/mol l^{-1}	i_p/nA	Sodium perchlorate concentration/mol l^{-1}	i_p/nA
0.01	5.5	0.09	132.5
0.03	20.0	0.10	90.0
0.05	21.0	0.12	40.0
0.07	15.0		

The interfacial and redox behaviour of the uranium–cephradine chelate can be evaluated from cyclic voltammetric measurements. Fig. 2(a) shows repetitive cyclic voltammograms for 5×10^{-6} mol l^{-1} cephradine in the presence of 0.05 mol l^{-1} sodium perchlorate at pH $\approx$ 6.5 after a deposition time of 60 s at an accumulation potential of 0 V. A very small cathodic peak was observed at -0.76 V, which is related to the reduction of the adsorbed drug;[2] this peak completely disappears in subsequent scans, *i.e.*, rapid desorption of the
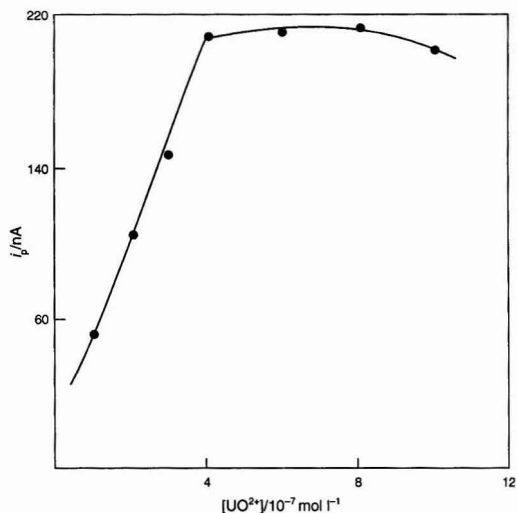
Fig. 1 Effect of cephradine concentration on the peak current in the presence of 1×10^{-7} mol l^{-1} uranium, 0.05 mol l^{-1} sodium perchlorate (pH $\approx$ 6.5), accumulation time 60 s and scan rate 100 mV s^{-1}.
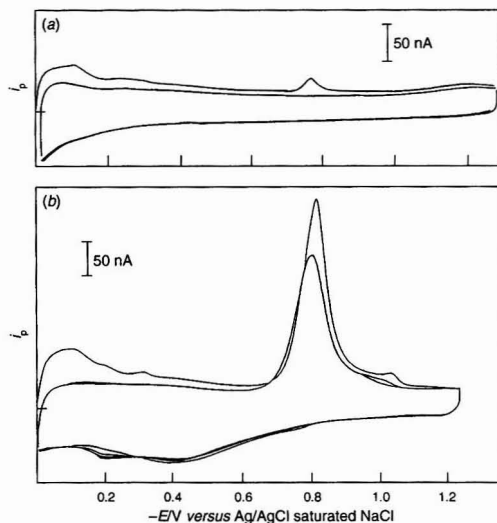
Fig. 2 Repetitive cyclic voltammograms following 60 s accumulation in the presence of 5×10^{-6} mol l^{-1} cephradine and 0.05 mol l^{-1} sodium perchlorate, accumulation potential 0.0 V, scan rate 100 mV s^{-1}. (a) In the absence; and (b) in the presence of 1×10^{-6} mol l^{-1} uranium.

reduced form of the drug. No peaks are observed on scanning in a positive direction. The cyclic voltammograms recorded after the addition of 1×10^{-6} mol l^{-1} UO^{2+} (238 µg l^{-1}) to the cell and a 60 s deposition time showed a sharp increase in the cathodic peak [Fig 2(b)] owing to the reduction of the adsorbed chelate, assuming that no adsorption occurred by the ligand itself and only the uranium–cephradine complex was adsorbed on the electrode surface.

Fig. 3 shows the direct current stripping voltammograms obtained with a hanging mercury drop electrode immersed in a stirred 5×10^{-9} mol l^{-1} uranium solution (1.19 µg l^{-1}) containing 5×10^{-6} mol l^{-1} cephradine and 0.05 mol l^{-1} sodium perchlorate (pH ≈ 6.5), with a scan rate of 100 mV s^{-1} and increasing the accumulation time. The amount of chelate absorbed on the electrode surface increased as the deposition time increased and also an enhancement of the peak current was observed. The uranium–cephradine complex yields a well defined peak at -0.75 V with a peak width at half-height of 42 mV. Hence the number of electrons involved is two.[20] The response obtained for a 300 s accumulation time (curve E) is 20 times greater than that attained without stirring (curve A). Hence convenient measurements at the µg l^{-1} level are feasible following a short deposition time.

The current *versus* accumulation time plots for (A) 2×10^{-9} mol l^{-1} (0.476 µg l^{-1}), (B) 5×10^{-9} mol l^{-1} (1.190 µg l^{-1}) (C) 5×10^{-8} mol l^{-1} (11.9 µg l^{-1}), (D) 5×10^{-7} mol l^{-1} (119.0 µg l^{-1}), and (E) 2×10^{-6} mol l^{-1} (476.0 µg l^{-1}) uranium in the presence of 5×10^{-6} mol l^{-1} cephradine and 0.05 mol l^{-1} sodium perchlorate (pH ≈ 6.5) are shown in Fig. 4. Straight lines were obtained and the magnitude of the peak current increased with increasing concentration of uranium. However, at higher concentrations (2×10^{-6} mol l^{-1}) of uranium a break was observed at a 120 s deposition time, which means that complete surface coverage was attained at this time. Therefore, the maximum charge obtained by integrating the area under the chelate stripping peak was found to be 9.0289×10^{-6} C.[21] Division of the charge by the conversion factor nFA ($n = 2$) indicates a surface coverage of 3.341×10^{-9} mol cm^{-2}. Each adsorbed chelate molecule occupies an area of 0.0497 nm^2.

The log i_p (peak current) *versus* log v (scan rate) in plot Fig. 5(A) is linear with a slope of 0.962 over the range 20–200 mV s^{-1} for 2×10^{-6} mol l^{-1} uranium in the presence of 5×10^{-6} mol l^{-1} cephradine and 0.05 mol l^{-1} sodium perchlorate (pH ≈ 6.5). A slope of 1 would be expected for an ideal redox couple immobilized on an electrode surface. A 20 mV negative shift in the peak potential from -0.77 to -0.85 V was observed on increasing the scan rate from 20 to 200

mV s^{-1}. The plot of peak potential *versus* log (scan rate) was also linear [Fig. 5(B)], the correlation coefficient being 0.998.

The adsorptive stripping peak for the uranium–cephradine chelate yields a well defined concentration dependence. The calibration plots over the uranium concentration range 23.8–238.0 µg l^{-1} (1×10^{-7}–1×10^{-6} mol l^{-1}) following 30, 60, 90, 180 and 240 s accumulation times are summarized in Table 3. The limit of linearity was extended to 2×10^{-6} mol l^{-1} uranium, which indicates strong adsorption of the uranium–cephradine complex for all of the deposition times applied.

The reproducibility of the adsorption process was tested by repeating 10 experiments on 1×10^{-7} mol l^{-1} uranium and 5×10^{-6} mol l^{-1} cephradine in the presence of 0.05 mol l^{-1} sodium perchlorate (pH ≈ 6.5) with a 60 s accumulation time. The relative standard deviation was 4.4%.

The major sources of interference in adsorptive stripping measurements are likely to be organic surfactants that compete with the chelate for space on the mercury surface and
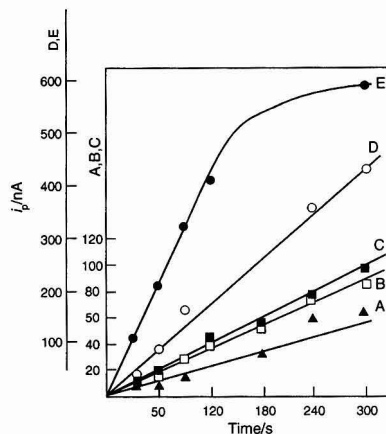
Fig. 4 Peak current *versus* accumulation time in the presence of 5×10^{-6} mol l^{-1} cephradine and 0.05 mol l^{-1} sodium perchlorate (pH ≈ 6.5), scan rate 100 mV s^{-1}, for A, 2×10^{-9}, B, 5×10^{-9}; C, 5×10^{-8}; D, 5×10^{-7} and E, 2×10^{-6} mol l^{-1} uranium.

Fig. 3 Voltammograms for 5×10^{-9} mol l^{-1} uranium and 5×10^{-6} mol l^{-1} cephradine in the presence of 0.05 mol l^{-1} sodium perchlorate (pH ≈ 6.5), scan rate 100 mV s^{-1}, following the accumulation periods: A, 0; B, 60; C, 120; D, 180; and E, 300 s.

Fig. 5 Log v (scan rate) *versus* log i_p (peak current, A) and log v *versus* E_p (peak potential, B) for 1×10^{-6} mol l^{-1} uranium and 5×10^{-6} mol l^{-1} cephradine in the presence of 0.05 mol l^{-1} sodium perchlorate (pH ≈ 6.5).

other metal ions that form chelates with the drug. Interferences of several metal ions were tested for 1×10^{-6} mol l^{-1} uranium, 5×10^{-6} mol l^{-1} cephradine in the presence of 0.05 mol l^{-1} sodium perchlorate (pH $\approx$ 6.5). The addition of 6×10^{-6}, 1×10^{-5}, 1×10^{-5} and 1×10^{-4} mol l^{-1} of Zn^{2+}, Cu^{2+}, Ni^{2+} and Ca^{2+}, respectively, has no effect on the peak height of uranium–cephradine. This means that no intereferences occur with 6-, 10-, 10- and 100-fold molar excesses of Zn^{2+}, Cu^{2+}, Ni^{2+} and Ca^{2+}, respectively, over UO_2^{2+}. On the other hand, on addition of 1×10^{-6} mol l^{-1} Fe^{3+}, Pb^{2+} or Cr^{6+} to 1×10^{-6} mol l^{-1} uranium the peak height of the uranium–cephradine complex decreased by half.

Interferences by organic surfactants were tested for a cell containing 5×10^{-6} mol l^{-1} cephradine and 1×10^{-6} mol l^{-1} uranium. The signal of the uranium–cephradine peak decreased by 16.3, 25.6, 37.2, 48.8 and 55.8% in the presence of 0.2, 0.3, 0.5, 0.7 and 0.8 mg l^{-1}, respectively, of Triton X-100. A similar depression was observed, *i.e.*, 20.5, 34.6 and 45.8%, on adding 0.3, 0.5 and 0.8 mg l^{-1}, respectively, of sodium dodecyl sulfate.

The method was applied to the determination of uranyl ion in uranyl nitrate hexahydrate (Merck) and uranyl acetate dihydrate (Merck), using the standard additions method. The results obtained indicate that the concentrations of uranium in the two samples were 98.2% and 99.3%, respectively, which are in good agreement with the results of labelled acidimetric methods, *viz.*, 98.10% and 99.10%, respectively.

Table 3 Characteristics of uranium–cephradine complex calibration graphs (0.05 mol l^{-1} sodium perchlorate, pH $\approx$ 6.5)

Deposition time/s	Linearity range/mol l^{-1}	Equation*	Correlation coefficient
30	1×10^{-7}–10×10^{-7}	$y = 11.36\,x$	0.9997
60	1×10^{-7}–10×10^{-7}	$y = 21.82\,x - 5$	0.9996
90	1×10^{-7}–10×10^{-7}	$y = 25.00\,x + 2.5$	0.9998
180	1×10^{-7}–10×10^{-7}	$y = 47.06\,x + 5$	0.9995
240	1×10^{-7}–10×10^{-7}	$y = 59.38\,x + 17.5$	0.9995

* Peak height (y) in nA, concentration (x) in 10^{-7} mol l^{-1}.

References

1 Katzung, R. G., *Basic and Clinical Pharmacology*, Appleton and Lange, East Norwalk, CT, 1987, 3rd edn.
2 Ali, A. M. M., *Bioelectrochem. Bioenerg.*, 1994, **33**, 201.
3 Halzbecher, J., and Ryan, D. E., *Anal. Chim. Acta*, 1980, **119**, 405.
4 Amos, M. D., and Willis, J. B., *Spectrochim. Acta*, 1966, **22**, 1325.
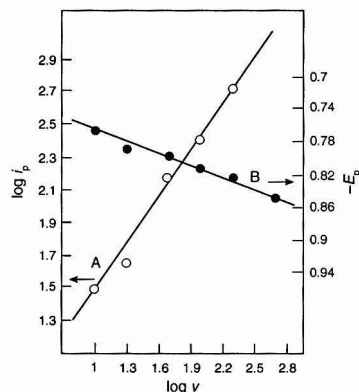5 Bond, A. M., Biskupsky, V. S., and Wark, D. A., *Anal. Chem.*, 1974, **46**, 155.
6 Marsh, S. E., Betts, M. R., and Rein, J. E., *Anal. Chim. Acta*, 1980, **119**, 401.
7 Sick, R. F., Richard, J. J., Iverson, K., and Barks, C. V., *Anal. Chem.*, 1971, **43**, 913.
8 Van den Berg, C. M. G., and Haung, Z. Q., *Anal. Chim. Acta*, 1984, **164**, 209.
9 Lam, N. K., Kalvoda, R., and Kopanica, M., *Anal. Chim. Acta*, 1983, **79**, 154.
10 Milner, G. W. C., Wilson, J. D., Barnett, G. A., and Smales, A. A., *J. Electroanal. Chem.*, 1961, **2**, 25.
11 Van den Berg, C. M. G., and Nimo, N., *Anal. Chem.*, 1987, **59**, 924.
12 Farias, P. A. M., and Ohara, A. K., *Electroanalysis*, 1991, **3**, 985.
13 Wang, J., and Zadii, J. M., *Talanta*, 1987, **34**, 247.
14 Zhao, Z. F., Cai, X. H., and Li, P. B., *Talanta*, 1987, **34**, 623.
15 Pournughi-Azar, M. H., and Golabi, S. M., *Talanta*, 1991, **38**, 1469.
16 Newton, M. P., and Van den Berg, C. M. G., *Anal. Chim. Acta*, 1987, **199**, 59.
17 Mlkar, M., and Branica, M., *Anal. Chim. Acta*, 1989, **221**, 279.
18 Lubert, K. H., Schnurrbusch, M., and Thoma, A., *Anal. Chim. Acta*, 1982, **144**, 123.
19 Izutsu, K., Nakamura, T., and Ando, T., *Anal. Chim. Acta*, 1983, **152**, 285.
20 Parry, E. P., and Osteryoung, R. A., *Anal. Chem.*, 1965, **37**, 13.
21 Gurira, R. C., and Bowers, L. D., *J. Electroanal. Chem.*, 1983, **146**, 109.

Electroanalytical Study of the Industrial Extractant LIX 54

Izaskun Alava, María P. Elizalde and Marta M. Huebra

Departamento de Química Analítica, Facultad de Ciencias, Universidad del País Vasco, Apdo 644, 48080 Bilbao, Spain

The voltammetric behaviour of 1-phenyldecane-1,3-dione, the active component in the commercial extractant LIX 54, was studied in the aqueous–alcoholic medium 0.1 mol l⁻¹ KCl–methanol (60 + 40 v/v) as a function of pH using polarographic and cyclic voltammetric techniques. Reduction processes of the extractant depending on the acidity conditions are proposed. The electrochemical reduction of the industrial formulation (LIX 54) under the same experimental conditions was also studied and found to exhibit similar behaviour. In order to determine the percentage of the active component in the commercial extractant, differential-pulse polarographic methods for the determination of 1-phenyldecane-1,3-dione were developed and compared with the results obtained for LIX 54.

Keywords: Voltamperometry; liquid–liquid extraction; LIX 54; 1-phenyldecane-1,3-dione

Introduction

1-Phenyldecane-1,3-dione has been found to be the active component in the industrial extractant LIX 54, manufactured by Henkel in 1976 to remove copper from ammoniacal solutions.[1,2] Although its metal extractant properties, acid–base equilibrium in aqueous–alcoholic solutions[3] and keto–enol tautomerism in different solvents are known,[3] the electrochemical behaviour of this component and of most other industrial extractants is still unknown.

A literature search on the reduction of diketones showed that the electrochemical behaviour depends on the structural position of the two carbonyl groups and on the presence of aromatic groups in the molecule.

1,3-Diketones show weak interactions between the two carbonyl groups, and are more easily reduced than the corresponding monoketones.[4] Studies of thenoyltrifluoroacetone[5] showed that it exhibits a complex electrochemical behaviour related to different equilibria such as acid–base, hydration and tautomerism. The symmetrical β-diketone 1,3-diphenylpropane-1,3-dione has been studied in protic solvents[6] and in aprotic media.[7,8] In a protic medium an intermediate dimeric product and an enediol were identified.

The reagent 1-phenylbutane-1,3-dione is the most similar to the active component in LIX 54. The replacement of the methyl group by a heptyl group confers on the industrial compound greater insolubility in aqueous media. The polarographic reduction of 1-phenylbutane-1,3-dione[9,10] showed different reduction waves in different electrolytes but the type of process involved was not described. Philp *et al.*[10] discussed the relationship of the current peaks to its possible enolization, but no definite conclusion was drawn. The most detailed work was carried out in an aqueous–alcoholic medium (2% ethanol) by Nisli *et al.*[9] They reported the formation of 4-hydroxy-4-phenylbutan-2-one in a series of reduction processes following the sequence enolate < unprotonated

β-diketone < monoprotonated diketone < diprotonated diketone. The currents were found to be governed by the rate of protonation of the carbonyl groups and of the enolate under neutral and alkaline conditions, respectively. They assumed that the diketo form is the only electroactive species and no evidence of any reduction products involving one electron was found.

The electrochemical reduction of 1-phenyldecane-1,3-dione as a function of the operational and chemical variables is described in this paper. The aims were to obtain fundamental properties concerning its redox stability and to search for methods for the determination of the active component in the commercial extractant LIX 54.

Experimental

Apparatus

Voltammetric measurements were made using an Inelecsa (Seville, Spain) PDC 1212 electrochemical system equipped with an Acer (Taiwan) Model 500 personal computer. A thermostatically controlled cell of 50 ml capacity and a three-electrode system, incorporating a dropping mercury electrode or a hanging mercury drop electrode as the indicator electrode, Ag/AgCl/KCl (3 mol l⁻¹) as the reference electrode and a platinum wire as the auxiliary electrode, were used. Measurements of pH were carried out using a Radiometer (Copenhagen, Denmark) pHM64 digital pH–voltmeter with a combined glass–Ag/AgCl/KCl (3 mol l⁻¹) electrode.

Reagents

A stock standard solution (10⁻³ mol l⁻¹) of 1-phenyldecane-1,3-dione (99.9% purity), previously isolated from the commercial LIX 54 extractant by column chromatography and characterized by elemental analysis and spectroscopic techniques,[1] was prepared in Lab-Scan HPLC-grade methanol. A stock standard solution of LIX 54 (321 mg l⁻¹), supplied by Henkel (batch No. MX 10425), was prepared in Lab-Scan HPLC-grade methanol. A stock standard Britton–Robinson buffer solution, which was 0.04 mol l⁻¹ in each of glacial acetic acid, phosphoric acid and boric acid, was prepared from analytical-reagent grade chemicals. Buffer solutions were prepared by adding the necessary amount of potassium hydroxide to obtain the appropriate pH values. Hydrochloric acid was added for the more acidic conditions. The ionic strength was adjusted to 0.1 mol l⁻¹ by addition of potassium chloride (Merck, analytical-reagent grade). The water used was obtained using a Waters (Milford, MA, USA) Milli-RO and Milli-Q system.

Procedure

Polarography in the sampled dc and differential-pulse modes and cyclic voltamperometry were applied.

In order to carry out the polarographic study of the extractant under the optimum conditions, the instrumental variables were optimized and the following parameters were used: drop time, 1 s; amplitude, 2 mV; scan rate, 2 mV s⁻¹; pulse level, 70 mV; and delay, 40 mV.

All the experiments were performed at 298 K. Dissolved air was removed from the solutions by bubbling oxygen-free nitrogen through the cell for 5 min.

Results

The current–voltage peaks (i_p–E) were investigated by recording polarograms of 1-phenyldecane-1,3-dione solutions (1.3×10^{-4} mol l⁻¹) in 0.1 mol l⁻¹ KCl–methanol (60 + 40 v/v) at different pH values. In the whole pH range studied the chelating reagent shows four reduction peaks in the range −800 to −1800 mV, as can be seen in Fig. 1. It can be seen that the third peak appears very close to the second, and its current increases with increase in pH until both peaks overlap and disappear, at the same time that the fourth peak is observed.

The variation of the potential (E_p) as a function of pH for the different reduction peaks is illustrated in Fig. 2. Three straight lines can be seen for the first peak [pH < 7.39, $E_p = -0.789 - 6.4 \times 10^{-2}$pH ($r^2 = 0.997$); 7.66 < pH < 9.18, $E_p = -1.191 - 8.62 \times 10^{-3}$pH ($r^2 = 0.998$); 9.98 < pH < 10.83, $E_p = -2.428 + 0.122$pH ($r^2 = 1.000$)], which break at pH 7.26 and 9.47. The last value is acceptably close to that obtained in 1.0 mol l⁻¹ KCl–ethanol (75 + 25 v/v) by spectrophotometric techniques (9.73 ± 0.05) and corresponds to the pK_a value for the acid–base equilibrium of the reagent.[3]

The second and third reduction peaks show a linear variation of E_p *versus* pH in acidic media, whereas under neutral conditions the potential approaches a constant value that seems to coincide with the last straight line of the first peak, so the confluence of the three peaks can be deduced under these conditions.
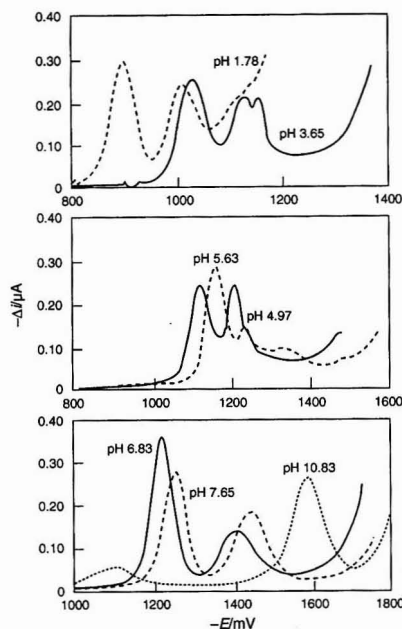
For the fourth peak, two different linear parts can be observed [6.83 < pH < 9.18, $E_p = -1.145 - 3.77$pH ($r^2 = 0.966$); 9.92 < pH < 11.42, $E_p = -0.863 - 6.73$pH ($r^2 = 0.995$)], which break at pH 9.51.

The reversibility of the electrodic process was studied using sampled d.c. polarography and cyclic voltamperometry.

Logarithmic analysis applied to sampled d.c. polarograms for the first and fourth reduction waves gave straight lines with similar slopes. Assuming that the reduction process involves two electrons,[4] the αn values obtained (Table 1) show a tendency for the process to be irreversible. It should be pointed out that d.c. polarograms do not permit a complete treatment of the different reduction waves as they overlap.

The results obtained using cyclic voltamperometry were similar to those obtained using the differential-pulse mode. Four reduction peaks and an anodic peak in the whole range of pH were observed, as can be seen in Fig. 3. The variation of the potential with pH obtained by this technique acceptably agrees with the corresponding functions obtained by differential-pulse polarography.

The irreversibility of the process for the first and third reduction peaks under acidic conditions was confirmed by the almost linear relationship between E_p and log v (scan rate). The slope values, around −30 mV per pH unit, suggest that the αn values are close to unity, in concordance with the results of the previous logarithmic analysis.

Whereas the reduction corresponding to the first peak is irreversible under acidic conditions, the same reduction seems to be reversible under alkaline conditions, as E_p is constant when varying the scan rate. The facts that the anodic peak is observed over almost the whole range of pH and that it does not show the difference ($E_p^c - E_p^a$) characteristic of a reversible process seem to indicate that oxidation of some reduced products, which have experienced a subsequent transformation, has taken place. On the other hand, the linear relationship between the peak current (i_p) and the scan rate for the anodic peak [pH = 4.35, $i_p = -0.3747 - 0.3394v$ ($r^2 = 0.9982$); pH = 9.22, $i_p = -0.7565 - 0.2228v$ ($r^2 = 0.9815$); pH = 10.94, $i_p = -0.4387 - 0.1061v$ ($r^2 = 0.9857$)] could indicate that the process is predominantly adsorptive controlled.[11]

The variation of the first and fourth current peaks with reagent concentration using the differential-pulse polaro-

Fig. 1 Differential-pulse polarograms of 1-phenyldecane-1,3-dione solutions [1.3×10^{-4} mol l⁻¹ in 0.1 mol l⁻¹ KCl–MeOH (60 + 40 v/v)] at different pH values.
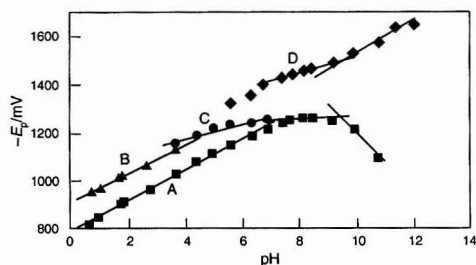
Fig. 2 Variation of the peak potential of 1-phenyldecane-1,3-dione solutions [1.3×10^{-4} mol l⁻¹ in 0.1 mol l⁻¹ KCl–MeOH (60 + 40 v/v)] with pH by differential-pulse polarography. A, first; B, second; C, third; and D, fourth peaks.

Table 1 Values at different pH values for αn and $E_{1/2}$ studied for the first and fourth reduction waves at different pH values

Reduction wave	pH	$E_{1/2}$/mV	αn
First	1.78	934.3	1.20
	7.63	1277.6	1.37
Fourth	7.63	1471.3	0.96
	10.90	1618.8	0.84

graphic technique at pH 6.81, where the maximum sensitivity is obtained, is illustrated in Fig. 4. The variation of the current is linear, so it can be deduced that the process is predominantly diffusion controlled.

Discussion

The results of the electrochemical study reveal a complex behavioural pattern that would need to be studied using additional techniques to detect intermediate species originated in the reduction process. The probability of finding hydrated keto forms in 1-phenyldecane-1,3-dione is limited and it seems more probable that surface protonation reactions take place in accordance with Nisli *et al.*,[12] although reactions involving the formation of radicals that can dimerize to generate pinacol, according to Buchta and Evans,[8] cannot be disregarded. An interpretation of the voltammetric behaviour observed for the extractant in terms of reactions of keto species with different degrees of protonation has been made. The scheme illustrated in eqns. (1)–(7) represents a simplification of the most important reactions which probably generate the reduction compound, 1-phenyl-1-hydroxydecan-3-one. In this scheme it has been assumed that the reduction processes involve two electrons, in accordance with studies made on compounds of a similar nature.[4]
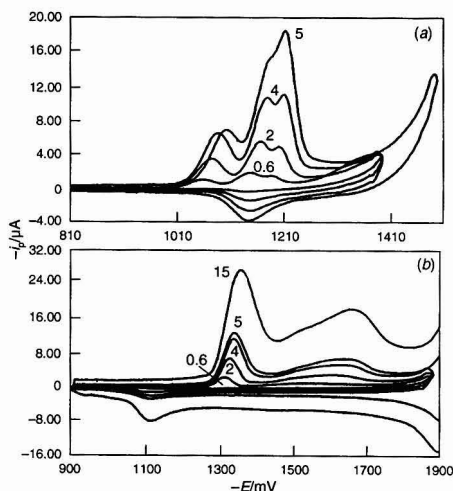
Fig. 3 Cyclic voltammograms of 1-phenyldecane-1,3-dione solutions [1.3 × 10⁻⁴ mol l⁻¹ in 0.1 mol l⁻¹ KCl–MeOH (60 + 40 v/v)] at different scan rates (V s⁻¹) at (*a*) pH 2.65 and (*b*) pH 6.86.
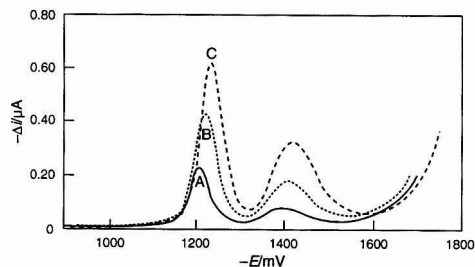
Fig. 4 Variation of the first and fourth peaks with reagent concentration at pH 6.8: A, 5.49 × 10⁻⁵; B, 1.3 × 10⁻⁴; and C, 2.17 × 10⁻⁴ mol l⁻¹.

$$PhC(OH^+)CH_2C(OH^+)R \rightleftharpoons PhC(OH^+)CH_2COR + H^+ \quad (1)$$
$$\updownarrow$$
$$PhCOCH_2C(OH^+)R$$

$$PhC(OH^+)CH_2C(OH^+)R \xrightarrow{2e^-} PhCH(OH)CH_2COR \quad (2)$$

$$PhC(OH^+)CH_2COR \rightleftharpoons PhCOCH_2COR + H^+ \quad (3)$$
$$\updownarrow \qquad\qquad \updownarrow$$
$$PhCOCH_2C(OH^+)R \qquad PhC(OH)CH=COR$$
$$\updownarrow$$
$$PhCO=CHC(OH)R$$

$$PhC(OH^+)CH_2COR \xrightarrow[H^+]{2e^-} PhCH(OH)CH_2COR \quad (4)$$
$$\updownarrow$$
$$PhCOCH_2C(OH^+)R$$

$$PhCOCH=COR \xrightarrow[2H^+]{2e^-} PhCH(OH)CH_2COR \quad (5)$$

$$PhCOCH_2COR \rightleftharpoons PhCO^-CH=COR + H^+ \quad (6)$$
$$\updownarrow$$
$$PhCO=CHCO^-R$$

$$PhCO^-=CHCOR \xrightarrow[3H^+]{2e^-} PhCH(OH)CH_2COR \quad (7)$$
$$\updownarrow$$
$$PhCOCH=CO^-R$$
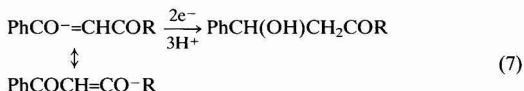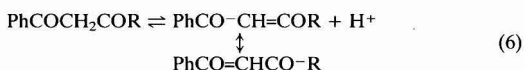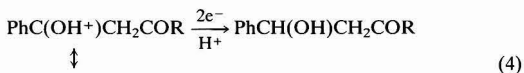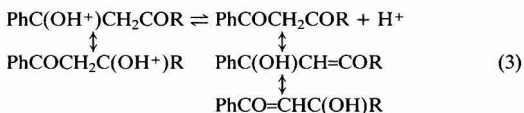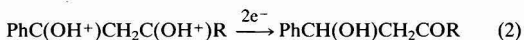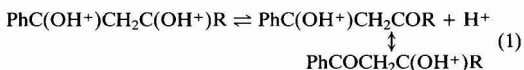
In the proposed scheme of reactions, the first reduction peak could correspond to the reduction of the diprotonated form [eqn. (2)] originating from a surface protonation [eqn. (1)]. The monoprotonated β-diketone, which is reduced depending on the protonation rate of the keto form [eqn. (3)], could give rise to the second reduction peak [eqn. (4)]. Since protonation can take place either in the benzoyl group or in the second ketonic group, unfolding and overlapping of the reduction waves are observed. The second reduction peak is observed only under the most acidic conditions and it reaches a minimum at pH 4.5, whereas the third reduction peak presents a maximum. This pH value could correspond to the predominance of the monoprotonated form. As protonated acetyl compounds are usually stronger acids than protonated benzoyl compounds,[13] it seems more probable that the third reduction peak involves the protonation of the benzoyl group which is observed over a wide pH range.

The first, second and third peaks meet at a constant potential value which can correspond to the unprotonated β-diketone [eqn. (5)], probably in the keto form. The reduction peak observed at the most negative potential values can be attributed to the enolate ion reduction [eqn. (7)]. Under alkaline conditions, in which the enolate is dominant, the current (i_p) can decrease owing to its slow decomposition, which has also been observed using spectrophotometric techniques.[14]

Finally, the oxidation of some reduction products, probably involving other transformation reactions and adsorption processes, can be postulated, but more experimental work needs to be carried out to clarify the type of reactions involved.

Analytical Applications

Fig. 5 shows a comparison between the polarographic behaviour of the commercial extractant LIX 54 and its active component, 1-phenyldecane-1,3-dione. It can be seen that the industrial formulation behaves in a similar way to the pure reagent and there is no new polarographic peak due to other

co-products, additives or solvents present in LIX 54. The polarographic peaks for LIX 54 present the same potential values, although the current is lower.

The above indicates the possibility of developing a method for the determination of 1-phenyldecane-1,3-dione in the commercial extractant LIX 54. It must be pointed out that no such analytical method has been published previously, mainly owing to the difficulties involved in the isolation of the pure active component.

In order to check the amount of 1-phenyldecane-1,3-dione present in the industrial formulation, methods for the determination of the β-diketone were developed. The procedure was based on the detection of the first and fourth peaks where maximum sensitivity is obtained (pH 6.8) using the parameters (drop time, pulse level, delay, amplitude and scan rate) given under Experimental. For the pure reagent, the first and fourth peaks show a linear dependence on concentration in the range 2.5×10^{-5}–1.7×10^{-4} and 2.5×10^{-5}–1.5×10^{-4} mol l^{-1}, respectively. The corresponding calibration lines fit the equations i_p (μA) $= 2837 C_{HL}$ and $i_p = 896 C_{HL}$, respec-

tively. On the other hand, the industrial extractant LIX 54 gives, under the same conditions, the calibration lines i_p (μA) $= 936 C_{LIX\ 54} - 0.0095$ with a linear range from 3.36 to 44.92 mg l^{-1} (first peak) and i_p (μA) $= 471 C_{LIX\ 54} - 0.021$ with a linear range from 13.25 to 51.00 mg l^{-1} (fourth peak). By comparison of the results obtained for the pure reagent and LIX 54, an average of 33% (m/v) of 1-phenyldecane-1,3-dione in the industrial formulation can be derived.

References

1   Zapatero, M. J., Elizalde, M. P., and Castresana, J. M., *Anal. Sci.*, 1989, **5**, 591.
2   Mickler, W., and Uhleman, E., *Sep. Sci. Technol.*, 1992, **27**, 1171.
3   Zapatero, M. J., Elizalde, M. P., and Castresana, J. M., *Anal. Sci.*, 1991, **7**, 935.
4   *Encyclopaedia of Electrochemistry of the Elements*, ed. Bard, A. J., and Lund, H., Marcel Dekker, New York, 1984, Vol. XIII.
5   Elving, P. J., and Grodzka, P. G., *Anal. Chem.*, 1961, **33**, 2.
6   Evans, D. H., and Woodbury, E. C., *J. Org. Chem.*, 1967, **32**, 2158.
7   Buchta, R. C., and Evans, D. H., *Anal. Chem.*, 1968, **40**, 2181.
8   Buchta, R. C., and Evans, D. H., *J. Electrochem. Soc.*, 1970, **117**, 1494.
9   Nisli, G., Barnes, D., and Zuman, P., *J. Chem. Soc. B*, 1970, 778.
10 Philp, R. H., Flurry, R. L., and Day, R. A., Jr., *J. Electrochem. Soc.*, 1964, **111**, 328.
11 Nicholson, R. S., and Shain, I., *Anal. Chem.*, 1964, **36**, 706.
12 Nisli, G., Barnes, D., and Zuman, P., *J. Chem. Soc. B*, 1970, 764.
13 Perrin, D. D., Dempley, B., and Serjeant, E. P., *pK$_a$ Prediction for Organic Acids and Bases*, Chapman and Hall, London, 1981.
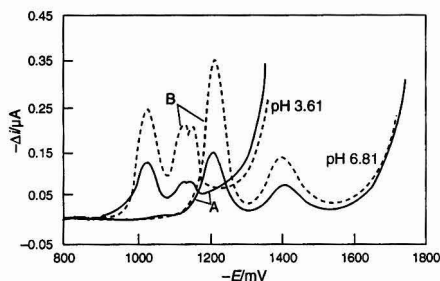14 Zapatero, M. J., *PhD Thesis*, University of the Basque Country, Bilbao, 1988.

Fig. 5 Comparison of the electrochemical behaviour of A, the commercial extractant LIX 54 and B, its active component (1-phenyldecane-1,3-dione) at different pH values.

Voltammetric Behaviour of Puerarin and Its Determination by Single-sweep Oscillopolarography

Jingbo Hu and Qilong Li*

Department of Chemistry, Beijing Normal University, Beijing, 100875, China

In 0.1 mol dm^{-3} H$_2$SO$_4$ solution, a sensitive reductive wave of puerarin was obtained by single-sweep oscillopolarography. The peak potential was -1.00 V (*versus* SCE). The peak height was proportional to the concentration of purearin over the range 4.0×10^{-7}–6.0×10^{-6} mol dm^{-3} and the detection limit was 5.0×10^{-8} mol dm^{-3}. The behaviour of the reduction wave was studied and applied to the determination of puerarin in tablets. The reduction process was irreversible with the adsorptive characteristics and the behaviour obeyed the Frumkin adsorptive isotherm. The adsorption coefficient β was 1.14×10^5 and the interaction factor α was 1.54.

Keywords: Single-sweep oscillopolarography; voltammetric behaviour; puerarin

Introduction

Puerarin (PRR) is an effective ingredient of the root of the kudzu vine (Chinese herbal medicine). The root of the kudzu vine is known for its effective treatment of hypertension, angina pectoris and sudden deafness. Its structure is shown in Fig. 1; it is a kind of flavonoid. The determination of puerarin by the coulometric titration, colorimetric analysis, ultraviolet spectrophotometry, a film photodensity method and high-performance liquid chromatography (HPLC) have been reported.[1-5] HPLC has the highest sensitivity of these methods, 1.92×10^{-6} mol dm^{-3}. However, the voltammetric behaviour of puerarin and its determination have not been reported so far.

In this work, the voltammetric behaviour of puerarin and its electrode reaction mechanism were studied and a new method for the trace determination of puerarin is proposed. The detection limit is 5.0×10^{-8} mol dm^{-3} using single-sweep oscillopolarography. This method, especially the derivative method, has the following characteristics over previous methods: the sensitivity is higher, particularly for the adsorption species, because it has an accumulation time of 5 s before

Fig. 1   Structure of puerarin.

* To whom correspondence should be addressed.

scanning and a fast scan rate, the selectivity is better, the operating method is more convenient and the structure of the instrument is simpler and cheaper. Hence this method should prove useful in the field of geological and metallurgical analysis.

Experimental

Apparatus

A Jp-2A single-sweep oscillopolarograph (Chengdu Instrumental Factory, China) was used. The conditions for derivative polarography were drop-time 7 s, scan rate 250 mV s^{-1}, potential scan range 500 mV in the negative direction and scanning from -0.8 to -1.30 V. A three-electrode system was used with a dropping mercury working electrode (DME), a platinum counter electrode and a saturated calomel reference electrode (SCE). A Model 370-8 Electrochemistry System (EG & G, Princeton Applied Research, Princeton, NJ, USA) was used for linear-sweep voltammetry and cyclic voltammetry, with a three-electrode system consisting of hanging mercury drop electrode (HMDE) as working electrode, a platinum counter electrode and an Ag–AgCl (saturated KCl) reference electrode. The electrolytic cell was a 10 cm^3 beaker. All experiments were performed at room temperature and dissolved oxygen was removed from the solutions.

Chemicals

Puerarin was obtained from the Institute of Materia Medica, Chinese Academy of Medical Science, with a purity of 99%, mp 189–190 °C (decomposition). A 1.0×10^{-3} mol dm^{-3} stock standard solution of puerarin in ethanol was prepared; working standard solutions of 1.0×10^{-5} and 1.0×10^{-6} mol dm^{-3} were prepared by dilution with water. All reagents were of analytical-reagent grade and water distilled in a fused-silica still was used throughout.

Procedure

A 10 cm^3 volume of 0.1 mol dm^{-3} sulfuric acid containing a specific amount of sample solution was added to the cell and purged with purified nitrogen for 5 min to remove oxygen. The derivative oscillographic polarogram was recorded from -0.8 to -1.3 V (*versus* SCE) and the height of the peak was measured at -1.00 V. The determination was performed by the standard additions method.

Results and Discussion

Selection of Experimental Conditions

Various supporting electrolytes, such as H$_2$SO$_4$, HCl, HOAc–NaOAc, KCl, NH$_3$–NH$_4$Cl, NaOH and Britton–Robinson buffer solution were tested by single-sweep oscillopolaro-
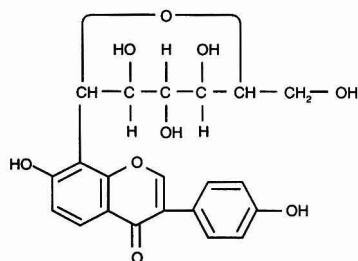
graphy; H_2SO_4 was found to be the best because the polarogram of puerarin was well defined and the sensitivity was reasonably high. In 0.1 mol dm^{-3} H_2SO_4 solution the peak potential is -1.00 V (*versus* SCE).

Calibration Graph and Detection Limit

A calibration graph was established by determining various concentrations of purified puerarin by single-sweep oscillopolarography. The relationship between the peak current and the concentration of puerarin was linear from 4.0×10^{-7} to 6.0×10^{-6} mol dm^{-3} with a linear correlation coefficient of 0.9998. The detection limit was 5.0×10^{-8} mol dm^{-3} of puerarin. Hence the proposed method permits the determination of puerarin over a wide concentration range.

Analysis of Samples

Measurement of puerarin in tablets was performed by oscillopolarography. The excipients in the tablets (starch, talc, *etc.*) did not affect the polarogram. No sample preparation was used other than dilution with the supporting electrolyte. The determination was performed by the standard additions method and the results of a few analyses are given in Table 1. These results were in good agreement with those obtained by a film photodensity method[3] and a fluorescence method.[6] The relative standard deviation was about 0.031–0.71%.

In addition, some recovery experiments were carried out and the results are given in Table 2. The recovery was 98.5–101.9%. These results confirm the usefulness of the proposed method for the determination of puerarin.

Study of Voltammetric Behaviour

Repetitive cyclic voltamperograms

Fig. 2 shows repetitive cyclic voltamperograms for 5.0×10^{-7} mol dm^{-3} puerarin, recorded after preconcentration at -0.5 V (*versus* Ag–AgCl) for 90 s. A large and well defined cathodic peak is observed in the first scan (curve A) at -0.96 V. Subsequent scans exhibit a decrease in the peak to a stable value. This indicates that puerarin has adsorptive character-

istics at the mercury electrode. No peak is observed on the anodic branch, indicating that the reduction of puerarin at the mercury electrode is irreversible.

Effect of accumulation time

Fig. 3 shows plots of the cathodic peak current (I_{pc}) of linear sweep voltammetry *versus* accumulation time (t) for different concentrations of puerarin. At first, I_{pc} increased linearly with t at both levels, indicating that before adsorptive equilibrium is reached, the longer the accumulation time, the more puerarin is adsorbed and the larger is the peak current. However, after a specific period of accumulation time, the peak current at different concentration levels tended to become stable, showing that adsorptive equilibrium of puerarin on the mercury electrode surface is achieved.

Effect of scan rate

Fig. 4 shows the effect of scan rate on I_{pc} at different accumulation times. When $t = 0$, I_{pc} showed a linear relationship with $v^{1/2}$, illustrating that the reduction of puerarin is diffusion controlled [Fig. 4(*a*), A]. When $t = 180$ s, the I_{pc} *versus* $v^{1/2}$ curve showed an upward slope [Fig. 4(*a*), B] and the I_{pc}–v curve became a straight line [Fig. 4(*b*), B], indicating that the system is adsorption controlled.[7,8]
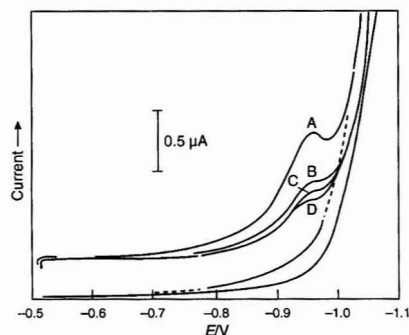
Fig. 2 Repetitive cyclic voltamperograms: 0.1 mol dm^{-3} H_2SO_4; 5.0 $\times 10^{-7}$ mol dm^{-3} puerarin; scan rate, 50 mV s^{-1}; accumulation time, 90 s.

Table 1 Analytical results for puerarin in tablets

	Puerarin found/mg per tablet			
	This method			
Sample No.	Found	Mean s_r (%)	Film photodensity method	Fluorescence method
1	29.94, 29.73, 29.52	29.73, 0.71	29.86	30.64
2	32.06, 31.85, 32.27	32.06, 0.66	32.58	33.20
3	31.85, 31.84, 31.86	31.85, 0.031	31.42	30.28

Table 2 Results of recovery experiments

Initial puerarin/ μg	Added/μg	Total found/μg	Recovery of added puerarin (%)
5.78	4.16	9.99	101.9
5.91	8.33	14.16	99.0
6.00	12.49	18.32	98.6
6.08	16.66	22.49	98.5
6.29	16.66	22.90	99.7

Fig. 3 Effect of accumulation time on the peak current: 0.1 mol dm^{-3} H_2SO_4; scan rate, 50 mV s^{-1}; initial potential, -0.50 V; $s =$ 0.5 μA; puerarin concentration, A, 5.0×10^{-7}; and B, 1.0×10^{-6} mol dm^{-3}.

Effect concentration of puerarin

The effect of the concentration of puerarin on the peak current at two different accumulation times is shown in Fig. 5. When $t = 0$, the relative peak current expressed as the ratio I_{pc}/c_{PRR} is very small and remains nearly constant with increasing concentration of puerarin (curve A). This indicates that the reduction of puerarin at the mercury electrode is almost totally diffusion controlled. However, when $t = 90$ s, the values of I_{pc}/c_{PRR} are much greater than those for curve A at lower concentrations of puerarin because of the adsorption of puerarin on the mercury electrode surface. At higher concentrations of puerarin, the adsorption of puerarin reaches saturation and its contribution to the peak current does not increase further. The ratio then declines very rapidly with increasing concentration of puerarin, and eventually tends toward the constant value of curve A (curve B). All of these results show the gradual transformation of the system from adsorption controlled to diffusion controlled with increasing concentration of puerarin.[9]

In summary, the reduction of puerarin at a mercury electrode is contributed to by the reduction of both surface species adsorbed on the electrode surface and solution species diffusing to the electrode surface. However, because the adsorption of puerarin is not strong enough, both the adsorbed and solution species are reduced at the same potential. The cathodic peak current I_p is thus made up of two parts: adsorption current I_{pa} and diffusion current I_{pd}, with $I_p = I_{pa} + I_{pd}$. The accumulation time t, scan rate v and concentration of puerarin c have different effects on I_{pa} and

I_{pd}. Generally, with lower c, faster v and longer t, the system manifests itself mainly with adsorptive properties and I_{pd} may be neglected, but with higher c, slower v and shorter t, the system essentially exhibits diffusion properties and I_{pa} can be neglected. This is characteristic of the system when the reactant is weakly adsorbed. According to this, we can study different electrode processes of electroactive species under different conditions.[9-11]

Measurement of the number of electrons transferred

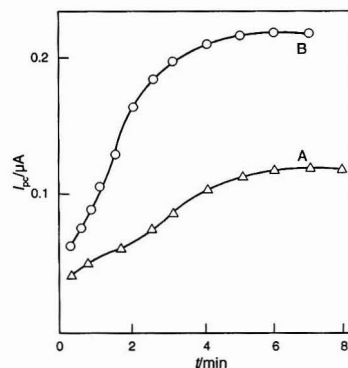The number of electrons was determined by constant potential coulometry with a large area of the mercury cathode. Three 50.0 cm³ portions of 0.1 mol dm⁻³ H_2SO_4 and 2.0×10^{-4} mol dm⁻³ puerarin were electrolysed for 2.5 h at -0.95 V (*versus* SCE), with consumption of 0.95, 1.08 and 1.05 C, respectively. The values of n, the number of electrons transferred, thus obtained were 0.98, 1.12 and 1.09, respectively, hence $n = 1$.

Determination of αn and α

The equation for the irreversible reduction wave is

$$E = E_{1/2} + RT/(\alpha nF) \ln [(I_d - I_{irr})/I_{irr}]$$

A plot of $\ln[(I_d - I_{irr})/I_{irr}]$ *versus* E, as shown in Fig. 6, is linear with slope $\alpha nF/RT$. The product of the electrode transfer coefficient and the number of electrons, αn, can be calculated

Fig. 4 Effect of scan rate: (*a*) $I_{pc}-v^{1/2}$ and (*b*) $I_{pc}-v$ curves. Concentrations, 0.1 mol dm⁻³ H_2SO_4, 1.0×10^{-6} mol dm⁻³ puerarin; $s = 1$ μA; accumulation time, A, 0 s and B, 180 s.

Fig. 6 Plot of $\ln[I_{irr}/(I_d - I_{irr})]$ *versus* potential: 0.1 mol dm⁻³ H_2SO_4, 1.0×10^{-6} mol dm⁻³ puerarin; $s = 2$ μA; initial potential, -0.70 V.

Fig. 5 Effect of concentration of puerarin on relative peak current as the ratio of peak current to puerarin concentration: accumulation time, A, 0 s and B, 90 s. Other conditions as in Fig. 3.
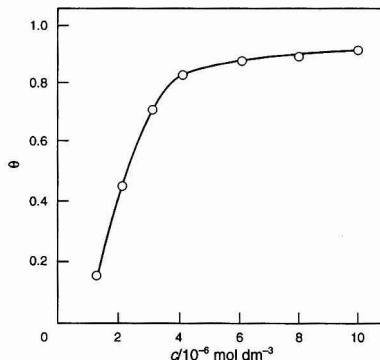
Fig. 7 Adsorption isotherm: 0.1 mol dm⁻³ H_2SO_4; $f = 40.5$ Hz; $v = 10$ mV s⁻¹; modulation amplitude = 50 mV; $s = 1$ mA; $E_i = -0.10$ V; and $t_{acc} = 60$ s.

from the slope of this system to be 0.42; puerarin undergoes a one-electron reduction, *i.e.*, $n = 1$, hence $\alpha = 0.42$. This belongs to an irreversible process.

Adsorption isotherm

From serial curves of differential capacitance at different concentrations of puerarin, the surface fraction of adsorbed species θ may be calculated. Fig. 7 illustrates the relationship between θ and c_{PRR}. When the concentration of puerarin is small, the surface coverage increases linearly with increasing c_{PRR}. However, at higher concentrations of puerarin, $c_{PRR} \approx 4.0 \times 10^{-6}$ mol dm^{-3}, the curve tends to level off, and full surface coverage is reached. A linear relationship between $\ln[c(1 - \theta)/\theta]$ and θ was found. This indicates that the adsorption of puerarin obeys the Frumkin isotherm,[12] with an adsorption coefficient $\beta = 1.14 \times 10^5$ and an interaction factor $\alpha = 1.54$. The adsorption coefficient β depends on the interaction between the adsorbed species and the electrode

surface, thus relating to the Gibbs energy of adsorption. A 25 °C, the Gibbs energy of adsorption $\Delta G° = -28.82$ kJ mol^{-1}, indicating that the reaction species has a stronger adsorption. The value of α depends primarily on the structure of the adsorbed particles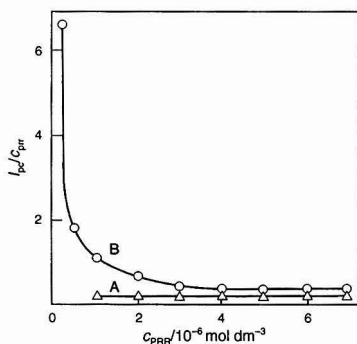 and may also be a function of potential. The value of α is positive, indicating that the interactions between the adsorbed species on the electrode surface are attractive.

Conclusion

As mentioned above, the number of electrons transferred per puerarin molecule is $n = 1$, the structure of puerarin is like that of a morin. Li and Xu[13] studied the electrochemical behaviour of morin and its electrode reaction mechanism, and considered that the reduction of morin is a two-step, one-electron process. Hence from all the experimental and calculated results, it can be concluded that the electrode reaction mechanism of puerarin is as follows:

(1) On scanning to -0.96 V (*versus* Ag–AgCl), the first-step reduction of puerarin, involves one electron:
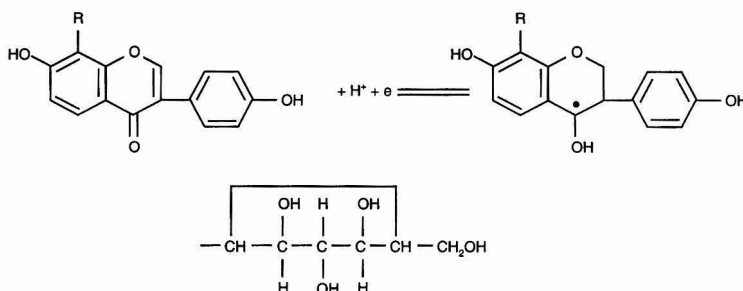
(2) On scanning further than -1.1 V, the second-step reduction, a discharge of hydrogen ion into the electrolyte solution interferes with the second peak:
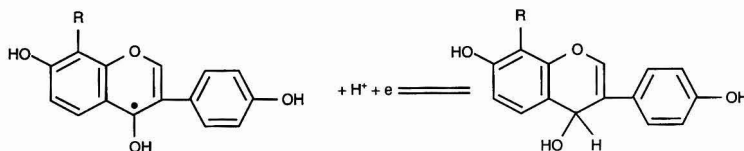
References

1 Xu, L. X., and Liu, A. R., *Fenxi Huaxue*, 1976, **4**, 372.
2 Xu, L. X., and Liu, A. R., *Zhongcaoyao*, 1975, **6**, 9.
3 Zhao, S. P., and Zhang, X. Z., *Yaoxue Xuebao*, 1985, **20**, 203.
4 Xu, L. X., and Liu, A. R., *Yaoxue Tongbao*, 1980, **15**, 40.
5 Xu, L. X., and Liu, A. R., *Yaoxue Xuebao*, 1991, **26**, 475.
6 Zhao, H. C., and Fang, X., unpublished results.
7 Osteryoung, A., Lauer, G., and Anson, F. G., *Anal. Chem.*, 1962, **34**, 1833.
8 Li, Q. L., and Chen, S. A., *Anal. Chim. Acta*, 1994, **282**, 145.
9 Li, Q. L., Chen, S. A., and Shang, J., *Gaodeng Xuexiao Huaxue Xuebao*, 1994, **15**, 339.
10 Wopschall, R. H., and Shain, I., *Anal. Chem.*, 1967, **39**, 1514.
11 Li, Q. L., *Huaxue Tongbao*, 1994, **10**, 13.
12 Moncelli, M. R., Nucci, L., Mariani, P., and Guidelli, R., *J. Electroanal. Chem.*, 1985, **183**, 285.
13 Li, N. Q., and Xu, H. W., *Wuli Huaxue Xuebao*, 1993, **9**, 175.

Indirect, Ion-annihilation Electrogenerated Chemiluminescence and Its Application to the Determination of Aromatic Tertiary Amines

Andrew W. Knight and Gillian M. Greenway*

Department of Chemistry, University of Hull, Hull, North Humberside, UK HU6 7RX

A novel method for the determination of aromatic tertiary amines has been developed, based on indirect, ion-annihilation electrogenerated chemiluminescence detection, using simplified flow injection instrumentation. The method has been used for the determination of a model compound, *N,N,N′,N′*-tetramethyl-*p*-phenylene diamine. Various experimental conditions including applied potentials, electrolyte type and concentration, and flow rate have been optimized, leading to a detection limit of 4×10^{-7} mol l^{-1}, with a log-linear range over three decades of concentration. The expected general formula of potential analyte compounds compatible with this technique is postulated to be ArNR$_2$, where R is a methyl or Ar group, and Ar is a simple aromatic system.

Keywords: Electrogenerated chemiluminescence; ion annihilation; aromatic tertiary amine

Introduction

Electrogenerated chemiluminescence (ECL) is a technique by which a chemiluminescent reaction is initiated at an electrode by application of a selected potential. ECL offers all the analytical advantages of conventional chemiluminescence (CL) methodology, including high sensitivity and selectivity, with the added benefits of increased control over the rate and course of the reaction, the ability to generate reagents, especially unstable reactive species, *in situ* when required at the electrode from passive precursors in the carrier stream, and the option to electrochemically modify an analyte prior to CL detection.

Only recently, however, has the analytical usefulness of this technique begun to be fully realized, and the analytical applications of ECL become the subject of comprehensive reviews.[1,2] This work concerns the area of ion-annihilation ECL reactions between organic radical ions. Although the oldest and most studied area of ECL, in terms of mechanisms and excited state production efficiencies, the reactions have received little attention in quantitative analytical chemistry. This is mainly owing to solvent limitations, the need to vigorously exclude water and oxygen to prevent quenching of the ECL reaction, and the complexity of the ion-annihilation mechanism.

Anion and cation radicals of polyaromatic hydrocarbons (A) can be sequentially generated at a single electrode in non-aqueous aprotic solvents, by application of a double step potential, alternating between the reduction and oxidation potentials of the compound, respectively. The subsequent exothermic electron transfer reaction between these radical ions generates the excited singlet species ^{1}A*, which emits

light with a spectrum characteristic of the fluorescence emission.

$$A - e^- \rightarrow A^{+\cdot} \qquad \text{Electro-oxidation} \qquad (1)$$

$$A + e^- \rightarrow A^{-\cdot} \qquad \text{Electro-reduction} \qquad (2)$$

$$A^{+\cdot} + A^{-\cdot} \rightarrow A + {}^1A^* \qquad \text{Electron transfer} \qquad (3)$$

$$^1A^* \rightarrow A + h\nu \qquad \text{Chemiluminescence} \qquad (4)$$

Fleet and co-workers[3,4] were amongst the first to propose the use of this type of ECL reaction for analytical determinations, and investigated the ECL of 24 aromatic compounds, achieving detection limits of 0.05–3 µg ml^{-1}. Sato *et al.*[5] used the reaction for the microanalysis of substituted anthracenes, and by careful selection of the applied potential wave form, trace amounts of diphenylanthracene were detected in a much larger concentration of dipropylanthracene. This demonstrated the added selectivity of ECL as both compounds have similar fluorescence spectra. Schaper[6] developed a thin-layer flow cell for normal phase HPLC–ECL detection, and used this to determine rubrene down to a detection limit of 25 pg. Later workers[7–10] developed various flow cell designs to determine aromatic hydrocarbons for use with reversed-phase HPLC–ECL, using high voltages (7–10 V) and low frequency pulsing (5–10 Hz). The determination of potentially ecologically toxic polyaromatic hydrocarbons in waste and other waters, has been successfully carried out by Rozhitskii *et al.*[11] Their method includes extraction of the sample by benzene, and transfer of the extract into an aprotic dipolar solvent for measurement of ECL intensity in specially constructed instrumentation.

In each of these instances the analysis is by 'direct' ECL detection, *i.e.*, the desired analyte is the emitting luminophore in the reaction. As only a limited number of compounds are directly electrochemiluminescent, this restricts the analytical applicability of the technique. Most CL and ECL methods, however, are essentially 'indirect', *i.e.*, a reaction occurs involving the analyte compound which leads to an emission from an added luminophore, and therefore the concentration of the analyte in some way effects the intensity of light generated in the reaction. For example the detection of metal ions that act as catalysts for the luminol CL and ECL reactions. Hence the indirect approach extends the technique to a much greater variety of compounds available to ECL detection. In the instance of the organic ECL reaction discussed, a suitable donor molecule such as a tertiary aromatic amine, can replace the cation precursor in reaction (1) to yield chemiluminescence from the polyaromatic hydrocarbon. In this work the polyaromatic hydrocarbon 9,10-diphenylanthracene (DPA) was used as the detector luminophore, and the cation precursor *N,N,N′,N′*-tetramethyl-*p*-phenylene diamine (TMPD) as the model analyte. Because the oxidation potential of TMPD (+0.35 V *versus* Ag wire) is lower than that of DPA (+1.80 V *versus* Ag wire), TMPD$^{+\cdot}$

radical ions could be produced selectively. The reaction proceeds as follows

$$TMPD - e^- \rightarrow TMPD^{+\cdot}$$
$$\text{Electro-oxidation} \qquad (6)$$

$$DPA + e^- \rightarrow DPA^{-\cdot}$$
$$\text{Electro-reduction} \qquad (7)$$

$$TMPD^{+\cdot} + DPA^{-\cdot} \rightarrow TMPD + {}^3DPA^*$$
$$\text{Electron transfer} \qquad (8)$$

$$2\,{}^3DPA^* \rightarrow DPA + {}^1DPA^*$$
$$\text{Triplet–triplet annihilation} \qquad (9)$$

$${}^1DPA^* \rightarrow DPA + h\nu \,\text{Chemiluminescence} \qquad (10)$$
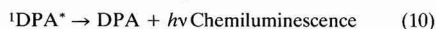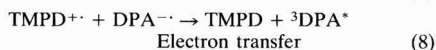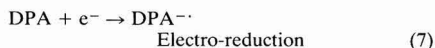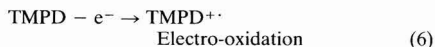
Owing to the lower energy available from the electron transfer reaction (8), the triplet excited state ${}^3DPA^*$ is formed, and a subsequent energy transfer reaction produces the emitting single state.[1] DPA was selected as the detector luminophore due to its high quantum efficiency for fluorescence, and low triplet energy for the electron transfer. TMPD was chosen as the model analyte due to its well characterized reversible one-electron oxidation, high stability of the radical ion, and known ECL reaction with DPA radical anions.

This approach has the unique characteristic of producing a non-destructive CL reaction in which both the reagent and the analyte species are regenerated during the course of the reaction. Hence each redox pair of molecules can emit several photons per measurement cycle, enhancing the sensitivity of the technique.

Analytical aspects of this indirect ECL approach have only been practically investigated in the past by Huret and Maloy,[12] and by Rozhitskii and Golovenko.[13] Huret and Maloy used a potential scan method for the determination of TMPD in the presence of excess DPA. As the method measured the ECL intensity as a function of potential, it represented the stationary electrode ECL equivalent of polarography. A calibration was obtained in the range $2–25 \times 10^{-5}$ mol l^{-1}, however, the method used an elaborate batch electrochemical cell, and was complicated by the procedures to exclude water and oxygen. The method included the transfer of solutions under high vacuum, on-line de-gassing by several freeze–thaw cycles, the weighing of the apparatus before and after reagent transfer and de-gassing, to ascertain volumes and hence concentrations used, and the preparation of reagent solutions within a glove box purged with nitrogen. ECL experiments were carried out in a dark room with a shuttered photomultiplier tube. Rozhitskii and Golovenko considered theoretically the indirect organic ECL approach for analytical applications, using numerical calculations based on diffusion equations for the reactants and products. They have shown that for diffusion-controlled reactions a linear concentration to ECL intensity relationship is obtained when the concentration of the detector luminophore is three to five orders of magnitude lower than the compound to be determined, in contrast to Huret and Maloy who employed an excess of luminophore.

The aim of the present work was to investigate the analytical potential of indirect ion-annihilation ECL detection, initially for the model analyte TMPD, and to implement more practical simplified apparatus, using flow injection instrumentation and an enclosed light-tight flow cell. Characteristics of the flow injection method were studied, and factors affecting the ECL intensity optimized, to achieve a lower detection limit and wider linear range than in previous investigations. Finally other classes of potential analyte compounds have been suggested to extend the technique.

Experimental

Reagents

All electrolyte and sample solutions were prepared using acetonitrile (HiPerSolv, HPLC grade, 99.7% containing only 0.1% H_2O; BDH, now Merck, Poole, UK). 9,10-Diphenylanthracene (99%) was obtained from Lancaster Synthesis, (Morecambe, UK). N,N,N',N'-tetramethyl-p-phenylene diamine (Purum, >98%), tetrabutylammonium hydrogensulfate (Puriss, >99%), tetrabutylammonium perchlorate (Puriss electrochemical grade, >99%), and tetrabutylammonium hexafluorophosphate (Puriss electrochemical grade, >99%) were all obtained from Fluka, (Gillingham, UK). All solid reagents were stored in dry conditions over calcium chloride, and used without further purification.

Instrumentation and Procedure

Fig. 1 shows the layout of the flow injection system and instrumentation used for the electrogeneration of CL. A blank electrolyte solution is constantly pumped through the system to maintain electrical contact between the electrodes, and provide a carrier stream. The two valves (Rheodyne Model 5020; Supelco, Poole UK) allow 100 μl volumes of sample solution to be injected into the carrier stream within an enclosed system, which excludes oxygen. PTFE (0.8 mm diameter) tubing was used throughout the manifold. The sample solution contains the same concentration of added electrolyte as the carrier stream. Both the background electrolyte and sample solutions were prepared in the open laboratory, purged with nitrogen for 5–10 min prior to use, and kept under a stream of nitrogen during the experiment. The nitrogen passes first through a wash bottle containing dry acetonitrile (not shown in Fig. 1), to saturate the gas, and reduce evaporation of the carrier and sample solutions during de-gassing.

As the reaction is electro-initiated within the flow cell, all the reagents can be mixed 'cold' prior to injection, forming the sample solution, and hence the flow injection manifold is simplified by reducing the number of reagents needing to be pumped separately to the reaction site as with more conventional CL flow injection manifolds. The solutions pass into a specially constructed light-tight PTFE flow cell, (built in-house), which incorporates a platinum disc working electrode, 4 mm in diameter, over which the reagents flow and the ECL reaction is initiated in view of a photomultiplier tube (PMT) (9789QB, Thorn EMI, Ruislip, UK) used for light detection. The PTFE flow cell is light-tight by virtue of a tight fitting aluminium housing which encapsulates the cell (for clarity not shown in Fig. 1), and is electrically insulated from the
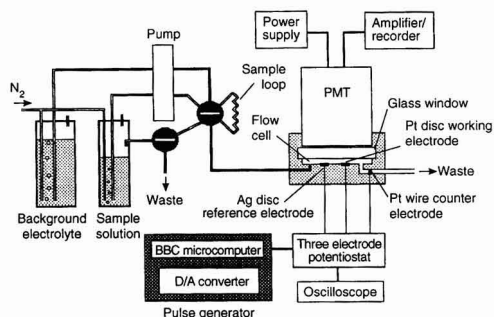

Fig. 1 Schematic diagram of the flow injection manifold and instrumentation used for the electrogeneration of chemiluminescence.

electrode control electronics. The housing has small holes drilled in appropriate positions to allow the insertion of, tubing for the in- and out-flow of reagents, and insulated wires to the electrodes. All the PTFE tubing is shielded with black PVC cover tubing to a suitable distance from the housing to prevent light entering the cell by light piping. The PMT is placed inside a steel housing, which screws *via* a long thread into the aluminium housing, such that the PMT is mounted directly in front of and as close as possible to, the flow cell window. The PMT is powered by a high voltage power supply, (Model 3000R, Thorn EMI), and the response is recorded using a chart recorder (Chessel, Worthing, UK).

The flow cell also incorporates a silver disc pseudo-reference electrode, 4 mm in diameter, within the cell, and a platinum wire counter electrode downstream of the cell. Although silver metal is not normally considered adequate as a reference electrode for electrochemical measurements, as it can be easily polarized and is hence subject to drift, it has proved to be sufficiently stable throughout an experiment in the solvent environment used. It also offers the advantages of simplicity, ease of construction, small size and minimum solution contamination. The effective flow cell volume is 150 μl, formed by an elliptical PTFE spacer, held between a glass window, and a PTFE back plate which houses the disc electrodes. Potentials are applied to the electrodes *via* a computer-controlled three-electrode potentiostat, designed and built in-house.

The software allows the flexible application of a square wave potential waveform, where the positive and negative pulsing limits (maximum ±2.5 V), and the applied frequency (maximum 245 Hz), can be controlled. The potential waveforms created are observed *via* an oscilloscope (Telequipment-Serviscope D52; Tektronix UK, Marlow, UK).

Experimental

Static System

The electrochemical characteristics of the reaction were first studied using static volumes of sample solution within the cell, in contact with all three electrodes. The working electrode was pulsed between −2.0 V (producing DPA⁻·), and a linearly increasing positive potential. The ECL appearance potentials were +0.37 V for a mixed TMPD–DPA solution (sample), and +1.75 V for a DPA only solution (blank), closely matching the oxidation potentials of TMPD and DPA respectively (*versus* Ag wire). The greatest ECL intensity is observed at the optimum pulsing frequency of 70 Hz, and owing to the cyclic nature of the reaction, with continued pulsing an ECL signal can be maintained over several minutes.

In a static system the analysis is carried out by a stopped-flow method, passing a sample solution to the cell, and pulsing with the appropriate square-wave voltage for a period of time (typically 2–10 s), to just achieve a steady ECL reading. The ECL decays very rapidly on removal of the voltage as there is no large build up of radical species in the vicinity of the electrode owing to their short lifetime in solution, and hence a response 'peak' is observed on the recorder and a peak height is measured. However, the signals obtained for any particular solution were observed to increase with each measurement pulse as shown in Fig. 2. The effect makes it difficult to obtain a reproducible set of peaks for a sample until the plateau in the peak heights is reached. This behaviour resembled an accumulation of an ECL active species on the electrode, or a sensitizing of the electrode surface, although the exact cause of this effect has not been determined. The effect is also observed for solutions of DPA only (blank solutions), and the rate at which the plateau is reached is effected by the ratio of the concentrations of TMPD to DPA. The effect is related to

the length of time the sample solution is in contact with the electrodes, even when they are held at zero volts, and not the length of the voltage pulsing time, hence the signal enhancement was not thought to be due to the electro-deposition of a species from solution. Fig. 2 also demonstrates this, showing how the enhancement effect is related to the length of time the sample solution is in contact with the electrode, by taking several ECL measurements at differing time intervals for separate sample solutions.

Various electrochemical cleaning pre-treatments were tried between samples in order to achieve reproducible peaks for each sample without the irreproducible enhancement effect, however, the most effective method was simply to pass blank clean electrolyte solution through the cell for typically 30–120 s, to wash the flow cell and electrode surface. Hence a flow injection method was developed using a continuously pulsing voltage, a flowing carrier stream of blank electrolyte solution, and the injection of sample solutions at regular time intervals, producing a transient ECL signal, interspersed with periods of electrode cleaning. In this way reproducible peaks could be obtained and ECL peak heights measured.

Flow Injection System

Background and blank emissions

Weak background ECL emissions are observed from acetonitrile solutions containing only electrolyte with no added luminescors, when the electrode is pulsed. Pulsing the voltage between the limits of interest (+0.5 to −2.0 V) at 71 Hz, the background ECL was measured above the photomultiplier tube dark current, for various tetrabutylammonium salts commonly used as electrolytes, and the effect of nitrogen de-gassing observed. Fig. 3 illustrates that de-gassing had the greatest effect on solutions of tetrabutylammonium hydrogen-
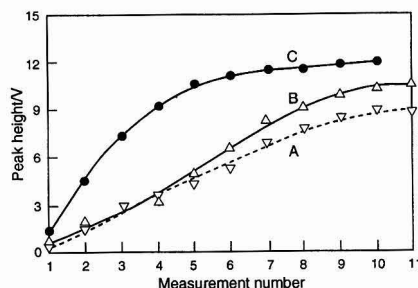
Fig. 2 Effect of the delay time left between successive measurements of ECL peak height: A, 0; B, 5; and C, 30 s. Concentrations: 1×10^{-4} mol l⁻¹ DPA; 1×10^{-5} mol l⁻¹ TMPD; 0.020 mol l⁻¹ TBAHSO₄.
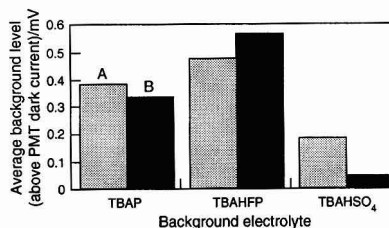
Fig. 3 ECL background emission for various electrolytes in dry acetonitrile. TBAP, tetrabutylammonium perchlorate; TBAHFP, tetrabutylammonium hexafluorophosphate; and TBAHSO₄, tetrabutylammonium hydrogen sulfate. A, Not de-gassed, and B, de-gassed.

sulfate (TBAHSO$_4$), greatly reducing background levels. TBAHSO$_4$ also demonstrated lower average noise levels, about half that of TBAP or TBAHFP measured peak to peak. The ECL background emission is postulated to arise from reactions involving radicals deriving from the tetrabutylammonium ion and the respective anion, although the exact mechanism has not been investigated. Dissolved oxygen in the solution may play two opposing roles depending on the reactions concerned, and either be involved in the reaction and hence enhance the background ECL, or quench radical ions involved in the reaction and hence reduce the background ECL. This may explain the differing behaviour of TBAHFP and TBAHSO$_4$ (see Fig. 3). While de-gassing enhances the ECL analytical signal by reducing quenching by dissolved oxygen, it also reduces the background noise, and hence this is a desirable situation. As TBAHSO$_4$ had no detrimental effect on the ECL reaction, is not electrochemically active under the experimental conditions used, and gave the lowest background and noise levels, it was used as the electrolyte throughout the study. The optimum electrolyte concentration was 0.02–0.03 mol l^{-1}, higher concentrations (>0.7 mol l^{-1}) noticeably reduced the ECL emission.

Although TBAHSO$_4$ is extremely soluble in acetonitrile, care was taken to avoid trace amounts of moisture contaminating the electrolyte or solvent, as this led to the formation of a fine white precipitate of the sulfate, produced by the following reaction

$$2N(C_4H_9)_4HSO_4 + 2H_2O \rightarrow 2H_3O^+ + SO_4{}^{2-} + \\ [N(C_4H_9)_4]_2SO_4 \downarrow \quad (11)$$
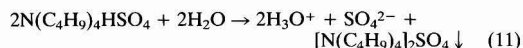
The precipitate redissolved on adding an excess of water. The presence of the precipitate slightly reduces the ECL intensity, and a problem of blockages in flow tubes and connections was observed with prolonged pumping of the slightly turbid solution.

A larger ECL background emission is observed for solutions containing electrolyte and the fluorescent detector (DPA) in acetonitrile, when pulsed between −2.0 V, producing DPA$^{-\cdot}$, and positive potentials lower than that required to produce DPA$^{+\cdot}$. Such an emission constitutes a blank signal, in the absence of TMPD, when pulsing to the oxidation potential of TMPD. This phenomenon is known as pre-annihilation electrogenerated chemiluminescence (PAECL),[14] and the chemiluminescence is generally ascribed to reactions involving the radical ion such as DPA$^{-\cdot}$, and solvent molecules, electrolytes or unspecified impurities. The emission had an intensity of about 2% of the corresponding ion-annihilation reactions [(3) and (4)] under similar conditions. The presence of the fluorescent DPA may also sensitize the weak background ECL resulting from the electrolyte and solvent.

Effect of applied voltage frequency

The effect of the applied frequency of the square-wave pulsing voltage was investigated in the range 25–245 Hz, for a sample and blank solution. The ECL intensity showed a clear maximum around 125 Hz for the blank, and 200 Hz for the sample solution, as shown in Fig. 4. Hence the possibility of discriminating between the signal and blank reactions on the basis of frequency has been demonstrated, as the reactions are likely to possess different electrode diffusion characteristics. The optimum frequencies would appear to lie in the region 175–245 Hz, where the maximum signal to blank ratio is observed. However, the flow injection peaks obtained for sample solutions in this region, although large, were ill-defined in shape, particularly noisy and hence possessed low reproducibility, limiting the analytical value of the measurements. The frequency range 90–170 Hz was avoided owing to

the large blank signal obtained. Hence a local maximum in the range 55–75 Hz had to be selected for the study, which gave a reasonable signal-to-blank ratio, with smooth well defined reproducible peaks. The optimum frequency lay in the narrow range 58–62 Hz, and slight adjustments to the frequency were required within this range for different experiments, depending on experimental conditions, to obtain optimum analytical performance.

Positive pulse voltage

Sample and blank solutions were injected, and the ECL intensity recorded, whilst the working electrode was pulsed between −2.0 V (producing DPA$^{-\cdot}$) and a set of linearly increasing positive potentials (see Fig. 5). The optimum voltage for the TMPD sample solution was +0.32 V, corresponding to the oxidation potential of the compound, and the ECL appearance potential as seen in the static system. The blank signal for DPA only becomes significant above 1.5 V, and hence a window is created from 0 to 1.5 V (*versus* Ag wire), where the oxidation potential for analyte compounds should lie in order to give the maximum S/N ratio.

Effect of flow rate

The ECL intensity, measured as the flow injection peak height, was observed to increase with flow rate as shown in Fig. 6, over the full range of pump speeds attainable. The ECL reaction when pulsed at 60.5 Hz was sufficiently rapid as to not be significantly disturbed by flow rates up to at least 2.6 ml min^{-1}, and in each instance using higher concentrations of reagents the ECL could be visually observed to be confined only to the electrode surface. The flow rate was chosen at 1.8
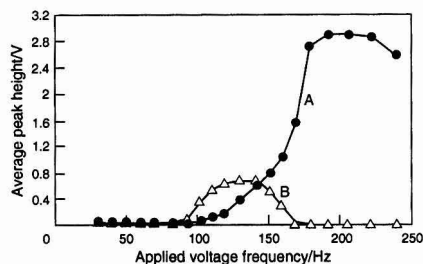
Fig. 4 Variation of ECL peak height with applied potential pulsing frequency (+0.5/−2.00 V). A, TMPD–DPA (sample); and B, DPA only (blank) concentrations: 1 × 10^{-4} mol l^{-1} DPA; 1 × 10^{-5} mol l^{-1} TMPD; and 0.030 mol l^{-1} TBAHSO$_4$.
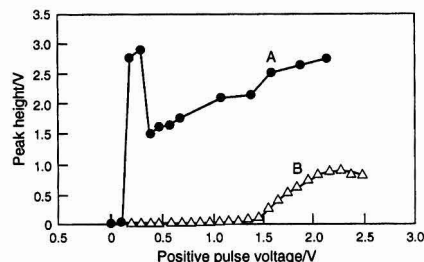
Fig. 5 Variation of ECL intensity with applied positive pulse voltage. Negative pulse −2.00 V, at 60.50 Hz. A, TMPD–DPA (sample); and B, DPA only (blank) concentrations: 1 × 10^{-4} mol l^{-1} DPA; 1 × 10^{-4} mol l^{-1} TMPD, and 0.025 mol l^{-1} TBAHSO$_4$.

ml min^{-1}, to give near optimum peak height without excessive consumption of the reagents.

Calibration characteristics

Using the optimum conditions: voltage profile, square wave +0.35 to −2.00 V (*versus* Ag wire), applied at 58 Hz; [DPA] = 1 × 10^{-5} mol l^{-1}; electrolyte, [tetrabutylammonium hydrogensulfate] = 0.025 mol l^{-1}; flow rate, 1.8 ml min^{-1}, a near linear log–log calibration could be obtained over 3 decades of concentration, with a correlation coefficient of 0.991 (see Fig. 7). The limit of detection achieved was observed to be 4 × 10^{-7} mol l^{-1}, which produced a signal three times as intense as that of the blank (DPA only) solution, under the same conditions. For shorter range calibrations the most reproducible peaks were obtained when the concentration of the detecting luminophore DPA was 10–100 times larger than the concentration of the analyte TMPD. Such a calibration graph is shown in Fig. 8. The average s_r value for the top four standards is 1.3% (n = 5), each point on the calibration graph being the average of five replicate injections. The increase in signal intensity with increased detecting luminophore concentration is evident by comparison of the two calibration graphs. For example an increase in DPA concentration from 1 × 10^{-5} mol l^{-1} (Fig. 7) to 2 × 10^{-4} mol l^{-1} (Fig. 8), gives an approximately 30-fold increase in signal for TMPD concentrations in the range 1 × 10^{-4}–1 × 10^{-5} mol l^{-1}.

Conclusions

The method described herein has been shown to be suitable for the analysis of TMPD in acetonitrile solutions, to a lower limit of detection and wider dynamic range than previously
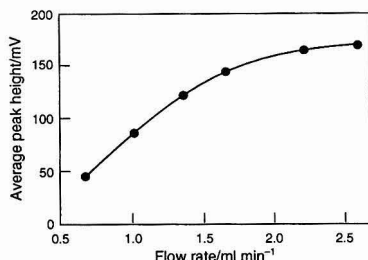
Fig. 6 Effect of flow rate on ECL peak height. Concentrations: 1 × 10^{-4} mol l^{-1} DPA, 1.4 × 10^{-5} mol l^{-1} TMPD, and 0.030 mol l^{-1} TBAHSO$_4$.
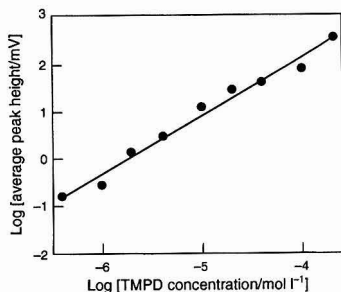
Fig. 7 Wide concentration range TMPD log–log calibration. Concentrations: 1 × 10^{-5} mol l^{-1} DPA, and 0.025 mol l^{-1} TBAHSO$_4$.

attained. A considerable simplification in both the apparatus and methodology used for organic ion-annihilation ECL has also been successfully implemented. The use of this method is obviously limited to compounds the electrochemically-generated oxidant of which will react with DPA$^{-\cdot}$ to produce ECL. However, it is postulated that the general formula of potential analyte compounds, that should form sufficiently stable cation radicals by reversible one-electron oxidation, is ArNR$_2$, where R is a methyl group or Ar, and Ar is a simple aromatic system. For example further work in this laboratory has shown that analytical signals can be obtained for dimethylaniline and some of its derivatives such as the insecticide 4-dimethyl-amino-*m*-toyl-methylcarbamate (Aminocarb).

Furthermore, as many other indirect ion-annihilation ECL reactions are known, the method should be more widely applicable than indicated in this work. Such reactions include the ECL generated from aromatic hydrocarbons and the cation precursors: 1,4-dihydropyridines,[15] halogen ions,[16] *n*-butylamine and triethylamine,[17] peroxydisulfate,[18] tetraphenylporphins,[19] tetrathiafulvalene,[20] 10-methylphenothiazine,[21] 2,5-diphenyl-1,3,4-oxadiazole,[22] reduced nicotinamide adenine dinucleotide (NADH),[23] triphenylamine derivatives,[24] and aromatic sulfonyl compounds.[25] The sulfur analogue of TMPD, dithiohydroquinone dimethylether,[26] although not as yet investigated for ECL activity, has been shown to exhibit reversible one-electron oxidation producing a radical species in the same way as TMPD, and hence this compound and some of its derivatives may also be potential candidates for the reaction.

Future work will be concerned with the preconcentration of selected compounds such as suitable agrochemicals, *e.g.*, pesticides, and subsequent transfer from aqueous to the aprotic organic solvent system. One limitation of the method, however, was that water was observed to quench the reaction reducing the ECL intensity to only a few percent of the original signal, when 1–3% water was added to the acetonitrile solution. This is not thought to be a major disadvantage as many procedures for pesticide analysis involve a preconcentration and sorbent extraction stage into an organic solvent. Attention must, however, be paid to the purity and dryness of the final solvent. ECL has been carried out in a variety of solvents, such as acetonitrile, dimethyl formamide (DMF), toluene, propylene carbonate and 1,2-dimethoxyethane, or mixtures of these solvents, although acetonitrile and DMF have proved to be the most suitable. Other work has also demonstrated the effect of water quenching is less severe using much higher pulsing frequencies in the region of kHz applied to microelectrodes, where 10% water could be tolerated.[27]

Currently work is continuing to assess the influence of the concentration of the luminophore (DPA) with respect to the concentration of the analyte, on the analytical response and calibration characteristics, and to assess relationships between the tertiary amines structural attributes and the ECL activity, in order to consider further potential applications for the technique.
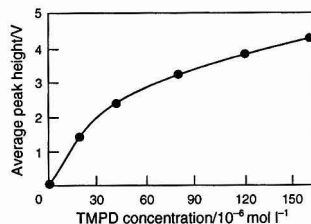
Fig. 8 Short concentration range TMPD calibration. Concentrations: 2 × 10^{-4} mol l^{-1} DPA, and 0.025 mol l^{-1} TBAHSO$_4$.

References

1 Knight, A. W., and Greenway, G. M., *Analyst*, 1994, **119**, 879.
2 Rozhitskii, N. N., *J. Anal. Chem. USSR (Engl. Transl.)*, 1992, **47**, 1288.
3 Fleet, B., Kirkbright, G. F., and Pickford, C. J., *Talanta*, 1968, **15**, 566.
4 Fleet, B., Keliher, P. N., Kirkbright, G. F., and Pickford, C. J., *Analyst*, 1969, **94**, 847.
5 Sato, M., Yamada, T., and Fujino, M., *Nippon Kagaku Kaishi*, 1981, **1**, 74; *Chem. Abstr.*, 1981, **94**, 149742s.
6 Schaper, H., *J. Electroanal. Chem. Interfacial Electrochem.*, 1981, **129**, 335.
7 Blatchford, C., and Malcolme-Lawes, D. J., *J. Chromatogr.*, 1985, **321**, 227.
8 Blatchford, C., Malcolme-Lawes, D. J., and Humphreys, E., *J. Chromatogr.*, 1985, **329**, 281.
9 Hill, E., Humphreys, E., and Malcolme-Lawes, D. J., *J. Chromatogr.*, 1986, **370**, 427.
10 Hill, E., Humphreys, E., and Malcolme-Lawes, D. J., *J. Chromatogr.*, 1988, **441**, 394.
11 Rozhitskii, N. N., and Belash, E. M., *Instrum. Metody. Anal. Ekol.*, 1991, **1**, 142; *Chem. Abstr.*, 1993, **118**, 51514h.
12 Huret, T. M., and Maloy, J. T., *J. Electrochem. Soc.*, 1974, **121**, 1178.
13 Rozhitskii, N. N., and Golovenko, V. M., *Sov. Electrochem. (Engl. Transl.)*, 1991, **27**, 178.
14 Blatchford, C., and Malcolme-Lawes, D. J., *J. Chem. Soc., Faraday Trans. 2*, 1986, **82**, 423.
15 Ludvik, J., Volke, J., and Pragst, F., *J. Electroanal. Chem. Interfacial Electrochem.*, 1986, **215**, 179.
16 Kihara, T., Sukigara, M., and Honda, K., *Electrochim. Acta*, 1973, **18**, 639.
17 Hercules, D. M., Landsbury, R. C., and Roe, D. K., *J. Am. Chem. Soc.*, 1966, **88**, 4578.
18 Becker, W. G., Seung, H. S., and Bard, A. J., *J. Electroanal. Chem. Interfacial Electrochem.*, 1984, **167**, 127.
19 Tokel, N. E., Keszthelyi, C. P., and Bard, A. J., *J. Am. Chem. Soc.*, 1972, **94**, 4872.
20 Wallace, W. L., and Bard, A. J., *J. Electrochem. Soc.*, 1978, **125**, 1430.
21 Bezman, R., and Faulkner, L. R., *J. Am. Chem. Soc.*, 1972, **94**, 6331.
22 Keszthelyi, C. P., Tachikawa, H., and Bard, A. J., *J. Am. Chem. Soc.*, 1972, **94**, 1522.
23 Ludvik, J., and Volke, J., *Anal. Chim. Acta*, 1988, **209**, 69.
24 Sharifian, H. A., and Park, S., *Photochem. Photobiol.*, 1982, **36**, 83.
25 Pragst, F., and Kaltofen, B., *Electrochim. Acta*, 1982, **27**, 1181.
26 Zweig, A., Hodgson, W. G., Jura, W. H., and Maricle, D. L., *Tetrahedron Lett.*, 1963, **26**, 1821.
27 Collinson, M. M., and Wightman, R. M., *Anal. Chem.*, 1993, **65**, 2576.

Development of a Novel Luminol-related Compound, 3-Propyl-7,8-dihydropyridazino-[4,5-*g*]quinoxaline-2,6,9(1*H*)-trione, and Its Application to Hydrogen Peroxide and Serum Glucose Assays

Junichi Ishida, Hiromi Arakawa, Maki Takada and Masatoshi Yamaguchi*

Faculty of Pharmaceutical Sciences, Fukuoka University, Nanakuma, Johnan-ku, Fukuoka 814-80, Japan

Manual and flow injection methods with chemiluminescence detection were developed for the determination of hydrogen peroxide (H_2O_2) using a novel luminol-related compound, 3-propyl-7,8-dihydropyridazino[4,5-*g*]quinoxaline-2,6,9(1*H*)-trione (PDIQ), having a higher efficiency than luminol. The methods are based on the chemiluminescence produced by the reaction of H_2O_2 with PDIQ in the presence of microperoxidase in alkaline media. Detection limits for manual and flow injection methods are 13 pmol per 100 µl of test solution and 1.3 pmol per 100 µl injection volume, respectively, at a ratio of chemiluminescence intensities (or peak heights) of test to blank of 2. The manual method was applied to the determination of glucose in human serum. The method correlated well with the conventional spectrophotometric method ($r = 0.998$).

Keywords: 3-Propyl-7,8-dihydropyridazino[4,5-g] quinoxaline- 2,6,9(1H)-trione; chemiluminescence detection; hydrogen peroxide determination; glucose determination; human serum

Introduction

The determination of hydrogen peroxide (H_2O_2) is very important in biological and clinical investigations. Spectrophotometric and fluorimetric methods based on the coupling oxidation of dyes with H_2O_2 using horseradish peroxidase as a catalyst have been reported for the determination of H_2O_2.[1,2] Recently, luminol[3-11] and peroxyoxalate chemiluminescence (CL) methods have been successfully introduced for the highly sensitive determination of H_2O_2.[12-18] Conventional luminol reaction methods were based on the CL generated from luminol itself. Therefore, the use of a luminol-related compound having a higher efficiency than luminol may increase the sensitivity of H_2O_2 determination.

Recently, we synthesized 3-propyl-7,8-dihydropyridazino[4,5-*g*]quinoxaline-2,6,9(1*H*)-trione (PDIQ) as a novel CL compound (Fig. 1).[19] Both PDIQ and luminol generate CL by reaction with H_2O_2 in the presence of microperoxidase in neutral and alkaline media (Fig. 1).

In this work, we evaluated PDIQ and luminol as CL compounds using microperoxidase, which is widely used as a catalyst in H_2O_2 determination.[13,18] As a result, we found that PDIQ gives more intense CL than luminol. Based on this finding, we propose novel manual and flow injection (FI) methods with CL detection for the sensitive determination of

H_2O_2 by using PDIQ. We also applied the manual method to the determination of glucose in human serum.

Experimental

Reagents and Solutions

All chemicals were of the highest purity available and were used as received. Distilled water, purified with a Milli-Q system (Japan Millipore, Tokyo, Japan), was used to prepare all aqueous solutions. Hydrogen peroxide (30% v/v) was purchased from Mitsubishi Gas Kagaku (Tokyo, Japan). Glucose and a glucose assay kit for the 4-aminoantipyrine method (Glucose B-Test, Wako) were obtained from Wako (Osaka, Japan). Glucose oxidase (GOD; EC 1.1.3.4) as type X with a specific activity of 128 000 units g^{-1} was purchased from Sigma (St. Louis, MO, USA). Mutarotase derived from porcine kidney with a specific activity of 10 000 units ml^{-1} was obtained from Wako.

PDIQ was prepared as described previously.[19] It was stable in the crystalline state for 1 year or longer even in daylight.

A 1 mmol l^{-1} PDIQ stock standard solution was prepared in dimethyl sulfoxide and diluted further with 10 mmol l^{-1} phosphate buffer (pH 7.0 and 8.0 for the manual and FI methods, respectively) to give the required concentrations before use. The PDIQ stock standard solution could be used for at least 1 month. Microperoxidase solutions were prepared in 10 mmol l^{-1} phosphate buffer (pH 7.0 and 8.0 for the manual and FI methods, respectively).

Serum Samples

Normal and clinical human serum specimens were obtained from healthy volunteers in our laboratories and from patients with diabetes in hospital (Kyushu Cancer Centre Hospital, Fukuoka, Japan), respectively.

Procedure for Evaluation of PDIQ and Luminol

CL intensities and reaction time courses were measured with an MLR-100 Microluminoreader (Corona Electric, Tokyo, Japan) equipped with a Corona DP-50 autopipetter.

A 100-µl portion of the PDIQ (or luminol) solution was placed in a well of a black microplate. The CL reaction was initiated by automatic injection of 100 µl of 50 µmol l^{-1} microperoxidase solution and 100 µl of 0.1 µmol l^{-1} hydrogen peroxide solution into the well. CL intensities were monitored immediately after the injection. The integrated CL intensity between 1.5 and 60 s after the injection was used for the evaluation of PDIQ and luminol.

---

* To whom correspondence should be addressed.

Manual Assay Procedure for H₂O₂

A 100 μl portion of H_2O_2 test solution was placed in the well of a black microplate. The CL reaction was initiated by automatic injection of 100 μl of 5 μmol l^{-1} microperoxidase solution and 100 μl of 10 μmol l^{-1} PDIQ solution into the tube. CL intensities were monitored immediately after the injection. For the blank, a 100 μl portion of water in place of H_2O_2 test solution was used. The integrated CL intensity between 15 and 60 s after the injection was used for the determination of H_2O_2.

FI Procedure for H₂O₂

A 100 μl volume of an H_2O_2 test solution was injected into the FI–CL system, which consisted of a pump (Model 880-PU; Jasco, Tokyo, Japan), a sample injector valve (Rheodyne Model 7125) with a 100 μl loop, a CL detector (AC-2220 luminometer; Atto, Tokyo, Japan) equipped with a 60 μl flow cell and a recorder (Model 561; Hitachi, Tokyo, Japan). Stainless-steel tubing (0.5 mm id) was used for the FI–CL system. The length of the reaction tube between the injector and detector was set at 100 cm. The test solution injected was mixed in the reaction tube with the PDIQ solution delivered at a flow rate of 0.5 ml min^{-1} by the pump; the reagent solution was a mixture containing PDIQ (20 μmol l^{-1}) and microperoxidase (12 μmol l^{-1}) in 10 mmol l^{-1} phosphate buffer (pH 8.0). The CL generated was monitored by the CL detector.

For the blank, a 100 μl portion of water was injected into the FI–CL system instead of H_2O_2 test solution.

Assay Procedure for Glucose in Human Serum

Human sera were diluted 100-fold with water. To a test-tube were successively added 200 μl of 100 mmol l^{-1} imidazole buffer (pH 6.75), 100 μl of the diluted serum sample, 100 μl of GOD (30 U ml^{-1}) and 20 μl of mutarotase solution (100 U ml^{-1}). After mixing, the mixture was allowed to stand at 37 °C for 10 min. The mixture was then cooled in ice–water to stop the enzymic reaction. A 100 μl volume of the mixture was treated as in the manual assay procedure.

The amount of glucose in human serum was calibrated by means of the standard additions method: the diluted plasma (100 μl) was replaced with 100 μl of the diluted plasma containing glucose (20 pmol–5 nmol). The net CL intensity was plotted against glucose concentration.

Spectrophotometric Method for the Determination of Glucose in Human Serum

Glucose levels in human sera were determined by a spectrophotometric method using a Glucose B-Test Wako kit with 4-aminoantipyrine.

Results and Discussion

Evaluation of PDIQ and Luminol as CL Compounds

PDIQ and luminol were evaluated as CL compounds. For luminol CL, microperoxidase, some transition metal ions (Cu^{2+}, Co^{2+} and Fe^{3+}) and hexacyanoferrate (III) have been widely used as catalysts.[20] From preliminary examinations, it was found that microperoxidase is the most suitable of these catalysts in the CL with PDIQ. When the other catalysts were used, a higher blank CL was observed. Further, it was confirmed that PDIQ gave the most intense CL when 50 μmol l^{-1} microperoxidase, 0.1 μmol l^{-1} hydrogen peroxide and 10 mmol l^{-1} phosphate buffer (pH 7.0) were used. Their optimum concentrations for PDIQ were almost identical with those for luminol. Under the optimum CL conditions, the integrated CL intensities for PDIQ and luminol were determined. As shown in Table 1, PDIQ produced approximately 2.5 times greater CL than luminol. This indicates that PDIQ is more useful than luminol as a CL compound for the determination of H_2O_2.

The kinetics of light emission from PDIQ seem to be the same as those from luminol. 3-Propyl-1,2-dihydro-2-oxoquinoxaline-6,7-dicarboxylic acid, which occurred in the reaction mixture, is expected to emit light under the present conditions (Fig. 1).

Manual Assay for H₂O₂

The time course of the CL reaction is shown in Fig. 2. The maximum intensity was obtained at <1.5 s after the injection of the microperoxidase and PDIQ solutions; the intensity at 60 s after the injection was approximately 1/100 of that at 1.5 s after the injection. The pattern of the curve was not affected by the concentrations of PDIQ, microperoxidase and phosphate buffer. On the other hand, the CL from the blank, which interfered with the determination of H_2O_2, almost disappeared within 15 s after the injection. Therefore, the integrated intensity was monitored at 15–60 s after the injection to give the maximum ratio of the test and blank intensities ($T : B$).

The optimum conditions for the determination of H_2O_2 were examined by using the manual method. The concentrations of PDIQ and microperoxidase and the pH of the phosphate buffer influenced the integrated CL intensities for

Table 1 Integrated CL intensities of PDIQ and luminol

Concentration/mol l^{-1}	Luminol*	PDIQ
1×10^{-6}	100	255
1×10^{-5}	1058	2408
1×10^{-4}	12 055	29 200

* Integrated CL intensity of 1 μmol l^{-1} luminol was taken as 100.

3-Propyl-7,8-dihydropyridazino-
[4,5-*g*]quinoxaline-2,6,9(1*H*)-trione
(PDIQ)
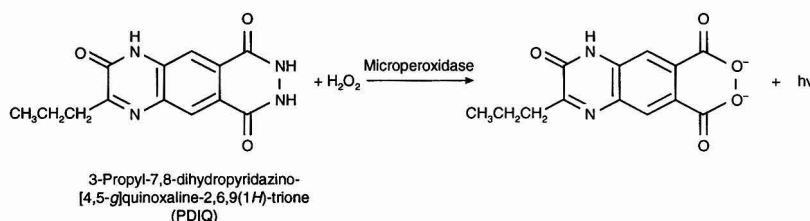
Fig. 1 Chemiluminescence reaction of PDIQ with hydrogen peroxide.

both the test and the blank. The conditions giving the highest CL intensity for the test were slightly different from those giving the highest ratio of the intensities for the test and blank $(T:B)$. We employed the conditions giving the highest $T:B$ ratio for the determination of H_2O_2. The concentrations of these reagents and the pH of the phosphate buffer were varied one at a time to establish the maximum $T:B$ ratio obtainable. Based on these experiments, 10 µmol l^{-1} PDIQ, 5 µmol l^{-1} microperoxidase and 10 mmol l^{-1} phosphate buffer (pH 7.0) were employed in the manual assay procedure.

The calibration graph was linear over the concentration range 0.2–50 µmol l^{-1} (20 pmol–5.0 nmol per 100 µl of test solution) $(r = 0.999)$. The precision was established by repeated analyses of 1.0 and 5.0 µmol ml^{-1} H_2O_2 solutions. The relative standard deviations were 4.5 and 5.8%, respectively $(n = 8$ in each instance). The detection limit was 13 pmol per 100 µl of test solution, which gave a CL intensity of twice the blank. The sensitivity was 2–3 times more sensitive than that with luminol.

FI Procedure for H_2O_2

As described above, the reproducibility in the manual method was relatively low. In order to improve the reproducibility, an FI system was introduced for the CL determination of H_2O_2.

The optimum CL reaction conditions for FI were examined using 1 µmol l^{-1} hydrogen peroxide (Figs. 3 and 4). PDIQ gave almost the largest CL peak height in the range 10–40 µmol l^{-1} in the reagent solution [Fig. 3(a)]. The peak height of the blank increased slightly in proportion to the PDIQ concentration. Therefore, 20 µmol l^{-1} PDIQ giving the maximum $T:B$ ratio was used as a suitable concentration. The microperoxidase concentration affected the peak height of the test and blank [Fig. 3(b)]. The peak height of the test was almost maximum in the concentration range 7.5–20 µmol l^{-1}. On the other hand, the height for the blank became smaller at microperoxidase concentrations <5 µmol l^{-1} and >30 µmol l^{-1}. As a result, the $T:B$ ratio was independent of the microperoxidase concentration; 10 µmol l^{-1} was adopted for the FI method. The CL peak height for the test solution increased with increasing pH of phosphate buffer in the PDIQ solution (Fig. 4). The peak height of the blank, however, also increased considerably with increase in pH. The phosphate buffer concentration did not influence the peak heights of either the test or blank solutions. Therefore, 10 mmol l^{-1} phosphate buffer (pH 8.0) was employed in the FI method. The length of the reaction tube affected the peak height of the test and blank solutions (Fig. 5). A 100 cm tube length giving the highest $T:B$ ratio was adopted.

The relationship between the peak height and the amount of H_2O_2 was linear from 3 pmol up to at least 300 pmol per 100 µl injection volume $(r = 0.999)$. Fig. 6 shows a typical recorder response for the H_2O_2 standard solution (0–50 pmol per 100 µl). The precision was established by repeated determinations $(n = 6)$ using an H_2O_2 test solution (50 pmol per 100 µl). The relative standard deviation was 2.0%. The detection limit was 1.3 pmol per 100 µl injection volume at a ratio of CL peak heights for the test and blank of 2.
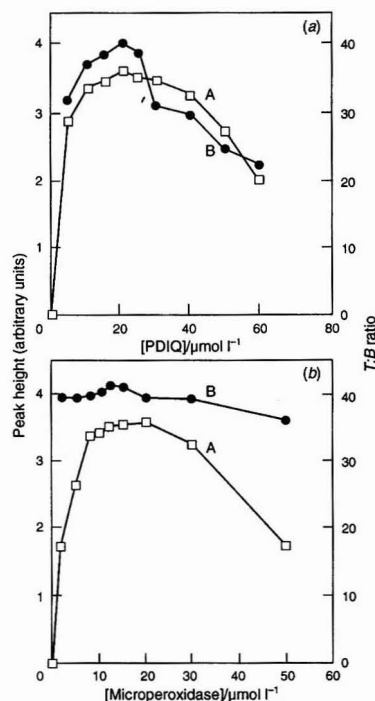
Fig. 3 Effects of (a) PDIQ and (b) microperoxidase concentrations on the CL peak height for A, the test and B, the $T:B$ ratio. Portions (100 µl) of a H_2O_2 test solution (1 µmol l^{-1}) were treated as in the FI method at various concentrations of the reagents.

Fig. 2 Time course of the CL reaction. A 100 µl portion of A, a 1 µmol l^{-1} H_2O_2 test solution (or B, water) was treated according to the manual method.
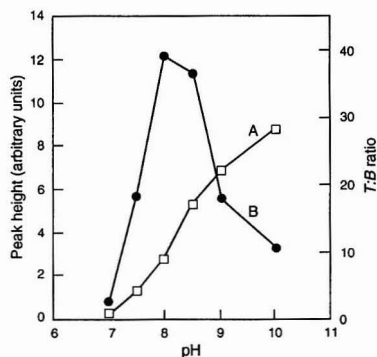
Fig. 4 Effect of pH of 10 mmol l^{-1} phosphate buffer on the CL peak height for A, the test and B, the $T:B$ ratio.

Plasma Glucose Assay

The manual method was applied to the determination of glucose in human serum. The method is based on the formation of H_2O_2 by the oxidation of glucose with glucose oxidase (GOD) and subsequent CL detection of H_2O_2 using the manual method.

The conditions for the conversion of α-D-glucose into β-D-glucose with mutarotase and enzymic conversion of D-glucose into H_2O_2 and D-gluconic acid with GOD were examined. The resulting optim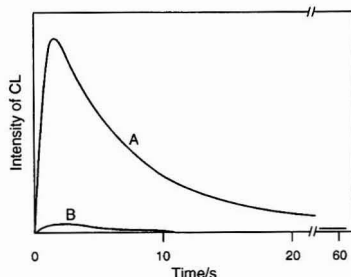um conditions were similar to those described by Nakashima *et al.*[17] The relationship between the net CL intensity and the amount of glucose was linear up to at least 20 μmol ml^{-1} serum ($r = 0.999$). The detection limit of the method for the determination of serum

Fig. 5 Effect of the tube length between the injector and CL detector on the peak height for A, the test and B, the $T:B$ ratio.

Fig. 6 Recorder responses for replicate injection of hydrogen peroxide. Numbers on the signals indicate the concentrations of hydrogen peroxide injected (in pmol l^{-1}).

glucose was 52 nmol ml^{-1} plasma. The present method with PDIQ is very sensitive and allowed the determination of glucose in an extremely small amount (1 μl) of human serum. The proposed method (y) was compared with the conventional spectrophotometric method with 4-aminoantipyrine (x) for the determination of glucose in normal and clinical human serum (5–340 mg dl^{-1}). A good correlation was obtained ($y = 1.022x + 3.317$; $r = 0.998$; $n = 22$).

Conclusion

The luminol-related compound PDIQ is easily synthesized and fairly stable in air and daylight. The reagent was found to be excellent for the determination of H_2O_2; the CL intensity generated from PDIQ is approximately 2.5 times that from luminol. Hence PDIQ could be used instead of luminol for the sensitive determination of H_2O_2.

The development of an FI method for the determination of serum glucose is in progress using normal and clinical serum samples.

References

1　Zaitsu, K., and Ohkura, Y., *Anal. Biochem.*, 1980, **109**, 109.
2　Capalidi, D. J., and Taylor, K. E., *Anal. Biochem.*, 1983, **129**, 326.
3　Segawa, T., Kamidate, T., and Watanabe, H., *Anal. Sci.*, 1990, **6**, 763.
4　Armstrong, W. A., and Humphreys, W. G., *Can. J. Chem.*, 1965, **43**, 2326.
5　Bostick, D. T., and Hercules, D. M., *Anal. Lett.*, 1974, **7**, 347.
6　Bostick, D. T., and Hercules, D. M., *Anal. Chem.*, 1975, **47**, 447.
7　Auses, J. P., Cook, S. L., and Maloy, J. T., *Anal. Chem.*, 1975, **47**, 244.
8　Partrovsky, V., *Talanta*, 1976, **23**, 553.
9　Gorus, F., and Schram, E., *Arch. Int. Physiol. Biochem.*, 1977, **95**, 981.
10　Kok, G. K., Moller, T. P., Lopez, M. B., Nachtrieb, H. A., and Yuan, M., *Environ. Sci. Technol.*, 1978, 1072.
11　Olsson, B., *Anal. Chim. Acta*, 1982, 113.
12　Ek, N., Lonber, E., Maehly, A. C., and Stromber, L., *J. Forensic Sci.*, 1972, **17**, 456.
13　Imai, K., *Methods Enzymol.*, 1986, **133**, 435.
14　Mellbin, G., and Smith, B. E. F., *J. Chromatogr.*, 1984, **312**, 203.
15　Kozilo, T., Grayeski, M. L., and Weiberger, R., *J. Chromatogr.*, 1984, **317**, 355.
16　Mann, B., and Grayeski, M. L., *J. Chromatogr.*, 1987, **386**, 149.
17　Nakashima, K., Maki, K., Kawaguchi, S., Akiyama S., Tsukamoto, Y., and Imai, K., *Anal. Sci.*, 1991, **7**, 709.
18　Nakashima, K., Hayashida, N., Kawaguchi, S., Akiyama, S, Tsukamoto, Y., and Imai, K., *Anal. Sci.*, 1991, **7**, 715.
19　Arakawa, H., Ishida, J., Yamaguchi, M., and Nakamura, M., *Chem. Pharm. Bull.*, 1990, **38**, 3491.
20　Seitz, W. R., *CRC Crit. Rev. Anal. Chem.*, 1981, **13**, 1.
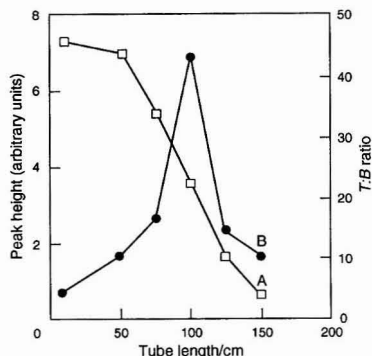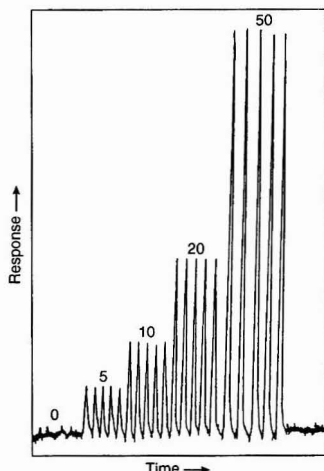
Involvement of Sulfhydryl Groups in the Stable Fluorescent Derivatization of Proteins by o-Phthalaldehyde

Ayses Kuralay, Oya Ortapamuk, Selma Yılmaz, Nilgün Sümer and Inci Özer*

Department of Biochemistry, School of Pharmacy, Hacettepe University, Ankara 06100, Turkey

Treatment of human α-1-proteinase inhibitor (α-1-PI) with o-phthalaldehyde (OPA) at pH 8.0 and 25 °C, in the absence of added thiol resulted in the formation of a mixed population of fluorescent and non-fluorescent isoindoles. The stoichiometry of isoindole formation was tentatively calculated to be 6 : 1 for unreduced α-1-PI and 10 : 1 for inhibitor treated with dithioerythritol, implicating not only cysteine but also non-sulfur nucleophilic centres as reaction partners. Despite the apparent involvement of the single cysteine residue in α-1-PI in the over-all derivatization process, the extent of fluorescent derivatization was independent of the redox state of the inhibitor. Hence the fluorescing moiety was not a 1-alkylthio-2-alkyl-substituted isoindole, as generally observed. The finding that isoindole formation in proteins is not limited by sulfhydryl content and that fluorescent products may originate from amino acid(s) other than cysteine cautions against interpreting fluorescent derivatization by OPA as evidence for cross-linking of lysine to cysteine residues.

Keywords: α-1-Proteinase inhibitor; o-phthalaldehyde; fluorescence labelling

Introduction

o-Phthalaldehyde (OPA) is a fluorogenic reagent widely used in the micro-determination of primary amines, amino acids and proteins.[1–5] In the presence of a thiol (such as 2-mercaptoethanol or ethanethiol), the derivatization reaction proceeds at mildly alkaline pH to yield 1-alkylthio-2-alkyl-substituted isoindoles.[6–10] The stoichiometry in the reaction of proteins indicates that lysine side-chains and the amino terminus are the sole reacting centres.[10] Proteins may react also in the absence of added thiol. It has been shown in a number of instances that an intramolecular reaction is involved, selectively cross-linking lysine to cysteine side-chains.[11,12] Based on this observation, and the reportedly inferior stability of 1-alkoxy-substituted isoindoles,[7] lysine and cysteine residues have been accepted as necessary partners in the reaction of proteins with OPA and isoindole formation has come to be taken as sufficient evidence for the cross-linking of lysine to cysteine residues.[13–15]

The present study on the reaction of OPA with human α-1-proteinase inhibitor (α-1-PI) indicates that a free sulfhydryl group is not an absolute requirement for the stable fluorescent derivatization of proteins with this reagent. A plasma protein with a relative molecular mass (M_r) of 51 000, α-1-PI has a single cysteine residue (Cys 232), which is positioned in the partial sequence NIQHCKK.[16] This residue readily forms mixed disulfides with endogenous and exogenous thiols.[17] It was expected that reduced α-1-PI would be

selectively labelled at a single point, and that the disulfide form of the inhibitor would be unreactive. The results pointed to multiple reactive sites in both reduced and oxidized species. The extent of fluorescent derivatization was independent of the oxidation state of the cysteine residue.

Experimental

Bovine pancreatic trypsin [N-tosyl-L-phenylalanine chloromethyl ketone (TPCK) treated] was obtained from Sigma. All other chemicals were purchased from Sigma or Merck.

α-1-PI was purified from human blood samples obtained from the blood bank of Hacettepe University Hospital close to the expiry date for clinical use. Plasma was dialysed against 20 mmol l⁻¹ potassium phosphate buffer (pH 6.8) and subjected to successive ion-exchange chromatography on DEAE-Trisacryl M and PBE 94 at the same pH. In both chromatographic steps elution was carried out using a linear gradient from 0 to 0.25 mol l⁻¹ KCl. Active fractions collected from the PBE 94 column were pooled and stored at 4 °C in 20 mmol l⁻¹ potassium phosphate (pH 6.8) containing 50 mmol l⁻¹ KCl and 0.02% sodium azide. Sodium dodecyl sulfate polyacrylamide gel electrophoresis (SDS-PAGE) according to Laemmli[18] revealed one major component, centred at M_r 50 000, which constituted >90% of Coomassie Brilliant Blue-stainable material. Protein concentration was determined (a) by the method of Lowry *et al.*,[19] using bovine serum albumin as standard, (b) by measurement of the absorbance at 280 nm, A_{280}, using a molar absorptivity of ε = 28 l mmol⁻¹ cm⁻¹,[20] and (c) by determination of sulfhydryl content (see below). The results agreed within ±10%. The specific activity of different preparations ranged between 11 and 15 nmol of trypsin-active α-1-PI per milligram of protein, corresponding to an active inhibitor population of 56–77%.

Determination of Inhibitor Activity

α-1-PI was assayed by pre-incubating appropriate aliquots of the inhibitor with 1 μmol l⁻¹ trypsin for 2 min in 20 mmol l⁻¹ potassium phosphate buffer (pH 6.8) at 25 °C. Residual tryptic activity was determined after diluting 200 μl of the pre-incubation mixture into 1 ml of 10 mmol l⁻¹ TRIS buffer (pH 8.0) containing 0.5 mmol l⁻¹ N-benzoylarginine ethyl ester as substrate. The hydrolytic reaction was monitored at 253 nm. Under the conditions of the assay, 1 μmol l⁻¹ α-1-PI caused a change in observed tryptic activity equivalent to 0.74 ± 0.085 absorbance min⁻¹.

Reduction and Determination of Sulfhydryl Content

The sulfhydryl content of the stock α-1-PI (14.9 μmol l⁻¹ protein, based on Lowry *et al.*'s method;[19] inhibitory activity equivalent to 8.24 μmol l⁻¹ of trypsin) was determined by

treating a sample with 100 µmol l^{-1} 5,5'-dithiobis(2-nitrobenzoic acid) (DTNB) in 100 mmol l^{-1} potassium phosphate buffer (pH 8.0) at 25 °C and recording the increase in A_{412}. The TNB released corresponded to 1.92 µmol l^{-1} SH [based on ε = 13.6 l mmol^{-1} cm^{-1} (ref. 21)]. The process was repeated after reduction of the stock α-1-PI with 0.5 mmol l^{-1} dithioerythritol (DTE) for 2 h at pH 8.0 and 25 °C and removal of excess of the reductant by dialysis against 20 mmol l^{-1} potassium phosphate (pH 6.8). The sulfhydryl content increased to 13.6 µmol l^{-1}.

Reaction With OPA

Reagent stock standard solutions were prepared daily in methanol. The reaction was carried out at 25 °C. The medium contained 100 mmol l^{-1} potassium phosphate buffer (pH 8.0), α-1-PI (unreduced, unless specified otherwise), 0–5 mmol l^{-1} OPA and 10% v/v methanol. The absorbance was measured at 337 nm; fluorescence was monitored at 405 nm (excitation at 337 nm; slit width 5 nm for both monochromators). Absorption and fluorescence spectra were taken following dialysis against 20 mmol l^{-1} potassium phosphate (pH 6.8).

Determination of Lysine Content

Unmodified and OPA-modified (dialysed) inhibitor were treated with 1.7% SDS at 100 °C for 15 min. Aliquots were analysed for lysine content using 2,4,6-trinitrobenzenesulfonic acid (TNBS). The reaction medium contained 120 mmol l^{-1} 3-(cyclohexylamino)-1-propane sulfonic acid (pH 9.3), 0.5% SDS and 1 mmol l^{-1} TNBS. The absorbance at 346 nm was measured following incubation at 35 °C for 60 min. 6-Aminocaproic acid was used as a standard. The efficiency of the reaction in OPA-modified samples was tested by using 6-aminocaproic acid as an internal standard. The samples (and any traces of OPA not removed by dialysis) had no effect on the reaction of the standard with TNBS.

Results

Reaction of OPA With α-1-PI, Monitored Spectrophotometrically

A typical time course for the increase in A_{337} during the reaction of OPA with α-1-PI is shown in Fig. 1. The absorbance increased and reached a constant slope that
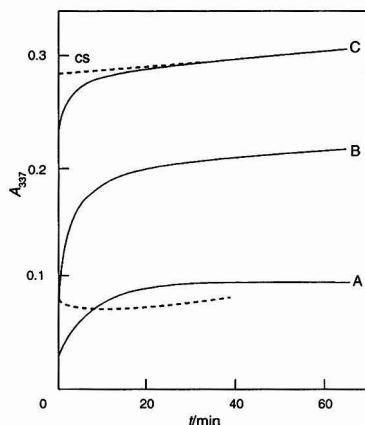
Fig. 1 Spectrophotometric time course for the reaction of OPA with α-1-PI. [OPA] = A 0.2, B 1 and C 5 mmol l^{-1}; [α-1-PI] = 6 µmol l^{-1} (total protein); pH 8.0, 25 °C. Broken line, reagent blank at 5 mmol l^{-1} OPA; cs, constant slope.

matched that of the reagent blank. The segment with constant slope (cs) was extrapolated back to $t = 0$, and the difference between the virtual and experimental data points ($A_{cs} - A_{exp}$) was used in diagnostic plots for determining reaction order with respect to (α-1-PI). At [α-1-PI] ≤ 0.03 [OPA], a plot of $1/(A_{cs} - A_{exp})$ *versus* t was linear at high [OPA], but showed an upward curvature at low [OPA] (data not shown). In contrast, semi-logarithmic plots of $(A_{cs} - A_{exp})$ *versus* t consistently revealed two linear components (Fig. 2), irrespective of reagent concentration. This suggested that the reaction was first order in [α-1-PI], with apparent conformity to second-order kinetics at high [OPA] fortuitously arising from complexities in a basically first-order system. The data were analysed assuming parallel (or sequential) pseudo-first-order processes.

The faster component was complex and showed a non-linear dependence on [OPA] with respect to both k' and amplitude, I (Table 1). Both parameters levelled out at high reagent concentration; k'_{max} and I_{max} were 1.9 min^{-1} and 0.200 absorbance, respectively, as determined from double reciprocal plots (not shown). Whereas the hyperbolic dependence of k' on [OPA] could be accounted for by complex
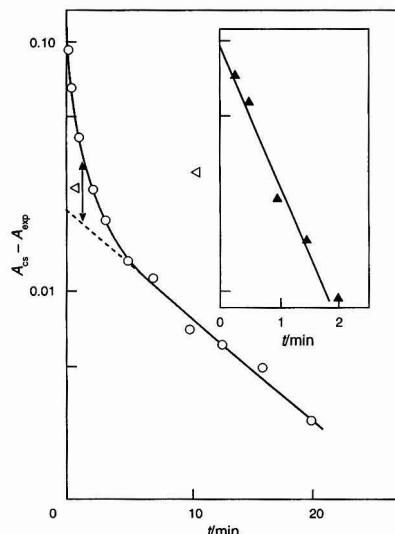
Fig. 2 Semi-logarithmic plot of Fig. 1C. Inset: corrected re-plot of the first phase.

Table 1 Spectrophotometric data relating to the reaction of OPA with α-1-PI. [α-1-PI] = 6.0 µmol l^{-1} (total protein).

Parameter	[OPA]/mmol^{-1}			
	0.2	0.5	1.0	5.0
Total I*	0.100 ± 0.009	0.147 ± 0.020	0.188 ± 0.008	0.200 ± 0.006
Fast component—				
k'/min^{-1}	nd‡	0.5 ± 0.05	0.8 ± 0.1	1.5 ± 0.3
$I(A_{337})$†	0.040	0.097	0.138	0.170
Slow component—				
k'/min^{-1}			0.12 ± 0.025	
$I(A_{337})$			0.05 ± 0.019	

* Value of $(A_{cs} - A_{blank})$ at $t = 0$.

† Inferred from the average values of total I and I for the slow component.

‡ nd, Amplitude too low to allow a reliable estimate.

formation between protein and reagent prior to covalent modification:

$$P + R \rightleftharpoons P \cdot R \rightarrow P\text{--}R \qquad (1)$$
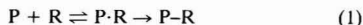
the sensitivity of I to [OPA] was unexpected. Several lines of evidence exclude the possibility of an artifact arising from reagent depletion. (*i*) Reconstructed semi-logarithmic plots of the fast components (inset, Fig. 2) were linear for at least three half-lives, indicating that the process was pseudo-first-order with respect to [OPA] throughout. (*ii*) The I_{max} value of 0.200 for the fast component corresponds to a maximum isoindole concentration of 26 μmol l^{-1} (based on $\varepsilon = 7.66$ l mmol^{-1} cm^{-1} reported for proteins[12]), so that at least in the 0.2–5.0 mmol l^{-1} range, the reagent concentration must have remained effectively constant. [OPA is itself stable under the reaction conditions. The slight changes in absorbance observed in the reagent blank (Fig. 1, dashed line) apparently have no significant bearing on the population of reacting species, as incubation for 1 h prior to the addition of α-1-PI did not alter the absorbance *versus* time profile given in Fig. 1.] (*iii*) Fluorescence changes occurring on the same time scale (see below) also indicate no significant reagent depletion. The spectrophotometric data for the reaction of OPA with α-1-PI in the fast phase most likely reflect alternative pathways for derivatization, depending on the level of the reagent. There appear to be multiple equilibria involving protein and OPA that yield products with different absorptivities.

The rate constant and amplitude of the slower component were independent of [OPA] in the range studied. The average amplitude corresponded to 6.5 μmol l^{-1} isoindole.

The total maximum amplitude indicated an approximate stoichiometry of 6 mol isoindole: 1 mol protein. The reaction resulted in loss of trypsin inhibitory capacity. The product (or mixture of products) was stable: A_{337} did not change noticeably on dialysis. A typical spectrum of the dialysed product is given in Fig. 3.

Reaction of OPA with α-1-PI, Monitored Spectrofluorimetrically

The fluorescence time course of the reaction of OPA with α-1-PI (Fig. 4) also revealed two first-order components (Fig. 5). However, the kinetic and end-point parameters (Table 2) differed from those determined spectrophotometrically. (*i*) Compared with 1 mmol l^{-1} OPA, k' for the first phase leading to a highly fluorescent intermediate was twice as large as k' derived from the spectrophotometric traces. (*ii*) The slow phase, which led to a product with lower fluorescence intensity, was [OPA] dependent. Compared with 1 mmol l^{-1} OPA, k' (spectrofluorimetric) was approximately three times smaller than k' (spectrophotometric). (*iii*) The end-point for the fast component (F_{max}) was insensitive to reagent concentration, as was the final fluorescence intensity (F_∞).
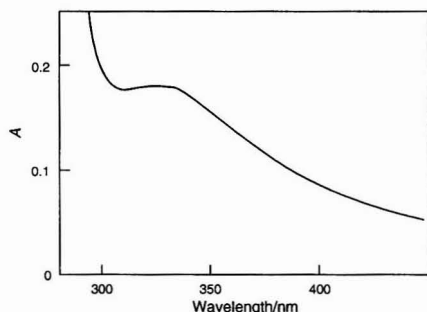
Fig. 3 UV spectrum of OPA-modified α-1-PI. [α-1-PI] = 6 μmol l^{-1}. [OPA] = 1 mmol l^{-1} in the original reaction mixture; removed by dialysis against 20 mmol l^{-1} potassium phosphate solution (pH 6.8).
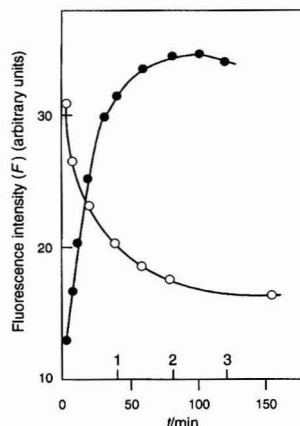
Fig. 4 Fluorescence time course for the reaction of OPA with α-1-PI. [OPA] = 1 mmol l^{-1}; [α-1-PI] = 6 μmol l^{-1}. pH 8.0, 25 °C. ●, approach to F_{max} (upper time scale); ○, decay to F_∞ (lower time scale); λ_{ex}, 337 nm; λ_{em}, 405 nm.
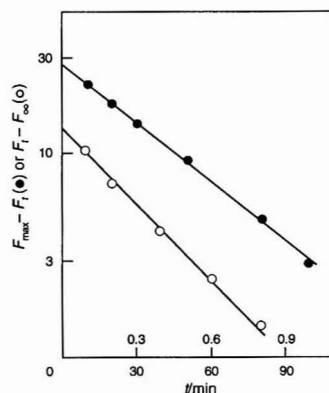
Fig. 5 Semi-logarithmic plot of the data in Fig. 4. Symbols and scales as in Fig. 4.

Table 2 Spectrofluorimetric data relating to the reaction of OPA with α-1-PI

[OPA]/ mmol l^{-1}	[α-1-PI]*/ μmol l^{-1}	Fast component (F increase)[†]		Slow component (F decay)[†]	
		k'/min^{-1}	F_{max}	k'/min^{-1}	F_∞
0.2	3.0	0.53	16	0.01	10
	3.8[‡]	0.30	13	nd[¶]	9
	6.0	0.53	28	0.01	16
1.0	3.0	1.8	19[§]	0.03	9
	3.8[‡]	1.5	13	nd	9
	6.0	1.8	34	0.03	16

* Based on total protein.

[†] Values of k' and F are the averages of at least two determinations which agree within ±<10%.

[‡] DTE treated.

[§] For comparison, this value matches the maximum F value obtained with 20 μmol l^{-1} 6-aminocaproic acid treated with 1 mmol l^{-1} OPA–3 mmol l^{-1} 2-mercaptoethanol under otherwise identical reaction conditions.

[¶] nd = Not determined.

More than one type of fluorescent product was apparently formed. While F_∞ was stable in storage for at least 20 h, removal of OPA by dialysis against 20 mmol l^{-1} potassium phosphate (pH 6.8) caused a 70–80% decrease in fluorescence (which could not be reversed by restoring the original pH and methanol content of the medium).

Reduction of α-1-PI with DTE did not significantly affect the spectrofluorimetrically determined kinetic and end-point parameters. The fluorescence spectra of the products were also similar (Fig. 6). End-point measurements of A_{337}, on the other hand, indicated more extensive derivatization in DTE-treated than in unreduced protein; the difference between the end-point absorbances with reduced and unreduced samples corresponded to four additional isoindoles formed per SH generated. This disproportionate increase in isoindole stoichiometry from 6:1 to 10:1 may have been induced by the conformational change that the inhibitor undergoes on reduction,[17] bringing a larger number of residues within reacting distance.[11]

Discussion

The results of this study point to several uncertainties regarding the reaction of OPA with proteins in the absence of added thiols. (1) It appears that isoindole formation is not limited by the availability of cysteine side-chains. With α-1-PI, a protein with a single cysteine residue, a total of ten sites are modified, as judged by the magnitude of the absorbance change at 337 nm. The stoichiometry of 10:1 is tentative, as it is based on the molar absorptivity for 1-alkylthio-2-alkyl-substituted isoindoles, owing to a lack of spectral data relating to non-sulfur-containing analogues. However, a >80% reduction in the number of TNBS-reactive groups in OPA-treated inhibitor (data not shown) implies that a significant degree of rigidity has been imposed on the molecule, and supports the premise that multiple cross-links have been formed. Regardless of the true stoichiometry, this finding requires that non-sulfur nucleophiles be involved in the reaction. (2) The fact that both reduced and unreduced α-1-PI result in

comparable maximum and end-point fluorescence intensities and products with identical fluorescence spectra indicates that the cysteine side-chain is not directly involved in the formation of the fluorophore. It has been observed previously that thio-substituted isoindoles are not necessarily fluorescent.[22] A further qualification may be justified: not all fluorescent isoindoles are thio-substituted. [The non-identity of the spectrophotometrically and spectrofluorimetrically determined rate constants relating to the first (fast) phase of the derivatization process might even suggest that the fluorescing moiety is not an isoindole, despite the characteristic fluorescence excitation and emission spectra given in Fig. 6. However, the observed discrepancy could easily arise if the fluorescent isoindole were making an insignificant contribution to the over-all absorbance change, or if the isoindole-related fluorescence were making an insignificant contribution to the over-all fluorescence change. The latter alternative is more likely to be valid, considering that the fluorescence of the stable fluorophore (in the dialysed sample) corresponds to only 10–15% of F_{max}.]

In conclusion, the potential for extended specificity in the reaction of OPA with proteins and the possibility of atypical fluorescence properties in the products should be taken into consideration when relating absorbance changes to isoindole-:protein stoichiometries and fluorescent derivatization to covalent linkage of lysine to cysteine residues.

References

1 Kremzner, L. T., *Anal. Biochem.*, 1966, **15**, 270.
2 Hakanson, R., and Rönnberg, A.-L., *Anal. Biochem.*, 1973, **54**, 353.
3 Cooper, J. D. H., Ogden, G., McIntosh, J., and Turnell, D. C., *Anal. Biochem.*, 1984, **142**, 98.
4 Petersen, G. L., *Methods Enzymol.*, 1983, **91**, 95.
5 Fried, V. A., Ando, M. E., and Bell, A. J., *Anal. Biochem.*, 1985, **146**, 271.
6 Simons, S. S., Jr., and Johnson, D. F., *J. Am. Chem. Soc.*, 1976, **98**, 7098.
7 Simons, S. S., Jr., and Johnson, D. F., *J. Org. Chem.*, 1978, **43**, 2886.
8 Stobaugh, J. F., Repta, A. J., Sternson, L. A., and Garren, K. W., *Anal. Biochem.*, 1983, **135**, 495.
9 Svedas, V.-J. K.; Galaev, I. J., Borisov, I. I., and Berezin, I. V., *Anal. Biochem.*, 1980, **101**, 188.
10 Church, F. C., Porter, D. H., Catignani, G. L., and Swaisgood, H. E., *Anal. Biochem.*, 1985, **146**, 343.
11 Puri, R. N., Bhatnagar, D., and Roskoski, R. R., Jr., *Biochemistry*, 1985, **24**, 6499.
12 Puri, R. N., Bhatnagar, D., and Roskoski, R. R., Jr., *Biochim. Biophys. Acta*, 1988, **957**, 34.
13 Puri, R. N., and Roskoski, R., Jr., *Biochem. Biophys. Res. Commun.*, 1988, **150**, 1088.
14 Yılmaz, S., and Özer, I., *Arch. Biochem. Biophys.*, 1990, **279**, 32.
15 Puri, R. N., and Colman, R. W., *Arch. Biochem. Biophys.*, 1991, **286**, 419.
16 Huber, R., and Carrell, R. W., *Biochemistry*, 1989, **28**, 8951.
17 Tyagi, S. C., and Simon, S. R., *Biochemistry*, 1992, **31**, 10584.
18 Laemmli, U. K., *Nature (London)*, 1970, **227**, 680.
19 Lowry, O. H., Rosebrough, N. J., Farr, A. L., and Randall, R. J., *J. Biol. Chem.*, 1981, **193**, 265.
20 Herve, M., and Ghelis, C., *Arch. Biochem. Biophys.*, 1991, **285**, 132.
21 Ellman, G. L., *Arch. Biochem. Biophys.*, 1959, **82**, 70.
22 Simons, S. S., Jr., Thompson, E. B., and Johnson, D. F., *Biochemistry*, 1979, **18**, 4915.
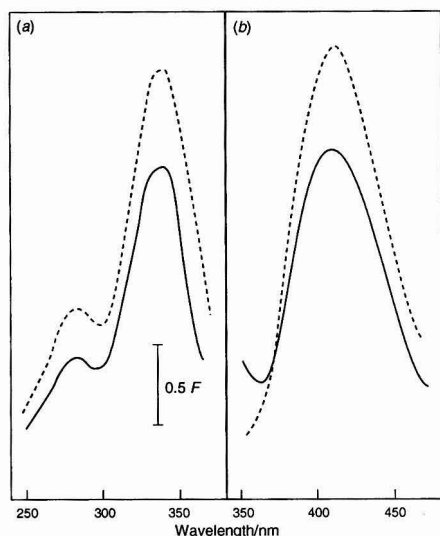
Fig. 6 Fluorescence excitation (*a*) and emission (*b*) spectra of 3 µmol l^{-1} α-1-PI (broken line) and 3.8 µmol l^{-1} DTE-treated α-1-PI (solid line). Both samples were dialysed against 20 mmol l^{-1} phosphate solution (pH 6.8), following reaction with 0.2 mmol l^{-1} OPA. λ_{ex}, 337 nm; λ_{em}, 405 nm.

Determination of Substrates Using Poly(ethylene glycol)-stabilized Dehydrogenase Enzymes by Microlitre per Minute Flow Injection

James R. Marsh and Neil D. Danielson*

Department of Chemistry, Miami University, Oxford, OH 45056, USA

Flow injection (FI), at a flow rate of µl min⁻¹, is an effective method for enzymic substrate determinations using low concentrations of poly(ethylene glycol) (PEG)-stabilized soluble enzymes. PEG stabilizes dehydrogenase enzymes for at least several days by promoting sub-unit association. Band broadening of knitted open tubular reactors is reduced as flow rate decreases below 300 µl min⁻¹ and a small tubing diameter is important for a faster rate of absorbance signal increase with residence time. Small (0.5 µl) sample injections also ensure narrow FI peaks. The determination of several substrates such as pyruvate, lactate, and cortisone using appropriate PEG-stabilized enzymes is demonstrated with this FI instrument at 25 or 50 µl min⁻¹ with sample throughputs of the order of 2–3 min per sample. The determination of lactate in serum samples is also possible. The advantage of this method, sample throughput, is not sacrificed but enzyme consumption is considerably less, compared to standard ml min⁻¹ FI.

Keywords: Lactate; pyruvate; cortisone; dehydrogenase enzyme; flow injection

Introduction

In clinical analysis, the use of enzyme reagents is essential in determining the concentration of substrates in plasma and serum. One of the most important enzymes as an analytical reagent (either immobilized or in solution) for the determination of pyruvate or lactate is lactate dehydrogenase (LDH). Although the determination of pyruvate is straightforward, it is usually only estimated for the diagnosis of severe thiamine deficiency of heavy-metal poisoning.[1] The difficulty in lactate determinations is the unfavourable equilibrium constant, $K = 2.76 \times 10^{-12}$ mol l^{-1} at pH 7 and 25 °C.[2] The reaction strongly favours the reverse reaction, the formation of lactate and NAD⁺ instead of the oxidation of lactate by NAD⁺. If the pH is raised to between 9 and 10, which neutralizes the H⁺ liberated, and a trapping agent such as hydrazine is added to remove pyruvate, the equilibrium constant increases by about six orders of magnitude and the forward reaction will be more favourable.[3]

Knowledge of serum lactate concentration has been important in the diagnosis of lactate acidosis in diabetic patients undergoing therapy with biguanide and in the clinical investigation of acute myocardial infarction complicated by shock.[4] Routine analysis of lactate samples is important in the discipline of sports medicine. The use of blood lactate concentration is a widely accepted method of evaluating an athlete's condition and training in terms of aerobic threshold, lactate threshold or breaking point (the onset of blood lactate accumulation), and maximal steady state.[5–9] Excessive quantities of lactate are produced during strenuous exercise and it is well known that the work load at which blood lactate starts to accumulate (lactate threshold) is higher for endurance-trained subjects than for untrained subjects.[8]

The application of flow injection (FI) with immobilized LDH has been described in detail by Sundaram and Hinsch.[4] They described the use of a continuous-flow clinical analyser with an immobilized coupled-enzyme nylon tube reactor and an immobilized single-enzyme nylon tube reactor for the routine estimation of lactate and pyruvate, respectively, in serum. For pyruvate determinations, the single-enzyme reaction maintained considerable activity upon storage at 4 °C for 18 months. The determination of lactate necessitated the use of a second reactor containing alanine aminotransferase (ALT) to remove pyruvate. The stability of this system was limited by ALT to 4 weeks. Newirth *et al.*[10] obtained a linear range for pyruvate of $0.5–10 \times 10^{-4}$ mol l^{-1} and a 4 min analysis time using a packed-bed LDH reactor. Recently, an on-line enzymic amplification method for lactate has been reported using immobilized lactate oxidase and LDH.[11] Substrate recycling between these two enzymes permits the production of H_2O_2 above the stoichiometric limit resulting in electrochemical detectability at the fmol l^{-1} level.

The application of FI using soluble LDH to the determination of blood lactate has been described in detail by Rydevik *et al.*,[12] Karlsson *et al.*,[13] and Weicker *et al.*[14] Each system was similar and used two carrier steams, one containing the soluble LDH and the other NAD⁺. The latter report[14] described a peristaltic pumping rate of 1.2 ml min⁻¹ and a sample injection of 30 µl. Prior to injection, it was necessary to employ a mixing coil to mix the reagent streams. The sample was then propelled to a 0.5 mm × 0.5 m reaction coil where the enzymic reaction took place. A linear range of 2–20 nmol l^{-1} lactate was obtained with a 1 min sample analysis time.

Determination of pyruvate by FI has also been carried out. Weicker *et al.*[14] used the same FI system as was used in the determination of lactate, except that the flow rate was lowered to 0.8 ml min⁻¹. Two measurements were necessary to calculate substrate concentrations because the loss in NADH fluorescence is measured and the injection of a blank results in a large negative peak. They concluded that the pyruvate determination was less reliable in comparison with the lactate FI assay.

Although enzyme substrate determinations using ml min⁻¹ FI are well known, the usefulness of this technique at µl min⁻¹ flow rates for a variety of enzyme reactions has not been established. Microlitre per minute flow rates not only offer more flexibility of reaction (without the need to lengthen reactor tubing) but, more importantly, can make the use of soluble enzymes more economically favourable with the addition of poly(ethylene glycol) (PEG) to enhance enzyme

---

stability at small concentrations. It has been reported that 15% PEG in solution can enhance LDH stability for the FI assay of pyruvate.[15] In this report, the determination of pyruvate and lactate in a μl min^{-1} FI system using PEG-stabilized LDH is demonstrated. Extension to the determination of cortisone using hydroxysteroid dehydrogenase (HSD) is also made. Although the use of immobilized HSD for a post-column HPLC method has been reported,[16] this enzyme is quite expensive and was not used in the soluble form with FI. Characterization of the FI instrument with respect to band broadening and signal as a function of flow rate was also carried out.

Experimental

Chemicals

All chemicals were of analytical-reagent grade and the water was distilled and doubly de-ionized. Lactate dehydrogenase [EC 1.1.1.27; L-2500; LDH, Type II from rabbit muscle, 955 (1U = 16.67 nkat mg^{-1} of protein), 11 mg of protein ml^{-1}], β-nicotinamide adenine dinucleotide, reduced form (N-8129; NADH$^+$, disodium salt), β-nicotinamide adenine dinucleotide, oxidized form (N-1511; NAD$^+$), pyruvic acid (P-2256; α-ketopropionic acid), L(+)-lactic acid (L-1750; 2-hydroxypropionic acid), cortisone (C-2755), 3α,20β-hydroxysteroid dehydrogenase (H-2267), and Trizma base (T-1503; TRIS were purchased from Sigma (St. Louis, MO). PEG polymer, with an average M_r of 8000 (P-5413), was also obtained from Sigma. Perchloric acid (70% HClO$_4$) was obtained from Fisher (Fairlawn, NJ). Hydrazine sulfate (H1018) and hydrazine monohydrate 98% (20,7942-2) were obtained from Spectrum Chemical (Gardena, CA) and Aldrich (Milwaukee, WI), respectively.

Instrumentation

An ISCO (Lincoln, NB) Model μLC-500-syringe pump with a 50 ml capacity capable of a flow rate range of 0.02–600 μl min^{-1} with an accuracy of ±1% and a precision of ±0.9% was used to propel the carrier stream. All connecting tubing and reactor tubing was Teflon from Supelco (Bellefonte, PA). All stainless steel nuts, ferrules and connection fittings were low, dead volume type and purchased from Alltech Associates (Deerfield, IL). Samples were introduced into the flow system by way of a Rheodyne (Cotati, CA) Model 7410 manual injection valve with an internal loop of 1.0 or 0.5 μl.

A knitted open-tubular (KOT) figure eight design was constructed to induce quick directional changes of radial mixing. The Teflon tubing 0.5 m × 0.24 mm was interwoven into a piece of 0.25 inch steel wire mesh in a figure eight configuration (5 figure eights 10 mm^{-1}), thereby ensuring periodic flow reversal as previously described.[17]

A Kratos Analytical (Ramsey, NJ) Model Spectroflow 757 variable absorbance detector with a variable time constant set at 0.045 s and equipped with a 2.5 μl flow cell was used for UV detection at 340 nm. A Waters (Milford, MA) Model 420-AC fluorescence detector with a time constant of 1.2 s was fitted with a 338 nm bandpass excitation filter and a 425 nm longpass emission filter and equipped with a 8 μl flow cell. A Waters temperature control system was used to bring the carrier stream to 30 °C prior to injection. The detector output signal was generated on either a Linear Model 1202 (Reno, NV) or a Fisher Record-All Series 5000 (Houston, TX) chart recorder for gathering data.

Calculations

Absorbance values were calculated from recorded peak heights. Plate height (H) was used to characterize band broadening or dispersion of the injected samples. Traditionally, plate height is calculated assuming the peak is Gaussian in shape by:

$$H = \frac{L}{16(t_R/w)^2} \tag{1}$$

where, L = reactor length; t_R = retention time at the peak centroid; and w = baseline peak width. However, when using FI there is often tailing which causes non-Gaussian peaks. To correct for peak skewness, a corrected plate height value, H_{corr} has been adopted.[17]

$$H_{corr} = \frac{L}{n} \tag{2}$$

where

$$n = \frac{4.179(t_R/w_{0.1})^2}{(b/a) + 1.25} \tag{3}$$

and L is the reactor length, b/a is the asymmetry or tailing factor, $w_{0.1}$ is the peak width at 10% maximum peak height, and t_R is the retention time at peak centroid.[18]

The limit of detection (LOD) and limit of quantification (LOQ) are defined as $k(\sigma_{blank})$/slope where $k = 3$ for LOD and $k = 10$ for LOQ.

Substrate Assays

For the determination of pyruvate, the decrease in NADH absorbance was measured at 340 nm. The carrier stream consisting of 0.067 mmol l^{-1} NADH, 2.6 U ml^{-1} LDH and 15% PEG-8000 all in a 0.2 mol l^{-1} TRIS buffer pH 7.3, was flowing at 25 μl min^{-1} or 55 cm min^{-1}. The NADH component was stable in this solution throughout the period of analysis. Owing to matrix interferences, standards had to be diluted to volume with the working mobile phase minus the enzyme. All injections were performed at ambient conditions.

For the determination of lactate, the formation of NADH was measured spectrofluorometrically. The carrier stream, consisting of 3.6 mmol l^{-1} NAD$^+$, LDH, and 15% PEG-8000 was prepared in a hydrazine buffer, pH 9.0, made in accordance to Weicker.[14] Standards were diluted by a factor of 10 with 7% HClO$_4$ (deproteinizing agent), which is consistent with serum sample preparations.[13] Neutralization was unnecessary and, therefore, was not performed.[13,14]

For the determination of cortisone, the decrease in NADH absorbance was measured at 340 nm. The carrier stream consisted of 0.5 U ml^{-1} HSD, 0.067 mmol l^{-1} NADH, and 15% PEG in 0.03 mol l^{-1} TRIS buffer, pH 7.6.

Results and Discussion

Reactor Design

The quality of mixing within a reactor type over a wide flow rate range was first observed. Fig. 1 gives the trend of peak absorbance upon injection of phenolphthalein in a borate buffer at different flow rates for a straight tube and a KOT reactor. As expected, the KOT reactor provided more efficient mixing at high flow rates. However, use of a KOT reactor instead of a straight tube, even at low flow rates, is recommended.

A response comparison of KOT reactors made with Teflon tubing of only slightly different diameters showed a measurable difference. The 0.24 and 0.30 mm id reactors, both 0.5 m long, have total volumes of approximately 23 and 35 μl, respectively. By decreasing only the id of the reactor tubing from 0.30 to 0.24 mm, a marked effect on signal response upon injection of phenolphthalein in borate buffer was noted. The

0.24 mm id KOT reactor shows a gain in signal by a factor greater than 3 throughout most of the flow rate range compared to the larger tube. In Fig. 2, there is a dramatic increase in absorbance with decreasing residence time. Both reactors show similar trends. The rate of increase below 10 s appears to be equal for both reactors. For the 0.30 mm id tubing, this increase occurs at approximately 5 s and for the 0.24 mm id tubing, the increase occurs at a slightly shorter time of 4 s. Although the rate of increased absorbance with decreasing residence time is equal for both reactors, the rate of increased absorbance with increased residence time occurs at a much faster rate for the smaller diameter tubing. At a residence time of 40 s, the 0.25 and the 0.30 mm id reactors provide signals of 0.225 and 0.073 absorbance units, respectively, representing an improvement in signal by a factor of approximately 3 for the narrower tubing. This can be explained in terms of band broadening, whereby, for longer residence times and lower flow rates, band broadening is dictated by a diffusion controlled process. Since the rate of diffusion is constant within both diameters (*i.e.*, both having identical carrier streams), the theoretical number of stream-lines crossed (or distance travelled) by the analyte per unit length travelled is constant, but for the larger diameter tubing there are more theoretical streamlines to cross. Therefore, a sample plug within the large diameter tubing will distribute itself more in the axial direction per unit length travelled than within the smaller diameter tubing.

PEG Stabilization of Dehydrogenase Enzymes

Previously, it was necessary to use 15% PEG to stabilize LDH activity, particularly at low concentrations.[15] However, the mechanism of stabilization is not well understood. As PEG is commonly used as a salting-out agent in purification methods of enzymes,[19] the solubility of LDH in PEG was investigated. The formation of enzyme aggregates could be the cause of stabilization. Solutions (50 ml) of 10, 50, and 100 U ml^{-1} LDH in 10, 15, 20 and 25% PEG-8000 were prepared in 0.2 mol l^{-1} TRIS buffer, pH 7.0. Previously, it has been shown that 15% PEG is the optimum percentage for maintenance of stable enzyme activity.[15] Within 10 min of preparation, the solutions were centrifuged at 13 000 rpm for 15 min. Precipitation occurred using 20 and 25% PEG for all three LDH solutions. Below 20% PEG there was no formation of aggregates for any of the LDH solutions. Therefore, stabilization at 15% PEG is not attributed to the formation of aggregates. It is possible that LDH is in a more compact form. To further support the assumption that enzyme aggregates did not form in 15% PEG, a small aliquot of the top half of the solution in the 50 ml centrifuge tube was tested for activity prior to and following centrifugation. In addition, a control without PEG was carried out. No significant loss in LDH activity for a solution of 15% PEG-8000 following centrifugation, by virtue of the constant values of $t_{\frac{1}{2}}$ (the time required for the NADH concentration to decrease by a factor of 2) was noted.

To determine if PEG could provide an environment to hold enzyme sub-units together, LDH denaturation and loss in activity at acidic pH was tested. Fritz[20] reported a loss in LDH activity at acidic pH values and concluded that LDH denatures as a result of sub-unit dissociation. Moreover, Lovell, and Winzor[21] have reported that the tetramer LDH dissociates completely into two dimers in an acetate–chloride pH 5 buffer. Fig. 3 represents residual activity of LDH in an acetate buffer of pH 5 as a function of time. It can be seen that the rate of deactivation for 2.5 U ml^{-1} of LDH is much slower than when 1.0 U ml^{-1} of LDH is present. Such an observation is consistent with other reports showing enzyme solutions with a high concentration of protein (such as albumin) are more stable.[22] After only 1 h in solution, the $t_{\frac{1}{2}}$ values have increased markedly for both LDH solutions at 1.0 and 2.5 U ml^{-1} of activity by factors of 6 and 12, respectively. More importantly, when 15% PEG-8000 was present in either LDH solution, little loss of activity occurred over a period of nearly 7 h. After

Fig. 1 Peak absorbance profiles obtained at various flow rates using either A, a KOT reactor or B, a straight tube made of 0.5 m × 0.24 mm id Teflon tubing. Injection of 0.5 μl phenolphthalein into a pH 10 borate buffer carrier. Time constant = 0.045 s, flow cell = 2.5 μl.

Fig. 2 Absorbance as a function of residence time for a 0.5 m KOT reactor having internal diameters of A, 0.30 and B, 0.24 mm. Flow rate range represented is from 500 to 25 μl min^{-1} for the 0.24 mm KOT reactor. Other conditions as in Fig. 1.

Fig. 3 Residual activity of LDH at pH 5.0 using 0.2 mol l^{-1} ammonium acetate buffer. (*a*) 1.0 and (*b*) 2.5 U ml^{-1} LDH. ($t_{\frac{1}{2}}$ Is defined as the time necessary for the NADH concentration to be reduced by half.) A, No PEG; and B, 15% PEG.

7.2 h, $t_{\frac{1}{2}}$ increased by a factor of 13 for the LDH solution without PEG. The 1.0 U ml^{-1} of LDH solution containing 15% PEG-8000 did show a slight residual loss in activity. For this solution the initial $t_{\frac{1}{2}}$ was 0.2 min whereas, after 6.7 h, the $t_{\frac{1}{2}}$ was 0.30 min. After almost 93 h, the solution with PEG resulted in a $t_{\frac{1}{2}}$ of only 3.7 min whereas, without PEG $t_{\frac{1}{2}}$ soared to 37.3 min. The rate of enzyme denaturation decreased when the pH was raised to 5.75, but the protective effect of PEG was still evident. Without PEG, $t_{\frac{1}{2}}$ increased from 0.17 to 2.5 min in 84 h representing a loss in activity by a factor of 15. After 84 h there was only a factor of 2 loss in LDH activity when PEG was present. Therefore, the mechanism of LDH activity stabilization is the ability of 15% PEG to prevent sub-unit dissociation, even at extreme pH values. It should be noted that LDH solutions used for the pyruvate method at pH 7.5 can be stable for at least 4 d. A 15% PEG-8000 matrix was definitely necessary to stabilize LDH and prevent loss in activity during the lactate determination at 30 °C. Upon repetitive injections of 10 mmol l^{-1} lactate there was a 15% loss in signal after 90 min, and a 47% loss in signal after 4.5 h without the use of PEG. When 15% PEG-8000 was present, no residual loss in signal occurred for at least 8.5 h. Higher temperature settings of 37 and 50 °C resulted in loss of signal attributed to thermal denaturation of LDH even in the presence of PEG. However, the stabilization of dehydrogenase enzymes using PEG does vary. Equine liver alcohol dehydrogenase (ADH) (2 sub-units) was stabilized by 15% PEG starting on day 3 for at least 24 d.

Pyruvate Determination

Band broadening (H_{corr}) for the negative peak due to the decrease in NADH as a function of flow velocity is shown in Fig. 4(*b*). This profile is different to that obtained from the simple injection of 1.0 mmol l^{-1} of nicotinic acid [Fig 4(*a*)]. For the nicotinic acid band broadening *versus* flow rate plot, the H_{corr} value is 3.0 from 150 to 350 μl min^{-1} and then decreases to about 1.5 at 60 μl min^{-1} and to 0.5 at 10 μl min^{-1}.
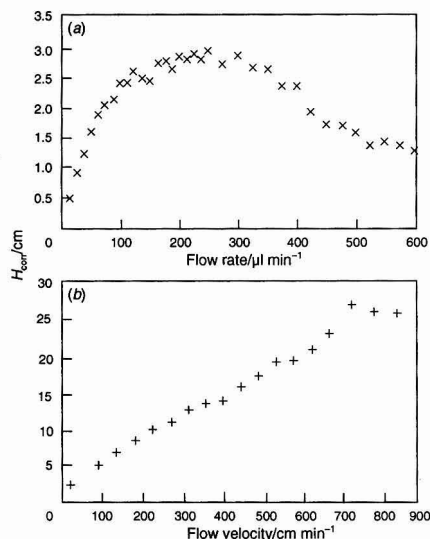
Similar H profiles as a function of flow rate have been shown for the enzyme assay of ethanol.[23] The relatively high values for the pyruvate H_{corr} compared to those for nicotinic acid can be attributed to the increased viscosity of the carrier stream with PEG present. Viscosity also appears to affect the hydrodynamics at higher flow rates with levelling off of H_{corr} values greater than 325 μl min^{-1}. This is possibly due to the inability of secondary flow patterns to develop caused by increased viscosity of the carrier stream. Additional support to this idea is given by Fig. 5 which shows no difference in signal when fast and slow detector time constants are used. A previous study[17] with nicotinic acid injections at different detector time constants, resulted in significant absorbance differences at flow rates greater than 300 μl min^{-1}. For that study, an increased signal was due to decreased band broadening caused by formation of secondary flow patterns. Owing to a fast moving carrier stream, the detector (when set to a slower detector time constant) was not able to sample the sample plug quickly enough to measure the increased response due to a decrease in band broadening. In addition, Fig. 5 shows there is an increase in absorbance by a factor of 10 when the flow rate has been decreased from 500 to 40 μl min^{-1}. It can be concluded that FI at lower flow rates should be more favourable, particularly when the mobile phase has an increased viscosity.

A calibration plot for pyruvate indicated linearity from 0.010 to 0.50 mmol l^{-1} with a correlation coefficient of 0.9999. Relative standard deviation values are generally less than 2%. This linear range is better than that (0.040–0.20 mmol l^{-1}) found previously[14] using standard FI. The linear regression analysis for the plot of absorbance units *versus* mmol l^{-1} pyruvate yielded a slope of $0.14 \pm 1.19 \times 10^{-3}$ and an intercept of $2.21 \times 10^{-4} \pm 3.04 \times 10^{-4}$. The LOD and LOQ were 0.008 and 0.028 mmol l^{-1}, respectively.

Lactate Determination

In order to minimize the use of LDH, calibration plots at 50 μl min^{-1} were obtained using varying amounts of LDH (200, 100, 50, and 10 U ml^{-1}). The statistical data and linear regression data are presented in Table 1. As expected, sensitivity increased with LDH activity. By using 200 U ml^{-1} of LDH, there was a significant improvement in sensitivity and LOD/LOQ (0.13 and 0.43 mmol l^{-1}). However, a concentration of 50 U ml^{-1} was chosen for the determination of lactate in serum samples. The s_r values were generally less than 1% at 1.0 mmol l^{-1} lactate or greater concentrations.

Flow injection was applied for the determination of lactate in serum taken from three athletes. Representative FI peaks

Fig. 4 Band broadening, H_{corr} as a function of (*a*) flow rate for the injection of 1.0 mmol l^{-1} nicotinic acid and (*b*) flow velocity for the determination of pyruvate.
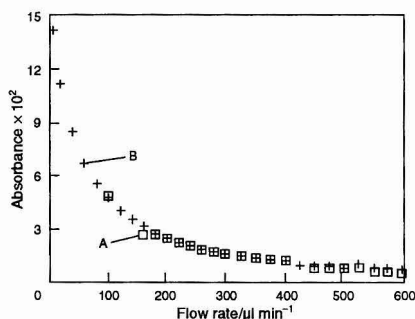
Fig. 5 Absorbance as a function of flow rate for detector time constants of A, 0.909 and B, 0.045 for the determination of pyruvate.

for standards and samples are shown in Fig. 6. Table 2 compares the result of lactate determinations in athletes at rest, during exercise, and during psychological stress for three subjects. From Table 2, it can be seen that lactate levels increase during exercise but not markedly during the psycho-

Table 1 Linear regression data* for lactate determination at 50 µl min⁻¹ for 200, 100, 50, and 10 units ml⁻¹ of LDH

| LDH/ U ml⁻¹	Sensitivity/ cm mmol l⁻¹	y-Intercept/ cm	Linear range/ mmol l⁻¹	r
200	7.06 ± 0.040	2.08 ± 0.44	0.50–20.0	0.9999
100	3.02 ± 0.040	−0.31 ± 0.45	0.50–20.0	0.9997
50	2.14 ± 0.024	−1.96 ± 0.25	0.30–20.0	0.9994
10	1.55 ± 0.020	0.017 ± 0.22	0.50–20.0	0.9997

* Blanks were not included and not subtracted.
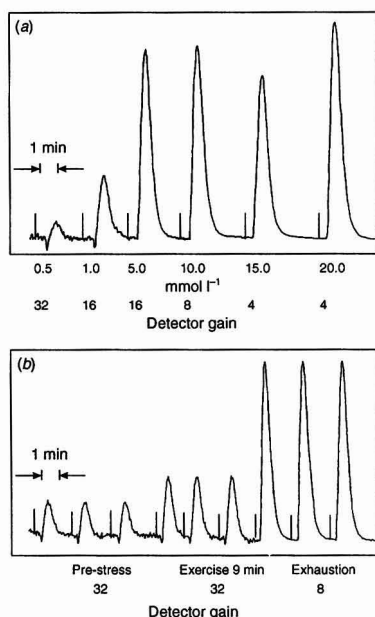
Fig. 6 Representative FI peaks for (*a*) lactate standards and (*b*) serum samples. See Table 2 for concentrations of serum (subject 2).

Table 2 Concentration of lactate levels (*n* = 3) for athletes at rest, during exercise, and during psychological stress

	Concentration/mmol l⁻¹		
Patient situation	Subject 1	Subject 2	Subject 3
Pre-stress	1.25 ± 0.30	0.86 ± 0.31	1.22 ± 0.30
Exercise for 9 min	1.80 ± 0.30	1.28 ± 0.30	1.98 ± 0.30
Exhaustion	10.32 ± 0.26	11.43 ± 0.24	6.21 ± 0.27
Post exhaustion	10.24 ± 0.26	11.47 ± 0.26	8.46 ± 0.26
Post exhaustion after 5 min	12.59 ± 0.27	8.77 ± 0.26	8.77 ± 0.65
Psychological after 1 min	0.96 ± 0.31	0.77 ± 0.31	1.97 ± 0.31
Psychological after 5 min	1.08 ± 0.31	0.93 ± 0.31	—
Psychological after 20 min	1.13 ± 0.31	0.91 ± 0.31	1.12 ± 0.31

logical stress test. The lactate levels found are in the typical range. A throughput of 2 min per sample at 50 µl min⁻¹ was acquired. This is not too dissimilar to 1–1.3 min per sample described previously for lactate.[14] Enzyme consumption was only 2.5 U per sample as compared to 20 U per sample using standard FI.[12] Sensitivity of both assays, if required, could be raised by increasing the LDH concentration and reducing the flow rate. However, LOD and LOQ values were 0.28 and 0.94 mmol l⁻¹, respectively, at a flow rate of 50 µl min⁻¹ with a LDH concentration of 50 U ml⁻¹.

Cortisone Determination

Although LDH is relatively inexpensive, this µl min⁻¹ FI method can be applied to a wide variety of enzymic methods which employ more expensive enzymes that traditionally require immobilization to permit their re-use. Cortisone will be reduced to 20-dehydrocortisone when injected into a carrier stream containing HSD and NADH. When a series of five 0.5 mmol l⁻¹ cortisone injections were run as a function of flow rate, the signal change increased with a decrease in flow rate. At 500 µl min⁻¹, a response of only 0.0075 absorbance units is observed, whereas for flow rates of 25 and 10 µl min⁻¹, values of 0.310 and 0.490 absorbance units were found, respectively. This is attributed to the decrease in band broadening at low flow rates and also longer reaction time. At 25 µl min⁻¹, the residence time is approximately 2.2 min with a sample throughput of 3 min per sample. A calibration plot for cortisone obtained at a flow rate of 25 µl min⁻¹ showed good linearity from 0.05 to 2.0 mmol l⁻¹ with a correlation coefficient of 0.9997, a slope of $0.076 \pm 6.78 \times 10^{-4}$, and a y intercept of $-2.72 \times 10^{-3} \pm 6.45 \times 10^{-4}$. Further research with other enzymes and polymers has been initiated using capillary electrophoresis in an FI mode.

In conclusion, we have shown that µl min⁻¹ FI can provide sample throughputs similar to standard ml min⁻¹ FI without the excessive consumption of enzyme reagent. This is important particularly for expensive enzymes such as HSD. The presence of PEG to stabilize soluble dehydrogenase enzymes is important for extended reagent lifetime.

References

1 Laurence, D. R., *Clinical Pharmacology*, Churchill Livingstone, New York, 4th edn., 1973, p. 284.
2 Hakala, M. T., Glaid, A. J., and Schwert, G. W., *J. Biol. Chem.*, 1956, **221**, 191.
3 Carr, P. W., and L. D. Bowers, *Enzymes in Analytical and Clinical Chemistry*, Wiley, New York, 1980.
4 Sundaram, P. V., and Hinsch, W., *Clin. Chem.*, 1979, **25**, 285.
5 Lehmann, M., Huber, G., and Gastmann, U., *Int. J. Sports Med.*, 1990, **11**, 379.
6 Weltmann, A., Snead, D., Stein, P., Seip, R., Schurrer, R., Rutt, R., and Weltman, J., *Int. J. Sports Med.*, 1990, **11**, 26.
7 Mercier, J., Mercier, B., and Prefaut, C., *Int. J. Sports Med.*, 1991, **12**, 17.
8 Ivy, J. L., Withers, R. T., van Handel, P. J., Elger, D. H., and Costill, D. L., *J. Appl. Physiol: Respir., Environ. Exercise Physiol.*, 1980, **48**, 523.
9 Hopkins, W. G., *Sports Med. (Auckland)*, 1991, **12**(3), 161.
10 Newirth, T. L., Diegelman, M. A., Pye, E. K., and Fallen, R. G., *Biotechnol. Bioeng.*, 1973, **15**, 1089.
11 Raba, J., and Mottola, H. A., *Anal. Biochem.*, 1994, **220**, 297.
12 Rydevik, U., Nord, L., and Ingham, F., *Int. J. Sports Med.*, 1982, **3**, 47.

13 Karlsson, J., Jacobs, I., Sjodin, B., Tesch, P., Kaiser, P., Sahl, O., and Karlberg, B., *Int. J. Sports Med.*, 1983, **4**, 45.
14 Weicker, H., Hagele, H., Kornes, B., and Werner, A., *Int. J. Sports Med.*, 1984, **5**, 47.
15 Marsh, J. R., and Danielson, N. D., *Microchem. J.*, 1991, **44**, 4.
16 Kawasaki, T., Maeda, M., and Tsuji, A., *Biomed. Chromatogr.*, 1986, **1**, 1.
17 Marsh, J. R., and Danielson, N. D., *Mikrochim. Acta*, 1991, **3**, 147.
18 Foley, J. P., and Dorsey, J. G., *Anal. Chem.*, 1983, **55**, 730.
19 Ingham, K. C., *Methods Enzymol.*, 1984, **104**, 351.
20 Fritz, P. J., *Science (Washington, D.C., 1883–)*, 1967, **156**, 82.
21 Lovell, S. J., and Winzor, D. J., *Biochemistry*, 1974, **13**, 3527.
22 Gerhardt, W., Louderback, A., and Waldenstrom, J., *Clin. Chem. (Winston-Salem, N.C.)*, 1982, **28**, 719.
23 Kojima, T., Hara, Y., and Morishita, F., *Bunseki Kagaku*, 1983, **32**, E101.

Selective Complexometric Determination of Mercury Using Acetylacetone as Masking Agent

Biju Mathew, B. Muralidhara Rao and B. Narayana*

Department of Studies in Chemistry, Mangalore University, Mangalagangothri—574 199, Karnataka, India

A complexo-titrimetric method for the determination of mercury(II) in the presence of other metal ions is described, based on the selective masking ability of acetylacetone. Mercury and other ions in a given sample solution are initially complexed with excess of EDTA and the surplus EDTA is titrated with lead nitrate solution at pH 5.0–6.0 (adjusted with hexamine) using Xylenol Orange as indicator. An excess of a 10% alcoholic solution of acetylacetone is then added to decompose the Hg^{II}–EDTA complex and the EDTA released is titrated with lead nitrate solution. Reproducible and accurate results are obtained for 3–55 mg of mercury with relative errors of <0.3% and standard deviations of <0.04 mg. The lack of effect of foreign ions on the accuracy and precision of the method reveals that the method may be suitable for the determination of mercury in its alloys. The method was successfully applied for the determination of mercury in complexes and synthetic alloy solutions.

Keywords: *Mercury determination; EDTA complex; titrimetry; acetylacetone*

Introduction

Mercury forms useful amalgams with alkali metals and heavy non-transition metals, such as Sn, Pb, Bi and Ba. Transition metals also form alloys; mercury–thallium alloy[1,2] is an unusual alloy that forms a eutectic at 8.7% thallium and freezes at −59 °C, about 20 °C below the freezing-point of mercury. Because of the extensive applications and toxic nature of mercury amalgams and its compounds, a selective analytical method for the determination of mercury is essential.

Direct titrations of mercury[3] are of poor selectivity owing to the interference of other metal ions. The usual practice is to determine the sum of mercury and the associated cations and then to decompose the mercury–EDTA complex selectively with masking agents such as thiosemicarbazide[4] and titrate the liberated EDTA using standard metal ion solutions. Interference of copper is severe in the above method. In alkaline medium, potassium iodide is used as a masking reagent for the determination of Hg^{II} in the presence of Cu^{II}, but several other cations interfere.[5] Copper interference can be avoided by using thiourea[6] as the masking agent, by controlling the pH at 5.5 and cooling the solution below 15 °C. Good results are obtainable provided that thiourea is in only a slight excess over the stoichiometric proportions. However, it is difficult to ensure the stoichiometric proportions with unknown concentrations of mercury. At pH 1.0, thiocyanate is used to mask Hg^{II} during the determination of Bi^{III}. Using silver ions the mercury–thiocyanate complex could then be decomposed and

the liberated Hg^{II} titrated with EDTA at pH 5.0–6.0 in the same solution.[7] The method using *N*-allylthiourea is not convenient as it involves heating for decomposition of the Hg–EDTA complex and precipitation of HgS.[8] Determination of Hg^{II} using 4-amino-5-mercapto-3-propyl-1,2,4-triazole,[9] thiocyanate,[10] 2-imidazolidene thione[11] or hexahydropyrimidine-2-thione[12] as replacing agents were found to be reliable and convenient. However, some of these reagents[9,11,12] require tedious and time-consuming preparations. Even though 2-mercaptoethanol[13] is a good masking agent, it is unpleasant to use because of its smell. Sulfite[14] as masking agent overcomes all the above difficulties but the interference of Tl^{III} and Pd^{II} is avoided by using secondary masking agents. In this work, acetylacetone was used as a masking agent for the indirect complexometric determination of mercury and all the drawbacks of the earlier methods were obviated.

Experimental

Reagents and solutions

All reagents used were of analytical-reagent grade.

Mercury(II) nitrate solution. Standardized by the ethylenediamine method.[15]

Lead nitrate solution, 0.02 mol l^{-1}.

EDTA solution, approximately 0.02 mol l^{-1}. Prepared by dissolving the disodium salt of EDTA in distilled water.

Xylenol Orange. Prepared by grinding 1 g of indicator with 100 g of potassium nitrate crystals.

Acetylacetone. Used as a 10% ethanolic solution.

Procedure

An excess of 0.02 mol l^{-1} EDTA solution is added to an aliquot of an acidic solution containing 3–55 mg of Hg^{II} and diluted to about 100 ml. About 0.03 g of solid Xylenol Orange indicator is added and the pH of the solution is adjusted to 5.0–6.0 using hexamine (10 ± 2 g). The excess of EDTA is titrated using lead nitrate solution to a sharp end-point. To this solution an excess of a 10% ethanolic solution of acetylacetone is added and mixed well by shaking. The EDTA liberated is then titrated against lead nitrate solution. The second titre value corresponds to the Hg^{II} present.

Results and Discussion

The conditional stability constant (log β) of Hg–EDTA is 15.3. Acetylacetone is a well known complexing agent and forms a stable complex with mercury[16] with a stability constant of 21.5.[17] At pH 5–6, instantaneous release of EDTA from the Hg–EDTA complex is observed on addition of excess of acetylacetone solution. The release of EDTA from the Hg–EDTA complex is quantitative and reproducible.

Precision and Accuracy

The determination of Hg^{II} in mercury(II) nitrate solution (Table 1) shows that accurate and reproducible results are obtainable with acceptable relative errors of <0.3% and standard deviations lower than 0.04 mg. A large excess of the reagent has no adverse effect and the absence of any precipitate in the reaction mixture favours a sharp end-point. On comparing the calculated Student's t value (Table 1) with the tabulated value for a 5% level of significance, it can be observed that there is no significant difference between the reference values [calculated for lower aliquots using the value obtained for 30 ml of mercury(II) nitrate solution by ethylenediamine method[15]] and the values obtained with the proposed method.

Effect of Foreign Ions

The effect of different cations and anions on the determination of Hg^{II} was investigated with 21.81 mg of Hg^{II} in solution. No interference was observed when the following ions were present: 50 mg of Cd^{II}, Co^{II}, Ni^{II} or Cu^{II}, 25 mg of Bi^{III} or Tl^{III}, 20 mg of V^{IV}, Zr^{IV}, Ti^{IV} or Cr^{III}, 15 mg of Al^{III}, Pd^{II}, Ce^{III}, Pt^{IV} or Fe^{III} and 100 mg of acetate, oxalate tartarate, nitrate or phosphate. The interference from Sn^{IV} can be eliminated by

using fluoride as a secondary masking agent (10% NH_4F, 3–5 ml) for 50 mg of Sn^{IV}.

Applications

Mercury forms solid alloys with zinc and tin containing 42% and 15% of mercury, respectively. It also forms amalgams with Na, Mg, Cu as $NaHg_2$, $MgHg$ and $CuHg$. Artificial mixtures of these metal ions with mercury(II) were prepared and analysed using acetylacetone as masking agent; the results are given in Table 2.

A number of Hg^{II} complexes with sulfur-containing ligands were prepared by the conventional methods and their purity was checked by elemental analysis. About 0.1–0.2 g of the complex was decomposed by evaporation to dryness with concentrated HNO_3. The residue was then cooled, dissolved in water and diluted to 100 ml. Aliquots of 10 ml were used for titration with the recommended procedure. The results are summarized in Table 3. Good recoveries and standard deviations were obtained.

Conclusions

The masking agent acetylacetone is readily available and does not form a precipitate with either the metal ion to be determined or the titrant, under the experimental conditions. This facilitates sharp end-points.

The method is simple, rapid and accurate. It does not require heating or cooling before the titration and also does not require standardization of EDTA.

Reproducible and accurate results are obtained in the concentration range 3–55 mg of Hg^{II} with a relative error of less than 0.3% and a standard deviation of less than 0.04 mg.

There is no interference from Tl^{III} and Pd^{II} in amounts up to 25 and 15 mg, respectively, and interference from Sn^{IV} can be eliminated by using fluoride as a secondary masking agent. The lack of effect of foreign ions on the accuracy and precision indicates that the method may be suitable for the determination of mercury in its alloys and complexes.

Table 1 Determination of mercury(II) in mercury(II) nitrate solution

Hg^{II} present/ mg	Hg^{II} found*/ mg	Standard deviation/ mg	Relative error (%)	Student's t value
4.37	4.36	0.01	−0.2	2.236
10.91	10.89	0.02	−0.2	2.236
21.81	21.83	0.02	+0.1	2.236
31.72	32.69	0.03	−0.1	2.236
43.63	43.64	0.02	+0.1	1.118
54.53	54.56	0.04	+0.1	1.677

* Average of five determinations.

Table 2 Determination of mercury(II) in artificial mixtures of salts corresponding to alloy compositions

Mixture	Composition (%)	Hg^{II} found* (%)	Relative standard deviation (%)
$Hg + Zn$	42 + 58	42.1	0.05
$Hg + Na$	66.7 + 33.3	66.7	0.05
$Hg + Cu$	50 + 50	49.8	0.02
$Hg + Sn^{†}$	15 + 85	14.8	0.20

* Average of three determinations.
† Fluoride used to mask Sn^{IV}.

Table 3 Analysis of mercury complexes

Complex	Hg^{II} present (%)	Hg^{II} found* (%)	Relative standard deviation (%)
$Hg(C_3H_5N_4S)_2$†	43.56	43.51	0.03
$Hg(C_3H_6N_2S)_2Cl_2$‡	42.18	42.26	0.03
$Hg(C_4H_8N_2S)_2Cl_2$§	39.84	39.75	0.04
$Hg(_{10}H_{11}N_4OS)_2$¶	29.91	29.85	0.02

* Average of three determinations.
† Mercury complex of 4-amino-5-mercapto-3-methyl-1,2,4-triazole.
‡ Mercury complex of imidazolidine-2-thione.
§ Mercury complex of hexahydropyrimidine-2-thione.
¶ Mercury complex of 4-amino-5-mercapto-3-(o-tolyloxymethyl)-1,2,4-triazole.

References

1 Brauer, G., *Handbook of Preparative Inorganic Chemistry*, Academic Press, New York, 2nd edn., 1963, vol. 1.
2 Foley, W. T., and Liu, M. T. H., *Can. J. Chem.*, 1964, **42**, 2607.
3 West, T. S., *Complexometry with EDTA and Related Reagents*, BDH, Poole, 1969.
4 Korbl, J., and Pribil, R., *Chem. Listy*, 1957, **51**, 667.
5 Ueno, K., *Anal. Chem.*, 1957, **29**, 1669.
6 Singh, R. P., *Talanta*, 1969, **16**, 1447.
7 Barcza, L., and Koros, E., *Chemist Analyst*, 1959, **48**, 94.
8 Vasilikiotis, G. S., and Apostolopoulou, C. D., *Microchem. J.*, 1975, **20**, 66.
9 Gadiyar, H. R. A., Gadag, R. V., and Gajendragad, M. R., *Talanta*, 1982, **29**, 941.
10 Raoot, K. N., and Raoot, S., *Talanta*, 1983, **30**, 611.
11 Narayana, B., and Gajendragad, M. R., *Talanta*, 1983, **35**, 719.
12 Narayana, B., Kuchinad, G. T., and Gajendragad, M. R., *Chin. J. Chem.*, 1992, **10**, 394.
13 Muralidhara Rao, B., and Narayana, B., *Chim. Acta Turc.*, 1993, **21**, 27.
14 Muralidhara Rao, B., and Narayana, B., *Microchim. Acta*, 1993, **111**, 251.
15 Vogel, A. I., *A Text Book of Quantitative Inorganic Analysis*, Longmans, London, 3rd edn., 1973, p. 487.
16 Paoloni, L., *Gazz. Chim. Ital.*, 1959, **89**, 2171.
17 Kotrly, S., and Sucha, L., *Hand Book of Chemical Equilibria in Analytical Chemistry*, Ellis Horwood, Chichester, 1985, p. 189.

ERRATUM

Titrimetric Determination of Free and Total Acidity and the Subsequent Deduction of Zirconium Content in Process Samples of Zirconium Nitrate

A. Umamaheshwari, B. Narasimha Murty, R. B. Yadav and S. Syamsundar

Analyst, 1995, **120**, 1099

On page 1099 the sentence:
'Hahn suggested that sodium fluoride may be used for the determination of free acid associated with zirconium salts,[3] but sodium fluoride was not used in the present work as prolonged use of glass electrodes in acidic solutions containing fluoride affect the performance of the electrode[4] or can ruin it completely.'
should read
'Hahn suggested that sodium fluoride may be used for the determination of free acid associated with zirconium salts,[3] but this fact was not exploited on the actual samples as prolonged use of the glass electrode in acidic solutions containing fluoride affects the performance of the electrode[4] or can spoil it completely.'

Titrimetric Determination of Free and Total Acidity and the Subsequent Deduction of Zirconium Content in Process Samples of Zirconium Nitrate

A. Umamaheshwari, B. Narasimha Murty, R. B. Yadav and S. Syamsundar
Control Laboratory, Nuclear Fuel Complex (DAE), Hyderabad-500 762, India

A simple titrimetric method for the rapid determination of free nitric acid concentration and total acidity in process samples of zirconium nitrate is described. This paper also details a theoretical method of deducing the zirconium oxide content of these samples based on the free and total acidity values. Sodium fluoride is used to complex the hydrolysable ions and sodium hydroxide is used as the titrant for the free acid. A mixed indicator of Bromocresol Purple and Bromothymol Blue (sodium salt, 0.1% each in water) was used to detect the end-point where there is a sharp change in colour from yellow to deep blue. A precision of ± 0.02 mol l^{-1} and ± 0.5 g l^{-1} is attainable for acidity values and zirconium oxide concentrations, respectively. The free acidity values are in good agreement with those calculated, based on the total acidity and total concentration of the hydrolysable ions present in the medium. The zirconium throughput values calculated from the total and free acidities compared favourably with the gravimetric values estimated by precipitating zirconium (hafnium) as mandelate followed by ignition to produce the oxide. Applicability of various ligands such as oxalate, tartrate, citrate and ethylenediaminetetraacetic acid as alternative complexants is also investigated and it is observed that the zirconium complexes formed with these complexants (except that with cupferron) hydrolyse significantly and cannot be used as complexants for the direct determination of free acidity. The use of cupferron was found to be limited because of poor precision.

Keywords: *Free acidity; total acidity; sodium fluoride; mixed indicator; titrimetry; oxalate; citrate; tartrate; cupferron; ethylenediaminetetraacetic acid; zirconium nitrate*

Introduction

The concentration of free nitric acid in zirconium(hafnium) nitrate feed solution (ZNFS) greatly influences the efficiency of separation of hafnium from zirconium by solvent extraction.[1] When free acidity (FA) in the aqueous phase is about 4 mol l^{-1}, the separation factor of the Zr/Hf separation by tri-*n*-butyl phosphate (TBP) is at a maximum. This necessitates the control of FA in ZNFS before the introduction of ZNFS into the solvent extraction system and, hence, the determination of FA on a routine basis is absolutely essential.

Using the values of total acidity (TA) and total oxide (TO) in the feed, the FA of ZNFS can be calculated. Total acidity, which is the sum of FA and the contribution of the hydrolysable ions, is usually obtained titrimetrically and TO by gravimetry.[2] The latter procedure is time consuming and involves the use of platinum ware, which is expensive. Alternatively, the content of ZrO_2 and HfO_2, obtained by wavelength-dispersive X-ray fluorescence spectrometry (WDXRF), and a value of 8 g l^{-1} can be added together to obtain TO. This deals with the contribution of the impurities towards the oxide content and is justified because these impurities originate from the starting material and their concentration in the feed solution is not expected to vary significantly (as observed at our plant during its operation). Although XRF is quite rapid, it is not cost effective and TA has to be determined titrimetrically.

Free acidity can be determined directly by titration with standard alkali, provided that the hydrolysable ions are prevented from interfering by means of a suitable ligand, which forms highly stable complexes with them. Hahn suggested that sodium fluoride may be used for the determination of free acid associated with zirconium salts,[3] but sodium fluoride was not used in the present work as prolonged use of glass electrodes in acidic solutions containing fluoride affect the performance of the electrode[4] or can ruin it completely. This significant drawback of using fluoride may be avoided by either changing the method of end-point detection to an acid–base indicator or by using conductimetric titrimetry.[5] As the detection of the end-point in the presence of fluoride was reported to be unsatisfactory with a single acid–base indicator,[6] studies were carried out in our laboratory to avoid these problems by using a mixed indicator. Also, the applicability of ligands such as oxalate, citrate, tartrate, ethylenediaminetetraacetic acid (EDTA) and cupferron for the determination of FA were studied in detail.

Knowledge of concentration of zirconium oxide in the ZNFS and zirconium nitrate pure solution (ZNPS) was essential for monitoring the process and was obtained either by gravimetry or by XRF. Nevertheless, these methods suffered from the disadvantages mentioned earlier.

Hence, a systematic study was undertaken to develop a simple and rapid cost-effective method to determine FA and TA and a simple theoretical method of calculation for deducing the zirconium content of the zirconium nitrate process samples is presented.

Experimental

Reagents

All reagents used were of analytical-reagent grade. Aqueous solutions (20%) of potassium oxalate, disodium tartrate, trisodium citrate and saturated solutions of sodium fluoride and Na_2EDTA (pH adjusted to 10.8), 6% aqueous solution of cupferron (containing small quantities of methanol) and 0.5 mol l^{-1} standard sodium hydroxide solution were prepared. Mixed-indicator solution was prepared as follows: 0.1% each of Bromothymol Blue and Bromocresol Purple in water were mixed in equal quantities and the pH was adjusted to 6.8. ZNFS and ZNPS were diluted ten times and used as stock solution for all experiments.

Determination of FA

In the presence of oxalate/tartrate/citrate/EDTA

To a 10 ml sample, 20 ml of the complexant were added and titrated against standard alkali. The end-point was detected using a pH meter. The equivalence-point pH values for oxalate, tartrate, citrate and EDTA were 8.03, 8.2, 8.85, and 10.8, respectively.

In the presence of cupferron

To a 10 ml sample, 10 ml of cupferron were added and titrated until pH 7 was reached.

In the presence of fluoride

To a 10 ml sample, 10 ml of sodium fluoride solution and 1 ml of the indicator were added and titrated until a permanent, deep-blue colour was formed.

Determination of TA

To a 10 ml sample, 1 ml of indicator was added and titrated until a permanent, deep-blue colour was formed.

Determination of TO

For the estimation of TO, the usual gravimetric procedure was followed where the sample aliquot was treated with aqueous ammonia solution, followed by filtration and finally the precipitate was ignited to oxide and weighed.

Determination of the Content of Zirconium

The sample aliquot was initially treated with aqueous ammonia solution and the precipitate was dissolved in hydrochloric acid (6 mol l^{-1}). Zirconium (hafnium) was selectively precipitated as mandelate which was ignited to form the oxide and weighed.

Results and Discussion

ZNFS is obtained by the alkali fusion of zircon($ZrSiO_4$), followed by leaching with water and dissolution of hydrolysed sodium zirconate in nitric acid. A chemical analysis of zircon[7] and ZNFS is provided in Table 1. Apart from free nitric acid, ZNFS contains dissolved silica and hydrolysable ions,[8] such as hafnium, iron, aluminium, titanium, *etc*. To determine FA in ZNFS, these ions, together with zirconium (which is itself a hydrolysable ion), cause serious interference as FA is simply the acidity obtained in the absence of hydrolysable ions. The interference can be eliminated either by quantifying the extent of interference in terms of the contribution of hydrolysable ions towards TA and subtracting that value from the TA, or by performing an acid–base titration in the presence of a suitable complexant which prevents the hydrolysable ions from causing interference.

In order to obtain a reasonable estimate of the contribution of the hydrolysable ions towards the TA, without loss of generality the following stoichiometric equations can be used:

$$Zr^{4+} + 4OH^- \rightarrow ZrO_2 \cdot 2H_2O \xrightarrow{800-850\,°C} ZrO_2 + 2H_2O$$

$$Hf^{4+} + 4OH^- \rightarrow HfO_2 \cdot 2H_2O \xrightarrow{800-850\,°C} HfO_2 + 2H_2O$$

$$TiO^{2+} + 2OH^- \rightarrow TiO_2 \cdot H_2O \xrightarrow{800-850\,°C} TiO_2 + H_2O$$

$$H_2SiO_3 + 2OH^- \rightarrow SiO_3^{2-} + 2H_2O$$

$$2Fe^{3+} + 6OH^- \rightarrow 2Fe(OH)_3 \xrightarrow{800-850\,°C} Fe_2O_3 + 3H_2O$$

$$2Al^{3+} + 6OH^- \rightarrow 2Al(OH)_3 \xrightarrow{800-850\,°C} Al_2O_3 + 3H_2O$$
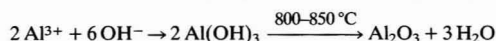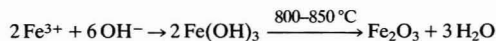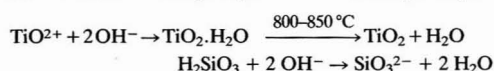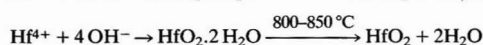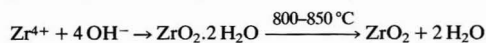
Therefore, the contribution of the hydrolysable ions towards TA can be expressed as

$$X_1\,(mol\,l^{-1}) = \frac{m_{oxide}\,(mol\,l^{-1}) \times \text{Molecular mass of oxide}}{\text{Equivalent mass of oxide}} \tag{1}$$

$$= 4M_{ZrO_2} + 4M_{HfO_2} + 2M_{TiO_2} + 2M_{SiO_2} + 6M_{Fe_2O_3} + 6M_{Al_2O_3} \tag{2}$$

where, M_{ZrO_2}, M_{HfO_2}, M_{TiO_2}, M_{SiO_2}, $M_{Fe_2O_3}$ and $M_{Al_2O_3}$ are the individual concentrations (in mol l^{-1}) of the oxides of zirconium, hafnium, titanium, silicon, iron and aluminium in ZNFS, respectively. As these impurities originate from the starting material zircon, the concentration of the ions Hf^{4+}, Ti^{4+}, Al^{3+}, Fe^{3+} and SiO_3^{2-} are expected to remain almost constant. Therefore, the following equation has been devel-

Table 1 Composition of Indian zircon and chemical analysis of ZNFS

Constituents	Zircon (% by mass)	ZNFS/ $g\,l^{-1}$
ZrO_2	63.5–64.5	82.5
HfO_2	2.0–2.5	2
SiO_2	31.0–32.0	2.0
Al_2O_3	0.70	1.5
Fe_2O_3	0.1–1.0	2.0
TiO_2	0.3–1.5	2.5
ThO_2	0.02	—
P_2O_5	0.1	—

Table 2 Comparison between calculated and volumetrically determined FA in ZNFS using sodium fluoride as the complexant

Sample No.	Sample code	TO/ $g\,l^{-1}$	FA/mol l^{-1} Calculated	Titrimetry	Corrected
1	F-19	96	4.29	4.58	4.34
2	F-34	67	2.95	3.11	2.87
3	F-35	77	2.85	3.05	2.81
4	F-36	89	3.99	4.22	3.98
5	F-37	89	3.89	4.17	3.93
6	F-38	98	4.65	4.87	4.63
7	F-39	71	4.15	4.28	4.04
8	F-42	88	4.33	4.63	4.39
9	F-45	93	4.44	4.69	4.45
10	F-46	74	4.01	4.22	3.98

Table 3 Comparison of content of zirconium–hafnium oxide in ZNFS obtained gravimetrically with that calculated from TA and FA by the present method

Sample No.	Sample Code	Content of ZrO_2–HfO_2/$g\,l^{-1}$ Gravimetry	Titrimetry
1	F-19	88.5	87.1
2	F-34	61.9	61.7
3	F-35	70.2	71.0
4	F-36	80.2	81.8
5	F-37	79.6	78.4
6	F-38	87.8	90.8
7	F-39	64.7	67.3
8	F-42	80.2	78.4
9	F-45	85.6	85.6
10	F-46	67.8	67.3

Table 4   Comparison of FA and content of zirconium oxide in ZNPS

Sample No.	Sample code	TA/ mol l⁻¹	FA/mol l⁻¹			Content of ZrO₂/g l⁻¹	
			Titrimetry	Calculated	Corrected	Gravimetry	Titrimetry
1	R-16	5.54	3.12	2.95	2.98	80	79
2	R-21	5.89	3.52	3.40	3.38	77	74
3	R-23	5.71	3.46	3.32	3.32	74	74
4	R-24	6.06	3.29	3.18	3.15	89	90
5	R-59	5.83	3.29	3.04	3.15	86	83
6	R-63	4.73	3.12	3.06	2.98	52	54

oped to obtain a reliable estimate of the contribution of hydrolysable ions towards TA

$$X_2 \ (\text{mol l}^{-1}) = 4\text{TO} \qquad (3)$$

where, TO is the sum of the individual concentrations (in mol l⁻¹) ZrO_2, HfO_2, TiO_2, SiO_2, Fe_2O_3 and Al_2O_3 present in the sample. The deviation (D) in the acidity value, owing to the use of the simplified eqn. (3) instead of eqn. (2), was obtained by the difference between the two equations

$$D = -2.7097 M_{HfO_2} - 0.5806 M_{TiO_2} + 0.0645 M_{SiO_2} + \\ 0.08710 M_{Fe_2O_3} + 2.7097 M_{Al_2O_3}$$

Substituting the typical values for M_{HfO_2}, M_{TiO_2}, $M_{Al_2O_3}$, M_{SiO_2} and $M_{Fe_2O_3}$ obtained in the process streams of our zirconium oxide plant during operation over the years yields a D value of 0.002 mol l⁻¹, which is negligible and falls within the precision of the method and, thus, does not affect the accuracy of the analysis, especially for a process sample.

Hence, the following simplified equation for the calculation of FA is proposed.

$$FA \ (\text{mol l}^{-1}) = TA - 4\text{TO} \qquad (4)$$

In the presence of sodium fluoride, zirconium is precipitated as sodium hexafluorozirconate (Na_2ZrF_6),[9] and other hydrolysable ions form stable fluoro-complexes. The presence of the precipitate in the solution did not pose any problem in the detection of the end-point. Table 2 shows a comparison of FA values in ZNFS obtained by this method and those by the use of eqn. (4) with TO determined by gravimetry, and TA, by direct titration in the absence of a complexant. Clearly, there is a constant positive bias of about 0.24 mol l⁻¹ in the values obtained by titrimetry using sodium fluoride. This may be attributed to the hydrolysis of the soluble $Na_2ZrF_6(Na_2HfF_6)$. This reasoning is supported by the low magnitude (0.14 mol l⁻¹) of this bias observed in the case of FA values of ZNPS where hafnium is present only in very low levels. Therefore, a value of 0.24 and 0.14 mol l⁻¹, respectively, has to be subtracted from the FA values obtained for ZNFS and ZNPS to obtain the actual FA value.

Use of potassium fluoride also gives similar results. In the presence of ammonium fluoride, however, the detection of the end-point is relatively difficult.

The zirconium complexes of oxalate, tartrate, citrate and EDTA undergo extensive hydrolysis and, hence, these ligands are not suitable for the direct determination of FA. The use of cupferron gives poor precision.[10]

The zirconium content of ZNFS can be calculated from the FA and TA values by simply rewriting eqn. (4) as

$$TO \ (\text{mol l}^{-1}) = \frac{(TA - FA)}{4} \qquad (5)$$

If one substitutes the value of uncorrected FA into eqn. (5), the equation gives the content of zirconium, directly, instead of TO. This may be because of the contribution of impurities towards TA is nearly equal to the extent of hydrolysis of soluble Na_2ZrF_6. Table 3 shows the comparison of the results obtained using this equation and those determined by gravimetry. Table 4 presents the FA values and zirconium content in ZNPS.

Conclusions

The method proposed for the determination of FA in zirconium nitrate solution involves direct titration with sodium hydroxide, in the presence of sodium fluoride as complexant and a mixed indicator of Bromocresol Purple and Bromothymol Blue for the detection of the end-point. This method is rapid, economical and sufficiently accurate for the process samples. The content of zirconium can also be calculated, based on the values of TA and FA.

References

1 Yagodin, G. A., and Sinegribova, O. A., in *Handbook of Solvent Extraction*, ed. Lo, T. C., Baird, M. H. I., and Hanson, C., Wiley, New York, 1983, p. 808.
2 Vogel, A. I., in *A Text Book of Quantitative Inorganic Analysis*, ELBS, Longman, London, 3rd edn., 1975, p. 17.
3 Hahn, R. B., in *Treatise on Analytical Chemistry*, ed. Kolthoff, P. J., Wiley, New York, Part II, vol. 5, 1961, p. 97.
4 Ahrland, S., *Acta. Chem. Scand.*, 1960, **14**, 2035.
5 Shepherd, M. J. Jr., and Rein, J. E., Technical Report IDO-14316, Idaho Opertions Offices, 1955.
6 Osborn, G. H., *Analyst*, 1953, **78**, 220.
7 Krishnan, T. S., *Symposium on Non-ferrous Metals Technology*, National Metallurgical Laboratory, Jamshedpur, Vol. III, 1968, p. 223.
8 Narasimha Murty, B., Yadav, R. B., and Syamsundar, S., *Sep. Sci. Technol.*, 1994, **29**, 249.
9 Bluementhal, W. B., in *Chemical Behaviour of Zirconium*, D. von Nostrand, New York, 1958, p. 195.
10 Narasimha Murty, B., Yadav, R. B., and Syamsundar, S., unpublished work.

Automatic Extraction–Spectrofluorimetric Method for the Determination of Imipramine in Pharmaceutical Preparations

Tomás Pérez-Ruiz, Carmen Martínez-Lozano, Virginia Tomás and Ciriaco Sidrach

Department of Analytical Chemistry, Faculty of Chemistry, University of Murcia, 30071 Murcia, Spain

The spectrofluorimetric determination of trace amounts of imipramine was carried out by liquid–liquid extraction using Erythrosine B with a flow injection system. The determination of imipramine in the range 0.12–2.80 µg ml^{-1} was possible with a sampling frequency of 45 h^{-1}. The method was satisfactorily applied to the determination of imipramine in pharmaceutical preparations.

Keywords: Imipramine determination; Erythrosine B ion-pair extraction; spectrofluorimetry; flow injection; pharmaceutical preparation

Introduction

Imipramine   (10,11-dihydro-N,N-dimethyl-5H-dibenz[b,f]-azepin-5-propanamine), a dibenzazepine derivative, is widely used for the treatment of depression. Because of its structure, it is often referred to as a tricyclic antidepressant. Studies have indicated that the efficacy of this drug in alleviating depression might be due to the enhancement of noradrenergic activity through the blockage of norepinephrine re-uptake in peripherical and central noradrenergic neurons.

A variety of methods for the determination of imipramine have been developed and these have been reviewed by Scoggins *et al.*[1] All these methods normally require one to three steps of extraction depending on the method of analysis followed, such as non-aqueous titrimetry,[2] ultraviolet and visible spectrophotometry,[2–11] spectrofluorimetry,[12,13] voltammetry,[14,15] ion-selective electrode potentiometry,[7] atomic-absorption spectrometry,[7,16] radioimmunoassay,[17] gas–liquid chromatography,[18,19] thin-layer chromatography,[20] high-performance liquid chromatography[21,22] and stopped-flow mixing methods[23].

The formation and extraction in organic solvents of ion pairs using Bromothymol Blue,[3] Methylthymol Blue,[4] picric acid,[5] reineckate[6,7] and bismuth hexaiodide[8] have been used to determine imipramine by molecular and atomic absorption spectrometry. However, these methods are not very sensitive and have the additional disadvantage that manual extraction with organic solvents is troublesome and hazardous. In this context, flow injection minimizes the above shortcomings as the organic solvents are kept in closed vessels.

The purpose of this work was to investigate systematically the formation and extraction behaviour of ion pairs of imipramine with fluorophores in order to develop a sensitive and automatic spectrofluorimetric method for its determination. Our results showed that Erythrosine B offered the best possibilities for use in unsegmented flow configurations. The proposed automatic method offers significant improvements over manual methods as regards safety, reagent consumption and throughput.

Experimental

Apparatus

A Hitachi (Tokyo, Japan) F-3010 spectrofluorimeter was used for recording spectra; excitation and emission spectra were corrected. The detector used in the flow system was a Perkin-Elmer (Norwalk, CT, USA) Model 3000 spectrofluorimeter. A Gilson (Villiers-le-Bel, France) Minipuls-4 peristaltic pump fitted with Tygon and Acidflex tubes and an Omnifit (Cambridge, UK) injection valve were also used.

Reagents

Analytical-reagent grade chemicals and doubly distilled water were used throughout.

Imipramine hydrochloride was obtained from Sigma (St. Louis, MO, USA) and used as received. A 1.00×10^{-2} mol l^{-1} standard solution was prepared by dissolving the drug in water; this solution remained stable for 2 weeks if kept refrigerated and in the dark. Working solutions of lower concentrations were freshly prepared by appropriate dilution of the standard solution.

A 2×10^{-3} mol l^{-1} Erythrosine B (tetraiodofluorescein, CI 45 430) stock standard solution was prepared by dissolving the required amount of the dye (sodium salt) (BDH, now Merck, Poole, Dorset, UK) in water. Solutions of lower concentration were prepared by dilution of the stock standard solution.

Manifold Design

The manifold for the proposed flow injection method is shown in Fig. 1. Acetate buffer (pH 5.0) and Erythrosine B solutions were pumped through Tygon tubes and chloroform was

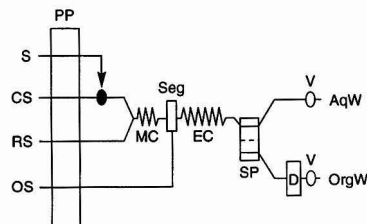**Fig. 1** Schematic diagram of the proposed flow injection method. S, sample; CS, carrier solution (0.2 mol l^{-1} acetate buffer, pH 5); RS, reagent solution (5×10^{-4} mol l^{-1} Erythrosine B); OS, organic solution (chloroform); PP, peristaltic pump; MC, reaction coil; Seg, segmenter; EC, extraction coil; SP, phase separator; D, spectrofluorimetric detector; V, needle valve; AqW, aqueous waste; and OrgW, organic waste.

pumped through the Acidflex tube. The sample (100 μl) was introduced into the buffer stream by means of an Omnifit rotary valve at which a volume control loop was attached. All connecting tubing was made of PTFE. The segmenter was a T-shaped connector, in which the organic phase is continuously added at right-angles to the aqueous phase flowing straight through. A grooved phase separator with a PTFE porous membrane was used. The fluorescence of the organic phase was measured with a Perkin- Elmer Model 3000 spectrofluorimeter equipped with a Helma (Müllheim, Germany) 176.052 QS flow cell (inner volume 25 μl) and was recorded with a Linseis (Selb, Germany) Model 6215 recorder. The spectrofluorimeter parameters were $\lambda_{ex} = 544$ nm, $\lambda_{em} = 560$ nm and excitation and emission slits = 10 nm. A needle valve restrictor was placed at each outlet of the aqueous and organic streams.

Results and Discussion

Imipramine is a tertiary amine and can be readily protonated. The formation of ion pairs of imipramine with fluorescent acid dyes was investigated. Imipramine formed associates with fluorescein dyes, which have potential application in the spectrofluorimetric determination of this drug.

Imipramine can be transferred from the aqueous phase into the organic phase in the form of an ion pair with the anion of these dyes. The extraction equilibria can be represented as follows:

$$HIm^+ + D^- \rightleftharpoons (HIm^+ D^-)$$

$$(HIm^+ D^-) \rightleftharpoons (HIm^+ D^-)_o$$
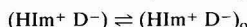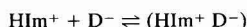
where HIm^+ and D^- denote the protonated imipramine and the anion of the dye, respectively, and the subscript o refers to the organic phase.

The dyes studied for imipramine ion-pair formation were fluorescein, dichlorofluorescein, eosin, phloxin, Erythrosine B and Rose Bengal. The degree of extraction of the complex

Table 1 Effect of the extracting solvent on the fluorescence intensity

	Relative fluorescence intensity (%)	
Solvent	Ion pair	Reagent blank
Chloroform	100	1
1,2-Dichloroethane	112	14
Isobutyl methyl ketone	128	62
Ethyl acetate	114	89
Isopentyl acetate	88	36
Toluene	18	1

Fig. 2 Influence of pH on extraction of the ion pair. Conditions: [imipramine] = 2.0×10^{-5} mol l^{-1}; [Erythrosine B] = 5×10^{-4} mol l^{-1}.

with fluorescein dyes decreased with decrease in halogenation and with decrease in the atomic number of the halogen substituent. Of the dyes tested, only Erythrosine B and phloxin appeared to display significant ion-pair formation with imipramine. Erythrosine B showed the greatest ion-pair extraction efficiency with the smallest reagent blank extraction.

The effect of the extracting solvent used was examined. The polarity of a solvent affects both the extraction efficiency and fluorescence intensity. The results using Erythrosine B are given in Table 1, in which the response using chloroform was normalized to 100.

Both 1,2-dichloroethane and chloroform are useful solvents, but the latter was selected because of its slightly higher sensitivity and considerably lower background.

Extraction Behaviour of Imipramine With Erythrosine B

Both Erythrosine B and its ion associate have identical maximum excitation and emission and so they must be separated if the ion pair is to be determined.

The effect of the pH of the aqueous phase on ion-pair extraction was studied using universal buffer solutions over the pH range 2.0–8.0. The fluorescence intensity of the chloroform extract was maximum and constant in the pH range 4.6–5.2 (Fig. 2).

The composition of the ion pair was established by Job's method of continuous variations and by the molar ratio method using both a variable dye concentration and a variable imipramine concentration. The results obtained with these methods showed that the composition of the associate was equimolar (1 : 1). The extraction constant for the above equilibrium was log $K_{ex} = 6.1 \pm 0.2$.

Shaking times from 0.5 to 5 min did not produce any change in the fluorescence intensity, suggesting that equilibrium between the two phases in the extraction of the ion pair can be attained rapidly. Reproducible fluorescence readings were always obtained after a single extraction. The over-all extraction efficiency was 96.7%.

Flow Injection Determination of Imipramine

The above extraction behaviour suggested that imipramine extracted with Erythrosine B might easily be used for the flow-injection determination of imipramine. The flow manifold for automation of the method is shown in Fig.1.

Flow Injection Variables

The variables studied were sample volume, lengths of the reaction coil and extraction coil, and the flow rate in each reagent line. The concentrations used in these experiments were as follows: buffer line, 0.2 mol l^{-1} acetate buffer (pH 5.0); Erythrosine B line, 5×10^{-4} mol l^{-1}; and sample solution, 5×10^{-5} mol l^{-1}.

The volume of sample injected was varied between 35 and 215 μl. The peak height increased with increasing sample size up to 60 μl, remained constant between 60 and 110 μl and decreased at greater volumes. The volume injected was selected as 100 μl.

The reaction coil connects the valve and segmenter (see Fig. 1). Experiments were carried out in which this coil length was varied. A 50 cm × 0.5 mm id coil was sufficient to yield the maximum signal because the ion pair is formed rapidly. The effects of the extraction coil length on the peak height were also examined by varying the length up to 400 cm. As the peak height hardly altered with extraction coils more than 100 cm long, a 100 cm coil × 0.5 mm id extraction coil was adopted.

The optimum flow rate of each stream is a compromise between sensitivity, peak resolution, phase separation, efficiency and rapidity of the analysis. The optimum flow rate for the aqueous phase was 2.0 ml min^{-1} (1.0 ml min^{-1} for each channel). The ratio of the organic to the aqueous phase adopted was 1 : 1 as ratios of 1 : 2 and 1 : 3 gave poorer results.

Effect of Reagent Concentration

With the concentration of Erythrosine B solution fixed at 5×10^{-4} mol l^{-1}, the buffer solution was varied over the pH range 3–6. The peak heights were maximum and constant from pH 4.7 to 5.1 and decreased outside this range. A 0.2 mol l^{-1} acetate buffer (pH 5.0) was used as carrier. With this carrier, the peak heights increased with increase in Erythrosine B concentration in the range 1×10^{-4}–5×10^{-4} mol l^{-1}, but a further increase up to 1×10^{-3} mol l^{-1} did not improve the sensitivity. Therefore, a Erythrosine B concentration of 5×10^{-4} mol l^{-1} was selected.

Calibration Graph and Statistical Data

As shown in Fig. 3, the flow signals for imipramine show good reproducibility under the above optimum conditions. The calibration graph was linear up to 2.80 µg ml^{-1} of imipramine. The detection limit, calculated according to IUPAC recommendations,[24] was 0.07 µg ml^{-1}. The relative standard deviations for eleven injections of each solution containing 0.56 and 2.24 µg ml^{-1} of imipramine were 1.4 and 0.84%, respectively. The sampling frequency of the proposed method was 45 h^{-1}.

Imipramine-*N*-oxide also forms an ion pair with Erythrosine B, which is useful for the determination of this drug using the manifold described above. Using the recommended conditions for imipramine hydrochloride, the calibration graph was linear between 0.30 and 2.96 µg ml^{-1} imipramine-*N*-oxide.

Fig. 3 (*a*) Flow signals for standard solutions of imipramine under the optimum conditions. All standard solutions were injected three times each. Values above the peaks are the concentrations of standard imipramine solutions (in µg ml^{-1}). (*b*) Calibration graph for imipramine.

Interferences

The influence of foreign substances that can commonly accompany imipramine in pharmaceutical preparations was studied. Solutions of imipramine and each compound tested were mixed to obtain samples containing 0.50 µg ml^{-1} of the drug and up to 50 µg ml^{-1} of the foreign compound. The tolerance ratio of each foreign compound was taken as the largest amount yielding an error of less than ±5% in the analytical signal of imipramine. Glucose, sucrose, lactose, galactose, saccharin, caffeine, starch, sodium bromide and magnesium nitrate were tolerated in large amounts (a 100-fold excess was the maximum tested) and a 50-fold excess of acetylsalicylic acid and a 20-fold excess of gelatin were also tolerated.

Table 2 Determination of imipramine in pharmaceutical preparations

		Found/mg	
Sample*	Drug	Proposed method†	Reference method‡
Tofranil	Imipramine chlorhydrate	49.2 ± 0.22	49.7
Paidenur	Imipramine chlorhydrate	8.3 ± 0.36	8.0
Imiprex	Imipramine-*N*-oxide	24.6 ± 0.29	24.8

* Composition of samples. Tofranil: imipramine hydrochloride, 50 mg; lactose; excipient. Paidemur: imipramine hydrochloride, 8 mg; atropine sulfate, 0.12 mg; γ-amino-β-hydroxybutyric acid, 150 mg; benzenesulfonimidic acid, sodium salt, 3 mg; excipient. Imiprex: imipramine-*N*-oxide hydrochloride, 25 mg; lactose; excipient.
† Average ± standard deviation for three determinations.
‡ BP spectrophotometric method.[2]

Analysis of Pharmaceutical Preparations

The method was applied to the determination of imipramine in commercially available pharmaceutical formulations. Interference from the tablet matrix or the dyes present in the capsules was not a problem. The data in Table 2 show that the imipramine contents were in good agreement with those obtained by the manual spectrophotometric reference method.[2] The recoveries obtained on adding imipramine or imipramine-*N*-oxide to each pharmaceutical formulation are shown in Table 3.

Table 3 Recovery of imipramine added to pharmaceutical formulations

Sample*	Drug	Added/ mg	Found/ mg†	Recovery (%)
Tofranil	Imipramine	10	9.8	98.0
		30	29.9	99.6
		60	59.2	98.6
Paidenur	Imipramine	4	4.1	102.5
		10	9.7	97.0
		20	19.7	98.5
Imprex	Imipramine-*N*-oxide	15	14.9	99.3
		30	30.4	101.3
		40	39.6	99.0

* See Table 2.
† Average of three determinations.

Conclusions

The proposed flow injection method has the advantages of simple operation, high sampling rate, high sensitivity, economy in use of reagents and decreased exposure to organic solvent vapours. In addition, the proposed method can be widely applied for quality control of pharmaceutical dosage forms.

References

1   Scoggins, B. A., Maguire, K. P., Norman, T. R., and Burrows, G. D., *Clin. Chem. (Winston-Salem, N.C.)*, 1980, **26**, 5.
2   *British Pharmacopoeia 1980*, HM Stationery Office, London, 1980, vol. 1, p. 238.
3   French, W. N., Matsui, F., and Truelove, J. F., *Can. J. Pharm. Sci.*, 1968, **3**, 33.
4   Person, B. A., and Eksborg, S., *Acta Pharm. Suec.*, 1970, **7**, 353.
5   Dembinski, B., *Pharm. Pol.*, 1983, **39**, 21.
6   Domagalina, E., and Przyborowski, *Chem. Anal. (Warsaw)*, 1962, **7**, 1153.
7   Elnemma, E. M., El Zawawy, F. M., and Hassan, S. S. M., *Mikrochim. Acta*, 1993, **110**, 79.
8   Dembinski, B., *Acta Pol. Pharm.*, 1977, **34**, 509.
9   Hamilton, H. E., Wallace, J. E., and Blum, K., *Anal. Chem.*, 1975, **47**, 1139.
10 Hussein, S. A., El-Kommos, M. E., Hassan, H. Y., and Mohamed, A. M. I., *Talanta*, 1989, **36**, 941.
11 Hussein, S. A., Mohamed, A. M. I., and Hassan, H. Y., *Talanta*, 1989, **36**, 1147.
12 Moody, J. P., Tait, A. C., and Todrick, A., *Br. J. Psychiatry*, 1967, **113**, 183.
13 Westerlund, D., Borg, K. O., and Lagerstroem, P. O., *Acta Pharm. Suec.*, 1972, **9**, 52.
14 Bishop, E., and Hussein, W., *Analyst*, 1984, **109**, 73.
15 Ghorochchian, J., Menghani, M., and Salahuddin, K., *Mikrochem. J.*, 1992, **45**, 62.
16 Alary, J., Villet, A., and Coeur, A., *Ann. Pharm. Fr.*, 1976, **34**, 419.
17 Brunswick, D. J., Needelman, B., and Mendels, J., *Life, Sci.*, 1978, **22**, 137.
18 Hucker, H. B., and Stauffer, S. C., *J. Chromatogr.*, 1977, **138**, 437.
19 Thompson, D., *J. Pharm. Sci.*, 1982, **71**, 536.
20 Villet, A., Alary, J., and Coeur, A., *Talanta*, 1980, **27**, 659.
21 Suekow, F. R., and Cooper, T. B., *J. Pharm. Sci.*, 1981, **70**, 257.
22 Segatti, M., Nisi, G., Grossi, F., and Mangiarotti, M., *J. Chromatogr.*, 1991, **536**, 319.
23 de la Peña, L., Gomez-Hens, A., and Pérez-Bendito, D., *Anal. Chim. Acta*, 1992, **269**, 137.
24 Long, G. L., and Winefordner, J. D., *Anal. Chem.*, 1983, **55**, 273.

Resolution of Mid-infrared Spectra by Factor Analysis Using Spherical Projections: Influence of Noise, Spectral Similarity, Wavelength Resolution and Mixture Composition on Success of the Method

Stephen P. Gurden and Richard G. Brereton*

School of Chemistry, University of Bristol, Cantock's Close, Bristol, UK BS8 1TS

John A. Groves

Health and Safety Laboratory, Health and Safety Executive, Broad Lane, Sheffield, UK S3 7HQ

A new method for the resolution and recovery of mid-infrared spectra by factor analysis is described. The key to the method is to determine a few 'composition-one' points in a set of mixture spectra, where one component uniquely absorbs. The method involves filtering the data using Savitzky–Golay filters, performing principal components analysis, elimination of composition-zero (noise) points, normalization of scores (projection onto the surface of a hypersphere), determining the best N composition-one points for each compound, and finally factor rotation/recovery of spectra. The method is evaluated using two criteria of success namely, the number of true composition-one points recovered and the correlation between true and recovered spectra. The influence of spectral similarity, spectral resolution, component concentration, noise levels, and cut-off threshold is investigated on two separate simulated datasets. Finally, the method is shown to work on a real dataset.

Keywords: Mid-infrared spectra; chemometrics; factor analysis; mixture analysis; resolution

Introduction

There has been limited work on resolving mid-infrared (MIR) spectra using chemometric methods. Recently we proposed an approach based on windows factor analysis[1] in which a set of spectra containing different proportions of three components was analysed by determining regions in the mixture set of composition one, *i.e.*, containing absorbances due to one unique compound. By this approach several composition-one wavelengths were identified for each proposed component, and factor rotation was used to recover the individual spectra. The window eigenvalue approach has been used effectively in areas such as diode array detector high-performance liquid chromatography (DAD–HPLC)[2–4] but the infrared (IR) problem is considerably more difficult to solve, because each compound may exhibit several different regions of unique absorbance over a series of spectra: thus finding 10 contiguous composition-one regions in a series of IR mixture spectra does not imply that there are 10 different compounds in the mixture set, as it would do in HPLC.

We can show that, providing composition-one regions are well defined, the step of factor rotation readily reproduces the

data, and the major problem is to define these composition-one regions. In this paper, we propose a new approach for finding the composition-one wavelengths. The method can be graphically illustrated using simple simulations and mixture sets.[5] If there are K components in a mixture, for each component the scores of the composition-one regions should be proportional to each other. If K principal components are used, and the scores vector at each wavelength in the mixture spectra is normalized to unit length, the scores should form a hypertriangle on the surface of a K-dimensional hypersphere (see Fig. 1). The wavelengths at the K corners of this hypertriangle should correspond to the composition-one points for the K components in the mixture. Hence, finding these corners allows us to identify composition-one regions, and hence the spectra and mixture profiles of each pure component.

For a three-component system it is possible to plot the triangle as a two-dimensional graph. An example of a spherical projection plot is given in Fig. 2.

Hyperspherical projections have several advantages over window eigenanalysis. Firstly, it is necessary to define a window, and this window needs to be several datapoints long because of the problems of noise and calculating ranks of small matrices, meaning that an 'average' composition is determined rather than a precise value. Secondly, we have shown[6] that there are many statistical factors influencing the size of
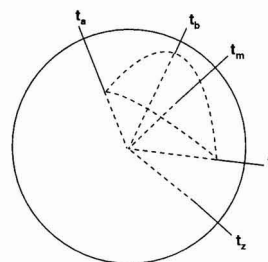
Fig. 1. Graphical description of a spherical projection for a three-component case. The scores vectors are normalized and so projected onto the surface of a sphere: t_a, t_b and t_c represent wavelengths of composition one (*i.e.*, pure A, B and C), and so fall at the corners of a triangular space; t_m represents a composition-three point (mixture of A, B and C); t_z represents a composition-zero point, which will not necessarily fall within the mixture space.

---

* To whom correspondence should be addressed.

eigenvalues, apart from the absolute amount of each component in the dataset. Thirdly, using eigenanalysis it is necessary to define significance thresholds for eigenvalues, which can cause considerable difficulty in the presence of heteroscedastic noise.

Notation

The main notation in this paper is given in the Appendix. Note that, optionally, for matrices, the dimensions are given as bottom left-hand side subscripts, the first being the number of rows, and the second the number of columns.

Methodology

A schematic diagram of some of the matrices used in this method is given in Fig. 3.

Savitzky–Golay Filter

The first step is to reduce the noise levels by using a filter function. In this work, we employ a seven-point quadratic/cubic function of the form

$$f_{x_{ij}} = \sum_{l=-3}^{3} c_l x_{i(j+l)} \tag{1}$$

where c_l are the Savitzky–Golay coefficients.[7] In this paper, we will not investigate the effect of changing the nature of this filter, although in the cases reported below, we find that a seven-point filter performs well.

Fig. 2 Example of a spherical projection plot.
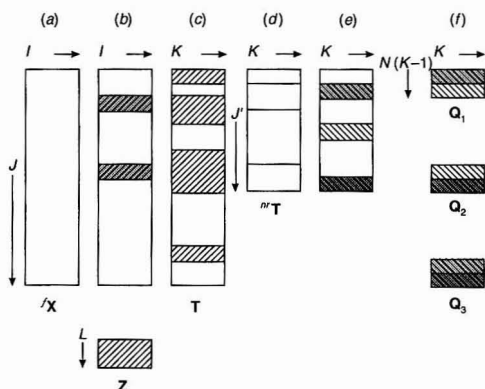
Fig. 3 Schematic of matrices. The filtered data matrix (a) is scanned for L composition-zero points (b), and from this sub-matrix, $_{L,L}Z$, a threshold, H, is found, in order to determine which of the scores vectors correspond to composition-zero wavelengths (c). The reduced scores matrix is then normalized (d), and N composition-one points are found for each component (e). For a $K = 3$ component system, three **Q** matrices are then used (f) to find the rotation matrix, $_{K,K}R$.

Principal Components Analysis

The next step is to perform principal components analysis (PCA) on the filtered mixture dataset. It is important that the PCA algorithm does not mean-centre the dataset as a pre-processing step, as this alters the geometry of the data.[6] K significant components are used, to give

$$_{J,I}\hat{X}' = {}_{J,K}T \cdot {}_{K,I}P \tag{2}$$

where $_{J,I}\hat{X}'$ is the estimated filtered matrix using K components, and **T** and **P** are the relevant scores and loadings matrices obtained from the filtered matrix. Finding the value of K is not always a trivial task. In this paper we do not discuss methods for finding K, but assume that we know the value, which is equal to the number of components in the mixture set. Note that we have a scores vector, t_j, for each wavelength.

Elimination of Composition-zero Points

Composition-zero points are defined as those wavelengths in the mixture spectra where there is no significant absorbance from any of the component spectra.[1] The difficulty with these points is that they tend to fall randomly within the mixture space when the data is normalized. In a previous paper on spherical projections,[5] we show that removing these points can make a dramatic improvement to the definition of the mixture space, and so performance of the factor analysis. In practice, some of these composition-zero points may contain small absorbances due to real compounds, but the aim of the algorithm described below is to find only a few points corresponding to each pure compound, so it is not always a serious problem rejecting wavelengths where pure compounds absorb. The difficulty occurs if there are some compounds present in trace amounts, with small absorbances, in which case these compounds may be rejected.

A threshold, H, is chosen so that scores vectors at wavelengths where the average absorbance at point j, $\bar{x}_j$, is greater than H are kept, and all other scores vectors are rejected. This can dramatically reduce the size of the scores matrix. The choice of H is important to the effectiveness of the algorithm as discussed below.

The value of H can be chosen by taking a submatrix of the spectra, $_{L,L}Z$, containing L composition-zero (i.e., only noise present) wavelengths, where $L = 50$, say, for a 1 cm^{-1} resolution mixture set. This submatrix can be chosen visually or computationally, and contains points that are known/assumed to be pure noise. The over-all mean is calculated, $\bar{z}_{i,l}$, as is the root mean square signal in this region, Z^{rms}. We can then define the average signal threshold, H:

$$H = \bar{z}_{il} + CZ^{rms} \tag{3}$$

where C is chosen to be an integer, typically between 1 and 10. Using the threshold H, further noise points are eliminated.

After reduction due to noise, J' wavelengths remain, where $J' < J$, and the scores matrix, $_{J,K}T$, is reduced to, $_{J',K}T$. This new matrix consists of the scores at the wavelengths that are assumed to be of composition > 0, i.e., contain significant signal intensity.

Normalization

Next, we normalize the scores at each of the J' wavelengths. If $r_{t_{jk}}$ is the score for the kth component at the jth wavelength, then the normalized score is defined by

$$^{nr}t_{jk} = \frac{^{r}t_{jk}}{\sqrt{\sum_{k=1}^{K} {}^{r}t_{jk}^{2}}} \tag{4}$$

giving a new matrix, $_{J',K}^{nr}\mathbf{T}$. As discussed previously, this operation results in the scores lying on the surface of a K-dimensional hypersphere of unit radius.[5]

Determining Best N Composition-one Points for Each Component

Assuming that all composition-zero wavelengths have been eliminated, all other wavelengths will fall within the mixture space, with composition-one points falling at the corners of the hypertriangle. Our aim is to find these corner points, as these are the wavelengths we will use as target vectors for subsequent factor rotations.

The average of the points, represented by a vector, $^{nr}\bar{\mathbf{t}}_{\mathbf{j}}$, is found, which gives a point within the mixture space. The distance, d_j, from each point to $^{nr}\bar{\mathbf{t}}_{\mathbf{j}}$ is then found:

$$d_j = \sqrt{\sum_{k=1}^{K} (^{nr}t_{jk} - ^{nr}\bar{t}_{jk})^2} \qquad (5)$$

If we wish to find, say, six points (*i.e.*, $N = 6$) which lie at the corner furthest from $^{nr}\bar{\mathbf{t}}_{\mathbf{j}}$, then we could merely take the six points which have the highest values for d_j. However, it is possible that some stray noise points are present outside of the mixture space, so we use a grouping algorithm, described as follows:

(*a*) Take the point with the highest value of d_j; this is the first member of the first group.

(*b*) Take the point which is next furthest and calculate the Pearson correlation coefficient[8] between this point and the first. If the correlation is high (*i.e.*, ≥ 0.95) then the second point is a member of the first group. If the correlation is low (*i.e.*, < 0.95) then the second point starts a new group.

(*c*) Continue with the third point *etc.*, until a group containing six points has been found.

Once the points at the first corner have been found, we use this information to find the points at the second corner. We calculate a new set of distances, this time from each point to the first corner. The grouping algorithm is then use to find the second corner. Once the second corner has been found, the distances are calculated again, this time an average of the distances from the first and second corners is used (not the distance from the average of the first and second corners) to find the third corner, and so on, until all the K corners have been found. Thus, N composition-one points for each of the K components are found.

Factor Rotation and Recovery of Spectra

The aim of factor analysis is to find the rotation matrix that will transform the abstract factors (given by PCA) into the real factors (chemical spectra and concentrations). The PCA on the smoothed data matrix, $_{I,J}^{f}\mathbf{X}$, gives us

$$_{I,J}^{f}\hat{\mathbf{X}} = _{I,K}\mathbf{T} \cdot _{K,J}\mathbf{P} \qquad (6)$$

The estimated pure component spectra, $_{K,J}\hat{\mathbf{S}}$, are given by the equation

$$_{K,J}\hat{\mathbf{S}} = _{K,K}\mathbf{R} \cdot _{K,J}\mathbf{P} \qquad (7)$$

where $_{K,K}\mathbf{R}$ is the rotation (or transformation) matrix we need to find.*

---

* As we are using uncentred PCA, the scores and loadings are interchangeable, with the latter usually being normalized. This means that the scores obtained in eqn. (2) can be transposed and normalized for use in eqn. (7), making a second PCA on the data unnecessary and, thus, saving computer time.

To find component k, a new matrix, $_{K,N(K-1)}\mathbf{Q}_k$, is defined as the subset of $_{K,J}\mathbf{P}$ which contains the loadings at the composition-one wavelengths for the other $K - 1$ components. Thus, if $K = 3$ and $N = 6$, then, to find the first component, we would use a matrix $_{3,12}\mathbf{Q}_1$, where the first six columns are the loadings at the composition-one points for component two, and the last six are the loadings at the composition-one points for component three. The rotation row vector, $\mathbf{r}_k$, is then found by solving the equation

$$_{1,K}\mathbf{r}_{kK,N(K-1)} \cdot \mathbf{Q}_k \approx 0 \qquad (8)$$

The above equation can be solved by setting $\mathbf{r}_{kK}$ to 1, and then using a standard regression method, such as the pseudo inverse,[9] to solve

$$_{1,K-1}\mathbf{r}_{,kK-1,N(K-1)} \cdot \mathbf{Q}_k \approx -_{1,N(K-1)}\mathbf{q}_k \qquad (9)$$

Once we have found a rotation vector, $\mathbf{r}_k$, for each of the K components we then have a rotation matrix, $_{K,K}\mathbf{R}$ for use in eqn. (7), and the estimated component spectra are found.

Criteria of Success

It is necessary to have some criteria by which the success of the method used can be ascertained. In this paper we use two criteria for determining how well the component spectra have been recovered, one indirect and one direct.

Number of Composition-one Points Estimated Correctly

It is obviously of critical importance that, for each pure compound, the correct composition-one wavelength area is selected. If these points are found, then the factor rotation will be successful, and the pure component spectra recovered. For the purpose of method validation, we can use our prior knowledge of the component spectra to predict the best composition-zero points. By comparing these points with the composition-one points estimated by the wavelength analysis, we have an indirect method of judging the success of the spectral deconvolution.

If the number of composition-one points found for each component is N, then we can define a measurement, $^{N,M}\psi_k$ as being, for component k, the number of predicted composition-one points which fall into the best M (as found by pre-knowledge of component spectra). Hence, a result of $^{6,6}\psi_k = 4$ means that of the six points estimated by the spherical projection, four fell into the actual best six. A result of $^{6,30}\psi_k = 6$ means that all of the six estimated points fell into the actual best thirty.

Correlation Between Recovered and True Spectra

A more direct method of measuring the success of recovery is to calculate the correlation coefficient between the recovered spectrum, $\hat{\mathbf{s}}_{\mathbf{k}}$, and the true spectrum, $\bar{\mathbf{s}}_{\mathbf{k}}$. Thus, for component k, we have

$$\varphi_k = \frac{\sum_{j=1}^{J} (\bar{s}_{kj} - \bar{\bar{s}}_k)(\hat{s}_{kj} - \bar{\hat{s}}_k)}{\sqrt{\sum_{j=1}^{J} (\bar{s}_{kj} - \bar{\bar{s}}_k)^2 \sum_{j=1}^{J} (\hat{s}_{kj} - \bar{\hat{s}}_k)^2}} \qquad (10)$$

The closer the magnitude of this coefficient is to one, the better the spectrum has been recovered.

Factors Influencing the Success of the Method

Spectral Similarity

Mid-infrared spectra of chemically closely similar compounds often have characteristic absorbances at similar wavelengths: for example, the carbonyl stretching frequency at around 1700 cm^{-1} is diagnostic of ketones, esters, carboxylic acids, *etc.* In order to distinguish different compounds, there must be some regions of unique absorbance; often this is in the high-wavelength 'fingerprint' region. The more similar the compounds, generally, the more similar the spectra, and so the harder it is to resolve out. It is important to be able to determine the influence of spectral similarity on methods for resolution of mixtures by factor analysis.

Two spectra sets of pure components were used. Set I consisted of A, ethyl methyl ketone; B, ethanol; and C, styrene. These spectra are relatively dissimilar, and are given in Fig. 4. Set II consisted of A, 1,2,3-trimethylbenzene; B, 1,3,5-trimethylbenzene; and C, *p*-xylene. These spectra are very similar and have few regions of unique absorbance. They are given in Fig. 5. The correlation coefficients between the component spectra for both of the sets are given in Table 1.

Spectral Resolution

Mid-infrared spectra can be measured at various digital resolutions, higher resolutions giving more points, and so more information, per spectrum. We expect the higher resolution spectra to give better results, especially for datasets where the component spectra are very similar. However, more datapoints mean that more computer calculation time is required, and so we do not want to use high-resolution spectra unless it is necessary.

Two different resolutions were used, 1 cm^{-1} (3501 points per spectrum) and 4 cm^{-1} (876 points).

Component Concentration

Components present in low concentration will be harder to resolve, especially as the signals may be overshadowed by other components present in much higher concentrations. Low concentrations also mean that the signal-to-noise ratio is low, which will cause difficulties.

We reduced the concentration of individual components in the mixture design in order to simulate these components being present in relatively low concentrations. Thus a concentration percentage for A of 10% means that component A was present at only a tenth of its normal concentration.

Noise Levels

In the simulations below, real IR component spectra have been added together computationally, and then simulated Gaussian noise of zero mean has been added. Some of the noise levels used are high, but this can be used to simulate datasets where the component concentrations are very low, and so the signal-to-noise ratio is low.

Two different noise levels were used, 0.1 and 1%. The amount of noise present is given as the distribution of the noise as a percentage of the maximum peak height in the dataset. Fig. 6 shows example mixture spectra for a noise level of 1% (*a*) before the use of the Savitzky–Golay smoothing filter and (*b*) after Savitzky–Golay filtering. Note that if a component has been reduced to a tenth of its normal concentration, then a 1% noise level will, in effect, appear to be 10% to this component.

Fig. 4   Pure component spectra for set **I** (*a*) ethyl methyl ketone, (*b*) ethanol and (*c*) styrene.
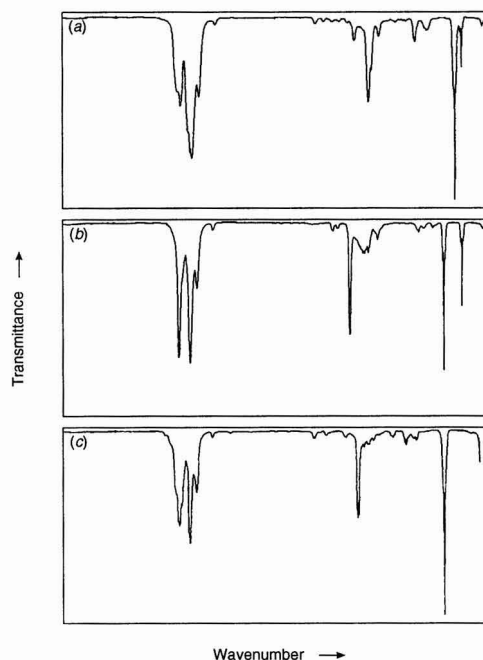
Fig. 5   Pure component spectra for set II (*a*) 1,2,3-trimethylbenzene, (*b*) 1,3,5-trimethylbenzene and (*c*) *p*-xylene.

Cut-off Threshold

The cut-off threshold, H, is of critical importance to the success of the method. The higher the value of H, the less wavelengths make up the spherical projection. If it is too low, then composition-zero points will interfere with the determination of a clear mixture space for the spherical projection. If it is too high, then important composition-one regions may be lost.

For our experiments, four different values of H were used, with $C = 2, 4, 6$ and 8 in eqn. (3).

Experimental

Spectroscopic Conditions

Vapour-phase spectra were recorded on a Perkin-Elmer System 2000 FT (Fourier transform) IR spectrometer by injecting appropriate quantities of the substances into a heated Accuspec gas cell with a pathlength of about 1 cm. All spectra were ratioed against the empty cell. The wavelength range was 4000–500 cm^{-1}. Spectra were Fourier transformed and converted to absorbance scale prior to subsequent analysis. The compounds chosen were typical of workplace pollutants.[10]

Table 1 Correlation coefficients between pure component spectra

Set I	A	B	C
A	1.0000	0.3162	−0.0044
B		1.0000	0.0108
C			1.0000
Set II	A	B	C
A	1.0000	0.7230	0.7218
B		1.0000	0.7475
C			1.0000
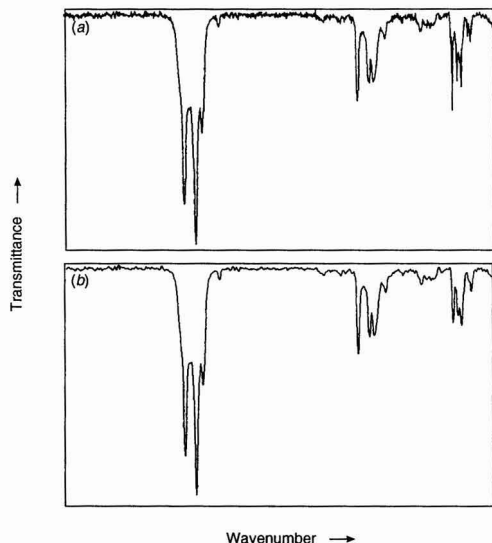
Fig. 6 Mixture spectra for (a) 1% noise before Savitzky-Golay filter, and (b) 1% noise after Savitzky-Golay filter.

Computing

All computing was performed on a 486DX with 33 MHz clock speed, and 4 Mb RAM. Routines were written in Visual Basic and C, running under Windows.

Results

The factor analysis method described above was evaluated by carrying out a comprehensive set of experiments, systematically altering the five main factors. A three-component design was used, the mixture set being simulated by multiplying the concentration matrix, given in Table 2, by the pure component spectra matrix, and then adding simulated random noise.

Spectral Similarity

For spectral set I, there was only one case, with the noise level at 1% and the concentration of C reduced to 10%, where the components could not be fully resolved. Otherwise, these component spectra are dissimilar enough that a composition-one region for each component is present, even at lower resolutions. For spectral set II, the results were also generally good, although at lower resolutions it was sometimes not possible to resolve the component spectra well.

Wavelength Resolution

For spectral set I (dissimilar components), not much difference was apparent in the success of the method: both resolutions gave good results in most cases. Where the 4 cm^{-1} resolution gave bad results (e.g., at very high noise levels), so did the 1 cm^{-1} resolution.

For spectral set II (similar components), the higher resolution spectra gave markedly better results than the lower resolution spectra. Table 3 gives two examples where this can be seen. By looking at the spherical projection plots for the second example, we can see why. Fig. 7(a) shows the plot for the low-resolution case. At the corner marked *, there are only two or three points, which are not enough to characterize a composition-one region for that component. Although the values for $^{6,6}\psi_k$ show us that the points that are most near to being composition-one have been found, these points are still not good enough for successful recoverance. Fig. 7(b), however, shows the plot for the higher resolution case, and the corner marked * now gives more points, which are enough to

Table 2 Concentration matrix used in simulations

	Component		
Mixture	A	B	C
1	1.0	0.6	0.6
2	0.2	0.6	0.6
3	0.6	1.0	0.6
4	0.6	0.2	0.6
5	0.6	0.6	1.0
6	0.6	0.6	0.2
7	1.0	1.0	1.0
8	1.0	1.0	0.2
9	1.0	0.2	1.0
10	1.0	0.2	0.2
11	0.2	1.0	1.0
12	0.2	1.0	0.2
13	0.2	0.2	1.0
14	0.2	0.2	0.2
15	0.6	0.6	0.6

give a composition-one region. As would be expected, in no cases did the lower resolution give better results than the higher resolution.

Component Concentrations

Table 4 gives some results displaying the effect of reducing component concentration for two noise levels. At low noise levels, the effect of lowering the concentration of an individual component was not very noticeable, and the component

spectra were still recovered well. However, at higher noise levels it was sometimes impossible to find composition-one regions for all of the components, and so not all of the pure spectra could be recovered. In general, we found that if the component concentration is at a concentration such that the noise level relative to that component is over 10%, then difficulties start to occur.

Cut-off Threshold

A cut-off threshold of $C = 4$ was usually found to be the best. For a noise level of 0.1%, this gave an absolute cut-off level of about 3% of the maximum peak height, and for a noise level of 1%, this gave an absolute cut-off level of about 6% of the maximum peak height. A low cut-off threshold may include too many noise points whereas a high threshold may eliminate genuinely useful points.

Application to Real Data

A set of 10 IR vapour spectra, containing A, ethyl methyl ketone; B, ethanol; and C, toluene in varying proportions, was measured. The mixture design is given in Table 5. The maximum injection volume of the components in the mixture set [and its relation to the Occupational Exposure Standard
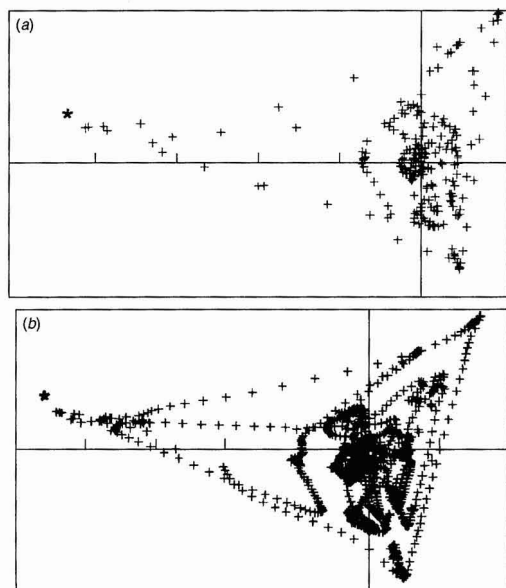
Fig. 7 Spherical projection plots as described in the text for a resolution of (a) 4 and (b) 1 cm^{-1}.

Table 5 Mixture design used for real data

	Component		
Mixture	A	B	C
1	1.0	1.0	1.0
2	0.1	1.0	1.0
3	1.0	0.1	1.0
4	1.0	1.0	0.1
5	0.1	0.1	0.1
6	0.01	0.1	0.1
7	0.1	0.01	0.1
8	0.1	0.1	0.01
9	0.01	0.01	0.01
10	0.001	0.001	0.001

Table 3 Effect of altering wavelength resolution

	Experimental						Success indices								
Set	Resolution /cm^{-1}	A (%)	B (%)	C (%)	Noise (%)	C	φ_1	$6.6\psi_1$	$6.30\psi_1$	φ_2	$6.6\psi_2$	$6.30\psi_2$	φ_3	$6.6\psi_3$	$6.30\psi_3$
II	4	10	100	100	1.0	2	0.9436	4	5	0.7102	4	5	0.9901	4	5
II	1	10	100	100	1.0	2	0.9506	0	6	0.9987	4	6	0.9960	4	6
II	4	100	10	100	1.0	4	0.9339	6	6	0.9569	6	6	0.7732	6	6
II	1	100	10	100	1.0	4	0.9986	5	6	0.9573	3	3	0.9975	5	6

Table 4 Effect of altering component concentrations

	Experimental						Success indices								
Set	Resolution /cm^{-1}	A (%)	B (%)	C (%)	Noise (%)	C	φ_1	$6.6\psi_1$	$6.30\psi_1$	φ_2	$6.6\psi_2$	$6.30\psi_2$	φ_3	$6.6\psi_3$	$6.30\psi_3$
II	1	100	100	100	0.1	4	0.9992	3	6	0.9993	5	6	0.9981	4	6
II	1	10	100	100	0.1	4	0.9986	0	5	0.9993	5	6	0.9978	3	6
II	1	100	10	100	0.1	4	0.9993	6	6	0.9987	3	3	0.9985	4	6
II	1	100	100	10	0.1	4	0.9992	0	6	0.9993	5	6	0.9965	3	4
II	1	100	100	100	1.0	4	0.9987	5	6	0.9987	4	5	0.9979	4	6
II	1	10	100	100	1.0	4	0.9506	1	4	0.7169	4	6	0.9956	4	6
II	1	100	10	100	1.0	4	0.9986	5	6	0.9573	3	3	0.9975	5	6
II	1	100	100	10	1.0	4	0.7273	4	6	0.9982	4	6	0.9101	3	6

(OES)] were as follows: (*a*) ethyl methyl ketone 8.8 μl (corresponds to a 25 ppm atmosphere or 1/8 of the OES); (*b*) ethanol 27.9 μl (corresponds to a 125 ppm atmosphere or 1/8 of the OES); (*c*) toluene 13.0 μl (corresponds to a 31.25 ppm atmosphere or 5/8 of the OES).

Before each sample spectrum was recorded, a background scan was made in order to minimize the levels of water vapour and carbon dioxide in the spectrum. The spectra were measured from 4000 to 500 cm^{-1} with a resolution of 4 cm^{-1} (*i.e.*, 876 data points). The spectra were then interpolated to give 3501 data points.

The noise levels of each spectrum were measured. Mixtures 1–4 had a noise level (*i.e.*, noise distribution as a percentage of maximum peak) of around 0.08%. Mixtures 5–8 had a noise level of around 0.13%. The noise levels for mixtures 9 and 10 were 0.46% and 4.9%, respectively.

A spherical projection factor analysis, as described above, was performed on all 10 mixture spectra, with $C = 4$. In this mixture set, the most favourable noise level was 0.08% (the worst being 4.9%). The spectra were recovered extremely well, the correlation coefficients between pure spectra and recovered spectra being 0.9987, 0.996 and 0.9953 for ethyl methyl ketone, ethanol and toluene, respectively.

Factor analysis was also performed on a subset of the data, mixtures 5–10. Here, the most favourable noise level was 0.13% (the worst being 4.9%), and there are less mixture spectra to extract information from. The spectra were still recovered very well, the correlation coefficients being 0.9934, 0.9997 and 0.9903 for ethyl methyl ketone, ethanol and toluene, respectively.

Thus the method was shown to have worked well on a real dataset, even when the components are present in relatively low concentrations.

Conclusion

The new method proposed in this paper is seen to be effective in most of the cases studied. The computational approach can easily be extended to more than three components: a four-dimensional hypersphere is perfectly easy to model computationally. On some occasions, poor recovery of spectra is found. In practice, for three components, this can be predicted, visually, from a projection of the normalized scores[5] as discussed in a previous paper. It is easy to see whether the data lie on a triangular projection or not, and this is a good approach for the selection of optimal cut-off threshold and reduction of noise points; it is also possible to interactively choose the composition-one points. For more than three components, this is not possible, and it is necessary to rely on computational algorithms.

In this paper, we have not studied non-additivity of spectra or heteroscedastic noise. Because we identify composition-one points, non-additivity of spectra is not a very serious problem, as there is only one significant spectrum in the regions selected for factor rotation; there may, however, be some inaccuracies in reconstructions in other regions, but for qualitative library searching this should not be a very major problem. Heteroscedasticity of IR spectroscopic noise could be allowed for by modifying the algorithm for reducing noise points. If C is high enough, and the L noise points are well selected, it should not pose serious difficulties: the importance is to have a sufficiently high signal-to-noise ratio so the signal is not accidentally eliminated.

This paper has presented a promising new approach for the resolution of multicomponent MIR spectra.

Appendix

List of Main Notation used in the Text

$_{I,J}\mathbf{X}$	Observed data matrix, *I* spectra of *J* wavelengths.
x_{ij}	Element of this matrix: absorbance of spectrum *i* at wavelength *j*.
$_{I,J}^{f}\mathbf{X}$	Data matrix, having been smoothed by Savitsky–Golay filter.
$_{I,J}^{f}\mathbf{X}'$	Transpose of this matrix.
K	Number of significant components in the mixture set.
$\mathbf{T}$	Scores matrix.
$\mathbf{P}$	Loadings matrix.
$_{I,L}\mathbf{Z}$	Submatrix of $_{I,J}^{f}\mathbf{X}$, containing *I* spectra at *L* composition-zero wavelengths.
$\bar{z}_{il}$	Mean value of the elements in $_{I,L}\mathbf{Z}$.
Z^{rms}	The root mean square of the absorbances in $_{I,L}\mathbf{Z}$.
$^{f}\bar{x}_j$	Mean absorbance (after smoothing) at wavelength *j*.
H	Absolute threshold: wavelengths are eliminated as being composition zero if $^{f}\bar{x}_j$ is below H.
J'	The number of non-composition-zero wavelengths, *i.e.*, $^{f}\bar{x}_j > H$.
$\mathbf{t}_j$	Scores vector for wavelength *j*.
$_{J',K}^{r}\mathbf{T}$	Reduced scores matrix.
$_{J',K}^{nr}\mathbf{T}$	Normalized, reduced scores matrix, where every scores vector, $^{nr}\mathbf{t}_j$, has been normalized to unit length.
$^{nr}\bar{\mathbf{t}}_j$	Mean vector of the J' normalized scores vectors.
$^{nr}\bar{\mathbf{t}}_{jk}$	Element of the vector $^{nr}\bar{\mathbf{t}}_j$.
d_j	Distance from $^{nr}\mathbf{t}_j$ to a point, as described in the paper.
N	Number of composition-one points to find for each component.
$_{K,J}\hat{\mathbf{S}}$	Matrix of estimated pure component spectra.
$_{K,J}\mathbf{S}$	Matrix of true pure component spectra.
$_{K,K}\mathbf{R}$	Rotation matrix used to transform abstract spectra into real component spectra.
$_{N,M}\psi_k$	The number of the N predicted composition-one points which match the M actual best composition-one points, for component k.
φ_k	Correlation coefficient between the estimated and true component spectra, for component k.
$_{K,N(K-1)}\mathbf{Q}_k$	Matrix which contains the loadings vectors at the N composition-one points for all the K components, except for the component we are trying to find.
$_{K,K}\mathbf{R}$	Rotation matrix.
$\mathbf{r}_k$	Row vector of the rotation matrix.

References

1 Gurden, S. P., Brereton, R. G., and Groves, J. A., *Chemom. Intell. Lab. Syst.*, 1994, **23**, 123.

2 Kvalheim, O. M., and Liang, Y.-Z., *Anal. Chem.*, 1992, **64**, 936.

3 Liang, Y.-Z., Kvalheim, O. M., Rahmani, A., and Brereton, R. G., *J. Chemom.*, 1993, **7**, 15.

4 Keller, H. R., and Massart, D. L., *Anal. Chim. Acta*, 1991, **246**, 379.

5 Gurden, S. P., Brereton, R. G., and Groves, J. A., *Anal. Proc.*, 1994, **31**, 205.

6 Brereton, R. G., Gurden, S. P., and Groves, J. A., *Chemom. Intell. Lab. Syst.*, 1995, **27**, 73.

7 Brereton, R. G., *Chemometrics: Applications of Mathematics and Statistics to Laboratory Systems*, Ellis Horwood, Chichester, 1993.
8 Czerminski, J., Iwasiewicz, A., Paszek, Z., and Sikorski, A., *Statistical Methods in Applied Chemistry*, Elsevier, Amsterdam, 1990.
9 Malinowski, E. R., *Factor Analysis in Chemistry*, Wiley, New York, 2nd edn., 1991.
10 Clayton, G., and Clayton, F. E., *Patty's Industrial Hygiene and Toxicology*, Wiley, Chichester, 1981, vol. 2A and 2B; 1982, vol. 2C, revised 3rd edn.

Orthogonal Array Design as a Chemometric Method for the Optimization of Analytical Procedures

Part 5.* Three-level Design and its Application in Microwave Dissolution of Biological Samples

Wei Guang Lan, Ming Keong Wong† and Ni Chen

Department of Chemistry, National University of Singapore, Kent Ridge, Singapore 0511, Republic of Singapore

Yoke Min Sin

Department of Zoology, National University of Singapore, Kent Ridge, Singapore 0511, Republic of Singapore

The theory and methodology of a three-level orthogonal array design as a chemometric method for the optimization of analytical procedures were developed. In the theoretical section, firstly, the matrix of a three-level orthogonal array design is described and orthogonality is proved by a quadratic regression model. Next, the assignment of experiments in a three-level orthogonal array design and the use of the triangular table associated with the corresponding orthogonal array matrix are illustrated, followed by the data analysis strategy, in which significance of the different factor effects is quantitatively evaluated by the analysis of variance (ANOVA) technique and the percentage contribution method. Then, a quadratic regression equation representing the response surface is established to estimate each factor that has a significant influence. Finally, on the basis of the quadratic regression equation established, the derivative algorithm is used to find the optimum value for each variable considered. In the application section, microwave dissolution for the determination of selenium in biological samples by hydride generation atomic absorption spectrometry is employed, as a practical example, to demonstrate the application of the proposed three-level orthogonal array design in analytical chemistry.

Keywords: *Experimental design; three-level orthogonal array design; response surface methodology; chemometric optimization; microwave dissolution, selenium determination; hydride generation atomic absorption spectrometry*

Introduction

Experimental design was first introduced by Fisher[1] as an agricultural research tool in the 1920s and introduced into the area of chemistry by Smallwood[2] in 1947. However, experimental design did not become generally known and applied until the 1970s [*c.f.*, the biennial/quadrennial fundamental reviews entitled 'Statistical and Mathematical Methods in Chemistry' before 1972 in *Analytical Chemistry*]. In 1971, Rubin *et al.*[3] published a renowned paper using experimental design to optimize specific transfer ribonucleic acid assay conditions. Since then, experimental design has found widespread application in optimizing analytical proce-

dures and much literature is now available [*c.f.*, the aforementioned reviews in 1976 and the reviews entitled 'Chemometrics' after 1980 in *Analytical Chemistry*]. Experimental design, as an effective and efficient optimization strategy, has found widespread application in all branches of analytical chemistry. Recently, a textbook by Deming and Morgan[4] dealing with experimental design as a chemometric approach has provided detailed information and comprehensive references on the use of different experimental design methods such as classical full/fractional factorial design, mixture design, central composite design, Plackett-Burman design, *etc.*, for chemists. However, in the presentation, although orthogonal design method as a type of experimental design had been dealt with, relatively little information was provided. This situation can be found in some other chemometric monographs of a similar nature.[5–7]

Statistically, orthogonal array design has been developed for many years.[8–13] However, this method was not introduced into analytical chemistry until 1989 by Oles and Yankovich,[14] whose paper, to the best of our knowledge, was the first publication in English applying the orthogonal array design method to analytical chemistry. Subsequently, some other papers on this topic have been published.[15–20] Nevertheless, the use of the orthogonal array design method in analytical chemistry is rather scarce. The reason for this might be that a large number of chemists are unfamiliar with the statistical steps and algorithms used in the orthogonal array design method.

For the reasons mentioned above, recently, we documented a series of papers in which the theory and methodology of an orthogonal array design for the optimization of analytical procedures were developed.[21–24] In the first part of this series,[21] a two-level orthogonal array design was proposed and the source and background of the orthogonal array design method were described in detail. There is no doubt that the two-level orthogonal array design is very useful, particularly for the experiments containing many factors to be screened, because a large amount of quantitative information can be extracted with a few experimental trials. However, a two-level orthogonal array design also suffers from two obvious disadvantages. Firstly, the response is highly dependent on the high and low levels chosen. For example, if the high and low levels are set too close, the effect of the factor may be negligible but may be significant if the high and low levels are set further apart. Secondly, the non-linear response surface cannot be expressed in a polynomial model. In other words,

---

for a two-level orthogonal array design, only a linear regression equation representing the response surface can be established, whereas in many instances the response surface cannot be adequately described by a linear regression equation. Such an example has been shown in Part 1 of this series. Hence, in Parts 2 and 3 of this series,[22,23] four-level and five-level orthogonal array designs were further introduced into the area of analytical chemistry. Both four-level and five-level orthogonal array designs can be used to deal with the non-linear response surface. However, they are strongly restricted by the presupposition of the absence of the two-variable interaction effects. Therefore, the practical applications of both four-level and five-level orthogonal array designs in analytical chemistry are rather limited. Consequently, it is desirable to develop an orthogonal array design in which the non-linear response surface and the interaction effect can be considered simultaneously.

For the reasons mentioned above, this paper introduces a three-level orthogonal array design into the area of analytical chemistry. Firstly, the matrix of a three-level orthogonal array design is described in detail and orthogonality is proved by using a quadratic regression model. This is followed by the assignment of experiments in the three-level orthogonal array matrix, the data analysis strategy including the ANOVA technique with the percentage contribution method, and the response surface methodology with the derivative algorithm. Subsequently, microwave dissolution for the determination of selenium in biological samples by hydride generation atomic absorption spectrometry (HGAAS), which has been employed to illustrate the use of two-level and four-level orthogonal array designs previously,[21,22] is used to demonstrate the application of the proposed three-level orthogonal array design and the data analysis strategy in analytical chemistry. For the definition of symbols in the text, the reader is referred to Parts 1–3 of this series.[21–23]

Theoretical

Matrix

A three-level orthogonal array design, denoted by $OA_{2S+1}(3^S)$, is a $(2S+1) \times S$ matrix, where S is the number of the columns, which corresponds to the factors, $2S+1$ is the number of the rows, which corresponds to the experimental trials. The intersections between the columns and rows indicate the level settings that apply to the factors for the experimental trials. The $OA_9(3^4)$ and $OA_{27}(3^{13})$ matrices, which are frequently used three-level orthogonal array matrices, are displayed in Tables 1 and 2 respectively, the methods of construction of which are given in Appendix A. From Table 1, it can be seen that, each of four columns is varied over three level settings, each level setting repeating three times, so a total of $3 \times 3 = 9$ experimental trials are necessary for each column. Similarly, from Table 2, it can be seen that each of thirteen columns is varied over three level settings, each level setting repeats nine times, and thus a total of $3 \times 9 = 27$ experimental trials are necessary for each column. Further, both Table 1 and Table 2 demonstrate that, in any two columns, the horizontal combination of any two level numbers appears the same number of times. This means that in the $OA_9(3^4)$ matrix (Table 1) each combination of the nine ordered pairs $(1, 1), (1, 2), (1, 3); (2, 1), (2, 2), (2, 3); (3, 1), (3, 2)$ and $(3, 3)$ appears exactly once, and in the $OA_{27}(3^{13})$ matrix (Table 2) each combination of the nine ordered pairs $(1, 1), (1, 2), (1, 3); (2, 1), (2, 2), (2, 3); (3, 1), (3, 2)$ and $(3, 3)$ appears exactly three times. Therefore, in Table 1 when the three rows for a column are at level 1, for any other columns, one of the three rows is at level 1, one at level 2, and one at level 3. Likewise, in Table 2 when the nine rows for a column

are at level 1, for any other columns, three of nine rows are at level 1, three at level 2, and three at level 3. Similar cases can be seen when this column is at other two level settings. The above features of the $OA_{2S+1}(3^S)$ matrix provide the orthogonality among all the S columns. This can be proved by the following statistical method.

First, let us consider the following statistical model:

(*i*) For a three-level factorial design, a quadratic regression model representing a response surface can be expressed as:

$$y = \beta_0 + \sum_{x=A}^{X} \beta_x \phi_x + \sum_{x \neq x'=A}^{X} \beta_{xx'} \phi_x \phi_{x'} + \sum_{x=A}^{X} \beta_{xx} \phi_x^2 + \varepsilon \quad (1)$$

where

$$\phi_x = \frac{Z_x - \bar{Z}_x}{H_x} \quad (2)$$

in eqn. (2), suppose that

$$H_x = Z_{x2} - Z_{x1} = Z_{x3} - Z_{x2} \quad (3)$$

then

$$\bar{Z}_x = \frac{Z_{x1} + Z_{x2} + Z_{x3}}{3} = Z_{x2} \quad (4)$$

Substituting eqns. (3) and (4) into eqn. (2) will lead to

$$\phi_{x1} = -1; \qquad \phi_{x2} = 0; \qquad \phi_{x3} = 1; \quad (5)$$

and

$$\sum_{k=1}^{3} \phi_{xk} = 0; \qquad \sum_{k=1}^{3} \phi_{xk}^2 = 2 \quad (6)$$

(*ii*) Considering that the $OA_9(3^4)$ matrix is relatively simple and easily understood, the $OA_{27}(3^{13})$ matrix is chosen as an example. Suppose all the thirteen columns in the $OA_{27}(3^{13})$ matrix are assigned an independent parameter, namely A, B, $\cdots$, and M, respectively, and no interactions exist between parameters; then the third term in eqn. (1) can be neglected, hence eqn. (1) can be rewritten as

$$y = \beta_0 + \sum_{x=A}^{M} \beta_x \phi_x + \sum_{x=A}^{M} \beta_{xx} \phi_x^2 + \varepsilon \quad (7)$$

Moreover, suppose that

$$E_x = \beta_x \phi_x + \beta_{xx} \phi_x^2 \quad (8)$$

Then, according to eqns. (7) and (8), the response, y_i, for each experimental trial in the $OA_{27}(3^{13})$ matrix can be described as follows:

$$y_i = \beta_0 + E_{Ak} + E_{Bk} + E_{Ck} + E_{Dk} + E_{Ek} + E_{Fk} + E_{Gk} \\ + E_{Hk} + E_{Ik} + E_{Jk} + E_{Kk} + E_{Lk} + E_{Mk} + \varepsilon_i \quad (9)$$

Table 1 The $OA_9(3^4)$ matrix

Trial no.	Column no.			
	1	2	3	4
			Construction*	
	f_1	f_2	f_3	f_4
1	**1**	**1**	1	1
2	**1**	**2**	2	2
3	**1**	**3**	3	3
4	**2**	**1**	2	3
5	**2**	**2**	3	1
6	**2**	**3**	1	2
7	**3**	**1**	3	2
8	**3**	**2**	1	3
9	**3**	**3**	2	1

* The basic columns are shown in bold.

where k represents the level setting numbers which are varied with the intersections in the $OA_{27}(3^{13})$ matrix. The statistical error (ε_i) is an independent random variable from an $N(0, \sigma^2)$ distribution. Therefore,

$$\frac{1}{I} \sum_{i=1}^{I} \varepsilon_i \simeq 0; \quad \frac{1}{L} \sum_{l=1}^{L} \varepsilon_l \simeq 0 \tag{10}$$

Now, a proof can be given as follows. Let us randomly select a factor at a level, *e.g.*, factor H at level 1, according to the eqn. (9), it can be concluded that

$$R_{H1} = y_1 + y_6 + y_8 + y_{10} + y_{15} + y_{17} + y_{19} + y_{24} + y_{26}$$

$$= 9\beta_0 + 3 \sum_{k=1}^{3} E_{Ak} + 3 \sum_{k=1}^{3} E_{Bk} + 3 \sum_{k=1}^{3} E_{Ck}$$

$$+ 3 \sum_{k=1}^{3} E_{Dk} + 3 \sum_{k=1}^{3} E_{Ek} + 3 \sum_{k=1}^{3} E_{Fk}$$

$$+ 3 \sum_{k=1}^{3} E_{Gk} + 9E_{H1} + 3 \sum_{k=1}^{3} E_{Ik}$$

$$+ 3 \sum_{k=1}^{3} E_{Jk} + 3 \sum_{k=1}^{3} E_{Kk} + 3 \sum_{k=1}^{3} E_{Lk}$$

$$+ 3 \sum_{k=1}^{3} E_{Mk}$$

$$+ (\varepsilon_1 + \varepsilon_6 + \varepsilon_8 + \varepsilon_{10} + \varepsilon_{15} + \varepsilon_{17} + \varepsilon_{19} + \varepsilon_{24} + \varepsilon_{26}) \tag{11}$$

When combined with eqns. (8) and (10), eqn. (11) can be rewritten as

$$R_{H1} = 9\beta_0 + 3\beta_A \sum_{k=1}^{3} \phi_{Ak} + 3\beta_{AA} \sum_{k=1}^{3} \phi_{Ak}^2$$

$$+ 3\beta_B \sum_{k=1}^{3} \phi_{Bk} + 3\beta_{BB} \sum_{k=1}^{3} \phi_{Bk}^2$$

$$+ 3\beta_C \sum_{k=1}^{3} \phi_{Ck} + 3\beta_{CC} \sum_{k=1}^{3} \phi_{Ck}^2$$

$$+ 3\beta_D \sum_{k=1}^{3} \phi_{Dk} + 3\beta_{DD} \sum_{k=1}^{3} \phi_{Dk}^2$$

$$+ 3\beta_E \sum_{k=1}^{3} \phi_{Ek} + 3\beta_{EE} \sum_{k=1}^{3} \phi_{Ek}^2$$

$$+ 3\beta_F \sum_{k=1}^{3} \phi_{Fk} + 3\beta_{FF} \sum_{k=1}^{3} \phi_{Fk}^2$$

$$+ 3\beta_G \sum_{k=1}^{3} \phi_{Gk} + 3\beta_{GG} \sum_{k=1}^{3} \phi_{Gk}^2$$

$$+ 9(\beta_H \phi_{H1} + \beta_{HH} \phi_{H1}^2) + 3\beta_I \sum_{k=1}^{3} \phi_{Ik}$$

$$+ 3\beta_{II} \sum_{k=1}^{3} \phi_{Ik}^2 + 3\beta_J \sum_{k=1}^{3} \phi_{Jk}$$

$$+ 3\beta_{JJ} \sum_{k=1}^{3} \phi_{Jk}^2 + 3\beta_K \sum_{k=1}^{3} \phi_{Kk}$$

$$+ 3\beta_{KK} \sum_{k=1}^{3} \phi_{Kk}^2 + 3\beta_L \sum_{k=1}^{3} \phi_{Lk}$$

$$+ 3\beta_{LL} \sum_{k=1}^{3} \phi_{Lk}^2 + 3\beta_M \sum_{k=1}^{3} \phi_{Mk}$$

$$+ 3\beta_{MM} \sum_{k=1}^{3} \phi_{Mk}^2 \tag{12}$$

Substituting eqn. (6) into eqn. (12) will lead to

$$R_{H1} = 9\beta_0 + 6 \sum_{x(\neq H)=A}^{M} \beta_{xx} + 9(\beta_H \phi_{H1} + \beta_{HH} \phi_{H1}^2) \tag{13}$$

Suppose that

$$9T_H = 9\beta_0 + 6 \sum_{x(\neq H)=A}^{M} \beta_{xx} \tag{14}$$

eqns. (13) can be rewritten as

$$r_{H1} = T_H + \beta_H \phi_{H1} + \beta_{HH} \phi_{H1}^2 \tag{15}$$

Correspondingly

$$r_{H2} = T_H + \beta_H \phi_{H2} + \beta_{HH} \phi_{H2}^2 \tag{16}$$

$$r_{H3} = T_H + \beta_H \phi_{H3} + \beta_{HH} \phi_{H3}^2 \tag{17}$$

Subtracting eqn. (15) from eqn. (16), and combining with eqn. (5), the following eqn. can be concluded:

$$r_{H2} - r_{H1} = \beta_H - \beta_{HH} \tag{18}$$

and similarly

$$r_{H3} - r_{H2} = \beta_H + \beta_{HH} \tag{19}$$

Consequently

$$\beta_H = \frac{1}{2}(r_{H3} - r_{H1}) \tag{20}$$

$$\beta_{HH} = \frac{1}{2}\{(r_{H3} - r_{H2}) - (r_{H2} - r_{H1})\} \tag{21}$$

By using a similar method, the following formula for each factor can be deduced

$$\beta_x = \frac{1}{2}(r_{x3} - r_{x1}) \tag{22}$$

$$\beta_{xx} = \frac{1}{2}\{(r_{x3} - r_{x2}) - (r_{x2} - r_{x1})\} \tag{23}$$

From eqns. (5), (8), (22) and (23), it is clear that the effect of the factor X at each level is only dependent on the level means for this factor at different levels and independent of the effect for any other factors. Hence, the orthogonality has been proven. By using the similar statistical model, the orthogonality of the other three-level orthogonal array design such as the $OA_9(3^4)$ and $OA_{81}(3^{40})$ matrices can also be proven. However, it should be pointed out that the $OA_{81}(3^{40})$ matrix is too large to be used in actual experimentation in analytical chemistry.

Note that from eqn. (23) it is convenient to judge whether second-order effects are present or absent. If for a factor X the difference of the level mean between level 2 and level 1 ($r_{x2} - r_{x1}$) is not significantly different from that between level 3 and level 2 ($r_{x3} - r_{x2}$), then the second-order effect of the factor X can be neglected. Interestingly, the above conclusion resulting from the statistical proof is the same as the interpretation based on experience given by Massart *et al.*,[25] who described a well balanced three-level screening design which is the half of the Plackett–Burman scheme. In fact, the features of the well balanced three-level design proposed by Massart *et al.*[25] are mathematically identical to those of the corresponding three-

level orthogonal array design except that the intersections between columns and rows need to be rearranged.

Assignment of Experiments

The $OA_{2S+1}(3^S)$ matrix can be viewed as a $(2S + 1)/3^S$ fraction of a full 3^S factorial design. In this matrix, the $2S + 1$ experimental trials provide a total of $2S$ degrees of freedom for the entire experiment. Owing to each column having three level settings, *i.e.*, two degrees of freedom, a total of S columns can be allocated. In principle, each column may be used to assign a factor. However, in order to measure the variance of error, it is preferable for at least one column to be used to assign a dummy factor, in which no actual factor can be assigned.

Generally, in the presence of dummy factors, no repetition is necessary for the same experimental trial, because replicated experiments have been performed for each factor at each level setting in the $OA_{2S+1}(3^S)$ matrix, and variance of error can be pooled from dummy variances. However, when all columns have to be assigned an actual factor, the error variance must come from the repetitions in each experimental trial since no dummies are available to estimate the variance of error.

In the statistical model considered above, all the interactions between columns are neglected. In practice, however, it is possible that a two-variable interaction may be considered.

In this event, as in the two-level orthogonal array design, each two-variable interaction is regarded as an independent parameter and assigned to a column in a two-level orthogonal array matrix according to the corresponding triangular table.[21] However, care should be taken that in the three-level orthogonal array design a two-variable interaction requires a total of $2 \times 2 = 4$ degrees of freedom, whereas one column just provides 2 degrees of freedom in the three-level orthogonal array design, hence, for a two-variable interaction, two columns must be occupied in the three-level orthogonal array matrix. This means that for a three-level orthogonal array design a two-variable interaction equals two independent parameters. As a result, if a two-variable interaction is expected to require consideration, for the $OA_9(3^4)$ matrix, in order to avoid confusion between the main effects and their interaction effects, only two columns are available for the main variables while the residual two columns have to be used to assign a two-variable interaction. For this reason, in general, the $OA_9(3^4)$ matrix is only to be used as a main-effect design. As a result, when two-variable interactions are expected to be considered in a three-level orthogonal array design, the $OA_{27}(3^{13})$ matrix is usually recommended.

The triangular table associated with the $OA_{27}(3^{13})$ matrix is displayed in Table 3, the method of construction of which is shown in Appendix B. As an example, the use of Table 3 is illustrated as follows. Suppose that variables A and B are assigned to columns 3 and 6 respectively, from Table 3 it can

Table 2 The $OA_{27}(3^{13})$ matrix associated with the analytical results

Trial no.	1 f_1	2 f_2	3 f_3	4 f_4	5 f_5	6 f_6	7 f_7	8 f_8	9 f_9	10 f_{10}	11 f_{11}	12 f_{12}	13 f_{13}	Experimental y	Polynomial $Y^\dagger$	$\hat{y}^\ddagger$	$y - \hat{y}$
1	1	1	1	1	1	1	1	1	1	1	1	1	1	66.4	−12.8	72.6	−6.2
2	1	1	1	1	2	2	2	2	2	2	2	2	2	71.2	−8.6	76.8	−5.6
3	1	1	1	1	3	3	3	3	3	3	3	3	3	67.8	−15.5	69.9	−2.1
4	1	2	2	2	1	1	1	2	2	2	3	3	3	89.1	2.2	87.6	1.5
5	1	2	2	2	2	2	2	3	3	3	1	1	1	84.8	−2.7	82.7	2.1
6	1	2	2	2	3	3	3	1	1	1	2	2	2	90.6	2.0	87.4	3.2
7	1	3	3	3	1	1	1	3	3	3	2	2	2	76.8	−9.2	76.2	0.6
8	1	3	3	3	2	2	2	1	1	1	3	3	3	96.4	7.4	92.8	3.6
9	1	3	3	3	3	3	3	2	2	2	1	1	1	97.8	75.4	95.0	2.8
10	2	1	2	3	1	2	3	1	2	3	1	2	3	71.7	−21.4	64.0	7.7
11	2	1	2	3	2	3	1	2	3	1	2	3	1	60.2	−26.3	59.1	1.1
12	2	1	2	3	3	1	2	3	1	2	3	1	2	67.3	−21.6	63.8	3.5
13	2	2	3	1	1	2	3	2	3	1	3	1	2	67.9	−18.8	66.6	1.3
14	2	2	3	1	2	3	1	3	1	2	1	2	3	89.5	−2.2	83.2	6.3
15	2	2	3	1	3	1	2	1	2	3	2	3	1	85.3	0.0	85.4	−0.1
16	2	3	1	2	1	2	3	3	1	2	2	3	1	77.4	−2.1	83.3	−5.9
17	2	3	1	2	2	3	1	1	2	3	3	1	2	79.9	2.1	87.5	−7.6
18	2	3	1	2	3	1	2	2	3	1	1	2	3	74.5	−4.8	80.6	−6.1
19	3	1	3	2	1	3	2	1	3	2	1	3	2	16.5	−69.4	16.0	0.5
20	3	1	3	2	2	1	3	2	1	3	2	1	3	33.7	−52.8	32.6	1.1
21	3	1	3	2	3	2	1	3	2	1	3	2	1	35.0	−50.6	34.8	0.2
22	3	2	1	3	1	3	2	2	1	3	3	2	1	40.1	−38.7	46.7	−6.6
23	3	2	1	3	2	1	3	3	2	1	1	3	2	45.4	−34.5	50.9	−5.5
24	3	2	1	3	3	2	1	1	3	2	2	1	3	41.9	−41.4	44.0	−2.1
25	3	3	2	1	1	3	2	3	2	1	2	1	3	54.5	−37.7	47.7	6.8
26	3	3	2	1	2	1	3	1	3	2	3	2	1	47.7	−42.6	42.8	4.6
27	3	3	2	1	3	2	1	2	1	3	1	3	2	48.6	−37.9	47.5	1.1
r_1	82.3	54.4	62.7	66.5	62.3	65.2	65.3	66.2	67.8	65.6	66.1	66.0	66.0				
r_2	74.8	70.5	68.2	64.6	67.6	66.1	65.6	64.8	70.0	66.4	65.7	66.3	62.7				
r_3	40.3	72.6	66.5	66.4	67.6	66.3	66.6	66.5	59.8	65.4	65.6	65.2	68.8				

Column no.

Construction*

$u \pm s = 65.8 \pm 21.4$
$\bar{Y} \pm s = -19.6 \pm 21.2$
$\bar{\hat{y}} \pm s = 65.8 \pm 21.2$
$\bar{y} - \bar{\hat{y}} \pm s = 0.0 \pm 4.4$

* The basic columns are shown in bold.
† Polynomial values excluding β_0 term.
‡ Polynomial values including β_0 term.

be seen that the intersection between columns 3 and 6 is numbers 10 and 11, and thus the interaction between A and B must be assigned to columns 10 and 11. Further, if another variable C is to be considered, it can be randomly assigned to one of these columns except columns 3, 6, 10 and 11. Suppose that variable C is assigned to column 5, then according to Table 3, the interaction between A and C must be assigned to columns 9 and 13, the interaction between B and C to columns 1 and 7, and so forth.

As a matter of convenience, the assignment table of the main variables and two-variable interactions in the $OA_{27}(3^{13})$ matrix is constructed according to the associated triangular table (Table 3) and is shown in Appendix C, from which it is clear that if three variables are expected to require consideration, a Resolution V design can be obtained; if four variables are expected to require consideration, a Resolution IV can be obtained. It should be pointed out that if more than four variables are expected to require consideration, apparently no Resolution IV can be achieved. In other words, when more than four variables are expected to be considered, it is apparent that only a Resolution III design can be obtained. However, because some interaction effects can be neglected based on experience in the areas studied (non-statistical knowledge), in many events, the $OA_{27}(3^{13})$ matrix containing

more than four variables can be considered as a Resolution IV design or even as a Resolution V design.

Data Analysis Strategy

After experimental design has been implemented, the ANOVA technique including the percentage contribution method should be employed to estimate the factor effects. The algorithm used is the same as that shown in our previous papers,[21–23] except that the equations used must be modified according to the change of the degrees of freedom. The modified equations are shown in Table 4. Note that when no replicate experiments are carried out, the computational formula for the variance of error given in Table 4 is not suitable because no degrees of freedom resulting from replicate experiments are available [$I(J-1) = 0$]. Hence, in this event the variance of error and its degrees of freedom need to be computed by pooling the variances of the dummy columns (in which no main variables and significant interactions are assigned) and their degrees of freedom. Alternatively, the total variance and total degrees of freedom can be computed by using the equations given in Table 4, then the error variance and its degrees of freedom can be calculated by the following equations:

$$SS_{error} = SS_{total} - \Sigma SS_X \qquad (24)$$

$$df_{error} = df_{total} - \Sigma df_X \qquad (25)$$

On the basis of the results obtained from ANOVA, according to eqn. (7), a quadratic regression equation representing a response surface can be expressed as follows:

$$y = \beta_0 + \sum_{x_s} \beta_{x_s} \phi_{x_s} + \sum_{x_s} \beta_{x_s x_s} \phi_{x_s}^2 + \varepsilon \qquad (26)$$

In which if x_s represents a two-variable interaction, *e.g.*, $A \times B$, the following formula must be employed:

$$\phi_{(A \times B)_1} = \phi_{(A \times B)_2} = \phi_A \phi_B \qquad (27)$$

According to the derivative algorithm given in Appendix D, the optimum ϕ_X value for each variable considered can be calculated, and then if each optimum ϕ_X value obtained is substituted into eqn. (2), the optimum input value (Z_X) for each variable considered can be achieved.

Experimental

Details of instrumentation, experimental procedures, reagents and reference materials have been described in our previous work.[21,22] In the present study only the new features are included as follows:

For each digestion, 0.100 g of National Institute of Environmental Studies (NIES) certified reference material No. 6 mussel were accurately weighed into the inner liner of a CEM lined digestion vessel made from Teflon PFA (CEM,

Table 3 Triangular table associated with the $OA_{27}(3^{13})$ matrix

Column no.	Column no.											
	2	3	4	5	6	7	8	9	10	11	12	13
1	3	2	2	6	5	5	9	8	8	12	11	11
	4	4	3	7	7	6	10	10	9	13	13	12
2		1	1	8	9	10	5	6	7	5	6	7
		4	3	11	12	13	11	12	13	8	9	10
3			1	9	10	8	7	5	6	6	7	5
			2	13	11	12	12	13	11	10	8	9
4				10	8	9	6	7	5	7	5	6
				12	13	11	11	13	11	9	10	8
5					1	1	2	3	4	2	4	3
					7	6	11	13	12	8	10	9
6						1	4	2	3	3	2	4
						5	13	12	11	10	9	8
7							3	4	2	4	3	2
							12	11	13	9	8	10
8								1	1	2	3	4
								10	9	5	7	6
9									1	4	2	3
									8	7	6	5
10										3	4	2
										6	5	7
11											1	1
											13	12
12												1
												11

Table 4 ANOVA equations including percentage contribution for a three-level orthogonal array design: SS, sum of square; df, degrees of freedom; MS, mean square; SS', purified sum of square; and PC, per cent contribution

Source of variance	SS	df	MS	F-value	SS'	PC
X	$LJ \sum_{k=1}^{3} (r_{xk} - u)^2$	2	SS_X	$\dfrac{MS_X}{MS_{error}}$	$SS_X - 2MS_{error}$	$\dfrac{SS'_X}{SS_{total}} \times 100\%$
Error	$\sum_{i=1}^{I} \sum_{j=1}^{J} (y_{ij} - \bar{y}_i)^2$	$I(J-1)$	$\dfrac{SS_{error}}{I(J-1)}$		$SS_{total} - \sum SS'_X$	
Total	$\sum_{i=1}^{I} \sum_{j=1}^{J} (y_{ij} - \bar{y}_i)^2$	$IJ - 1$				

Matthews, NC, USA). To this, A ml of nitric acid, B ml of sulfuric acid, C ml of perchloric acid, D ml of hydrogen peroxide and E ml of phosphoric acid were added, and the vessel cap was closed tightly. Then four digestion vessels with the same power and time level settings (*e.g.*, experimental trials: no. 1, 16 and 22 in Table 2) were placed into the turn-table of a CEM MDS-2000 microwave digestion system (2450 MHz, 0–630 ± 50 W in 1% increments), and the fibre-optic temperature probe and pressure sensing tube were fitted in the digestion vessel which contained a large volume of acid combinations so as to monitor temperature and pressure. Subsequently, the quick digest option in the computer programs was chosen and the operating parameters were loaded. The parameters chosen were (*i*) power F; (*ii*) pressure, 6.89×10^5 Pa; (*iii*) time G; (*iv*) fan speed, 100%; and (*v*) temperature, 170 °C. The running procedure was then carried out. For different experimental trials, the variables (A–G) were varied with the level setting shown in Table 4.

After completion of the heating cycle, the digestion vessels were removed and cooled in a water bath for about 10 min. The contents of each vessel were then quantitatively transferred into a glass tube so as to reduce selenate to selenite, followed by hydride generation atomic absorption spectrometric determination. Detailed procedures for the reduction and determination of selenium had been described previously.[26]

Results and Discussion

Experimental Design

From a review of the literature as reported earlier,[26] seven variables were considered in this work: (*i*) the composition and volume of digestion reagents: nitric acid (A), sulfuric acid (B), perchloric acid (C), hydrogen peroxide (D) and phosphoric acid (E); (*ii*) the microwave power (F); and (*iii*) the microwave dissolution time (G). In addition, possible two-variable interactions ($F \times G$) were investigated because of the inter-dependence between microwave power and the microwave dissolution time. Apparently, there are other two-variable interactions, which are italicized in Table 5. However, in fact, according to experimental knowledge, the italicized interactions can be considered to be negligible. Hence, the assignment shown in Table 5 can be considered to be a Resolution V design.

Data Analysis Strategy

The definition of the output response in this work is the same as that used in our previous work.[21] After conducting all the

experiments, the results obtained are given in Table 2. The average of the accuracy for each factor at levels 1, 2, and 3 (r_1, r_2, and r_3) are also calculated and given in Table 2 so as to facilitate ANOVA and establish a quadratic regression model.

In such experiments a direct estimate of the variance of error is not calculable because for each experimental trial only one experiment is carried out. Hence, as described under Theory, the variance of error must be computed by pooling the sums of squares of dummies (columns 4, 8, 10 and 12), and the variance of error pooled is shown in Table 6. Alternatively, the total variance and its degrees of freedom can be first calculated by using the equations given in Table 3. Then by using eqns. (24) and (25), the variance of error and its degrees of freedom can be obtained (shown in Table 6). From Table 6, it can be seen that the variance of error pooled from dummies is in good agreement with that computed by eqn. (24).

ANOVA including percentage contribution is calculated and shown in Table 6. Table 6 indicates that the main variables A, B, and G are statistically significant at $p < 0.001$ and the main variable F and the interaction $F \times G$ are significant at $p < 0.01$, whereas no statistical differences are observed for any other main variables (C, D, E) at $p > 0.1$. These figures further confirm the findings obtained from implementing two-level orthogonal array design in our previous work.[21] Moreover, from the percentage contribution calculated (shown in Table 6), it can be seen that the most significant effect contributing to the output response is A (75.9%), then in order, is B (14.9%), G (4.3%), $F \times G$ (2.4%) and F (1.3%). The percentage contribution due to errors (unknown and uncontrolled factors) is low (1.1%). This means that no important variables and/or interactions have been omitted in this work. Therefore, it is reasonable to neglect the italicized two-variable interactions mentioned earlier.

Establishment and Evaluation of the Quadratic Regression Model

By using eqns. (22) and (23), we can calculate β_x and β_{xx} for each factor that has a significant influence. Then, according to the eqns. (26) and (27), the following quadratic regression equation can be obtained:

$$y = \beta_0 - 21.00\phi_A - 13.50\phi_A^2 + 9.10\phi_B - 7.00\phi_B^2$$
$$+ 2.65\phi_F - 2.65\phi_F^2 - 4.00\phi_G - 6.20\phi_G^2$$
$$+ 3.30\phi_F\phi_G + 1.10\phi_F^2\phi_G^2 + \varepsilon \qquad (28)$$

As $-1 < \phi_F < 1$ or $-1 < \phi_G < 1$, the second-order effect of the interaction ($1.10\phi_F^2\phi_G^2$) can be incorporated into the ε item. In addition, for each experimental trial, by substituting

Table 5 Assignment of factors and levels for the microwave dissolution experiments by the $OA_{27}(3^{13})$ matrix along with the associated triangular table

Column no.												
1	2	3	4	5	6	7	8	9	10	11	12	13
							Factor*					
A	B	$(F \times G)_1$	#	F	C	D	#	G	#	E	#	$(F \times G)_2$
$(C \times F)_1$	$(E \times F)_1$	$(A \times B)_1$	$(A \times B)_2$	$(A \times C)$	$(A \times F)_1$	$(A \times F)_2$	$(A \times G)_1$	$(B \times C)_1$	$(A \times G)_2$	$(B \times F)_2$	$(A \times E)_1$	$(A \times E)_2$
$(D \times F)_1$	$(C \times G)_1$	$(C \times E)_1$	$(D \times G)_1$	$(A \times D)_1$	$(B \times G)_1$	$(A \times C)_2$	$(B \times F)_1$	$(D \times E)_2$	$(B \times D)_1$	$(D \times G)_2$	$(B \times C)_2$	$(B \times D)_2$
$(C \times D)_1$			$(D \times E)_1$	$(B \times E)_1$	$(A \times D)_2$	$(C \times F)_2$	$(B \times E)_2$		$(C \times E)_2$		$(B \times G)_2$	
			$(E \times G)_1$	$(C \times D)_2$	$(D \times F)_2$	$(E \times G)_2$	$(E \times F)_2$				$(C \times G)_2$	
8.0	0.0			30	0.6	0.0		15		0.0		
5.0	1.0			60	0.3	0.5		10		0.5		
2.0	2.0			90	0.0	1.0		5		1.0		

* A, Volume of nitric acid (ml); B, volume of sulfuric acid (ml); C, volume of perchloric acid (ml); D, volume of hydrogen peroxide (ml); E, volume of phosphoric acid (ml); F, microwave power (%); and G, microwave dissolution time (min).
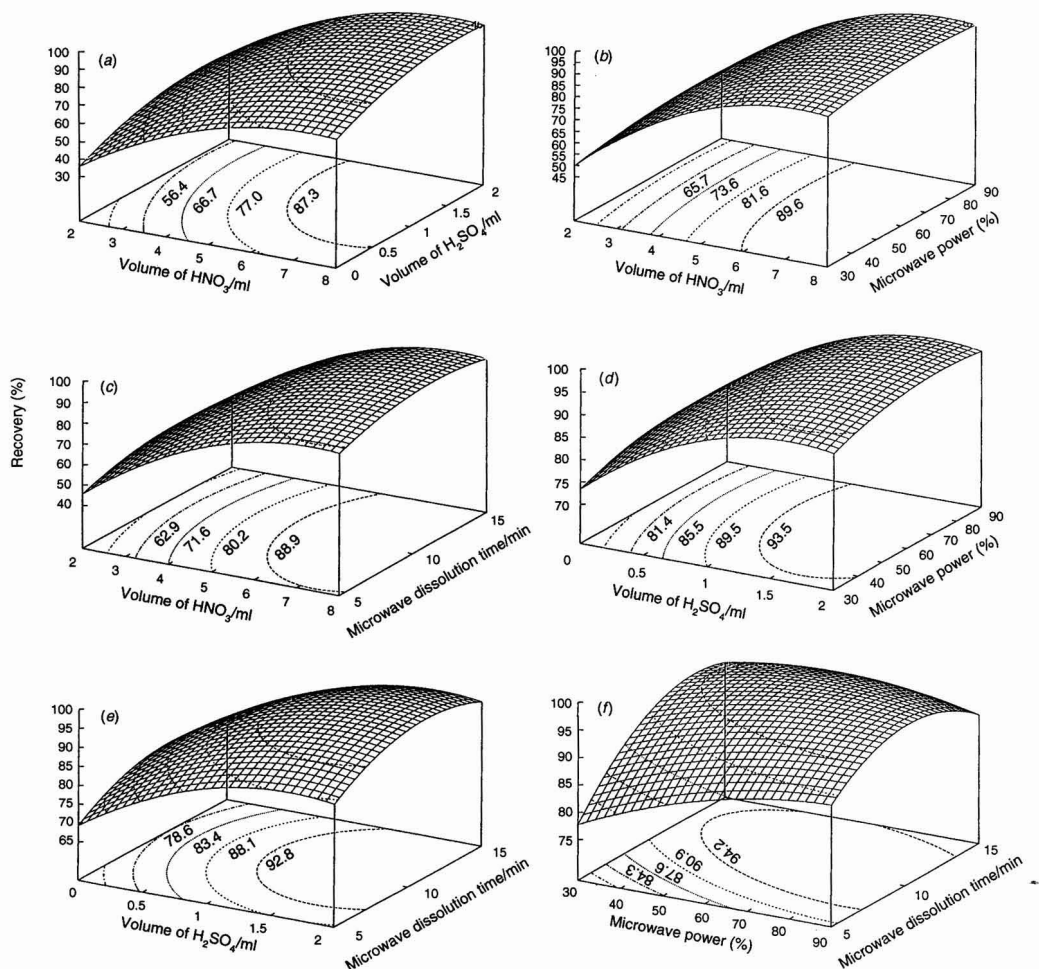
Fig. 1 Response surface for the effect of: (*a*) nitric and sulfuric acids on the recovery of selenium, with a microwave power of 71% and a microwave dissolution time of 11 min; (*b*) nitric acid and microwave power on the recovery of selenium, with a 1.7 ml volume of sulfuric acid and a microwave dissolution time of 11 min; (*c*) nitric acid and microwave dissolution time on the recovery of selenium, with a 1.7 ml volume of sulfuric acid and a microwave power of 71%; (*d*) sulfuric acid and microwave power on the recovery of selenium, with a 7.3 ml volume of nitric acid and a microwave dissolution time of 11 min; (*e*) sulfuric acid and microwave dissolution time on the recovery of selenium, with a 7.3 ml volume of nitric acid and a microwave power of 71%; and (*f*) microwave power and microwave dissolution time on the recovery of selenium, with a 7.3 ml volume of nitric acid and a 1.7 ml volume of sulfuric acid.

the ϕ_{xk} values [given in eqn. (5)], in which the level setting (k) for each factor is varied with the level number of the intersection in Table 2, into eqn. (28), the polynomial value excluding the β_0 item (Y) can be computed and the figures are given in Table 2. Combined with eqn. (10), it is clear that the mean of the difference between y and $Y(y - Y, i = 27$; shown in Table 2) can be considered as the β_0 item. Thus, eqn. (28) can be rewritten as

$$y = 85.4 - 21.00\phi_A - 13.50\phi_A^2 + 9.10\phi_B - 7.00\phi_B^2$$
$$+ 2.65\phi_F - 2.65\phi_F^2 - 4.00\phi_G - 6.20\phi_G^2 + 3.30\phi_F\phi_G + \epsilon \quad (29)$$

Hence, according to eqn. (29), the expected value ($\hat{y}$) (polynomial value including the β_0 term) and the random error

item ($\epsilon = y - \hat{y}$) for each experimental trial in the $OA_{27}(3^{13})$ matrix are calculated and given in Table 2. The results obtained show that the expected value for each experimental trial is in good agreement with the corresponding experimental value. The mean of the random error item ($y - \hat{y}$, $i = 16$) equals zero (see Table 1), which is in accordance with the assumption given in eqn. (10). Therefore, the quadratic regression equation given in eqn. (29) can adequately and accurately represent the described response surface.

According to the derivative algorithms given in Appendix D, the optimum ϕ value for each factor that has a significant influence is $\phi_A = -0.78$; $\phi_B = 0.65$; $\phi_F = 0.36$; and $\phi_G = -0.23$. Therefore, by means of eqn. (2), the following optimum conditions (*i*) 7.3 cm³ of nitric acid; (*ii*) 1.7 cm³ of

sulfuric acid; (*iii*) 71% of microwave power; and (*iv*) 11 min of the microwave dissolution time can be obtained. In addition, according to the results obtained from ANOVA, no perchloric acid, hydrogen peroxide, and phosphoric acid are necessary. Note that the above results are in very good agreement with that obtained by implementing the two-level orthogonal array design,[21] which must be followed by implementing the four-level orthogonal array design in order to describe the non-linear response surface represented.[22]

Further, in order to precisely express the functional relationship between the output response (y) and the input variable value (z), eqn. (2) with the known $\bar{Z}_x$ and H_x values should be substituted into eqn. (29), then the following equation can be obtained

$$y = -65.1 + 22.00Z_A - 1.50Z_A^2 + 23.10Z_B - 7.00Z_B^2 + 0.66Z_F - 0.0029Z_F^2 + 7.08Z_G - 0.248Z_G^2 - 0.022Z_FZ_G + \varepsilon \tag{30}$$

The response surfaces represented are displayed in Fig. 1. Finally, to confirm the validity of the optimization procedure, additional experiments using the optimum conditions obtained were performed. The result demonstrated that a satisfactory recovery value (98.0 ± 3.4%, $n = 6$) can be achieved. The theoretical value predicted by eqn. (30) is 97.5%, which is in accord with the mean experimental value of 98.0%.

Table 6 ANOVA including percentage contribution for output responses in the $OA_{27}(3^{13})$ matrix

Source	SS	v	MS	F^*	SS'	PC(%)
$HNO_3(A)$	9031.5	2	4518.8	752.6***	9019.5	75.9
$H_2SO_4(B)$	1784.6	2	892.3	148.7***	1772.6	14.9
$HClO_4(C)$	6.2	2	3.1	0.5		
$H_2O_2(D)$	8.3	2	4.2	0.7		
$H_3PO_4(E)$	1.3	2	0.6	0.1		
Power (F)	168.5	2	84.2	14.0**	156.5	1.3
Time (G)	518.6	2	259.3	43.2***	506.6	4.3
$(F \times G)_1$	142.7	(2)				
$(F \times G)_2$	167.8	(2)				
$F \times G$	310.5	4	77.6	12.9**	286.5	2.4
Column 4 (#)	20.6	(2)				
Column 8 (#)	14.8	(2)				
Column 10 (#)	5.0	(2)				
Column 12 (#)	5.8	(2)				
Pooled errors†	46.2	(8)				
Computed errors‡	47.6	8	6.0		135.4	1.1
Total	11877.1	26	—	—	11877.1	100

* Critical Value is 18.5 (***$p < 0.001$), and 8.6 (**$p < 0.01$).
† Resulted from pooling dummy variances.
‡ Computed by eqn. (24). The F value given is calculated by using computed error variance.

Conclusions

Based on the previous works, the present study further developed the theory and methodology of the three-level orthogonal array design for the optimization of analytical procedures. To the best of our knowledge, we are the first to prove the orthogonality of the three-level orthogonal array design by using a quadratic regression model. By means of the equations resulting from the proof of orthogonality, it is convenient to establish a quadratic regression equation representing the response surface for the three-level orthogonal array design. Moreover, the usefulness of the quadratic regression model established has been demonstrated in the application section.

The most important advantage of using a three-level orthogonal array design is that the non-linear response surface and the interaction effects can be considered simultaneously. In theory, when all of the interactions are expected to require consideration, no more than four main-variables can be assigned together in order to obtain a Resolution V or IV design. However, according to experience, some interactions can be omitted. Therefore, in practice, more than four main-variables can be assigned in the $OA_{27}(3^{13})$ matrix and the resulting design can be considered as a Resolution V design. Such an example has been shown in the present study. Nevertheless, it is worth mentioning that if no judgements can be made using non-statistical knowledge, it is difficult to differentiate an interaction from a main factor or another interaction in a Resolution III or IV design.

Note that although the optimum value for each factor that has a significant influence is readily obtained by using the derivative algorithm recommended, it may not always be necessary to choose the best condition according to the optimum value obtained. The reason is that the departure from the optimum value obtained may not always cause a significant variation. For instance, in this work, when the volume of nitric acid was changed from 6.0 to 8.0 cm³, according to eqn. (30), it was calculated that only 2.0 cm³ need to be added for the output response value. Obviously, it is reasonable that the variation of 2.0 is neglected. In addition, the above example has also demonstrated that the effect of relatively small changes of the input value for each factor that has a significant influence can be evaluated by a quadratic regression equation that was established in order to avoid further ruggedness testing being carried out.

Note also that because discrete factors can be assigned in the three-level orthogonal array matrix but cannot be quantitatively described in a quadratic regression model, care should be taken if the discrete factors chosen have significant influences. In such an event it is not suitable to establish a quadratic regression equation representing the response surface.

Appendix A
Construction of Three-level Orthogonal Array Design

An $OA_{2S+1}(3^S)$ matrix, here $2S + 1 = 3^m$, can be constructed by the following steps:

(i) The M basic columns specified by column numbers $\{(3^{m-1} - 1)/(3 - 1)\} + 1$ ($m = 1, 2, \cdots, M$) are first constructed by writing three level settings (1, 2 and 3). Each level setting repeats $\frac{1}{3}(2S + 1)$ times. Note that the left-most columns change less frequently than the right most columns. For the $OA_9(3^4)$ matrix, the basic columns are columns 1 and 2 (shown in Table 1 in bold); for the $OA_{27}(3^{13})$ matrix, the basic columns are columns 1, 2 and 5 (shown in Table 2 in bold).

(ii) The columns except for the M basic columns are constructed by the generating equations described as follows:

$$f_3 = f_2 + (f_1 - 1) \tag{A1}$$

$$f_4 = f_2 + 2(f_1 - 1) \tag{A2}$$

$$f_6 = f_5 + (f_1 - 1) \tag{A3}$$

$$f_7 = f_5 + 2(f_1 - 1) \tag{A4}$$

$$f_8 = f_5 + (f_2 - 1) \tag{A5}$$

$$f_9 = f_5 + (f_1 - 1) + (f_2 - 1) \tag{A6}$$

$$f_{10} = f_5 + 2(f_1 - 1) + (f_2 - 1) \tag{A7}$$

$$f_{11} = f_5 + 2(f_2 - 1) \tag{A8}$$

$$f_{12} = f_5 + (f_1 - 1) + 2(f_2 - 1) \tag{A9}$$

$$f_{13} = f_5 + 2(f_1 - 1) + 2(f_2 - 1) \tag{A10}$$

All calculations are carried out in modulo 3 arithmetic (that is, an integer larger than three is replaced with its remainder after division by three).

Hence, the $OA_9(3^4)$ and $OA_{27}(3^{13})$ matrices can be constructed, respectively. By using a similar method, the other $OA_{2S+1}(3^S)$ matrices can also be constructed.

Appendix B
Construction of the Triangular Table Associated with the $OA_{27}(3^{13})$ Matrix

Let us randomly choose two columns, for example, columns 4 and 7, according to eqns. (A2) and (A4), it can be inferred:
$f_4 + f_7 = f_2 + 2(f_1 - 1) + f_5 + 2(f_1 - 1)$

$$= f_5 + (f_2 - 1) + (f_1 - 1) + 3(f_1 - 1) + 1 \tag{B1}$$

When combined with eqn. (A6), eqn. (B1) can be rewritten as

$$f_4 + f_7 = f_9 + 3(f_1 - 1) + 1 \tag{B2}$$

As mentioned in the Appendix A, for the construction of a three-level orthogonal array design, all the calculations are done in modulo 3 arithmetic, and thus $3(f_1 - 1) + 1$ can be considered as a constant term. Therefore

$$f_4 + f_7 = f_9 + K_{C1} \tag{B3}$$

This means that one interaction between columns 4 and 7 is in column 9. On the other hand,

$$2f_4 + f_7 = 2[f_2 + 2(f_1 - 1)] + f_5 + 2(f_1 - 1)$$
$$= f_5 + 2(f_2 - 1) + 6(f_1 - 1) + 2$$
$$= f_{11} + K_{C2} \tag{B4}$$

This is to say that another interaction between columns 4 and 7 is in column 11.

By using a similar method, it can be concluded that the interactions resulting from columns 1 and 2 are in columns 3 and 4; the interactions resulting from columns 3 and 9 are in columns 5 and 13; the interactions resulting from columns 5 and 11 are in columns 2 and 8; and so forth. Therefore, the triangular table associated with the $OA_{27}(3^{13})$ matrix would be constructed.

Appendix C

Table C1 The assignment table of the factors for obtaining a Resolution V or IV design in the $OA_{27}(3^{13})$ matrix

Variable no.	Column no.												
	1	2	3	4	5	6	7	8	9	10	11	12	13
3	A	B	$(A \times B)_1$	$(A \times B)_2$	C	$(A \times C)_1$	$(A \times C)_2$	$(B \times C)_1$			$(B \times C)_2$		
4	A	B	$(A \times B)_1$ $(C \times D)_2$	$(A \times B)_2$	C	$(A \times C)_1$ $(B \times D)_2$	$(A \times C)_2$	$(B \times C)_1$ $(A \times D)_2$	D	$(A \times D)_1$	$(B \times C)_2$	$(B \times D)_1$	$(C \times D)_1$

Appendix D
Derivative Algorithm Used to Calculate the Optimum Values

Suppose a quadratic regression equation representing a response surface can be expressed as follows:

$y = \beta_0 + \beta_A\phi_A + \beta_{AA}\phi_A^2 + \beta_B\phi_B + \beta_{BB}\phi_B^2 +$
$+ \beta_C\phi_C + \beta_{CC}\phi_C^2 + \beta_{C \times D}\phi_C\phi_D + \beta_D\phi_D + \beta_{DD}\phi_D^2 + \varepsilon \tag{D1}$

Then, the following guidelines are used:
(1) For the factor without interaction effect (e.g., factor A), assume that

$$f(\phi_A) = \beta_A\phi_A + \beta_{AA}\phi_A^2 \tag{D2}$$

then the algorithm used is:

(*i*)   If it exists, find the ϕ_{A_c} value which is satisfied with
$$\frac{df}{d\phi_A}(\phi_{A_c}) = 0 \text{ and } \phi_{A_c} \epsilon[-1, 1].$$

(*ii*) Compute $f(-1)$, $f(1)$ and $f(\phi_{A_c})$ values if ϕ_{A_c} exists.

(*iii*) According to the optimum value expected (maximum or minimum), select the largest or smallest values computed in step (*ii*).

Hence, the optimum value for the factor without interaction effect can be found.

(2) For the factors with interaction effect (*e.g.*, factors C and D), assume that

$$f(\phi_C, \phi_D) = \beta_C\phi_C + \beta_{CC}\phi_C^2 + \beta_{C \times D}\phi_C\phi_D + \beta_D\phi_D + \beta_{DD}\phi_D^2 \tag{D3}$$

then the algorithm used is:

(*i*)   When $\phi_C = -1$, if it exists, find $\phi_{D_{-1}}$ value which is satisfied with
$$\frac{df}{d\phi_D}(\phi_{D_{-1}}) = 0 \text{ and } \phi_{D_{-1}} \epsilon[-1, 1].$$

(*ii*) When $\phi_C = 1$, if it exists, find the ϕ_{D_1} value which is satisfied with
$$\frac{df}{d\phi_D}(\phi_{D_1}) = 0 \text{ and } \phi_{D_1} \epsilon[-1, 1].$$

(*iii*) When $\phi_D = -1$, if it exists, find $\phi_{C_{-1}}$ value which is satisfied with
$$\frac{df}{d\phi_C}(\phi_{C_{-1}}) = 0 \text{ and } \phi_{C_{-1}} \epsilon[-1, 1].$$

(*iv*) When $\phi_D = 1$, if it exists, find ϕ_{C_1} value which is satisfied with
$$\frac{df}{d\phi_C}(\phi_{C_1}) = 0 \text{ and } \phi_{C_1} \epsilon[-1, 1].$$

(*v*)   Find ϕ_{C_c} and ϕ_{D_c} values which
$$\frac{\partial f}{\partial\phi_C}(\phi_{C_c}, \phi_{D_c}) = \frac{\partial f}{\partial\phi_D}(\phi_{C_c}, \phi_{D_c}) = 0.$$

(*vi*) Compute $f(-1, \phi_{D_{-1}})$, $f(1, \phi_{D_1})$, $f(\phi_{C_{-1}}, -1)$, $f(\phi_{C_1}, 1)$ and $f(\phi_{C_c}, \phi_{D_c})$ values if specified ϕ value exists.

(*vii*) According to the optimum value expected (maximum or minimum), select the largest or smallest values computed in step (*vi*).

Hence, the optimum value for the factor with interaction effect can be found.

References

1   Fisher, R. A., *J. Minist. Agric.*, 1926, **33**, 503.
2   Smallwood, H. M., *Ind. Eng. Chem., Anal. Ed.*, 1947, **19**, 950.
3   Rubin, I. B., Mitchell, T. J., and Goldstein, G., *Anal. Chem.*, 1971, **43**, 717.
4   Deming, S. N., and Morgan, S. N., *Experimental Design: a Chemometric Approach*, Elsevier, Amsterdam, 2nd edn., 1993.
5   Bayne, C. K., and Rubin, I. B., *Practical Experimental Designs and Optimization Methods for Chemists*, VCH, Deerfield Beach, FL, 1986.
6   Brereton, R. G., *Chemometrics: Applications of Mathematics and Statistics to Laboratory systems*, Ellis Horwood, New York, 1990.
7   Morgan, E., *Chemometrics: Experimental Design (Analytical Chemistry by Open Learning)*, Wiley, Chichester, 1991.
8   Tarry, G. C. R., *Ass. Franc. Av. Sci.*, 1900, **1**, 122.
9   Tarry, G. C. R., *Ass. Franc. Av. Sci.*, 1901, **2**, 170.
10 Rao, C. R., *Bull. Calcutta Math. Soc.*, 1946, **38**, 67.
11 Rao, C. R., *Proc. Edinburgh Math. Soc.*, 1947, **8**, 119.
12 Rao, C. R., *J. R. Stat. Soc. Suppl.*, 1947, **9**, 128.
13 Bose, R. C., *Sankhya*, 1947, **8**, 107.
14 Oles, P. J., and Yankovich, A., *LC-GC*, 1989, **7**, 579.
15 Oles, P., Gates, G., Kensinger, S., Patchell, J., Schumacher, D., Showers, T., and Silcox, A., *J. Assoc. Off. Anal. Chem.*, 1990, **73**, 724.
16 Oles, P. J., *J. Assoc. Off. Anal. Chem.*, 1993, **76**, 615.
17 Bilot, P., and Pitard, B., *J. Chromatogr.*, 1992, **623**, 305.
18 Wan, H. B., Lan, W. G., Wong, M. K., and Mok, C. Y., *Anal. Chim. Acta*, 1994, **289**, 371.
19 Wan, H. B., Lan, W. G., Wong, M. K., Mok, C. Y., and Poh, Y. H., *J. Chromatogr. A*, 1994, **677**, 255.
20 Lan, W. G., Wong, M. K., Chen, N., and Sin, Y. M., *Talanta*, 1994, **41**, 1917.
21 Lan, W. G., Wong, M. K., Chen, N., and Sin, Y. M., *Analyst*, 1994, **119**, 1659.
22 Lan, W. G., Wong, M. K., Chen, N., and Sin, Y. M., *Analyst*, 1994, **119**, 1669.
23 Lan, W. G., Wong, M. K., Chee, K. K., and Sin, Y. M., *Analyst*, 1995, **120**, 273.
24 Lan, W. G., Wong, M. K., Chee, K. K., Lee, H. K., and Sin, Y. M., *Analyst*, 1995, **120**, 281.
25 Heyden, Y. V., Khots, M. S., and Massart, D. L., *Anal. Chim. Acta*, 1993, **276**, 189.
26 Lan, W. G., Wong, M. K., and Sin, Y. M., *Talanta*, 1994, **41**, 195, and references cited therein.

Naphthalene Contamination of Sterilized Milk Drinks Contained in Low-density Polyethylene Bottles

Part 2. Effect of Naphthalene Vapour in Air

Oi-Wah Lau and Siu-Kay Wong

Department of Chemistry, The Chinese University of Hong Kong, Shatin, NT, Hong Kong

Ka-Sing Leung

Government Laboratory, Homantin, Hong Kong

A survey on naphthalene vapour in air was conducted, revealing that the ambient atmosphere contained concentrations of naphthalene in the range of 0.005–0.100 mg m^{-3}. The level of naphthalene vapour in air increased to 0.35 and 4.00 mg m^{-3} in places exposed to lacquer paint and naphthalene-based moth-repellent, respectively. The effect of naphthalene vapour in air on milk drinks contained in low-density polyethylene (LDPE) bottles was assessed. A mathematical model was suggested to describe the migration of naphthalene from the atmosphere into milk. The model was proved to be valid for milk drinks exposed to naphthalene-based moth-repellent during storage. Moreover, the extent of migration was found to increase with the fat content of foods, which might be ascribed to an increase in diffusion, in addition to the kinetic factor, that affects naphthalene migration.

Keywords: Naphthalene contamination; milk; low-density polyethylene; naphthalene vapour; fat content; mathematical model

Introduction

In our previous study,[1] we observed naphthalene contamination in sterilized milk drinks contained in low-density polyethylene (LDPE) bottles. The level of contamination in milk increased with storage time at room temperature, depending on the concentration of naphthalene in the packaging material.

Naphthalene in the environment was suspected as a possible source of naphthalene found in the milk drinks. Hence, this study investigated the effect of naphthalene vapour in air on the level of the compound observed in the milk drinks. A mathematical model was suggested to describe the migration of naphthalene from the atmosphere into the milk, and the effect of the fat content in foods on the extent of migration was assessed and is reported in this paper.

Experimental

Instruments and Apparatus

Gas chromatography was performed on a Hewlett-Packard Model HP-5890 II gas chromatograph equipped with a flame ionization detector. An HP-1 capillary column (30 m × 0.53 mm i.d.) and nitrogen as the carrier gas were used. Injector and detector temperatures were both 230 °C. The oven temperature was held at 70 °C for 5 min and then increased, at a rate of 6 °C min^{-1}, to 230 °C for 5 min.

Materials

The milk' samples used were purchased batchwise from different supermarkets. The vegetable oil used was a mixture of rapeseed, peanut and sesame oils, purchased from a local supermarket.

Reagents

Napthalene standard solution, tetramethylbenzene internal standard solution and all other reagents were of analytical-reagent grade.

Stock internal standard solution. This was prepared by dissolving 0.051 g of tetramethylbenzene in 50 ml of distilled heptane in a calibrated flask.

Working internal standard solution. An aliquot (0.5 ml) of the stock internal standard solution was diluted to 50 ml with distilled heptane in a calibrated flask.

Stock standard solution. This was prepared by dissolving 0.050 g of naphthalene in 50 ml of distilled heptane in a calibrated flask to give a concentration of 1000 µg ml^{-1}.

Working standard solutions. Standard solutions of 2.5, 5.0 and 10.0 µg ml^{-1} were prepared by mixing 0.125, 0.25 and 0.50 ml of the stock standard solution, respectively, with 0.5 ml of stock internal standard solution, and then diluting to 50 ml with distilled heptane in calibrated flasks.

Method

Survey on naphthalene vapour in air

The determination was based on the American Society for Testing and Materials (ASTM) standard methods D3686-89 and D3687-89 for the analysis of volatile organic solvents in air.[2] A known volume of air was drawn through a charcoal tube to trap the organic vapours present, which were then desorbed with carbon disulfide. The compounds in the desorbed samples were identified using a Varian Model 3700 gas chromatograph (Alltech, Arlkington Heights, IL, USA) equipped with a Finnigan-Mat 805-665670N ion-trap detector (Sunnyvale, CA, USA).

Migration studies

Naphthalene, in the packaging material, was extracted using Dean and Stark apparatus.[3] About 3 g of the packaging

material were cut into small pieces and placed in a 250 ml round-bottomed flask, followed by the addition of 2 ml of the working internal standard in heptane and 130 ml of aqueous saturated NaCl solution. The mixture was heated to boiling and refluxed for 2 h. The collected heptane extract was dried over anhydrous sodium sulfate and the naphthalene concentration in the extract was determined by gas chromatography.

Naphthalene in each milk sample was extracted and determined following the procedure for the packaging material, except that 100 g of the homogenized milk sample was used and placed in a 500 ml round-bottomed flask, and 180 ml of aqueous, saturated NaCl solution and 1 ml of antifoaming agent (an aqueous emulsion containing 30% m/m silicone) were employed.

Environment

Saturated naphthalene environment

This was established by placing about 40 g of solid naphthalene inside a closed desiccator (24 cm i.d.) and the whole system was left unattended for one month to achieve equilibrium. Following this, four 100 ml beakers containing 20.0 g of vegetable oil were each placed inside the desiccator, and the amount of naphthalene absorbed by the oil was then determined weekly by gas chromatography, after extraction of the packaging material using Dean and Stark apparatus, as described above.

Controlled environment

This was established by placing a beaker of vegetable oil with 1–2 g of dissolved naphthalene in a closed desiccator (24 cm i.d.) and the whole system was left unattended for one month to achieve equilibrium. Following this, four 100 ml beakers containing 20.0 g of vegetable oil were each placed inside the closed vessel, and the amount of naphthalene absorbed by the oil, in the controlled environment, was then determined weekly, again by gas chromatography, as described above.

Results and Discussion

Naphthalene in the Atmosphere

The concentration of naphthalene in the atmosphere was determined using the ASTM standard method for the analysis of volatile organic solvents in air,[2] and the results are shown in Table 1. From the survey, it can be seen that the naphthalene concentration was normally in the range of 0.005–

0.041 mg m^{-3}, which may be considered as low. However, the naphthalene concentration could be raised to a level of 0.35 or 4.0 mg m^{-3}, under certain special circumstances (such as that inside a cupboard with naphthalene-based moth-repellent or in a space close to freshly applied lacquer paint).

Controlled Environment for Migration Studies

In order to study the impact of napthalene vapour in air on milk drinks during storage, migration studies were conducted under a controlled environment, where the concentration of naphthalene vapour was kept constant. A simple way to generate a constant naphthalene environment is proposed, where a solution of naphthalene in vegetable oil is allowed to establish an equilibrium state with the surrounding atmosphere inside a desiccator, as described in the Experimental section.

A method has also been developed for the determination of naphthalene in a controlled environment. An empirical equation, eqn. (1) is suggested to relate the concentration of naphthalene in the vegetable oil, c_{oil}, to γ_{air},

$$c_{oil} = \gamma_{air} A e^{Bt} \tag{1}$$

where A and B are constants, t is the time of exposure, and $\gamma_{air} = c_{air}/c_{sat}$, where c_{air} is the concentration of naphthalene in air and c_{sat} is that under saturated conditions and has a value of 0.5895 µg cm^{-3} at 25 °C,[4] and c_{oil} is the concentration of naphthalene in 20 g of vegetable oil in contact with air. Using data for the c_{oil} under saturated conditions, where $\gamma_{air} = 1$, constants A and B in eqn. (1) were determined by plotting ln c_{oil} against t and were found to be 1900 µg g^{-1} and 1 × 10^{-6} s^{-1}, respectively.

In the controlled environment γ_{air} was calculated by two methods. First, by determining the concentration of naphthalene in 20 g of vegetable oil (after various times of exposure to the controlled environment) and then by determining the best fit of the experimental data to eqn. (1) using the non-linear least square method.

Mathematical Modelling

It was our aim to propose a mathematical model to describe the migration of naphthalene vapour into milk contained in LDPE bottles. However, the situation was complicated by the distribution of naphthalene vapour in air, the packaging material and milk. In the proposed model, we assume that naphthalene vapour is first absorbed by the packaging material, which then acts as a source of naphthalene for the milk sample, such that naphthalene will migrate from the packaging material into the milk.

Naphthalene Absorbed by the Packaging Material

When the packaging material (LDPE) was exposed to an environment containing a naphthalene vapour the concentration of naphthalene in the packaging material per unit mass, c_p (in µg g^{-1}), due to the absorption of naphthalene by the packaging material, can be derived using the kinetic theory of gases,[5] shown in eqn. (2).

$$c_p = \frac{\gamma_{air} c_{sat} K'}{\rho} (1 - e^{-\lambda t/K'}) \tag{2}$$

where c_{sat} is the saturated naphthalene concentration in air at 25 °C; $\gamma_{air} = c_{air}/c_{sat}$, and c_{air} is the actual naphthalene concentration in air; ρ is the density of LDPE and has a value of 0.9025 g cm^{-3}; K' is the partition coefficient of naphthalene between the packaging material and air; and λ is the kinetic factor, which includes the geometry and the collision frequency term.

Table 1 The level of naphthalene vapour in various places determined using the ASTM method

Sampling sites	[Naphthalene]/mg m^{-3}*
Open area	0.005
Residents' premises	0.013
Storeroom A	0.027
Storeroom B	0.029
Office A	0.041
Office B	0.008
Office C	0.005
Laboratory A	0.025
Laboratory B	0.100
Laboratory C	<0.003
Inside a cupboard stored with moth balls†	4.00
In a flat, freshly painted with lacquer paint	0.35

* Mean of duplicate determinations.
† Cupboard with dimensions 80 × 40 × 60 cm containing 10 moth-repellent balls with a total mass of about 36 g and γ_{air} of 0.007.

Naphthalene Absorbed by Milk

It is assumed that the milk sample contained within the LDPE bottle was subjected to a time dependent source of naphthalene the concentration of which, c_{source}, could be described by an equation having a form similar to that for c_p [see eqn. (2)] as shown in eqn. (3)

$$c_{source} = c'_{sat} \gamma_{air} (1 - e^{-\beta t}) \qquad (3)$$

where c'_{sat} is the saturated naphthalene concentration in the packaging material exposed under saturated naphthalene vapour (which has been determined experimentally in the present work to be 15 000 µg g⁻¹ or 15 mg g⁻¹) and β is a kinetic factor.

From eqn. (3), the concentration of naphthalene in milk caused by the naphthalene vapour in air, c_{Total} as given by eqn. (4), may be derived

$$c_{Total} = c'_{sat}\gamma_{air} \; \frac{\sqrt{Dt}}{\sqrt{\pi A}} \; (1.33\beta t - 0.54(\beta t)^2 + 0.15(\beta t)^3 - ...) \qquad (4)$$

where, D is the diffusion factor for naphthalene and A is the volume-to-surface area ratio of the packaging material. The parameters, D and β, were determined by fitting[6] eqn. (4) to the experimentally determined amount of naphthalene migrated into milk at different times of exposure for the sterilized milk drinks stored in controlled environments. The average values of β and D are found to be 4.1×10^{-8} s⁻¹ and 2.1×10^{-7} cm² s⁻¹, respectively.

Using the optimum values of D and β and the determined value of γ_{air} inside a cupboard (of dimensions $80 \times 40 \times 60$ cm³) with 10 napthalene-based moth-repellent balls (about 36 g), the naphthalene concentrations in the milk samples stored in the cupboard for various periods of time were calculated and compared with the experimental values, and the results are given in Table 2. The calculated values fitted well with the experimental data with a mean square error of 0.3, which implies that the proposed model is useful to predict the migration of naphthalene vapour from air into milk.

Table 2 Experimental and predicted concentrations of naphthalene in milk samples stored at 25 °C in polyethylene bottles inside a cupboard with γ_{air} of 0.007 for varying times

Storage time/d	[Napthalene in milk]/µg ml⁻¹	
	Found*	Predicted
7	0.68	0.67
14	2.17	1.90
21	3.77	3.43
28	5.17	5.22

* Mean of duplicate determinations.

Effect of Fat Content

As naphthalene is a fat-soluble compound, a study was conducted to assess the effect of the fat content of food on the migration of naphthalene into food stored in LDPE containers. In order to shorten the testing time, the tests were carried out in a controlled environment with $\gamma_{air} = 0.037$, and the proposed model was applied to calculate the values of D and β for each case. The results are shown in Table 3.

Both the kinetic factor, β, and the diffusion factor, D, increase greatly as the fat content of the food increases. From this study, it is clear that the fat content plays a crucial role in the migration of naphthalene (possibly by enhancing the interactions between the packaging material and food).

Effect of Naphthalene Vapour in Air

It is worthwhile to note that the level of naphthalene in the packaging material was found to vary batchwise, in the range of 0.7–2.0 µg g⁻¹,[1] which were higher than the corresponding saturated naphthalene concentration (*i.e.*, 0.4–0.5 µg g⁻¹) in the packaging material due to naphthalene vapour in the laboratory within the testing period. Under such circumstances, the effect of naphthalene vapour on milk contamination would be negligible, and the methods reported in Part 1 of this work[1] for the estimation of the level of naphthalene in milk are still valid.

Furthermore, the level of naphthalene in the packaging material for the milk bottles made of LDPE have been significantly reduced to the values of 0.1–0.4 µg g⁻¹. The reduction in naphthalene may be ascribed to the improved method in the packaging. Previously, bottles were packed in cardboard boxes, whereas now milk bottles are sealed in plastic bags, with aluminium lining, before being packed into cardboard boxes. This observation suggests that the high-naphthalene level in the packaging materials for milk, observed previously, were due to naphthalene picked up from the environment during transportation and/or storage.

Conclusion

The possibility and extent of naphthalene migration into milk stored in LDPE bottles from atmospheres having a relatively high level of naphthalene vapour, were studied. A mathematical model, accounting for the migration, was established and tested to be valid. The migration studies also showed that the fat content in food may increase the diffusion as well as the kinetic factor, leading to increased naphthalene migration.

Further, it is worthy to note that milk samples stored in LDPE bottles can pick up naphthalene vapour from the atmosphere when the naphthalene in the packaging material is below its saturated value. Hence, when low-density polyethylene is used as the packaging material, it is of vital importance to keep the concentration of naphthalene vapour low in the storage.

Table 3 Effect of fat content of foods on the migration of naphthalene from an atmosphere with γ_{air} of 0.037 inside a desiccator into foods stored in the desiccator for various periods of time

Type of food tested	Fat content (%)	[Naphthalene]*/µg g⁻¹				Calculated value for β × 10⁸/s⁻¹	Calculated value for D × 10⁷/cm² s⁻¹
		7d†	14d†	21d†	28d†		
Water	0	0.01	0.03	0.06	0.20	—	—
Low-fat milk	1.5	2.0	7.0	11.1	17.0	3.51	1.02
Sterilized milk	3.5	3.4	10.5	19.1	28.9	4.33	1.94
Oil	100	5.5	19.0	33.1	40.8	5.87	8.57

* Mean of duplicate determinations.
† Time of exposure.

References

1 Lau, O.-W., Wong, S.-K., and Leung, K.-S., *Analyst*, 1994,
   119, 1037.
2 American Society for Testing and Materials Methods D3686-89
   and D3687-89, ASTM Committee on Standards, Philadelphia,
   1989.
3 Egan, H. O., Kirk, R. S., and Sawyer, R., in *Pearson's
   Chemical Analysis of Food*, Churchill Livingstone, London, 8th
   edn., 1981, p. 314.
4 *Handbook of Chemistry and Physics*, ed. Weast, R. C., CRC
   Press, Boca Raton, Florida, 67th edn., 1987.
5 Atkins, P. W., *Physical Chemistry*, Oxford University Press,
   Oxford, 4th edn., 1990, p. 733.
6 Johnston, M. D., *Computational Chemistry*, Elsevier, Amster-
   dam, 1988, pp. 482–492.

Determination of Lasalocid in Eggs Using Liquid Chromatography–Electrospray Mass Spectrometry

W. John Blanchflower and D. Glenn Kennedy

Department of Agriculture, Veterinary Sciences Division, Belfast, UK BT4 3SD

A method is presented for the determination of the polyether ionophore, lasalocid, in eggs. Samples are extracted under acidic conditions using acetonitrile and the extracts are cleaned up using a simple liquid–liquid extraction step. Lasalocid is detected and quantified using liquid chromatography–electrospray mass spectrometry on a quadrupole bench-top instrument. The technique is highly sensitive, with a detection limit of about 0.5 ng g^{-1} of lasalocid in homogenized egg samples.

Keywords: Lasalocid; ionophore; eggs; high-performance liquid chromatography; electrospray mass spectrometry

Introduction

Lasalocid belongs to the group of carboxylic polyether antibiotics that are produced by the fermentation of *Streptomyces lasaliensis*. It is classified as a divalent ionophore because of its ability to complex divalent ions such as calcium and magnesium, as well as monovalent ions such as sodium and potassium. It is currently licensed for veterinary use as a coccidiostat for broiler and breeder chickens, turkeys and pheasants. For this purpose, it is sold as a premix under the trade name Avatec (Roche Products, Welwyn Garden City, Hertfordshire, UK) and is normally added to feed at the rate of 600–800 g tonne^{-1} to provide 90–120 mg kg^{-1} of lasalocid sodium in the final feed. It is licensed for turkeys and pheasants up to a maximum age of twelve weeks, and also for broiler chickens provided that a withdrawal period of at least five days is observed before slaughter. It can also be fed to layer replacement chickens up to a maximum age of sixteen weeks. It should not be fed after this period to prevent residues of lasalocid occurring in eggs. However, a recent report[1] showed that in a survey of eggs from retail outlets, approximately 7% contained residues of lasalocid above 40 ng g^{-1}. In a second report, high levels of lasalocid were found in the eggs from chickens which had been accidentally given 115–150 mg kg^{-1} in their feed.[2] The concentrations ranged from 2.5 µg g^{-1} in eggs collected 3 d after starting administration of lasalocid, to 18 µg g^{-1} in eggs collected after 14 d of administration.

Food for human consumption should contain either no residues of veterinary drugs, or levels that are below the maximum residue limits (MRLs) stipulated by regulatory authorities. At present no MRL has been stipulated for lasalocid in eggs, but National Reference Laboratories require sensitive confirmatory methods for the detection of such drugs in avian or animal products. Several methods, using high-performance liquid chromatography (HPLC) with fluorescence detection, have been published for the determination of lasalocid in tissues[3–5] but to date we are only aware of one publication[6] on the determination of lasalocid in eggs. The latter method also uses HPLC with fluorescence detection and claims a detection limit of 10 ng g^{-1}. For confirmatory purposes, however, it is recommended by the European Union (EU) that mass spectrometry (MS) be used where possible in order to increase specificity and to reduce the likelihood of false positives. We have already shown that liquid chromatography–mass spectrometry (LC–MS) is a suitable technique for the determination of a range of veterinary drug residues in biological samples, on a routine basis. These include compounds such as nitroxynil,[7] rafoxanide,[8] trenbolone,[9] furazolidone,[10] fenbendazole and oxfendazole[11] and penicillins.[12] In general, the technique is easy to perform and requires only relatively simple clean-up steps. In this paper we present a method for the determination of lasalocid in eggs using simple liquid–liquid extraction followed by detection using LC–electrospray mass spectrometry (EMS).

Experimental

Materials

Acetonitrile, methanol and tetrahydrofuran were of HPLC grade and were obtained from Rathburn Chemicals, Walkerburn, Scotland. Trifluoroacetic acid was obtained from Aldrich, Gillingham, Dorset. Distilled water was used throughout. The mobile phase comprised a mixture of acetonitrile, methanol, tetrahydrofuran, water and trifluoroacetic acid (TFA) (67 + 10 + 10 + 13 + 0.1). This was filtered and de-gassed using an HPLC solvent filter unit (Millipore-waters, Watford, Hertfordshire). Lasalocid was obtained as a sodium salt from Sigma, Poole, Dorset. A stock standard (1 mg ml^{-1}) was prepared in methanol and stored at 4 °C for up to 2 months. Dilute standards (10 µg ml^{-1} and 100 ng ml^{-1}) were prepared weekly in 80% v/v acetonitrile–water and were also stored at 4 °C. Orthophosphoric acid (1.7 g ml^{-1}) was standard AnalaR grade. Siliconizing fluid (SurfaSil) was obtained from Pierce and Warriner, Chester, Cheshire. Before use, tubes (65 × 14 mm Quickfit) were rinsed with a 4% v/v solution of SurfaSil in hexane, allowed to drain by inversion, dried briefly in a 60 °C hot air oven and rinsed with methanol.

Equipment

The HPLC system consisted of a Merck–Hitachi Model L6000 pump and AS2000 autosampler (Merck, Poole, Dorset) and an Intersil 4.6 × 150 mm ODS-2 (end-capped) reversed-phase column (GL Sciences, Tokyo, Japan). The flow rate of the mobile phase was set at 1 ml min^{-1}.

The HPLC system was coupled to the Megaflow probe of a VG Platform electrospray LC–MS system (VG Biotech, Altrincham, Cheshire). The instrument was operated in the positive-ion mode. Full scan data was collected in order to obtain spectra from standards and single-ion data (dwell time 0.5 s for each ion) was collected when analysing samples. The source of the instrument was maintained at 150 °C and the flow rates of the drying and nebulizing gases were optimized at 500

and 15 l h[-1], respectively. The cone voltage was set at 25 V. The position of the electrospray probe and the MS parameters (low and high mass resolution and ion energy) were optimized to give maximum sensitivity and symmetrical peak shape (approximately 1 u wide) using any of the solvent ions produced by the mobile phase. Once optimized, these rarely required changing.

Extraction of Lasalocid From Eggs

Whole egg samples were homogenized using a Silverson homogenizer and were either analysed fresh or stored at $-20\,^{\circ}\mathrm{C}$ until analysis. Portions (5 g) were weighed into 115 × 28 mm Quickfit centrifuge tubes. The assay recoveries were also established at this stage, by spiking portions of homogenized egg with lasalocid, allowing them to stand for 10 min, and then treating them as for normal samples. The samples were acidified using orthophosphoric acid (2 ml, 3.7 mol l^{-1}) and mixed. Acetonitrile (13 ml) was added singly to each sample followed by immediate homogenization (to prevent clumping of the precipitated protein) for 30 s using a Silverson homogenizer. The tubes were then placed in an ultrasonic bath for 10 min, mixed, and centrifuged for 10 min at 2000 rpm at 10–15 °C. Aliquots of the supernatants (2 ml) were transferred to 100 × 17 mm Quickfit tubes and water (4 ml) was added to each. The solutions were then extracted with a mixture (1 + 1) of hexane and toluene (2 ml and 1 ml,

Fig. 1 Chemical structure and positive ion electrospray spectra of lasalocid.

respectively) by inversion for 30 s and centrifuging for 5 min. Any slight emulsions formed were disrupted by swirling the tubes and again centrifuging. The extracts were combined in 65 × 14 mm Quickfit tubes and evaporated to dryness under nitrogen at 55 °C in a fume hood, using a needle manifold assembly. Residues were dissolved in acetonitrile–water (200 μl, 80% v/v) and transferred into autosampler vials for analysis by LC–MS.

LC–MS Analyses

The system was equilibrated by pumping mobile phase through the column for 15 min at a flow rate of 1 ml min^{-1}. A standard (20 μl, 100 ng ml^{-1} lasalocid) was injected and peak-area data was collected for the ion at m/z 613. Injections were repeated (typically three times) until constant peak areas were obtained. This was followed by injections of sample extracts, with a standard included after every four samples. The concentration of any lasalocid found in the sample extracts was determined with reference to the peak-area data for the ion at m/z 613 in the standard. The 100 ng ml^{-1} standard was equivalent to 40 ng g^{-1} of lasalocid in egg.

Results and Discussion

The molecular structure and positive ion electrospray spectra for lasalocid are shown in Fig. 1. The mono-isotopic mass of lasalocid is 590 Da. In electrospray LC–MS, the intensity and the number of ions produced can sometimes be changed by altering the fragmentation-cone voltage. With lasalocid, however, the only useful diagnostic ion obtained was at m/z 613 (M + Na). The protonated molecular ion (m/z 591) and the water adduct ion (m/z 608) are also apparent in the spectrum. Increasing the cone voltage above 25 V slightly increased the intensity of these ions, but decreased the intensity of the ion at m/z 613. This, therefore, effectively reduced the sensitivity of the assay when using this as the diagnostic ion. A cone voltage of 25 V was therefore used routinely. Ion ratio measurements can sometimes be used to increase the specificity of an assay and this depends on a constant ratio being obtained between samples and standards. We found that the ratios of the water adduct and protonated ions to the M + Na ion changed between samples and standards, however, so that ion ratio measurements were not valid in this case. This is probably due to the relatively low intensity of the other ions and to the high affinity of the ionophore for sodium.
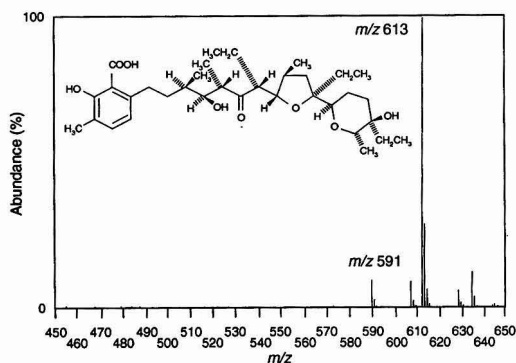
Fig. 2 Single-ion LC—EMS chromatograms at m/z 613 for (*a*) 100 ng ml^{-1} lasalocid standard, (*b*) a negative egg extract, and extracts from eggs containing (*c*) 15 and (*d*) 1.7 ng g^{-1} of lasalocid. The injection volume in each case was 20 μl. Lasalocid elutes at about 5.6 min. Chromatograms (*a*), (*b*) and (*c*) were scaled to the same relative intensity (vertical axis).

The negative ion electrospray spectra of lasalocid (not shown) produced an M − 1 ion, but acidic mobile phases are not suitable for negative ion LC–EMS. The omission of TFA from the m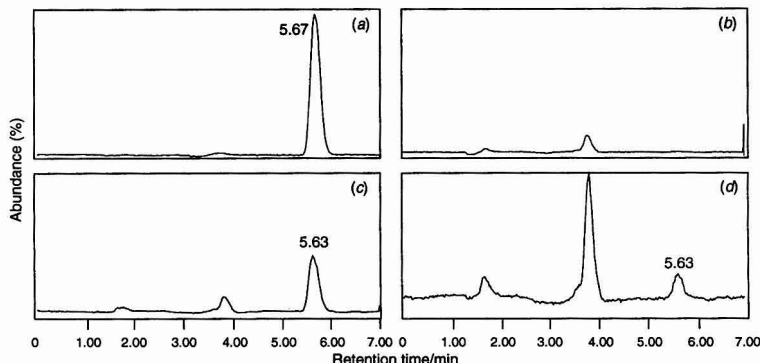obile phase resulted in poor chromatography, with severe peak tailing, thus ruling out the use of the negative-ion mode for measuring lasalocid.

Single-ion chromatograms at m/z 613 for a standard (*a*), a negative egg extract (*b*) and the extracts from eggs containing 15 ng g^{-1} (*c*) and 1.7 ng g^{-1} (*d*) of lasalocid are shown in Fig. 2. Lasalocid elutes at about 5.6 min. In several hundred egg samples which have been analysed using the described assay, we have found no evidence of interfering peaks from any other compounds in the proximity of this retention time. The retention time could be reduced by decreasing the water content of the mobile phase, but care needs to be taken to avoid ion suppression effects being introduced. In our experience, this can be a problem in Megaflow electrospray LC–MS and is caused when significant amounts of other compounds elute at the same retention time as the compound of interest. Even though these compounds cannot be seen on the single-ion chromatograms, because they may not produce ions of the same mass to charge ratios as those being monitored, they can reduce the signal intensity, leading to low results. This is particularly important when using relatively simple extraction procedures. In the assay described here, a mobile phase giving a retention time for lasalocid of about 3 min was used initially, but this sometimes gave low recoveries due to ion suppression. By extending the retention time to above 5 min, these effects were reduced or eliminated as can be seen by the recovery values (Table 1). It was also necessary to carry out the extraction of lasalocid from eggs under acidic conditions, using phosphoric acid, otherwise ion suppression effects were increased. Initially we also used a C_{18} Sep-Pak clean-up step in the assay, but this was unnecessary when acidic conditions were used.

Reproducibility and recovery values for the assay are shown in Table 1. Negative egg samples were spiked with 5, 10, 20 and 50 ng g^{-1} of lasalocid and each was analysed five times on three different occasions. The mean recoveries ranged from 76

to 88% and the relative standard deviations (s_r) ranged from 2.5 to 11.7%.

The use of an internal standard is generally recommended for quantitative analytical methods, but this depends on the availability of a suitable compound. For MS methods, stable isotopically labelled (generally deuterated) compounds are to be recommended, but unfortunately no labelled lasalocid is currently available. As an alternative, other ionophores such as monoensin, narasin and salinomycin were investigated for use as an internal standard, but only monoensin was extracted from spiked egg samples under the acidic conditions used. This gave a good diagnostic ion at m/z 693 (M + Na), which eluted shortly after lasalocid. However, recoveries of monensin from spiked egg were lower than lasalocid (about 60%) and led to over-compensation when lasalocid results were corrected for the monensin internal standard. This approach were therefore abandoned.

The linearity of the assay was determined by spiking negative egg samples with 20 to 200 ng g^{-1} of lasalocid and carrying them through the assay. The assay proved linear up to the highest concentration tested (linear regression coefficient, $r = 0.997$).

The detection limit of the assay is dependent on a number of factors including the cleanliness of the source of the LC–MS and the position of the electrospray probe. The latter could be optimized using one of the solvent ions procured by the mobile phase, and once set, did not need adjusting again unless the source had been removed for cleaning. Cleaning was carried out about every 3 d, during which time about 60 samples could easily be analysed by one operator. In general, the detection limit was about 0.5 ng g^{-1} of lasalocid in egg at a signal-to-noise ratio of 3 : 1. The relatively high sensitivity of the assay is illustrated in Fig. 2(*d*) which shows a single ion chromatogram from an egg sample containing 1.7 ng g^{-1} of lasalocid. We also found, however, that the sensitivity of the instrument towards lasalocid could be influenced by the composition of the mobile phase. The addition of 10% v/v methanol increased the peak areas for lasalocid three-fold, but there was no increase in sensitivity with higher concentrations. However, one batch of methanol used during development of the assay decreased the sensitivity by a factor of 10. It was concluded that this particular batch of methanol contained an impurity which was causing ion suppression. This is a factor to bear in mind should the sensitivity fall. Tetrahydrofuran is included in the mobile phase to improve peak symmetry and prevent tailing.

The assay has been used to determine the lasalocid concentrations in randomly sampled eggs and in those from experimental flocks. These results, to be published elsewhere, confirm that residues of lasalocid can be found in eggs from birds which are not receiving intentionally medicated feed. Accidental exposure may be caused by lasalocid carry over from medicated to non-medicated feeds in mills. The results also show that relatively high levels (up to 300 ng g^{-1}) can be found in eggs from birds fed contamination levels (0.1 to 5 mg kg^{-1}) in their diet.

The significance of these results is at present unknown because no MRL for lasalocid has yet been set. However, as with other veterinary drug residues, it is desirable to prevent them entering the human food chain. In addition, traces of antimicrobials could lead to drug resistance, reducing the efficacy of a drug when required therapeutically.

Table 1 Recovery (%) and intra- and inter-assay variation in the determination of lasalocid in eggs. Samples were spiked with 5, 10, 20 and 50 ng g^{-1} of lasalocid. Five replicates were analysed on each of 3 days.

	Level of fortification/ng g^{-1}			
	5	10	20	50
Day 1				
Mean Recovery (%)	87.4	76.0	77.0	82.4
s	3.58	7.81	3.74	2.41
s_r	4.1	10.3	4.9	2.9
n	5	5	5	5
Day 2				
Mean Recovery (%)	88.0	86.6	80.8	78.0
s	3.16	3.65	4.97	3.81
s_r	3.6	4.2	6.1	4.9
n	5	5	5	5
Day 3				
Mean Recovery (%)	83.2	85.6	80.6	83.2
s	8.04	2.88	9.4	2.05
s_r	9.7	3.4	11.7	2.5
n	5	5	5	5
Overall				
Mean Recovery (%)	86.2	82.7	79.4	81.2
s	5.47	6.93	6.21	3.55
s_r	6.3	8.4	7.8	4.4
n	15	15	15	15

References

1 *Medicines Act Veterinary Information Service*, 1994, **11**, 12.

2 Perelman, B., Pirak, M., and Smith, B., *Vet. Rec.*, 1993, **132**, 271.
3 Horii, S., Miyahara, K., and Momma, C., *J. Liq. Chromatogr.*, 1990, **13**, 1411.
4 Martinez, E., and Shimoda, W., *J. Assoc. Off. Anal. Chem.*, 1986, **69**, 637.
5 Weiss, G., Felicito, N. R., Kaykaty, M., Chen, G., Caruso, A., Hargroves, E., Crowley, C., and McDonald, A., *J. Agr. Food Chem.*, 1983, **31**, 75.
6 Tarbin, J. A., and Shearer, G., *J. Chromatogr.*, 1992, **579**, 177.
7 Blanchflower, W. J., and Kennedy, D. G., *Analyst*, 1989, **114**, 1013.
8 Blanchflower, W. J., Kennedy, D. G., and Taylor, S. M., *J. Liq. Chromatogr.*, 1990, **13**, 1595.
9 Hewitt, S. A., Blanchflower, W. J., McCaughey, W. J., Elliott, C. T., and Kennedy, D. G., *J. Chromatogr.*, 1993, **639**, 185.
10 Blanchflower, W. J., McCracken, R. J., and Kennedy, D. G., *Proceedings of the Euroresidue II, Conference Veldhoven, The Netherlands*, ed. Haagsma, N., Ruiter, A., and Czedik-Eysenberg, P. B., 1993, 201.
11 Blanchflower, W. J., Cannavan, A., and Kennedy, D. G., *Analyst*, 1994, **19**, 1325.
12 Blanchflower, W. J., Hewitt, S. A., and Kennedy, D. G., *Analyst*, 1994, **119**, 2595.

High-performance Liquid Chromatography With Diode-array Detection for the Determination of Pesticides in Water Using Automated Solid-phase Extraction

B. Nouri and B. Fouillet

Faculty of Pharmaceutical Sciences, Department of Toxicology, 8 Avenue Rockefeller, 69373 Lyon Cedex 08, France

G. Toussaint

Institut Pasteur de Lyon, Département d'Hygiène Appliquée à l'Homme et son Environnement, Avenue Tony Garnier, 69365 Lyon Cedex 07, France

P. Chambon

Faculty of Pharmaceutical Sciences, Department of Toxicology, 8 Avenue Rockefeller, 69373 Lyon Cedex 08, France and *Institut Pasteur de Lyon, Département d'Hygiène Appliquée à l'Homme et son Environnement, Avenue Tony Garnier, 69365 Lyon Cedex 07, France*

R. Chambon

Faculty of Pharmaceutical Sciences, Department of Toxicology, 8 Avenue Rockefeller, 69373 Lyon Cedex 08, France

An accurate, economical and sensitive method was developed for the simultaneous determination of phenylureas, phenoxy acids, some nitriles and nitrophenols in aqueous samples. The method is based on automated solid-phase extraction and high-performance liquid chromatography with diode-array detection. The analytes were separated on a 25 cm C_{18} analytical column and determined at three wavelengths simultaneously, 220, 240 and 270 nm. The solid-phase extraction time was less than 1 h for six water samples and the lowest detectable concentrations were in the range 25–100 ng l^{-1} The recoveries of the pesticides ranged from 85 to 99% and the relative standard deviations were in the range 1–10% at 200 ng l^{-1} ($n = 6$).

Keywords: Pesticide determination; solid-phase-extraction; high-performance liquid chromatography; diode-array detection; water analysis

Introduction

Herbicide combinations of substituted phenylureas, phenoxy acids and/or nitriles or nitrophenols are still common in liquid formulations for weed control. The commercial introduction of these pesticides has led to the need for rapid, selective and sensitive analytical methods for the control of environmental pollution levels.

Residue analysis of such pesticides in environmental samples is often based on GC methods,[1–5] which are not specific. Another serious disadvantage of GC is the necessity for intermediate steps such as hydrolysis and/or derivatization, which are time consuming. In this context, high-performance liquid chromatography (HPLC) has emerged as an interesting method for the analysis of this group of pesticides.[6–10]

In recent years, the requirements for water quality have been raised considerably and it is frequently necessary to monitor water contamination at low- to sub-microgram per litre levels.[11,12] Analysis at these levels requires a concentra-tion step. For this purpose, solid-phase extraction (SPE) has proved to be a good alternative to liquid–liquid extraction because of its simplicity, robustness and potential for automa-tion.[13,14]

In this study, an automated method was developed for the determination of trace amounts of 12 pesticides in water using SPE and HPLC with diode-array detection, providing simul-taneously structural information and quantitative data. The method allows the simultaneous extraction of six samples in less than 1 h. The SPE isolation step was performed with a Zymark Autotrace Workstation, providing complete auto-mation of cartridge conditioning, sample loading, cartridge air-drying and analyte elution. Parameters such as flow rate of samples through the SPE cartridges, efficiency of elution solvents and analyte elution step are discussed. In addition, the performance of C_{18} and graphitized carbon black car-tridges was compared.

Experimental

Reagents and Samples

Herbicides were supplied by Riedel-de Haën (Seelze, Ger-many) and Dr. S. Ehrenstorfer (Augsburg, Germany) with 95% purity. Pesticides used in this study are listed in Table 1. Individual standard solutions were prepared by dissolving 20 mg each of herbicide in 20 ml of methanol. A composite working standard solution was prepared by mixing 0.2 ml of each standard solution and diluting to 20 ml with methanol.

Ultra-pure water was prepared by ultrafiltration with a Milli-Q system (Millipore, Bedford, MA, USA). Orthophos-phoric acid (H_3PO_4) (85%) was obtained from Prolabo (Paris, France). HPLC gradient-grade acetonitrile and methanol were obtained from SDS (Peypin, France) and Prolabo, respectively. All other solvents were of analytical-reagent grade (SDS) and were used as supplied.

Supelclean ENVI-Carb, 120–400 mesh (0.5 g), and Supel-clean ENVI-C_{18} cartridges (1 g) were purchased from Supelco

(Bellefonte, PA, USA). These adsorbents were packed in poly(propylene) tubes (6 × 1.4 cm id).

Instrumentation

SPE was performed with a Zymark Autotrace Workstation 1.20.

The LC analyses were performed with an HP 1090 Series II liquid chromatograph (Hewlett-Packard, Waldbronn, Germany) equipped with a PV5 ternary solvent-delivery system, an injection valve with a 250 µl loop and an HP Model 1090 diode-array detector (DAD) equipped with a 10 mm flow cell. For multi-wavelength monitoring, the DAD was set at 240, 225 and 270 nm with a bandwidth of 4 nm. During recording of the absorbance spectra the diode optical slit-width was 4 nm and a sampling interval for recording of spectra in the all-spectra mode of 320 ms was used with a peak-width of 0.053 min. Absorbance spectra were recorded from 200 to 400 nm. Data from the DAD were collected and evaluated by the HPchem Workstation computer. The stainless-steel column (25 cm × 4.6 mm id) was packed with 5 µm Spherisorb ODS-2 (Hewlett-Packard).

For separating the pesticides on the C_{18} column, the initial mobile phase composition was as follows: solvent A, water containing 0.1% H_3PO_4; solvent B, methanol. The methanol concentration was programmed from 50% to 54% over 35 min, and then to 70% after 12 min and finally to 50% after 1 min, the last segment of the gradient programme being intended to return the system to its initial conditions in order to be ready for another run. All solvents were de-gassed with helium. The flow rate of the mobile phase was 1 ml min^{-1}. The temperature of the column was kept at 40 °C.

Procedure

The SPE was entirely automated from the conditioning step to the elution step. Solutions (water and solvents) were passed through cartridges under a gas pressure using nitrogen (positive pressure) and not by aspiration under vacuum (negative pressure).

ENVI-C_{18} cartridges were pre-washed with 5 ml each of acetonitrile, methanol and acidified water at a flow rate of 10 ml min^{-1} for the conditioning step. Samples of 500 ml of spiked water, acidified with 0.1% H_3PO_4, were allowed to flow through the cartridge at 10 ml min^{-1}. After the sample had been applied, each solid-phase cartridge was dried under a stream of nitrogen for 5 min to remove traces of water. A 1 ml volume of acetonitrile was added to each cartridge and left for 1 min before the eluting air pressure was applied. This time

period was chosen arbitrarily. The total amount of pesticides was eluted by passing 5 ml of acetonitrile through the cartridge at a flow rate of 5 ml min^{-1}. A 40 µl volume of dimethyl sulfoxide (DMSO) was added to the extract before concentration in order to avoid losses of analytes. The acetonitrile eluate was evaporated to 20–50 µl under a slow stream of nitrogen in a 30 °C water-bath. The residue was reconstituted with 0.25 ml of 0.1% orthophosphoric acid–methanol (1 + 1 v/v) mixture. A 100 µl aliquot of this solution was injected into the HPLC apparatus.

A similar procedure was used to extract pesticides from ENVI-Carb cartridges.

Results and Discussion

For the analysis of the 12 selected herbicides, we adopted an HPLC technique because these compounds are not easily analysed by standard GC methods. Use of a DAD gave advantages in acquiring UV spectra on-line and monitoring signals at up to eight wavelengths simultaneously. Thus, for different substances, optimum selectivity was attained by choosing the appropriate wavelength with maximum absorption (Table 1).

The chromatographic separation was effected in the gradient mode under previously described conditions. Substances that could not be separated chromatographically, such as diuron and MCPA [Fig. 1(a)], were differentiated by their
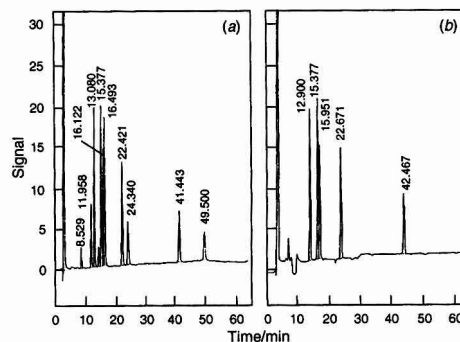

Fig. 1 HPLC traces obtained by injecting the composite working standard solution of 12 pesticides. Amount of each pesticide injected, 50 ng. Chromatograms were recorded with the DAD set at 240 nm with a bandwidth of 4 nm. (a) Mobile phase, water acidified with 0.1% H_3PO_4–methanol; and (b) mobile phase, water–methanol.

Table 1 Statistical parameters for the validation of the SPE method for spiked tap water

No.	Pesticide	Retention time/min	Maximum wavelength/nm	Correlation coefficient*	Recovery (%)†	LOD‡/µg l^{-1}
1	Dicamba	8.629	220	0.998	75 ± 2.2	0.05
2	Bromoxynil	11.958	220	0.998	98 ± 2.2	0.05
3	Chlortoluron	13.080	220	0.982	96 ± 1.2	0.05
4	2,4-D	14.541	240	0.999	95 ± 2.2	0.025
5	Isoproturon	15.377	220	0.998	90 ± 1.6	0.05
6	Diuron	16.122	240	0.998	90 ± 0.3	0.05
7	MCPA	16.122	220	0.998	85 ± 2.3	0.05
8	Ioxynil	16.493	240	0.999	92 ± 1.4	0.025
9	Linuron	22.421	220	0.999	112 ± 1.2	0.05
10	MCPP	24.340	240	0.996	97 ± 3.7	0.05
11	Diflubenzuron	41.443	240	0.989	96 ± 1.0	0.1
12	Dinoterbe	49.800	270	0.986	85 ± 1.1	0.05

* For a range of concentrations from 50 to 1000 µg l^{-1}.
† Mean values calculated from six determinations for a tap water spiked at 200 µg l^{-1}.
‡ Limit of determination.

specific absorbance maxima and their peak apex spectra (Fig. 2). When the two compounds (Diuron and MCPA) were present in the sample, the quantification was not possible by only comparison of absorbance maxima and apex spectra, a mobile phase change was necessary. When the mobile phase was not acidified, only the phenylureas were chromatographed and determined [Fig. 1(b)]. In environmental samples it is likely that other organic compounds will be present that could interfere with the compounds of interest. Therefore, we checked each peak by comparing the UV spectra obtained with those stored in a library (Fig. 3).

During the development of the above methodology, several experimental parameters were investigated. When acidified water was used for conditioning the cartridges, good recovery was achieved for the acidic pesticides whereas there was no change in recovery for the phenylurea herbicides. When
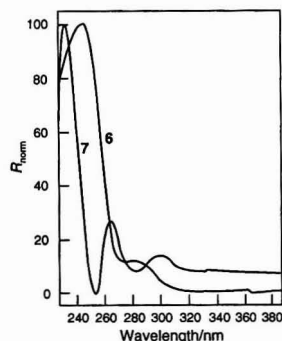

Fig. 2 Ultraviolet spectra of peak at 15.122 min in the chromatogram of the mixture of 12 pesticides extracted from a water sample. 6, Diuron; 7, MCPA.
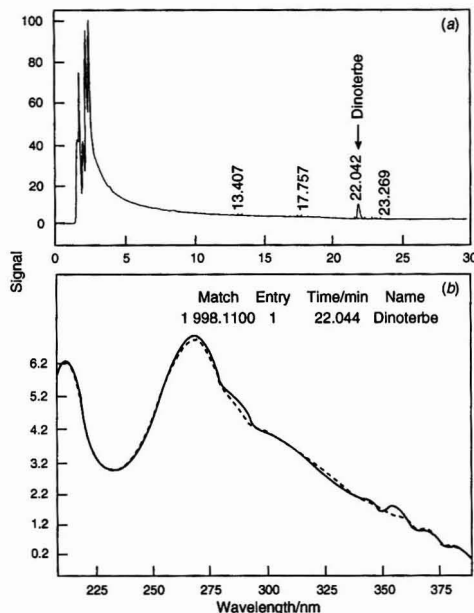

Fig. 3 Dinoterbe peak confirmation in river water. (a) Retention-time tagging; and (b) using a spectral library for pesticides. Dashed line, library spectrum; solid line, target spectrum.

loading the water sample, a flow rate of 10 ml min^{-1} through the cartridge was found to be optimum. At a flow rate of 20 ml min^{-1}, breakthrough of the early-eluting compounds (dicamba, bromoxynil and 2,4-D) was evident. This was confirmed by liquid extraction with methylene chloride of the water sample collected after passing it through the cartridge.

The ENVI-Carb and ENVI-C$_{18}$ cartridges were compared in order to determine the optimum extraction conditions. The air-drying step of 20 min under a stream of nitrogen did not totally remove the residual sample water from the ENVI-Carb cartridge. Consequently, when acetonitrile was passed through the ENVI-Carb cartridge, the percentage of water in the total eluted volume was above 50%. The residual water in ENVI-Carb cartridges is a disadvantage because it lowers the volatility of the eluted solvent under the stream of nitrogen. Forcing the evaporation of this eluate resulted in the loss of analytes. In contrast to the ENVI-Carb cartridge, an air-drying step of 5 min eliminated most of the residual sample water from the ENVI-C$_{18}$ cartridge. Recoveries of <50% were obtained with the ENVI-Carb cartridges when the drying time exceeded 30 min under vacuum. The great affinity of ENVI-Carb cartridges for water indicates that automation of the extraction with this type of adsorbent is unsatisfactory because the elimination of the water from the cartridges lengthens the time of the extraction method, in contrast to ENVI-C$_{18}$ cartridges. Therefore, our results suggest that not only are ENVI-C$_{18}$ cartridges efficient for the retention of all the compounds under the conditions described above, but also that they are adequate for the automation of the SPE method.

Table 2 gives the recoveries for 500 ml water samples spiked with herbicide mixture at the 500 ng l^{-1} level. The results indicate that acetonitrile was preferable to the other extraction solvents tried. Methanol and methylene chloride were poor extraction solvents, with recoveries <50% for most pesticides.

The volume of acetonitrile used to elute the pesticides from the ENVI-C$_{18}$ adsorbent was 6 ml. Before the elution step, the cartridges were soaked with acetonitrile in order to achieve equilibrium between the solid and liquid phases. Thus, the efficiency of desorption was increased and the recovery of analytes improved (Table 3). A 6 ml elution volume was found to be optimum as doubling this volume did not improve recovery of the pesticides.

In addition to the analysis of 500 ml samples reported above, we have also tried 1 l samples and there appeared to be no decrease in efficiency. On the basis of 500 ml water samples and concentration of the extract to 250 µl, the estimated limits of quantification ranged between 25 and 50 ng l^{-1}, except for

Table 2 Recovery of pesticides from the ENVI-C$_{18}$ cartridge using different eluents

		Recovery (%)*		
No.	Pesticide	Methylene chloride	Methanol	Aceto-nitrile
1	Dicamba	20	9	76
2	Bromoxynil	10	25	95
3	Chlortoluron	25	9	95
4	2,4-D	56	106	88
5	Isoproturon	35	30	92
6	Diuron	63	35	85
7	MCPA	ND	26	89
8	Ioxynil	52	84	88
9	Linuron	63	45	100
10	MCPP	82	40	96
11	Diflubenzuron	16	62	117
12	Dinoterbe	43	16	80

* Mean values calculated from two determinations.

diflubenzuron, the limit of quantification of which was 100 ng l^{-1} (Table 1). The concentrations of the pesticides in water were calculated by measuring the peak area of each pesticide and comparing them with those obtained from standard solutions. These were prepared by taking known volumes of the working standard solutions, evaporating the acetonitrile and reconstituting the residue with 250 µl of the mobile phase. Under the chromatographic conditions selected, the limits of detection of the method were calculated by assuming arbitrarily that 0.5 cm was the minimum peak area that could be used with reasonable confidence.

With the above-described method, the recoveries of pesticides from six replicate samples ranged from 85 to 99% (Table 1), the only exception being dicamba, with a recovery of 75% owing to its high water solubility (6.5 g l^{-1}). The same recoveries were obtained for the 12 pesticides at concentrations between 25 and 100 ng l^{-1}.

This technique has been validated for a group of 12 pesticides. The repeatabilities of the retention times and peak areas were determined using tap water (Table 1). The relative standard deviations of the retention times were in the range 0.2–2% and those of the peak areas were 1–10% ($n = 6$). The correlation coefficients of all the calibration graphs for water samples were over 0.998 for most of the pesticides.

Table 3 Influence of soaking of C_{18} cartridge before elution on recoveries for pesticides from water spiked at 200 ng l^{-1}

No.	Pesticide	Recovery (%)*	
		Without soaking	With soaking
1	Dicamba	70	76
2	Bromoxynil	80	98
3	Chlortoluron	92	98
4	2,4-D	89	99
5	Isoproturon	90	90
6	Diuron	88	102
7	MCPA	80	99
8	Ioxynil	86	105
9	Linuron	84	110
10	MCPP	80	97
11	Diflubenzuron	75	96
12	Dinoterbe	79	88

* Mean values for two determinations.

Conclusion

The automated SPE–HPLC method described here is accurate, efficient, economical and sensitive. It is also less hazardous than liquid–liquid extraction methods and is easier to perform and less time consuming than other existing methods. It can be used for the daily analysis of 24 water samples and it has sufficient sensitivity to be of value as a rapid screening technique for the detection and determination of these 12 pesticides in water samples.

References

1 Burchill, P., Herod, A. A., Marsh, K. M., and Pritchard, E., *Water Res.*, 1983, **17** (12), 1905.
2 De Kok, A., Vos, Y. J., Van Garderen, C., De Jong, T., Van Opstal, M., Frei, R. W., Geerdink, R. B., and Brinkman, U. A. Th., *J. Chromatogr.*, 1984, **288**, 71.
3 Senin, N. N., Filippov, Y. S., Tolikina, N. F., Smol'yaninov, G. A., Volkov, S. A., and Kukushkin, V. S., *J. Chromatogr.*, 1986, **364**, 315.
4 Lee, H.-B., Peart, T. E., Carron, J. M., and Tse, H., *J. Assoc. Off. Anal. Chem.*, 1991, **74**, 835.
5 Ngan, F., and Ikesaki, T., *J. Chromatogr.*, 1991, **537**, 385.
6 Stout, R. W., and Destefano, J. J., *J. Chromatogr.*, 1983, **261**, 189.
7 Jandera, P., Svoboda, L., Kubat, J., Schvantner, J., and Churacek, R., *J. Chromatogr.*, 1984, **292**, 71.
8 Walters, S. M., Westerby, B. C., and Gilvydis, D. M., *J. Chromatogr.*, 1984, **317**, 533.
9 Lindner, W., Ruckendorfer, H., Lechner, W., and Posch, W., *Int. J. Environ. Anal. Chem.*, 1987, **31**, 235.
10 Di Corcia, A., and Marchetti, M., *J. Chromatogr.*, 1991, **541**, 365.
11 Di Corcia, A., and Marchetti, M., *Anal. Chem.*, 1991, **63**, 6.
12 Miles, C. J., *J. Chromatogr.*, 1992, **595**, 283.
13 Liska, I., Brouwer, E. R., Ostheimer, A. G. L., Lingeman, H., Brinkman, U. A. Th., Geerdink, R. B., and Mulder, W. H., *Int. J. Environ. Anal. Chem.*, 1992, **42**, 267.
14 Brouwer, E. R., Van Iperen, D. J., Liska, I., Lingeman, H., and Brinkman, U. A. Th., *Int. J. Environ. Anal. Chem.*, 1992, **47**, 257.

Evaluation of a Split-type Flow Cell for a Polarized Spectrophotometric Detector

Atsushi Yamamoto, Akinobu Matsunaga and Eiichi Mizukami

Toyama Institute of Health, 17-1 Nakataikoyama, Kosugi-machi, Toyama 939-03, Japan

Kazuichi Hayakawa and Motoichi Miyazaki

Faculty of Pharmaceutical Sciences, Kanazawa University, 13-1 Takara-machi, Kanazawa 920, Japan

Masayuki Nishimura, Mitsuo Kitaoka and Tomio Fujita

Shimadzu Corporation, 1 Nishinokyo-kuwabara-cho, Nakagyo-ku, Kyoto 604, Japan

A split-type flow cell for a polarized spectrophotometric detector (PPD), in which the column effluent is simultaneously passed through both the sample and reference sides, is described. The improvement in detection sensitivity in PPD with the use of this cell is discussed. Its utility as a universal polarimetric detector for HPLC for the detection of coloured amino acid–copper(II) complexes is shown. A new possibility for this cell in the gradient elution separation of glucose syrup is demonstrated.

Keywords: Polarized spectrophotometric detector; split-type flow cell; high-performance liquid chromatography

Introduction

We have proposed a novel detector, a polarized spectrophotometric detector (PPD),[1] which measures the optical rotation of optically-active analytes as the change in absorbance, and have reported the fundamental theory[2] and applications[3,4] of this detector. The main advantage of the PPD is the easy use of a conventional absorbance detector as a polarimetric detector without any remodelling. However, the use of PPD has been limited by poor sensitivity, and the lack of distinction between optical rotation and absorbance at the absorption band of the analyte. As far as sensitivity is concerned, there is room for improvement in the former aspect,[2] but overcoming the latter problem is impossible with a conventional flow cell.

The photodetector in a conventional absorbance detector consists of two independent photodiodes, one of which merely receives the light from the empty cell as reference. If the column effluent is simultaneously passed through not only the sample side but also the reference side, the effects of light absorption of the analyte will compensate each other. Moreover, the inversion of the phase angle of two polarizers fitted to both the sample and reference cells will double the signal response by the optical rotation. We thought that the construction of a split-type cell assembly based on the above concept would improve the performance of the PPD without destroying the native properties of the absorbance detector. We report here the evaluation of a prototype split-type cell that can be inserted into an absorbance detector as a working cell for the HPLC of optically active-compounds.

Theoretical

If I_0 is the intensity of polarized light transmitted through the first polarizer, then the final intensity of this light, I, transmitted through the flow cell and the second polarizer is given by

$$I = I_0 K \cos^2 \alpha$$

where α is the phase angle of two polarizers across the flow cell and K is a constant for each polarizer and/or flow cell. When a light-absorbing compound enters the flow cell, I is changed to

$$I = I_0 e^{-\varepsilon c l} K \cos^2 \alpha$$

where ε and C are molar absorptivity and molarity of the compound, respectively, and l is the cell length. When this compound shows optical activity and rotates the plane of polarized light by an angle β, I is further changed to

$$I = I_0 e^{-\varepsilon c l} K \cos^2(\alpha + \beta)$$

If the assumption is made that the column effluent flows into both cells at the same velocity, then the output as an absorbance, *Abs*, from the detector equipped with the split cell can be expressed as

$$Abs = \log \left[\cos^2(\alpha_r + \beta) / \cos^2(\alpha_s + \beta) \right] \quad (1)$$

where the subscripts s and r indicate sample and reference sides, respectively. The effects of light absorption are offset in eqn. (1), see Fig. 1.

Next, we consider the case when $\alpha_r = -\alpha_s$ in eqn. (1). When the optically-active analyte is in the split cell, the signal intensity, ΔAbs, is given by

$$\Delta Abs = -\log \left[\cos^2(-\alpha_s + \beta) / \cos^2(\alpha_s + \beta) \right] \quad (2)$$

because the baseline absorbance is given by $\log(\cos^2 \alpha_r / \cos^2 \alpha_s)$. By substituting $f(x)$ for $\log(\cos x)$ in eqn. (2), ΔAbs can be rewritten as

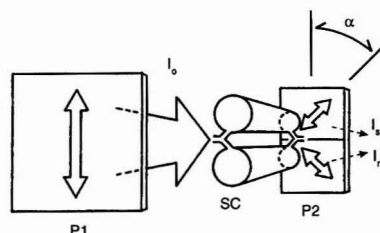$$\Delta Abs = -2[f(\alpha_s - \beta) - f(\alpha_s - \beta + 2\beta)]$$

Fig. 1 Experimental set-up of the split cell: SC, split-type flow cell; P1 and P2, polarizers; α, phase angle.

As $f(\alpha_s - \beta + 2\beta)$ is almost equal to $f(\alpha_s - \beta) + 2\beta f'(\alpha_s - \beta)$ by using Taylor's series, we obtain

$$\Delta Abs \approx 4\beta f'(\alpha_s - \beta) = 4\beta \log e \tan \alpha_s \quad (3)$$

Eqn. 3 shows that exactly twice as large a signal intensity is obtained by the split cell as with the normal, conventional single flow cell, which is derived from the previous fundamental theory [eqn.(6) in ref. 2].

Experimental

The split-type flow cell was constructed as shown in Fig. 2, with a pathlength and inner diameter of 12 and 1.5 mm, respectively. Three linear polarizers (Type HN32, 0.01 in. thick) obtained from Polaroid (Norwood, MA, USA) were placed on this cell assembly, one on the incident light side and
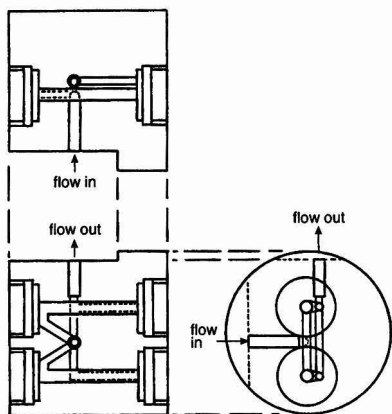

Fig. 2 Perspective drawings through the split-cell assembly equipped with two cylindrical flow cells of 1.5 mm id and 12 mm optical pathlength.
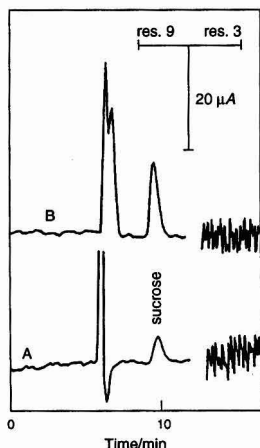

Fig. 3 Comparison of sensitivities of the split and normal cells. Conditions: eluent, acetone–water (5 + 3); flow rate, 0.5 ml min⁻¹; column temperature, 70 °C; detection wavelength, 530 nm; phase angle between two polarizers (α), ±0.9 rad (split) and +0.9 rad (normal); time constant, 10 s for res. 9 and 0.5 s for res. 3. See text for further conditions. A, Normal; B, split.

two on the transmitting light side, whose phase angles are the inverse of each other, as shown in Fig. 1. This assembly was inserted into a Shimadzu (Kyoto, Japan) SPD-10AV UV/VIS spectrophotometric detector, and used as the PPD. Regulation of this detector to obtain high PPD sensitivity was described in a previous paper.[4]

Chromatographic separations of sucrose and glucose syrup were carried out on a 250 × 4.6 mm id TSK-Gel Amide-80 column (Tosoh, Tokyo, Japan) maintained at 70 °C by a Shimadzu CTO-10AC column oven. Acetone–water eluents were delivered with isocratic or gradient elution using a Shimadzu LC-4A pump.

Enantiomeric resolution of D,L-proline was performed on a 50 × 4.6 mm id chiral column, MCI GEL CRS10W (Mitsubishi Kasei, Tokyo, Japan), maintained at 35 °C. An eluent containing 1 mmol l⁻¹ copper(II) sulfate was delivered at a flow rate of 0.8 ml min⁻¹. Another spectrophotometric detector, a Shimadzu SPD-6AV, was used in series with the PPD to monitor the elution of D,L-proline.

Sucrose, D,L-proline and copper(II) sulfate, purchased from Wako (Osaka, Japan), were of guaranteed grade. Acetone from Wako was of HPLC-grade. The glucose syrup sample (Fujioligo G67) was purchased from Nihon Shokuhin Kakou (Fuji, Japan).

Results and Discussion

Improvement of Detection Sensitivity

The split cell used in this work has a 1.2 times longer pathlength and 2.25 times larger sectional area than the normal cell (1 cm pathlength and 1 mm id). In the fundamental theory of PPD,[2] an increase in pathlength brings about an increase in signal response, and the increase in light intensity accompanying the increase in the sectional area produces a decrease in the noise level. Fig. 3 shows chromatograms obtained with both the split and normal cells with an injection of 10 µg of sucrose of each. The split cell makes the practical pathlength double (*i.e.*, 24 mm), so the signal response can be seen to increase in proportion to the pathlength of the cell. The baseline noise level is magnified after the sucrose signals owing to the decrease in the time constant of the detector. However, the split cell was not effective enough to reduce the noise level. It is thought that the total sectional areas through which the light passes in the split cell is not much larger than that in the normal cell, because the normal cell assembly has a hole as a reference about three times as large as the sample side. From the measured signal-to-noise ratio, the split cell showed an advantage in detection limit of about three times over that of the normal cell.

Offset of Light Absorption

In general, amino acid–Cu^{II} complexes show the Cotton effect in the range of 500–600 nm.[5] Especially the L-proline–Cu^{II} complex has a large specific rotation with a negative value around 580 nm, so this can be detected with high sensitivity by the polarimetric detector. However, coloured Cu^{II} complexes obstructed the measurement of optical rotation by the PPD with the normal cell. Fig. 4 shows chromatograms of D,L-proline obtained on a chiral column monitored at 580 nm by both visible and PPD methods. It is difficult to ensure that the linear velocities of the column effluent in both the sample and reference cells are identical. However, this difficulty in construction of the split cell can be avoided by enlargement of the phase angle, α, beyond the optimum angle (around 0.9 rad), although an increase in baseline noise is induced. In a situation where a solution of proline–Cu^{II} complex turns blue, showing absorption at the detection wavelength (upper trace),

the split cell could cancel the change in the baseline due to their absorption, and D-proline gave a positive peak as it is dextrorotatory and the L-form gave a negative peak as it is laevorotatory (bottom trace).

Many optically-active compounds readily chelate with metals. Chelation brings about a significant increase in the specific rotation of ligands, but is often attended by colour formation.[5] The split cell for PPD will be useful for the highly
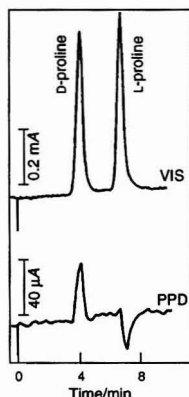

Fig. 4 Separation of D,L-proline on a chiral column with visible and polarized spectrophotometric detection. Conditions: eluent, 1 mmol l^{-1} CuSO$_4$; flow rate, 0.8 ml min^{-1}; column temperature, 35 °C; phase angle, ±1 rad; sample size, 50 nmol D,L-proline. See text for further conditions.
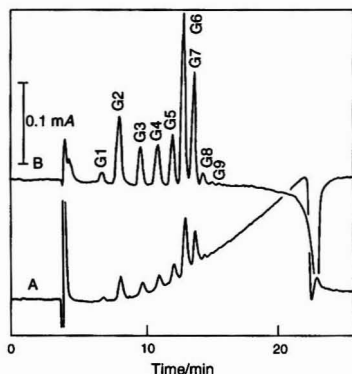

Fig. 5 Comparison of the split and normal cells in the analysis of glucose syrup with gradient elution: solvent gradient, 2 + 1 to 1 + 2 acetone–water over 15 min; flow rate, 0.7 ml min^{-1}; G1, glucose; G2, maltose; G3, maltotriose and higher sugars, with numbers indicating degree of polymerization. Other conditions as in Fig. 3. A, Normal; B, split.

sensitive detection of optically-active compounds as their metal complexes.

Effect of Refractive Index

In a conventional polarimetric detector for HPLC, the refractive index (RI) change of the eluent gives rise to baseline disturbances, and great care is necessary for the gradient elution analysis.[6,7] PPD is no exception, but the cancellation of the absorbance change by the split cell may contribute to stabilizing the baseline from the disturbances due to RI changes under gradient elution conditions. Investigations of gradient elution with various solvents revealed that the split cell produced a small baseline drift and an increase in noise levels in comparison with the normal cell. Typical chromatograms for a 10 μl injection of 5% m/v glucose syrup with linear gradient elution are shown in Fig. 5. The upper trace, obtained with the split cell, shows almost no baseline drift. The large disturbance observed around 22 min is attributed to rapid exchange of the eluents from (1 + 2) to (2 + 1) acetone–water. In contrast, the normal cell produced baseline drift that was equivalent to changes in the RI of the eluent. This result shows that the split cell is able to cancel the RI change and is useful in gradient elution separation.

Conclusion

We have constructed a split-type flow cell assembly in which the column effluent is passed through both the sample and reference sides to improve the performance of the PPD. In the split cell, the signal responses are doubled in comparison with a conventional cell. This cell is capable of determining the optical rotations of analytes at their absorption bands, and can also be used in gradient elution separation. The PPD with this split cell might be developed into an alternative polarimetric detector based on the Faraday effect.

References

1 Yamamoto, A., Matsunaga, A., Hayakawa, K., Mizukami, E., and Miyazaki, M., *Anal. Sci.*, 1991, **7**, 719.
2 Hayakawa, K., Yamamoto, A., Matsunaga, A., Mizukami, E., Nishimura, M., and Miyazaki, M., *Biomed. Chromatogr.*, 1994, **8**, 130.
3 Yamamoto, A., Matsunaga, A., and Mizukami, E., *Shokuhin Eiseigaku Zasshi*, 1992, **33**, 301.
4 Yamamoto, A., Matsunaga, A., Mizukami, E., Hayakawa, K., and Miyazaki, M., *J. Chromatogr. A*, 1994, **667**, 85.
5 Pfeiffer, P., and Christeleit, W., *Z. Physiol. Chem.*, 1937, **247**, 262.
6 Reitsma, B. H., and Yeung, E. S., *Anal. Chem.*, 1987, **59**, 1059.
7 Lloyd, D. K., Goodall, D. M., and Scrivener, H., *Anal. Chem.*, 1989, **61**, 1238.

Determination of Free Hydroxyproline and Proline in Human Serum by High-performance Liquid Chromatography Using 4-(5,6-Dimethoxy-2-phthalimidinyl)phenylsulfonyl Chloride as a Pre-column Fluorescent Labelling Reagent

Hirofumi Inoue, Kazuhiro Moritani, Yuuko Date, Kazuya Kohashi and Yasuto Tsuruta*

Faculty of Pharmacy and Pharmaceutical Sciences, Fukuyama University, Fukuyama, Hiroshima 729-02, Japan

A fluorescent labelling reagent, 4-(5,6-dimethoxy-2-phthalimidinyl)phenylsulfonyl chloride, was designed for the determination of amines by precolumn HPLC and was applied to the simultaneous determination of hydroxyproline and proline in serum. The reagent reacted with hydroxyproline and proline at 30 °C for 10 min to produce the fluorescent derivatives, which were separated on a reversed-phase column by gradient elution with phosphate buffer (1 mmol l^{-1}, pH 7) and acetonitrile and detected by fluorescence measurement at 315 nm (excitation) and 385 nm (emission). The detection limits (signal-to-noise ratio = 3) for both hydroxyproline and proline were 10 fmol per injection. The within-day ($n = 10$) and day-to-day ($n = 5$) relative standard deviations using human sera were less than 2.16% and 2.75%, respectively, for hydroxyproline and less than 2.30% and 3.25%, respectively, for proline. The concentrations of free hydroxyproline and proline in normal human sera ($n = 13$) were 5.6–18.0 and 137.6–252.6 µmol l^{-1}, respectively. The proposed method was also applied to the determination of hydroxyproline and proline in sera from patients with chronic renal failure. The mean concentrations of hydroxyproline and proline in chronic renal failure were about 2.6 and 1.6 times higher, respectively, than those in normal human sera.

Keywords: High-performance liquid chromatography; hydroxyproline and proline determination; fluorescence detection; 4-(5,6-dimethoxy-2-phthalimidinyl)phenylsulfonyl chloride; serum

Introduction

It is well known that proline (Pro) and hydroxyproline (Hyp) are characteristic imino acids that exist in collagen, and Hyp is formed by hydroxylation of Pro after its incorporation into peptides during collagen biosynthesis. The concentration of Hyp in biological fluids is associated with certain diseases such as metastatic bone disease,[1] breast cancer[2] and chronic uraemia,[3] which are accompanied by an increased concentration of free Hyp in plasma. Therefore, the determination of free Pro and Hyp in serum can afford useful information not in only the diagnosis but also in the prognosis of diseases.

Hitherto, a number of methods for the determination of Hyp in serum, urine and collagen have been developed. Among these methods, the simultaneous determination of Hyp and Pro has been achieved by use of gas chromatography (GC) and high-performance liquid chromatography (HPLC). However, the GC method required a two-step derivatization procedure to convert imino acids into *N*-dimethylthiophosphoryl methyl esters.[4] In HPLC methods, imino acids are determined using either post- or pre-column derivatization techniques with absorbance or fluorescence detection. Some of the post-column techniques using *o*-phthalaldehyde (OPA)–mercaptoethanol[5–7] and 4-chloro-7-nitrobenzofurazan (NBD-Cl)[8,9] as fluorescent reagents are time consuming and also those using OPA–mercaptoethanol require the oxidation of a secondary amino group of imino acids to a primary amino group by treatment with hypochlorite prior to the derivatization. On the other hand, the methods using pre-column techniques are fairly sensitive for Hyp and Pro by use of pre-labelling reagents, *e.g.*, 4-dimethylaminoazobenzene-4'-sulfonyl chloride,[10] dansyl chloride (DNS-Cl),[11] NBD-Cl[12,13] and 9-fluorenylmethyl chloroformate.[14] Among these methods, only DNS-Cl[11] and NBD-Cl[12] have been applied to the simultaneous determination of free Hyp and Pro in plasma. These reagents have been used for the selective labelling of imino acids after reaction of primary amino acids with formaldehyde and OPA, respectively. However, Hyp is partly altered to non-reactive products by treatment with formaldehyde, and the method using NBD-Cl has the disadvantages that it requires relatively large sample volumes and the NBD derivatives are light-sensitive.

We designed 4-(5,6-dimethoxy-2-phthalimidinyl)phenylsulfonyl chloride (DPS-Cl) as a labelling reagent for primary and secondary amines and found that it reacted with Pro and Hyp to give the corresponding fluorescent sulfonamides quantitatively. In this paper, the simultaneous determination of Hyp and Pro in small amounts of serum by HPLC using DPS-Cl is described.

Experimental

Instrumental Conditions

The HPLC system consisted of a Bip-1 HPLC pump (Jasco, Tokyo, Japan), a GP-A50A gradient programmer (Jasco), a Model 880-51 two-line degasser (Jasco), a Rheodyne Model 7161 injector (10 µl loop), an RF-530 spectrofluorimeter (Shimadzu, Kyoto, Japan) and a C-R6A Chromatopac integrator (Shimadzu). A Nova-Pak C_{18} column (150 × 3.9 mm id, 4 µm; Waters) connected with a TSK Guardgel ODS-80TM (15 × 3.2 mm id; Tosoh, Tokyo, Japan) as a guard column was used with a gradient system of (A) phosphate buffer (1 mmol l^{-1}, pH 7)–(B) acetonitrile at 25 °C. The

elution programme was a linear gradient from 10 to 22% of B for 12 min, followed by a stepwise increased in B to 80% to wash the column for 5 min and then a stepwise decrease to 10% B to re-equilibrate the column for 5 min. The flow rate was 1.0 ml min^{-1}. The fluorescence intensities were monitored at excitation and emission wavelengths of 315 and 385 nm, respectively. Uncorrected fluorescence spectra were measured with a Hitachi (Tokyo, Japan) Model 650-10S spectrofluorimeter using a quartz cell (optical pathlength 10 mm). Proton nuclear magnetic resonance (^{1}H NMR) spectra were obtained in [^{2}H]chloroform (CDCl$_3$) or [^{2}H]dimethyl sulfoxide ([^{2}H] DMSO) using tetramethylsilane as an internal standard with a JEOL FX-100 spectrometer (Nihondenshi, Tokyo, Japan). Mass spectra were measured with a GLUMS-6020 instrument (Shimadzu).

Chemicals and Solvents

All chemicals were of analytical-reagent grade, unless stated otherwise. 4,5-Dimethoxyphthalaldehyde was prepared from 3,4-dimethoxybenzoic acid *via* *m*-meconin and 4,5-dimethoxyphthalyl alcohol according to the method of Bhattacharjee and Popp.[15] Amino acids were purchased from Kyowa Hakko (Tokyo Japan), except hydroxyproline, from Wako (Osaka, Japan). DL-Nipecotic acid, *o*-phthalaldehyde (OPA) and Creatinine Test Wako were obtained from Wako. De-ionized, distilled water was used throughout. Organic solvents except acetonitrile (HPLC grade, Wako) were purified by distillation prior to use.

Synthesis of DPS-Cl labelling reagent

4,5-Dimethoxyphthalaldehyde (2.0 g) in dioxane (230 ml) and aniline (0.96 g) in dioxane (20 ml) were mixed and stirred at room temperature for 3 d. The reaction mixture was concentrated to about 5 ml by evaporation under reduced pressure and then diethyl ether was added. The precipitates were filtered off and recrystallized from ethanol to obtain 5,6-dimethoxy-2-phenylphthalimidine as colourless plates (yield 0.98 g, mp 198.7–199.3 °C). The crystals (0.5 g), in limited amounts, were dissolved in chlorosulfonic acid (approximately 1 ml) cooled in an ice-bath and the mixture was stirred at 50 °C for 5 min. After cooling at room temperature, the mixture was poured dropwise onto crushed ice (20 g) and then water (200 ml) was added. The product was extracted with chloroform (150 ml, three times). The organic layer, washed with water (200 ml, three times), was dried with anhydrous sodium sulfate for 2 h and then evaporated to dryness. The residue was chromatographed on a silica gel column (Wakogel C-200, 120 × 40 mm id) with chloroform as eluent. Immediately after eluting the first fluorescent fraction (approximately 200 ml), the non-fluorescent fraction was collected (approximately 200 ml) and evaporated to dryness under reduced pressure. The residue was recrystallized from acetonitrile to obtain DPS-Cl as white needles (yield 0.4 g, mp 214.4 °C). Analysis: calculated for $C_{16}H_{14}NO_5SCl$, C 52.25, H 3.84, N 3.81, S 8.72, Cl 9.64; found, C 52.29, H 3.67, N 3.82, S 8.61, Cl 9.37%. MS (*m/z*): 367 (M$^+$). ^{1}H NMR (δ, ppm, in CDCl$_3$): 3.98 and 4.00 (3H each, s each, –OCH$_3$ each), 4.83 (2H, s, –CH$_2$– of phthalimidine), 7.00 and 7.37 (1H each, s each, aromatic H of phthalimidine), 8.10 and 8.12 (2H each, d each, J = 9.14 Hz each, H of benzene ring).

Preparation of and Analytical Data for the DPS derivatives of Hyp and Pro

To the solution of Hyp (40 mg) or Pro (35 mg) in borate buffer (0.1 mol l^{-1}, pH 8.5) (40 ml), DPS-Cl (100 mg) in acetone (200 ml) was added and stirred for 30 min at room temperature.

The reaction mixture was evaporated to dryness under the reduced pressure. The suspension of the residue in acetone (200 ml) containing concentrated hydrochloric acid (300 µl) was filtered and the filtrate was evaporated to dryness. This operation was repeated. The DPS derivative of Hyp or Pro was recrystallized from ethanol and then from acetone-hexane.

DPS derivative of Hyp. White needles (yield 93 mg, m.p. 270–271.4 °C). Analysis: calculated for $C_{21}H_{22}N_2O_8S$, C 54.54, H 4.79, N 6.06, S 6.93; found, C 54.60, H 4.88, N 6.03, S 6.72%. MS (*m/z*): 417 (M$^+$ – COOH). ^{1}H NMR (δ, ppm, in [^{2}H] DMSO): 1.82–4.34 (6H, m, H of pyrrolidine ring), 3.86 and 3.89 (3H each, s each, –OCH$_3$ each), 4.91 (1H, s, –OH), 4.96 (2H, s, –CH$_2$– of phthalimidine), 7.25 (2H, s, aromatic H of phthalimidine), 7.91 and 8.10 (2H each, d each, J = 8.70 Hz each, H of benzene ring).

DPS derivative of Pro. White plates (yield 72 mg, m.p. 252.9–253.9 °C). Analysis: calculated for $C_{21}H_{22}N_2O_7S$, C 56.49, H 4.97, N 6.27, S 7.18; found, C 56.40, H 4.98, N 6.26, S 7.04%. MS (*m/z*): 401 (M$^+$ – COOH). ^{1}H NMR (δ, ppm, in [^{2}H] DMSO): 1.51–4.20 (7H, m, H of pyrrolidine ring), 3.86 and 3.89 (3H each, s each, –OCH$_3$ each), 4.96 (2H, s, –CH$_2$– of phthalimidine), 7.26 (2H, s, aromatic H of phthalimidine), 7.89 and 8.12 (2H each, d each, J = 9.04 Hz each, H of benzene ring).

Analytical Procedure

To human serum (10 µl) were added nipecotic acid (50 µmol l^{-1}, 20 µl) as an internal standard (IS), borate buffer (0.1 mol l^{-1}, pH 8.5, 270 µl) and OPA (4% in acetone, 50 µl). After standing for 3 min, the mixture was reacted with DPS-Cl (1.2 mmol l^{-1} in acetone, 450 µl) at 30 °C for 10 min. The reaction mixture was mixed with dichloromethane (0.8 ml), vortex mixed and then centrifuged (500 *g*) for 10 min. An aliquot of the aqueous layer was subjected to HPLC.

Results and Discussion

Structures and Fluorescence Spectra of DPS-Cl and DPS Derivatives of Hyp and Pro

Some phthalaldehydes, such as OPA, 4,5-methylenedioxyphthalaldehyde and 4,5-dimethoxyphthalaldehyde, react with certain aromatic primary amines to produce highly fluorescent 2-phenylphthalimidine derivatives, which are used as fluorophores for fluorescent labelling reagents.[16–18] The reaction of 4,5-dimethoxyphthalaldehyde with aniline also gave a fluorescent product, 5,6-dimethoxy-2-phenylphthalimidine, which was easily converted into DPS-Cl by treatment with chlorosulfonic acid. DPS-Cl, which itself was non-fluorescent, reacted with primary and secondary amino compounds in a basic medium to give a fluorescent product. As sulfonyl chlorides react with amines to form sulfonamides, the reaction products of DPS-Cl with Hyp and Pro should be the corresponding sulfonamides (as shown in Fig. 1); these were confirmed by elemental analyses and ^{1}H NMR spectral data.

The fluorescence spectra of DPS derivatives of Hyp and Pro in aqueous acetonitrile (10–90% v/v) and acetonitrile were measured. The excitation and emission maximum wavelengths of both DPS derivatives in aqueous acetonitrile were 315 and 385 nm, respectively, and the emission maximum wavelengths were shifted to shorter wavelengths in acetonitrile. The fluorescence intensities of both derivatives were observed to increase with increasing water content in the range 0–80% v/v in the medium and to decrease with water contents more than 80% v/v. Incidentally, the fluorescence intensities in water–acetonitrile (8 + 2 v/v) were about 7.7 times more intense than those in acetonitrile and about 1.2

times more intense than those in water–acetonitrile (9 + 1 v/v).

Chromatographic Separation

The derivatives of Hyp, Pro and the IS labelled with DPS-Cl were separated successfully on a reversed-phase column. Typical chromatograms obtained from a standard solution and human serum are shown in Fig. 2. The peaks corresponding to Hyp, Pro and the IS eluted at 6.8, 9.0 and 12.0 min, respectively, and were completely separated from the peaks due to the reagent blank and other serum components. The wavelengths of the fluorescence excitation and emission maxima of the eluates corresponding to Hyp, Pro and the IS were 315 and 385 nm, respectively. The sensitivity of the detector was reduced to 1/8 for detection of free Pro after the elution of the peak due to Hyp, because the concentration of Pro was about ten times higher than that of Hyp in serum. Gradient elution with (A) phosphate buffer–(B) acetonitrile was employed, as the peaks due to Pro and the IS were delayed and broadened by isocratic elution with less than 12% of acetonitrile and the peak due to Hyp overlapped with that of reagent blank with more than 12% of acetonitrile. The chromatographic separation was also affected by the concentration and pH of the phosphate buffer in the mobile phase. At concentrations lower than 0.5 mmol l^{-1}, the retention times of all peaks became shorter and the peak due to Hyp overlapped

partially with the tail of the reagent blank. At acidic pH of the phosphate buffer (pH 5 and 6), the peak of the IS was delayed and broadened, although the peaks of Hyp and the reagent blank eluted earlier. Therefore, the conditions described above were employed.

The peaks due to the fluorescent derivatives of Hyp and Pro in human serum were identified by comparing the retention times and fluorescence spectra with those of the prepared DPS derivatives and the standard solutions.

Dichloromethane Extraction

When the reaction mixture was directly subjected to HPLC without dichloromethane extraction, the DPS derivatives of Hyp, Pro and the IS were not retained on the column under the influence of acetone present in the reaction mixture. In addition, when DPS-Cl was present in excess in the sample subjected to HPLC, it caused the guard column to degrade and the retention times of peaks to be delayed after several injections. However, these problems were solved by extraction of the excess of DPS-Cl and acetone with dichloromethane from the reaction mixture, and fortunately the derivatives of Hyp, Pro and the IS were concentrated in the aqueous layer. The effect of the volume of dichloromethane on the peak heights of Hyp, Pro and IS is shown in Fig. 3. Dichloromethane was used in a volume of 800 μl, as almost constant peak heights were obtained at volumes of 750–1100 μl.

Selection of Internal Standard

Some secondary amino acids (1 nmol each in the labelling reaction mixture) were examined to select an internal standard. Although the peaks of isonipecotic acid, DL-pipecolic acid and thioproline labelled with DPS-Cl were eluted at 11.8, 11.3 and 10.6 min, respectively, the peak heights were very small (about one sixth in comparison with nipecotic acid). The peak of L-azetidine-2-carboxylic acid at a retention time of 8.6 min partially overlapped with that of Pro. The peak due to nipecotic acid eluted at 12.0 min and was successfully separated from those of Hyp, Pro, the reagent blank and other serum components, as shown in Fig. 2.

Reaction Conditions

As the labelling reaction of Hyp, Pro and the IS with DPS-Cl proceeded in a basic medium, the effect of the pH of borate buffer (0.1 mol l^{-1}) was examined by use of a standard solution (10 μmol l^{-1} Hyp and 200 μmol l^{-1} Pro). Above pH 8.5, the peak heights of Hyp, Pro and the IS labelled with DPS-Cl reached a maximum (Fig. 4). These derivatives were stable for at least 48 h in the reaction mixture at pH 8.5,
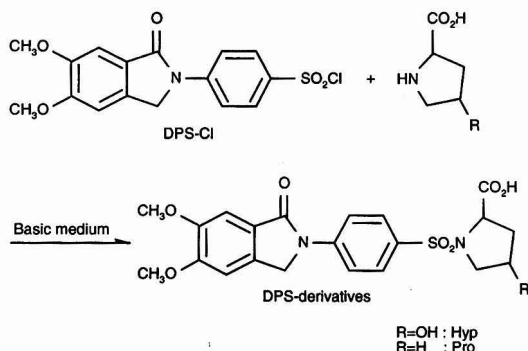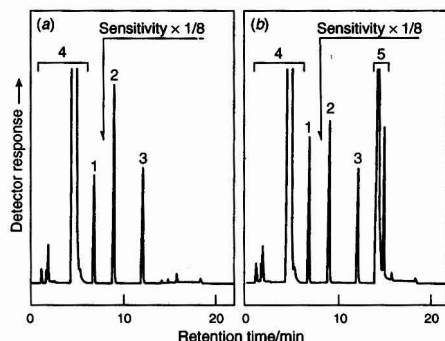

Fig. 1 Reaction of DPS-Cl with Hyp and Pro.

Fig. 2 HPLC traces obtained from (a) standard solution and (b) serum reacted with DPS-Cl. Peaks: 1, Hyp; 2, Pro; 3, IS; 4, reagent blank components; and 5, unknown. Concentration: (a) Hyp, 10.0 μmol l^{-1}; Pro, 200.0 μmol l^{-1}; (b) Hyp, 13.5 μmol l^{-1}; Pro, 164.5 μmol l^{-1}.
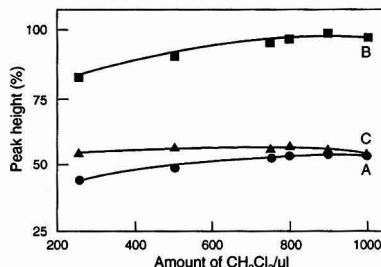

Fig. 3 Effect of volume of dichloromethane on the peak heights of A, Hyp; B, Pro and; C, IS labelled with DPS-Cl.

although the peak heights decreased to less than 70% after 5 h at pH > 9.5. The concentration of borate buffer (0.05–0.30 mol l^{-1}) did not affect the labelling reaction. When a phosphate buffer (0.1 mol l^{-1}, pH 8.5) or a carbonate buffer (0.1 mol l^{-1}, pH 8.5) was used instead of borate buffer, similar results were obtained.

The reaction time was examined at various temperatures (20, 30, 50 and 70 °C). The labelling reactions of Hyp, Pro and the IS with DPS-Cl were complete within 5 min regardless of the temperature.

The efficiencies of conversion of Hyp and Pro into the fluorescent derivatives were examined by comparing the peak heights under the analytical conditions with those of the prepared DPS derivatives of Hyp and Pro. The extents of conversion (mean, $n = 5$) were 99.1% for Hyp and 98% for Pro.

Concentration of DPS-Cl

The concentration of DPS-Cl in acetone was determined by use of serum spiked with Hyp and Pro at concentrations of 40 and 500 µmol l^{-1}, respectively. The most intense and constant peak heights were obtained when a concentration of the reagent solution of more than 0.6 mmol l^{-1} was used. Therefore, 1.2 mmol l^{-1} of DPS-Cl in acetone was employed in the present procedure.

Effect of OPA Treatment

It is known that primary amino compounds in serum are eliminated by reaction with some aldehydes such as OPA[4,12,14,19] and formaldehyde.[11] When the labelling reactions of Hyp and Pro with DPS-Cl were carried out in the presence of 25 amino acids (L-alanine, γ-aminolactic acid, ε-aminocaproic acid, L-arginine, L-asparagine, L-aspartic acid, L-citruline, L-cysteine, L-cystine, L-glutamic acid, L-glutamine, glycine, L-histidine, L-homoserine, L-isoleucine, L-leucine, L-lysine, L-methionine, L-ornithine, L-phenylalanine, L-threonine, L-tryptophan, L-tyrosine, L-valine and L-serine, 500 µmol l^{-1} each), a complicated chromatogram was obtained although the peaks of Hyp and Pro were separated from those of other amino acids, as shown in Fig. 5. However, when samples were treated with OPA at a concentration of more than 2% prior to the labelling reaction, the peaks due to primary amino acids disappeared completely. Incidentally, OPA treatment did not affect the labelling reaction of Hyp and Pro with DPS-Cl.
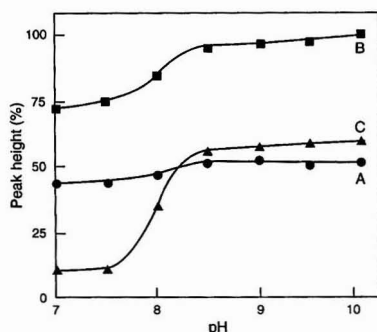
Precision and Recoveries

When the precision was calculated from peak height and peak area using a standard solution of Hyp and Pro (10 and 200 µmol l^{-1}, respectively), the relative standard deviations ($n = 8$) for peak-height measurement were 7.4 and 3.9%, respectively, and those for peak-area measurement were 1.9 and 2.6%, respectively. These results suggest that free Hyp and Pro in serum can be determined with a high accuracy by peak-area measurement. The within-day and day-to-day precisions were also tested using sera from normal subjects and patients with chronic renal failure by peak-area measurement. The within-day precision was examined with ten replicate assays in one day and the day-to-day precision by assays on five different days. As shown in Table 1, the within-day and day-to-day relative standard deviations (s_r) were 1.31–2.16% and 2.22–2.75%, respectively, for Hyp and 1.47–2.30% and 2.37–3.25%, respectively, for Pro.

Recovery tests were carried out by the use of IS solutions containing Hyp and Pro (50 pmol and 1.5 nmol, respectively, and 200 pmol and 3.0 nmol, respectively) added to a serum (Hyp, 13.9 µmol l^{-1}; Pro, 185.7 µmol l^{-1}). The recoveries (mean ± s, $n = 3$) were 96.9 ± 3.44% (50 pmol) and 98.0 ± 0.10% (200 pmol) for Hyp and 99.1 ± 0.72% (1.5 nmol) and 98.6 ± 2.03% (3.0 nmol) for Pro.
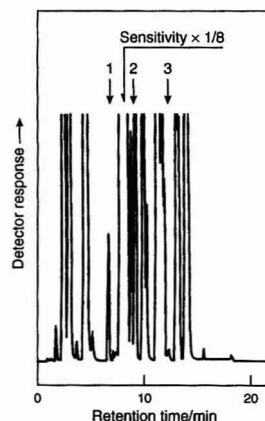

Fig. 5 HPLC trace obtained from a standard solution containing 25 amino acids (500 µmol l^{-1} each) according to the analytical procedure without OPA treatment. Peaks: 1, Hyp; 2, Pro; and 3, IS.

Table 1 Precision of determination of free Hyp and Pro in human sera

	Within-day* ($n = 10$)		Day-to-day† ($n = 5$)	
	Mean ± s/ µmol l^{-1}	s_r (%)	Mean ± s/ µmol l^{-1}	s_r (%)
Normal serum—				
Serum 1:				
Hyp	5.4 ± 0.09	1.67	5.4 ± 0.12	2.22
Pro	182.9 ± 2.68	1.47	185.2 ± 4.75	2.56
Serum 2:				
Hyp	13.0 ± 0.17	1.31	13.1 ± 0.36	2.75
Pro	177.7 ± 3.13	1.76	176.2 ± 5.73	3.25
Chronic renal failure serum—				
Hyp	25.9 ± 0.56	2.16	25.7 ± 0.65	2.53
Pro	357.3 ± 8.21	2.30	359.9 ± 8.54	2.37

* Within-day precision tested on ten replicate assays in one day.
† Day-to-day precision tested on five different days.

Fig. 4 Effect of pH of borate buffer (0.1 mol l^{-1}) on the labelling reactions of A, Hyp; B, Pro and; C, IS with DPS-Cl.

Linearities and Detection Limits

Linearity was studied over wide ranges of concentrations of Hyp and Pro (between 0.1 μmol l^{-1} and 1 mmol l^{-1} each). The peak-area ratios of Hyp and Pro to the IS (y) were linear in the concentration ranges (x) investigated. The regression equations at concentrations between 1 and 100 μmol l^{-1} for Hyp and between 10 μmol l^{-1} and 1 mmol l^{-1} for Pro were $y = 9.89 \times 10^{-3} x + 0.69 \times 10^{-3}$ ($r = 0.9999$) and $y = 7.92 \times 10^{-3} x + 1.41 \times 10^{-3}$ ($r = 0.9999$), respectively. The detection limits (signal-to-noise ratio = 3) of both Hyp and Pro were 10 fmol per injection.

Determination of Free Hyp and Pro in Human Serum

The concentrations of free Hyp and Pro in sera from thirteen normal subjects and five patients with chronic renal failure measured by the present method are given in Table 2. The mean values for normal sera (9.5 ± 3.58 μmol l^{-1} for Hyp and 200.0 ± 33.26 μmol l^{-1} for Pro) agreed with those reported previously.[7,12] Although the samples measured were small in number, the mean values of Hyp and Pro in sera from chronic renal failure patients (24.0 ± 6.53 and 328.1 ± 106.09

μmol l^{-1}, respectively) were about 2.6 and 1.6 times higher, respectively, than those in normal sera.

Conclusion

The newly designed reagent DPS-Cl is highly sensitive and suitable for the determination of Hyp and Pro in small amounts of serum by HPLC with fluorescence detection. The proposed HPLC method should be useful for physiological and biomedical studies of Hyp and Pro.

Table 2 Concentrations of free Hyp and Pro in normal serum and chronic renal failure serum

	Age (yr)	Sex*	Cre†/ mg l^{-1}	Hyp/ μmol l^{-1}	Pro/ μmol l^{-1}
Normal serum—					
1	22	M	10.9	10.4	170.8
2	22	M	10.2	13.3	202.1
3	22	M	7.8	8.3	232.3
4	23	M	8.7	13.5	164.5
5	43	M	10.7	18.0	245.4
6	21	F	8.5	5.6	188.1
7	21	F	7.3	6.4	194.9
8	22	F	7.3	7.7	196.5
9	22	F	7.6	7.1	252.6
10	23	F	7.6	6.8	204.1
11	23	F	7.6	10.3	187.3
12	23	F	7.6	6.8	232.3
13	23	F	6.9	9.0	137.6
Mean				9.5	200.7
s				3.58	33.26
Chronic renal failure serum—					
1	40	M	62.0	20.7	459.0
2	65	M	69.9	17.5	295.1
3	73	M	62.8	21.3	351.0
4	77	M	66.3	26.5	365.1
5	60	F	61.8	34.2	170.3
Mean				24.0	328.1
s				6.53	106.09

* M = male; F = female.
† Cre = serum creatinine, measured with the Creatinine Test Wako.

References

1 Kontturi, M. J., Sotaniemi, E. A., and Larmi, T. K. I., *Scand. J. Urol. Nephrol.*, 1974, **8**, 91.
2 Powles, T. J., Rosset, G., Leese, C. L., and Bondy, P. K., *Cancer*, 1976, **38**, 2564.
3 Dubovský, J., Dubovská, E., Pacovský, V., and Hrba, J., *Clin. Chim. Acta*, 1967, **19**, 387.
4 Kataoka, H., Nabeshima, N., Nagao, K., and Makita, M., *Clin. Chim. Acta*, 1993, **214**, 13.
5 Böhlen, P., and Mellet, M., *Anal. Biochem.*, 1979, **94**, 313.
6 Nakazawa, K., Tanaka, H., and Arima, M., *J. Chromatogr.*, 1982, **233**, 313.
7 Tanaka, H., Nakazawa, K., Arima, M., Morooka, K., Suzuki, F., Aoki, T., and Kohno, Y., *Brain Dev.*, 1983, **5**, 450.
8 Roth, M., *Clin. Chim. Acta*, 1978, **83**, 273.
9 Stratford, M. R. L., Watfa, R. R., Murray, J. C., and Martin, S. G., *J. Chromatogr.*, 1990, **526**, 383.
10 Ikeda, M., Sorimachi, K., Akimoto, K., and Yasumura, Y., *J. Chromatogr.*, 1993, **621**, 133.
11 Tsuchiya, H., Hayashi, T., Tatsumi, M., Fukita, T., and Takagi, N., *J. Chromatogr.*, 1985, **339**, 59.
12 Palmerini, C. A., Fini, C., Floridi, A., Morelli, A., and Vedovelli, A., *J. Chromatogr.*, 1985, **339**, 285.
13 Sessa, W. C., Jr., Rodgers, R. L., and Chichester, C. O., *J. Chromatogr.*, 1986, **382**, 258.
14 Nathans, G. R., and Gere, D. R., *Anal. Biochem.*, 1992, **202**, 262.
15 Bhattacharjee, D., and Popp, F. D., *J. Pharm. Sci.*, 1980, **69**, 120.
16 Tsuruta, Y., Date, Y., Tonogaito, H., Sugihara, N., Furuno, K., and Kohashi, K., *Analyst*, 1994, **119**, 1047.
17 Tsuruta, Y., Teranishi, T., Date, Y., and Kohashi, K., *J. Chromatogr.*, 1993, **617**, 213.
18 Tsuruta, Y., Moritani, K., Date, Y., and Kohashi, K., *Anal. Sci.*, 1992, **8**, 393.
19 Bellon, G., Malgras, A., Randoux, A., and Borel, J. P., *J. Chromatogr.*, 1983, **278**, 167.

High-performance Liquid Chromatography with Post-column Chemiluminescence Detection for Simultaneous Determination of Trace *N*-Nitrosamines and Corresponding Secondary Amines in Groundwater

Cheng-Guang Fu and Hong-Da Xu

Research Centre of Physical and Chemical Analysis, Hebei University, Baoding 071002, China

A sensitive, selective and reliable high-performance liquid chromatographic method with chemiluminescence detection is described for the determination of trace *N*-nitrosamines and corresponding secondary amines simultaneously in environmental water samples. The method combines solid-phase extraction on to a mini activated carbon column, followed by elution with acetone and concentration of the extracts by denitrosation and fluorogenic derivatization. The separation of derivatives was performed on a C_{18} column (3μm, 83×4.6 mm id) with a mobile phase consisting of acetonitrile–water–ethanol ($63.5 + 35.5 + 1.0$ v/v) containing 3.0 mmol l^{-1} imidazole and 0.5 mmol l^{-1} oxalic acid and with a pH of 6.2. Peroxyoxalate chemiluminescence detection was carried out by using bis(2-nitrophenyl) oxalate and hydrogen peroxide as chemilumigenic reagents. The quantitative data obtained (calibration graphs, detection limits, *etc.*) were analogous to those published previously. Groundwater samples were analysed using the proposed method. Data including the total amounts of secondary amines plus *N*-nitrosamines, the amount of secondary amines and results of blank experiments from the chromatograms for individual water sample were calculated, then the final concentrations of *N*-nitrosamines and secondary amines in each water sample were obtained simultaneously. The application of this procedure for determination of *N*-nitrosamines and corresponding secondary amines in water samples at pmol l^{-1} and fmol l^{-1} levels was successfully achieved. The recoveries of various *N*-nitrosamines and secondary amines added to groundwater samples were excellent ($\geqslant 95\%$ for all except two).

Keywords: High-performance liquid chromatography; chemiluminescence detection; nitrosamines; secondary amines; groundwater

Introduction

In recent years, there has been great interest in improving the analytical sensitivity and selectivity for the determination of trace amounts of *N*-nitrosamines and their parent compounds in environmental samples. In this respect, gas chromatography combined with a thermal energy analyser (TEA) provides a highly selective and sensitive method for trace amounts of *N*-nitrosamines,[1] but their sensitivity obtained with the TEA combined with high-performance liquid chromatography (HPLC) was more than two orders of magnitude lower.[2] These results showed that the TEA cannot be operated with the reversed-phase materials and inorganic buffer solutions used for HPLC. On the other hand, routine HPLC with UV detection provides detection limits that are only at nanogram levels for *N*-nitrosamines. For *N*-nitrosam-

ines, a more sensitive detection method using HPLC is needed.

There are two pre-column fluorescent derivatization techniques for the determination of trace amounts of *N*-nitrosamines and secondary amines that might provide a sensitive method. These derivatizations convert the nitrosamines and secondary amines into fluorogenic derivatives that can be determined by HPLC with fluorescence detection.[3–6] Peroxyoxalate chemiluminescence detection has been shown to be a highly sensitive detection method[7–9] in combination with reversed-phase HPLC for determination of *N*-nitrosamines and secondary amines[10,11] in our laboratory; the detection limits were at the femtomole level.

In this paper, a method for the simultaneous determination of *N*-nitrosamines and corresponding secondary amines in environmental water samples is described. A mini activated carbon column[12] was used for the solid-phase extraction of *N*-nitrosamines and secondary amines from groundwater samples, and with reversed-phase HPLC combined with bis(2-nitrophenyl)oxalate chemiluminescence detection allowed determinations at pmol l^{-1} or fmol l^{-1} levels. The sensitivity, precision, linearity and recovery of the method were satisfactory. The pre-column fluorigenic derivatization and peroxyoxalate chemiluminescence reactions are illustrated.

The proposed method was applied to the simultaneous determination of six *N*-nitrosamines and corresponding secondary amines in groundwater samples. It has been routinely used in our laboratory and may be suitable for application in the life sciences and cancer research.

Experimental

Reagents

Dimethylamine (DMA), pyrrolidine (Py), diethylamine (DEA), piperidine (Pip), dipropylamine (DPA) and dibutylamine (DBA) were obtained from Beijing Chemical Works (Beijing, China). Nitrosodimethylamine (NDMA), nitrosopyrrolidine (NPy), nitrosodiethylamine (NDEA), nitrosopiperidine (NPip), nitrosodipropylamine (NDPA) and nitrosodibutylamine (NDBA) were prepared and purified by a conventional procedure as described previously[13] and were identified by mass spectrometry. Bis(2-nitrophenyl) oxalate (2-NPO) was synthesized by a published method[14] and was further purified by washing with trichloromethane and recrystallization from ethyl acetate and identified by mass spectrometry. Hydrogen peroxide (30%), acetone, acetonitrile, dichloromethane, hydrobromic acid, acetic anhydride, ethyl acetate, imidazole, oxalic acid, sodium hydrogencarbonate and hydrochloric acid (all of analytical-reagent grade) were

obtained from Beijing Chemical Works and all reagents were used as received. Dansyl chloride (puriss.) was obtained from Fluka (Buchs, Switzerland). Triply distilled water was prepared in the laboratory.

Stock standard solutions of secondary amines and nitrosamines were prepared by dissolving six secondary amines in 0.01 mol l^{-1} hydrochloric acid and six nitrosamines in dichloromethane and diluting to a concentration of 10^{-6} mol l^{-1}.

A 10^{-5} mol l^{-1} dansyl chloride solution in acetone was prepared. A 10 mmol l^{-1} 2-NPO stock standard solution was prepared by dissolution in ethyl acetate. A hydrogen peroxide stock standard solution in ethyl acetate was prepared at a concentration of 3000 mmol l^{-1}. Hydrobromic acid–acetic anhydride solution was prepared by dissolving 1 ml of hydrobromic acid in 4 ml of acetic anhydride (1 : 4 v/v). Sodium hydrogencarbonate solution (0.25 mol l^{-1}) and hydrochloric acid solutions (0.01 and 0.1 mol l^{-1}) were prepared in triply distilled water.

Apparatus

The analytical system consisted of a Model 114M eluent-delivery pump (Beckman, Fullerton, CA, USA), a Model

E-120-S-2 reagent-delivery pump for chemiluminogenic solution (Eldex, San Carlos, CA, USA), a C$_{18}$ 3 µm analytical column (83 × 4.6 mm id) (Perkin-Elmer, Norwalk, CT, USA) and a Model 7125 injection valve with 20 µl loops (Rheodyne, Cotati, CA, USA). The mixing device and the chemiluminescence detector was made in our laboratory[10] and a chart recorder was used.

Chromatographic Conditions

All analyses were carried out isocratically on a 3 µm reversed-phase C$_{18}$ column with a mobile phase consisting of acetonitrile–water–ethanol (63.5 + 35.5 + 1.0 v/v), containing imidazole (3.0 mmol l^{-1}) as catalyst, the pH being adjusted to 6.2 with oxalic acid, and delivered at a flow rate of 0.4 ml min^{-1}. The chemilumigenic reagent solution contained 3.0 mmol l^{-1} 2-NPO and 10.0 mmol l^{-1} hydrogen peroxide in acetone–ethyl acetate solvent and was supplied at a flow rate of 100 µl min^{-1}.

Solid-phase Extraction and Elution

The water samples were adjusted to pH 7.0 with 0.1 mol l^{-1} hydrochloric acid, then the samples (100 ml) were passed
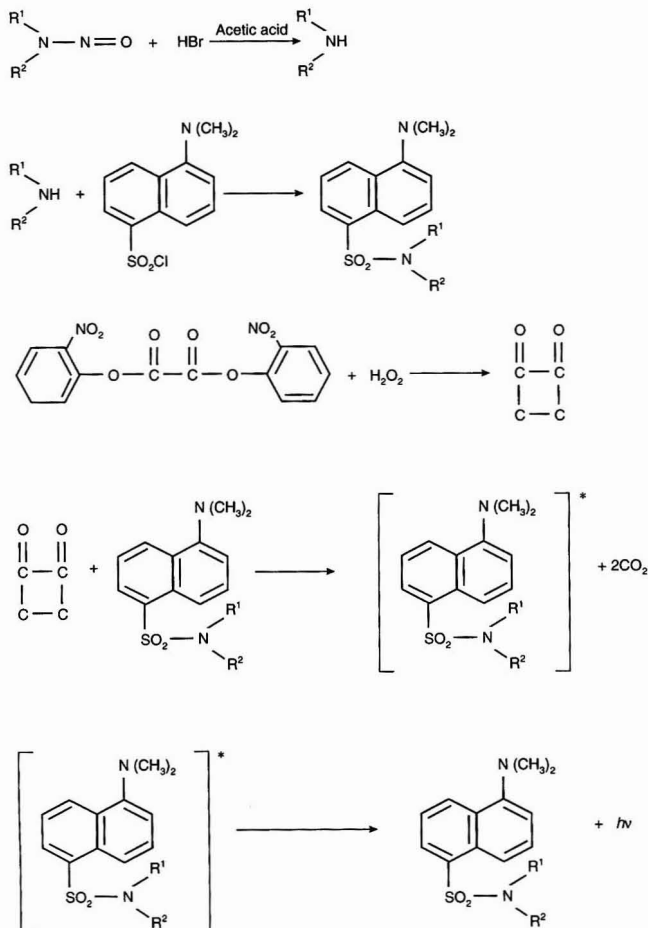
through a mini activated carbon column[12] (100–120 mesh, 20 × 1.2 mm id) by a sweep pump at a flow rate of 0.5 ml min⁻¹. The mini column used for solid extraction was used once only. When this step was finished, the activated carbon mini column was eluted with 1.0 ml of acetone and the eluate was collected in a 2 ml stoppered graduated test-tube, shaken, then divided into two equal parts and evaporated to dryness in a stream of dry nitrogen. One part of the dry residue was used for the measurement of secondary amines and the other for the determination of total amounts of nitrosamines and secondary amines. Blank tests were also carried out at the same time.

Fluorogenic Derivatization

To one part of the residue were added 20 µl of hydrobromic acid–acetic anhydride solution for denitrosation and the mixture was allowed to stand in the dark for 10 min at 70 °C. The mixture was then evaporated to dryness in a stream of nitrogen for determination of the total amounts of nitrosamines and secondary amines. The other part of the residue and a blank sample were analysed without denitrosation to provide measurements of the secondary amines in the sample and blank. After the above treatment, all the test-tubes for each water sample were treated simultaneously with the subsequent procedures.

The fluorogenic derivatization was performed as follows: 100 µl of 0.25 mol l⁻¹ sodium hydrogencarbonate solution and 100 µl of dansyl chloride solution were added to each graduated test-tube and the tubes stopped and shaken. The mixture was allowed to stand for 30 min at 40 °C and then was diluted with mobile phase to 1.0 ml for HPLC analysis.

Results and Discussion

Analytical Conditions

The proposed method for the determination of trace amounts of nitrosamines and secondary amines in groundwater involves a pre-treatment procedure consisting of solid-phase extraction, denitrosation and fluorogenic derivatization. The subsequent reversed-phase HPLC separation and post-column chemiluminescence detection mostly used methods published previously,[10,11] but some of the analytical conditions were re-optimized by examining the variables, such as the composition of the mobile phase. The mobile phase composition was varied slightly such that only 1% of ethanol

was added and the flow rate was decreased to 0.4 ml min⁻¹; all other conditions were as reported previously.[10,11] As a result of the modifications, lower background or chemical noise and more reproducible results than in the former experiments were obtained. Fig. 1 shows the chromatograms of (*a*) standard mixtures of six nitrosamines plus secondary amines, (*b*) standard mixtures of six secondary amines and (*c*) a blank sample.

In order to verify the linearity of the chemiluminescence detection response with respect to the concentrations of each nitrosamine and secondary amine, a series of standard solutions were treated according to the proposed procedures and injected into the HPLC–chemiluminescence detection system. The relationships between the peak heights and the amounts of each nitrosamine and secondary amine were evaluated over the range 0.05–20.00 pmol and linear least-squares regression was used to calculate the slope, intercept, correlation coefficient, detection limits and reproducibility (Table 1). These results were equivalent to or (in a few instances) better than those in our previous work.[10,11]
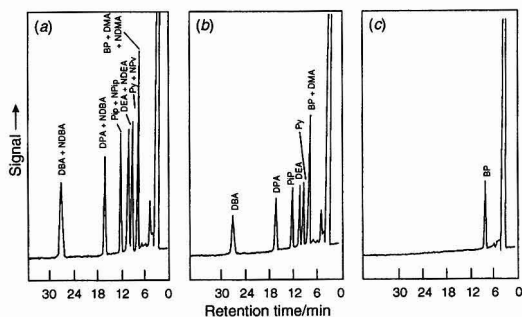

Fig. 1 Separation of (*a*) standard mixtures of six nitrosamines plus corresponding secondary amines, (*b*) standard mixtures of six secondary amines and (*c*) blank sample treated in the same way. Analytical column, Perkin-Elmer HS3 C₁₈ (83 × 4.6 mm id); mobile phase, acetonitrile–water–ethanol (63.5 + 35.5 + 1.0 v/v) containing 0.5 mmol l⁻¹ oxalic acid and 3.0 mmol l⁻¹ imidazole at pH 6.2 (flow rate, 0.4 ml min⁻¹); chemiluminogenic reagent solution, containing 3.0 mmol l⁻¹ 2-NPO and 10.0 mmol l⁻¹ H₂O₂ (flow rate, 100 µl min⁻¹). BP, Blank peak; for other abbreviations, see text.

Table 1 Linearity, detection limit and reproducibility of the proposed method

Compound	Slope	Intercept/mm	Correlation coefficient	Detection limit/fmol	Relative standard deviation (%)*
Nitrosamines—					
NDMA	0.52	1.4	0.999	4.3	3.6
NPy	0.54	2.8	0.999	4.4	3.3
NDEA	0.47	4.1	0.999	4.6	6.3
NPiP	0.48	3.0	0.999	5.0	1.9
NDPA	0.41	3.5	0.999	6.2	3.3
NDBA	0.31	0.8	0.999	8.3	4.7
Secondary amines—					
DMA	0.55	−1.7	0.999	4.8	3.9
Py	0.51	0.8	0.999	4.6	3.1
DEA	0.45	−0.2	0.999	4.8	7.1
Pip	0.45	0.1	0.999	4.9	2.6
DPA	0.35	0.4	0.999	5.6	2.9
DBA	0.30	0.3	0.999	7.3	3.9

* Results are means for seven standard mixtures subjected to the whole analytical method.
† The range of linearity is the same, 0.05–20.00 pmol, for each nitrosamine and secondary amine, and data were obtained from a seven-level calibration.

Blank Experiments

Triply distilled water (100 ml) was subjected to the proposed procedure with reversed-phase HPLC–chemiluminescence detection; a chromatogram of a blank of water sample was obtained [Fig. 2(*a*)] for verification of over-all analytical method. A small peak of constant height was obtained at a retention time corresponding to dansylnitrosodimethylamine and a trace peak eluting at a retention time close to that of dansylnitrosodiethylamine. These peaks in the blank extract were obtained each time when five serial analytical experiments were performed, so a stable and repeatable chromatogram was presented. It is probable that the peaks in the blank were produced by impurities in the reagents used in the analytical procedures.

Groundwater Analysis

When an environmental water sample such as groundwater (100 ml) was subjected to solid-phase extraction and elution, half of the residue of the extract was used without denitrosation for detection of secondary amines after fluorogenic derivatization, and a typical chromatogram is given in Fig. 2(*b*). It was observed that the peaks obtained were produced from trace amounts of secondary amines in groundwater. The other half of the residue was used with denitrosation for

measurement of the total amounts of nitrosamines plus secondary amines after fluorogenic derivatization, and a typical chromatogram is given in Fig. 2(*c*).

The peak height of the blank results in Fig. 2(*a*) were subtracted from the peak height that corresponded to the appropriate secondary amine results in Fig. 2(*b*) and the total amounts of nitrosamines plus secondary amines in Fig. 2(*c*). This permitted the accurate calculation of the results for secondary amines and the total amounts of nitrosamines plus secondary amines, respectively. The secondary amine results [Fig. 2(*b*)] were subtracted from the total amounts [Fig. 2(*c*)] to provide a value for the levels of nitrosamines present in the groundwater samples. Hence the procedures described in this paper are suitable for the determination of both nitrosamines and corresponding secondary amines.

Possible interferences in the analysis of groundwater samples were studied and were found to be minimal. The sole example of interference is an unknown peak observed in each chromatogram of the analysed water samples, such as the unknown peak in the chromatogram in Fig. 2, from which the neighbouring peak was well separated. The changes in the unknown peak height confirmed that the proposed method possessed good selectivity for the peaks of other compounds; *e.g.*, considering Fig. 2(*b*) and (*c*), the peak height of the unknown in Fig. 2(*c*) (nitrosamines plus secondary amines) is smaller than the peak height of the unknown in Fig. 2(*b*) (secondary amines), indicating that the unknown peak is neither a nitrosamine nor a secondary amine.
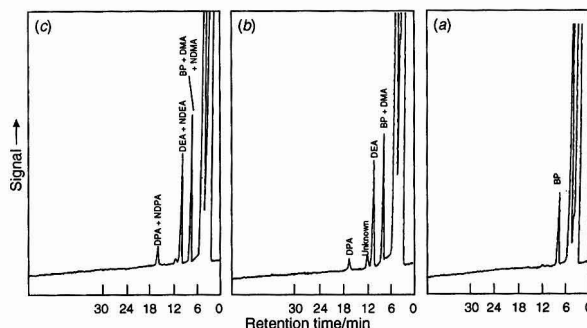

Fig. 2 Chromatograms obtained from (*a*) blank sample, (*b*) groundwater sample determining secondary amines and (*c*) for determining *N*-nitrosamines plus corresponding secondary amines. Chromatographic conditions as Fig. 1. BP, Blank peak; for other abbreviations, see text.

Table 2 Recoveries of nitrosamines and corresponding secondary amines from groundwater

| Compound | 1 | Recovery (%) | | | | Mean recovery (%) | Relative standard deviation (%) |
		2	3	4	5		
Nitrosamines—							
NDMA	78.5	77.5	74.0	75.1	76.4	76.3	2.4
NPy	97.5	101.9	99.8	100.6	96.5	99.3	2.2
NDEA	97.3	101.0	103.1	99.0	95.7	99.2	3.0
NPip	94.2	98.5	97.8	95.2	99.0	96.9	2.2
NDPA	98.0	99.8	101.2	97.7	100.6	99.5	1.6
NDBA	94.6	92.5	93.8	96.0	92.5	93.9	1.6
Secondary amines—							
DMA	100.5	97.0	99.6	102.4	100.7	100.0	2.0
Py	97.2	98.4	99.5	99.8	101.4	99.3	1.6
DEA	94.0	93.2	98.2	95.6	99.7	96.1	2.9
Pip	101.8	96.4	98.4	101.6	97.5	99.1	2.5
DPA	97.5	93.3	96.2	98.0	94.1	95.8	2.2
DBA	95.8	98.8	92.4	95.2	96.2	95.7	2.4

* The same amount of standard, 100 pmol, for each nitrosamine and secondary amine was added to each groundwater sample.

Table 3 Results of the simultaneous determination of nitrosamines and corresponding secondary amines in groundwater*

Compound	Sample no.					
	1	2	3	4	5	6
Nitrosamines—						
NDMA/pmol l^{-1}	—†	12.15	—	—	4.34	16.65
s_r (%)	—	2.1	—	—	1.1	1.6
NPy/pmol l^{-1}	—	—	—	—	—	—
s_r (%)	—	—	—	—	—	—
NDEA/pmol l^{-1}	54.45	39.32	22.18	26.56	—	3.37
s_r (%)	2.1	1.3	2.5	2.1	—	1.2
NPip/pmol l^{-1}	—	—	—	—	—	—
s_r (%)	—	—	—	—	—	—
NDPA/pmol l^{-1}	12.65	44.99	8.36	7.29	—	6.97
s_r (%)	1.1	1.2	1.0	1.1	—	1.2
NDBA/pmol l^{-1}	—	—	—	—	—	—
s_r (%)	—	—	—	—	—	—
Secondary amines—						
DMA/pmol l^{-1}	—	37.18	—	5.02	10.05	16.65
s_r (%)	—	1.3	—	1.4	1.2	1.6
Py/pmol l^{-1}	—	—	—	—	—	—
s_r (%)	—	—	—	—	—	—
DEA/pmol l^{-1}	16.51	36.24	51.36	27.32	—	52.56
s_r (%)	1.3	1.1	1.1	1.3	—	1.3
Pip/pmol l^{-1}	—	—	—	—	—	—
s_r (%)	—	—	—	—	—	—
DPA/pmol l^{-1}	6.09	20.87	17.4	8.71	8.74	11.76
s_r (%)	1.1	1.3	1.2	1.2	1.3	1.4
DBA/pmol l^{-1}	—	—	—	—	—	—
s_r (%)	—	—	—	—	—	—

* Results are means for five water samples subjected to the whole analytical method.
† Dashes indicate not detected.

Recovery of Nitrosamines and Secondary Amines From Groundwater

Simultaneous recovery studies were performed by adding known amounts of standards to groundwater samples. A synthetic standard mixture containing 100 pmol of each nitrosamine and secondary amine was added to 100 ml of fresh groundwater and the pH was adjusted to 7.0 with hydrochloric acid followed by five replicate analyses using the procedures described above. A blank experiment was also carried out. The recoveries of the various nitrosamines and corresponding secondary amines from the groundwater samples are given in Table 2.

The recoveries of individual compounds were 95% in all except two instances. These results show that the recoveries of trace amounts of nitrosamines and secondary amines in environmental water samples with the proposed method were satisfactory.

Application to Environmental Water Analysis

Some groundwater samples from an aquifer in Hebei Province were analysed using the proposed procedure and the results are given in Table 3.

These data for the average concentrations of all nitrosamines and corresponding secondary amines in groundwater obtained with five replicate analyses suggest that the proposed method is well suited for the simultaneous determination of these compounds in environmental water samples at the pmol l^{-1} or fmol l^{-1} level.

Conclusion

A sensitive, selective and reliable method has been developed for the simultaneous determination of six nitrosamines and corresponding secondary amines in environmental water samples. This method has been routinely used in our laboratory and could be extended for use in the life sciences and cancer research.

References

1 Oetinger, P. E., Huffman, F., Fine, D. H., and Lieb, D., *Anal. Lett.*, 1973, **6**, 731.
2 Baker, J. K., and Ma, C. Y., *IARC (Int. Agency Res. Cancer) Sci. Publ.*, 1978, No. 19, 19.
3 Wang, Z., and Fu, G. C., *Chin. J. Chromatogr.*, 1990, **8**, 325.
4 Wang, Z., Xu, H. D., and Fu, C. G., *J. Chromatogr.*, 1992, **589**, 394.
5 Zheng, M. H., Xu, H. D., and Fu, C. G., *Chin. J. Chromatogr.*, 1992, **10**, 164.
6 Zheng, M. H., Fu, C. G., and Xu, H. D., *Analyst*, 1993, **118**, 296.
7 Imai, K., Nishitani, A., and Tsukamoto, Y., *Chromatographia*, 1987, **24**, 77.
8 Kobayashi, K., and Imai, K., *Anal. Chem.*, 1980, **52**, 424.
9 Imai, K., and Wienberger, R., *Trends Anal. Chem.*, 1985, **4**, 170.
10 Fu, C. G., Xu, H. D., and Wang, Z., *J. Chromatogr.*, 1993, **634**, 221.
11 Fu, C. G., Xu, H. D., and Wang, Z., *Fenxi Ceshi Xuebao*, 1994, **13**(1), 28.
12 Fu, C. G., and Wan, Q. H., *Chin. J. Anal. Chem.*, 1985, **13**, 595.
13 Hwo, L. M., and Ma, L. S., *Analytical Methods for N-Nitroso Compounds*, Science Publishers, Beijing, 1980.
14 Mohan, A. G., and Turro, N., *J. Chem. Educ.*, 1974, **51**, 528.

Fractionation of an Antiserum to Progesterone by Affinity Chromatography: Effect of pH, Solvents and Biospecific Adsorbents

Cornelia Parini, Maria A. Bacigalupo and Stefano Colombi

Istituto di Chimica degli Ormoni–CNR, Via Mario Bianco 9, 20131 Milan, Italy

Nadia Corocher, Claudio Baggiani and Gianfranco Giraudi*

Dipartimento di Chimica Analitica, Università di Torino, Via Pietro Giuria 5, 10125 Turin, Italy

Several progesterone–AH Sepharose 4B matrices were prepared as biospecific adsorbents suitable for affinity chromatography to fractionate antibodies of different affinity and specificity from a polyclonal antiserum to progesterone-11α-hemisuccinate–BSA. From an affinity column of progesterone-11α-hemisuccinate–AH Sepharose 4B no antibodies can be eluted, even with glycine buffer (pH 2.6) and 30% of 2-methoxyethanol. The use of biospecific adsorbents, prepared by coupling with AH Sepharose 4B progesterone derivatives [5-pregnene-3,20-dione di(ethyleneacetal)-11α-ol-11α-hemisuccinate; 4-pregnene-11,20β-diol-3-one-11α-hemisuccinate 20β-benzoate; progesterone-3-carboxymethyloxime] having a low cross-reactivity with the antiserum, makes the elution of various antibody fractions of variable affinity and specificity possible. 2-Methoxyethanol or *N,N*-dimethylformamide gradients, in acetate or TRIS buffer, were equally efficient for fractionating the antiprogesterone serum, while a decreasing pH gradient was less effective and eluted antibody fractions that were further separated into various binding components by a solvent gradient. Antibodies eluted from the affinity columns by an eluent containing a high solvent concentration have affinities higher than antibodies eluted at lower solvent concentration.

Keywords: *Progesterone; affinity chromatography; biospecific adsorbent; cross-reaction; affinity constant*

Introduction

Polyclonal antisera to steroid hormones are still widely used in immunoassay owing to their generally high affinity and good specificity. In spite of this, the need for a low detection limit and/or greater specificity stimulated research into the fractionation of antisera by affinity chromatography to obtain antibodies of improved affinity[1,2] and/or specificity.[2,3] However, the high affinity of the interaction between the immobilized ligand and the antibody molecules makes the elution of bound antibodies difficult.[4]

The problem of eluting high-affinity antibodies to steroid hormones has been tackled in various ways. The most common desorption methods involved solvent gradients combined with acidic buffers,[4,5] an eluent containing the steroid[1] and electrophoresis.[1,4,6] All the methods reported can be considered as adsorption and desorption methods rather than chromatographic methods. Their drawbacks derive

mainly from a very low dissociation rate for the immobilized ligand–antibody complexes resulting from the high affinity for the specific immunoglobulins to be purified[4] for the stationary phase.

A true chromatographic procedure to elute antibodies to steroid hormones using a steroid–Sepharose stationary phase was reported by Lewis and Elder.[2] They were able to elute antibodies of improved affinity and specificity to cortisol from a column of cortisol–AH Sepharose 4B with a pH gradient containing 20% acetonitrile, and the eluted antibodies showed affinities that increased with decreasing pH. This successful separation seems to be due to the choice of a stationary phase bearing cortisol-21-acetate as a ligand with an affinity lower than that of cortisol, together with a further inhibition of the steroid–antibody interaction caused by a combination of organic solvent and acidic pH during elution.

As the rapid dissociation of a ligand–antibody complex is generally associated with a low affinity,[7] the condition for a chromatographic separation of antibodies by means of biospecific adsorbents requires a lowering of the antibody–stationary phase interaction to a suitable value during elution. This condition can even be fulfilled by derivatizing the solid phase with a low-affinity ligand, while retaining the ability to bind antibodies effectively during the loading and washing steps.

In order to develop a systematic approach to the fractionation of antibodies to steroid hormones, the effects of the structure of the biospecific adsorbent and the composition of the eluent were investigated by using the affinity chromatography of a high-affinity antiserum to progesterone as a model system.

Experimental

Materials

Progesterone (pregn-4-ene-3,20-dione), 11α-hydroxyprogesterone (pregn-4-en-11α-ol-3,20-dione), 11β-hydroxyprogesterone (pregn-4-en-11β-ol-3,20-dione), progesterone-3-carboxymethyloxime (pregn-4-ene-3,20-dione-3-carboxymethyloxime), progesterone-11α-hemisuccinate (pregn-4-en-11α-ol-3,20-dione-11α-hemisuccinate), 17α-hydroxyprogesterone (pregn-4-en-17α-ol-3,20-dione), pregn-5-en-3β-ol-20-one, dicyclohexylcarbodiimide (DCCD), 1-ethyl-3-(3-dimethylaminopropyl)carbodiimide chloride (EDAC) and bovine serum albumin (BSA) (Cohn fraction V, electrophoretic purity >99%) were obtained from Sigma–Aldrich (Milan, Italy). Silica gel 60 $F_{254}S$ plates for analytical and preparative thin-layer chromatography, all organic solvents and chemicals for buffers were purchased from Merck (Darmstadt, Germany). The Coomassie Protein Assay kit (pre-diluted dye and albumin standards) was supplied by Pierce (Rockford, IL,

---

USA). Polystyrene microtitre plates were obtained from Nunc (Naperville, IL, USA). Triitated progesterone ([1,2,6,7-^{3}H]-progesterone), specific activity 70 Ci mmol^{-1}, was purchased from Amersham (Amersham, UK). Picofluor 30 scintillation fluid was supplied by Packard Instruments (Downers Grove, IL, USA). Goat anti-rabbit immunoglobulin G (IgG) (H + L chains)–alkaline phosphatase conjugate, diethanolamine buffer and sodium *p*-nitrophenyl phosphate tablets were obtained from Bio-Rad (Hercules, CA, USA). Pre-packed Sephadex G-25 gel filtration columns and the low-pressure chromatographic apparatus were supplied by Pharmacia–LKB (Brussels, Belgium). Infrared spectra were recorded on a Perkin-Elmer Model 781 instrument. All UV measurements were recorded on a Varian Cary 219 double-beam spectrophotometer. A microtitre plate washer and reader were obtained from Sorin Biomedica (Saluggia, Italy).

Synthesis of 11α-Hydroxyprogesterone 3,20-Diethyleneacetal

Pregn-5-en-11α-ol-3,20-dione diethyleneacetal was synthesized from 2.0 g of 11α-hydroxyprogesterone according to the procedure given by Yoshida *et al.*,[8] and purified by preparative thin-layer chromatography on silica gel [mobile phase, light petroleum–acetone (7 + 3 v/v)]. A crystalline product was obtained (1.5 g, 60% yield). A small amount of 11α-hydroxyprogesterone 3-ethyleneacetal (pregn-5-en-11α-ol-3,20-dione 3-ethyleneacetal) was also separated as a spot with a lower R_F value. Infrared data were C=O (20) 1720 cm^{-1}, OH 3420 cm^{-1}.

Synthesis of Progesterone-11α-hemisuccinate 3,20-Diethyleneacetal

Pregn-5-ene-3,20-dione   diethyleneacetal-11α-ol-11α-hemisuccinate was synthesized from 1.0 g of 11α-hydroxyprogesterone 3,20-diethyleneacetal, according to the procedure given by Allen and Redshaw[9] but with a longer time of reflux (21 h). A glassy product was obtained (0.68 g, 55% yield), proved pure by thin-layer chromatography on silica gel [mobile phase ethanol–chloroform (1 + 9 v/v)]. Infrared data were COOH 1720 cm^{-1}, OH (carboxylic) 3200 cm^{-1} (broad).

Synthesis of 20β-Hydroxyprogesterone-11α-hemisuccinate

Pregn-4-ene-11α,20β-diol-3-one-11α-hemisuccinate   was synthesized from 1.0 g of progesterone-11α-hemisuccinate by selective reduction of the ketone group at the 20-position with sodium tetrahydroborate according to a modification of the procedure given by Norymberski and Woods,[10] by reaction overnight at 0 °C. A glassy product was obtained (0.80 g, 80% yield), proved pure by thin-layer chromatography on silica gel [mobile phase, chloroform–ethanol (9 + 1 v/v)]. The product was used in the subsequent reactions without further purification.

Synthesis of Progesterone-11α-hemisuccinate 20β-Benzoate

Pregn-4-ene-11α,20β-diol-3-one-11α-hemisuccinate   20β-benzoate was synthesized from 0.24 g of 20β-hydroxyprogesterone-11α-hemisuccinate. The steroid was dissolved in 5 ml of dry pyridine and, with continuous stirring, 0.58 ml of benzoic anhydride was added. The mixture was refluxed under nitrogen for 4 h and, after concentration under vacuum, it was diluted with ethyl acetate and washed with 1 mol l^{-1} HCl and then with water. The organic solution was dried over sodium sulfate and concentrated under vacuum to a small volume. The residue was purified by preparative thin-layer chromatography on silica gel [mobile phase, chloroform–ethanol (9 + 1 v/v)], dissolved in ethyl acetate and extracted with 4% m/v

potassium hydroxide solution. The solution was acidified with 1 mol l^{-1} HCl and extracted again with ethyl acetate. The organic solution was washed with water, dried over sodium sulfate and evaporated to dryness under vacuum. The residue was washed with light petroleum, giving a solid product (0.15 g, 50% yield), proved pure by thin-layer chromatography on silica gel [mobile phase, chloroform–ethanol (9 + 1 v/v)]. Infrared data were COOH and benzoate 1730 cm^{-1} with a shoulder at 1700 cm^{-1}, aryl and C=C (4) 1615 cm^{-1}, C=O (3) 1670 cm^{-1}, OH (carboxylic) broad 3300–3000 cm^{-1}.

Synthesis of Progesterone-11α-hemisuccinate 20β-Acetate

Pregn-4-ene-11α,20β-diol-3-one-11α-hemisuccinate 20β-acetate was synthesized from 0.4 g of 20β-hydroxyprogesterone-11α-hemisuccinate in the same way as for the benzoate derivative, but using acetic anhydride and performing the reaction at room temperature overnight. A crystalline product was obtained (0.26 g, 60% yield), proved pure by thin-layer chromatography on silica gel [mobile phase, chloroform–ethanol (9 + 1 v/v), acidified with a drop of glacial acetic acid]. Infrared data were COOH and acetate 1720 cm^{-1}, C=O (3) 1645 cm^{-1}, C=C (4) 1615 cm^{-1}, OH (carboxylic) broad 3200–3000 cm^{-1}.

Antiserum

Rabbit polyclonal antiserum to progesterone-11α-hemisuccinate–BSA was kindly furnished by G. Bolelli, Servizio di Fisiopatologia della Riproduzione, Ospedale S. Orsola, Bologna, Italy. Antibodies to albumin were precipitated by adding BSA to crude serum. The globulin fraction of the antiserum was obtained after removal of albumin and proteolytic enzymes by dye affinity chromatography as described.[11] The titre of the globulin fraction of the antiserum (*i.e.*, the working dilution of antiserum in each test that binds 50% of 0.05 nmol l^{-1} tritiated progesterone, in the absence of standard progesterone) was 1 : 7500.

Cross-reactions

The progesterone derivatives suitable for coupling with the stationary phase were chosen on the basis of cross-reactions between progesterone and several structurally related steroids. To 0.1 ml of solution of steroid containing increasing concentrations from 1 to 10^4 mmol l^{-1} in PBS–gelatine (0.1 mol l^{-1} phosphate, 50 mmol l^{-1} NaCl, 1 mmol l^{-1} EDTA, 0.1% m/v sodium azide, 0.1% m/v gelatine, pH 7.4) in duplicate test-tubes were added 0.1 ml of 1.5 nmol l^{-1} tritiated progesterone in PBS–gelatine and 0.1 ml of the globulin fraction of antiserum, diluted 1 : 7500 with PBS–gelatine. The mixture was equilibrated overnight at room temperature. The bound–free separation was performed by adding 0.5 ml of an ice-cold suspension of dextran-coated charcoal (0.25% m/v charcoal, 0.025% m/v dextran in PBS) to all the tubes except those for total activity. All tubes were vortex mixed for a few seconds, incubated for 10 min in an ice-bath and centrifuged for 10 min at 2000*g* in a refrigerated centrifuge. A 0.5 ml volume of the supernatant from each tube was transferred into a vial, mixed with 4.5 ml of scintillation fluid and the radioactivity was counted in a β-counter. Non-specific binding (*i.e.*, the radioactivity not bound by charcoal without specific antiserum) was measured by replacing the globulin fraction with the buffer. The actual count rates due to the steroid–antibody complex were calculated from raw count rates, total activity, non-specific binding and radiochemical purity as described elsewhere.[12] Cross-reactions were calculated according to Abraham.[13]

Preparation of the Biospecific Adsorbent

Several stationary phases were prepared by reacting AH Sepharose 4B with progesterone-11α-hemisuccinate, progesterone-11α-hemisuccinate 3,20-diethyleneacetal, progesterone-11α-hemisuccinate 20β-benzoate and progesterone-3-(*O*-carboxymethyl)oxime by means of a general procedure for amino-functionalized solid phases.[14]

An aliquot of dry gel, washed with 1 mol l^{-1} NaCl, was suspended in a suitable volume of water–dioxane (1 + 1). A solution of DCCD in dioxane, 10 mg ml^{-1} of swollen gel, and a 40-fold defect of ligand dissolved in dioxane were added. The mixture was brought to pH 5 with 1 mol l^{-1} HCl and stirred very gently overnight at room temperature. The yield of conjugation was about 50%, as determined by radioimmunoassay of the supernatant after gel sedimentation. After washing with water–dioxane (1 + 1), the swollen gel was resuspended in water and mixed with an excess of glacial acetic acid and EDAC, to block the residual active amino groups. The pH was again adjusted to 5 and the suspension was gently stirred for 3 h at room temperature; the swollen gel was then washed with PBS solution and stored at 4 °C.

Affinity Chromatography

The functionalized stationary phases were packed in C10/10 columns with flow adapters to obtain the affinity columns. The gel was equilibrated with the buffer selected for the first elution step, then 0.5 ml of the 1 + 9 diluted globulin fraction of antiserum in the same buffer was injected onto the column, which was then washed with 5–10 ml of the same buffer, with a flow rate of 0.5 ml min^{-1}, while monitoring the absorbance at 280 nm. At the end of the washing step absorbance always attained the baseline value.

Elutions were performed with a flow rate of 0.5 ml min^{-1}. The mobile phases used to elute antibodies were: TRIS buffer (pH 8.1) (0.05 mol l^{-1} TRIS, 0.1 mol l^{-1} NaCl, 1 mmol l^{-1} EDTA, 0.1% m/v sodium azide), acetate buffers (pH 3.5, 4.0, 4.5 and 5.7) (0.05 mol l^{-1} acetate, 0.1 mol l^{-1} NaCl, 1 mmol l^{-1} EDTA, 0.1% m/v sodium azide) and glycine buffer (pH 2.6) (0.05 mol l^{-1} glycine, 0.1 mol l^{-1} NaCl, 1 mmol l^{-1} EDTA, 0.1% m/v sodium azide), mixed with various amounts of 2-methoxyethanol or *N*,*N*-dimethylformamide (DMF). Fractions of 0.5 ml of the eluate were collected in test-tubes containing 2 ml of TRIS buffer (pH 8.1) and were immediately used or stored at −20 °C.

Assays for Antibodies in the Eluate

The antibody content in each of the fractions collected was measured (*a*) by evaluating the binding capacity for tritiated progesterone and (*b*) by determining the amount of antibody by means of a non-competitive, solid-phase, enzyme immunoassay (EIA), using a progesterone–BSA conjugate as immobilized antigen.

Binding capacity was measured in duplicate on fractions diluted ten-fold with TRIS buffer (pH 8.1) containing 0.1% m/v gelatine. Aliquots of 0.2 ml were reacted with 0.1 ml of 1.5 nmol l^{-1} tritiated progesterone in PBS–gelatine, as described for cross-reactions, and the ratio of antibody-bound to free progesterone (*B*/*F*) was plotted against the elution volume to obtain an elution curve. The *B*/*F* ratio indirectly measures the amount of antibody. In fact, from the law of mass action,

$$B/F = K(Ab_0 - B)$$

where K and Ab_0 are, the equilibrium association constant (affinity) and antibody sites concentration, respectively.

The solid-phase EIA directly measures the amount of antibody in the eluted fractions and was performed according to the following general procedure.[15] Microtitre plates (8 × 12 wells) were incubated overnight at 4 °C with 0.25 ml per well of a solution containing 10 μg ml^{-1} of progesterone-11α-hemisuccinate–BSA in 6 mol l^{-1} guanidine. The progesterone-11α-hemisuccinate–BSA conjugate (steroid-to-protein molar ratio = 26) was prepared and characterized as described.[16] The plates were washed five times with a solution of 0.05% v/v Tween 20, then to each well was added 0.3 ml of blocking buffer (pH 7.4, 0.02 mol l^{-1}, 0.15 mol l^{-1} NaCl, 1 mmol l^{-1} EDTA, 0.1% m/v sodium azide, 0.1% m/v gelatine, 5% m/v saccharose). After 1 h at room temperature, the plates were washed three times with a solution of 0.05% v/v Tween 20, and kept at 4 °C until used. In order to confirm the complete binding of the anti-progesterone antibodies, the assay was performed with the maximum amount of antigen absorbable on the solid phase.

Antibody assay was carried out in duplicate, by diluting the eluted fractions ten-fold with PBS–gelatine. Wells containing 0.2 ml of each sample were incubated for 2 h at room temperature, then washed three times with a solution of 0.05% v/v Tween 20. To each well 0.2 ml of goat anti-rabbit IgG–alkaline phosphatase conjugate, diluted 1:2000 with TRIS buffer (pH 8.1) containing 1% m/v gelatine, was added to react with immobilized anti-progesterone antibodies, and after 2 h of incubation at room temperature the plates were washed with a solution of 0.05% v/v Tween 20. The amount of enzymic activity detected in the wells is proportional to the level of anti-progesterone antibodies in each fraction and was determined spectrophotometrically using the substrate sodium *p*-nitrophenylphosphate [0.2 ml of 5 mmol l^{-1} sodium *p*-nitrophenyl phosphate in 0.05 mol l^{-1} diethanolamine buffer (pH 9.6)]. After 1 h of incubation at room temperature, the enzymic reaction was blocked with 0.1 ml of 0.5 mol l^{-1} sodium carbonate, and after 10 min the absorbance was read at 405 nm. Non-specific binding was measured by replacing the diluted fractions with an equivalent amount of PBS–gelatine buffer. The absorbance measured, which is proportional to the amount of eluted antibodies, was plotted against the elution volume.

Separate experiments with the diluted globulin fraction of the antiserum showed that neither 2-methoxyethanol nor DMF inhibited the progesterone–antibody binding at the percentages present in either binding capacity experiments or solid-phase EIA.

Equilibrium Constants

The equilibrium association constants (affinities) for the purified globulin fraction of the antiserum and for the chromatographic fractions collected were determined as described previously.[12] The undiluted chromatographic fractions were de-salted by gel filtration on Sephadex G-25 pre-packed columns with PBS buffer, to remove solvents and elution buffers. An amount of 0.2 ml of de-salted sample was reacted with 0.1 ml of tritiated progesterone (0.15–12 nmol l^{-1}) in PBS–gelatine as described for cross-reactions. Affinity constants were obtained from a Scatchard plot.[17]

Results and Discussion

Cross-reactions

The percentage values obtained for cross-reactions (CR_{50}) are reported in Table 1. These values show that the antiserum is able to recognize the spacer arm because of its higher cross-reaction with progesterone-11α-hemisuccinate than progesterone itself or 11α-hydroxyprogesterone. This 'bridge effect' can also be observed by comparing the cross-reactions with 11α-hydroxyprogesterone 3,20-diethyleneacetal and

progesterone-11α-hemisuccinate 3,20-diethyleneacetal. In both instances the hemisuccinate arm increases the cross-reactions about four-fold (52% *versus* 180% and 0.33% *versus* 1.1%). As a consequence, the interactions of the antibody with free steroid and immobilized ligand may not be the same.

The low values of CR_{50} obtained with some functionalized derivatives [progesterone-3-(O-carboxymethyl)oxime, progesterone-11α-hemisuccinate 3,20-diethyleneacetal and progesterone-11α-hemisuccinate 20β-benzoate] show that the affinity of the antiserum for these steroids is sharply decreased. Hence these molecules were considered suitable for preparing some stationary phases for affinity chromatography by derivatization of AH Sepharose 4B.

Affinity Chromatography

Progesterone-11α-hemisuccinate 3,20-diethyleneacetal–AH Sepharose 4B

A first group of elutions were performed on a 1.8 × 1.0 cm id column of progesterone-11α-hemisuccinate 3,20-diethyleneacetal–AH Sepharose 4B, using TRIS buffer (pH 8.1) as eluent, with a stepwise gradient of 2-methoxyethanol (0 to 20% v/v). This stationary phase retains the antiserum well, with a loss of antibodies of only about 1% during the washing step (10 ml). Elution in the presence of different amounts of 2-methoxyethanol gives several peaks of progesterone-binding activity.

It was not possible to measure the affinity constants of the eluted fractions because when elutions on the same stationary phase were repeated, no binding activity was observed in the eluate, even with concentrations of organic solvent up to 30% v/v. The same effect was obtained employing a more acidic buffer, such as glycine buffer (pH 2.6). We think that this may be due to the hydrolysis of the ethyleneacetal moieties, with a consequent large increase in the affinity of the stationary phase. This hypothesis was confirmed by attempting to elute the antiserum from a column functionalized with progesterone-11α-hemisuccinate, which also did not cause any detachment of antibodies.

Progesterone-3-CMO–AH Sepharose 4B

A second group of elutions were performed on a 1.8 × 1.0 cm id column of progesterone-3-(O-carboxymethyl)oxime–AH Sepharose 4B. A first elution using acetate buffer (pH 4.0) as eluent, with a linear gradient of 2-methoxyethanol (0 to 25% v/v), showed that this stationary phase retains the antiserum well, with a loss of antibodies of about 10% during the washing

step (10 ml), but complete elution of retained antibodies was only obtained by raising the amount of 2-methoxyethanol to 30% v/v (Fig. 1). To verify if a more acidic pH was able to detach the antibodies retained on the column more effectively, the same gradient of 2-methoxyethanol was developed in glycine buffer (pH 2.6). An elution pattern very similar to that obtained with acetate buffer in the eluent was observed. However, the *B/F* values measured were very low and total antibody recovery was estimated as <10%. The pooled fractions corresponding to the broad peak eluted were used to measure the mean affinity and antibody sites concentration. The very low value obtained for antibody affinity (4.2 × 10⁸ l mol⁻¹ compared with 1.1 × 10¹⁰ l mol⁻¹ for the antiserum *in toto*), together with a binding sites concentration slightly lower than that expected for a quantitative recovery, indicates that the low *B/F* values measured in the eluate were a consequence of the very low affinity of the eluted antibodies and not a poor recovery from the column. The actual recovery, calculated on the basis of binding sites concentration, was about 80%. This low affinity can be attributed to denaturation of the antibodies during the elution step, due to the exposure to an acidic pH for a long time (about 2 h). Immediate neutralization of the eluate seems insufficient to prevent this denaturing effect.
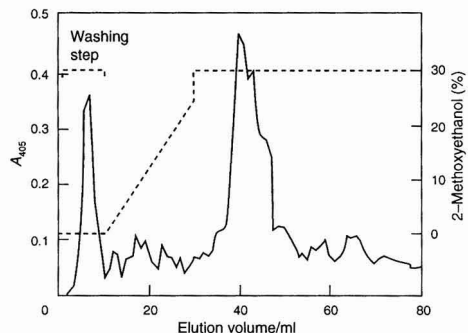

Fig. 1 Elution profile obtained from affinity chromatography of 0.5 ml of a 1 + 9 diluted globulin fraction of antiserum to progesterone-11α-hemisuccinate–BSA. Stationary phase: progesterone-3-(O-carboxymethyl)oxime–AH Sepharose 4B. Mobile phase: acetate buffer (pH 4.0), 2-methoxyethanol linear gradient (0–30% v/v).
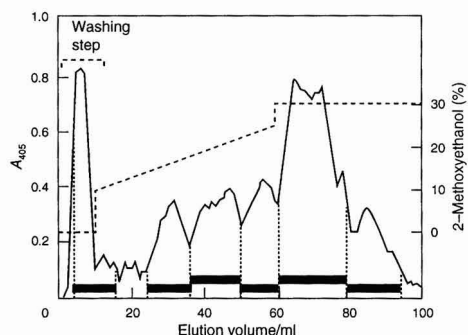

Fig. 2 Elution profile obtained from affinity chromatography of 0.6 ml of an undiluted globulin fraction of anti-progesterone antiserum. Stationary phase: progesterone-3-(O-carboxymethyl)oxime–AH Sepharose 4B. Mobile phase: TRIS buffer (pH 8.1), 2-methoxyethanol linear gradient (0–30% v/v). Fractions were diluted three-fold more than in Fig. 1. Peaks of binding activity were collected as indicated (broken lines and solid bars) and subjected to affinity measurements (see Table 2).

Table 1 Cross-reactions (% CR_{50}) of the antiserum to progesterone. Cross-reaction is defined as the ratio between the concentrations of steroid and progesterone that inhibit 50% of the binding of tritiated progesterone to antiserum. The cross-reactivity is a measure of the relative affinity of the antiserum

Steroid	% CR_{50}
Progesterone	100
11β-Hydroxyprogesterone	16
11α-Hydroxyprogesterone	52
Progesterone-11α-hemisuccinate	180
11α-Hydroxyprogesterone 3-ethyleneacetal	0.65
11α-Hydroxyprogesterone 3,20-diethyleneacetal	0.33
Progesterone-11α-hemisuccinate 3,20-diethyleneacetal	1.1
20β-Hydroxyprogesterone-11α-hemisuccinate	10.5
Progesterone-11α-hemisuccinate 20β-acetate	20
Progesterone-11α-hemisuccinate 20β-benzoate	2
Progesterone-3-(O-carboxymethyl)oxime	7.4
17α-Hydroxyprogesterone	0.4
5-Pregnen-3β-ol-20-one	0.05

A third elution was peformed after loading 0.6 ml of the undiluted globulin fraction of the antiserum onto the same stationary phase, with TRIS buffer (pH 8.1) as eluent and a solvent gradient of 2-methoxyethanol (0 to 30% v/v). The loss of antibodies in the washing step was higher (<15%), and the chromatographic pattern shows a series of overlapping peaks (Fig. 2), with a good recovery of antibodies (about 75%). The affinity constants measured for the pooled fractions corresponding to the various peaks of the chromatogram are reported in Table 2, and show clearly that high-affinity antibodies are eluted at solvent concentrations greater than those required to elute low-affinity antibodies. This trend can be expected if one considers that the lowering of the antibody–steroid interaction[18] is enhanced with increasing solvent concentration. As the desorption of antibodies with a higher affinity for the stationary phase require a stronger inhibition of the interaction, the elution can be obtained only at higher solvent concentrations in the eluent.

Progesterone-11α-hemisuccinate 20β-benzoate–AH Sepharose 4B

A third set of analyses using affinity chromatography were performed on a 1.2×1.0 cm id column containing a stationary phase functionalized with progesterone-11α-hemisuccinate 20β-benzoate. A first elution using a stepwise gradient with decreasing pH (5.7 to 2.6) showed that this stationary phase retains the antiserum well, with < 5% loss of antibodies during the washing step (10 ml), and the pH gradient makes the sharp elution of two progesterone-binding fractions at pH 4.5 and 3.5 possible (Fig. 3), with a recovery of >80%. The first fraction was tested for homogeneity by further affinity chromatography on the same stationary phase, but eluting with a stepwise gradient of *N,N*-dimethylformamide (2.5 to 10% v/v) in TRIS buffer (pH 8.1). This new elution gives three distinct peaks of binding activity (Fig. 4), with affinity constants of 3×10^9, 7×10^9 and 1.1×10^{10} l mol^{-1} for peaks 1, 2 and 3, respectively. The specificity of the eluted antibodies was tested with 11α-hydroxyprogesterone, the underivatized steroid with a high cross-reaction with progesterone. While the specificity of peaks eluted with 2.5% and 10% DMF was not different from that of antiserum *in toto*, it is remarkable that the peak eluted with 5% DMF shows a cross-reaction to 11α-hydroxyprogesterone lowered from 52% to 6%, indicating a much higher specificity of these antibodies. To test the stability of the affinity column, the elution of the antiserum (with the pH gradient and the DMF gradient) was repeated three times, without appreciable variation in the elution profile and with about the same recovery of antibodies (75–85%).

Conclusions

The results obtained from the different elutions clearly show that a proper choice of the steroid molecule to be immobilized on the Sepharose matrix appears to be an essential step in the development of affinity chromatography of high-affinity antisera to steroid hormones. In fact, stationary phases prepared by coupling steroid derivatives with high affinity for the antiserum [progesterone-3-(*O*-carboxymethyl)oxime] require strong eluting conditions to recover adsorbed

proteins. This causes a certain amount of denaturation of the eluted antibodies.

Near optimum conditions for the elution of high-affinity antibodies were achieved by using a stationary phase functionalized with a steroid derivative giving a decrease in affinity of about two orders of magnitude and remaining stable under the elution conditions (progesterone-11α-hemisuccinate 20β-benzoate). This results in a limited loss of antibodies during loading and washing of the column, still allowing elution under mild, non-denaturing conditions with a quantitative recovery of antibodies.

The use of a steroid derivative of lower affinity (progesterone-11α-hemisuccinate 3,20-diethyleneacetal) appears to be more effective for the elution of antibodies but the instability of the acetal at acidic pH makes it impossible to re-use the column for further separations.
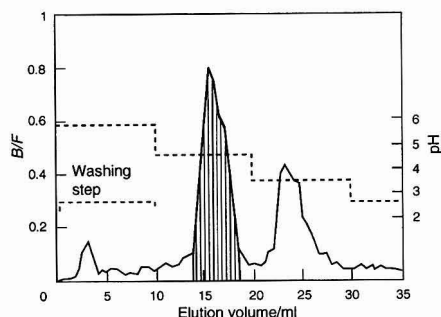

Fig. 3 Elution profile obtained from affinity chromatography of 0.5 ml of a 1 + 9 diluted globulin fraction of antiserum to progesterone-11α-hemisuccinate–BSA. Stationary phase: progesterone-11α-hemisuccinate 20β-benzoate–AH Sepharose 4B. Mobile phase: acetate buffer, stepwise pH gradient between 5.7 and 3.5, glycine buffer (pH 2.6). The peak eluted at pH 4.5 (highlighted area) was re-chromatographed with a solvent gradient in the same stationary phase (see Fig. 4).
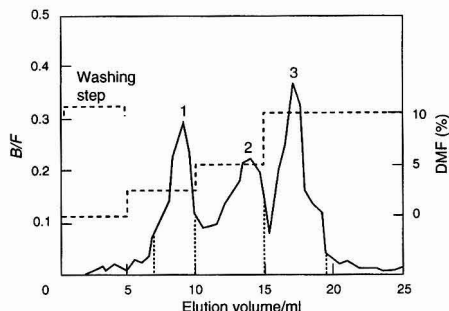

Fig. 4 Elution profile obtained from affinity chromatography of the antibodies eluted at pH 4.5 (see Fig. 3) in the progesterone-11α-hemisuccinate 20β-benzoate–AH Sepharose 4B stationary phase. Mobile phase: TRIS buffer (pH 8.1), DMF stepwise gradient (2.5–10% v/v). Peaks 1, 2 and 3 were collected as indicated by broken lines and subjected to affinity measurements.

Table 2 Affinity constants measured on pooled fractions eluted from a column of progesterone-3-(*O*-carboxymethyl)oxime–AH Sepharose 4B. Mobile phase: TRIS buffer (pH 8.1), 2-methoxyethanol linear gradient (10–30% v/v)

Volume of eluate/ml	4–16	24–36	37–50	51–61	62–80	81–94
Affinity/l mol^{-1}	7.1×10^8	1.6×10^9	1.9×10^9	2.6×10^9	3.3×10^9	6.2×10^9

Increasing concentrations of organic solvent and a decreasing pH gradient appear suitable for lowering the affinity of the immobilized antibody, thus allowing the elution of the antibodies retained in the column. However, using a pH gradient alone appears to be unsuccessful in separating several antibody fractions. A further fractionation can be obtained with a solvent gradient. As expected, an increase in the solvent concentration in the eluent increases the affinity of eluted antibodies, because the solvent inhibits the steroid–antibody interaction more efficiently.

References

1   Grenot, C., and Cuilleron, C. Y., *Steroids*, 1979, **34**, 2261.
2   Lewis, J. G., and Elder, P. A., *J. Steroid Biochem.*, 1985, **22**, 713.
3   Podestà, A., Luisi, M., and Montagnoli, G., *J. Steroid Biochem. Mol. Biol.*, 1991, **39**, 63.
4   Bouzerna, N., Hammadi, H., Richard, C., Formstecher, P., and Dautrvaux, M., *J. Immunol. Methods*, 1988, **112**, 251.
5   Formstecher, P., Hammadi, H., Bouzerna, N., and Dautrevaux, M., *J. Chromatogr.*, 1986, **369**, 531.
6   Müller, R. F., Palluk, R., and Kemple, M. A., *J. Chem. Tech. Biotechnol.*, 1984, **34B**, 263.
7   Smith, T. W., and Skubitz, K. M., *Biochemistry*, 1975, **14**, 1496.
8   Yoshida, H., Nakai, S., Nimbari, F., Yoshimoto, K., and Nishimura, T., *Steroids*, 1989, **53**, 727.
9   Allen, R. M., and Redshaw, R. M., *Steroids*, 1978, **32**, 467.
10 Norymberski, J. K., and Woods, G. F., *J. Chem. Soc.*, 1955, 3426.
11 Giraudi, G., Baggiani, C., and Costa, L., *Ann. Chim.*, 1990, **80**, 111.
12 Giraudi, G., Cenderelli, G., and Patrito, G., *Steroids*, 1983, **42**, 475.
13 Abraham, G. E., *J. Clin. Endocrinol. Metab.*, 1969, **29**, 866.
14 Abercrombie, D. H., and Chaiken, I. M., in *Affinity Chromatography: a Practical Approach*, ed. Dean, P. D. G., Johnson, W. S., and Middle, F. A., IRL Press, Oxford, 1st edn., 1985, pp. 173–175.
15 Tijssen, P., in *Laboratory Techniques in Biochemistry and Molecular Biology. Vol. 15, Practice and Theory of Enzyme Immunoassays*, ed. Burdon, R. H., and van Knippenberg, P. H., Elsevier, Amsterdam, 1985, p. 329.
16 Giraudi, G., and Baggiana, C., *Analyst*, 1990, **115**, 1531.
17 Scatchard, G., *Ann. N. Y. Acad. Sci.*, 1949, **51**, 660.
18 Giraudi, G., and Baggiani, C., *Biochem. Biophys. Acta*, 1993, **1157**, 211.

Air Sampling and Determination of Airborne Phenetole in the Workplace: A Regulatory Method Development and Validation for Establishing an Exposure Guideline in Ontario

Weh S. Wu and Paul K. Fung

Occupational Health Laboratory, Ontario Ministry of Labour, Weston, Ontario, Canada M9P 3T1

A regulatory method was developed and validated for establishing an exposure guideline for monitoring phenetole at workplaces in Ontario. Phenetole vapours were sampled into a charcoal tube and then desorbed into carbon disulfide for gas chromatography (GC) analysis. By spiking the phenetole solution into charcoal tubes, it was found that the recoveries for up to 100 µg (equivalent to 5 times the suggested exposure limit in a 2 dm³ sample) levels were excellent after the tubes were aerated for 1 h at an aeration rate of 0.2 dm³ min⁻¹. For validation of the method, the vapour pressure of phenetole was established experimentally in order to assess the efficiency of simulated air sampling using a test atmosphere generation system. Recoveries of phenetole vapours at the approximate levels of 0.3, 0.7, and 1.5 times the suggested exposure limit (10 mg m⁻³) were all over 90%. Phenetole in simulated air samples was identified using gas chromatography–mass spectrometry (GC–MS) in the electron impact (EI) scan mode.

Keywords: Airborne phenetole; gas chromatography; test atmosphere generation system; validation

Introduction

Phenetole, an ethyl phenyl ether of the homologous series of anisole characterized by a strong pleasant odour, is one of the important commercial phenolic ethers. Low molecular mass phenolic ethers are chemically stable and used as heat-transfer media and antioxidants. Other common applications are for uses as industrial solvents and cleaning agents, in addition to the widespread use in the perfume industry.

Phenetole vapours can be absorbed by inhalation, ingestion or through the skin and, hence, phenetole is generally regarded as a skin and respiratory irritant. Although there have been no reports of serious adverse health effects on humans caused by exposure or contact with phenetole,[1] workers' concern of prolonged occupational exposure during the industrial use of phenetole has prompted a need to develop a sampling method to monitor the air concentration of the agent in the work environment. In pursuit of a method to determine the atmospheric concentrations of phenetole, the Occupational Health Laboratory of Ontario undertook a project to develop a sampling and analytical method for the agent. At present, there are no human exposure guidelines established by the Occupational Safety and Health Administration (OSHA), American Conference of Governmental Industrial Hygienists (ACGIH) or Health and Safety Executive (HSE) of the UK for phenetole. An exposure limit of 10 mg m⁻³ has been stipulated for anisole by the Russian agency.[2] In view of the similarity in chemical structure and possibly the metabolic pathway[1] for phenetole and anisole, there is a proposal under the consideration of the Ontario Ministry of Labour to apply the same value of anisole exposure limit to phenetole as an interim measure until more information becomes available.

A regulatory method for sampling and analysing phenetole vapours in the workplace was developed by using gas chromatographic techniques for quantification after the vapours were sampled onto a charcoal adsorption tube. An important aspect for the ministry of labour in developing a regulatory method is that the method should be reasonably validated in addition to the preference that the method should be easily applied by ordinary laboratories in industry for self compliance to the exposure guideline. In order to validate the method, the correct value of phenetole vapour pressure at the temperature for conducting investigation on air sampling was obtained experimentally. By spiking both the liquid and vapour phase of phenetole onto charcoal tubes under aerated conditions, results indicated that the recoveries were satisfactory. The final validation of the method in the laboratory was successfully performed on a test vapour generation system (TAGS) for simulated air sampling at the approximate levels of 0.3, 0.7 and 1.5 times the suggested exposure limit.

Experimental

Reagents and Apparatus

Phenetole (99%) was purchased from Aldrich Chemical (Milwaukee, WI, USA). Carbon disulfide (certified-reagent grade) was from Caledon Laboratory (Georgetown, Ontario, Canada). Charcoal tubes (Cat. No. 226-01) for air sampling were supplied by SKC (Eighty Four, PA, USA).

Portable air sampling pumps were MSA Model C-210 (Pittsburgh, PA). Glass gas sampling bulbs (with a side arm) were supplied by ACE Glass (Vineland, NJ, USA). TAGS for simulation of air sampling was manufactured by SRI International (Mento Park, CA, USA). The operation of TAGS was illustrated in detail in a previous publication[3] except all three cone-shaped vapour chambers (1, 2, 3) were utilized this time. Concentrations of generated phenetole vapours from the ration lines of TAGS to the vapour chambers (c_1, c_2, c_3) are consecutively reduced by half, *i.e.*, $c_2 = (1/2)c_1$ and $c_3 = (1/2)c_2$.

The chromatograph was an HP model 5880A with an analytical column (12 ft. × 0.125 in. od) of 10% free fatty acid phase (FFAP) on Chrom W H.P. (80/100). The injection temperature was 220 °C and the oven temperature was programmed at 140 °C for 7 min, ramped up to 170 °C at 15 °C min⁻¹ with a total run time of 15 min. The detector was a flame ionization detector (FID) operating at 250 °C. The nitrogen carrier gas flow rate was 30 cm³ min⁻¹.

The gas chromatography–mass spectrometry (GC–MS) system contained an HP 5890 Series II gas chromatograph and

an HP 5989A mass spectrometer. The GC column was a cross-linked 5% Me Silicon type, 25 m × 0.32 mm; film thickness, 1.05 μm. The injection temperature of the GC was 130 °C and the oven temperature was started at 80 °C for 5 min, ramped up at the rate of 20 °C to 130 °C for 2 min. The electron impact (EI) scan mode was used for the identification.

Evaluation of Phenetole Vapour Pressure

The vapour pressure of phenetole given in the literature[4,5] shows that the corresponding temperatures for 1, 5, 10 and 20 mm Hg are at 18.1, 43.7, 56.4 and 70.3 °C, respectively. The vapour pressure corresponding to the temperature at which the simulation of air sampling was conducted on the TAGS can be extrapolated from Fig. 1. Because the calculated recovery based on the TAGS study depends largely on the vapour pressure of phenetole, a separate investigation was also conducted (the experimental procedure is fully described in previous publications[6,7]). A 5 ml aliquot of air withdrawn using an air-tight syringe from a 250 ml glass gas sampling bulb was released into a cap-crimped 20 ml vial containing 1 cm³ of CS_2. The vial was then thoroughly agitated to ensure that all phenetole vapours dissolved in the CS_2. The vial was de-capped immediately prior to GC injection.

Recovery of Phenetole Spiked Onto Charcoal Tubes

A 10 mm³ volume of CS_2 solution containing levels of phenetole of 2, 10, 50 and 100 μg were spiked into charcoal tubes by using a 10 mm³ Hamilton syringe. Care was taken to direct the spiking solution into the centre of the charcoal and to minimize the spreading on the wall of the tube. All tubes were immediately aerated with MSA air sampling pumps for 1 h at an air flow rate of 0.2 dm³ min⁻¹. The charcoal was then removed from each tube into a standard 1.5 cm³ capacity borosilicate glass vial. After the addition of 1 cm³ of CS_2, the vial was crimped for closure with a Teflon-lined septum for GC analysis *via* an autosampler. Detection responses were linear for all the above mentioned concentrations and the lower detection limit can be easily established at the level of 1 μg in 1 cm³ of CS_2.

Recovery of Phenetole Vapours Spiked Onto Charcoal Tubes

Vapour phase phenetole was prepared[6,7] in a 500 cm³ glass gas sampling bulb with an overnight equilibration between the liquid and vapour phase of phenetole. A 5 cm³ air sample was withdrawn from the bulb and slowly injected through the side arm of a 250 ml glass gas sampling bulb for which the top opening was exposed to atmospheric air and the bottom was connected to an SKC charcoal sampling tube followed by an MSA portable air sampling pump operated at the air flow rate of 0.2 dm³ min⁻¹. The sampling time was set for 1 h. Reference standard was prepared, in duplicate, by a similar method by withdrawing 5 cm³ and directly discharged into a cap-crimped vial containing 1 cm³ of CS_2. Sample preparation for GC analysis was identical to the previously described procedure under Evaluation of Phenetole Vapour Pressure. A typical chromatogram from this experiment is shown in Fig. 2.

Stability of Charcoal Adsorbed Phenetole Vapours

Phenetole vapours sampled onto charcoal tubes *via* a portable sampling pump, as described earlier, were studied for stability. Desorption and quantification of phenetole vapours adsorbed on charcoal tubes were carried out on days 0, 7, and 14 after sampling. All samples were stored at room temperature and away from light prior to analysis.

Simulated Air Sampling Using TAGS

The TAGS was operated under the following conditions: 61 dm³ min⁻¹ flow rate of dilution air (F_{air}); 150 kPa purging pressure of nitrogen, which corresponds to a flow of 51.37 cm³ min⁻¹ when a 0.002 in (No. 2B) orifice was used. Charcoal sampling tubes were connected to the multiple sampling ports of all three vapour chambers. Sampling time and air flow rate for all samplers were set for 25 min and 0.2 dm³ min⁻¹, respectively. After sampling, samplers were treated for GC analysis as described earlier.

Identification of Phenetole Using GC–MS

A concentration of about 30 μg cm⁻³ phenetole prepared through vapour phase sampling *via* a portable sampling pump (as described earlier) was diluted to 3 μg cm⁻³ with CS_2. Electron input scan mode was used to monitor ions. The solvent delay time was set for 2 min.

Results and Discussion

An estimation of phenetole vapour pressure from the extrapolation of the pressure–temperature curve (Fig. 1) indicated that a 1.2 mm Hg pressure was expected at the laboratory's temperature of 22 °C under which the simulated air sampling
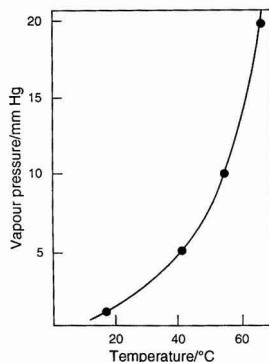

Fig. 1 Profile graph of vapour pressure of phenetole *versus* temperature.
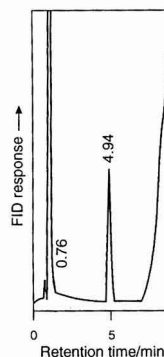

Fig. 2 Chromatogram of phenetole (16.8 ng) from simulated air sampling. Retention time, 4.9 min.

experiments were performed. A more precise figure, resulting from the experimental work conducted, yielded 0.98 mm Hg which showed a 20% discrepancy compared with the estimated value. Recoveries of direct spiking of CS_2 solution containing phenetole (Table 1) show that phenetole was effectively retained in the SKC charcoal tubes. Desorption of phenetole from charcoal was effectively achieved by placing charcoal in only 1 cm³ of CS_2 instead of using an excess amount to elute. As all charcoal tubes were aerated after spiking, the high recoveries also reflect that the charcoal adsorbed phenetole was relatively stable under open atmosphere conditions. Atmospheric oxidation and depletion owing to evaporation were not a problem of concern when charcoal tubes were used. Table 2 further confirms that charcoal adsorbed phenetole vapours were stable with no depletion observed for up to two weeks.

The calculated amount of phenetole in the reference standard for the evaluation of recoveries of phenetole vapours spiked onto charcoal tubes was 32.6 µg based on the experimentally obtained vapour pressure of 0.98 mmHg at 22 °C. The present findings through GC analysis were 32.6 and 30.8 µg, for which the averaged value of 31.7 µg was used as the reference amount for the evaluation of recoveries (Table

3). Accordingly, an averaged relative recovery of 95.6 ± 2.3% was obtained.

For the simulated air sampling study, the concentration of phenetole vapours generated in chamber 1 of the TAGS can be calculated based on the following eqn:

$$c_1 = (F_n/F_{air})\,(P_0/T_0)\,(16.0325 \times M)\,[P_a/(P_0 - P_a)]$$

where T_0 is the ambient temperature (in K); P_0 the pressure (in mm Hg); M the molecular mass of phenetole; F_n and F_{air} the flow rates (in dm⁻³ min⁻¹) at T_0 and P_0 for nitrogen purging gas and dilution air, respectively; and P_a is the vapour pressure of phenetole. Consequently, vapour concentrations in chamber 2 (c_2) and chamber 3 (c_3) are half of those in chamber 1 and 2, respectively. The amount of phenetole vapours collected in each charcoal sampler at the sampling port of chamber 1 was calculated to be 27.5 µg based on the TAGS settings. Recoveries of simulated air sampling conducted on TAGS are shown in Table 4.

The identity of phenetole was characterized by using a GC–MS system. The retention time of phenetole was about

Table 1 Recoveries of phenetole spiked on charcoal tubes

Level of spiking/µg	Amount recovered/µg	Yield (%)
2.0	1.9	95.0
	1.9	95.0
	1.9	95.0
	1.8	90.0
	1.7	85.0
		Average 92.0 ± 4.5
10.0	10.0	100.0
	9.8	98.0
	9.9	99.0
	9.9	99.0
	9.7	97.0
	10.2	102.0
		Average 99.2 ± 1.7
50.0	49.6	99.2
	50.6	101.2
	49.4	98.8
	49.1	98.2
	48.8	97.6
	48.3	96.6
		Average 98.6 ± 1.6
100.0	100.3	100.3
	100.4	100.4
	101.7	101.7
	98.4	98.4
	92.5	92.5
	98.0	98.0
		Average 98.6 ± 3.3

Table 2 Stability of phenetole vapours adsorbed on charcoal tubes

Time lapse before desorption/d	Amount of phenetole vapour found/µg
0	30.5
	33.2
	31.5
7	33.9
	32.4
14	35.4
	35.6
	31.5

Table 3 Recoveries of phenetole vapours spiked onto charcoal tubes

Sample No.	Amount recovered/µg	Relative yield (%)
	31.7	100
1	29.4	92.7
2	30.8	97.2
3	31.0	97.8
4	30.7	96.8
5	29.7	93.7
		Average 95.6 ± 2.3

Table 4 Recoveries of phenetole from simulated air sampling conducted on TAGS

Theoretical level of vapour generated/µg	Amount recovered/µg	Yield (%)
27.5	26.8	97.5
(Chamber 1)	24.6	89.5
	24.4	88.7
	26.8	97.5
	25.4	92.4
	30.9	112.4
	30.9	112.4
	25.9	94.2
		Average 98.1 ± 9.4
13.8	13.9	100.7
(Chamber 2)	12.3	89.1
	12.9	93.5
	13.2	95.7
	12.0	87.0
	14.6	105.8
	13.9	100.7
	14.8	107.2
	12.9	93.5
	14.8	107.2
		Average 98.0 ± 7.4
6.9	7.3	105.8
(Chamber 3)	6.9	100.0
	7.5	108.7
	7.7	111.6
	6.9	100.0
	7.6	110.1
	7.0	101.4
	7.5	108.7
	6.5	94.2
	6.4	92.8
		Average 103.3 ± 6.7

4.5 min. The EI mode of MS (Fig. 3) indicated that phenol was one of the intermediates with dominant abundance of its molecular ion m/z 94 as the base ion. The molecular ion of phenetole was also identified at m/z 122.

Although the maximum exposure limit (WEG-MAX) of phenetole in the workplace is still to be determined by the Ontario Ministry of Labour, a value of 10 mg m^{-3} is likely to be set based on the Russian occupational exposure limit (OEL-STEL) set for anisole. Analytical method validation from our simulated air sampling study indicates that the method can be satisfactorily applied to monitor phenetole exposure at levels of approximately 0.3, 0.7, 1.5 times the proposed WEG-MAX based on a 10 min sampling time at the rate of 0.2 dm^3 min^{-1}.

As a governmental regulatory laboratory to enforce chemical exposure regulations and guidelines, we have experienced that many of the newly set regulatory exposure levels are often upgraded to considerably lower levels in a relatively short time period. Therefore, our future direction in analysing phenetole will focus on lower detection levels. One consideration is to

use a GC–electron capture detector (ECD). Because the ethoxy group of phenetole is an electron-donating group, halogenation or nitration on phenetole to substantially increase detection sensitivity on ECD is possible. Conditions for those reactions should be controlled for yielding a predominant product. To upgrade and simplify future validation techniques employing a permeation tube[8] containing phenetole standard in addition to the use of TAGS to regulate the release of phenetole vapour for study is also being considered.

As the accurate vapour pressure of an organic chemical is vital in validating air sampling recovery, we also plan to extend the present technique for obtaining phenetole vapour pressure to other organic chemicals for which the air sampling recoveries were less than satisfactory.

References

1 Clayton, G. D., and Claytonand, F. E., *Patty's Industrial Hygiene and Toxicology*, John Wiley & Sons, New York, revised edn., 1981, Vol. IIA, pp. 2521–2525.
2 United Nations Environment Program *IRPTC* (*International Register of Potentially Toxic Chemicals*)—*Legal Database*, 1993.
3 Wu, W. S., and Gaind, V. S., *Analyst*, 1992, **117**, 9.
4 Chemical Society of Japan *Kagaku Benran*, ed. Nagai, S., Maruzen Kabushiki Kaisha, Tokyo, 1958, p. 526.
5 *CRC Handbook of Chemistry and Physics*, Weast, R. C., CRC Press, Boca Raton, FL, 69th edn., 1988, p. D-204.
6 Wu, W. S., and Gaind, V. S., *J. High Resolut. Chromatogr.*, 1992, **15**, 479.
7 Wu, W. S., and Gaind, V. S., *Analyst*, 1993, **118**, 1285.
8 Gaind, V. S., Wu, W. S., and Chai, F., *J. High Resolut. Chromatogr.*, 1992, **15**, 840.

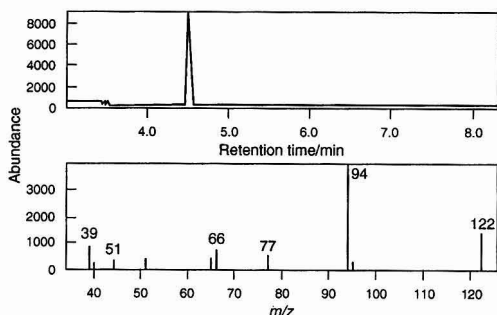**Fig. 3** Identification of phenetole by using GC–MS on simulated air sample. Phenetole, 3 μg cm^{-3} (retention time, 4.5 min).

Chromatographic Methods for the Determination of Alkylketene Dimer in Pulp and Paper Matrices

B. Bruce Sitholé, Samuel Nyarku and Lawrence H. Allen

Process Chemistry Division, Pulp and Paper Research Institute of Canada, 570 St. John's Boulevard, Pointe Claire, Quebec, Canada H9R 3J9

Chromatographic procedures for the determination of alkylketene dimer (AKD) and stearone were evaluated. The best results were obtained when AKD was converted into its ketone form before determination by GC. Bound AKD in paper samples is best removed by digestion of the paper with either hydrochloric acid or sodium carbonate. A separation scheme based on solid-phase extraction was developed for the determination of hydrolysed AKD in deposits from alkaline paper mills. As different AKD emulsions have different chromatographic patterns, it is recommended that standards be prepared from the same AKD that was used in the sizing process. The GC determination of AKD and stearone can be significantly expedited by using Soxtec extraction (rather than Soxhlet extraction) and by employing short capillary GC columns.

Keywords: Alkylketene dimer; alkaline papers; gas chromatography; papermaking; sized papers

Introduction

In recent years, many mills have been converted from acid to alkaline papermaking owing to such factors as the greater permanence of alkaline paper and customer demand.[1-4] Conventional sizing with aluminum resinate (also referred to as rosin sizing), which is commonly used in acid papermaking, does not work in alkaline papermaking. Instead, sizing agents such as alkylketene dimer (AKD), alkenylsuccinic anhydride (ASA) and neutral rosin systems have to be used.[5,6]

Problems associated with sizing in alkaline papermaking include low retention in the sheet, wet press picking due to tacky hydrolysis products of the size and loss of sizing on storage.[7-9] In order to find solutions to these problems, reliable methods for the determination of the sizing agents and their hydrolysis products in the sheet and in white waters (drainage from wet stock in pulping and papermaking operations) are needed. For example, the problem of low size retention can be assessed by conducting a mass balance of the size in the sheet and in the white water.

From the chemistry of AKD, it is evident that its determination will not be straightforward. AKD is generally considered to have the structure shown in Fig. 1. However, by virtue of its manufacturing process (dimerization of aliphatic acid chlorides), it is not a pure material because it is made from commercial stearic acid, which contains a range of fatty acid impurities with chain lengths varying from C_{14} to C_{20} (see Table 1). This is why the term AKD is sometimes pluralized to alkylketene dimers. AKD can undergo hydrolysis to form a ketone as shown in Fig. 1. The structures in Fig. 1 indicate there are no functional groups that can be easily exploited to facilitate the determination of these compounds. Several methods for the determination of AKD in paper have been reported;[11-16] the methods entail extraction of AKD from paper, treatment of the extract (derivatization or hydrolysis) and analysis by gas chromatography, GC–MS, HPLC, spectrophotometry, NMR and IR spectrometry and pyrolysis GC. These procedures are so diverse that it is difficult to assess which ones give the most reliable results. Consequently, an evaluation of methods and procedures based on GC analysis has been made. This paper gives an overview of the evaluations that were conducted and also outlines new procedures that have been developed for the determination of AKD and its primary hydrolysis product (stearone) in white waters and deposits.

Experimental

Materials

Solid AKD and AKD emulsions (Hercon-70 and Hercon-72S), as used by mills, were obtained from Hercules. The keto form of AKD, stearone, was prepared by first boiling a sample of AKD in 6 mol l⁻¹ HCl for 1 h and then cooling and decanting the aqueous phase. The solid product, impure stearone, was dissolved in hot chloroform, quickly filtered and finally cooled to precipitate the ketone. Several recrystallizations were performed in the manner mentioned above, until no AKD was detected in the purified ketone by gas chromatography.

Doubly distilled tall oil was used as model wood resin and calcium oleate was used as a model calcium soap.

HPLC-grade solvents and analytical-reagent grade reagents obtained from Fisher or Canlab were used. Tetramethylammonium hydroxide (25% in methanol) was obtained from Aldrich.

Methods

AKD is believed to react with cellulosic fibres to render the surface hydrophobic.[3,16-19] However, not all of the AKD

Fig. 1 Hydrolysis reaction of AKD (**1**) to form stearone (**2**).

reacts with fibres; some of it undergoes hydrolysis to form stearone. Thus, one can distinguish three types of AKD in a sized paper sample: unbound AKD, which is trapped in the fibres; bound or reacted AKD, which forms β-esters with cellulose; and hydrolysed AKD (stearone). In addition there is AKD in the white water, which may be in the free and hydrolysed forms.

Preparation and analysis of AKD solutions

Currently, there are two types of methods in use for the analysis of AKD: methods that involve hydrolysis of AKD to yield the corresponding ketone, followed by determination of the ketone by various chromatographic techniques, notably HPLC and GC,[14,15] and techniques that involve conversion of the AKD into its methyl ester, followed by gas chromatographic analysis of the ester.[11]

These two types of analysis were investigated and compared with the simple method, that entails gas chromatographic determination of AKD without prior chemical treatment such as hydrolysis or methylation. The following AKD solutions were prepared in acetone in concentrations ranging from 20 to 1000 mg l^{-1} and analysed by capillary gas chromatography (as described later) to prepare calibration graphs: (1) non-hydrolysed AKD; (2) hydrolysed AKD, prepared by acidic hydrolysis using the method of Dart and McCalley;[14] (3) methylated AKD, using diazomethane as methylating agent; and (4) methylated AKD, using methyl iodide.[11]

Extraction and determination of free AKD in paper

The following methods of extracting and determining free AKD in paper were investigated:

(1) extraction of AKD from handsheets with chloroform followed by derivatization of the AKD extracts with methyl iodide and analysis by gas chromatography with flame ionization detection;

(2) the same as in (1) except that the AKD was derivatized with diazomethane before analysis by GC;

(3) the same as in (1) except that the AKD was converted into stearone before GC;

(4) solvent extraction with a Soxtec system *versus* Soxhlet extraction. A Soxtec system is a rapid extraction unit that can be used to extract soluble extractives from various sample matrices. A comparison of features and performances of Soxtec and Soxhlet systems was made recently.[20]

Extraction and determination of bound AKD in paper

About 0.55 g of accurately weighed samples were used in all instances. The following procedures were used to extract and determine reacted or bound AKD in paper.

Digestion of handsheets with acid. Once the free AKD had been removed, the paper samples were digested with 6 mol l^{-1} HCl for 30 min to break cellulose–AKD bonds. The acid was removed and the charred samples were extracted by refluxing for 1 h with chloroform. The chloroform extracts were

evaporated to a final volume of 1.0 ml, spiked with an internal standard (nonacosane) and analysed for AKD content by capillary gas chromatography.

Digestion of handsheets with sodium hydroxide. An alternative digestion procedure was carried out with 2 mol l^{-1} sodium hydroxide using the same conditions as applied to acid digestion. In this instance the samples turned yellow after digestion.

Digestion with sodium carbonate. Paper samples were digested with 25 ml of 0.1 mol l^{-1} sodium carbonate by refluxing for 2 h in round-bottom flasks. The liquid phases were evaporated nearly to dryness before Soxtec extraction (1 h) with chloroform and analysed by gas chromatography. This was a modification of a literature procedure[14] in which the evaporated sample was extracted for 4 h with acetone, evaporated to dryness and the ketones were extracted with three 5 ml aliquots of boiling hexane.

Digestion with tetramethylammonium hydroxide (TMAH). Paper samples were digested with 16 ml of 25% tetramethy-lammonium hydroxide by boiling for 1 h.[11] As it is not clear from the literature how the analysis was done (that is, how the authors did not describe their experimental approach fully; for example, does the AKD migrate into the TMAH or does it have to be extracted by a solvent from the paper after the digestion?), we determined AKD after digestion by four procedures, which are described in the Results section. **[Caution]**: TMAH is foul smelling and very reactive; it should be handled in a well ventilated fume-hood.

Photochemical reaction. It is well known that paper sized with AKD sometimes loses its sizing during storage and transportation.[9] There is some speculation that this could be due to photochemically induced rupture or cleavage of the cellulose–AKD bonds. We studied the effect of light on sized paper samples by exposing them to room light (fluorescent) and UV light (380 nm) for 24 h. The papers were then extracted with chloroform for 1 h using a Soxtec extractor and the extracts were analysed by gas chromatography (after volume reduction and addition of the internal standard).

Determination of free and hydrolysed AKD in white waters

The objective here was to develop a solid-phase extraction (SPE) method for trace enrichment of AKD and its hydrolysis product from white waters. Known amounts of AKD and stearone were prepared in distilled water (to give 10 mg l^{-1} solutions) and a variety of solid phases and elution solvents were tested to ascertain their efficiencies in retaining and eluting the compounds from 10 ml aliquots of spiked sample. The most promising procedure was then used for trace enrichment of AKD from white water. The amounts of AKD and stearone found by SPE were compared with those found by filtration of white waters through an 0.8 μm membrane filter. The filter retains AKD and stearone particles, which were subsequently extracted into chloroform before GC analysis.

Determination of hydrolysed AKD in deposits

The objective here was to develop a method for the determination of stearone in deposits. As stated earlier, one of the problems with sizing in alkaline papermaking is hydrolysis of AKD to yield stearone, which is tacky and contributes to deposition problems. The determination of stearone in mill deposits can indicate whether or not the compound is a major source of the problem. Deposits typically contain wood resin, calcium soaps, stearone and defoamer components. Current technologies for the analysis of mill deposits entail solvent extraction with acetone to give a fraction containing wood resin and/or oil, followed by extraction with chloroform to

Table 1 Fatty acid composition of commercial stearic acid used to prepare AKD[10]

Formula	Fatty acid	% of total
C_{14}	Myristic	0–5
C_{16}	Palmitic	3–40
C_{18}	Stearic	55–96
C_{20}	Arachidic	0–3

give a fraction containing metal soaps.[21,22] However, because stearone is soluble in the solvents used (see Table 2), erroneous results will be obtained for deposits that contain this compound; a method that can permit fractionation of alkaline paper mill deposits into wood resin/oil, metal soaps and AKD (stearone) is needed. A procedure based on solid-phase extraction was developed for this purpose and is described below.

A weighed amount of sample (250 mg) was deposited on a pre-washed solid-phase extraction tube packed with 0.5 g of octadecylsilane (C_{18}) sorbent. The tube was then placed in a heated water-bath at 50 °C as shown in Fig. 2 and eluted with 15 ml of hot acetone to obtain a fraction (A), containing stearone and wood resin, and with 15 ml of hot chloroform to obtain a fraction (B), containing metal soaps. Fraction A was cooled and filtered through a 0.2 μm solvent-resistant membrane filter (made of PTFE, supplied by Sartorius) to separate stearone (precipitate) from the wood resin, which remains in solution. The solids collected on the filter were washed with 2 ml of acetone and dried to constant mass in a desiccator. The wood resin and metal soap fractions were evaporated using a gentle stream of nitrogen at room temperature, then freeze-dried and weighed. The procedure was tested on an artificial mixture of wood resin, stearone and calcium soaps of wood resin. The purity of the separated fractions was tested using either GC or FTIR spectrometry.

Determination of AKD by gas chromatography

Literature reports[11,14] indicate that capillary GC can be used in the determination of AKD and stearone. In these reports, a

Table 2 Solubility tests for stearone and calcium soap in organic solvents

Solvent	Temperature	Stearone	Calcium soap
Methanol	Cold	No	No
	Hot	No	No
Acetone	Cold	No	No
	Hot	Yes	No
Dichloromethane	Cold	~50%	Yes
	Hot	Yes	Yes
Chloroform	Cold	Yes	Yes
	Hot	Yes	Yes
Toluene	Cold	~50%	Yes
	Hot	Yes	Yes
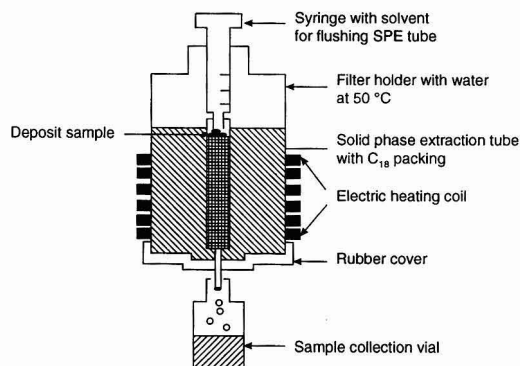
Fig. 2 Schematic diagram of the apparatus used in the solid-phase extraction of samples containing a mixture of wood resin, stearone and calcium soaps of resin and fatty acids. A filter holder for a membrane filtration unit was adapted and used as a laboratory-made water-bath.

30 m column coated with methylsilicone was used. In the current study, the following conditions were used.

A Hewlett-Packard (Avondale, PA, USA) Model 5890 Series II gas chromatograph, equipped with electronic pressure programming, and FID and a capillary injection port, was used. The injection port was fitted with an unpacked fused-silica split liner, which was deactivated as described previously.[23] Both the injector and detector were maintained at 320 °C. Analytes were separated on a 10 m × 0.25 mm id DB-5 (0.25 μm thickness) fused-silica capillary column (J&W Scientific, Rancho Cordova, CA, USA). The oven temperature was raised from 200 to 320 °C at 15 °C min^{-1} and held isothermal at 320 °C for 3 min. Data processing was performed by Chemstation software from Hewlett-Packard.

A recent report showed that GC–MS could be used for the determination of AKD and stearone in paper extracts.[14] This technique was also evaluated in this work.

Determination of AKD by potentiometric titration

A potentiometric titration procedure for the determination of AKD was developed. The procedure entails reacting an AKD solution with an excess amount of a primary amine followed by back-titration of the excess amine with perchloric acid. Details of the procedure, which is useful for monitoring the stability of AKD emulsions at mills, are given elsewhere.[24]

Preparation of handsheets

Sized handsheets were prepared as shown in Fig. 3 using a Mark V Dynamic Handsheet Mold (Paper Chemistry Laboratories, Syracuse, NY, USA). The pulp mixture (90% hardwood–10% softwood) was stirred under dynamic conditions, drained by gravity flow and a vacuum was applied at the end to remove excess of water. The handsheets were pressed at 420 kPa, dried on a cylinder speed drier at 105 °C and cured for 10 min in an oven at 110 °C. The basis mass of the sized sheets was 70 g m^{-2}.

Results and Discussion

Determination of AKD solutions by GC

Chromatograms from all the AKD solutions in acetone showed three prominent peaks and a number of small peaks (that is, several peaks arise from the mixture present in the AKD); analysis of AKD solutions did not result in extra multiple peaks attributed to thermal decomposition as previously reported.[13] Peak areas of the prominent peaks, which are C_{16}–C_{16}, C_{18}–C_{16} and C_{18}–C_{18} clusters of AKD or hydrolysed stearone, were summed and used to plot calibra-
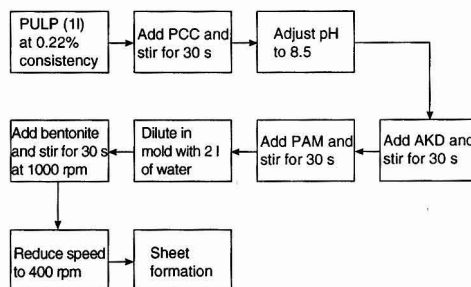
Fig. 3 Flow diagram of the procedure used for making sized handsheets using the Mark V dynamic handsheet mold. (PULP, fully bleached kraft pulp; PCC, precipitated calcium carbonate; and PAM, polyacrylamide retention aid.)

tion graphs. Using the chromatographic conditions described, all the prominent peaks eluted between 6 and 9 min, which is much shorter than the elution times of around 20 min reported previously.[11,14] The prominent peaks were used for both qualitative and quantitative analysis of AKD and stearone, with the exceptions noted below. Analysis of AKD solutions after conversion into the stearone form by hydrolysis resulted in three prominent peaks also, but their retention times shifted to slightly lower values.

Chromatograms of AKD samples, after methylation, gave peaks that were smaller than those obtained from analysis of non-derivatized AKD solutions. Chromatograms of the methylated samples showed extra peaks, presumably from methylation products of impurities in the AKD starting material. Their calibration graphs were not linear. Methylation with diazomethane resulted in chromatograms with larger areas than peaks from methylation with methyl iodide. Evidently, the methylation methods were more time consuming than the other methods mentioned in the preceding paragraph. It is not clear why AKD should respond to derivatization as it does not have functional groups amenable to methylation.

Considering the factors of extra peaks and linearity of calibration graphs, hydrolysis to the ketone form was the most reliable method for the determination of AKD. A similar conclusion has been reported.[14] However, in this work the analysis time is about one third of that reported previously.[11,14] The analysis time was reduced by using much shorter capillary columns. As the GC determination of AKD and stearone gives rise to several peaks, quantification is best performed by summing all peak areas. The use of an internal standard, besides correcting for losses during sample preparation, is very useful for this purpose. The detection limit was 25 mg l^{-1} and the relative standard deviation was less than 2.5%. It is striking that AKD has such a high detection limit, as FID has the potential to offer much lower detection limits.

The determination of stearone by GC–MS has been reported by Dart and McCalley.[14] A similar GC–MS analysis was attempted in this work. However, because of the low volatility of AKD and stearone, fouling of the mass spectrometer components occurred after a few runs. Conse-

quently, the use of GC–MS is not recommended for the routine analysis of AKD samples.

In analysing for AKD in mill samples, it is imperative to use standards derived from the size being used in the process, because different AKD emulsions can give rise to different GC patterns owing to differences in amounts of various fatty acids used in the synthesis of AKD. For example, Figs. 4 and 5 illustrate differences in chromatograms of AKD and stearone from two AKD supplier formulations. The chromatograms clearly illustrate the differences between the two emulsions; the ratios of the C_{16}–C_{16}, C_{18}–C_{16} and C_{18}–C_{18} peaks were not the same in the two emulsions; the C_{16}–C_{16} and C_{16}–C_{18} peaks were predominant in the emulsion from supplier A whereas the C_{16}–C_{18} and C_{18}–C_{18} peaks were predominant in the emulsion from supplier B.

Determination of Various AKD Forms in Paper

The schematic diagram in Fig. 6 illustrates the procedures involved in the determination of AKD in its various forms in paper. The various forms are (1) free AKD, which may be
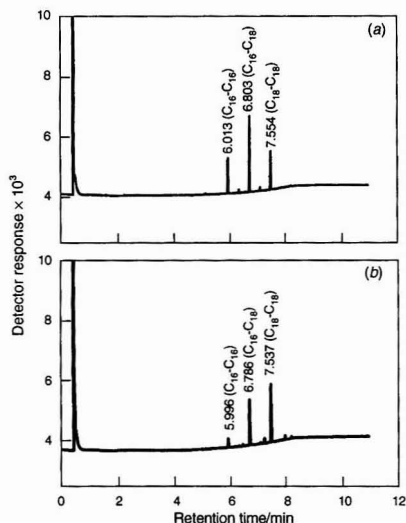
Fig. 5 Chromatograms of 500 mg l^{-1} stearone samples prepared from AKDs from two different suppliers: (a) supplier A and (b) supplier B.
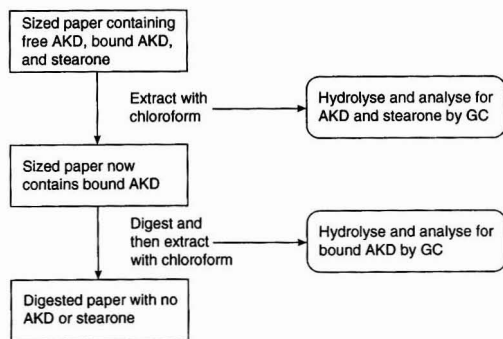
Fig. 6 Flow diagram illustrating the extraction of various forms of AKD from paper.

Fig. 4 Chromatograms of 500 mg l^{-1} AKD samples from two different suppliers: (a) supplier A and (b) supplier B.

non-hydrolysed or hydrolysed to form stearone, and (2) bound AKD, which is chemically bonded to fibres.

Free AKD in paper

As in the previous section, conversion of AKD in extracts into the stearone form gave the best results. Depending on the emulsion used, hydrolysis to the stearone may not be required as all the free AKD was found to be in the form of ketones. For example, Fig. 7, which shows chromatograms for non-hydrolysed AKD extracts of papers sized with Hercon-70 and Hercon-72S, indicates that all the AKD in the extract of the paper sized with Hercon-72S was in the ketone form whereas the extract from Hercon-70 sized paper showed the presence of both free and hydrolysed AKD. However, it is best to perform the hydrolysis step to ensure any free AKD that may be present is converted into the ketone form. The results in Fig. 7 offer a further demonstration of the importance of using standards prepared from the same emulsions used in the sizing process.

Reacted or bound AKD in paper

Table 3 shows the results obtained using various digestion procedures. Of the first three, only digestion with sodium hydroxide did not extract bound AKD from paper. It was found that hydrolysis of AKD to the stearone form was partial in the absence of precipitated calcium carbonate and complete in its presence. Perhaps this was due to the difficulty of removing all of the AKD bound to the fibres; in the presence of precipitated calcium carbonate some of the AKD may be hindered from reacting with the fibres. (This observation may lend credence to the belief that AKD does chemically bond with fibres, contrary to some recent reports.[25])
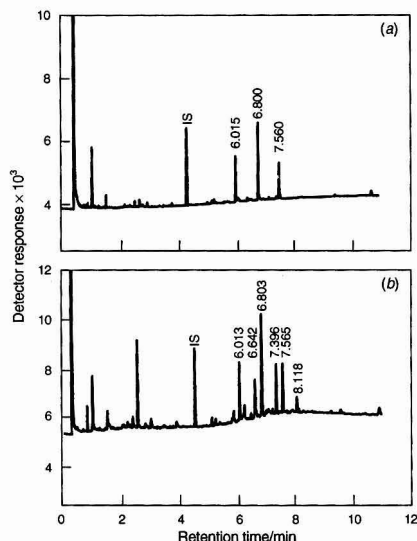
Fig. 7 Chromatograms for non-hydrolysed extracts of paper sized with two different AKD emulsions from Hercules: (*a*) Hercon-72S and (*b*) Hercon-70. Peaks corresponding to AKD are at 6.4, 7.4 and 8.1 min; those corresponding to stearone are at 6.0, 6.6 and 7.6 min. (Hercon-70 needs an effective retention aid system and contains a 2 : 1 starch to AKD ratio, whereas Hercon-72S contains a resin sizing promoter and less cationic starch.) IS, Internal standard.

Digestion with TMAH gave curious results. The samples were processed in four ways:

(1) After digestion, the TMAH was removed by filtration before extraction with chloroform. Neither AKD nor stearone peaks were found in the chromatogram of the chloroform extract.

(2) After digestion, the TMAH was removed from the sample which was then digested with sodium carbonate for 1 h followed by extraction with chloroform. The chromatogram showed only one stearone peak (C_{16}–C_{18}) instead of the three that had been expected. No AKD peaks were found.

(3) After digestion, the TMAH was removed by evaporation to almost dryness and the mixture was extracted with chloroform. Two peaks (C_{16}–C_{16} and C_{18}–C_{18}) corresponding to AKD were found.

(4) After digestion, the TMAH was removed by evaporation almost to dryness, the mixture was neutralized with HCl and boiled for 1 h before extraction with chloroform. Two AKD peaks (C_{16}–C_{16} and C_{18}–C_{18}) were found. This was unexpected, as hydrolysis should produce only stearone and not free AKD.

The AKD values in Table 3 obtained after digestion with TMAH seem to be significantly higher than the results obtained after digestion with either acid or carbonate. However, it is not certain that the peaks found did really correspond to AKD or stearone. Consequently, it is believed that the results obtained with acid or carbonate digestion are more reliable as their chromatograms display a complete spectrum of stearone peaks. Thus digestion with acid or carbonate leads to results that enable both qualitative (from the chromatographic patterns) and quantitative determination of AKD in paper.

Table 3 Amount of bound AKD in sized handsheets as determined, after digestion, by a variety of procedures

Digestion procedure	AKD added in the sizing process/mg	Bound AKD/mg	Bound AKD (% of AKD added)	Bound AKD (% of oven dried sheet)
HCl	3.5	0.2	5.7	0.008
NaOH	3.5	0	0	0
Na$_2$CO$_3$	3.5	0.2	5.7	0.008
TMAH*	3.5	0	0	0
TMAH†	3.5	0.5	14.3	0.02
TMAH‡	3.5	0.4	11.4	0.02
TMAH§	3.5	0.4	11.4	0.02

* After digestion, the TMAH was removed from the sample before extraction with chloroform.

† After digestion, the TMAH was removed from the sample which was then digested with sodium carbonate for 1 h, followed by extraction with chloroform.

‡ After digestion, the TMAH was removed by evaporation almost to dryness and the mixture was extracted with chloroform.

§ After digestion, the TMAH was removed by evaporation almost to dryness and the mixture was neutralized with HCl then boiled for 1 h before extraction with chloroform.

Table 4 Effect of photochemical irradiation on papers sized with AKD

	AKD in extracts (%)			
	Handsheet samples		Paper machine samples	
Light source	Control	Exposed	Control	Exposed
Fluorescent	0.05	0.04	0.02	0.02
UV	0.05	0.04	0.02	0.02

The results for the photochemical studies, shown in Table 4, indicate that exposure to UV and fluorescent light caused no significant decrease in the amount of stearone found in extracts from handsheets and no significant changes in extracts from machine-made paper. From these limited results, it can be concluded that exposure of sized papers to light for a period of 24 h does not affect the amount of bound AKD in sized paper.

Soxtec versus Soxhlet Extraction

Extraction of sized handsheets and machine-made samples by the two methods gave similar results. Prior swelling of fibres by soaking in water as reported[11] was found to be unnecessary. It is therefore recommended that Soxtec extraction be used instead of Soxhlet extraction as this leads to considerable savings in time (extraction time of 1 h *versus* 4 h). Soxtec extraction affords rapid extraction of pulp and paper matrices.[20]

Free and Hydrolysed AKD in White Waters

Solid-phase extraction was ideal for isolating AKD and stearone from white waters. An investigation of a variety of solid-phase sorbents showed that AKD in dilute aqueous solution was retained on a neutral alumina phase and not on silica, NH_2, CN, diol or C_{18} phases. The SPE column became plugged after filtration of 60–70 ml of white water. The best solvent for eluting the adsorbed AKD and stearone was dry ethanol. Recoveries of stearone and AKD from spiked samples were over 97% and 82%, respectively. The lower recoveries for AKD were probably due to hydrolysis in water or adsorption on the surfaces of containers used in the study.

Similar recoveries of stearone were obtained by filtration, confirming the validity of the solid-phase extraction procedure. Stearone particles in white water are large enough to be retained on membrane filters.

Mass Balance of AKD in Sheet and in White Water

Results of a mass balance of AKD in white water and in handsheets after sizing with 3.5 mg of AKD are shown in Table 5; there was an 89% recovery of the original AKD added in the sizing process. A recovery of this magnitude is good considering that some of the AKD may be lost by adsorption on the equipment used in the sizing process. The results also show there was 71% retention of AKD in the sheet, which is higher than the 50% 'best' value achieved on paper machines.[26] This is probably a reflection of the handsheet-making equipment not fully simulating real paper machine conditions.

Hydrolysed AKD in Deposits by Solid-phase Extraction

In order to find a suitable solvent for quantitative extraction of stearone from deposits, solubility tests were performed as shown in Table 2. The results show hot acetone was a good solvent for separating stearone and wood resin from calcium soaps. The separation scheme depicted in Fig. 8 was developed for the fractionation of a mixture of wood resin, calcium

Table 5 Mass balance of AKD in handsheets and in white water

AKD added/mg	Free AKD in paper/mg	Bound AKD in paper/mg	AKD in white water/mg	Total AKD found/mg	AKD found (%)
3.5	2.3	0.2	0.6	3.1	89
3.5	2.5	0.2	0.6	3.3	94

soaps and stearone. As shown in Table 6 for triplicate analyses of an artificial mixture containing known amounts (50–80 mg each) of stearone, wood resin and calcium soap, there were good recoveries of the components with the exception of stearone, which is possibly due to sample loss during the filtration step. The purity of the fractions was confirmed by GC for stearone and wood resin and by FTIR spectrometry for calcium soaps. Hence a scheme is now available for the determination of the major components in deposits from mills where AKD is used for sizing.

Conclusions

Gas chromatographic determination of AKD is best performed by prior hydrolysis of the AKD to the stearone form. The determination of AKD in paper can be significantly expedited by solvent extraction with a Soxtec system instead of the traditional Soxhlet system and by using a short capillary column. Digestion of sized papers with hydrochloric acid or sodium carbonate should be used for releasing AKD bound in paper. Solid-phase extraction can be used to fractionate major components, namely wood resin, calcium soaps and stearone, in deposits from alkaline paper mills. Different supplies of AKD emulsions lead to different chromatographic patterns during GC analysis. Consequently, AKD standard should be

Table 6 Mass percentage recoveries of wood resin (tall oil), calcium soap (oleate) and hydrolysed AKD from a mixture. Separation by solid-phase extraction with a C_{18} column packing

Replicate sample	Stearone (%)	Calcium soap (%)	Wood resin (%)
1	86.7	102.6	103.5
2	89.2	98.7	104.6
3	92.5	98.5	104.7

Fig. 8 Schematic diagram of the solid-phase extraction procedure used to fractionate wood resin, stearone and calcium soaps in alkaline paper mill deposits.

prepared from the same batches of AKD that were used in the sizing process.

Impurities in the AKD lead to the formation of multiple peaks in gas chromatographic analysis. Consequently, the determination of AKD and its hydrolysed form necessitates summation of all the peaks observed. As different formulations will have various amounts of impurities, this becomes a problem if one does not have samples that were used in the sizing process. A way to overcome this is to synthesize the entire range of AKDs (R groups ranging from C_{14} to C_{20}) according to procedures mentioned by Bottoroff and Sullivan.[16] With each of these standards one could then obtain GC calibration graphs (response *versus* concentration), enabling one to quantify the various AKDs present in any commercially available preparation. In addition, the various keto forms of each synthesized AKD could be prepared easily from the above standards, facilitating the preparation of GC calibration graphs for all the major keto forms one would expect to encounter from hydrolysis of commercial AKD preparations. We are currently working on the synthesis of these compounds.

References

1   Crouse, B., and Wimer, D. G., *Tappi J.*, 1991, **74**, 152.
2   Panchapakesan, B., *Pulp Pap.*, 1992, **66**, 57.
3   Evans, D. B., in *The Sizing of Paper*, ed. Reynolds, W. F., Tappi Press, Atlanta, GA, 2nd edn., 1989, ch. 2.
4   Meier, R., and Baly, C., in *Technical Conference Proceedings—Pacific Paper Expo Conference*, Vancouver, Canada, 1990, vol. 5, p. 67.
5   Corry, P. A., *Pap. Technol.*, 1992, **33**, 33.
6   Herner, B., *Pulp Pap.*, 1990, **63**, 141.
7   Scalfarotto, R. E., *Pulp Pap.*, 1985, **59**, 126.
8   Walkden, S. A., *Neutral/Alkaline Papermaking*, TAPPI Short Course Notes, Tappi Press, Atlanta, GA, 1990, p. 67.
9   Moyers, B., *Proceedings—TAPPI Papermakers Conference*, Tappi Press, Atlanta, GA, 1991, p. 245.
10 Arnson, T., Crouse, B., and Griggs, W., in *The Sizing of Paper*, ed. Reynolds, W. F., Tappi Press, Atlanta, GA, 2nd edn., 1989, ch. 5.
11 Odberg, L., Lindstrom, T., Liedberg, B., and Gustavsson, J., *Tappi J.*, 1987, **70**, 135.
12 Kropholler, H., and de Sousa, A. M., *Appita*, 1993, **46**, 123.
13 Yano, T., Ohtani, H., Tsuge, S., and Obokata, T., *Analyst*, 1992, **117**, 849.
14 Dart, P. J., and McCalley, D. V., *Analyst*, 1990, **115**, 13.
15 Kamutzki, W., and Krause, Th., *Papier*, 1982, **36**, 311.
16 Bottorff, K. J., and Sullivan, M. J., *Nord. Pulp Pap. Res. J.*, 1993, **8**, 86.
17 Colasurdo, A. R., and Thorn, I., *Tappi J.*, 1992, **75**, 143.
18 Gess, J. M., and Lund, R. C., *Tappi J.*, 1991, **74**, 111.
19 Odberg, L., and Lindstrom, T., in *Proceedings—International Symposium on Wood and Pulping Chemistry*, Vancouver, Canadian Pulp and Paper Association, Montreal, 1985, p. 41.
20 Sitholé, B. B., Vollstaedt, P., and Allen, L. H., *Tappi J.*, 1991, **74**, 187.
21 Dorris, G., Douck, M., and Allen, L. H., *J. Pulp Pap. Sci.*, 1983, **9**, TR1.
22 Dorris, G., Douck, M., and Allen, L. H., *J. Pulp Pap. Sci.*, 1985, **11**, J149.
23 Sitholé, B. B., Sullivan, J. L., and Allen, L. H., *Holzforschung*, 1992, **46**, 409.
24 Nyarku, S., and Sitholé, B. B., *Can. J. Chem.*, 1994, **72**, 274.
25 Isogai, A., Taniguchi, R., Onabe, F., and Usuda, M., *Nord. Pulp Pap. Res. J.*, 1992, **8**, 193.
26 Girardi, F. P., in *Proceedings—TAPPI Papermakers Conference*, Tappi Press, Atlanta, GA, 1989, p. 205.

Ultrasonic Treatment of Molluscan Tissue for Organotin Speciation*

J. L. Gomez-Ariza, E. Morales, R. Beltran, I. Giraldez and M. Ruiz-Benitez
Departmento de Química y Ciencia de los Materiales, Escuela Politécnica Superior, Universidad de Huelva, Huelva, Spain

A method is described for the extraction of nanogram amounts of mono-, di- and tributyltin compounds from bivalves. The procedure is based on treatment of lyophilized samples with 0.08% m/v tropolone solution in methanol in successive sonication steps. The method was applied to oyster and cockle samples from southwest Spain and the results compared favourably with those given by typical leaching methods based on the use of acid reagents, owing to the absence of degradation processes.

Keywords: Mono-, di- and tributyltin; speciation; sonication; gas chromatography; mollusc

Introduction

Organotin compounds are of important environmental concern owing to their wide use for industrial purposes. Increasing interest is focused on triorganotin compounds, which have been used as biocides owing to their high toxicity towards molluscs and fungi. Triorganotins, especially tributyltin (TBT), are used in antifouling paints, and are of recent growing concern as significant toxic effects have been found on non-target organisms. Consequently, determining levels of organotin species in sea-water, sediments and biological samples is necessary in order to assess whether environmental contamination is occurring.

Analytical techniques for organotin speciation in waters are well established,[1] but for sedimentary and biological samples the techniques are less developed, especially in the extraction step. Few methods have been developed for the determination of organotins in biological matrices owing to the difficulty of applying the analytical techniques for tin speciation to such complex systems.

The main procedures described for leaching organotins from biological samples are based on the use of acid reagents that may be grouped in several classes: (*i*) digestion of samples with 0.2 mol l^{-1} acetic acid[2] (algal tissues and marine invertebrates); (*ii*) crushing in a grinder with soft parts and tissues in 0.04 mol l^{-1} hydrochloric acid[3] (limpets and fish tissues); (*iii*) homogenization of tissues in 0.02 mol l^{-1} sorbitol–0.01 mol l^{-1} TRIS–acetate buffer solutions[4] (fresh algal tissues); (*iv*) drying and freezing the tissues in liquid nitrogen followed by crushing and homogenization with distilled water, the final mixture being digested with 1 mol l^{-1} sodium hydroxide for 48 h and acidified to pH 2 with 5 mol l^{-1} nitric acid;[5] (*v*) alkaline leaching with sodium hydroxide;[6] (*vi*) extraction with an organic solvent after acid or alkaline leaching, the solvent sometimes containing a chelating agent;[7] and (*vii*) acid leaching with HBr followed by extraction with 0.04% tropolone in dichloromethane.[8]

Other workers have considered the use of sonication to enhance the extraction of organotins. Tugrul *et al.*[3] proposed sonication of dried and homogenized limpet shells in 40 ml of water for 1 h. Han and Weber[9] extracted methyl- and butyltin compounds from oyster tissue with a methanol–8.4 mol l^{-1} HCl (1 + 5) in a capped centrifuge tube that was sonicated at 50–60 Hz in a 60 °C water-bath for 1 h. Batley and Scammel[10] used ultrasonication with concentrated HCl and methanol before extraction of tributyltin with tropolone in dichloromethane. Higashiyama *et al.*[11] used 0.5% tropolone–benzene and 1 mol l^{-1} HBr–ethanol solution containing L-ascorbic acid, under ultrasonication for 30 min, for extraction of butyl- and phenyltins from mussels.

However, these leaching procedures based on the use of an acid reagent are time consuming and they can cause degradation of the organotins. For this reason, an alternative simpler and faster extraction method based on sonication of samples with non-acid leaching reagents was studied in this work, and the procedure was successfully applied to the speciation of butyltin compounds in molluscan tissues, comparing the results with those from acid extraction.

Experimental

Reagents

All organic solvents were of HPLC grade. Organotin standards were obtained from Aldrich and were used without further purification, as purity tests did not reveal any detectable impurities. The purity of organotin standards was tested by chromatographic confirmation of the absence of other organotin species in the standard, followed by determination of the tin content by AAS. The other chemicals were of analytical-reagent grade. Water used in all the experiments was distilled and de-ionized and gave blank readings in all analyses.

Materials

Molluscs, particularly mussels and oysters, frequently bioaccumulate organotin species and they were used for the ultrasonic extraction study.

Samples O1 and O2. About 30 specimens of oysters (*Crassostrea giga*) of size between 50 and 100 mm were collected from rocks and man-made structures below half-tide, at two stations, Estero de Pinillos on the Carreras river and Agua del Pino on the Piedras river (Huelva, southwest Spain), respectively.

Samples C1 and C2. About 50 specimens of cockles (*Gerastoderma edulis*) of size between 18 and 24 mm were collected from a sandy bank below low tide at two sites located downstream and upstream, respectively, on the San Pedro river (Cadiz, southwest Spain).

Sample M1. This sample from the Carreras river coastal area consisted of 40 specimens of mussels (*Mytilus edulis*) of

size between 20 and 50 mm, collected from rocks below half-tide.

All the specimens were collected in February 1992 and kept for 24 h in a container with clean sea-water before the analysis.

Chemical Extraction

A suitable mass of wet homogenized biological tissue (1–20 g) was placed in a 100 ml Erlenmeyer flask with a PTFE screw closure and treated with 25 ml of hydrobromic acid–water (1 + 1) with vigorous shaking at room temperature for 1 h, then extracted with 50 ml of 0.04% (m/v) tropolone solution in dichloromethane for 2 h. The phases were separated in 50 ml Teflon tubes by centrifugation at 10 000 rpm for 10 min and both the aqueous and organic phases were transferred into a separating funnel in which the organic phase was separated and dried with anhydrous sodium sulfate. The resulting extract was reduced in volume to about 1 ml by rotary evaporation. The solid phase was washed in the centrifuge tube with 5 ml of hexane and centrifuged. The resulting hexane extract was used to re-extract the previously separated aqueous phase for 3 min and then added to the dichloromethane extract. The mixture was again reduced in volume to 1 ml, the dichloromethane being replaced by hexane owing to the higher boiling-point of the latter. This manipulation avoids the subsequent reaction of dichloromethane with the Grignard reagent used in the derivatization step.

Ultrasonic Extraction

Samples were lyophilized, for elimination of water, before ultrasonic extraction. A Maxi-Dry lyophilizer (FTS, Stone Ridge, NY, USA) was used for this purpose, fixing the temperature at −100 °C and the pressure at 40 mTorr. Samples were treated under these conditions for 24 h.

A 5 g amount of lyophilized biological sample, weighed exactly, was placed in a 100 ml Erlenmeyer flask with a PTFE screw closure, 25 ml of 0.08% m/v tropolone solution in methanol were added and the mixture was treated for 15 min in an ultrasonic bath (Ultrasons 3000513 Selecta, size 15 × 30 × 14 cm, power 150 W, frequency 50 Hz) in which the temperature was maintained between 30 and 35 °C. The methanolic phase was separated by centrifugation at 10 000 rpm for 10 min, the supernatant was removed with a Pasteur pipette, the residue was washed with 5 ml of methanol and centrifuged and the two methanolic extracts were combined and dried over anhydrous sodium sulfate. The residue was extracted again in the ultrasonic system, as previously, and all the extracts were combined and reduced in volume to about 1 ml by rotary evaporation. Finally, the extract was treated with 10 ml of hexane and reduced again to 1 ml to replace the methanol in the extract, as this solvent reacts with the Grignard reagent during the derivatization process.

Analysis

Derivatization

The hexane extract was treated with 4 ml of 1 mol l⁻¹ pentylmagnesium bromide solution in diethyl ether for 1 h in a Pyrex glass tube, injecting the Grignard reagent through a septum with a syringe to avoid losses caused by its vigorous reaction with the fats present in the samples. Derivatization reaction was continued in the same tube to complete the reaction time (1 h), replacing the septum with a standard glass cap.

Clean-up

The excess of reagent was removed with 0.5 mol l⁻¹ sulfuric acid and the organic extract was reduced to 1 ml and passed through a Florisil column, then treated with 25 ml of 1 mol l⁻¹ sodium hydroxide at 40 °C with mechanical stirring for 30 min. The phases were separated in a funnel, and the organic phase was reduced to 1 ml and again passed through the Florisil column, the organotin species being eluted with pentane and transferred into a microevaporator together with the internal standard (dimethyldipentyltin). Finally, the pentane extract was concentrated to 0.5 ml under a stream of nitrogen.

Measurement of organotin concentration

Organotin species were determined using GC with flame photometric detection (FPD), following a procedure reported previously.[12,13] A Perkin-Elmer Model 8140 gas chromatograph fitted with a split–splitless injector, glass capillary column (Supelco SPB-1, 15 m × 0.53 mm id, film thickness 1.5 µm). The flame photometric detector was operated with a 610 nm cut-off interference filter at 250 °C, using hydrogen and air flow rates of 46.5 and 88.0 ml min⁻¹, respectively. The injector temperature was set at 250 °C and helium (9.5 ml min⁻¹) served as the carrier gas using a splitting ratio of 3.8 : 1. Sample aliquots of 5–10 µl were injected and the compounds of interest were eluted with the following temperature programme: initial column temperature 50 °C, heating to 250 °C at 10 °C min⁻¹ and isothermal at 250 °C for 7 min.

Calibration and analytical quality control

Organotin concentrations were deduced from calibration graphs derived from derivatized standard solutions using peak heights. Calibration experiments were not directly carried out on molluscan tissues. The calibration graphs were linear for amounts of tin less than 40 ng for most organotin species; this limit increased to 55 and 60 ng for diphenyltin (DPT) and triphenyltin (TPT), respectively. The determinations were carried out using Me_2SnPe_2 as internal standard, which improved the precision.

Quality control of results was monitored by preparing a calibration graph each week and injecting a derivatized standard with all the tin species every day to test the instrument signal. The absolute limit of Sn that could be detected with the instrument, evaluated as three times the standard deviation of the blank, was in the range of about 0.3 ng for butyltins and 0.5 ng for phenyltin species. The detection limits in molluscan tissue, including the extraction step, were TBT 0.61, DBT 0.75, MBT 0.76, MPT 2.8, DPT 3.2 and TPT 2.7 ng g⁻¹.

Table 1 Influence of lyophilization on organotin concentration* (as ng g⁻¹ of Sn) in biological samples

Sample	Form	TBT	DBT	MBT
O1	Fresh	430	71	12.6
	Lyophilized	430	71	11.8
O2	Fresh	170	24	5.2
	Lyophilized	160	25	7.1
C1	Fresh	390	140	82
	Lyophilized	380	130	83
C2	Fresh	350	93	36
	Lyophilized	350	94	35

* Mean of three determinations.

Results and Discussion

The use of non-acid reagents for organotin extraction from a natural matrix under ultrasonication can eliminate some loss problems caused by treatment with a strong acid (HCl, HBr), which could lead to organotin degradation. However, these leaching reagents make it necessary to lyophilize the sample before ultrasonic extraction for elimination of water if the solvent used is water-soluble, to avoid the subsequent reaction of water with the Grignard reagent in the derivatization step prior to the GC determination.

Several experiments were carried out to check for possible losses of tin species during the lyophilization. For this purpose organotins were determined in both lyophilized and non-lyophilized samples of oyster (O1 and O2) and cockle (C1 and

C2) after extraction of species with $HBr–CH_2Cl_2$.[8] The results, in Table 1, show that lyophilization does not affect the presence of organotin compounds in the samples, particularly butyltins, the only species detected in this assay.

The sonication extraction was tested with molluscan tissues using six different leaching solvents in the presence of tropolone: pentane, chloroform, dichloromethane, acetone, tetrahydrofuran and methanol. Different successive periods of sonication (15 min each) were also tested. With pentane and methanol the experiments were also carried out in the absence of tropolone. In Table 2 are given the results obtained for samples O1 and C1, which were sampled in a coastal area in southwest Spain near a boatyard, and these results were compared with those corresponding to chemical extraction using $HBr–CH_2Cl_2$.[8] It can be observed that the recoveries are

Table 2 Optimization of sonication procedure for biological samples: organotin concentrations[*] (as ng g^{-1} of Sn)

Solvent	Sequential sonication/min	O1			A1		
		TBT	DBT	MBT	TBT	DBT	MBT
C_5H_{12}	0–15	150	12.1	<DL[†]	140	28	<DL
	15–30	33	<DL	<DL	27	9.9	<DL
	30–45	13.6	<DL	<DL	20	<DL	<DL
	Residue	250	56	11.2	200	88	79
	Total	440	68	11.2	390	130	79
	(Σ of fractions)						
C_5H_{12}–tropolone	0–15	210	22	<DL	190	48	<DL
	15–30	52	10.6	<DL	38	16	<DL
	30–45	<DL	<DL	<DL	<DL	<DL	<DL
	Residue	170	35.1	11.9	160	61	85
	Total	430	68	11.9	380	130	85
	(Σ of fractions)						
$CHCl_3$–tropolone	0–15	270	39	8.1	220	92	50
	15–30	37	11.1	<DL	25	14.9	12.1
	30–45	11.1	<DL	<DL	9.7	<DL	<DL
	Residue	8.9	8.1	<DL	11.6	7.9	8.1
	Total	320	58	8.1	260	114	70
	(Σ of fractions)						
CH_2Cl_2–tropolone	0–15	250	37	4.1	200	75	24
	15–30	49	10.1	<DL	52	14.4	6.6
	30–45	26	<DL	<DL	15.4	<DL	<DL
	Residue	103	25	5.1	113	35	56
	Total	420	72	9.2	380	120	87
	(Σ of fractions						
Acetone–tropolone	0–15	210	34	<DL	210	54	<DL
	15–30	69	10.4	<DL	73	16.8	<DL
	30–45	17.2	<DL	<DL	35	<DL	<DL
	Residue	100	28	10.9	76	56	79
	Total	430	73	10.9	390	130	79
	(Σ of fractions)						
THF–tropolone	0–15	210	29	5.1	160	61	41
	15–30	109	14	1.9	100	28	20
	30–45	52	5.0	<DL	54	<DL	7.2
	Residue	68	21	4.9	73	48	11.8
	Total	430	69	11.9	340	140	80
	(Σ of fractions)						
CH_3OH	0–15	330	36	3.0	310	71	24
	15–30	108	22	<DL	69	43	4.6
	30–45	<DL	9.1	<DL	<DL	12.9	<DL
	Residue	<DL	<DL	7.9	<DL	<DL	52
	Total	440	68	10.9	380	127	81
	(Σ of fractions)						
CH_3OH–tropolone	0–15	350	56	8.6	320	99	3.1
	15–30	82	12.7	3.4	66	36	79
	30–45	<DL	<DL	<DL	<DL	<DL	<DL
	Residue	<DL	<DL	<DL	<DL	<DL	<DL
	Total						
	(Σ of fractions)	430	69	12	390	134	82
Acid leaching		430	71	11.8	380	131	83

[*] Mean of three determinations.
[†] DL = detection limit.

not good with most of the solvents. Pentane extracts low concentrations of dibutyl- and monobutyltin and acetone does not show a high extraction of monobutyltin, but the results are better using dichloromethane and tetrahydrofuran, and especially methanol, which makes possible (in the presence of tropolone) the quantitative extraction of all the species with only two successive sonication steps.

Sonication of molluscan tissues with methanol–tropolone leaching agent gave similar results to acid extraction[8] (HBr–CH_2Cl_2). Table 3 gives the concentration levels obtained with both methods, using oysters, cockles and mussels sampled from five different locations in southwest Spain (see Experimental).

The results in Table 3 show that the sonication extraction procedure based on the use of non-acid reagents can replace the acid leaching of organotins from bivalve tissues. In addition, the proposed method requires only about 30 min for total extraction of the organotin species against the 3 h necessary for the acid non-ultrasonic leaching. Finally, the number of manipulations needed for ultrasonic extraction have been reduced and hence the possibility of sample losses.

An additional study was carried out to achieve the simultaneous pentylation (derivatization) and extraction of organotins from the molluscan tissues, in order to have a simpler and less time-consuming procedure. For this purpose lyophilized oyster and mussel tissues were treated with 25 ml of 1 mol l^{-1} pentylmagnesium bromide solution in diethyl ether under reflux at 30 °C for different times from 1 to 24 h, and the extract was centrifuged in Teflon tubes at 10 000 rpm. The organic phase was separated and the excess of reagent removed with 25 ml of 0.5 mol l^{-1} sulfuric acid. The organic extract was finally cleaned up and organotin species were determined following the described chromatographic procedure. However, the low recoveries obtained (TBT 42–53%,

Table 3 Comparison of sonication and acid extraction methods to evaluate the presence of organotin species in molluscs

Sample	Method	Concentrations*/ng g^{-1} of Sn (dry mass)		
		TBT	DBT	MBT
O1	Sonication	440	66	10.8
	Acid leaching	430	68	10.9
O2	Sonication	156	26	6.9
	Acid leaching	159	25.0	7.1
C1	Sonication	380	137	87
	Acid leaching	380	141	83
C2	Sonication	350	92	33
	Acid leaching	350	94	35
M1	Sonication	172	73	51
	Acid leaching	178	80	59

* Mean of three determinations.

DBT 20–27% and MBT 28–29%) make the method unsuitable for practical purposes.

Conclusions

The sonication procedure proposed for the extraction of organotins from bivalve tissues, based on the use of non-acid reagents, makes possible the extraction of butyltin species from these samples with recoveries similar to those given by acid treatment and extraction. The use of methanol as extracting agent under sonication makes the procedure simpler and faster than traditional acid treatment and extraction, which, in addition, could produce degradation of organotin species. Therefore, this method represents a good alternative to acid treatment.

References

1 Donard, O. F. X., and Pinel, R., in *Environmental Analysis Using Chromatography Interfaced With Atomic Spectroscopy*, ed. Harrison, R. M., and Rapsomanikis, S., Ellis Horwood, Chichester, 1989, pp. 193–310.
2 Seidel, S. L., Hodge, V. F., and Goldberg, E. D., *Thalassia Jugosl.*, 1980, **16**, 209.
3 Tugrul, S., Balkas, T. I., and Goldberg, E. D., *Mar. Pollut. Bull.*, 1983, **14**, 197.
4 Ishii, I., *Bull. Jpn. Soc. Sci. Fish*, 1982, **48**, 1609.
5 Donard, O. F. X., Short, F. T., and Weber, J. H., *Can. J. Fish. Aquat. Sci.*, 1986, **44**, 140.
6 Rapsomanikis, S., and Harrison, R. M., *Appl. Organomet. Chem.*, 1988, **2**, 151.
7 Tsuda, T., Nakanishi, H., Morita, T., and Takebayashi, J., *J. Assoc. Off. Anal. Chem.*, 1986, **69**, 981.
8 Gomez-Ariza, J. L., Morales, E., Beltran, R., Giraldez, I., Ruiz-Benitez, M., and Pozas, J. A., *Fresenius' J. Anal. Chem.*, 1995, in the press.
9 Han, J. S., and Weber, J. H., *Anal. Chem.*, 1988, **60**, 316.
10 Batley, G. E., and Scammel, M. S., *Appl. Organomet. Chem.*, 1991, **5**, 99.
11 Higashiyama, T., Shiraishi, H., Otsuki, A., and Hashimoto, S., *Mar. Pollut. Bull.*, 1991, **22**, 585.
12 Gomez-Ariza, J. L., Morales, E., and Ruiz-Benitez, M., *Analyst*, 1992, **117**, 641.
13 Gomez-Ariza, J. L., Morales, E., and Ruiz-Benitez, M., *Appl. Organomet. Chem.*, 1992, **6**, 279.

Determination of Formation Quotients by a Flow Injection Procedure

Roger T. Echols and Julian F. Tyson*

Department of Chemistry, University of Massachusetts, Box 34510, Amherst, MA 01003-4510, USA

A method is described for determining equilibrium constants for reactions of 1 : 1 stoichiometry in which a flow injection procedure is used to generate absorbance–time data that are analysed by two iterative computational procedures. A two-line manifold was used with a well stirred mixing chamber downstream of the confluence point. The physical dispersion of the system was characterized first by the passage of an absorbing solution through the manifold in the absence of chemical reaction. Three chemical systems were then studied at controlled pH and ionic strength in which a metal ion was injected into a carrier and merged with a stream of ligand. These systems were the reaction of iron(III) with salicylic acid, the reaction of iron(III) with thiocyanate and the reaction of lanthanum(III) with Methyl Thymol Blue. Absorbance–time data were taken from the trailing edge of the peak profile between dispersion coefficient values of 5 and 25. Results for the formation quotients in agreement with previously reported values were obtained, except that iron(III) thiocyanate would appear to be more stable when formed in a flow injection (FI) manifold than when formed in a static batch procedure. The flow injection method greatly simplifies the experimental procedure compared with that of Job's method or the method of continuous variation, and the iterative computational methods account for absorbance by the ligand at the wavelength monitored. The educational aspects of this approach are critically evaluated and it is proposed that the FI method would form the basis of a set of teaching experiments.

Keywords: Formation quotients; equilibrium constants; flow injection; spectrophotometry

Introduction

The equilibrium expression for an ML-type complexometric reaction includes activity coefficients. For a reaction of the general form

$$M + L \rightleftharpoons ML \tag{1}$$

the formation constant (K_f) is

$$K_f = \frac{[ML]f_{ML}}{[M][L]f_M f_L} \tag{2}$$

for which [M], [L] and [ML] are the respective equilibrium concentrations of the metal, ligand and complex and f_M, f_L and f_{ML} are the respective activity coefficients of the metal, ligand and complex.

Only rarely are true formation constants reported in the literature. It is common practice to report the ratio of concentrations of products to reactants at certain ionic strengths rather than to calculate activity coefficients and report a true K_f at infinite dilution.[1–3] This is a reasonable

practice considering the experimental difficulties encountered in determining formation constants. The issue is further complicated when side reactions are ignored. To avoid confusion over the definition and to define precisely the constant being determined, the term formation quotient (Q) will be used in this paper:[4]

$$Q = \frac{[ML]}{[M][L]} \tag{3}$$

The most widely used method for determining formation constants (K_f) of metal–ligand complexes is the method of continuous variation, or Job's method.[5,6] The Job's plot procedure is simple, but requires several solutions over a range of mole fractions. The absorbance of the complex is plotted *versus* mole fraction of the metal species (x_M). The formation quotient is determined by drawing tangents to the curves (low and high x_M); extrapolation of these lines to the point of intersection provides an absorbance for the condition of all metal converted to the complex.[6]

An experimental procedure that uses a flow injection (FI) system to generate data from ML-type reactions is presented. Two iterative methods of data treatment[4,7] are used to process the data. These methods are used because they allow the determination of Q values from several data points and accommodate the common situation in which both the free ligand and complex absorb at the wavelength of interest. Use of the FI method to generate the data removes the need for the preparation of a large number of discrete solutions.

Experimental Methods of Data-Handling

The iterative methods of determining formation quotients from absorbance–time data from an FI peak profile are based on a model for which the reaction stoichiometry is a 1 : 1 complexometric reaction model and for which the molar absorptivity of the complex (ε_{ML}) is unknown; the model accounts for the common situation of the free ligand absorbing at the wavelength at which the formation of the complex is monitored (Fig. 1). At the wavelength of interest (λ), the contribution of the absorbance due to the ligand to the overall absorbance is not negligible. Often the free ligand does not have a chromophore in the visible spectrum, or the absorbance maximum of the complex is red shifted sufficiently that ε_L is negligible. The two methods used for the determination of Q in this work are similar in that an initial guess is required to begin the process. The analytical (total) concentration of metal and ligand and the absorbance of the product are required at each data point (time on the FI peak profile).

Long and Drago Method

The method of Long and Drago[7] is based on minimizing the sum of the squared deviations (χ^2) between experimentally obtained absorbance (A^{exp}) and calculated absorbance (A^{calc}). The method requires an initial guess of Q, from which the

---

* To whom correspondence should be addressed.

equilibrium concentration of the complex, [ML], is calculated [eqn. (3)]. The difference ($\Delta\varepsilon$) in molar absorptivity between the complex (ε_{ML}) and the free ligand (ε_L) is calculated from the complete data set of A^{exp} and [ML], based on the initial guess of Q:

$$\Delta\varepsilon = \frac{\sum_{i=1}^{n} \{(\Delta A_i^{exp})[ML]_i\}}{\sum_{i=1}^{n} [ML]_i^2} \quad (4)$$

The corresponding sum of squared deviations,

$$\chi^2 = \sum_{i=1}^{n} \left(\Delta A_i^{exp} - \Delta A_i^{exp} \right)^2 \quad (5)$$

for which $\Delta A^{calc} = \Delta\varepsilon$ [ML] and $\Delta A^{exp} = A^{exp} - A^0$ (absorbance of free ligand) is calculated for each Q and $\Delta\varepsilon$. The formation quotient is varied stepwise until a minimum χ^2 is obtained. The computer program allows for the size of the step to be varied by any amount.

Ramette Method

The method proposed by Ramette[4,8] follows the model chemical system (Fig. 1) in which the free ligand and the complex absorb at the wavelength of interest (*i.e.*, $\varepsilon_L \neq 0$). An apparent molar absorptivity (ε) is established with the assumption that all of the ligand is unbound,

$$\varepsilon = \frac{A}{bc_L} \quad (6)$$

where A is absorbance, b is pathlength and c_L is the analytical concentration of the ligand. The following mathematical relationship can be established:

$$A^{exp} = \varepsilon c_L = \varepsilon_L [L] + \varepsilon_{ML} [ML] \quad (7)$$

with the assumption that $b = 1$ cm. Substitution and rearrangement of eqn. (7) leads to the ratio of the two forms of the ligand:

$$\frac{[ML]}{[L]} = \frac{\varepsilon - \varepsilon_L}{\varepsilon_{ML} - \varepsilon} \quad (8)$$

Substitution of eqn. (8) into eqn. (3) leads to the working equation for the method:

$$Q = \frac{1}{[M]} \times \frac{\varepsilon - \varepsilon_L}{\varepsilon_{ML} - \varepsilon} \quad (9)$$

Eqn. (9) can be rearranged for the general situation in which [M] and ε_{ML} are unknown:

$$\varepsilon = -\varepsilon_{ML} - \frac{1}{Q} \times \frac{\varepsilon - \varepsilon_L}{[M]} \quad (10)$$

An initial guess of ε_{ML} is used to calculate initial metal equilibrium concentrations ([M]); the intercept of a plot of ε
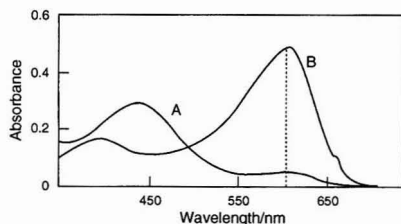
Fig. 1 Spectra of the model chemical system. A, Spectrum of the free ligand (MTB); B, spectrum of the complex (La^III–MTB).

versus $\varepsilon - \varepsilon_L/[M]$ provides the subsequent value of ε_{ML}, from which the second [M] are calculated. The iteration is continued until the slope ($= -1/Q$) does not change. Linear regression equations are included in the computer program; the program continues until stopped by the user.

Several methods for determining acid dissociation constants by flow injection techniques have been described.[9–14] A limited number of previous publications show the feasibility of determining formation constants for metal–ligand complexes.[14–16] Yoza *et al.*[15] designed a method for determining K_f of Mg and Ca complexes that relied on an empirical relationship between peak height and known K_f values for the displacement reaction of Methyl Thymol Blue (MTB) from the metals. The ligand of interest was injected into a carrier stream, which was merged with a metal–MTB reagent stream. The decrease in absorbance (from the competitive equilibrium) was plotted *versus* known formation constants to construct a calibration graph that could be used for unknowns. Tyson[16] proposed determining formation constants from FI data obtained from FI doublet peaks; formation constants were calculated from the peak maximum absorbance and the initial concentrations of reagent and sample.

The method described by Vithanage and Dasgupta[14] is of most relevance to this work. A modified Job's plot was used for determining K_f for two chemical systems: Fe^II–1,10-phenanthroline and Mg^II–methyl thymol blue. Data on dispersion and the product were obtained simultaneously in a single injection by monitoring the progress of the reaction by means of a diode-array spectrometer at a wavelength at which the product absorbs and at the isosbestic wavelength.

Experimental

Apparatus

A double-line FI manifold was used for all experiments (Fig. 2). Components of the system included a variable-speed peristaltic pump (Ismatec), a six-port injection valve (Rheodyne) and a UV/VIS photodiode-array spectrophotometer (Hewlett-Packard Model 8451A), equipped with an 8 µl flow cell (Hellma). Absorbance–time data for reactions was collected using the Hewlett–Packard Kinetics program. Flow tubing and injection loops were constructed from 0.8 mm i.d. flow tubing. Injection volumes and flow rates for the experiments are listed in Table 1.

A well stirred tank was employed as the mixing chamber in these experiments. The two parts of the approximately 1.2 ml tank were machined from Perspex.[17,18] The cylindrical part of the chamber, 10 mm in diameter and 20 mm deep, housed a standard cuvette magnetic follower (stir bar); the upper part was conical with a height of approximately 4 mm and a base of 10 mm. An inlet was bored into the lower section and an outlet into the upper section. The well stirred tank was chosen as the mixing device because of the broad concentration gradients it produces. Other mixing devices can be used in lieu of this mixing device: single-bead string reactors, packed-bed reactors, knotted tubular reactors[19,20] or alternating helical reactors.[21]
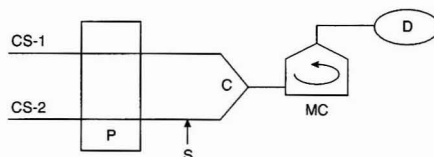
Fig. 2 Double-line flow injection system. CS-1 and CS-2 = carrier streams; P = pump; S = sample injection valve; C = confluence point; MC = well stirred mixing chamber; and D = UV/VIS detector.

Chemical Systems and Reagents

Three chemicals systems were chosen for studying the FI procedure for determining formation quotients. The only rigorous criteria for choosing the reactions was whether they fit the 1 : 1 model. The reactions between iron(III) and salicylic acid and between iron(III) and thiocyanate were used to test the FI method for a reaction for which $\varepsilon_L = 0$. The Fe^{III}–salicylic acid complex is a violet complex that has a λ_{max} of 510 nm and the Fe^{III}–thiocyanate complex is a red complex that has a λ_{max} of 546 nm. The reaction between lanthanum(III) and MTB was used to test the method for the situation for which $\varepsilon_L \neq 0$. The blue complex was monitored at 610 nm; the yellow free ligand also absorbs at that wavelength ($\varepsilon_{MTB} = 2069$). Metal solutions were prepared from iron(III) nitrate and lanthanum chloride analytical-reagent grade salts. Analytical-reagent grade salicylic acid (dry acid) and potassium thiocyanate were used; methyl thymol blue sodium salt (Aldrich) was of 95% technical grade. Metal and ligand solutions were prepared in the appropriate ionic strength and pH buffer. Solution concentrations and buffers are listed in Table 1, along with values of some experimental parameters.

Procedure

The three steps of the experimental procedure are summarized in Table 2 and are discussed briefly below. In a typical FI experiment an inert dye is used to characterize dispersion by means of the dispersion coefficient (D). To simplify solution preparation, it is recommended that the metal or ligand solution be used in steps 1 and 2 rather than prepare an additional dye solution. The absorbance of the undiluted solution at some wavelength (λ_1) should be determined prior to beginning the experiments. A second wavelength (λ_2) at which the metal–ligand complex absorbs is selected for step 3.

The following procedure was followed (refer to Table 2 and Fig. 2). (1) The dispersion of CS-1 (*i.e.*, the dilution due to the merging at the confluence point) was established by determining the steady-state absorbance (at λ_1) of the metal or ligand solution after dilution with CS-2. In the examples discussed below, D for CS-1 was approximately 2.5. (2) The concentration gradient of S was determined by monitoring (at λ_1) the injection of metal or ligand solution into two buffered carrier streams. (3) The absorbance–time profile of the product was established by monitoring (at λ_2) the reaction between the metal and ligand; metal solution (S) was injected into buffer (CS-2), which was merged with ligand carrier (CS-1).

Injections had to be timed with reasonable precision such that the data from the first injection could be correlated with that of the second. After data collection was begun, a mental count of 1 s was made and the valve turned. Slow flow rates of 0.6–0.8 ml min^{-1} were used in order to ensure that peaks were broad and that the reactions had time to come to equilibrium. Absorbance–time data in the region in which $D = 5$–25 were collected from the trailing edge of the FI peaks. Data analysis was performed using the methods outlined above. Iterations were performed using BASIC programs that read data from text

files of total metal concentration, total ligand concentration and absorbance of complex. Listings of the QuickBASIC (Microsoft) programs are available from the authors on request.

Results and Discussions

Chemical Systems

The results for steps 2 and 3 from the procedure described above are shown in Fig. 3 for the iron(III)–salicylic acid system. Results from the experiments to determine Q are listed in Table 3. Confidence intervals were obtained through repeating step 3 of the experimental procedure. Thus, the uncertainty in Q values include the imprecision in the manual timing procedure and the normal variations in pump tubing that are inherent in FI experiments. The confidence intervals are large in relation to those typically seen for analytical determinations, but are similar to other formation constant confidence intervals reported in the literature. Literature values for each reaction are discussed below.

Table 2 Summary of experimental procedure

Step	CS-1*	CS-2*	S	Wavelength monitored
1	Metal or ligand	Buffer	No injection	λ_1
2	Buffer	Buffer	Metal or ligand	λ_1
3	Ligand	Buffer	Metal	λ_2

* Carrier streams of the FI system (see Fig. 1).
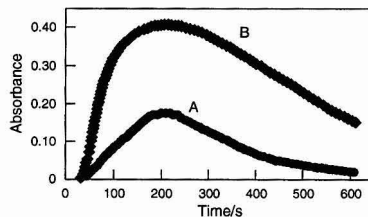
Fig. 3 Plots of absorbance against time for the iron(III)–salicylic acid system. A, when iron(III) solution was injected into buffered carrier streams (this was used to establish the dispersion profile for the injected solution) and B, when the iron(III) was injected into buffered carrier and merged with the ligand solution at the confluence point.

Table 3 Results from determination of formation quotients by the flow injection procedure

Chemical system	Long and Drago method*	Ramette method*	Mean $\log Q$
Fe^{III}–salicylic acid	$2\,045 \pm 276$	$2\,074 \pm 258$	3.31
La^{III}–MTB	$37\,560 \pm 5300$	$37\,010 \pm 5140$	4.57
Fe^{III}–SCN$^-$	553 ± 60	565 ± 56	2.74

* The $\pm$ terms are 95% confidence intervals ($n = 4$).

Table 1 Experimental parameters and solution concentrations of chemical systems

Chemical system	Concentration of solutions/mol l^{-1}		Buffer solution (ionic strength, pH)	Injection volume/μl	Flow rate/ ml min^{-1}	Wavelength/nm	
	Metal	Ligand				λ_1	λ_2
Fe^{III}–salicylic acid	9.136×10^{-3}	6.111×10^{-4}	NaClO$_4$–HNO$_3$ ($I = 0.25$ mol l^{-1}, pH = 1.66)	852	0.6	350	510
La^{III}–MTB	8.460×10^{-5}	5.9×10^{-4}	Acetate–acetic acid ($I = 0.1$ mol l^{-1}, pH = 6.20)	852	0.6	458	600
Fe^{III}–SCN$^-$	3.009×10^{-2}	6.972×10^{-4}	NaClO$_4$–HNO$_3$ ($I = 0.2$ mol l^{-1}, pH = 1.35)	783	0.8	372	460

Iron(III)–salicylic acid

Eight data points were collected from the trailing edge of the absorbance–time profile in the region from $D = 4$ to 13. The calculated mean formation quotient of 2060 (log $Q = 3.31$) is in reasonable agreement with literature conditional formation constants. Colleter[22] reported a log K of 16.48 for the Fe^{III}–salicylic acid reaction at $I = 0.25$ mol l^{-1}. Consideration of the hydrolysis of Fe^{III} and the protonation of the acid ($\alpha_{Fe} = 0.774$, log $\alpha_{SA} = -13.07$) yields a conditional formation constant (K') of 1989. Other reported values for log K are 16.4 ($I = 0.1$)[23] and 15.8 ($I = 3.0$).[24] There was a slight curvature in the plot of data obtained using the Ramette method. It is thought that this is the result of formation of the 1 : 2 product.

Lanthanum(III)–Methyl Thymol Blue

Nine data points over the range of $D = 3.5–25$ were used in computing the formation quotient of the La–MTB complex. It is difficult to compare the mean log Q of 4.57 with literature values of K for this reaction. A log K of 6.1 (at pH 6.0) was reported for the 1 : 1 reaction[25] and a log K of 35.8 has been reported for a 2 : 2 La^{III}–MTB complex (log $K = 7.4$ at pH 5.84).[26] In the latter study, the side reaction coefficients of all six protons were used to determine K at various pH. This approach neglects the conclusions of other researchers that MTB forms complexes as a protonated ligand (H_3L^{3-}, for example).[27] In the absence of a reliable reference value, log $Q = 4.57$ is reasonable, considering both the fit of the data to the 1 : 1 model (Fig. 4) and the La^{III}–acetate side reaction, which would decrease the conditional formation constant.

Iron(III)–thiocyanate

The reaction between Fe^{III} and SCN^- can form several species depending on the concentration of the ligand; the formation of the 1 : 2 and 1 : 3 products is negligible only if the SCN^- concentration is maintained below 1×10^{-3} mol l^{-1}. Calculated Q values were consistently high for the FI method. A mean Q of 559 (log $Q = 2.74$) was computed for the conditions noted in Table 1. Literature values of log Q for the 1 : 1 reaction at similar ionic strength are lower: 2.37 for $I = 0.128$ and 2.14 for $I = 0.5$.[28] When the experiment was performed in the batch mode using the same solutions, the results were in agreement with the literature values: log $Q = 2.37$. The kinetic aspect of the FI method is illustrated by the difference between the results of the batch and FI methods: equilibrium is not established on the time scale of the FI experiment. Although the FI method cannot be used to determine accurately formation quotients for this reaction,

Fig. 4 Plot of eqn. (10) for the determination of Q for the La–MTB system. Slope $= -1/Q$; intercept $= \varepsilon_{ML}$. Scatter of the data from the straight-line fit illustrates the uncertainty that gives rise to the large confidence intervals (Table 3).

the linearity of the data shows that the 1 : 1 complex is being formed in a ratio described by the experimental value of Q. It is an interesting facet of the chemistry that the complex is slightly more stable under the regime of continuous flow than the conventional methods that employ calibrated glassware.

Features of the FI method

The proposed FI method for determining formation quotients simplifies the generation of experimental data such that the more complicated iterative methods of data handling can be more readily used in computing Q values. The iterative methods proposed by Long and Drago[7] and Ramette[4,8] can account for the situation of a free ligand that absorbs at the wavelength of interest; metals generally do not absorb in the UV/VIS region of the spectrum, but many common complexometric reagents absorb in the spectral regions of interest to chemists. The iterative methods also provide a measure of the precision of the determination and a measure of the fit of the data to the model.

The FI experiment provides the data required for the iterative methods of determining Q with a minimum of two injections. Absorbance data can be readily imported into computer programs through text files. Thus, the focus of the experiment is shifted from the preparation of a series of experiments to the collection of data obtained from an experiment that requires three solutions: metal, ligand and buffer solutions. In contrast, the Job's plot method requires several data points that must be obtained from the same number of solutions.

Educational Aspects

Equilibrium data on most chemical systems of interest have been tabulated in well known and widely available reference books.[1–3] The need to determine K_f values from a research standpoint has diminished, but experimental methods for determining K_f and acid dissociation constants (K_a) are useful teaching experiments, usually conducted by students in quantitative analysis classes. An experiment to determine an equilibrium constant helps students acquire a good understanding of the fundamental concepts of chemical equilibrium and many subtopics such as side reactions (metal hydrolysis and ligand protonation), successive or competing equilibria (α-plots), buffer action and the effect of ionic strength. It is advantageous to use an FI system for this experiment to shift the focus of the laboratory work from solution preparation to handling of the data and understanding of the chemistry. This type of experiment, in which the amounts of reagents consumed are minimized, is part of the general trend in chemical education to 'miniaturize' experiments.

The simplification of the procedure for determining formation quotients makes the experiment attractive for use in a teaching laboratory. Traditional methods have the aforementioned problem of being too solution intensive. In the FI method, data for one injection is collected in 5–6 min. A student should be able to conduct the experiment with the FI system and obtain eight or more data points in 15–20 min. Only 3–4 ml of metal solution are required for each injection, the extra solution being required to wash the injection loop; thus, less than 20 ml of buffered carrier and 10 ml of ligand solution are required for steps 1–3. The experimental procedure can be simplified further by characterizing the dispersion of metal in the FI system (step 2) prior to the beginning of the experiment (step 3).

Monographs on complexometric or titrimetric analysis are sources of reactions that can be studied with the FI system.[6,29] The 1 : 1 stoichiometry condition is a limitation of the
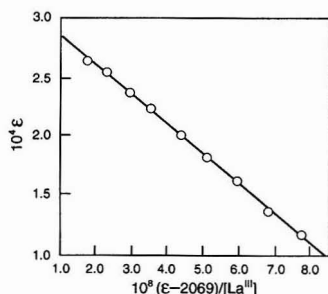
experiment, but there are ways to establish conditions such that only the first complex is formed. Setting the pH and ligand concentration to appropriate values are two important ways to accomplish this. The use of α-plots (fraction of complex formed *versus* concentration of ligand) can be incorporated into the experiment to establish proper conditions. The rate of the reaction must be considered in order to avoid kinetic effects although, as in the case of the Fe^{III}–SCN reaction, a formation quotient can be calculated from the data. Although the FI method cannot be used to determine formation constants accurately for this reaction, the use of the proposed method as a teaching experiment is not prohibited because a 1:1 complex is formed and good linearity is obtained when the data are plotted (Ramette method).

The FI system can be used to demonstrate other aspects of chemical equilibrium such as the effect of ionic strength. The reaction of a series of Fe^{III} solutions of increasing ionic strengths with salicylic acid or thiocyanate will result in absorbance–time profiles of different shapes and data from which *Q* values can be determined. The FI peaks can be plotted on a common time axis to illustrate the effect in a quantitative manner.

References

1 Martell, A. E., and Smith, R. M., *Critical Stability Constants*, Plenum Press, New York, 1977.
2 Sillen, L. G., and Martell, A. E., *Stability Constants of Metal–Ion Complexes*, Chemical Society, London, 1964.
3 Sillen, L. G., and Martell, A. E., *Stability Constants of Metal–Ion Complexes, Supplement No. 1*, Chemical Society, London, 1971.
4 Ramette, R. W., *Chemical Equilibrium and Analysis*, Addison-Wesley, Reading, MA, 1981.
5 Job, P., *Ann. Chim. Phys.*, 1928, **9**, 113.
6 Inczedy, J., *Analytical Applications of Complex Equilibria*, Ellis Horwood, Chichester, 1976.
7 Long, J. R., and Drago, R. S., *J. Chem. Educ.*, 1982, **59**, 1037.
8 Ramette, R. W., *J. Chem. Educ.*, 1967, **44**, 647.
9 Turner, D. R., Knox, S., Whitfield, M., dos Santos, M., Pescada, C., and Goncalves, M. L., *Anal. Chim. Acta*, 1989, **226**, 239.
10 Brooks, S. H., and Rullo, G., *Anal. Chem.*, 1990, **62**, 2059.
11 Marcos, J., Rios, A., and Valcarcel, M., *Anal. Chem.*, 1990, **62**, 2237.
12 Norgaard, L., *Anal. Chim. Acta*, 1991, **255**, 143.
13 Turner, D. R., Dossantos, M. M. C., Coutinho, P., Goncalves, M. D., and Knox, S., *Anal. Chim. Acta*, 1992, **258**, 259.
14 Vithanage, R. S., and Dasgupta, P. K., *Anal. Chem.*, 1986, **58**, 326.
15 Yoza, N., Shuto, T., Baba, Y., Tanaka, A., and Ohashi, S., *J. Chromatogr.*, 1984, **298**, 89.
16 Tyson, J. F., *Analyst*, 1987, **112**, 527.
17 Růžička, J., Hansen, E. H., and Mosback, H., *Anal. Chem.*, 1977, **92**, 235.
18 Tyson, J. F., *Analyst*, 1987, **112**, 523.
19 Valcarcel, M., and Luque de Castro, M. D., *Flow Injection Analysis: Principles and Applications*, Ellis Horwood, Chichester, 1987.
20 Růžička, J., and Hansen, E. H., *Flow Injection Analysis*, Wiley, New York, 2nd edn., 1988.
21 Echols, R. T., and Tyson, J. F., *Anal. Chim. Acta*, 1994, **286**, 169.
22 Colleter, J., *Ann. Chim.*, 1960, **5**, 415.
23 Babko, A. K., *Zh. Obshch. Khim.*, 1945, **15**, 745.
24 Agren, A., *Acta Chem. Scand.*, 1954, **8**, 1059.
25 Serdyuk, L. S., and Smirnaya, V. S., *Zh. Anal. Khim.*, 1965, **20**, 161.
26 Budesinsky, B., and Antonescu, E., *Collect. Czech. Chem. Commun.*, 1963, **28**, 3264.
27 Yoshino, T., Imada, H., Murakami, S., and Kagawa, M., *Talanta*, 1974, **21**, 211.
28 Frank, H. S., and Ostwald, R. L., *J. Am. Chem. Soc.*, 1947, **69**, 1321.
29 Ringbom, A., *Complexation in Analytical Chemistry*, Robert E. Kreiger, Huntington, NY, 1979.

Multicomponent Techniques in Sequential Injection

E. Gómez, C. Tomás, A. Cladera, J. M. Estela and V. Cerdà*

Departamento de Química, Universitat de les Illes Balears, E-07071 Palma de Mallorca, Spain

The application of multicomponent techniques in sequential injection analysis is considered. Such a scarcely selective chromogenic reagent as 4-(2-pyridylazo)resorcinol allowed the simultaneous spectrophotometric determination of Ca and Mg in environmental samples. The process was carried out in a fully automated fashion by using a personal microcomputer running software for instrumental control and data acquisition and processing. The ensuing method features a linear determination range of 1–20 and 2–40 mg l⁻¹ for magnesium and calcium, respectively, and a sample throughput of 60 h⁻¹. The results are compared with those provided by batch and flow injection methodology.

Keywords: Multicomponent analysis; segmented flow; sequential injection analysis; calcium and magnesium determination; water analysis; spectrophotometry

Introduction

Sequential injection (SI), developed by Růžička and Marshall,[1] has a number of attractive advantages, including instrumental simplicity, flexibility, automatability and as sparing use of reagents, over its parent technique, flow injection (FI). However, only two publications on the application of this novel technique,[2,3] in addition to one about its theoretical foundation,[4] have so far been reported. In one of them,[3] the potential of SI for automated implementation of sophisticated analytical procedures was demonstrated by developing a method for the determination of factor XIII enzyme. The scant literature on SI can probably be ascribed to the fact that the liquid drive originally used in this technique (a low-pressure piston pump delivering a sinusoidal flow) was specifically designed for it, and to the lack of software for accurately controlling the circular motion of the cam and synchronizing the steps of the process. Recently, Ivaska and Růžička[5] compared the performance of peristaltic and piston pumps in order to facilitate the implementation of this technique and found the former type to provide less reproducible, but still acceptable results.

In previous work,[6] we used autoburettes actuated by a stepper motor in order to simplify SI operation. In addition to being easier to operate and more widely available, autoburettes have longer lives than peristaltic pump tubing and provide more precise results than PTFE tubes. In addition, an autoburette frees one of the channels of the switching valve as it can be loaded with carrier by using its own, two-position valve.

After the initial technical shortcomings had been overcome, our group started to address the practical problems encountered in using multicomponent techniques in SI, *viz.*, those posed by changes in the refractive index of the sensing microcell and the high absorbance of chromogenic reagents.

In this work, we used a multilinear regression program for the simultaneous determination of calcium and magnesium in mixtures, which is of interest in the analysis of hard waters. The assay relies on the formation of the Ca and Mg complexes with the chromogenic reagent 4-(2-pyridylazo)resorcinol (PAR); the complex mixture can be readily resolved, notwithstanding the extensive spectral overlap involved. This reaction was previously used in a batch[7] and an FI method[8] for the determination of the two alkaline earth metals in drinking and waste waters.

Experimental

Reagents

The reagents were all of analytical-reagent grade and were used to prepare the following solutions: a 3.0×10^{-3} mol l⁻¹ PAR solution, made from the monohydrated monosodium salt (Merck) and stored in a dark polyethylene flask, a 0.5 mol l⁻¹ tris(hydroxymethyl)aminomethane (TRIS) buffer of pH 9.6, adjusted with HCl, and 1000 mg l⁻¹ calcium and magnesium standard solutions.

Apparatus and Software

Fig. 1 depicts the instrumental set-up used for the automatic determinations. All tubing was PTFE of 0.8 mm id. The capacity of the burette syringe was 5 ml and the piston delivered a flow rate of 2.11 ml min⁻¹.

The procedure is based on the use of two computer programs, *viz.* DARRAY v.2.0[6] and MULTI3,[9] both developed by the authors (the software used in this work can be obtained on request from SCIWARE, Banco de Programas, Departamento de Química, Universitat de les Illes Balears, E-07071 Palma de Mallorca, Spain). DARRAY v. 2.0 is a program for using an HP 8452A spectrophotometer (Hewlett-Packard) as a detector in SI. It allows automatic control of the autoburette, detector, sample changer and customized valve-based electrochemical actuator. After SI recordings for the sample have been acquired, spectra are corrected in order to avoid the effect of changes in the refractive index inside the sensing microcell and subtracted for the absorbance of the chromogenic reagent.

In this work we used MULTI3 with the option of multiple standard calibration of pure components. For a mixture of N absorbing components in the absence of matrix effects and chemical interaction, Beer's law can be written as

$$A_j = \sum_{i=1}^{N} \varepsilon_{ij} b c_i; \ \forall j = 1 \ldots M \qquad (1)$$

where A_j is the absorbance of the mixture at wavelength j, ε_{ij} is the molar absorptivity of component i at wavelength j, b is the optical pathlength and c_i is the concentration of component i in the mixture. If a number M of wavelengths greater than that of components is used, then eqn. (1) can be converted into an

---

* To whom correspondence should be addressed.

overdimensioned equation system which, once all ε_{ij} values are known, can be solved by least-squares multiple linear regression in order to obtain the concentration of each component in the mixture minimizing the sum of the squares of the residues ($A_{exp} - A_{cal}$). In the resolution, an independent term (a) can be introduced that allows one, in part, to compensate for the matrix effects and chemical interactions that may cause significant deviations from a zero intercept. In our case the ε_{ij} values were determined by regression from standards of different concentrations of each component.

Procedure

The file that stores the operational sequence starts with a sentence commanding cleaning of all tubes. Then, R_1 is used to aspirate 200 µl of 1.2×10^{-3} mol l^{-1} PAR, 100 µl of sample and 200 µl of 0.5 mol l^{-1} TRIS at pH 9.6, in this order. If the PAR solution has previously been buffered, then 200 µl of the mixed reagent are aspirated, followed by 100 µl of sample. Finally, the mixture is propelled by R_2 to the detector.

The reaction is monitored *via* absorbance readings at 500 nm, from which are subtracted those at 650 nm, where no reactant or product absorbs, in order to minimize potential effects from differences in the refractive index. However, because PAR is a coloured reagent and absorbs in the same visible spectral region as its complexes with various metals, the peaks obtained will always be the summation of two contributions, *viz.*, that from unreacted PAR and that from its complexes (Mg–PAR and Ca–PAR here). Hence the actual peak height for each complex can be determined by subtracting the blank spectrum from that for an injected sample or standard. The amount of reacted PAR is assumed to be negligible relative to that of unreacted reagent, which is plausible as the complexes formed are highly labile and a large excess of reagent is used.

Results and Discussion

Recording of Spectra

Multicomponent determinations involving chromogenic reagents in SI are more complicated than their batch and FI counterparts,[7,8] as direct acquisition of the sample spectrum can be hindered by two effects. One arises from changes in the refractive index when the injected products reach the detector. These changes give rise to a non-spectral, sample-dependent variation of the signal, but can be readily corrected for by subtracting the absorbance at a wavelength at which neither the reagents nor the products absorb. The other effect originates from the absorbance of the chromogenic reagent and cannot be suppressed by instrumental zeroing because the reagent is injected into a non-absorbing carrier and its absorption is variable.

Both effects must be corrected in order to obtain reproducible spectra consisting of the sole contribution of the analyte complexes. This entails taking the following steps:

(a) The SI recordings for a blank, standards and samples are obtained as the difference between the absorbances at 500 and 650 nm.

(b) A point in the peaks corresponding to the maximum extent of complex formation and ensuring acceptable reproducibility is chosen based on the dispersion profile for the flow system. The selected point must also ensure that the spectra for standards and samples are recorded at equivalent times.

(c) The spectra for the blank, standards and samples at the selected point are acquired and corrected to cancel the effect of refractive index changes by subtracting the absorbance at 650 nm.

(d) The spectra for the standards and samples are corrected for the contribution of PAR by subtracting the corrected blank spectrum. Fig. 2 shows the absorption bands exhibited by PAR and the two analyte complexes.
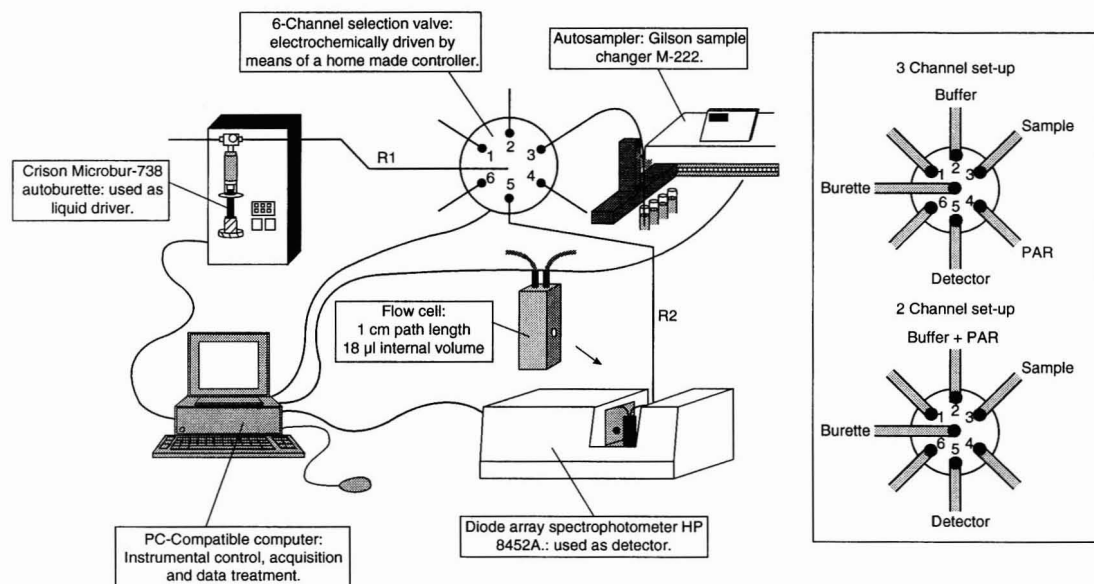
Fig. 1 SI instrumental set-up.

(*e*) Finally, the previous spectra are used to implement the multicomponent technique.[9]

Optimization of Experimental Variables

Based on the theoretical considerations established in previous work,[6] the sample volume used, V_s, was half of that resulting in a sample-to-reagent dispersion coefficient ratio of 2, $V_{1/2}$, in order to ensure efficient mixing and formation of the complex. Also, the reagent volume employed, V_R, was equal to $V_{1/2}$.

To obtain $V_{1/2}$ we used the equation

$$-\log\left(1 - \frac{A_{max}}{A_0}\right) = \frac{0.693}{2.303\, V_{1/2}} V_s \qquad (2)$$

where A_{max} is the maximum absorbance for each peak and A_0 is the initial absorbance (without dispersion). The $V_{1/2}$ value was calculated from the slope of the plot of $-\log(1 - A_{max}/A_0)$ against V_s and for the type of tubing used (0.8 mm id) was approximately 200 µl. Therefore, V_s and V_R were 100 and 200 µl, respectively.

We tested two sample-dispensing arrangements based on the use of two or three channels for delivering PAR, the buffer and the sample (Fig. 1). In the former instance, PAR and the buffer were previously mixed and then aspirated *via* a single channel. In the latter, the reagent and buffer were loaded separately, so the sample aspiration tube was placed between the two. Both configurations were found to require PAR to be aspirated first (Fig. 3) in order to ensure efficient mixing of sample and reagent. Based on reported data,[10] the two-channel configuration would entail preparing the mixtures immediately prior to use; otherwise, they might be absorbed on the tube walls to some extent. However, we encountered no absorbance decrease by virtue of this effect in our experiments.

We used TRIS buffer at pH 9.6 as the reaction medium as a lower pH hindered the complex formation and a higher value resulted in no further increase in the analytical signal. The TRIS buffer proved to be optimum for the intended purpose, even though the signal was slightly smaller than it was in its absence; however, the results were not as reproducible if the buffer was excluded. Alternative buffers of the same pH such as phosphate and borax gave rise to markedly decreased signals relative to TRIS.

Finding the optimum PAR concentration was made difficult by the appreciable absorbance of this reagent and the need to use it in a large excess relative to the metal ions. The concentration used, 1.2×10^{-3} mol l^{-1}, was therefore a compromise. Although higher concentrations resulted in further increased signals, they shifted the spectral maxima for the complexes, probably as a result of too high an absorbance for PAR.

By using the optimum working conditions and the two-channel manifold, the analytical response was linearly related to the metal concentrations over the ranges 1–10 and 2–40 mg l^{-1} for Mg and Ca, respectively. Hence the determination limits were similar to those of the FI method.[8] The three-channel configuration provided roughly half the sensitivity of the previous configuration as the absorbance signal was also approximately half by virtue fo the sample and reagent dispersion.

Reproducibility

Spectral reproducibility is crucial in multicomponent analysis. In order to check the proposed application, we carried out a series of 10 injections of a sample containing 10 mg l^{-1} each of calcium and magnesium. Figs. 4 and 5 show the SI recordings and corrected spectra obtained. The analyte concentrations
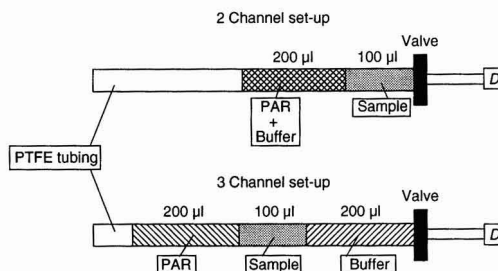
Fig. 3 Position of the stacked zones in the two sample-dispersing arrangements tested.
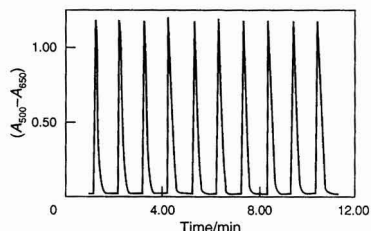
Fig. 4 Sequential injection register obtained by injection of 10 replicates of a sample containing 10 mg l^{-1} each of Ca and Mg.
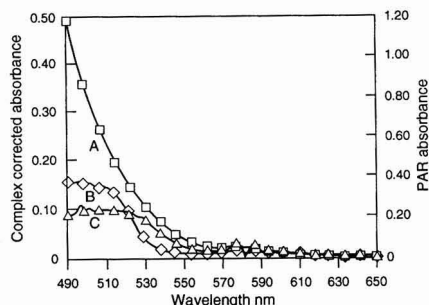
Fig. 2 Absorption spectra for PAR and its Ca and Mg complexes. A, PAR; B, PAR–Mg (10 mg l^{-1}); C, PAR–Ca (10 mg l^{-1}).
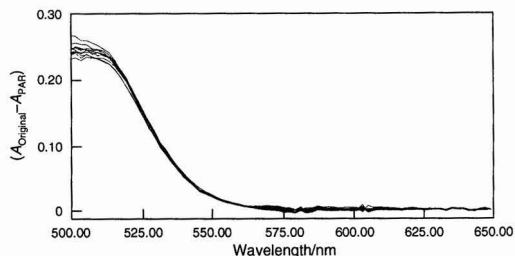
Fig. 5 Corrected spectra of metal complexes corresponding to the peak maxima in Fig. 4.

found were 9.7 mg l^{-1} Ca (s_r = 2.0%) and 10.1 mg l^{-1} Mg (s_r = 4.0%). The higher relative standard deviation for Mg compared with Ca was the result of its resolution being more affected by the high absorbance of PAR owing to the lower wavelength of the Mg maximum.

Resolution of Mixtures

Table 1 gives the results obtained by using the two types of configuration. As can be seen, they were similar for various Ca–Mg mixtures. Therefore, the two-channel manifold was the natural choice as it provided a higher sensitivity.

As in the batch and FI methods,[7,8] the sole interferences from metal ions usually present in water samples were posed by Cu^{II} and Zn^{II}. In fact, the maximum, tolerated concentrations for the two-channel SI configuration were 0.05 mg l^{-1} Cu^{II} and 0.1 mg l^{-1} Zn^{II}. However, if the concentration of Zn and Cu exceeds its tolerated limit after the sample has been diluted to accommodate the Ca and Mg concentrations within the linear determination range, the problem can be solved by determining the two analytes simultaneously.[8]

Analysis of Real Samples

The proposed method was applied to the determination of Ca and Mg in drinking and waste waters from Palma de Mallorca.

Table 1 Results obtained in the resolution of Ca–Mg mixtures by use of the proposed method. All concentrations in mg l^{-1}

Added		Found, two-channel system*		Found, three-channel system*	
Ca	Mg	Ca	Mg	Ca	Mg
5.0	20.0	5.7 ± 0.2	19.4 ± 0.4	3.5 ± 0.2	19.4 ± 0.3
20.0	5.0	18.4 ± 0.2	6.8 ± 0.4	20.3 ± 0.1	5.2 ± 0.3
5.0	5.0	4.8 ± 0.1	4.6 ± 0.2	4.1 ± 0.2	4.7 ± 0.3
10.0	10.0	9.6 ± 0.1	10.8 ± 0.2	9.8 ± 0.1	10.0 ± 0.2
0.0	20.0	0.1 ± 0.1	19.8 ± 0.1	0.0 ± 0.1	20.0 ± 0.1
20.0	0.0	20.2 ± 0.1	0.0 ± 0.1	20.8 ± 0.1	0.0 ± 0.1

* Mean ± standard deviation (n = 3).

Table 2 Determination of Ca and Mg in water samples by using the proposed and an ICP-AES reference method. All concentrations in mg l^{-1}. Dilution factor = 1 : 10

Type of water	Proposed method*		Reference method	
	[Ca]	[Mg]	[Ca]	[Mg]
Drinking	121 ± 2	24 ± 4	139	26
Waste 1 (paint inflow)	193 ± 2	93 ± 4	182	81
Waste 2 (plant outflow)	189 ± 3	86 ± 5	176	75
Waste 3 (large lake)	170 ± 3	80 ± 5	171	71
Waste 4 (small lake)	171 ± 2	77 ± 3	172	72

* Mean ± standard deviation (n = 3).

Table 2 gives the results obtained and those provided by an inductively coupled plasma atomic emission spectrometric (ICP-AES) method used for reference. No interference from Cu or Zn was observed as their concentrations were below 0.02 mg l^{-1} in all the samples.

Conclusions

The proposed method allows multicomponent techniques to be implemented in SI. The multiple linear regression procedure used allows one to validate the method experimentally, as would any similar alternative. Some of the technical difficulties to be overcome include changes in the refractive index inside the sensing microcell and the overlap of a major band in the spectrum of the chromogenic reagent with those of the analytes owing to the lack of specific channel for cancelling its effect in SI. Nevertheless, the use of a single channel to aspirate and propel the sample and reactants by means of the burette piston allows the working conditions to be readily and conveniently modified, and results in substantial savings as regards reagent consumption. The diffusion profile for sample and reagents allows one to choose the most suitable configuration for the particular purpose, and also the point where spectra are to be acquired to ensure the best possible resolution in multicomponent analyses.

References

1 Růžička, J., and Marshall, G. D., *Anal. Chim. Acta*, 1990, **237**, 329.
2 Růžička, J., and Gübeli, T., *Anal. Chem.*, 1991, **63**, 1680.
3 Guzmán, M., Pollema, C., Růžička, J., and Christian, G. D., *Talanta*, 1993, **40**, 81.
4 Gübeli, T., Christian, G. D., and Růžička, J., *Anal. Chem.*, 1991, **63**, 2407.
5 Ivaska, A., and Růžička, J., *Analyst*, 1993, **118**, 885.
6 Cladera, A., Tomàs, C., Gómez, E., Estela, J. M., and Cerdà, V., *Anal. Chim. Acta.*, in the press.
7 Gómez, E., Estela, J. M., and Cerdà, V., *Anal. Chim. Acta.*, 1991, **249**, 513.
8 Cladera, A., Gómez, E., Estela, J. M., Cerdà, V., Alvarez Ossorio, A., Rioncón, F., and Salvá, *Int. J. Environ. Anal. Chem.*, 1991, **45**, 143.
9 Cladera, A., Gómez, E., Estela, J. M., and Cerdà, V., *Anal. Chim. Acta*, 1992, **267**, 95.
10 Jezorek, J. R., and Freiser, H., *Anal. Chem.*, 1979, **51**, 373.

Spectrophotometric Determination of Tannin in Tanning Effluent With a Flow Injection System

Valderi L. Dressler, Enio L. Machado and Ayrton F. Martins*

Department of Chemistry, UFSM, 97119-900 Santa Maria, RS-Brazil

The use of the Folin–Ciocalteu reagent in the spectrophotometric determination of polyphenolic substances (total tannins) in tanning effluent by means of a chemical analysis system based on flow injection (FI) is described. Chemical variables and variables related to the FI system were evaluated. The proposed method permits the execution of up to 250 determinations per hour, with good precision (relative standard deviation <3%, $n = 10$) and a broad linear range (5.0–100.0 mg l^{-1} tannin). The results are comparable to those obtained by the conventional method for the determination of tannic acid (114.3 ± 6.4 and 111.7 ± 3.2 mg l^{-1} tannin for the proposed FI system and the conventional method, respectively).

Keywords: Flow injection; spectrophotometry; tannin; tanning effluent

Introduction

Tannins represent a group of substances of variable chemical composition and complex structure, basically formed by glycoside phenols with relative molecular masses of 500–3000. Their main characteristics are good solubility in water and the ability to bind to and/or precipitate water-soluble proteins.

Gravimetric,[1] volumetric,[2] chromatographic[3] and spectrophotometric[4–13] techniques have been used most frequently for the determination of tannin. Among the spectrophotometric methods, the reagent prepared by Folin and Denis[4] and later modified by Folin and Ciocalteu[5] has been widely applied to the determination of tannin in different matrices.[2,7–10] The reagent consists of a mixture of phosphomolybdic acid and phosphotungstic acid which are reduced by phenols to their respective oxides in alkaline medium,[13] resulting in the formation of a blue colour. Only one report[10] of the use of this reagent in spectrophotometric determinations by means of a chemical analysis system based on flow injection (FI) exists in the literature.

In the present study the application of the Folin–Ciocalteu reagent (FCR) to the spectrophotometric determination of tannic acid in tanning effluent using a chemical analysis system based on FI was investigated. After optimization of the parameters of the system, the results obtained were compared with those obtained by a conventional method[7,9] under the same conditions in terms of reagent concentrations.

Experimental

Equipment

Fig. 1 is a schematic representation of the FI system used. The reagents were propelled with an eight-channel peristaltic pump (Abimed Gilson) of variable velocity, equipped with Tygon tubes. The sample was injected manually with an acrylic double commuter-injector,[14] and polyethylene tubing

(0.8 mm i.d.) was used throughout the analytical module. The absorbance was measured at 670 nm using a Perkin-Elmer Model 124B ultraviolet–visible spectrophotometer and the signals were recorded as peak heights with a Perkin-Elmer Model 54 recorder and evaluated manually.

Reagents and Solutions

All reagents used were of analytical-reagent grade and all solutions were prepared in distilled, de-ionized water. All laboratory material was carefully cleaned before use by first washing with a neutral detergent solution and then with distilled, de-ionized water.

Reagents and Solutions

All reagents used were of analytical-reagent grade and all solutions were prepared in distilled, de-ionized water. All laboratory material was carefully cleaned before use by first washing with a neutral detergent solution and then with distilled, de-ionized water.

A stock solution containing 1000 mg l^{-1} tannin was prepared from the same product as used in the industrial tanning process. The solution was heated to boiling in order to achieve better solubilization and appropriate dilutions were obtained therefrom. A 10% m/v NaOH solution was prepared and subsequently diluted.

The FCR was prepared as described by Folin and Ciocalteu,[5] except that lithium sulfate was not added.

The reagent and the stock tannin solutions were stored under refrigeration at 4 °C in the dark.

Sample Treatment

The tanning effluent was collected and stored under refrigeration (4 °C) in a polyethylene flask. A 50 ml aliquot of the sample was placed in a beaker, acidified with 5% v/v HCl to pH 2, heated to boiling and allowed to cool. The pH of the

Fig. 1 Configuration of the FI system. A = Sample (4 ml min^{-1}), B = reaction coil (150 cm), C = sample carrier (water; 6 ml min^{-1}), W = waste, M = spectrophotometer (670 nm), R_1 = 2% NaOH (2 ml min^{-1}), R_2 = FCR (2 + 8; 1 ml min^{-1}), L = sampling loop (200 µl). x–y = 7 cm.

---

* To whom correspondence should be addressed.

solution was then adjusted to 11 with 5% m/v NaOH and the solution was again boiled for 5 min, allowed to cool to room temperature, filtered through Selecta No. 595½ filter-paper and neutralized to pH 6 with 5% v/v HCl. The final volume was adjusted to 100 ml with distilled, de-ionized water.

The residue on the filter-paper was washed and acidified with 5% v/v HCl to pH 2. The solution was heated to boiling, adjusted to pH 11 with 5% m/v NaOH and boiled again for 5 min. After reaching room temperature, the solution was filtered, neutralized to pH 6 and adjusted to a final volume of 50 ml with distilled, de-ionized water. Tannin was then determined in the two solutions.

Chemical Analysis System Based on FI

On the basis of the standard conditions suggested for the determination of tannin with the FCR by the conventional method,[7,9] several parameters for application of the method to the proposed FI system (Fig. 1) were determined. The FI arrangement consists of a confluent system[15] with recovery of the reagent (FCR) in which the sample is inserted into an inert carrier (water) and successively flows together with NaOH and the FCR.

The chemical variables were optimized in a univariate manner. First, with fixed concentrations of NaOH (2%) and tannin (40 mg l^{-1}) (injection volume 200 µl), the effect of the FCR concentration was studied at dilutions from $1 + 9$ to $3 + 7$ (dilution from the stock solution and adjustment to pH 4–5 with 5% m/v NaOH). Subsequently, with the FCR dilution fixed at $2 + 8$, NaOH concentrations from 0.5 to 4% were tested. The relationship between the flow rates of the reagents and of the sample carrier and the total flow rate was also investigated. Finally, after the optimum conditions for the proposed system had been obtained, the effect of reactor length (50–250 cm) and injection volume (100–350 µl) was studied. The influence of the temperature on the reaction rate was also investigated. After optimization of all the system parameters, the linear range of the method was determined.

Study of Interferents

Using the configuration illustrated in Fig. 1, some ions known to be interferents in the conventional method for the determination of tannin[9] or to be present at higher concentrations in the sample, *viz.*, in the range 1–300 mg l^{-1}, were studied. Iron, Fe[(NH$_4$)$_2$(SO$_2$)$_2$·6H$_2$O], aluminium (AlCl$_3$), sulfide (Na$_2$S) and chloride (NaCl) were selected and their individual and synergistic effects were studied by adding them to a 40 mg l^{-1} tannin solution.

Results and Discussion

For the FI system illustrated in Fig. 1, using a 150 cm coiled reactor and injecting 200 µl of tannin solution (40 mg l^{-1}), it was found that the best response, with minimum reagent consumption, was obtained at a $2 + 8$ FCR dilution, pH 4–5 and 2% NaOH concentration. Under the conditions employed, more dilute FCR solutions were found to cause a considerable decrease in the signal, and more concentrated solutions were found to have little effect. Hence, at dilutions of more than $2 + 8$ there is insufficient reagent to oxidize all the tannin present in the solution because the intensity of the blue colour developed is proportional to the amount of FCR reduced by the polyphenols. For the NaOH concentration, however, a constant increase in the signal was observed up to about 2% NaOH, with stabilization at higher concentrations; this may be explained by the fact that the reaction had a higher sensitivity within a certain alkaline pH range (between 10 and 11).[9]

Table 1 Study of interferents in the determination of 40 mg l^{-1} tannin with the proposed FI system

Interferent	Concentration/ mg l^{-1}	Relative error (%)
Cl$^-$	1.0–300.0	0
Al^{3+}	1.0	0
	10.0	−7.7
	50.0–200.0	−12.8
Fe^{2+}	1.0	5.5
	10.0	−12.8
	25.0	−32.3
	50.0	−48.7
	75.0	−34.9
	100.0	89.7
S^{2-}	1.0–10.0	0
	25.0	5.4
	50.0	12.8
	100.0	84.6
Fe^{2+} +Cl$^-$	1.0	−7.7
	10.0	−13.0
	25.0	−31.7
	50.0	−45.6
	75.0	−36.2
	100	87.1
S^{2-} + Cl$^-$	1.0–10.0	0
	25.0	6.5
	50.0	28.2
	100.0	89.7
Fe^{2+} + S^{2-}	1.0–10.0	−11.7
	25.0	17.4
	50.0	43.6
Fe^{2+} +Al^{3+} + Cl$^-$ + S^{2-}	1.0–10.0	−12.8
	25.0	15.2
	50.0	43.6

Table 2 Study of interferents in the determination of 6.0 mg l^{-1} tannin by the conventional method

Interferent	Concentration/ mg l^{-1}	Relative error (%)
Cl$^-$	10–300.0	0
Al^{3+}	1.0	0
	10.0–25.0	14.0
	50.0–200.0	18.7
S^{2-}	1.0	40.4
	10.0	140.4
Fe^{2+}	1.0	22.8
	10.0	261.7
Fe^{2+} + Cl$^-$	1.0	26.6
	10.0	273.3
S^{2-} + Cl$^-$	1.0	17.7
	10.0	287.7
Fe^{2+} + S^{2-}	1.0	45.5
	10.0	419.3
Fe^{2+} + Al^{3+} + S^{2-} + Cl$^-$	1.0	48.7
	10.0	456.1
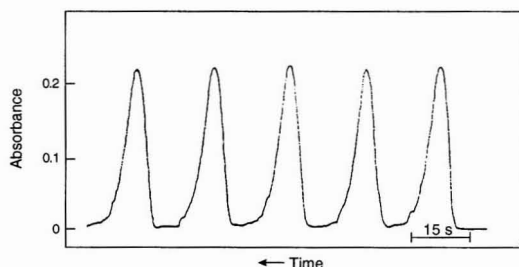
Fig. 2   Absorbance profile of a 40 mg l^{-1} tannin solution (at 670 nm).

A 150 cm reactor was adopted because only a small variation in sensitivity was observed when reactors of 50–250 cm were used. A considerable increase in the analytical signal was observed with the injection of up to 200 μl of the sample, with a less significant increase occuring with larger volumes.

As regards the flow rates of the reagents (FCR and NaOH), the sample (A) and the sample carrier (C), the best ratio obtained was $1:2:4:6$ (FCR:NaOH:A:C). A total flow rate of 9 ml min⁻¹ provided a good determination rate and only a small variation in sensitivity was observed between 4.5 and 17 ml min⁻¹.

The interference of iron[7,9] and sulfide[9] ions was confirmed. It was also observed that chloride ions do not interfere and that aluminium ions have little effect in the concentration range studied. In all iron and/or sulfide ion combinations

Table 3 Determination of tannin in tanning effluent samples with the proposed FI system and conventional method

	Tannin/mg l⁻¹	
Sample	FI system	Conventional method
B*	0	0
1	108.5	108.7
2	111.7	112.8
3	114.9	121.2
$x \pm s$†	111.7 ± 3.2	114.3 ± 6.4

* Blank.
† Mean ± standard deviation.
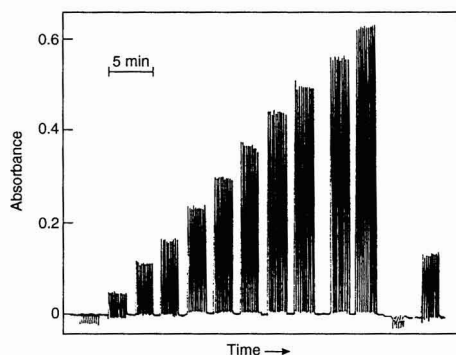
Fig. 3 Recordings of routine analyses at 670 nm. From left to right: signals for 0–100 mg l⁻¹ tannin standards, followed by the blank and the effluent sample.

Table 4 Features of the proposed FI system and of the conventional method

Parameter	FI system	Conventional method
Reagent volume/ml: FCR (2 + 8)	0.2	2.5*
NaOH (2%)	0.4	2.0
Sample volume/ml†	0.2	8.0
Sample throughput (determinations per hour)	250	1.5
Linearity/mg l⁻¹	5.0–100.0	0–20.0
Sensitivity/A l mg⁻¹	0.0063	0.0313
Detection limit/mg l⁻¹	1.04	0.96

* Final volume = 25 ml.
† 40 mg l⁻¹ Tannin solution.

studied, significant interference was noted. On the other hand no synergistic effect of chloride ions on the interference from aluminium ions was found (Table 1). The measured positive interference values for higher iron concentrations (100 mg l⁻¹) result from the formation of insoluble iron hydroxide in the solution. Owing to the complexation of iron ions with tannin, no interference was found at lower concentrations. Table 2 shows the extent of the interference of different ions in the determination of 6.0 mg l⁻¹ of tannin by the conventional method.

As regards the effect of temperature on the spectrophotometric determination of tannin with the proposed FI system, no effect on the signal was noted in the range 15–35 °C.

The calibration graph was linear from 5.0 to 100.0 mg l⁻¹ tannin, and was described by the following equation: $y = -0.015 + 0.00628x$ (where y is the absorbance and x the tannin concentration); the correlation coefficient was 0.999. Fig. 2 illustrates the peak profile of a 40 mg l⁻¹ tannin solution. The relative standard deviation (s_r) was 2.9% ($n = 10$). The detection limit (3σ) was calculated as recommended by IUPAC,[16] and the value obtained was 1.04 mg l⁻¹ tannin.

Table 3 shows the results obtained with the proposed FI system and with the conventional method for the determination of the tannin concentration of samples collected from the decanter (primary treatment) of a tanning effluent treatment system.

The signals for standard solutions containing 10.0–100.0 mg l⁻¹ of tannin and for routine analyses, obtained at 670 nm, are shown in Fig. 3. The solutions from the filtration residues (see under Sample Treatment) were also analysed and no perceptible signal was observed for tannin. Negative peaks were observed for blank assays and for diluted solutions, a phenomenon that may be attributed to the fact that the FCR is coloured and to variations in the refractive index (particularly between NaOH and FCR).

The main features of the proposed FI system and of the conventional method are presented in Table 4.

Conclusion

The proposed FI system is suitable for the determination of tannin in tanning effluent and in similar matrices. When compared with the conventional method for the determination of tannin, the FI method has advantages such as reduced reagent consumption, increased analytical speed and wider linear range (5.0–100.0 and 0–20.0 mg l⁻¹ tannin, respectively). The effect of interferents is also minimized by using the FI-based system. It is possible to perform up to 250 determinations per hour using 200 μl of the FCR per determination. Furthermore, the results obtained by the two methods in the determination of tannin in a sample of tanning effluent are equivalent. Hence, the precision ($s_r < 3\%$, $n = 10$) of the FI method is good but, as expected, its sensitivity is relatively low compared with that of the conventional method.

References

1 Hagerman, A. E., and Butler, L. G., *J. Agric. Food Chem.*, 1987, **26**, 809.
2 *Official Methods of Analysis of the Association of Official Analytical Chemists*, ed. Horwitz, W., AOAC, Washington, D.C., 11th edn., 1970, pp. 154, 188.
3 Verleze, M., and Delahaye, P., *J. Chromatogr.*, 1983, **268**, 469.
4 Folin, O., and Denis, W., *J. Biol. Chem.*, 1912, **12**, 239.
5 Folin, O., and Ciocalteu, V., *J. Biol. Chem.*, 1927, **73**, 626.
6 Snell, F. D., and Snell, C. T., *Colorimetric Methods of Analysis*, Van Nostrand, Princeton, NY, 3rd edn., 1950, vol. III, pp. 458–462.
7 Kloster, M. B., *J. Am. Water Works Assoc.*, 1974, **66**, 44.

8 Reicher, F., Sierakowski, M. R., and Corrêa, J. B. C., *Arq. Biol. Tecnol.*, 1981, **24**, 407.
9 Box, J. D., *Water Res.*, 1983, **17**, 511.
10 Celeste, M., Tomás, C., Cladera, A., Estela, J. M., and Cerdà, V., *Anal. Chim. Acta*, 1992, **269**, 21.
11 Willemot, J., and Parry, G., *Ann. Pharm. Fr.*, 1970, **28**, 391.
12 Lau, O.-W., Luk, S.-F., and Huang, H.-L., *Analyst*, 1989, **114**, 631.
13 Tempel, A. S., *J. Chem. Ecol.*, 1982, **8**, 1289.
14 Bergamin, F⁰, H., Zagatto, E. A. G., Krug, F. J., and Reis, B. F., *Anal. Chim. Acta*, 1978, **104**, 17.

15 Růžička, J., Hansen, E. H., and Zagatto, E. A., *Anal. Chim. Acta*, 1977, **88**, 1.
16 Commission on Spectrochemical and Other Optical Procedures for Analysis. Nomenclature, Symbols, Units and Their Usage in Spectrochemical Analysis—II, *Spectrochim. Acta, Part B*, 1978, **33**, 241.

Utility of Certain π-Acceptors for the Spectrophotometric Determination of Norfloxacin

Alaa S. Amin and Gamal O. El-Sayed

Chemistry Department, Faculty of Science, Benha University, enha, Egypt

Yousry M. Issa

Faculty of Science, Cairo University, Giza, Egypt

Simple, rapid, accurate and sensitive spectrophotometric methods are described for the determination of norfloxacin. The methods are based on the reaction of this drug as a π-electron donor with 2,3-dichloro-5,6-dicyano-*p*-benzoquinone (DDQ), 7,7,8,8-tetracyanoquinodimethane (TCNQ), *p*-chloranil (CL) or chloranilic acid (CLA) as π-acceptors to give highly coloured complex species. The coloured products are measured spectrophotometrically at 460, 843, 550 and 531 nm for DDQ, TCNQ, CL and CLA, respectively. Optimization of the different experimental conditions is described. Beer's law is obeyed in the range 10–400 µg ml^{-1} and colours were produced in non-aqueous media and were stable for at least 3 h. Applications of the suggested methods to representative pharmaceutical dosage forms are presented and compared with the official method. Interferences from additives and common degradation products were investigated.

Keywords: Norfloxacin determination; spectrophotometry; π-acceptor; charge-transfer complex

Introduction

Norfloxacin [1-ethyl-6-fluoro-1,4-dihydro-4-oxo-7-(1-piperazinyl)-3-quinolonecarboxylic acid] (CAS 70458-96-7) has broad-spectrum antibacterial activity against gram-positive and gram-negative aerobic pathogens and is considered to be the first commercially available member of the modern fluoroquinolones.[1,2] Norfloxacin is specifically prescribed for the treatment of complicated urinary tract infections. Its mode of action has advantages over the other common antibiotics; it is thought to inhibit the DNA gyrase enzyme that catalyses chromosomal DNA supercoilings and the promotion of double-stranded DNA breakage. The fluorine atom at the 6-position provides increased potency against gram-negative organisms and the piperazine moiety at the 7-position is responsible for antipseudomonal activity.
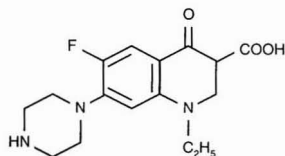
Most published assay methods for norfloxacin are suitable for its determination in biological fluids.[3–8] On the other hand, methods based on the spectrophotometric determination of norfloxacin in pharmaceutical formulations using FeCl$_3$,[9] Fe(NO$_3$)$_3$,[10] Bromothymol Blue[11] and tetrachlorobenzoquinone[12] have been reported. Various potentiometric titration[13,14] and high-performance liquid chromatographic[15–18] procedures for the determination of the drug have been used. Only one official method,[19] based on the titration of norfloxacin dissolved in glacial acetic acid with 0.1 mol l^{-1} perchloric acid using a suitable anhydrous electrode system, is considered. This paper reports spectrophotometric methods for the assay of norfloxacin using 2,3-dichloro-5,6-dicyano-*p*-benzoquinone (DDQ), 7,7,8,8,-tetracyanoquinodimethane (TCNQ), *p*-chloranil (CL) or chloranilic acid (CLA) as chromogenic reagents. The proposed methods were applied successfully to the determination of norfloxacin either pure or in dosage forms, with good accuracy and precision. The results were compared with those given by the official method.[19]

Experimental

Apparatus

A Perkin-Elmer Lambda 3B recording spectrophotometer equipped with 10 mm matched silica cells was used for all spectral measurements.

Norfloxacin

Norfloxacin was obtained from the Egyptian International Pharmaceutical Industries Co. (EIPICO) under licence from Merck (Rahway, NJ, USA).

Formulations

The following commercial formulations were subjected to the analytical procedures: Noroxin tablets (EIPICO) containing 400 mg of norfloxacin per tablet, Neofloxin tablets (Alexandria Company for Pharmaceuticals and Chemical Industries, Alexandria, Egypt) containing 400 mg of norfloxacin per tablet and Spectrama tablets [Amoun Pharmaceutical Industries Co. (APIC), El-Salam City, Cairo, Egypt] containing 400 mg of norfloxacin per tablet.

Reagents

DDQ solution (5 × 10^{-3} mol l^{-1}) in methanol was freshly prepared. TCNQ 5 × 10^{-3} mol l^{-1} solution in acetonitrile is stable for at least 1 week at 4 °C. *p*-Chloranil and chloranilic acid solutions, 5 × 10^{-3} mol l^{-1} in acetonitrile, were prepared.

Stock Standard Solutions

For the DDQ method, weigh accurately 500 mg of norfloxacin into a 100 ml calibrated flask, dissolve the drug in methanol and dilute to volume with methanol. For the TCNQ, CL and

CLA methods, dissolve the drug in 2 ml of methanol and dilute to volume with acetonitrile.

Working Standard Solutions

Weigh accurately 500 mg from a composite of the mixed contents of ten tablets, then follow the procedure as for the stock standard solutions.

General Procedure

Method using DDQ

Place a 2 ml aliquot of a solution of the standard or pharmaceutical preparation in methanol containing 0.5–10.0 mg of the drug in a 25 ml calibrated flask. Add 2.5 ml of DDQ solution and allow the mixture to stand at 20–25 °C for about 10 min. Dilute to volume with methanol and measure the absorbance at 460 nm against a reagent blank prepared in the same manner.

Method using TCNQ

Place a 2 ml aliquot of a solution of the standard or pharmaceutical preparation in acetonitrile containing 0.25–7.5 mg of the drug in a 25 ml calibrated flask. Add 2.5 ml of TCNQ solution and allow the mixture to stand at 20–25 °C for 20 min. Dilute to volume with acetonitrile and measure the absorbance at 843 nm against a reagent blank prepared in the same manner.

Method using CL or CLA

Place a 2 ml aliquot of a solution of the standard or pharmaceutical preparation dissolved in acetonitrile containing 0.25–5.75 and 0.5–6.25 mg of the drug in a 25 ml calibrated flask. Add 2.5 ml of CL or CLA solution and heat in a water-bath at 60 °C for 10 min. Cool, dilute to volume with acetonitrile and measure the absorbance at 550 or 531 nm for CL or CLA, respectively, against a reagent blank prepared in the same manner.

Stoichiometric Relationship

Job's method of continuous variation was employed; a 1×10^{-3} mol l^{-1} standard solution of norfloxacin and a 1×10^{-3} mol l^{-1} solution of DDQ, TCNQ, CL or CLA were used. A series of solutions was prepared in which the total volume of norfloxacin and reagent was kept at 4 ml. The reagents were mixed in various proportions and diluted to volume in a 25 ml calibrated flask with the appropriate solvent following the above-mentioned procedure.

Results and Discussion

The reaction of DDQ with norfloxacin results in the formation of an intense orange–red product which exhibits an absorption maximum at 460 nm. This spectrum is similar to that of the radical anion obtained by reduction with iodide.[20]

In acetonitrile, a solution of norfloxacin and TCNQ yields an intense blue colour, causing characteristic long-wavelength absorption bands, frequently with numerous vibrational maxima in the electronic spectrum (Fig. 1). The predominant chromogen with TCNQ is the blue radical anion TCNQ$^-$, which was probably formed by the dissociation of an original donor–acceptor (DA) complex with norfloxacin:

$$D^{\cdot\cdot} + A \rightleftharpoons \underset{\text{DA complex}}{D^{\cdot\cdot}\!-\!A} \xrightarrow{\text{polar solvent}} \underset{\text{radical ions}}{D^{\cdot+} + A^{\cdot+}}$$
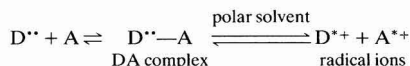
The dissociation of the DA complex is promoted by the high ionizing power of the solvent, acetonitrile.[21] Further support for this assignment was provided by comparison of the absorption band with those of the TCNQ$^{\cdot-}$ radical anion produced by the iodide reduction method.[22]

In addition to the TCNQ and DDQ radical anions, the resulting bands for the complexes of norfloxacin with CL and
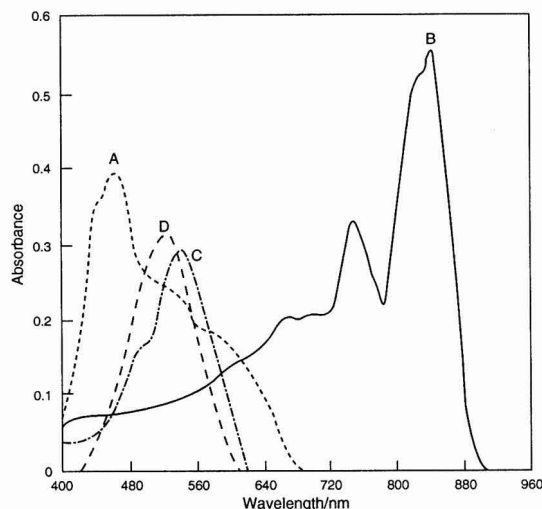
Fig. 1 Absorption spectra of norfloxacin complexes with: A, DDQ; B, TCNQ; C, CL; and D, CLA. Concentration of: norfloxacin = 5 mg per 25 ml; and reagent = 5×10^{-4} mol l^{-1}.

Table 1 Quantitative parameters for the complexation of norfloxacin with DDQ, TCNQ, CL and CLA

Parameters	DDQ	TCNQ	CL	CLA
Beer's law limits/μg ml^{-1}	20–400	10–300	10–230	20–250
Molar absorptivity/l mol^{-1} cm^{-1}	4.1×10^3	8.8×10^3	1.2×10^3	1.1×10^3
Sandell sensitivity/μg cm^{-2}	0.017	0.013	0.027	0.028
Slope (specific absorptivity)	0.025	0.028	0.011	0.010
Intercept	0.012	0.016	−0.013	0.009
Correlation coefficient	0.9996	0.9984	0.9986	0.9988
Standard deviation (%)	0.67	0.83	0.91	0.78
Range of error (%)	±0.8	±1.3	±1.5	±1.5
Ringbom optimum concentration range/μg ml^{-1}	20–370	20–280	20–220	20–240

CLA, obtained by reaction in acetonitrile at 60 °C, are similar to the maxima of the radical anions of these acceptors obtained by the reduction method.[20]

Acetonitrile was found to be the best solvent for TCNQ, CL and CLA because it has a high relative permittivity which ensures the maximum yield of TCNQ*⁻, CL*⁻ and CLA*⁻ species. On the other hand, methanol affords maximum sensitivity with DDQ, and in addition it is a good solvent for the reagent. Of the other solvents examined, dichloromethane and 1,2-dichloroethane are possible substitutes but benzene and chloroform were unsuitable owing to the limited solubility of the reagents in these solvents. In 1,4-dioxane other orange products, and not TCNQ*⁻, were obtained on addition of the reagent. It is likely that the formation of this product also involves interaction with solvent molecules.[23]

The relative sensitivities of the four acceptors can be determined by comparing the molar absorpitivities (ε) of the chromogens (Table 1). DDQ and TCNQ exhibited the most intense bands and were therefore selected for all further work. The most important spectral characteristics of the reaction of DDQ and TCNQ with norfloxacin investigated are presented in Table 1.

When various concentrations of DDQ or TCNQ were added to a fixed concentration of norfloxacin, 2.5 ml of 5×10^{-3} mol l⁻¹ solution were found to be sufficient for the production of maximum and reproducible colour intensity. Higher concentrations of reagent did not affect the colour intensity (Fig. 2).

The optimum reaction time was determined by following the colour development at ambient temperature (20–25 °C). Complete colour development was attained after 10 and 20 min for DDQ and TCNQ, respectively, whereas for CL and CLA complete colour development was attained after 90 min; after heating on a water-bath at 60 °C for 10 min, complete colour development was obtained. The colour remained stable for 3, 2.5, 2 and 2.5 h for DDQ, TCNQ, CL and CLA, respectively.

Job's continuous variation graph for the reaction between norfloxacin and different reagents (Fig. 3) shows that the interaction between these two compounds occurs on an equimolar basis. The reaction of norfloxacin with DDQ, TCNQ, CL or CLA occurs through the formation of a charge-transfer complex. The coloured reaction product can be represented, taking DDQ as an example, by the following structure:
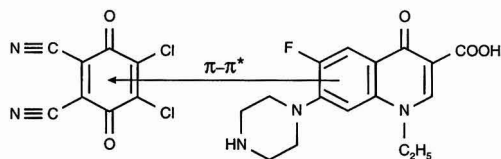
Quantification

A linear correlation was found between absorbance and concentration in the ranges given in Table 1. The correlation coefficients, intercepts and slopes for the calibration data for norfloxacin are calculated using the least-squares method.

The reproducibility of the procedure was determined by running five replicate samples, each containing 130 micrograms of norfloxacin per millilitre of the final assay solution. At this concentration, the relative standard deviation was 0.67, 0.83, 0.91 and 0.78% for DDQ, TCNQ, CL and CLA complexes, respectively.

The performance of the methods was assessed by calculation of the t- and F-values compared with the official method.

Mean values were obtained in a Student's t- and F-test and 95% confidence limits for five degrees of freedom,[24] and the results showed that the calculated t- and F-values did not exceed the theoretical values.

Sensitivity, Accuracy and Precision

The mean molar absorptivity (ε) and Sandell sensitivity (S) as calculated from Beer's law are presented in Table 1. For more accurate results, Ringbom optimum concentration ranges were obtained (Table 1). In order to determine the accuracy and precision of the method, solutions containing six different concentrations of norfloxacin were prepared and analysed in quintuplicate. The measured standard deviations (s), relative standard deviations (s_r), the standard analytical errors and confidence limits (Table 2) can be considered satisfactory, at least for the levels of concentrations examined.

Comparison of the results obtained by the proposed methods using chloranil with those obtained by Zhou *et al.*[12] using the same reagent in aqueous buffer medium showed a wider range of determination, higher accuracy and less time consumption with the non-aqueous methods proposed here.

Comparison of the recovery obtained with the proposed methods with the purity of the studied compounds as determined according to the *US Pharmacopoeia*[19] showed a high accuracy of the present methods. The proposed methods
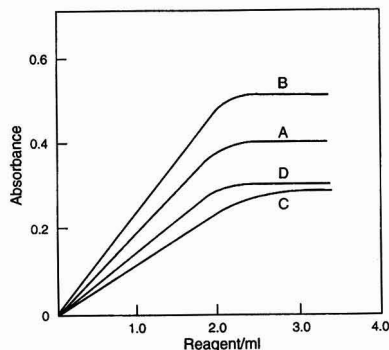
Fig. 2 Effect of reagent concentration (5×10^{-3} mol l⁻¹) on the formation of norfloxacin complexes with: A, DDQ; B, TCNQ; C, CL; and D, CLA.
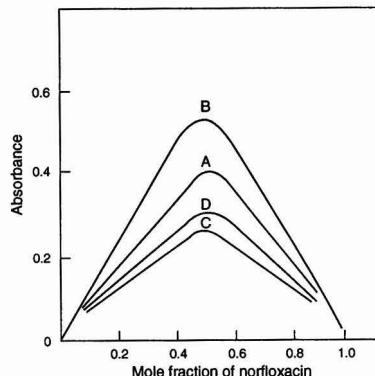
Fig. 3 Job's method for the norfloxacin complexes. Total molar concentration = 1.6×10^{-4} mol l⁻¹. A, DDQ; B, TCNQ; C, CL; and D, CLA.

Table 2 Evaluation of accuracy and precision of the proposed method

Reagent	Taken/ $\mu g\ ml^{-1}$	Found*/$\mu g\ ml^{-1}$ O	P	s	s_r (%)	Standard error	Confidence limits
DDQ	50	48.2	50.4	0.04	0.53	0.016	50.4 ± 0.050
	150	145.6	149.1	0.03	0.46	0.012	149.1 ± 0.035
	250	244	253.8	0.05	0.68	0.020	253.8 ± 0.060
	350	358	347.2	0.03	0.39	0.012	347.2 ± 0.035
	Mean				0.52	0.015	
TCNQ	70	72.5	69.1	0.06	0.76	0.024	69.1 ± 0.070
	140	135.3	141.8	0.07	0.91	0.029	141.8 ± 0.080
	210	214.8	208.4	0.04	0.56	0.016	208.4 ± 0.050
	280	287.5	283.2	0.05	0.66	0.020	283.2 ± 0.060
	Mean				0.73	0.022	
CL	60	63.1	59.1	0.08	1.07	0.033	59.1 ± 0.095
	120	125.7	118.5	0.09	1.16	0.037	118.5 ± 0.110
	170	174.3	172.6	0.07	0.94	0.029	172.6 ± 0.080
	220	228.1	217.8	0.05	0.69	0.020	217.8 ± 0.060
	Mean				0.97	0.030	
CLA	40	38.1	40.6	0.09	1.19	0.037	40.6 ± 0.110
	100	102.3	99.1	0.07	0.96	0.029	99.1 ± 0.080
	160	164.6	157.6	0.06	0.78	0.024	157.6 ± 0.070
	240	233.3	243.2	0.08	1.04	0.033	243.2 ± 0.095
	Mean				0.99	0.031	

* Average of six determinations. O = Official method.[19] P = Proposed method.

Table 3 Determination of norfloxacin in different pharmaceutical formulations using DDQ, TCNQ, CL and CLA reagents

Tablets	Manufacturer	Content/ mg per tablet	Found* DDQ	TCNQ	CL	CLA	O[†]
Noroxin	EIPICO	400	401	398	396	403	395
Spectrama	APIC	400	398	399	403	402	406
Neofloxin	Alexandria	400	402	401	397	398	396

* Average of six determinations.
[†] O = Official method.[19]

are simpler, less time consuming and more sensitive than the official method. Moreover, the proposed methods could be used for the routine determination of norfloxacin in pure form or in pharmaceutical formulations.

Analytical Applications

The proposed methods were applied to some pharmaceutical formulations containing norfloxacin. The results in Table 3 indicate high accuracy. The proposed methods are suitable for the determination of norfloxacin in drug formulations without interferences from excipients such as starch and glucose or from common degradation products.

Conclusion

The proposed methods are simpler, less time consuming and more sensitive than the official method (based on the titration of norfloxacin dissolved in glacial acetic acid with 0.1 mol l^{-1} perchloric acid using a suitable anhydrous electrode system). Although the colour development of CL and CLA complexes at room temperature requires 90 min for completion, this can be shortened to 10 min by raising the temperature to 60 °C. Moreover, the CL procedure has the advantages over an aqueous method[12] of a wider range of determination, higher sensitivity and less time consumption. The presence of the F atom acting as an electron-withdrawing group does not affect the formation of the charge-transfer (CT) complex owing to the existence of the 1-methyl and 7-piperazinyl electron-donating groups in the molecule. Regarding the interference of degradation products, the energy of the CT (E_{CT}) depends

on the ionization potential (I_p) of the donor and the electron affinity of the acceptor (E_A) hence the λ_{max} values of the other π-donors mostly differ from that of the investigated compound if they are able to form CT complexes. The proposed methods are suitable for the determination of norfloxacin in dosage forms without interferences from excipients such as starch and glucose or from common degradation products, suggesting applications in bulk drug analysis.

References

1 Grohe, K., *Chem. Br.*, 1992, **28**, 34.
2 Zeiler, H., and Grohe, K., *J. Clin. Microbiol.*, 1984, **3**, 339.
3 Schoenfeld, W., Knoeller, J., Bremm, K. D., Dahlhoff, A., Weber, B., and Koenig, W., *Zentralbl. Bakteriol. Mikrobiol. Hyg., Ser. A.*, 1986, **261**, 338.
4 Morton, S. J., Shull, V. H., and Dick, J. D., *Antimicrob. Agents Chemother.*, 1986, **30**, 325.
5 Nelson-Ehle, I., *J. Chromatogr.*, 1987, **416**, 207.
6 Lagana, A., Curini, R., D'Ascenzo, G., and Miano, L., *J. Chromatogr.*, 1987, **417**, 135.
7 Lagana, A., Rototori, M., Curini, R., D'Ascenzo, G., and Miano, L., *J. Pharm. Biomed. Anal.*, 1988, **6**, 221.
8 Carlucci, G., Mazzeo, P., and Palumbo, G., *Biomed. Chromatogr.*, 1993, **7**, 126.
9 Bhowal, S. K., and Das, T. K., *Anal. Lett.*, 1991, **24**, 25.
10 Chowdary, K. P. R., and Annapuma, A., *Indian Drugs*, 1992, **29**, 612.
11 He, X., *Yaowu Fenxi Zazhi*, 1992, **12**, 107.
12 Zhou, X. G., Feng, J. Z., and Tong, S. S., *Fenxi Huaxue*, 1993, **21**, 184.
13 Li, G. X., and Zheng, R. Q., *Zhongguo Yaoxue Zazhi*, 1992, **27**, 24.

14 Shen, X., Wang, S., and Liu, Z., *Yaowu Fenxi Zazhi*, 1993, **13**, 107.
15 Zhao, L., Chan, Y., Dai, Q., and Yang, Q., *Zhongguo Yaoke Daxue Xuebau*, 1992, **23**, 127.
16 Jain, R., and Jain, C. L., *LC–GC*, 1992, **10**, 707.
17 Zhong, H. R., Cai, B. Q., Li, A. C., Hao, L. X., and Zhang, A. L., *Yaowu Fenxi Zazhi*, 1993, **13**, 27.
18 Carlucci, G., Mazzeo, P., and Palumbo, G., *Biomed. Chromatogr.*, 1993, **7**, 126.
19 *US Pharmacopeia, XXII Revision*, US Pharmacopeial Convention, Rockville, MD, 1990.
20 Terrey, H. A., and Hunter, W. H., *J. Am. Chem. Soc.*, 1912, **34**, 702.

21 Liptay, W., Briegleb, G., and Schnindler, K., *Z. Elektrochem.*, 1962, **66**, 331.
22 Melby, L. R., Harder, R. J., Hertler, W. R., Mahler, W., Benson, R. E., and Mochel, W. E., *J. Am. Chem. Soc.*, 1962, **84**, 3374.
23 Diekmann, J., and Pedersen, C. J., *J. Org. Chem.*, 1963, **28**, 2874.
24 Miller, J. C., and Miller, J. N., *Statistics in Analytical Chemistry*, Ellis Horwood, Chichester, 2nd edn., 1988.

Determination of Manganese in Chinese Tea Leaves by a Catalytic Kinetic Spectrophotometric Method

Renmin Liu, Aimei Zhang, Daojie Liu and Shuhao Wang

Department of Chemistry, Liaocheng Teachers College, Liaocheng, Shandong, China

The catalytic effect of manganese(II) on the oxidation of Rhodamine B with potassium periodate in the presence of 1,10-phenanthroline in acetic acid–sodium acetate was studied. A catalytic kinetic spectrophotometric method for determination of manganese(II) was developed. Manganese in the range 0.1–5.0 ng ml^{-1} can be determined, and the detection limit is 0.02 ng ml^{-1}. Manganese in Chinese tea leaves was successfully determined.

Keywords: Manganese determination; tea leaves; catalytic kinetic method; spectrophotometry

Introduction

Manganese is an essential microelement for human body. It participates in haemopoietic function and transmission of genetic information.[1,2] Manganese deficiency in humans is related to delayed blood coagulation and hypercholesterolaemia, and abnormal manganese metabolism can contribute to diabetes mellitus.[3] Hence the determination of manganese in food is of great interest. Many kinetic methods have been reported for the determination of manganese based on its catalytic effect on the oxidation of organic compounds. The oxidants most frequently used are hydrogen and potassium periodate. The organic compounds used include hydroxyanthraquinones,[4] triphenylmethane,[5] Schiff base,[6–12] and azo dyes.[13–15] Among the most sensitive methods of this type reported so far are the method of Bartkus and Nauekaitis,[4] based on the oxidation of purpurin by hydrogen peroxide, that of Hirayama and Unohara,[16] based on the oxidation of N,N-diethylaniline by periodate, the method of Rubio *et al.*,[10] based on the oxidation of pyridoxal 2-pyridylhydrazone by hydrogen peroxide, and the method of Tarin and Blanco,[14] based on the oxidation of 3-(2-hydroxyphenylazo)pyridine-2,6-diol by hydrogen peroxide.

In this work, the catalytic effect of manganese(II) on the oxidation of Rhodamine B (RhB) with potassium periodate in the presence of 1,10-phenanthroline (Phen) was studied. A catalytic kinetic spectrophotometric method for the determination of manganese was developed. The method can be used for the determination of manganese in the range 0.1–5.0 ng ml^{-1} by the fixed-time method with a detection limit of 0.02 ng ml^{-1}. The precision and accuracy and the influence of 26 foreign ions were studied. The method is one of the most sensitive methods developed so far. Manganese in Chinese tea leaves was determined by this method with good results.

Experimental

Reagents

All chemicals were of analytical-reagent grade and solutions were prepared with doubly distilled water.

Standard manganese(II) solution, 100 µg ml^{-1}. Provided by Shandong University.

RhB solution, 0.02%. Third Reagent Plant of Shanghai.

Potassium periodate solution, 0.015 mol l^{-1}.

Phen solution, 0.025% in aqueous ethanol (1 + 9).

Sodium fluoride solution, 0.5 mol l^{-1}.

pH *Buffer solution*. 0.5 mol l^{-1} acetic acid–sodium acetate (pH 3.8).

Apparatus

A Shimadzu UV-365 recording spectrophotometer and a Model 180-80 atomic absorption spectrophotometer were used. A CS 501 super thermostat was used to control the temperature.

General Procedure

Pipette into a 10 ml graduated tube, 0.4 ml of 0.02% RhB solution and 1.6 ml of a mixture of 0.025% Phen, 0.015 mol l^{-1} potassium periodate, 0.5 mol l^{-1} sodium fluoride and pH buffer solution (prepared just before use in volume proportions 1 + 1 + 1 + 7). To this add the sample solution containing 0.4–20 ng of manganese and dilute to 4.0 ml. Heat the mixture at 80 °C for 8.5 min, then cool it quickly to terminate the reaction. Transfer the solution into the spectrophotometer cell and measure the absorbance at 550 nm against a reagent blank. Manganese(II) is determined according to the absorbance *A*.
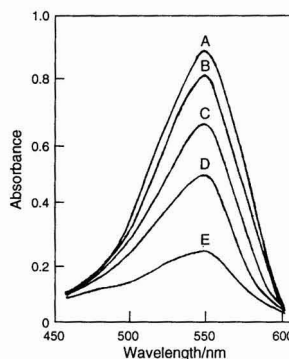
Fig. 1 Absorption spectrum against water: A, RhB; B, RhB + KIO$_4$; C, RhB + KIO$_4$ + Phen; D, RhB + KIO$_4$ + Mn^{II}; E, RhB + KIO$_4$ + Phen + Mn^{II}. RhB, 0.002%; KIO$_4$ 6 × 10^{-4} mol l^{-1}; Phen, 0.001%; Mn^{II}, 3 ng ml^{-1}; pH 3.8; time, 8.5 min; and temperature, 80 °C.

Results and Discussion

The oxidation of RhB by potassium periodate in weakly acidic media results in decoloration of the solution. Fig. 1 shows the absorption spectra of solutions of RhB, RhB + KIO_4, RhB + KIO_4 + Phen, RhB + KIO_4 + Mn^{II} and RhB + KIO_4 + Phen + Mn^{II} after heating at 80 °C for 8.5 min according to the above procedure. Fig. 1 indicates that the oxidation of RhB by potassium is catalysed by the presence of small amounts of manganese(II). The oxidation reaction was also accelerated by Phen, and this acceleration effect was greater when manganese was present in the system. The mechanism of this accelerative reaction is not clear. RhB has an absorption maximum at 550 nm, which was chosen as the measurement wavelength.

Optimum Conditions

The oxidation of RhB was influenced by the concentrations of RhB, Phen and potassium periodate and by the pH buffer and temperature. The effects of these on the catalysed reaction were studied.

The effect of RhB concentration was investigated. The results showed that the absorbance of the blank was very high when much more RhB was used, and the linear range for manganese was too narrow if a small amount of RhB was used. Considering these two factors, 0.002% RhB was used, while the absorbance of the blank was less than 1.2.

The influence of pH was studied by adjusting the pH with acetic acid and sodium acetate. The results are shown in Fig. 2. A pH value of 3.8 was selected as optimum.

The dependence of the reaction rate on temperature was studied between 40 and 90 °C (Fig. 3). A temperature of 80 °C was chosen as the optimum.

Fig. 4 shows the influence of reaction time; 8.5 min was selected for the determination.

The influence of the concentrations of potassium periodate and Phen was also studied and the results are shown in Figs. 5 and 6, respectively. Concentrations of 6×10^{-4} mol l^{-1} potassium periodate and 0.001% Phen were used.
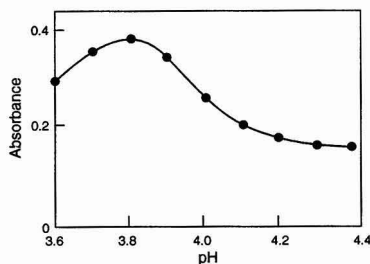
Fig. 2 Influence of pH. Other conditions as in Fig. 1.
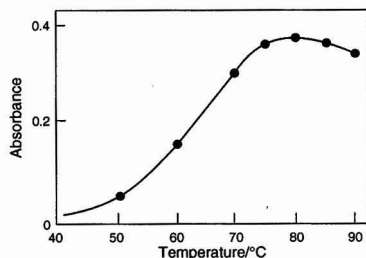
Fig. 3 Influence of temperature. Other conditions as in Fig. 1.

Calibration Graph

A linear calibration graph for manganese from 0.1 to 5.0 ng ml^{-1} was obtained under the optimum conditions. The regression equation of the calibration graph was $A = 0.019 + 0.121C$ where C is concentration (ng ml^{-1}) and the correlation coefficient was 0.998.

The proposed method yields a relative standard deviation of 1.1% for 11 determinations of a blank. The detection limit was 0.02 ng ml^{-1}, calculated as three times the standard deviation of the blank.

Interferences

The influence of 26 foreign inorganic ions on the determination of manganese was investigated. The tolerated limits for the ions assayed are given in Table 1 (with relative errors less than 5%). Caffeine and other organic compounds found in tea leaves were also investigated and no influence on the determination of manganese was found.
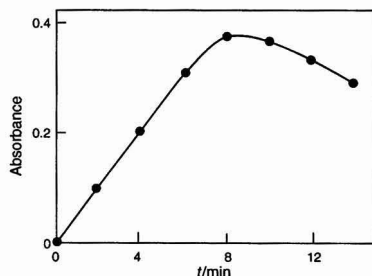
Fig. 4 Influence of reaction time. Other conditions as in Fig. 1.
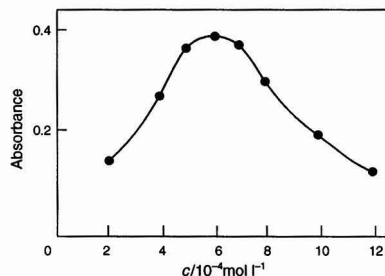
Fig. 5 Influence of KIO_4 concentration. Other conditions as in Fig. 1.
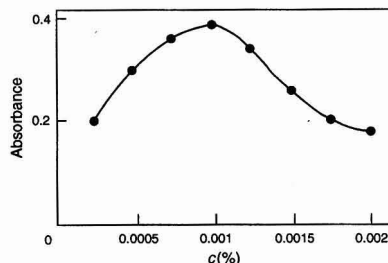
Fig. 6 Influence of Phen concentration. Other conditions as in Fig. 1.

Table 1 Effect of foreign ions on the determination of manganese (3 ng ml^{-1})

Foreign ion	Tolerated mass ratio, ion : Mn^{II}
K$^+$, Na$^+$, NH$_4$$^+$, Mg^{2+}, Ca^{2+}, Ba^{2+}, F$^-$, Cl$^-$, NO$_3$$^-$, SO$_4$$^{2-}$	300 000
Al^{3+}, PO$_4$$^{3-}$	5000
Br$^-$, Ag$^+$	2500
Fe^{3+}	1000*
I$^-$	500
Pb^{2+}, Cd^{2+}, Hg^{2+}	200
Cr^{VI}	150
NO$_2$$^-$, Cu^{2+}, Cr^{3+}	100
Zn^{2+}	50
Ni^{2+}	20
Co^{2+}	5
Fe^{3+}	1

* In the presence of 0.02 mol l^{-1} sodium fluoride.

Table 2 Determination of manganese in Chinese tea leaves

No.	Sample*	Concentration obtained by proposed method/ μg g^{-1}	Concentration obtained by AAS/ μg g^{-1}	Relative error (%)
1	Jasmine tea (Zhenghe, Fujian)	372.1	364.6	2.1
2	XianYin Oolong tea (Fuzhou, Fujian)	512.8	497.3	3.1
3	Ti Kun Yin (Anxi, Fujian)	486.4	492.8	−1.3
4	Early-Spring brand Jasmine tea You Country, Hunan)	395.8	384.6	2.9

* The names in the parentheses are the areas producing the tea leaves.

Table 3 Determination of percentage of manganese extracted from tea leaves by immersion in boiling water

Sample No.*	Mn content after 1st immersion/ μg g^{-1}	Mn content after 2nd immersion/ μg g^{-1}	Mn extracted of 1st immersion (%)	Mn further extracted on 2nd immersion (%)
1	240.7	174.3	35.3	27.6
2	429.2	398.2	16.3	7.2
3	396.6	364.7	18.5	8.0
4	274.3	212.8	30.7	22.4

* Samples as same in Table 2.

Applications

Some tea samples were analysed by the proposed method and by atomic absorption spectrometry. Tea samples were treated according to the ref. 17. The results are summarized in Table 2.

Tea leaves were immersed in boiling water and the percentage of manganese extracted was determined as follows. A 2.0 g amount of tea leaves was immersed in 100 ml boiling water for 5 min, the solution was poured out and the manganese was determined in the residue by the proposed method. After a second immersion in boiling water the manganese in the residue was determined again. The results are given in Table 3 and show that certain amounts of manganese can be ingested by drinking a tea infusion.

References

1 Li, S., *Essential Elements and Health*, Light Industry Press, Beijing, 1988, p. 141.
2 Chen, Q., in *Microelements and Health*, ed. Chen, Q., and Lu, G., Beijing University Press, Beijing, 1989, p. 106.
3 Castillo, J. R., and Fernanden, A., *Microchem. J.*, 1989, **39**, 224.
4 Bartkus, P., and Nauekaitis, A., *Nauchn. Konf. Khim. Anal. Pribalt. Resp. BSSR (Tesizy Dokl)*, *1st*, 1974, 190.
5 Fukasawa, T., Yamane, T., and Yamakazi, T., *Bunseki Kagaku*, 1977, **26**, 200.
6 Perez Bendito, D., Valcarcel, M., Ternero, M., and Pino, F., *Anal. Chim. Acta*, 1977, **94**, 405.
7 Moreno, A., Silva, M., Perez Bendito, D., and Valcarcel, M., *Talanta*, 1983, **30**, 107.
8 Raya Saro, T., and Perez Bendito, D., *Analyst*, 1983, **108**, 857.
9 Perez Bendito, D., Peinado, J., and Toribio, F., *Analyst*, 1984, **109**, 1297.
10 Rubio, S., Gomez Hens, A., and Valcarcel, M., *Analyst*, 1984, **109**, 717.
11 Vazqez Ruiz, J., Garcia de Torres, A., and Cano Pavon, J. M., *Talanta*, 1984, **31**, 29.
12 Salinas, F., Berzas Nevado, J. J., and Valiente, P., *Talanta*, 1987, **34**, 321.
13 Yamane, T., and Fukasawa, T., *Bunseki Kagaku*, 1977, **26**, 300.
14 Tarín, P., and Blanco, M., *Analyst*, 1988, **113**, 433.
15 Zhang, Z., and Ahang, G., *Yankuang Ceshi*, 1989, **8**, 13.
16 Hirayama, K., and Unohara, N., *Bunseki Kagaku*, 1984, **33**, E517.
17 Chen, S., *Huaxue Shijie*, 1990, **31**, 172.

Highly Selective Spectrophotometric Determination of Chlorine Dioxide in Water Using Rhodamine B

Zhang Xin and Zhao Jinyu

Department of Applied Chemistry, Anhui Agricultural University, Hefei 230036, China

A method for the spectrophotometric determination of chlorine dioxide in the presence of other chlorine species, *viz.*, free chlorine, hypochlorite, chlorite, chloramine and chlorate, was developed. The detection limit is 0.04 mg l^{-1} of chlorine dioxide; the calibration graph is linear over the range 0–1.5 mg l^{-1} of chlorine dioxide. The results show that free chlorine concentrations up to 40 mg l^{-1} and excess of oxychlorine species could be tolerated without interference. the method is rapid, sensitive and highly selective.

Keywords: Chlorine dioxide determination; water; spectrophotometry; Rhodamine B

Introduction

Many spectrophotometric reagents have been described for the determination of chlorine dioxide,[1–6] and they are claimed to be selective for chlorine dioxide. However, some of these reagents, although selective, do not possess the necessary sensitivity to determine low levels of chlorine dioxide, and only *N,N'*-diethyl-*p*-phenylenediamine (DPD) reagent is recommended in standard procedures.[7]

This paper describes a spectrophotometric reagent that is both selective and sensitive for the determination of low levels of chlorine dioxide in the presence of free chlorine, hypochlorite, chlorite, chloramine and chlorate. Using this reagent, free chlorine concentrations up to 40 mg l^{-1} could be tolerated without interference in chlorine dioxide determinations.

Experimental

Reagents and Standards

Stock standard chlorine dioxide solution, 200–400 mg l^{-1}. Prepared as described in ref. 8. In a gas-generating glass bottle, a 10 g amount of sodium chlorite was dissolved in 500 ml of water. Sulfuric acid (20%) was added intermittently from a separating funnel. Chlorine dioxide gas was synthesized by reaction of sulfuric acid and sodium chlorite and passed through a scrubber containing a saturation solution of sodium chlorite using a slow-moving air flow. The stock standard solution of chlorine dioxide was prepared as required by bubbling the chlorine dioxide gas through distilled water and stored at 4 °C in a dark-glass bottle. Dilute standard solutions of chlorine dioxide were prepared daily from the stock standard solution and were also stored in dark. The solutions were standardized by iodimetric titration prior to use.

Stock standard chlorine solution, 1000 mg l^{-1}. The solution was prepared by bubbling chlorine gas through distilled water and was stored in a dark-glass bottle at 4 °C. The solution was standardized by iodimetric titration prior to use.

Rhodamine B standard solution, 10 mg l^{-1}. A 100 mg l^{-1} stock standard solution was prepared by dissolving 100 mg of Rhodamine B in and diluting to 1 l with distilled water. A 10 mg l^{-1} solution was prepared by tenfold dilution of the stock standard solution.

Apparatus

Absorbance measurements were performed at 553 nm using a Model 751G UV–visible spectrophotometer, fitted with a 30 mm cell and was used with distilled water as a reference blank.

Procedure

Place 2 ml of Rhodamine B solution in a 25 ml calibrated flask. Add 2 ml of NH$_3$–NH$_4$Cl buffer (pH 10.0), followed by

Fig. 1 Calibration graph for the determination of chlorine dioxide in the range 0–1.5 mg l^{-1}.

Fig. 2 Dependence of sensitivity (dA/dc) on pH for the determination of chlorine dioxide using Rhodamine B.

various amounts of the chlorine dioxide stock standard solution. Dilute to volume and measure the absorbance at 553 nm.

Results and Discussion

Calibration

A calibration graph for chlorine dioxide over the range 0–1.5 mg l⁻¹ was obtained (Fig. 1). The chlorine dioxide concentra-

Fig. 3 Absorbance stability studies for the reaction of chlorine (40 mg l⁻¹) with Rhodamine B using different buffers (pH 10.0). A, ammonia buffer; and B, carbonate buffer.

Table 1 Effect of other substances on the determination of chlorine dioxide by the NH_3–NH_4 Cl–Rhodamine B method (chlorine dioxide absent)

Substance	Concentration/ mg l⁻¹	Apparent chlorine dioxide concentration/ mg l⁻¹
Free chlorine (hypochlorous acid)	40	0.000
Hypochlorite (sodium)	1000	0.005
	500	0.015
Monochlorimine*	500	−0.010
Chlorate (sodium)	1000	0.020
Chlorite (sodium)	1000	0.045
* Prepared as described in ref. 6.		

Table 2 Results of analysis of raw waters with chlorine dioxide and free chlorine added

Sample No.	ClO_2 added/ mg l⁻¹	Cl_2 added/ mg l⁻¹	ClO_2 concentration found/mg l⁻¹	s_r (%)
1	0.40	0.75	0.21, 0.19, 0.18, 0.20, 0.20, 0.24, 0.17, 0.23	2.4
2	1.05	3.40	0.73, 0.76, 0.78, 0.72, 0.74, 0.74, 0.75, 0.76	1.9

tion (c mg l⁻¹) and the absorbance (A) are well correlated, the regression equation being $A = -0.2828c + 0.5254$ ($r = -0.9996$; $n = 10$).

The within-batch precision was investigated using ten replicate analyses of a blank and 0.10 mg l⁻¹ chlorine dioxide standard solution. The results show that the detection limit of the proposed method is 0.04 mg l⁻¹.

Effect of pH

The effect of pH was demonstrated by establishing calibration graphs for a series of standard buffers. The results showed that the reaction pH has a marked effect on the sensitivity of the method (Fig. 2). Using the slope of the calibration graph as a measure of sensitivity, the optimum pH lay between 10 and 11.

Interferences

The behaviour of free chlorine and oxychlorine species towards Rhodamine B was studied at pH 10.0 using different buffers. The results are shown in Fig. 3. Chlorine, hypochlorite, chlorite and chlorate produced no measurable effect in any buffer at pH 10.0. Free chlorine produced a measurable effect with pH 10.0 carbonate buffer. The results show that ammonia–ammonium chloride buffer is a good masking reagent for free chlorine. Free chlorine concentrations up to 40 mg l⁻¹ could be tolerated without interference (Table 1).

Application

The proposed method was applied to the analysis of raw water samples. Chlorine dioxide and free chlorine were added and measured about 2 h later. The results are summarized in Table 2.

References

1 Hodgden, H. W., and Ingols, R. S., *Anal. Chem.*, 1954, **26**, 1224.
2 Aston, R. N., *J. Am. Water Works Assoc.*, 1950, **42**, 151.
3 Masschelein, W., *Anal. Chem.*, 1966, **38**, 1839.
4 Palin, A. T., *Water Sewage Works*, 1960, **107**, 457.
5 Fletcher, I. J., and Hemnings, P., *Analyst*, 1985, **110**, 695.
6 Chiswell, B., and O'Halloran, K. R., *Analyst*, 1991, **116**, 657.
7 American Public Health Association, American Water Works Association and Water Pollution Control Federation, *Standard Methods for the Examination of Water and Wastewater*, American Public Health Association, Washington, DC, 16th edn., 1985, p. 323.
8 American Public Health Association, American Water Works Association and Water Pollution Control Federation, *Standard Methods for the Examination of Water and Wastewater*, American Public Health Association, Washington, DC, 16th edn., 1985, pp. 320 and 321.

Catalytic Determination of Iodide Using the Promethazine–Hydrogen Peroxide Redox Reaction

Ashraf A. Mohamed and Masaaki Iwatsuki

Department of Applied Chemistry and Biotechnology, Faculty of Engineering, Yamanashi University, Takeda-4, Kofu-shi 400 Japan

Mohamed F. El-Shahat

Department of Chemistry, Faculty of Science, Ain Shams University, Abbassia, Cairo, Egypt

Tsutomu Fukasawa

Department of Applied Chemistry and Biotechnology, Faculty of Engineering, Yamanashi University, Takeda-4, Kofu-shi 400 Japan

A highly selective and sensitive spectrophotometric method was developed for the determination of iodide based on its catalytic effect on the oxidation of promethazine hydrochloride (PM) with H_2O_2. The red oxidation product of PM is monitored at 516 nm for 40 s. Using the recommended procedure, iodide can be determined with a linear calibration graph up to 12 ng ml^{-1} at 25 °C. The limit of detection is about 0.1 ng ml^{-1}. The mechanism of the reaction is inferred. The method was successfully applied to the determination of iodide in river waters.

Keywords: *Catalytic analysis; iodide determination; promethazine–hydrogen peroxide redox reaction; hypoiodite; river water*

Introduction

Promethazine hydrochloride (PM) is an important antihistaminic phenothiazine derivative that is very susceptible to oxidation. It is first oxidized to a red, free radical, PM*, showing a maximum absorbance at 516 nm. It is further oxidized to a colourless sulfoxide derivative as shown in eqn. (1):[1,2]

$$\begin{array}{ccc}
\text{PM} & \overset{\text{oxidant}}{\rightleftharpoons} & \text{PM}^* \xrightarrow{\text{oxidant}} \\
\text{(colourless)} & & \text{(red, free radical)}
\end{array}$$

$$\text{PM(O)}$$
$$\text{(colourless sulfoxide)} \quad (1)$$

Owing to these characteristics, PM has been used as a redox indicator in titrimetric analysis.[1,3] However, there are no reports on the application of PM in catalytic analysis.

The determination of trace amounts of iodine has been receiving increased interest in a variety of fields, especially in river waters.[4,5] Current techniques for the sensitive determination of iodine include neutron activation analysis,[6] ion chromatographic[7] and catalytic methods. Catalytic methods using the well known Ce^{IV}–As^{III} and other reaction systems catalysed by iodine have been reported,[8] and are sensitive and inexpensive. Also, more sensitive reactions catalysed by iodide have recently been described,[9–12] but they seem to have a problem for reliable application to the determination of iodide in river waters owing to serious interference by nitrite and iron(III) ions.

The oxidation of PM with H_2O_2 in a mixed acid medium of H_2SO_4 and H_3PO_4 is a slow process that can be catalysed by

iodide ions. This paper describes a highly selective, sensitive and simple method for the determination of iodide based on its catalytic effect on the PM–H_2O_2 reaction and its application to river water. The mechanism of the indicator reaction is discussed.

Experimental

Reagents and Apparatus

All chemicals were of analytical-reagent grade and all solutions were prepared with distilled, de-ionized water. A stock standard solution of PM (100 mmol l^{-1}) was prepared by dissolving promethazine hydrochloride (Wako, Osaka, Japan) in water and stored in the dark at 4 °C. A stock standard iodide solution (1000 μg ml^{-1}) was prepared by dissolving potassium iodide in water. Working standard solutions of 20 mmol l^{-1} PM and 125 ng ml^{-1} iodide ion were prepared daily by dilution of their respective stock standard solutions with water. A reagent of 30% H_2O_2 was used without any dilution. A 2% sulfamic acid solution was prepared daily by dissolving the reagent in water. An acid mixture of 3.5 mol l^{-1} H_2SO_4, 5.0 mol l^{-1} H_3PO_4 and 1.0 mol l^{-1} (NH_4)$_2SO_4$ was also prepared. Eppendorf micropipettes (100–1000 μl) were used to deliver accurate volumes.

A Shimadzu (Kyoto, Japan) UV-160A double-beam spectrophotometer with 10 mm cells was used for recording absorbance (A)–time (t) graphs. The temperature of the cell compartment was kept constant (within ±0.1 °C) by circulating the water from a thermostated water-bath regulated at the reaction temperature.

Recommended Procedure

The reagent solutions, water and 20 ml stoppered glass test-tubes are kept at 25 °C in the thermostated water-bath. Treated samples (as described later) are kept at 4 °C until analysed. Transfer 2.80 ml or less of the sample, which contains less than 60 ng of iodide, into a test-tube and dilute to 2.80 ml with water. Add 0.10 ml of the sulfamic acid solution and 1.0 ml of the acid mixture, shake and allow to stand for 10 min in the water-bath to decompose nitrite and attain the equilibrium temperature. Add 0.35 ml of the working PM standard solution, shake and allow to stand for 1 min to assist the reduction of iodate with the reagent. Start the reaction by adding 0.75 ml of the H_2O_2 solution, shake well and

immediately transfer a portion of the reacting solution into the spectrophotometric cell to record the A–t graph at 516 nm against water. The rate (tan α) can be calculated from the slope of the initial linear part of the A–t graph. (In routine analysis the rate, within 40 s after the addition of H_2O_2, was automatically output using a built-in program of the spectrophotometer.) The iodide concentration in the unknown sample is determined from a calibration graph similarly prepared with the iodide working standard solution.

Results and Discussion

Effect of Acidity

As the red, free radical obtained from the oxidation of PM is stable only in acidic media,[1] the catalysed reaction was extensively studied in different acidic media. It was not possible to follow the reaction in hydrochloric acid because the rate of the uncatalysed reaction was too rapid. Phosphoric acid gave very low rate values for both the catalysed (k_c) and uncatalysed (k_u) reactions and showed a very low sensitivity ($k_c - k_u$). The reaction was then studied in detail in a sulfuric acid medium, but it was subject to severe interference from iron. Therefore, in order to improve the selectivity of the method, a mixture of sulfuric and phosphoric acids was studied as the medium. Fig. 1 shows the dependences of k_c and k_u on acid concentration. A mixed acid medium of 0.7 mol l^{-1} sulfuric acid and 1.0 mol l^{-1} phosphoric acid was adopted, because it gave a lower reagent blank.

Effect of PM Concentration

As shown in Fig. 2(a), the reaction rates k_c and k_u changed slightly in the PM concentration range 1.0–1.8 mmol l^{-1}. Therefore, a PM concentration of 1.4 mmol l^{-1} was adopted in the recommended procedure.

Effect of H_2O_2 Concentration

The reaction rate increased with increasing H_2O_2 concentration, as shown in Fig. 2(b). However, the linearity of the A–t graph in the presence of iodide became poor at H_2O_2 concentrations higher than 3 mol l^{-1}, so 1.5 mol l^{-1} was chosen in the recommended procedure.

Fig. 1 Effect of acid concentrations on the reaction rate. Except for the abscissa variable, reaction conditions are as in the recommended procedure; data with poor precision resulting from non-linear A–t graphs are indicated by asterisks; k_u, reagent blank; k_c, 5 ng ml^{-1} iodide; A and A', H_2SO_4 (in the presence of 1 mol l^{-1} H_3PO_4); B and B' H_3PO_4 (in the presence of 0.7 mol l^{-1} H_2SO_4).

The partial orders of the individual reaction variables mentioned above were determined using the initial rate data, and are given in Table 1.

Fig. 2 Effects of (a) PM and (b) H_2O_2 concentrations, and (c) the reaction temperature on the reaction rate. Reaction conditions and symbols as in Fig. 1, except for 2.5 ng ml^{-1} iodide in (c).

Table 1 Partial orders for the reactants in the promethazine–H_2O_2 reaction

Variable	Uncatalysed reaction c^*	n^*	Iodide-catalysed reaction c^*	n^*
PM	$(0.04–0.8) \times 10^{-3}$	0.3	$(0.04–0.3) \times 10^{-3}$	0.9
	$(1.2–2.0) \times 10^{-3}$	1.8	$(1.0–2.0) \times 10^{-3}$	0
H_2O_2	0.4–3.0	1.0	0.4–3.0	1.1
H^+ (total) acidity)	0.34–2.24	1.6	0.36–2.24	1.2

* c = Concentration range (mol l^{-1}); n = partial reaction order.

Effect of Ionic Strength

The rate of both the catalysed and uncatalysed reactions increased with increasing $(NH_4)_2SO_4$ concentration higher than 0.2 mol l^{-1}, but the sensitivity remained almost constant. In the recommended procedure, 0.2 mol l^{-1} $(NH_4)_2SO_4$ was adopted, and lower concentrations of $(NH_4)_2SO_4$ should be added to water samples with high salt content so as to maintain a constant ionic strength of 1.5 mol l^{-1}.

Effect of Temperature

Fig. 2(c) shows that k_c and k_u increased with increase in temperature, but the increase in rate above 28 °C was less than that predicted from the Arrhenius equation, and 25 °C was convenient for the operation. The Arrhenius plot was linear up to 28 °C. The deviation from linearity at higher temperatures may be attributed to the increased rate of disproportionation of the red, free radical with temperature. The activation energy for the uncatalysed reaction was 20.5 kcal mol^{-1} and that for the reaction catalysed by 2.5 ng ml^{-1} iodide was 10.3 kcal mol^{-1}.

Effects of Foreign Ions

The effects of foreign ions on the determination of 5 ng ml^{-1} iodide were investigated. The tolerance limit was defined as the maximum concentration of foreign ions that produce a determination error of less than 5%. Table 2 shows the high selectivity of the method. However, Ag^I and Hg^{II} at a 1:1 molar ratio to iodide seriously interfered. Nitrite ion was a serious interferent, as shown in the last line in Table 2. The nitrite interference was successfully eliminated by the addition of sulfamic acid as described in the recommended procedure, so that the method can easily tolerate up to 10 µg ml^{-1} of nitrite.

Calibration Graph and Detection Limit

A linear calibration graph for up to 12 ng ml^{-1} of iodide was obtained using the recommended procedure. The equation of the calibration graph was $100(\tan \alpha) = 0.43 + 0.52[I^-]$ with a correlation coefficient of 0.9999, where $[I^-]$ is the iodide concentration expressed in ng ml^{-1}. The detection limit was about 0.1 ng ml^{-1} of iodide and was obtained from the criterion of three times the standard deviation (s) of the blank. The relative standard deviations (s_r) for six replicate determinations of 1, 3, 7 and 12 ng ml^{-1} of iodide were 5.5, 1.9, 1.0 and 1.5%, respectively.

Table 2 Tolerance limits of foreign ions in the determination of 5 ng ml^{-1} iodide. Other experimental conditions: 1.4 mmol l^{-1} PM, 1.5 mol l^{-1} H_2O_2, 0.7 mol l^{-1} H_2SO_4, 1.0 mol l^{-1} H_3PO_4, 0.2 mol l^{-1} $(NH_4)_2SO_4$ and 4.12 mmol l^{-1} sulfamic acid at 25 °C

Tolerance limit/ µg ml^{-1}	Foreign ions
>1000	Acetate, citrate, oxalate, tartrate, EDTA, sulfamic acid, Na^+, K^+, NH_4^+, NO_3^-, Mg^{II}
100	Cl^-, F^-, Al^{III}, Cd^{II}, Ni^{II}, Zn^{II}, Th^{IV}
10	SO_3^{2-},* NO_2^-, Fe^{III}
2	Co^{II}, Cu^{II}, Mn^{II}, Cr^{III}, Mo^{VI},* W^{VI}*
0.8	Br^-
0.3	V^V
0.05	SCN^-
0.02	S^{2-}
0.01	NO_2^-*,†

* Ions that produced negative interference.
† In the absence of sulfamic acid.

Determination of Iodate and Periodate

The exact chemical form of iodine in natural waters is not definitely known, but may be mainly iodide;[11] however, in some instances, iodate[4,13] may constitute an appreciable fraction of the total iodine present in river waters. As PM can reduce iodate and periodate to iodide, this allows their determination. The percentage reduction depends slightly on the standing time after the addition of PM. In the determination of 5 ng ml^{-1} iodate and periodate (as iodide), a 1 min standing time was found adequate to give recoveries of about 93 and 94% for iodate and periodate, respectively. Hence, the present method rapidly gives the total inorganic iodine present in a given sample.

Kinetics and Mechanism of the Reaction

According to the partial orders of the individual reaction variables shown in Table 1, the following rate equations may be formulated to describe the uncatalysed and catalysed reactions, respectively:

$$d[PM^*]/dt = k_1 [PM]^2 [H^+]^2 [H_2O_2] \qquad (2)$$

$$d[PM^*]/dt = k_2 [H^+] [I^-] [H_2O_2] \qquad (3)$$

where k_1 and k_2 are the rate constants for the uncatalysed and catalysed reactions, respectively. In the rate-determining step (r.d.s.), a catalytic redox reaction utilizing iodide as a catalyst usually involves elemental iodine in a higher oxidation state, e.g., I_2 or hypoiodite.[14] The involvement of I_2 in the r.d.s. implies a second-order dependence on iodide. However, the linearity of the calibration graph (reaction rate *versus* iodide concentration) suggests a first-order dependence on iodide. Therefore, hypoiodite was suggested rather than I_2 as an intermediate in the catalysed reaction, thus, eqn. (4) and eqns. (5) and (6) may be used to describe the mechanisms of the uncatalysed and catalysed reactions, respectively:

$$2\ PM + 2\ H^+ + H_2O_2 \rightleftharpoons 2\ PM^* + 2H_2O \qquad (4)$$

$$\overset{slow}{H^+ + {}^-I + H_2O_2 \rightleftharpoons H_2O + HIO\ (r.d.s.)} \qquad (5)$$

$$\overset{fast}{2\ PM + H^+ + HIO \rightleftharpoons 2\ PM^* + I^- + H_2O} \qquad (6)$$
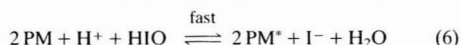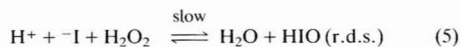
However, the participation of a protonated form of PM may also be possible.

Determination of Iodide in River Waters

After the collection of a sample, it was filtered through a Millipore (Millipore-Waters, Milford, MA, USA) MF-HA membrane filter with a pore size of 0.45 µm. The analytical results for such samples varied with the standing time after collection, showing 20–35% losses in their iodide contents within 1 h of collection. Such behaviour may be attributed to the effect of micro-organisms, which was greatly retarded by treating the sample by adding 2.5 ml of the acid mixture per 250 ml of sample, filtering the sample through a 0.45 µm membrane filter and storing at 4 °C until the analysis step. Such pre-treatment was effective and the treated samples were stable for 5 h after their collection.

Table 3 shows the results for river samples collected at Kofu City, Japan. Samples that were not treated with sulfamic acid showed a much lower iodide content than the treated samples. This may be attributed to the presence of low concentrations of nitrite, which usually constitute an appreciable fraction of the total nitrogen content of river waters. These results show the importance of sulfamic acid for eliminating the serious interference of nitrite.

Table 3 Determination of iodide in water samples from polluted rivers. Reaction conditions as in Table 1

Sample no.[*]	pH	Sample taken/ ml	Iodide added/ ng ml^{-1}	Iodide found (mean)/ ng ml^{-1}	s/ng ml^{-1}	s_r (%)	n[†]	Recovery (%)
1	7.9	2.90[‡]	0	1.88			1	
		2.80	0	3.45	0.09	2.7	5	
		2.30	0	3.29	0.12	3.6	5	
				Total: 3.37	0.15	4.5	10	
		1.90	2.00	5.49	0.03	0.5	5	106
2	8.3	2.90[‡]	0	0.55			1	
		2.80	0	1.94	0.07	3.5	5	
		2.30	0	1.83	0.08	4.4	5	
				Total: 1.88	0.09	4.9	10	
		1.90	2.00	3.75	0.07	1.9	5	94

[*] Collected at Kofu City, No. 1 from Ara river on August 14, 1994, and No. 2 from Ai river on August 16, 1994.
[†] Number of determinations.
[‡] In the absence of sulfamic acid.

References

1 Puzanowska-Tarasiewicz, H., in *Phenothiazines and 1,4-Benzo-thiazines, Chemical and Biomedical Aspects*, ed. Gupta, R. R., Elsevier, New York, 1988, ch. 16, pp. 861–898.
2 Massie, S. P., *Chem. Rev.*, 1954, **65**, 797.
3 Gowda, H. S., and Ahmed, S. A., *Talanta*, 1979, **26**, 233.
4 Yonchara, N., Kozono, S., and Sakamoto, H., *Anal. Sci.*, 1991, **7**, 229.
5 Tomiyasu, T., Sakamoto, H., and Yonehara, N., *Anal. Sci.*, 1992, **8**, 293.
6 Johansen, O., and Steinnes, E., *Analyst*, 1976, **101**, 455.
7 Han, K., Koch, W. F., and Pratt, K. W., *Anal. Chem.*, 1987, **59**, 731.
8 Perez-Bendito, D., and Silva, M., *Kinetic Methods in Analytical Chemistry*, Ellis Horwood, Chichester, 1988, ch. 2, pp. 48–69.
9 Vinas, P., Hernandez-Cordoba, M., and Sanchez-Pedreno, C., *Talanta*, 1987, **34**, 351.
10 Lopez-Cueto, G., and Ubide, C., *Talanta*, 1990, **37**, 849.
11 Liang, B., Iwatsuki, M., and Fukasawa, T., *J. Jpn. Soc. Air Pollut.*, 1993, **28**, 168.
12 Liang, B., Kawakubo, S., Iwatsuki, M., and Fukasawa, T., *Anal. Chim. Acta*, 1993, **282**, 87.
13 Jones, S. D., Spencer, C. P., and Truesdale, V. W., *Analyst*, 1982, **107**, 1417.
14 Yatsimirskii, K. B., *Kinetic Methods of Analysis*, Pergamon Press, New York, 1966, pp. 86–91.

Automated Determination of Inorganic Mercury in Blood after Sulfuric Acid Treatment Using Cold Vapour Atomic Absorption Spectrometry and an Inductively Heated Gold Trap

Ingvar A. Bergdahl, Andrejs Schütz and Gert-Åke Hansson

Department of Occupational and Environmental Medicine, University Hospital, S-221 85 Lund, Sweden

Inorganic mercury (InoHg) in whole blood and erythrocytes was determined by cold vapour atomic absorption spectrometry (CVAAS) after overnight treatment with sulfuric acid at 45 °C and reduction with Sn^{II} in the acidic mixture. Total mercury (TotHg) was determined after digestion with a mixture of nitric and perchloric acids. Mercury vapour was preconcentrated on an amalgamation trap made of gold wire. The mercury was rapidly released by inductive heating of the trap. InoHg could be determined specifically in the presence of methylmercury (MeHg). The concentration of MeHg could be calculated by subtracting the concentration of InoHg from that of TotHg. Calculated concentrations of MeHg in erythrocytes showed a strong correlation with the results of a gas chromatographic method, though a discrepancy in calibration was indicated. The detection limits (3 s) in blood (0.5 g) were 0.06 ng g^{-1} for TotHg and 0.04 ng g^{-1} for InoHg and s_r for a 5 ng g^{-1} whole blood sample was 2% ($n = 10$) for both TotHg and InoHg.

Keywords: *Inorganic mercury determination; blood; amalgamation; inductive heating; cold vapour atomic absorption spectrometry*

Introduction

Human blood usually contains both methylmercury (MeHg) and inorganic mercury (InoHg). In the general population, the organic mercury is MeHg from fish and the InoHg stems mainly from amalgam tooth fillings. High consumption of fish from mercury-contaminated waters and occupational exposure to metallic mercury may cause toxic blood levels of MeHg and InoHg, respectively.[1,2] The metabolism and toxic effects differ between MeHg and InoHg. It is therefore essential to have analytical methods that can differentiate between MeHg and InoHg.

Methods for the determination of mercury in biological samples have been reviewed recently.[3] For the determination of total mercury (TotHg), analytical techniques based on cold vapour generation with atomic absorption detection dominate. These techniques involve reduction of dissolved ionic mercury by SnCl$_2$ or NaBH$_4$ into its atomic state, Hg^0, followed by aeration of Hg^0 into a gas cell of the detector.

A variety of methods for the specific determination of MeHg in biological samples are based on gas chromatography. Some of these methods are also capable of determining InoHg after alkylation,[3] but the methods involve time-consuming work-up procedures. Methods with conventional gas chromatographic detectors normally lack the sensitivity required for blood analysis, but spectrometric detectors (atomic emission, atomic fluorescence or mass) may be used to enhance the sensitivity of gas chromatographic methods.[3] Another approach to the differentiation between InoHg and MeHg in biological samples was introduced by Magos and Cernik.[4] They used a cold vapour atomic absorption spectrometric (CVAAS) method with selective reduction of InoHg with Sn^{II} in alkaline solution, after addition of an excess of alkali to acidified samples. Velghe *et al.*[5] described a CVAAS method for the determination of InoHg in fish samples treated with sulfuric acid, without addition of alkali. For reduction of mercury, they used Sn^{II} in the presence of large amounts of cadmium.

In this paper, we present a method for the automated CVAAS determination of InoHg in blood and erythrocytes after treatment with sulfuric acid. The reduction of mercury was carried out with Sn^{II} without any addition of cadmium. To increase the sensitivity, we included a preconcentration step consisting of an amalgamation trap of thin gold wire,[6] from which mercury was released by inductive heating to obtain rapid heating and cooling characteristics.

Experimental

Automated Apparatus for Mercury Determination

Einarsson *et al.*[7] described the automated apparatus used in this work. It was modified for enrichment of Hg^0 on a gold trap (see below). Peristaltic pumps are used for the transport of sample and reagents to and from the reaction vessel (Fig. 1). After the sample has been pumped from an autosampler into the reaction vessel, 0.8 ml of 5% SnCl$_2$ solution is added. The
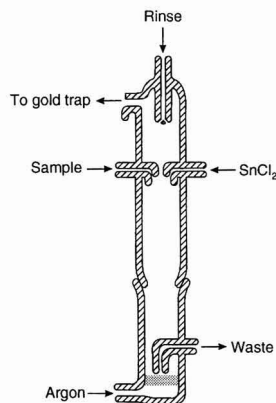
Fig. 1 The glass reaction vessel is made in two pieces, joined by a ground taper joint. The purging gas (argon) is blown through a G4 sintered-glass filter.

mercury (TotHg or InoHg, depending on what sample treatment has been used) is thereby reduced to Hg^0. Hg^0 is purged from the solution by bubbling argon (50 s, 270 ml min^{-1}) through the reaction vessel to the gold trap. Droplets in the gas stream are removed by a glass-wool filter. During heating of the trap, the reaction vessel is by-passed, and the argon is introduced through a tee-connection between the glass-wool filter and the gold trap. This is done to reduce interference on the baseline when the mercury is released and swept to a gas cell in an AAS detector. The reaction vessel and sample uptake tubing are rinsed with water between each sample. Each determination takes 140 s.

The AAS detector used was a Perkin-Elmer (Norwalk, CT, USA) Model 305 B equipped with a windowless gas cell, which was made of a 22 cm × 6 mm i.d. Plexiglas tube. An inlet was made at the middle of the tube. The AAS signal was fed to a Perkin-Elmer Model 56 chart recorder and the results were calculated from peak heights.

Gold Trap and Heating Device

The gold trap was made from gold wire (diameter 0.05 mm) (Johnson Matthey, Royston, UK), from which a 20–30 mm long coil-shaped wad was formed by loosely winding 5 m (0.2 g) of the gold wire around a piece of plastic tubing of 1.5 mm o.d. The wad was introduced into a quartz tube (4 mm i.d.) and the plastic tubing was retracted. The gold trap was held in place by a boiling stone (sintered quartz), supported by a constriction on the quartz tube, and two glass-wool wads, one at each end of the trap.

The quartz tube with the gold trap was placed in an induction coil made of copper wire (diameter 1.7 mm). The coil had 12 turns, a diameter of 12 mm and a length of 32 mm. It was connected to a 1.75 MHz (sine wave) radiofrequency generator (Martin Elektrotom 170 RF originally made for diathermy; Gebrüder Martin, Tuttlingen, Germany), which was slightly modified to match the load of the coil. The copper coil was connected in parallel with a 10 nF capacitor, to make the system work as a resonance circuit. During heating, the voltage over the copper coil was approximately 60 V_{RMS}. The time from the baseline to the peak maximum for the mercury signal was 2.5 s, and the peak width at 10% peak height was 4.5 s and was independent of concentration within the calibrated range. The time required for cooling of the trap after a heating step was tested by blowing a continuous flow of argon (270 ml min^{-1}) containing mercury vapour of approximately 0.1 ng ml^{-1} through the trap. At 11 s after cessation of heating, the absorption of mercury was better than 98%.

Purging Gas

Passivation or inactivation of the gold surface has been reported when gold traps are used for the analysis of acid-digested samples. The reason for this phenomenon is not known, but deposition of acidic aerosols,[8] adsorption of volatile chlorides[9] or elemental chlorine[10] have been suggested. Initially, when we tried to use air as the purging gas for the determination of TotHg (see below), only a few samples could be analysed before the gold trap ceased to function. This could be prevented by the insertion of a bubbler, containing a solution of 1% sodium tetrahydroborate and 1% sodium hydroxide, between the reaction vessel and the gold trap. However, when argon was used, no bubbler was needed.

Although argon was used throughout this work, we also tested nitrogen for purging. This gave a 35% decrease in peak height. This decrease may be explained by a higher (45%) thermal conductivity of nitrogen compared with that of argon, which slows the heating of the gold trap and thus broadens the

peaks. This could be compensated for by increasing the heating power.

Reagents

The water was de-ionized. All chemicals were of at least analytical-reagent grade, except ungraded 2-octanol (from Janssen Chimica, Beerse, Belgium). Sulfuric acid (Merck, Darmstadt, Germany) was diluted to 16 mol l^{-1}. The mercury content of the sulfuric acid was determined and was approximately 0.1 ng ml^{-1}. A digestion reagent was prepared from concentrated perchloric and nitric acids (5 + 1) (both from Merck). A 25% urea (AnalaR grade from Merck, Poole, UK) solution was prepared in water. A 5% $SnCl_2$ (Merck, Darmstadt) solution was prepared in 10% v/v sulfuric acid. Mercury(II) chloride stock standard solution for AAS was 1.00 mg ml^{-1} Hg from Merck, UK. This stock standard solution was diluted with 2% v/v nitric acid to give a working standard solution of 1.00 µg ml^{-1}. Argon N57 and nitrogen N52 were supplied by Alfax (Malmö, Sweden). All glassware was acid washed in 20% nitric acid.

Sample Treatment for Determination of InoHg

The samples (0.5 g of whole blood or erythrocytes) were weighed into glass test-tubes. Immediately after addition of 1.5 ml of 16 mol l^{-1} sulfuric acid, the sample and acid were mixed using a vortex mixer. The test-tubes were placed in a heating block and digested overnight (16 h) at 45 ± 2 °C. After cooling to room temperature, 1 ml of water was added and the samples were cooled again. After addition of five drops of octanol (anti-foaming agent), the test-tubes were placed in the autosampler for automatic analysis.

Digestion for Determination of TotHg

This method was adapted from Lindstedt and Skare.[11] The samples (0.5 g whole blood or erythrocytes) were weighed into glass test-tubes. A 3 ml volume of the digestion reagent was added and the samples were digested overnight (16 h) at 65 ± 2 °C in a heating block under an extraction hood connected to a scrubber (at this temperature, very small amounts of perchloric acid fumes are evolved). After cooling to room temperature, 0.5 ml of the 25% urea solution was added as a weak reductant. A 2 ml volume of water was added and the test-tubes were placed in an ultrasonic bath for 10 min, to release nitrous gases. After addition of two drops of octanol, the samples were then analysed, using the same procedure as for the determination of InoHg.

Calibration

Blood from a blood donor was spiked with the working standard solution to give an addition of 2, 4 and 8 ng g^{-1}, respectively. These blood standards, including an unspiked sample, were kept refrigerated in plastic bottles (high-density polyethylene). At least two blood standard series and one commercial reference sample (Seronorm Trace Elments Whole Blood from Nycomed, Oslo, Norway) were incorporated in each run. All samples, references and blood standards were analysed in duplicate.

Laboratory Intercomparison

Erythrocyte samples from nine subjects were analysed for MeHg at another laboratory using a gas chromatographic separation after butylation of the mercury compounds, coupled to microwave-induced plasma atomic emission spectrometry (GC–MIP-AES).[12] The detection limit was 0.2

ng g^{-1} (3 s criterion) after modification of the sample introduction system. This method was one of the very few published methods capable of measuring mercury species in 'normal' blood samples. The samples were chosen to represent different levels of, and ratios between, InoHg and MeHg. The extreme values among the samples (InoHg/MeHg) were 0.3/0.5, 1.0/13.3 and 10.6/0.6 ng g^{-1}. Although the method is also capable of determining InoHg, this could not be done owing to accidental contamination of the samples with InoHg at the laboratory or during shipment.

Results

Detection Limits and Precision

The absolute detection limits, calculated as three times the standard deviation for the reagent blanks ($n = 10$), were 0.03 ng for TotHg and 0.02 ng for InoHg, corresponding to 0.06 and 0.04 ng g^{-1} in the sample, respectively. The precision for the analysis of a 5 ng g^{-1} sample was 2% (s_r for ten consecutive samples) for both TotHg and InoHg. The day-to-day precision for a sample with low InoHg concentration (Seronorm Trace Elements Whole Blood, Batch No. 010011, recommended InoHg concentration 0.9 ng g^{-1}) was 7% (s_r for 26 determinations within 7 d).

Interference from MeHg

The overnight treatment with sulfuric acid for the determination of InoHg caused some degradation of MeHg into InoHg. After overnight treatment (16 h) at 45 ± 2 °C of MeHg-spiked samples (100 ng g^{-1}), approximately 2% of the MeHg degraded. A correction coefficient derived through analysis of MeHg spiked samples was applied to compensate for the degradation when determining InoHg in the presence of MeHg. The degradation seemed to increase exponentially with decreasing sample mass, and was approximately 6% for a 0.3 g sample and 15% for a 0.1 g sample. The degradation was proportional to time and was approximately doubled by a rise in temperature of 10 °C.

Analytical Application

Erythrocytes from 20 persons with known fish intake and number of amalgam-filled teeth were analysed for InoHg and TotHg (Figs. 2 and 3). Fourteen of the subjects had a high intake of fish (they ate fish almost every day, mainly salmon and herring from the Baltic Sea) and six had a low or no intake of fish. The mean InoHg concentration in erythrocytes was 0.5 (range 0.0–1.0) ng g^{-1} and the mean TotHg concentration was 7.8 (range 0.8–29) ng g^{-1}. The correlation between InoHg in erythrocytes and the number of amalgam filled teeth ($r = 0.74$, Fig. 2), decreased ($r = 0.63$) when no correction was made for the 2% degradation of MeHg. There was no significant correlation between TotHg concentration and the number of amalgam-filled teeth ($r = 0.11$, Fig. 3).

We also analysed erythrocytes from there occupationally exposed men working in fluorescent tube production. The TotHg results were 11.2, 9.6 and 4.4 ng g^{-1}, while the results for InoHg were 10.6, 6.7 and 3.9 ng g^{-1}, respectively. This corresponds to 70–95% as InoHg.

Interlaboratory Comparison

MeHg concentrations calculated from CVAAS results were compared with results from species-specific determination of MeHg by GC–MIP-AES. There was a strong correlation throughout the whole concentration range (0.5–13.3 ng g^{-1}) between the results obtained by the two methods; no points

lay more than 1 ng g^{-1} from the linear regression line. However, the CVAAS results were higher than the GC–MIP-AES results; the slope of the regression line was 1.23.

Analysis of Reference Samples

To establish the accuracy of the method further, six reference samples were analysed. To our knowledge, the only commercially available reference blood samples with 'normal' mercury levels are those batches of lyophilized Seronorm Trace Elements Whole Blood which are not spiked with mercury. The Seronorm samples are not certified reference materials, but some of them have recommended values for mercury. Our results are given in Table 1.

Discussion

Determination of InoHg

The described method allows the specific determination of InoHg in blood in the presence of MeHg. The principle of selective reduction of InoHg with Sn^{II} is the same as in the method of Magos and co-workers.[4,13,14] However, the main difference is that no alkali is used; the blood is simply treated with sulfuric acid, followed by reduction of InoHg with Sn^{II}.
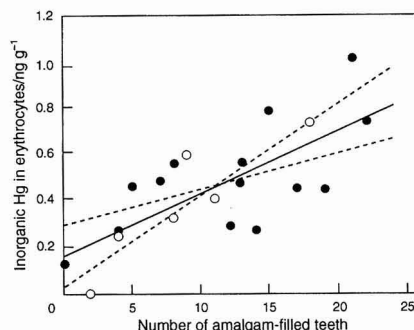
Fig. 2 Correlation between inorganic Hg in erythrocytes and the number of amalgam-filled teeth from groups of people with different fish consumptions, giving an MeHg concentration of up to 27 ng g^{-1} (Fig. 3). The regression line ($r = 0.74$) and 95% confidence interval for the slope of the regression line are displayed. Closed symbols, high fish intake; open symbols, low fish intake.
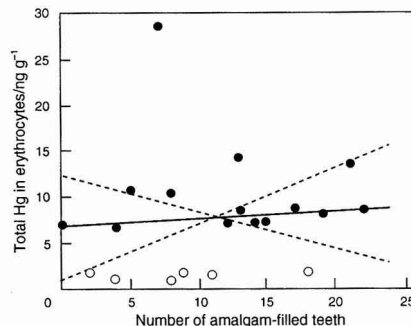
Fig. 3 Correlation between total Hg in erythrocytes and the number of amalgam-filled teeth in groups of people with differing intakes of MeHg through fish consumption. The linear regression line ($r = 0.11$) and 95% confidence interval for the slope of the regression line are displayed. Closed symbols, high fish intake; open symbols, low fish intake.

The problems associated with the considerable amount of heat generated on mixing acid and alkali were thus avoided. We used approximately the same reduction conditions as described by Velghe *et al.*[5] for the analysis of fish samples, but found that the addition of cadmium was unnecessary for the reduction of InoHg in blood. The absence of large amounts of cadmium minimizes the risk of reduction of MeHg and makes our method more attractive to trace element laboratories, considering the risk of cadmium contamination.

The MeHg concentration may be calculated as the difference between TotHg and InoHg concentrations. InoHg and MeHg are the only mercury species that are normally expected to appear in human blood at appreciable concentrations. Other mercury species may be present after direct exposure to the compounds, but such exposure is very uncommon.

The detection limit obtained is sufficient for the determination of InoHg in blood samples from the normal population. The detection limit may be improved by the use of sulfuric acid with a lower mercury content, leading to lower blanks.

The observed approximately 2% degradation of MeHg into InoHg is of significance only for samples with high levels of MeHg. This has to be considered in cases of high fish intake, and may be handled using mathematical correction. The present principle for the determination of InoHg in blood has previously been used manually without the heating step,[15]

Table 1 Inorganic Hg (mean and range) determined in commercial reference samples (Seronorm Trace Elements Whole Blood)

Batch No.	No. of determinations	InoHg/ ng g^{-1}	Recommended value and range/ng g^{-1}
010010*	4	0.9 (0.8–0.9)	1.2 (1.0–1.4)
010011*	26	0.9 (0.8–1.0)	0.9 (0.7–1.0)
010012*	4	0.9 (0.9–0.9)	1.1 (0.9–1.3)
205052	4	0.4 (0.4–0.4)	No recommendation, no Hg added
203056†	4	5.6 (5.5–5.7)	No recommendation, 5 ng g^{-1} added
205053	4	11.4 (11.1–11.6)	No recommendation, 10 ng g^{-1} added

* These three batches originate from the same pooled blood, two of them spiked with elements other than mercury.

† Batch No. 203056 does not originate from the same pooled blood as do 205052 and 205053.

Fig. 4 Interlaboratory comparison of three samples low in MeHg but with widely varying inorganic Hg concentrations. The results were obtained by GC–MIP-AES and CVAAS. Hatched, MeHg (GC–MIP-AES); solid, inorganic Hg (CVAAS); difference total − inorganic Hg (CVAAS).

giving no detectable interference from MeHg. Blood does, however, clot on mixing with sulfuric acid, making pumping of the mixture impossible in the automated system. This drawback was eliminated by overnight heating of the sample. The use of a lower heating temperature resulted in excessive foaming in the reaction vessel. The reason for using 16 mol l^{-1} sulfuric acid, instead of concentrated (18 mol l^{-1}) acid, is to lessen the heat generated when the acid is mixed with blood.

No interlaboratory comparison of InoHg results was made, owing to the accidental contamination with InoHg during shipment or at the laboratory performing the gas chromatographic analysis. However, the comparison of our calculated MeHg results (TotHg minus InoHg) with those obtained by GC–MIP-AES gives an indication of the accuracy of our InoHg determination As our MeHg results were calculated as the difference between the TotHg and InoHg results, an error in our InoHg determination would considerably influence the MeHg results for samples with high InoHg concentration. Such an influence would be most obvious in samples with low MeHg concentrations. Fig. 4 shows the results for the samples with an MeHg concentration below 1 ng g^{-1} and indicates that the calculated MeHg results are not significantly affected by high InoHg concentrations. This indicates good accuracy in the InoHg determination. The systematic difference between the MeHg results obtained by the two methods might be explained by a calibration error in one, or both, of the laboratories.

Three out of the six reference samples analysed had recommended values for InoHg. For two of them, we obtained results within the recommended ranges (Table 1). In fact, the three samples were identical with reference to the mercury concentration, but two of them were spiked with other elements.[16]

InoHg in blood is approximately evenly distributed between erythrocytes and plasma, whereas the concentration of MeHg is about 20 times higher in erythrocytes than in plasma.[1] To study the interference from MeHg in authentic samples, we therefore determined InoHg in erythrocytes from two groups of subjects, one with a high fish intake and the other with a low or no fish intake. Despite the high levels of TotHg (mainly MeHg) in the group with a high fish intake (Fig. 3), our method gave similar concentrations of InoHg for both groups (Fig. 2). Further, we obtained a good correlation between InoHg in erythrocytes and the number of amalgam-filled teeth ($r = 0.74$). The correlation was similar to that between TotHg in plasma and the number of amalgam surfaces ($r = 0.71$) reported by Molin *et al.*,[17] who studied 20 persons with moderate to low fish intake. These results indicate that the method has good specificity for InoHg in blood samples.

Further, the high percentage of InoHg obtained in the blood of subjects occupationally exposed to mercury vapour indicates that the method does not give any large underestimation of the InoHg concentration.

This method is now being used for routine analyses in our laboratory to distinguish between exposure to InoHg and MeHg. The simple sample preparation procedure makes it easy to adapt the method to CVAAS laboratories that wish to determine InoHg in blood samples.

Inductively Heated Gold Trap

The main advantages of the inductively heated gold wire trap may be summarized as follows: the temperature increases uniformly in the inner and outer regions of the trap; the low mass of the trap facilitates a rapid change in temperature; and unnecessary heating of the surrounding material and, thus, delay in heating and cooling of the trap are minimized.

When making the gold trap, it is essential to ensure a uniform distribution of the gold wire in the wad, otherwise the heating of the wire wad will not be uniform. This may result in peak broadening, double peaks and changes in peak height due to deformation of the trap, caused by excessive heating of some parts of the trap. On the other hand, if a uniform distribution of the gold wire is obtained, the lifetime of such a trap can be very long; in our laboratory, the same trap was used in routine analysis for 1 year. During that year, it was used for more than 10 000 determinations.

A constant gas flow is necessary to minimize variations in peak width and height. In addition to the mere dilutory effect of the gas flow, even small changes in the flow will affect the heating characteristics of the trap, thus changing the desorption rate. It is also necessary, of course, to avoid gas leakages. Here the gold wire wad has an advantage with its low flow resistance compared with the use of gold-coated sand as proposed by other workers.[18]

Information on the time characteristics of other types of gold traps is scarce, and the data are not always comparable because of differences in, *e.g.*, the gas flow and the dead volume of the gas cell. Fast heating characteristics have been demonstrated for a commercially available cold vapour equipment with an oven-heated gold gauze trap.[19] From Fig. 4 in that paper, the time for the signal to increase from the baseline to the peak maximum can be estimated as 3.5 s, and the peak width at 10% peak height can be estimated to 7.4 s, which are slightly longer than our 2.5 and 4.5 s, respectively. The cooling time was not reported. Considerably longer heating and cooling times (2 min for each step) were reported in another recent paper,[18] using a trap made of gold-coated sand.

References

1 World Health Organization, International Programme on Chemical Safety, *Environmental Health Criteria 101: Methylmercury*, WHO, Geneva, 1990.
2 World Health Organization, International Programme on Chemical Safety, *Environmental Health Criteria 118: Inorganic Mercury*, WHO, Geneva, 1991.
3 Schütz, A., Skarping, G., Skerfving, S., and Malmquist, K., in *Trace Element Analysis in Biological Specimens*, ed. Herber, R. F. M., and Stoeppler, M., Elsevier, Amsterdam, 1994, pp. 403–467.
4 Magos, L., and Cernik, A. A., *Br. J. Ind. Med.*, 1969, **26**, 144.
5 Velghe, N., Campe, A., and Claeys, A., *At. Absorpt. Newsl.*, 1978, **17**, 139.
6 May, K., Forchungszentrum Jülich, Jülich, personal communication, 1988.
7 Einarsson, Ö., Lindstedt, G., and Bergström, T., *J. Autom. Chem.*, 1984, **6**, 74.
8 Vermeir, G., Vandecasteele, C., Temmerman, E., Dams, R., and Versieck, J., *Mikrochim. Acta*, 1988, **3**, 305.
9 Horvat, M., and Lupsina, V., *Anal. Chim. Acta*, 1991, **243**, 71.
10 Mertens, H., and Althaus, A., *Fresenius' Z. Anal. Chem.*, 1983, **316**, 696.
11 Lindstedt, G., and Skare, I., *Analyst*, 1971, **96**, 223.
12 Bulska, E., Emteborg, H., Baxter, D. C., Frech, W., Ellingsen, D., and Thomassen, Y., *Analyst*, 1992, **117**, 657.
13 Magos, L., *Analyst*, 1971, **96**, 847.
14 Magos, L., and Clarkson, T. W., *J. Assoc. Off. Anal. Chem.*, 1972, **55**, 966.
15 Brunmark, P., Skarping, G., and Schütz, A., *J. Chromatogr.*, 1992, **573**, 35.
16 Wiken, A.-G., SERO, Billingstad, Norway, personal communication, 1994.
17 Molin, M., Bergman, B., Marklund, S. L., Schütz, A., and Skerfving, S., *Acta Odontol. Scand.*, 1990, **48**, 189.
18 Liang, L., and Bloom, N. S., *J. Anal. At. Spectrom.*, 1993, **8**, 591.
19 McIntosh, S., *At. Spectrosc.*, 1993, **2**, 47.

Atomic Emission Spectrometric Determination of Antazoline, Hydralazine and Amiloride Hydrochlorides, and Quinine Sulfate Based on Formation of Ion Associates With Manganese Thiocyanate

Adel F. Shoukry, Yousry M. Issa, H. Ibrahim and Sabry K. Mohamed

Department of Chemistry, Faculty of Science, Cairo University, Giza, Egypt

Ion associate complexes of the hydrochlorides of antazoline (1), hydralazine (2) and amiloride (3), and quinine sulfate (4) with $[Mn(SCN)_4]^{2-}$ were precipitated and their solubilities were studied as a function of pH, ionic strength and temperature. The optimum conditions for the complete precipitation of the ion associate were, thus, elucidated. An accurate and precise method using atomic emission spectrometry for the determination of the investigated drugs in pure solutions and in pharmaceutical preparations is reported. The drugs can be determined by this method in the ranges 0.3–3.0, 0.19–1.96, 0.3–3.0 and 0.78–7.82 mg per 25 ml solutions of (1), (2), (3) and (4), respectively.

Keywords: Antazoline; hydralazine; amiloride; quinine; drug analysis; atomic emission spectrometry

Introduction

The drugs studied in this work are important pharmaceutical compounds. Antazoline hydrochloride [91-75-8] has local antihistaminic and also some anticholinergic properties. Hydralazine hydrochloride [304-20-1] is used as a vasodilator in the treatment of hypertension. Amiloride hydrochloride [17440-83-4] is recommended in oedema of cardiac origin, in hepatic cirrhosis with ascites and in hypertension. Quinine sulfate [6119-70-6] is used specifically for the treatment of malaria. These pharmaceutical properties led us to prepare new ion associates containing these drugs and to study and elucidate their chemical structures. This paper also reports a rapid method for the determination of these drugs after transformation into the ion associates.

Several methods have been reported for the determination of the hydrochlorides of antazoline,[1–3] hydralazine[4–6] and amiloride,[7,8] and quinine sulfate.[9–11] Although direct current plasma atomic emission spectrometry, DCP-AES, can be used to obtain a rapid determination of these drugs even at trace levels unachievable by other methods, it has not yet been applied to the determination of these drugs. In this work, DCP-AES has been used to determine these drugs using a method based on precipitation of the ion associate formed between drugs and $[Mn(SCN)_4]^{2-}$. The equilibrium concentration of the metal ion present in the form of soluble inorganic complex ion in the supernatant of saturated solution of the ion associates was determined using DCP-AES.

Experimental

Reagents and Materials

Doubly distilled water and analytical-reagent grade reagents were used to prepare all solutions. Antazoline hydrochloride,

hydralazine hydrochloride, amiloride hydrochloride, and quinine sulfate were provided by Misr for Pharmaceutical Industries, Egypt. Manganese chloride and potassium thiocyanate were supplied by Aldrich. The pharmaceutical preparations assayed were: Antistine tablets (antazoline HCl 100 mg per tablet), Apresoline ampoules (hydralazine HCl 20 mg ml^{-1}), and Ser-Ap-Es tablets (hydralazine HCl 25 mg per tablet) obtained from Ciba, Swiss-pharma, Cairo, Egypt; Calazole lotion (1% antazoline HCl, Misr); quinine sulfate tablets (quinnine SO_4 200 mg per tablet, Nile for Pharmaceutical and Chemical Industries, Cairo); and Moduretic tablets (amiloride HCl 5 mg per tablet, El-Kahira for Pharmacuetical and Chemical Industries, Cairo).

Apparatus

The pH of the solutions was measured by a Chemtrix Type-62 digital pH meter (USA). Direct current plasma atomic emission spectrometry was carried out using a Beckman Spectra Span V emission spectrometer. Conductimetric measurements were carried out using a conductivity meter Model CM-1 (TOA Electronics, Japan).

Preparation of Ion Associates

The solid ion associates were prepared by mixing solutions containing manganese(II) (1×10^{-3} mol) with a solution containing potassium thiocyanate (4×10^{-3} mol) with the calculated amount of the drugs. The precipitates obtained were filtered off, thoroughly washed with distilled water and dried at room temperature. Elemental analyses were performed, their IR spectra measured, and their metal contents determined.

Determination of Solubility of the Ion Associate

The solid ion associate was added in excess to a solution of a particular pH and ionic strength. The solution was shaken for 4–6 h, left for a week to reach equilibrium, and filtered into a dry beaker (rejecting the first few ml of filtrate). Concentrated nitric acid (1 ml) and 1 ml of the filtrate were mixed and diluted to 100 ml with distilled water. The equilibrium concentration of the metal ion present, in the form of the soluble inorganic complex ion, was measured using DCP-AES, from which the solubility (S) of the ion associate was evaluated, and the solubility product of the ion-associate calculated.

Preparation of the Standard Solution

A standard solution (1000 ppm) of manganese(II) was prepared by dissolving manganese oxide (1.29 g) in concen-

trated nitric acid (50 ml), followed by dilution to 1 l. The solution was stored in a plastic bottle which had been presoaked in dilute nitric acid; the solution was stable for approximately one year.

Calibration of the DCP-AES

Under the recommended conditions, calibration graphs were constructed for standard aqueous solutions of manganese(II) in 1 mol l^{-1} nitric acid by performing triplicate measurements using solutions containing 0, 10, 20 and 50 ppm analyte concentrations. The graphs obtained were straight lines passing through the origin.

Conductimetric Measurements

The stoichiometry of the ion associates was elucidated by conductimetric titration of the drugs with a solution of manganese thiocyanate complex, using a Model CM-1 K (TOA Electronics, Japan) conductivity meter.

Emission Measurements

The manganese was measured at: wavelength 257.61 nm, order 87, plasma position 0.0, detection limit 0.003 ppm, linear dynamic range 0.03–100 ppm, background equivalent concentration 0.1 mg, entrance slits 50 × 300 µm and exit slits 100 × 300 µm.

Analytical Determination of the Drugs

Aliquots (1–10 ml) of 0.001 mol l^{-1} drug solutions were quantitatively transferred into 25 ml calibrated flasks. Standard manganese thiocyanate solution (1.0 ml; 0.01 mol l^{-1}) was added and the mixture diluted to 25 ml with an aqueous solution of the optimum pH and ionic strength (Table 2). The solutions were shaken well, left for 15 min, then filtered through Whatman P/S paper; the equilibrium metal ion concentration in the filtrate was determined using DCP-AES. The amount of metal ion consumed in the formation of the ion associates was calculated and the drug concentration was,
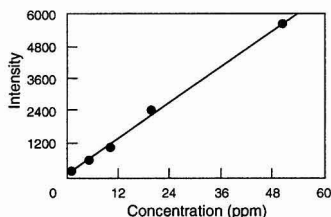
Fig. 1 Calibration curve for determination of Mn^{2+} using DCP-AES.

thus, determined indirectly. A representative calibration curve is shown in Fig. 1.

Assay of Pharmaceutical Preparations

For analysis of antazoline HCl, 12 tablets of Antisine were ground, and 0.35–3.0 mg dissolved in water (25 ml), or 10 bottles of Calazole lotion were mixed and 4–15 ml samples (containing 0.4–1.5 mg) were used. For analysis of hydralazine HCl, Apresoline solution (0.3–4.5 ml; 0.24–1.85 mg of hydralazine HCl) was used; alternatively, 20 tablets of Ser-Ap-Es were ground and dissolved in water (25 ml). Amirolide HCl was analysed by dissolving 0.35–2.62 mg of ground tablets in water (25 ml). Ten tablets of quinine sulfate were ground and 1.05–5.5 mg samples dissolved in water (25 ml).

These samples were analysed in the same way as the pure solutions.

Results and Discussion

The results of elemental analysis (Table 1) and determination of the metal content of the solid ion associates show that in all cases the stoichiometry of the drug cation: [Mn(SCN)$_4$]$^{2-}$ is 2 : 1. These results were confirmed by IR spectroscopy and are

Table 2 Optimum conditions of pH and ionic strength (μ) values at 25 °C

Ion associate	pH	μ/mol l^{-1}
Antazolinium manganese thiocyanate	8	0.4
Hydralazinium manganese thiocyanate	6	0.8
Amiloridium manganese thiocyanate	4	0.7
Quininium manganese thiocyanate	8	0.4

Table 3 Determination of the drugs in pure solutions and in pharmaceutical preparations by DCP-AES

Sample	m/mg	Mean recovery (%)	Mean s_r* (%)
Antazoline solution	0.30–3.00	101.1	1.15
Antistine tablets	0.35–3.00	103.0	1.42
Calazol lotion	0.40–1.50	100.4	1.16
Hydralazine solution	0.19–1.96	100.0	0.98
Apresoline ampoules	0.24–1.85	100.05	1.03
Ser-Ap-Es tablets	0.20–1.65	100.3	1.22
Amiloride solution	0.30–3.00	101.1	0.91
Moduretic tablets	0.35–2.62	100.2	0.65
Quinine solution	0.78–7.82	100.2	1.22
Quinine sulfate tablets	1.00–5.50	101.0	1.16

* s_r: Relative standard deviation (5 determinations).

Table 1 Elemental analysis, composition and some physical properties of the 2 : 1 drug ion associates

Drug	Ion associate composition	M.p., t/°C	Colour	Found (Calc.) (%)			
				C	H	N	Metal
Antazoline	(C$_{17}$H$_{19}$N$_3$)$_2$[Mn(SCN)$_4$]	149	White	55.8 (55.8)	4.6 (4.7)	17.1 (17.1)	6.8 (6.7)
Hydralazine	(C$_8$H$_8$N$_4$)$_2$[Mn(SCN)$_4$]	198	White	39.55 (39.5)	2.7 (2.65)	27.3 (27.7)	9.0 (9.0)
Amiloride	(C$_8$H$_8$ClN$_7$O)$_2$[Mn(SCN)$_4$]	272	Pale yellow	26.3 (26.3)	2.2 (2.2)	34.5 (34.5)	7.5 (7.5)
Quinine	(C$_{20}$H$_{24}$N$_2$O$_2$)$_2$)$_2$[Mn(SCN)$_4$]	123	White	56.3 (56.65)	5.1 (5.2)	12.0 (12.0)	5.9 (5.9)

comparable to those previously reported by Lemli.[12] Conductimetric titrations of the drugs with $[Mn(SCN)_4]^{2-}$ also confirmed the formation of 2:1 (Drug:X) ion associates.

The solubilities of the ion associates were determined under the optimum conditions; pS ($-$ log solubility) values of 5.19, 5.16, 4.44 and 5.44 for antazolinium, hydralazinium, amiloridium and quininium manganese thiocyanate ion associates, respectively, were found. Furthermore, the solubility products (pK_{sp}) were calculated using the relation $K_{sp} = 4S^3$, and found to be 14.97, 14.87, 12.71 and 13.71, respectively, for the above-mentioned ion associates.

Analytical Determination of Drugs in Pure Solutions and in Pharmaceutical Preparations

The hydrochlorides of antazoline, hydralazine and amiloride, and quinine sulfate were determined precisely and accurately using the proposed method in pure solutions and in their pharmaceutical preparations (Table 3) under optimum conditions of pH and ionic strength (Table 2). Recovery values of approximately 100% (Table 3) within the concentration ranges investigated reveal a high accuracy; the low relative standard deviations show that the method is highly precise.

Generally, the proposed method is as good as that reported in the US Pharmacopoeia.[13] It is applicable over relatively wide concentration ranges: 0.3–3.0, 0.19–1.96, 0.3–3.0 and 0.78–7.82 mg per 25 ml solutions of the hydrochlorides of antazoline, hydralazine and amiloride, and quinine sulfate, respectively. Statistical analysis of the results using the t-test at a 95% confidence limit was satisfactory. Comparison of the precision of the proposed method with that of the US Pharmacopoeia method by the F-test showed that it was reliable.

The proposed method also has the advantage that no extraction is needed to separate the ion associates formed, because they are insoluble in the aqueous medium. The DCP-AES measurements are fast and simple in comparison with other techniques such as chromatography,[14] spectrophotometry,[15] potentiometry[16] and gravimetry.[17]

References

1 Badawy, S. S., Shoukry, A. F., and Omar, M. M., *Anal. Chem.*, 1988, **60**, 758.
2 Korany, M. A., Wahbi, A. M., Mandour, S., and El-sayed, M. A., *Anal. Lett.*, 1985, **18**, 21.
3 Ayad, M. M., and Abdel-Hady, M. A., *Analyst*, 1984, **109**, 1431.
4 Badawy, S. S., Shoukry, A. F., Rizk, M. S., and Omar, M. M., *Talanta*, 1988, **35**, 487.
5 Mopper, B., *J. Assoc. Off. Anal. Chem.*, 1987, **42**, 70.
6 Mahrous, M. S., Issa, A. S., Abdel-Salam, M. A., and Soliman, N., *Anal. Lett.*, 1986, **19**, 901.
7 Sastry, C. S. P., Prasad, T. N. V., Sastry, B. S., and Rao, E. V., *Analyst*, 1988, **113**, 255.
8 Sastry, C. S. P., Prasad, T. N. V., Rao, A. R. M., and Rao, E. V., *Indian Drugs*, 1988, **25**, 206.
9 Miroslav, M., *Anal. Chem. Acta*, 1979, **109**, 191.
10 Anzai, J., Isomara, C., and Osa, T., *Chem. Pharm. Bull.*, 1985, **33**, 236.
11 Zen'Ko, I. V., *Farmatsiya*, 1938, **37**, 73.
12 Lemli, J., and Konck, C. H. L., *Pharm. Weekbl., Sci. Ed.*, 1983, **5**, 142.
13 United States Pharmacopoeia, 18th edn., Mack, Easton, 1970.
14 Meer, M. J., and Brown, L. W., *J. Chromatogr.*, 1987, **423**, 351.
15 Shah, M. H., and Stewart, J. T., *J. Pharm. Sci.*, 1984, **73**, 989.
16 Tuyen, Q., and Ioan, G., *Rev. Chim.* (Bucharest), 1977, **28**, 585.
17 Dean, R. B., and Dixon, W. J., *Anal. Chem.*, 1951, **23**, 636.

Potassium Determination by Slurry Technique

Judy Heinen Brown and Jesus E. Vaz

*Unidad de Tecnología Nuclear, Instituto Venezolano de Investigaciones Científi-
cas (IVIC), Apartado 21827, Caracas 1020A, Venezuela*

Zully Benzo and Manuela Velosa

*Centro de Química, Instituto Venezolano de Investigaciones Científicas (IVIC),
Apartado 21827, Caracas 1020A, Venezuela*

A variety of soil types (lime, clay, sandy-clay-loam,
stream-deposits, and sandstone) were analysed by the slurry
technique. The samples were dried, homogenized, ground,
sieved, weighed, suspended in nitric acid solution and
calibrated against aqueous standards. The results obtained by
this technique were then compared with those from digested
samples of the same soil. In order to establish optimum
conditions for the slurry method, the following variables were
studied: slurry concentration, acid concentration, aspiration
rate, time and temperature of the ultrasonic agitation bath.
The results have shown that only for soils with a high content of
silicon oxide are there significant differences between the two
methods.

Keywords: Potassium; slurry; atomic absorption spectrometry

Introduction

Many authors have pointed out the need for methods with
minimum sample preparation, or that do not require any prior
dissolution of the sample, for the analysis of soils. Usually, the
time needed for preparation of the samples exceeds by an
order of magnitude the actual instrument time needed for the
measurement. The time and effort of analysis become critical
factors in determining the feasibility and cost of monitoring
programmes. The determination of total potassium concentra-
tion in the sediment is a measurement required in the dating of
sediments *via* thermoluminescence. This technique produces
an error of the order of 12%. In the conventional atomic
absorption spectrometry (AAS) method, the complex dissolu-
tion procedures required prior to the test and the fact that a
large number of samples have to be handled make the assay
much more time-consuming than the direct analysis of soils by
sampling of slurries. A number of techniques have been used
to introduce solid samples into an air–acetylene flame.

Previous Literature

Gilbert[1] was the first to introduce soil suspensions directly into
a flame for analysis, and suggested that an adequately fine
grinding would be essential. Lebedev[2] suggested a new
method for determining alkaline elements in suspended
samples of rocks and minerals by flame emission and found
the sensitivities of solutions to be consistently higher than
those of slurries, and the intensity of emission of the analysed
element to be dependent upon the particular mineral. He also
observed that when the slurry particle size is sufficiently
reduced, emission intensity becomes independent of this
parameter and remarked that the need for chemical treatment
of the samples is 'completely eliminated'. Kashiki and
Oshima[3] proposed a new method for the nebulization of solid
sample in suspension into a flame, without the requirement of

prior dissolution of the sample, and determined cobalt and
molybdenum in alumina catalysts. Harrison and Juliano[4-6]
studied the atomization of tin(IV) oxide, tin(IV) sulfide and
tin(II) oxide suspensions in air–hydrogen and oxygen–acetyl-
ene flames.

They concluded that the results were dependent on the
physical nature of the sample. Burrows *et al.*[7] determined
trace amounts of the wear metals copper, chromium, iron,
lead and silver in used lubricating oil by use of premixed
air–acetylene. Following these, several fundamental studies
on the efficiency of atomization of suspended iron particles
have been reported (Lacour *et al.*;[8] Bartels and Slater;[9] Kriss
and Bartels;[10] Taylor *et al.*[11]. Muzgin and Lisienko[12] deter-
mined silicon, magnesium and zinc in limestone by spraying
suspensions into a spark discharge and measuring the emission
of the analyte, keeping the sample in suspension by bubbling
air through the mixture during the analysis. Ramírez-Muñoz
et al.[13] have analysed insoluble materials by slurry techniques.
Willis[14] has studied the factors influencing the atomization
efficiencies of metals such as copper, nickel, cobalt, man-
ganese, zinc, and lead when suspensions of geological
materials are sprayed into the flame for analysis by AAS. He
concluded that only particles of less than 10–12 µm diameter
contribute significantly to the observed atomic absorption and
that constant mixing of the suspended material, using either
ultrasonic agitation or a magnetic stirrer, is required during
the analysis. Langmyhr[15] reviewed the literature concerning
the advantages and possibilities of direct analysis of solid
suspension by AAS and pointed out the problems of sample
homogeneity which arise from these types of samples. Fuller
and co-workers[16-18] have shown that with the use of elec-
trothermal atomization it is possible to tolerate larger particle
sizes for the sample. This advantage is borne out by work
carried out on the direct introduction of powdered solid
samples to electrothermal atomizers (Langmyhr and co-work-
ers;[19-22] Gong and Suhr[23]). Stupar and Ajlec[24] have used the
soil suspension technique in the determination of iron,
manganese, magnesium and copper by flame AAS. Rygh and
Jackson[25] determined cadmium in soil slurries by micro-
sampling cup AAS and results were compared with those from
slurry ETAAS and flame AAS with acid digestion. Halicz and
Brenner[26] have introduced slurries of silicate rocks and their
glasses and suspensions of clay minerals into an ICP with use
of a high solids nebulizer. They observed that grinding time
and associated particle size appeared to control the reliability
of analytical calibration functions and reliable calibration
methods could be obtained only for clay mineral fractions
(0.5–2 µm). Ebdon and co-workers[27-30], Sparkes and
Ebdon,[31] and Goodall *et al.*[32] have studied the particle size
effects on kaolin slurry and refractory slurries, and several
different nebulizers, spray chambers and injector tubes have
been compared for slurry atomization ICP-AES. Epstein
et al.[33] evaluated the application of an automated slurry

sample and determined arsenic, iron, manganese and lead by GFAAS. Darke *et al.*[34] have studied laser ablation and slurry nebulization of samples for the analysis of geochemical materials by ICP. Laird *et al.*[35] have studied recoveries for clay minerals by ICP using slurry nebulization. Jarvis[36] has studied the role of slurry nebulization for the analysis of geological samples by inductively coupled plasma mass spectrometry. It was concluded that this is a useful additional method for the determination of volatile elements.

In view of the increasing application of the slurry technique to the analysis of soils and sediment, we became interested in developing a method for the determination of potassium by flame AAS using this technique in different types of soil samples which would eliminate time consuming procedures in the chemical dissolution of geological materials. A study of sample drying, grinding, particle size influence and standardization was carried out to determine whether the air–acetylene flame is suitable for the determination of potassium in slurry samples. The accuracy of the present method has been checked by using the standard additions technique and also by comparing the results with those obtained by the analysis of digested samples because there is no availability of certified standards for these types of soils.

Experimental

Apparatus

Elementary determinations were performed with a Varian Model 875 atomic absorption spectrometer. A single element hollow-cathode lamp was used. An X-ray diffractometer, Philips Model PW1730, was used for the identification of crystalline materials, and an X-ray Princeton Gammatech fluorescence spectrometer, Model LD13155, was used for the qualitative identification of the metal. Powdered samples were dried in an oven (Cole-Palmer, Model 5015-54). Grinding of the samples was carried out by using a vibrational Retsch High Speed Planetary Mixer Mill with a porcelain cylinder and zirconium balls, and sieving through a bronze screen of 400 mesh, which retained particles with nominal diameters of 38 μm. The measurement of particle size was carried out by electron microscopy. Samples used in the dissolution process were weighed in an analytical balance (Mettler, Model H20T), then fused in a muffle (K. H. Huppert, Model 439DL) and homogenized. Samples used in suspension were weighed and dispersed with an ultrasonic agitator (Cole-Palmer, Model 8851).

Reagents

Analytical-reagent grade chemicals and de-ionized water (Milli-Q) were used throughout. *Pro analysi* nitric acid and caesium chloride–aluminium nitrate buffer solution, from Merck, were used in the preparation of standards. Samples were fused with lithium metaborate from Merck. Potassium nitrate stock standard solution (1000 μg ml^{-1}) from BDH (now Merck) was diluted to provide the working standards.

Sample Preparation

Geological samples were collected from different Venezuelan regions. In this study we concentrated on five common soil types: lime soils from Acarigua (Fig. 1), clay from Camaguan (Fig. 2) and Corozo, sandy-clay-loam from Cunaviche, stream deposits from San Fernando and sandstone (Fig. 3) from the shores of the Apure river. These are used in the determination of potassium for dating of sediments in connection with edaphological studies. After collection, each wet soil sample was mixed thoroughly and separately and a portion oven-dried

at 80 °C for 6 h. For the digestion process and slurry analysis, approximately 3 g of the sample were homogenized in a porcelain mortar, then ground in a mill, which was cleaned between samples by grinding a small amount of quartz and washing thoroughly with distilled, de-ionized water and then dried. In order to eliminate any possible contamination coming from the cleaning procedure, small amounts of each sample were ground before the grinding step.

Analysis of Soil Slurries

Preparation of suspensions

Stock suspensions were prepared by weighing approximately 100 mg of material into a calibrated flask (100 ml); powdered samples (<400 mesh) were dispersed in concentrated nitric acid for 90 min at 45 °C by ultrasonic agitation. For lime soil, 1 ml of nitric acid was added, 15 ml of nitric acid for clayey soil, and 20 ml of nitric acid for sandy-clay-loam, stream deposits and sandstone. By pipetting aliquots from the stock solution, the required volume was transferred by pipette into a polystyrene tube (10 ml), aliquots of CsCl were added to both standards and samples and then the mixture was diluted with de-ionized water. In the normal time required for the pipetting step no settling problem was noted in the test-tube. When absorption readings were taken for three duplicate aliquot suspensions from a common stock, reproducibility was within the reading error of the instrument, with good signal response. A properly formed slurry could easily be volumetrically manipulated and aspirated.

Sample digestion

A 100 mg portion of sample and 800 mg of lithium metaborate were weighed into a graphite crucible and fused in a muffle furnace at 900 °C for 15 min; this process has to be carried out gradually in order to avoid damaging the sample with the moisture from lithium metaborate dihydrate. This step takes 1.5 h to reach 900 °C. The fused material was digested in a beaker with 50 ml of 5% v/v nitric acid, then diluted to the mark with de-ionized water.
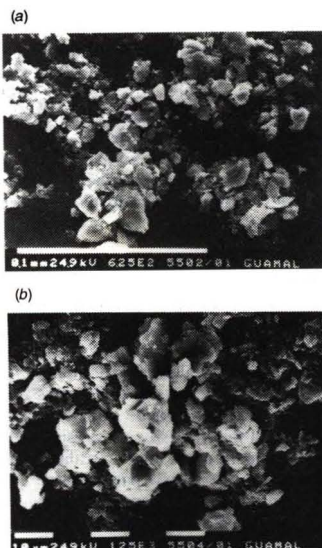
Fig. 1 (*a*) General view of Guamal Acarigua sample; (*b*) greater magnification.

Measurement of Absorption

For analytical determination stock standard potassium solution was prepared over a concentration range (0.2–2.0 µg ml^{-1}) by dilution from standard potassium nitrate solution (1000 mg l^{-1}). The absorption line at 766.5 nm was used, with a spectral bandpass of 0.1 nm and a lamp current of 5 mA. Owing to the effect of the wide concentration range studied the calibration graph is linear up to 1.0 ppm: it then flattens out until 2 ppm. Samples were shaken prior to aspiration in order to minimize the effect of settling. Readings were taken as soon as the signal stabilized, a process which normally required no more than 5 s of suspension aspiration. Five readings were always taken.

For soil characterization two methods of analysis were carried out: X-ray diffraction and X-ray fluorescence spectrometry. For X-ray diffraction analysis, all data were collected by using copper radiation KL, wavelength 1.541 78 Å, nickel filter, swept from 3° to 50°. A 4 g amount of sample was weighed and transferred into a graduated cylinder (100 ml) and de-ionized water added. The suspension was homogenized by ultrasonic agitation for 1 h and allowed to settle for 30 min, then pipetted onto glass slides and left to evaporate until dry for the analysis.

X-ray Fluorecence Spectrometry

For qualitative analysis of the samples the system consisted of three excitation sources (^{109}Cd, ^{55}Fe and ^{241}Am), a Si(Li) spectrometer (*i.e.*, detector, preamplifier and bias supply) and an analogue-to-digital converter which was interfaced to a computer (Apple II-e). The detector used in this system was a 30 mm^2 × 3 mm Si(Li) detector with a resolution of 200 eV (FWHM) at 5.9 keV.

Results and Discussion

X-ray Fluorescence and Diffraction Results

The results for fluorescence analysis showed that Si, K, Ca, Ti, Fe, Cu, Zn, Rd, Sr, Zr and Y are present in soil samples, and the diffraction pattern that the clay separates contained a mixture of kaolinite, muscovite, gibbsite, pirofilite, dicktite, mica, chlorite and berthierine in approximately equal amounts, with lesser amounts of silicon oxide. For agricultural soils the results showed micas (taeniolite), with a lesser amount of silicon oxide. Stream deposits contained mostly quartz with minor quantities of feldspar and clay; sandstone contained sanidine and feldspar (potassium aluminium silicate). The latter is very stable even when exposed to temperatures of more than 500 °C.[37,38]

Sample Drying and Grinding

Drying is an indispensable procedure in sample treatment which facilitates the grinding step described below. The duration of the drying step was optimized, with a minimum time of 6 h. Depending on soil texture, it is advisable to leave the samples overnight in order to guarantee optimum grinding. For the determination of the influence of the grinding time on the particle size distribution, soil samples were ground for periods of 2, 4 and 6 h to achieve a final representative sample that was 95% m/m, with a minimum particle size. It was observed that increasing the grinding time to more than 2 h did not reduce 95% of the particles finer than the minimum particle size. With this procedure it was possible to obtain samples with a mean particle size below 10 µm. The grinding time chosen for analysis was 2 h.

Influence of Particle Size

The particle size of the sample is known to be of major importance in atomization. Slurries with particle sizes in the ranges 1–10 and 10–40 µm were measured in order to check whether there is any influence from the particle size on the atomic absorption signal of the analyte. The results from calibration curves presented in Fig. 4 for Corozo soil show that particle sizes of 5 µm led to an increase in absorption signal of about 19% over those produced by the 38 µm particle size fractions. This is due to the lower slurry concentration studied
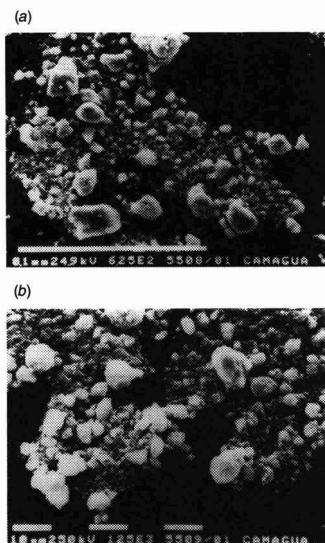
Fig. 2 (*a*) General view of Palmar Camaguan sample; (*b*) greater magnification.
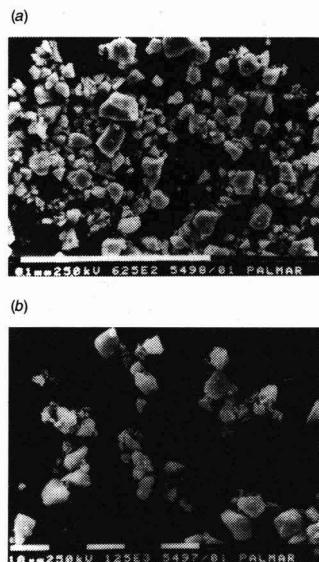
Fig. 3 (*a*) General view of Palmar Apure sample; (*b*) greater magnification.

in the calibration curve and could possibly affect the analytical signal response. That figure also indicates that only suspensions containing particles of less than 10 μm in diameter show significant atomic absorption when sprayed into the flame. Particles above 10 μm can be eliminated through the drainage of the mixing chamber. The lighter mineral fractions, representing 95% of the sample, contain mostly clay with minor amounts of quartz. It follows that the bulk of the potassium must be in the lighter fraction, probably in the clay.

Aspiration Rate Optimization

This study was carried out in order to make the aspiration rate of both standards and analyte solution identical. There is a difference between nebulizing a suspension and a liquid. More viscous solutions will be aspirated more slowly into the flame and will affect sensitivity.

The instructions that come with the AAS equipment suggest that the aspiration rate be fixed between 4 and 6 ml min^{-1}, because liquid nebulization occurs more efficiently in this range. In probing the variability effect of the aspiration rate with slurry concentration, as shown in Fig. 5, it can be observed that from 3 ml min^{-1} onwards the slurry signal appears, then increases with the aspiration rate; it remains stable from 6.5 ml min^{-1} onwards as the plateau is reached. Therefore, 6.8 ml min^{-1} was taken as the optimum aspiration rate. Measurements revealed that no significant difference in

rates could be observed between the aqueous solution and suspensions in an air–acetylene flame. To compensate for any potassium impurity that might be present in reagents, appropriate blanks were prepared for each test solution and suspension.

Nitric Acid Optimization

In the study of optimization of the nitric acid concentration for lime soils, Fig. 6 shows that the slurry signal increases progressively between 0–0.7% of acid. It remains stable from 0.7%, therefore the optimum concentration taken for slurry analysis was 1% v/v.

For clayey soils, Fig. 7 shows that the slurry signal is constant between 0–3% of acid; from 3% it increases progressively until 8%, and then stabilizes. Eventually, 15% of acid was taken as optimum concentration for slurry analysis.

The study of nitric acid concentration for sandy-clay-loam, stream deposits and sandstone shows, in Fig. 8, that the slurry signal is constant between 0 and 5% of nitric acid, increases progressively from 5 until 10% and then remains constant; 20% v/v was taken as the optimum concentration.

Slurry Concentration

In this work we optimized the slurry concentration with and without nitric acid. We observed that the slope of the curve (Fig. 9) corresponding to the inclusion of nitric acid was due to the fact that the concentration of potassium in the slurry increased the calibration graph which became more non-

Fig. 4 Particle size distribution: ▤, $10 < x < 44$ μm $(x = 38)$; ▦, $1 < x < 10$ μm $(x = 5)$; ■, standard. Determined, Corozo soil.
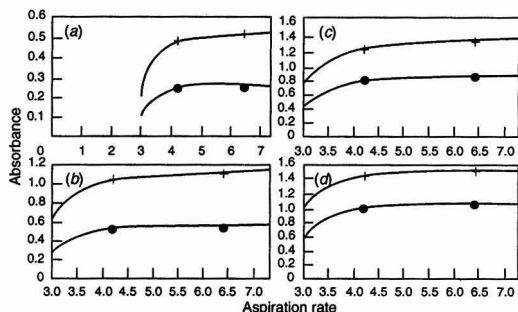
Fig. 5 Variability effect of aspiration rate with slurry concentration: (*a*) 25 mg per 100 ml; (*b*) 50 mg per 100 ml; (*c*) 75 mg per 100 ml; (*d*) 100 mg per 100 ml. ●, Without acid; +, with acid.
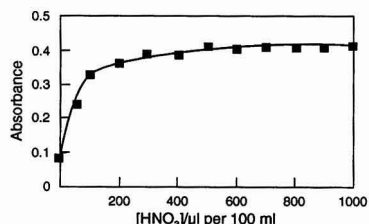
Fig. 6 Optimization of acid concentration for lime soil.
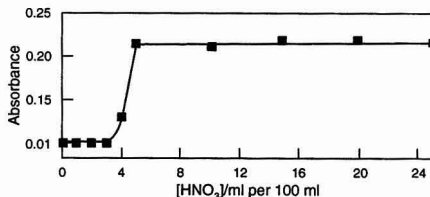
Fig. 7 Optimization of acid concentration for clayey soil.
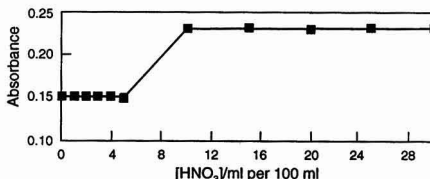
Fig. 8 Optimization of acid concentration for sandy-clay-loam, stream deposits and sandstone.

linear. It can be observed also with aqueous standards. In no case can this be attributed to saturation of the slurry signal by the high level of slurry, a result also confirmed in the procedure without nitric acid. This graph also shows that the absorbance increases linearly with the slurry concentration. Therefore, 0.1% m/v was taken as optimum slurry concentration for the analysis. For higher concentrations capillary obstruction may occur, and in lower concentrations a decrease in absorption signal is observed. This study was performed fixing the aspiration rate at 6.8 ml min^{-1}.

Matrix Effect

In order to check whether an interference effect could result from the matrix, two methods of analysis were used: calibration using aqueous standards and standard additions.

Calibration Method

In this study two calibration curves were produced, one using aqueous standards and the other with stock suspension, having previously carried out a potassium determination by use of a digestion method. The slurry calibration was achieved by taking different aliquots from as stock solution. It can be observed in Fig. 10 that the points of both measures are superposed, forming one slope. The graph indicates that there is no interference when the slurry is atomized. Equally, a light sloping of the curve due to the effect of the wide range of concentration (0.2–2 ppm of potassium) studied is observed, and normally it decreases at high levels of concentration. This effect occurs in the determination of potassium and other elements which can be quantified by use of AAS.

Standard Additions

The study of standard additions was carried out by the comparison of calibration curves from slurry and dissolution. Different aliquots from standard potassium nitrate solution (1000 mg l^{-1}) were added to every stock solution and suspension. The calibration curves were made by successive dilutions from each stock solution. The results of this study are
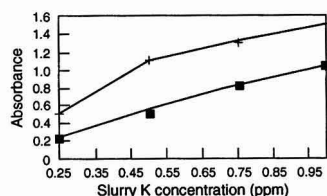
shown in Table 1. A Camaguan soil was used as a representative sample for this study.

Slurry and Digestion Results

Table 2 summarizes the results obtained by use of the proposed method, compared with the values given by the conventional method. It is observed that the analytical results for potassium by the slurry technique are in good agreement with the digested samples.

Suspension or Extraction

To clear any doubt whether the potassium determination by use of the slurry technique is a suspension or extraction, we studied the potassium concentration by measuring different aliquots of decanted liquid and suspension from a common stock, which was acidified by adding 20% v/v of nitric acid. The results shown in Table 3 show that the high value for

Table 1 Standard additions results on Camaguan soil

Soil	Total dissolution (%)	Slurry standard addition (%)
0–10 cm	0.219 ± 0.003	0.215 ± 0.019
10–25 cm	0.282 ± 0.015	0.296 ± 0.014
50–75 cm	0.546 ± 0.010	0.542 ± 0.026
100–125 cm	0.640 ± 0.035	0.658 ± 0.019

Table 2 Comparison of results obtained by use of proposed and conventional methods for potassium

Soils	Total dissolution (%)	Slurry (%)
Corozo—		
0–10 cm	0.466 ± 0.013	0.460 ± 0.001
10–25 cm	0.500 ± 0.024	0.487 ± 0.010
50–75 cm	0.464 ± 0.006	0.461 ± 0.010
125–150 cm	0.549 ± 0.009	0.540 ± 0.002
Camaguan—		
0–10 cm	0.219 ± 0.003	0.215 ± 0.001
10–25 cm	0.282 ± 0.015	0.268 ± 0.012
50–75 cm	0.546 ± 0.010	0.544 ± 0.001
100–125 cm	0.640 ± 0.035	0.640 ± 0.001
San Fernando—		
0–10 cm	1.602 ± 0.004	1.561 ± 0.005
10–25 cm	1.661 ± 0.013	1.622 ± 0.013
75–100 cm	1.636 ± 0.020	1.647 ± 0.001
100–125 cm	1.648 ± 0.014	1.659 ± 0.024
Acarigua—		
0–10 cm	1.570 ± 0.020	1.560 ± 0.020
10–25 cm	2.230 ± 0.020	2.220 ± 0.020
50–75 cm	2.430 ± 0.020	2.400 ± 0.020
100–125 cm	2.480 ± 0.020	2.470 ± 0.020
Cunaviche—		
0–7 cm	0.266 ± 0.008	0.254 ± 0.007
10–30 cm	0.800 ± 0.002	0.734 ± 0.070
60–90 cm	0.930 ± 0.001	0.926 ± 0.003
130–150 cm	1.010 ± 0.001	1.007 ± 0.003

Fig. 9 Optimization of slurry concentration with fixed aspiration rate (6.8 ml min^{-1}): ■, without acid; +, with acid.

Fig. 10 Comparative calibration curves: ■, slurry; +, standard.

Table 3 Determination of potassium decanted liquid and suspension (Apure soil)

Soil	Suspension (%)	Decanted (%)
0–10 cm	0.360 ± 0.004	0.196 ± 0.007
10–30 cm	1.207 ± 0.008	1.028 ± 0.001
90–105 cm	1.530 ± 0.008	1.306 ± 0.001
105–130 cm	1.295 ± 0.017	1.050 ± 0.001

potassium concentration corresponds to the slurry assay. Therefore, particles of less than 10 μm in diameter are nebulized and efficiently transported through the mixing chamber as a liquid.

Conclusions

The determination of potassium in soil samples by aspiration of suspension into the flame showed that an air–acetylene flame is indeed suitable for decomposing crystalline clay material in order to provide accurate elemental analyses of clay suspensions. The method can be applied to most types of soils as a routine analysis. One of the advantages of this technique is that the tedious and time-consuming step of dissolution for geochemical analyses is avoided at lower cost for chemicals and equipment. In addition, this technique uses direct calibration with aqueous standards. The accuracy of the determination using the slurry technique was ±5% and the values have errors of less than 5%. Applications of the slurry technique to chemical analysis showed that results were dependent on the physical nature of the samples.

References

1 Gilbert, P. T., *Anal. Chem.*, 1962, **34**, 1025.
2 Lebedev, V. I., *Zh. Anal. Khim.*, 1969, **24**, 337.
3 Kashiki, M., and Oshima, S., *Anal. Chim. Acta*, 1970, **51**, 387.
4 Harrison, W. W., and Juliano, P. O., *Anal. Chem.*, 1971, **43**, 248.
5 Harrison, W. W., and Juliano, P. O., *Anal. Chem.*, 1969, **41**, 1016.
6 Juliano, P. O., and Harrison, W. W., *Anal. Chem.*, 1970, **42**, 84.
7 Burrows, J. A., Heerdt, J. C., and Willis, J. B., *Anal. Chem.*, 1965, **37**, 579.
8 Lacour, A., Teinturier, C., and Isabelle, D. B., *Méthodes Phys. Anal. (GAMS)*, 1971, **7**, 49.
9 Bartels, T. T., and Slater, M. P., *At. Absorpt. Newsl.*, 1970, **9**, 75.
10 Kriss, R. H., and Bartels, T. T., *At. Absorpt. Newsl.*, 1970, **9**, 78.
11 Taylor, J. H., Bartels, T. T., and Crump, N. L., *Anal. Chem.*, 1971, **43**, 1780.
12 Muzgin, V. N., and Lisienko, D. G., *Zh. Anal. Khim.*, 1969, **24**, 666.
13 Ramírez-Muñoz, J., Roth, M. E., and Ulrich, W. F., *20th Pittsburgh Conference on Analytical Chemistry and Applied Spectroscopy, Cleveland, Ohio, March 2–7, 1969*.
14 Willis, J. B., *Anal. Chem.*, 1975, **47**, 1752.
15 Langmyhr, F. J., *Analyst*, 1979, **104**, 993.
16 Fuller, C. W., and Thompson, I., *Analyst*, 1977, **102**, 141.
17 Fuller, C. W., Hutton, R. C., and Preston, B., *Analyst*, 1981, **106**, 913.
18 Fuller, C. W., *Analyst*, 1976, **101**, 961.
19 Langmyhr, F. J., and Thomassen, Y. Z., *Anal. Chem.*, 1973, **264**, 122.
20 Langmyhr, F. J., Stubergh, J. R., Thomassen, Y., Hanssen, J. E., and Dolezal, J., *Anal. Chim. Acta*, 1974, **71**, 35.
21 Langmyhr, F. J., and Rasmussen, S., *Anal. Chim. Acta*, 1974, **72**, 79.
22 Langmyhr, F. J., *Fresenius' Z. Anal. Chem.*, 1985, **322**, 654.
23 Gong, H., and Suhr, N. H., *Anal. Chim. Acta*, 1976, **81**, 297.
24 Stupar, J., and Ajlec, R., *Analyst*, 1982, **107**, 144.
25 Rygh, G., and Jackson, K. W., *J. Anal. At. Spectrom.*, 1987, **2**, 397.
26 Halicz, L., and Brenner, B. I., *Spectrochim. Acta, Part B*, 1987, **42**, 207.
27 Ebdon, L., and Collier, A. R., *Spectrochim. Acta, Part B*, 1988, **43**, 355.
28 Ebdon, L., and Collier, A. R., *J. Anal. At. Spectrom.*, 1988, **3**, 557.
29 Ebdon, L., Foulkes, M. E., and Hill, S., *J. Anal. At. Spectrom.*, 1990, **5**, 67.
30 Ebdon, L., and Goodall, P., *J. Anal. At. Spectrom.*, 1992, **7**, 1111.
31 Sparkes, S. T., and Ebdon, L., *J. Anal. At. Spectrom.*, 1988, **3**, 563.
32 Goodall, P., Foulkes, M. E., and Ebdon, L., *Spectrochim. Acta, Part B*, 1993, **48**, 1563.
33 Epstein, M. S., Carnrick, G. R., Slavin, W., and Miller-Ihli, N. J., *Anal. Chem.*, 1989, **61**, 1414.
34 Darke, S. A., Long, S. E., Pickford, C. J., and Tyson, J. F., *Fresenius J. Anal. Chem.*, 1990, **337**, 284.
35 Laird, D. A., Dowdy, R. H., and Munter, R. C., *J. Anal. At. Spectrom.*, 1990, **5**, 515.
36 Jarvis, K. E., *Chem. Geol.*, 1992, **95**, 73.
37 Barth, T. F. W., *Feldspars*, Wiley Interscience, New York, 1969, pp. 2–10.
38 Hurlbut, J. R., *Dana's Manual of Mineralogy*, John Wiley and Sons, New York, 18th edn., 1971, pp. 458–464.

Dilute Acid Digestion Procedure for the Determination of Lead, Copper and Mercury in Traditional Chinese Medicines by Atomic Absorption Spectrometry

P. Y. T. Chow, T. H. Chua, K. F. Tang and B. Y. Ow
*Department of Scientific Services, Institute of Science and Forensic Medicine,
Outram Road, Singapore 0316*

A sample preparation procedure using 10% v/v HNO_3 was successfully applied to the determination of Pb, Cu and Hg in traditional Chinese medicines. It provides good recoveries of Pb, Cu and Hg, requires small volumes of concentrated acid and is free from reagent and procedural blank problems. A number of Chinese medicines were analysed using the proposed method. The results obtained were comparable to those obtained by other standard procedures. Using a 3 g sample, the detection limit for Pb was about 4 µg g^{-1}, for Cu about 0.2 µg g^{-1} and for Hg about 0.03 µg g^{-1}. The precision of the method, obtained by calculation of the relative standard deviations for six replicate measurements, was 0.7% for Pb, 0.7% for Cu and 6.5% for Hg.

Keywords: Chinese traditional medicines; acid digestion; atomic absorption spectrometry; lead; copper; mercury

Introduction

The use of medicinal plants for traditional therapeutic treatment has been practised in many countries in the Asian Pacific Region and traditional Chinese medicines have been used for several thousand years to cure various illnesses. They are readily available to the general public and are sold over the counter in many Chinese medicine shops. Although Western medicine is also available, the Chinese community still prefers to use Chinese medicines because they believe in their therapeutic effects.

Some of the traditional Chinese medicines have been found to contain toxic metals such as Hg, Pb and Cu. These toxic metals are introduced into the medicines either as contaminants or as active ingredients. Under the Sale of Drugs (Prohibited Substances) Regulations of Singapore, the regulatory limits for Hg, Pb and Cu in any drug, including Chinese medicines, are 0.5, 20 and 150 µg g^{-1}, respectively. It is therefore necessary to develop a precise and accurate method for the determination of these toxic metals in traditional Chinese medicines.

Traditional Chinese medicines are complex mixtures and are available as tablets, capsules, pills, powders, syrups, injections, *etc*. Obviously there is a need to find an effective sample preparation procedure that is capable of solubilizing the toxic metals completely. Sample preparation procedures for the determination of toxic metals in traditional Chinese medicines have been reported,[1] but most of them are in Chinese. They usually employ wet digestion methods, using concentrated acids to oxidize the organic matter completely, and are often tedious and time consuming.

In the early days, the determination of trace elements was mainly carried out by spectrophotometry. Therefore, classical sample preparation procedures demand complete decomposi-

tion of organic matter, which would otherwise interfere with the process of colour development. For analysis by atomic spectrometric techniques, however, the criterion that should be applied is complete dissolution of the trace elements but not necessarily complete digestion of the sample.[2]

Extraction with dilute nitric acid at room temperature is a simple and safe sample preparation technique that has been applied with some success for the determination of a range of elements in bovine liver (NIST SRM 1577a), rat liver and citrus leaf tissue.[3,4] In this work, a simple sample preparation procedure involving digestion with 10% v/v nitric acid at 100 °C was investigated for the determination of Pb, Cu and Hg in traditional Chinese medicines.

Experimental

Instrumentation

Lead and copper in all sample digests were determined by flame atomic absorption spectrometry (flame AAS) on a Perkin-Elmer Model 3100 atomic absorption spectrometer. The conditions used are given in Table 1. Mercury in all sample digests was determined by cold vapour AAS on the Perkin-Elmer Model 3100 instrument in conjunction with an MHS-20 Hg/hydride system. The conditions used are given in Table 2.

Reagents

Analytical-reagent grade chemicals and distilled water were used for the preparation of all solutions.

Stock standard solutions for AAS, containing individually 1000 µg ml^{-1} of Pb, Cu and Hg, were purchased from Merck (Poole, Dorset, UK). Working standard solutions of Pb, Cu and Hg were freshly prepared by appropriate dilution with 1% v/v HNO_3.

The certified reference material (CRM) olive leaves (*Olea europaea*, BCR 62) was purchased from the Commission of the European Communities (Brussels, Belgium).

Table 1 Instrumental conditions used for the determination of Pb and Cu by flame AAS

	Pb	Cu
Source	HCL*	HCL*
Wavelength/nm	283.3	324.8
Slit width/nm	0.7	0.7
Lamp current/mA	10	25
Background correction	On	Off
Calibration range/µg ml^{-1}	0–3	0–2
Integration time/s	3	3

* Hollow-cathode lamp.

The reductant for cold vapour AAS was a freshly prepared 3% m/v solution of $NaBH_4$ in 1% m/v NaOH. It was prepared by dissolving NaOH and $NaBH_4$ powder in distilled water and filtering.

Procedures

The sample was ground into powder or cut into small pieces to produce a homogeneous mixture. About 3 g of sample were accurately weighed into an acid-washed 100 ml Nessler tube. A duplicate sample was used in each run. About 20 ml of 10% v/v HNO_3 were added to the sample and the tube was covered with a layer of sealing film. The tube was heated in a water-bath at 100 °C for 3 h with occasionally swirling. The digest was cooled and filtered into a 50 ml calibrated flask, then diluted to volume with distilled water. A blank was carried out simultaneously with 10% v/v HNO_3 in the same manner as for the samples. Both Pb and Cu were determined by flame AAS, and Hg by cold vapour AAS. The concentrations of Pb, Cu and Hg in the sample solution were obtained from their respective calibration graphs. After the blank correction, the amounts of Pb, Cu and Hg present in the sample were calculated.

Results

CRM olive leaves (BCR 62) were used for evaluation of the suggested method, and selected for two reasons. First, it has a reasonable match of matrix with that of the traditional Chinese medicine that is usually made up of medicinal plant materials, and second, it contains suitable amounts of the elements of interest. The reference material was dried at 105 °C for about 3 h before analysis.

To establish the minimum heating time for complete extraction of Pb, Cu and Hg, a set of 2 g samples of CRM olive

leaves were digested with 10% v/v HNO_3 for 2, 2.5, 3, 4 and 6 h. After dilution to volume, the diluted digests were analysed for the elements. The results, illustrated in Fig. 1, show that maximum extraction was achieved for Pb and Hg after 2 h. For Cu, only 93% extraction was achieved after 2 h and 100% after 3 h. For this reason, a 3 h heating period was selected in all further work.

Table 3 shows the results for Pb, Cu and Hg obtained by heating 2–3 g of CRM olive leaves in 10% v/v HNO_3 for 3 h. There was good agreement with the certified values and the blank values for Pb, Cu and Hg were not significant.

Traditional Chinese medicines in the form of pills, powder and tablets, with known Pb, Cu and Hg levels obtained by this method, were spiked with Pb, Cu and Hg, then digested with 10% v/v HNO_3 and analysed according to the described procedures. The recoveries were good, ranging from 94 to 104% for Pb, from 94 to 102% for Cu and from 100 to 110% for Hg (Table 4). Again, the results indicate that 3 h of digestion should be sufficient for extraction of the three elements from traditional Chinese medicine samples.

A 3 g sample was used in this study because it would increase the absorption signal of Pb in flame AAS. It would also provide a more representative sample for the determination of trace elements such as Hg. Traditional Chinese medicines are composed of complex mixtures of medicinal plant materials, which by their nature show a high degree of variability in elemental distribution. Heavy metals, such as Hg in particular, tend to be inhomogeneously distributed in such a matrix owing to their nature and possible speciation.[5] Hence, it is important to obtain a representative sample for analysis.

Table 3 Pb, Cu and Hg determined in BCR olive leaves using the proposed method

Analyte	Certified value/$\mu g\,g^{-1}$	Found value/$\mu g\,g^{-1}$ dry mass
Pb	25.0 ± 1.5	26.4
Cu	46.6 ± 1.8	44.9
Hg	0.28 ± 0.02	0.29

* Average of six replicates.

Table 2 Instrumental conditions used for the determination of Hg by cold vapour AAS

Source	HCL*
Wavelength/nm	253.6
Slit width/nm	0.7
Lamp current/mA	6
Calibration range/ng ml^{-1}	0–25
Integration time/s	10
MHS-20 settings—	
Cell temperature/°C	200
Purge I/s	5
Reaction/s	10
Purge II/s	30

* Hollow-cathode lamp.

Table 4 Recoveries of Pb, Cu and Hg added to Chinese medicines using the proposed method

Metal	Sample*	Metal added/μg	Metal found†/μg	Recovery (%)
Pb	Pill A	—	ND‡	—
		50.0	47.2	94
	Powder	—	ND	—
		50.0	51.9	104
	Tablet A	—	ND	—
		50.0	51.0	102
Cu	Pill A	—	7.7	—
		30.0	38.3	102
	Powder	—	26.9	—
		30.0	55.0	94
	Tablet A	—	16.3	—
		30.0	45.3	97
Hg	Pill A	—	ND	—
		0.50	0.55	110
	Powder	—	1.02	—
		0.50	1.52	100
	Tablet A	—	1.18	—
		0.50	1.70	104

* Pill A is a mixture of herbal plants and plant extracts in pill form. Powder is a mixture of herbal plants and plant extracts in powder form. Tablet A is a mixture of herbal plants and plant extracts in tablet form.
† Average of two values.
‡ ND = not detected.

Fig. 1 Effect of heating time on the measured concentrations of Pb, Cu and Hg in CRM olive leaves.

Table 5 Comparison of Pb, Cu and Hg measurements by the proposed and existing methods

Sample*	Proposed method			Existing methods[†]		
	Pb/µg g^{-1}	Cu/µg g^{-1}	Hg/µg g^{-1}	Pb/µg g^{-1}	Cu/µg g^{-1}	Hg/µg g^{-1}
Capsule A	ND[‡]	10.7	2.7	ND	9.3	3.9
Capsule B	ND	6.9	0.64	ND	6.7	0.67
Capsule C	ND	7.6	0.26	ND	7.4	0.26
Pill B	9.4	4.5	0.12	9.2	5.4	0.15
Pill C	8.2	36.0	3.1	6.7	36.7	3.9
Tablet B	ND	4.4	0.41	ND	4.2	0.40
Tablet C	ND	65.3	0.74	ND	53.0	0.70
Tablet D	12.8	6.0	45.1	14.0	4.7	46.3

* Capsules A, B and C are mixtures of herbal plants and plant extracts packed in capsules. Pills B and C are mixtures of herbal plants and plant extracts in pill form. Tablets B, C and D are mixtures of herbal plants and plant extracts in tablet form.
[†] Pb and Cu by dry ashing method and Hg by wet oxidation method.
[‡] ND = not detected.

The described procedure has been used to determine Pb, Cu and Hg in several traditional Chinese medicines. The results were satisfactory and comparable with those given by existing procedures used in this laboratory using conventional dry ashing with magnesium nitrate as an ashing aid for Pb and Cu and wet oxidation with concentrated nitric acid for Hg (Table 5).

The method is simple, easy to follow and is able to determine Pb, Cu and Hg in one sample preparation with the minimum use of concentrated nitric acid. There is also very little evolution of acid fumes and digestion is carried out at a low temperature (100 °C). It is free from reagent and procedural blank problems. The final diluted sample solution has a low acid concentration (less than 4% v/v HNO$_3$) and is suitable for AAS and inductively coupled plasma measurements with minimum interference and without causing corrosion,[4,6] and the electrothermal AAS without causing matrix effects.[7–9]

References

1 Lau, O. W., Han, P. K., Cheung, C. Y., and Chau, M. H., *Analyst*, 1985, **110**, 483.
2 Niazi, S. B., and Littlejohn, D., *Analyst*, 1993, **118**, 821.
3 Luterotti, S., Zanic-Grubisic, T., and Juretic, D., *Analyst*, 1992, **117**, 141.
4 Basson, W. D., and Bohmer, R. G., *Analyst*, 1972, **97**, 482.
5 Colinet, E., Griepink, B., and Muntau, H., *BCR Information on Reference Materials, Report EUR 8119 EN*, Commission of the European Communities, Brussels, 1982, p. 10.
6 Williams, M. C., Stallings, E. A., Foreman, T. M., and Gladney, E. S., *At. Spectrosc.*, 1988, **9**, 110.
7 Smeyers-Verbeke, J., Michotte, Y., Van den Winkel, P., and Massart, D. L., *Anal. Chem.*, 1976, **48**, 125.
8 Lau, O. W., Hon, P. K., Cheung, C. Y., and Wong, M. C., *Analyst*, 1984, **109**, 1175.
9 Tong, S. L., *Anal. Chem.*, 1978, **50**, 412.

CUMULATIVE AUTHOR INDEX
JANUARY–APRIL 1995

Book Reviews

Chemical Analysis by Nuclear Methods
Edited by Z. B. Alfassi. Pp. xx + 556. Wiley. 1994. Price £90.00. ISBN 0-471-93834-3.

This text, written by a group of 25 specialist authors from ten different countries, provides a comprehensive review of the wide range of nuclear techniques that can be employed in chemical analysis. The book comprises 20 self-contained chapters with appropriate references up to 1993. The text is divided into five sections dealing with: (1) basic background in nuclear physics and chemistry; (2) elemental analysis with neutron sources; (3) elemental analysis with particle accelerators; (4) use of radioactive (alpha, beta and gamma) sources; and (5) use of radiotracers. The book provides a good balance between rigorous, mathematically-based treatment of theoretical aspects of the subject and reviews of practical applications.

The 5 chapters forming Part 1 provide essential background information on interaction of radiation with matter, instrumentation, radiation sources, prompt and delayed measurements and radiation protection. Part 2, containing 4 chapters devoted to the use of neutrons in chemical analysis, includes detailed consideration of the various methods of neutron activation analysis and descriptions of neutron thermalization, scattering and absorption techniques. Part 3, with 5 chapters, deals with analysis using particle accelerators and includes charged particle activation analysis, charged particle scattering and recoil methods, particle induced X-ray emission and microprobes. In Part 4, which contains 4 chapters, descriptions are given of the use of radioactive sources for X-ray fluorescence analysis, radiation scattering techniques, Mossbäuer spectroscopy and analytical methods based upon positron annihilation. Finally, Part 5 has two chapters dealing with isotope dilution analysis and radio-immunoassay.

'This text, written by a group of 25 specialist authors from ten different countries, provides a comprehensive review of the wide range of nuclear techniques that can be employed in chemical analysis.'

The last two decades have seen a rapid expansion in the use of nuclear techniques for analytical purposes and this book provides a valuable addition to the literature by bringing together descriptions of more than 70 of such methods (and their acronyms). The growing importance of nuclear analytical methods is indicated by the applications described in a diverse range of disciplines including medicine, biology, environmental studies, agriculture, geology, archaeology, metallurgy, semiconductors, on-line production monitoring, nuclear fuel analysis, monitoring of nuclear fuel storage pond water, oil-well borehole logging and airport security.

The text is generally well written, but with a surprising number of typographic errors and considerable variations in style and ease of reading between chapters. There is some degree of repetition of aspects that are common to more than one method (*e.g.*, radiation sources and instrumentation) but this has been minimized to a level consistent with making each chapter self contained. This book, providing a detailed, quantitative treatment of the subject matter, will primarily be of value to chemists and physicists at honours degree or research level and would be a useful addition to appropriate libraries or for individual use by those actively involved in this area. The background information and descriptions of appli-cations will also be of considerable value for 'customers' in other disciplines who make use of the analytical methods.

A. B. MacKenzie
Scottish Universities Research & Reactor Centre
Glasgow, UK

Flame Chemiluminescence Analysis by Molecular Emission Cavity Detection
Edited by David Stiles, Anthony Calokerinos and Alan Townshend. *Volume 129 in Chemical Analysis: A Series of Monographs on Analytical Chemistry and its Applications.* Series Editor, J. D. Windfordner. Pp. vii + 206. Wiley. 1994. Price £50.00. ISBN 0-471-94340-1.

Molecular emission cavity analysis (MECA) was first reported in 1973 by Belcher, Bogdanski and Townshend. It was developed from a qualitative flame test for bismuth (from Feigl's Spot Tests in Inorganic Analysis) which, when mixed with alkaline earth carbonates, gives a cornflower-blue colouration to a hydrogen flame. This phenomenon is now known as candoluminescence and MECA is essentially the quantitative measurement of this phenomenon. The sulfur/phosphorus detector (flame photometric detector) used in gas chromatography is probably the most well known example of qualitative analysis based on emissions from cool hydrogen-based flames. For the potential user, MECA instrumentation is no longer commercially produced but purpose built appa-ratus can be constructed relatively easily from a flame photometer.

'Recommended for its complete coverage of the historical development and current status of MECA and for the obvious enthusiasm that the contributors have for the technique'.

The major attraction of the technique is its good sensitivity for non-metals, particularly sulfur, phosphorus and the halides, a fact that is emphasized by the contents of this book. The first three chapters cover historical aspects, basic principles, instrumentation and automation. Particularly important in this regard is the design of the cavity itself, which is most commonly a metallic or carbon rod in which a small aperture is cut to accommodate the sample. The remaining four chapters cover in detail the application of the technique to the determination of various groups of compounds, namely; sulfur, selenium and tellurium; arsenic, antimony, boron, silicon, germanium and tin; nitrogen, phosphorus and carbon; and halogens and metals. The most significant aspects of these chapters are that the technique can be used for analysis of solids (as well as gases and liquids), *e.g.*, sulfur in coal, and for the speciation of elements, *e.g.*, the determination of organic and inorganic species containing phosphorus and the analysis of S^{2-}, SO_3^{2-} and SO_4^{2-} in a single run.

This book, which is volume 129 in the *Chemical Analysis* series published by Wiley, is well presented and easy to read and is the only comprehensive account of a niche technique in atomic spectrometry. It may well be that with modern array detectors there is some scope for revisiting a technique that is currently pursued by a small but dedicated band of research-ers. The reference lists cited at the end of each chapter show that there was a steady output of papers throughout the 1970s and 1980s.

It is recommended for its complete coverage of the historical development and current status of MECA and for the obvious enthusiasm that the contributors have for the technique.

P. J. Worsfold
Department of Environmental Sciences
University of Plymouth, UK

Fluorescent Chemosensors for Ion and Molecule Recognition
Edited by Anthony W. Czarnik. *ACS Symposium Series 538*. Pp. x + 236. Price US $69.95. American Chemical Society. 1994. ISBN 0-8412-2728-4.

This book, developed from a symposium of similar title, contains a series of specialist papers consisting of past and current research plus reviews on the topic, and is written by experts from a wide range of fields. It is presented in a camera ready type publication format in order that the symposium papers could be published as soon as possible. All papers address the fluorescent chemosensor field and the valuable contributions that synthetic organic chemists can make to this important technology. Application papers deal with sensing of many biological analytes of importance in the biomedical field. The book, on the whole, stresses the need for the design and synthesis of a wide variety of receptors for ions and molecules, and the need for more basic research to accomplish and realise working chemosensory systems.

'The book stresses the need for the design and synthesis of a wide variety of receptors for ions and molecules, and the need for more basic research to accomplish and realise working chemosensory systems'.

The book contains 13 chapters, all dealing with some fundamental aspect of fluorescent chemosensors. Chapter 1 deals with the basics of supramolecular chemistry, fluorescence and sensing supported by an excellent bibliography. The synthesis of crown ether-type reagents are discussed in Chapter 2 with a view to develop alkali metal ion sensors and also includes a discussion on the different schemes used to accomplish this. Chapters 3 and 4 present comprehensive notes on the detection of ions and molecules using photo-induced energy transfer mechanisms. Molecular recognition of organic compounds are discussed in Chapters 5 and 6; while the former discusses a variety of new supramolecular systems with fluorescence emission of the receptor molecule tunable to the guest molecule, the latter presents molecular recognition by the use of chromophore modified cyclodextrin molecules. Both chapters emphasize the structural aspects of recognition molecules. Chapter 7 deals with the incorporation of chromophores and fluorophores into the structure of a synthetic molecular receptor resulting in 'intrinsic' chemosensor systems. Chapter 8 discusses the mechanisms of recognition and of fluorescent signal transduction using a variety of examples involving guests such as cations, anions and carbohydrates. Chapters 9 to 11 discuss, in somewhat detail, the use of fluorescent probes for the detection and measurements of ions/molecules in cells and blood, particularly calcium and potassium ions. Chapter 12 similarly discusses the use/application of fluorescent probes in studies pertaining to proteases. Finally, Chapter 13 is devoted to sensors based on fluorescence lifetime measurements with discussions on the advantages of the technique by the use of flow-cytometry and its potential use in fluorescence microscopy. The references

provided at the end of each chapter are fairly comprehensive and cover the literature up to 1992.

This book provides information of great value of those involved, or those that wish to become involved in the field of optical fluorescence based sensors, and is considered to be a useful reference text. The material is well presented and the choice of topics reflects a good balance. The book has been produced in hardback form and is priced at a reasonable level for a book of this type. It is highly recommended.

R. Narayanaswamy
Department of Instrumentation and Analytical Science
UMIST, Manchester

LIMS: Implementation and Management
By Allen S. Nakagawa. Pp. xiv + 180. Royal Society of Chemistry. 1994. Price £37.50. ISBN 0-85186-824-X.

The preface of the text has some well chosen aims for the volume. It asks, in respect of Laboratory Information Management Systems (LIMS), the following questions. Are the costs justified? Do they make organizations stronger or do they just increase overheads? Are LIMS only appropriate for certain laboratories? How should the technology be evaluated and implemented?

The measure of the book's value is best judged by how well the above are answered. For many laboratories (deciding on LIMS purchase) the purchase decision is made on the basis of a consultant's investigation and report. The book could well be regarded as a consultant's methodology and would form a sound basis for a laboratory manager to perform a DIY exercise on LIMS purchase and implementation.

The book contains several potentially interesting case studies, but deals with them in a superficial manner, which contrasts with its more comprehensive approach to the issues surrounding LIMS. One case study cites the software development needing 25 years of effort, but with a projected benefit of 15 to 20 years of effort per year, both difficult concepts to digest in that type of unit measure. Another study suggests an over-all productivity improvement of 30%, with payback of the system occurring within one year. The studies are there to attempt to answer the question; are LIMS costs justified and the intended answer is that for some laboratories they appear to be cost effective. Other examples suggest an increase in workload concomitant with staff reduction. In those instances one is left pondering if the LIMS introduction may have provided a convenient opportunity for re-organization, thus, clouding the actual benefits of the LIMS introduction.

'The book is genuinely honest and helpful in its treatment of common misconceptions of LIMS introduction'.

A chapter is devoted to the effects of LIMS on the laboratory operation and includes consideration on individual work patterns and methods of work. This is a novel and useful piece of narrative to those who live in a laboratory environment, but one suspects the ideas are closely derived from manufacturing industry and the impact of automation. The book is genuinely honest and helpful in its treatment of common misconceptions of LIMS introduction. The book adequately demonstrates LIMS strengthening of laboratory management, simply by the availability of timely and useful information. Without such systems, how many large laboratories would accurately know their workload and current output?

In respect of technology employed, LIMS are simply a reflection of general hardware and software computer development. Nothing is demonstrated in the text that shows LIMS to be unique or especially demanding in the technology applied.

The text is a useful and essential aid in laboratory management (with or without LIMS) and I recommend it to all concerned with labratory management.

David Best
Yorkshire Water
Bradford, UK

The Colloidal Domain: Where Physics, Chemistry, Biology and Technology Meet
By D. Fennel Evans and Håkån Wennerström. Pp. xxxii + 516. VCH (Weinheim). 1994. Price. DM98.00. ISBN 1-56081-525-6.

Every book naturally reflects the interests of the author(s), and this one is no exception. Evans and Wennerström have approached their explanation of 'The Colloidal Domain' by concentrating on association colloids formed by molecular self-assembly, rather than relying on the more traditional lyophobic colloids as examples. The book is based on lectures given by the authors at the University of Minnesota and its primary value will be as an aid for teaching colloid science in university or college courses. It forms part of the *Advances in Interfacial Engineering Series* published by VCH Publishers.

As a text book, it covers the usual aspects found in 'traditional' works, albeit in the unconventional style of approaching colloid and interface science from the different perspective of self-assembled structures. The authors have taken the trouble to explain their reasoning behind this approach. To aid learning, the authors have used sentences/statements as chapter headings and sub-headings, and the provision of 'concept maps' summarizing the contents of each chapter. At the end of each chapter, examples/questions (which are particularly useful) and a limited bibliography based on established texts are provided.

To anyone experienced in the field, this book offers limited new material or interpretation. Some areas have been covered well, especially the treatment of colloidal forces, phase behaviour, solvency, micellization and the role of polymers in colloid science, whereas other aspects normally regarded as being fundamental to the subject, have been given less attention. For example, even considering their technological importance, lyophobic colloids have mainly been used to illustrate principles, and the authors have avoided dealing specifically with experimental methods in their own right, preferring instead to describe or discuss techniques where and when they are associated with, or relevant to, a particular topic. In taking this approach, some discussions are far from comprehensive, *e.g.*, rheology is briefly covered in connection with polymer systems, and in the section on surface/interfacial tension, only passing reference is made to the importance of 'dynamic' surface effects, with no reference being made to the measurement of dynamic tensions.

'Students of colloid science may benefit from its modern style, and the principles which it describes are sound. For the more experienced reader or researcher, however, it is unlikely to displace established texts as a reference book.'

Even though amphiphiles provide the foundation of the book, discussion on commercial aspects and applications (technology) of surfactants are largely absent (the HLB concept, however fragile it may be regarded, is mentioned once!). In fact, as one attracted by the title, I was disappointed that examples of the meeting of physics, chemistry, biology and (unashamedly as an industrialist, especially) technology that have been discussed in any detail in 'The Colloidal Domain' are themselves only dispersed very thinly throughout the 500+ pages.

In their introduction, the authors observe, rightly in my opinion, that 'Nearly all industrial processes involve colloidal systems'. However, the attention given to association colloids has restricted the scope of the book almost exclusively to aqueous-based systems, with some brief excursions into the realms of polar non-aqueous solvent systems, in line with the authors' interests. A further disappointment is that little or no consideration has been given to non-polar systems which, arguably, form the basis of many industrial processes and products which 'involve colloidal systems.'

Notwithstanding the shortcomings of this book in terms of content and approach, 'The Colloidal Domain' has been well-produced, with newcomers to the subject in mind. Students of colloid science may benefit from its modern style, and the principles which it describes are sound. For the more experienced reader or researcher, however, it is unlikely to displace established texts as a reference book.

S. E. Taylor
Applied Science Group
BP Research and Engineering Centre
Middlesex, UK

Environmental Analysis
By Roger N. Reeve. *Analytical Chemistry by Open Learning.* Pp. xx + 264. Wiley. 1994. Price £19.50. ISBN 0-471-93833-5.

Environmental Analysis is one of a series of *ACOL (Analytical Chemistry by Open Learning)* books, of which there are already 32 books and 8 computer-based packages. The books are designed to be easy to read and are for training, continuing education and updating in the various fields of analytical chemistry. Details are given in the book about how to achieve full benefit from them.

In addition to a study guide and bibliography the book discusses the reasons for concern about the environment and has chapters on the transport of pollutants in the environment, the analysis of water (both for main components and for trace analysis), analysis of gases, of solids, of particulates in the atmosphere, and a chapter about ultra-trace analysis.

Throughout the book there are numerous small 'boxes' containing 'self-assessment questions' pertinent to the immediate text, spaces being left, presumably, for the answers and for discussion.

'The importance of careful and meaningful sampling procedures is stressed throughout, and types of samplers and analysers are discussed where relevant'.

Analytical techniques to which references are made in this book, and of which a basic knowledge by the reader is assumed, include: atomic absorption spectrometry and fluorescence; chemiluminescence; inductively coupled plasma–mass spectrometry; inductively coupled plasma–optical emission spectrometry; gas, ion, and high-performance liquid chromatography; emission and X-ray spectrometry; and infrared spectrometry, among others.

The importance of careful and meaningful sampling procedures is stressed throughout, and types of samplers and analysers are discussed where relevant. There are numerous useful illustrations throughout, some of which appear to be hand drawings (with rather an unusual perspective shown in the drawing of Kjeldahl apparatus).

There appears to be an error in the formula shown for *o,p'*-DDT inasmuch as an additional chlorine is included, and this affects the example illustrating increase of water solubility. Nevertheless, this is a useful little book, not over-expensive, and I would recommend it for purchase by people involved in such environmental studies and by libraries (although it is not to be expected that the latter would appreciate borrowers writing or drawing in the book in the spaces provided).

D. Simpson
Analysis For Industry
Essex, UK

Cationic Surfactants. Analytical and Biological Evaluation

An earlier volume on cationic surfactants in the *Surfactant Science Series* devoted 64 pages to analytical evaluation but now John Cross, the author of that 1970 review and co-editor of this new volume, has assembled a group of authors whose chapters on analysis cover 232 pages. This expansion demonstrates not only the improvement in analytical techniques but also the increasing importance of being able to detect and analyse cationic surfactants in particular.

Although cationic surfactants have a wider variety of applications than any other type of surfactant their share of the total surfactant market is less than 10%. Nevertheless, annual usage is several hundred kilotonnes and is still rising. Most of this comes from the use of cationic surfactants as textile conditioners and fabric softeners. However, the biological activity of cationic surfactants, which incidentally gives them several useful applications, produces a greater risk of environmental damage than with anionic and non-ionic surfactants and it is for this reason that analysis of cationics has received increasing attention.

The biological aspects are dealt with in the section edited by Edward Singer. Chapters on 'Biological Properties and Applications of Cationic Surfactants' (Fredell), 'Current Topics on the Toxicity of Cationic Surfactants' (Drobeck), and 'Environmental Aspects of Cationic Surfactants' (Boethling) give comprehensive coverage of properties, test methods and references.

'An essential addition to the libraries of any institution; academic, research or industrial, that has an interest in cationic surfactants.'

The second section covers analytical evaluation. Chapters written by experienced practitioners on 'Volumetric Analysis' (Cross), 'Potentiometry' (Moody and Thomas), 'Tensammetric Determination' (Bos), 'Analysis of Low Concentrations of Cationic Surfactants in Laboratory Test Liquors and Environmental Samples' (Waters), 'Mass Spectrometry' (Kalinoski), 'Chromatography' (McPherson and Rasmussen), and 'Molecular Spectroscopy' (Mozayeni) will be useful to anyone planning to analyse cationic surfactants in almost any system. Important practical details specific to cationic surfactants, such as ways of overcoming the interfering effects of ubiquitous anionic surfactant and the difficulties caused by the surfactant's propensity to adsorb strongly on solid surfaces, are adequately described.

This book is a valuable addition to the *Surfactant Science Series* and a useful companion to Volume 37 ('Cationic Surfactants; Physical Chemistry'). Its cost is likely to deter private owners but it should be an essential addition to the libraries of any institution; academic, research or industrial, that has an interest in cationic surfactants.

B. T. Ingram
Procter & Gamble Limited
Newcastle Upon Tyne, UK

Solution Calorimetry

Some years ago calorimetry was a branch of research that was pursued in a reasonable number of University Research Schools in Chemistry within the UK. This area of research has seen a decline in interest within the UK and most development and interest is now shown by continental Europeans, together with American and East European colleagues. Perhaps the time has arrived for there to be a resurgence in calorimetry in the UK, although the volume reviewed here has (strictly) only one contributor from the UK. Proving that the subject is very much alive and perceived as important is evidenced by the appearance of these IUPAC sponsored volumes.

'rich variety of material to be found within this volume, however, the information is for the specialist'

This book, the fourth in the series, is a pleasure to review. It, like the previous volumes, has an impressive list of contributors; all experts in the field. The contributions range widely from; Reduction to Standard States (Vanderzee: to whom, together with Stanley Gill, the book is dedicated) through Excess Enthalpies by Flow Microcalorimetry (Ott and Wormald) *via* Aqueous and Biological Systems (Wadso) to Calorimetric Determination of Pressure Effects (Randzio). This, incomplete, listing gives some idea of the rich variety of material to be found within this volume. It also, however, gives a clear indication that the information is for the specialist although the calorimetrist with a desire to be informed over the range of solution phase calorimetry should emerge from reading this book well informed and stimulated. Necessarily in a book of this coverage of a particular, and hugely important area, a reviewer can find some, albeit small, deficiencies. Amongst these I am surprised at the rather limited coverage given to titration calorimetry, especially in the area of biological studies, given the appearance of high sensitivity, rapid titration equipment. This small objection apart, the book is welcomed as a most useful addition to, in the main, library shelves.

A. E. Beezer
Chemical Laboratory
The University, Canterbury, Kent, UK

Conference Diary

Date	Conference	Location	Contact
1995 **May**			
3	**New Techniques in Bioanalysis**	Bradford, UK	**A. J. Crooks,** 'Cartref', 35 Queensbury Road, Salisbury, Wiltshire, UK SP1 3PH **Tel:** +44 (0)1722 334974.
7–10	**Handling of Environmental and Biological Samples in Chromatography**	Lund, Sweden	**Mrs. M. Frei-Häusler,** Postfach 46, CH-4123 Allschwil 2, Switzerland **Fax:** +41 61 482 0805
7–11	**86th AOCS Annual Meeting & Expo**	Texas, USA	**AOCS Education/Meetings Department,** P.O. Box 3489, Champaign, IL 61826-3489, USA **Tel:** +1 217 359 2344. **Fax:** +1 217 351 8091
7–11	**Seventeenth International Symposium on Capillary Chromatography and Electrophoresis**	Virginia, USA	**Dr. Milton L. Lee,** Department of Chemistry, Brigham Young University, Provo, UT 84602-4672, USA **Tel:** +1 801 378 2135. **Fax:** +1 801 378 5474
9–12	**Metal Compounds in Environmental and Life Sciences 6—Analysis, Speciation and Specimen Banking**	Jülich, Germany	**H. W. Dürbeck,** Institute of Applied Physical Chemistry, Research Center Jülich (KFA), P.O. Box 1913, D-5170 Jülich, Germany
14–18	**EMAS 95 on Modern Developments and Applications in Microbeam Analysis**	St Malo, France	**EMAS Secretariat,** RIKILT-DLO, P.O. Box 230, 6700 AE Wageningen, The Netherlands
16–18	**Fourth International Conference on Progress in Analytical Chemistry in the Steel and Metals Industry**	Luxembourg	**R. Jowitt,** British Steel plc, Technical, Teesside Laboratories, P.O. Box 11, Grangetown, Middlesbrough, Cleveland, UK TS6 6UB **Fax:** +44 (0)1642 460321
20–24	**Electron Microscopy in Solid State Science**	Lund, Sweden	**A. Sjögren,** The Swedish National Committee for Chemistry, Walligatan 24 3 Tr, 11124 Stockholm, Sweden
21–25	**ASMS Conference on Mass Spectrometry**	Atlanta, USA	**ASMS,** 815 Don Gaspar, Santa Fe, NM 87501, USA **Tel:** +1 505 989 4517
21–26	**CLEO '95: Conference on Lasers and Electro-Optics**	Baltimore, USA	**Meetings Department,** Optical Society of America, 2010 Massachusetts Avenue, NW, Washington, DC 20036-1023, USA **Tel:** +1 202 223 9034. **Fax:** +1 202 416 6100
21–26	**QELS '95: Quantum Electronics and Laser Science Conference**	Baltimore, USA	**Meetings Department,** Optical Society of America, 2010 Massachusetts Avenue, NW, Washington, DC 20036-1023, USA. **Tel:** +1 202 223 9034. **Fax:** +1 202 416 6100
22–24	**Eighth International Symposium on Polymer Analysis and Characterization (ISPAC-8)**	Sanibel Island, USA	**ISPAC Registration,** 815 Don Gaspar, Sante Fe, NM 87501, USA **Tel:** +1 505 989 4735. **Fax:** +1 505 989 1073
28–2/6	**19th International Symposium on Column Liquid Chromatography**	Innsbruck, Austria	**HPLC '95 Secretariat,** Tyrol Congress, Marktgraben 2, A-6020 Innsbruck, Austria **Tel:** +43 512 575600. **Fax:** +43 512 575607
June			
5–7	**Image Techniques and Analysis in Fluid Mechanics**	Rome, Italy	**A. Cehedese,** Department of Mechanics and Aeronautics, University La Sapienza, Via Eudossiana 18, 00184 Rome, Italy
5–8	**5th Symposium on our Environment and 1st Asia–Pacific Workshop on Pesticides**	Convention City, Singapore	**The Secretariat,** 5th Symposium on our Environment, c/o Department of Chemistry, National University of Singapore, Kent Ridge, Republic of Singapore 0511 **Fax:** +65 779 1691
6–9	**8th International Symposium on Loss Prevention and Safety Promotion in the Process Industries**	Antwerp, Belgium	**The Organising Committee,** 8th International Symposium on Loss Prevention, c/o Ingenieurshuis V2W, Desguinlei 214, B-2018 Antwerpen, Belgium

Date	Conference	Location	Contact
7	**Joint Meeting of the Molecular Spectroscopy Group and the Infrared and Raman Discussion Group—Vibrational Spectroscopy and Imaging**	Oxford, UK	**Dr. J. M. Chalmers,** ICI plc, Wilton Research Centre, P.O. Box 90, Wilton, Middlesbrough, UK TS90 8JE
7–9	**LIMS 95—International Conference and Exhibition**	Bonn, Germany	**JAY Conference Services,** 45 Hilltop Avenue, Hullbridge, Hockley, Essex, UK SS5 6BL
11–14	**1995 International Symposium, Exhibit and Workshops on Preparative Chromatography, Ion Exchange, and Adsorption/Desorption Processes**	Washington DC, USA	**Mrs. Janet Cunningham,** PREP '95 Symposium/ Exhibits Manager, Barr Enterprises, 10120 Kelly Road, P.O. Box 279, Walkersville, MD 21793, USA **Tel:** +1 301 898 3772. **Fax:** +1 301 898 5596
12–16	**50th Annual Molecular Spectroscopy Symposium**	Columbus, USA	**T. A. Miller,** International Symposium on Molecular Spectroscopy, Department of Chemistry, Ohio State University, 120 West 18th Avenue, Columbus, Ohio 43210, USA
13–16	**ESIS 95—New Infrared Spectroscopy and Microspectroscopy: FTIR and Raman**	Lyon, France	**G. Lachenal,** Laboratoire des Materiaux Plastiques et Biomateriaux, Université Claude Bernard Lyon 1, 43 Boulevard du 11 Novembre, 69622 Villeurbanne Cedex, France

July

Date	Conference	Location	Contact
2–6	**VII International Congress of Toxicology**	Seattle, USA	**Jada Hill,** The Sterling Group, 9393 W, 110th Street, Suite, Overland Park, KS 66210, USA **Tel:** +1 913 345 2228. **Fax:** +1 913 345 0893
2–7	**12th International NMR Meeting**	Manchester, UK	**Dr. J. E. Gibson,** Royal Society of Chemistry, Burlington House, Piccadilly, London, UK W1V 0BN
9–13	**3rd International Symposium on Applied Mass Spectrometry in Health Sciences and 3rd European Tandem Mass Spectrometry Conference**	Barcelona, Spain	**Professor Emilio Gelpi,** Palau de Congressos, Departamento de Convencions, Avda, Reina Ma Christina, 08004 Barcelona, Spain
9–14	**13th Australian Symposium on Analytical Chemistry/4th Environmental Chemistry Conference**	Darwin, Australia	**13AC/4EC, Symposium Secretariat,** Convention Catalyst Int., GPO Box 2541, Darwin NT 0801, Australia **Tel:** +61 89 811 875. **Fax:** +61 89 411 639
9–15	**SAC 95**	Hull, UK	**Analytical Division,** The Royal Society of Chemistry, Burlington House, Piccadilly, London, UK W1V 0BN **Tel:** +44 (0)171 437 8656. **Fax:** +44 (0)171 734 1227
10–13	**Vth COMTOX Symposium on Toxicology and Clinical Chemistry of Metals**	Vancouver, Canada	**F. William Sunderman, Jr., M.D.,** Departments of Laboratory Medicine and Pharmacology, University of Connecticut Medical School, P.O. Box 1292, Farmington, CT 06034-1292, USA **Tel:** +1 203 679 2328. **Fax:** +1 203 679 2154
30–5/8	**XXIInd International Conference on Phenomena in Ionized Gases**	Hoboken, USA	**E. E. Kunhardt,** Physics Department, Stevens Institute of Technology, Hoboken, NJ 07030 USA **Tel:** +1 201 216 5099. **Fax:** +1 201 216 5638

August

Date	Conference	Location	Contact
5–10	**1995 International Symposium on Soil and Plant Analysis**	Wageningen, The Netherlands	**Soil and Plant Analysis Council,** Georgia University Station, P.O. Box 2007, Athens, GA 30612-2007, USA **Tel:** +1 706 546 0425. **Fax:** +1 706 548 4891
6–11	**NIR '95—The Future Waves**	Montreal, Canada	**NIR '95, The Canadian Grain Commission,** Grain Research Laboratory, 1403-303 Main Street, Winnipeg, Manitoba, Canada R3C 3G8
13–17	**ICFIA '95, 7th International Conference on Flow Injection Analysis and JAFIA, Japanese Association for Flow Injection Analysis**	Seattle, USA	**Gary D. Christian,** Department of Chemistry, BG-10, University of Washington, Seattle, WA 98195, USA **Tel:** +1 206 685 3478. **Fax:** +1 206 543 5340. **E-Mail:** christia@chem.washington.edu
14–16	**41st International Conference on Analytical Science and Spectroscopy**	Windsor, Canada	**William E. Jones,** Department of Chemistry and Biochemistry, University of Windsor, Windsor, Ontario, Canada N9B 3P4

Date	Conference	Location	Contact
20–25	**12th International Symposium on Plasma Chemistry**	Minneapolis, USA	**L. Graven,** 315 Pillsbury Drive, SE, University of Minnesota, Minneapolis, MN 55455-0139, USA **Tel:** +1 612 625 9023. **Fax:** +1 612 626 1623
27–2/9	**CSI XXIX: Colloquium Spectroscopicum Internationale**	Leipzig, Germany	**GDCh-Geschäftsstelle, Abt. Tagungen,** Varrentrappestr. 40–42, Postfach 90 04 40, D-6000 Frankfurt am Main 90, Germany **Tel:** +49 69 791 7358. **Fax:** +49 69 791 7475
27–1/9	**46th Annual Meeting of the International Society of Electrochemistry (ISE46)**	Xiamen, China	**Secretariat,** XLVIth ISE Annual Meeting, P.O. Box 1995, Xiamen University, Xiamen 361005, China **Tel:** +86 592 208 5349. **Fax:** +86 592 208 8054
27–1/9	**Third International Conference on Magnetic Resonance Microscopy**	Würzburg, Germany	**Dr. A. Haas,** Physikalisches Institute, Universität Würzburg, Am Hubland, D-97074 Würzburg, Germany
27–30	**EUROTOX**	Prague, Czech Republic	**Czech Medical Association J. E. Purkyně,** EUROTOX '95, P.O. Box 88, Sokolská 31, 120 26 Prague 2, Czech Republic **Tel:** +42 2 24 915195. **Fax:** +42 2 24 216836

September

Date	Conference	Location	Contact
1–4	**CSI XXIX, Post-symposium ICP-MS and 11th German ICP-MS Users Meeting**	Wernigerode, Germany	**Professor Lieselotte Moenke,** Department of Chemistry, Martin-Luther University, Halle-Wittenberg, Institute of Analytical and Environmental Chemistry, Weinbergweg 16, D-06120 Halle, Germany
3–6	**Third International Meeting on Recent Advances in Magnetic Resonance Application to Porous Media**	Louvain la Neuve, Belgium	**Professor J. M. Dereppe,** Université de Louvain, Place L. Pasteur 1, B-1348, Louvain la Neuve, Belgium
3–8	**6th European Conference on the Spectroscopy of Biological Molecules**	Villeneuve d'Ascq, France	**Professor J. C. Merlin,** ECSBM '95, LASIR, UST Lille Bât. C5, 59655 Villeneuve d'Ascq Cedex, France
5–8	**RSC Autumn Meeting. Analytical and Faraday Symposium: Ions in Solution**	Sheffield, UK	**Dr. J. F. Gibson,** The Royal Society of Chemistry, Burlington House, Piccadilly, London, UK W1V 0BN **Tel:** +44 (0)171 437 8656. **Fax:** +44 (0)171 734 1227
6–8	**5th Symposium on Chemistry and Fate of Modern Pesticides**	Paris, France	**Mrs. Frei-Häusler,** IAEAC Office, Postfach 46, CH-4123 Allschuril 2, Switzerland **Fax:** +41 61 482 08 05
6–9	**Joint Meeting of the Royal Society of Chemistry Fast Reactions in Solution Discussion Group and the Molecular Spectroscopy Group on Ultrafast Processes in Laser Spectroscopy**	Norwich, UK	**Professor B. H. Robinson,** School of Chemical Sciences, University of East Anglia, Norwich, UK NR4 7TJ
10–14	**Ion-Ex '95, The Fourth International Conference and Industrial Exhibition on Ion Exchange Processes**	Wrexham, UK	**Ion-Ex '95 Conference Secretariat,** Faculty of Science, The North East Wales Institute, Connah's Quay, Deeside, Clwyd, UK CH5 4BR **Fax:** +44 (0)1244 814305
12–15	**5th International Symposium on Drug Analysis**	Leuven, Belgium	**Professor J. Hoogmartens,** Institute of Pharmaceutical Sciences, Van Evenstraat 4, B-3000 Leuven, Belgium **Tel:** +32 16 32 34 40. **Fax:** +32 16 32 34 48
12–16	**European Symposium on BiOS Europe '95: The European Biomedical Optics Symposium Week**	Barcelona, Spain	**Ms. Karin Burger,** BiOS Europe '95, EUROPTO Series, c/o Direct Communications GmbH, Xantener Strasse 22, D-10707 Berlin, Germany **Tel:** +49 30 881 50 47. **Fax:** +49 30 881 50 40 **E-Mail:** Burger,100140.3211@compuserve.com
17–20	**6th Surrey Conference on Plasma Source Spectrometry**	Jersey, UK	**Dr. Kym Jarvis,** NERC ICP-MS Facility, CARE, Imperial College, Silwood Park, Ascot, Berkshire, UK SL5 7TE **Tel:** +44 (0)1344 294517/6. **Fax:** +44 (0)1344 873997

Date	Conference	Location	Contact
17–21	**109th AOAC International Annual Meeting and Exposition**	Tennessee, USA	**Meetings and Education Department,** AOAC International, 2200 Wilson Boulevard, Suite 400, Arlington, Virginia, 22201-3301, USA **Tel:** +1 703 522 3032.
24–28	**11th Asilomar Conference on Mass Spectrometry—Molecular Structure Determination: Activation, Mass Analysis and Detection**	Pacific Grove, USA	**Professor R. Graham Cooks,** Department of Chemistry, 1393 Brown Building, Purdue University, West Lafayette, IN 47907, USA
25–28	**5th Symposium on 'Kinetics in Analytical Chemistry' (KAC '95)**	Moscow, Russia	**Dr. I. F. Dolmanova,** Analytical Chemistry Division, Chemical Department, Lomonosov Moscow State University, 119899 Moscow, Russia **Tel:** +7 095 939 3346. **Fax:** +7 095 939 2579

October

Date	Conference	Location	Contact
1–5	**21st World Congress of the International Society for Fat Research (ISF)**	The Hague, The Netherlands	**Mrs. J. Wills,** ISF Secretariat, P.O. Box 3489, Champaign, IL 61826–3489, USA **Tel:** +1 217 359 2344. **Fax:** +1 217 351 8091
9–13	**ECASIA '95**	Montreux, Switzerland	**EPEL-ECASIA 95,** Department des Materiaux/ LMCH, CH-1015 Lausanne, Switzerland **Fax:** +41 21 693 3946
15–20	**22nd Annual Conference of the Federation of Analytical Chemistry and Spectroscopy Societies**	Cincinnati, USA	**Joseph A. Caruso,** FACSS National Office, 198 Thomas Johnson Dr., Suite S-2, Frederick, MD 21702, USA **Tel:** +1 301 694 8122. **Fax:** +1 301 694 6860
19–20	**Biotechnology Now and Tomorrow**	Bucharest, Romania	**Mrs. Gestiana Munteanu,** Biotechnos S.A., Str. Dumbrava Rosie, nr. 18, Bucuresti 70254, Romania **Tel:** +40 1 210 20 15. **Fax:** +40 1 210 97 05
24–27	**BCEIA '95—The International Sixth Beijing Conference and Exhibition on Instrumental Analysis**	Beijing, China	**General Service Office,** The International Sixth BCEIA, Room 585, Chinese Academy of Science Room, San Li He, Xi Jiao, P.O. Box 2143, Beijing 100045, China
26–27	**Sensors and Signals**	County Dublin, Ireland	**Dr. D. Diamond,** School of Chemical Sciences, Dublin City University, Glashevin, Dublin, Ireland **Tel:** +353 1 704 5308. **Fax:** +353 1 704 5503

November

Date	Conference	Location	Contact
5–10	**1st Mediterranean Basin Conference on Analytical Chemistry**	Cordoba, Spain	**Professor Alfredo Sanz-Medel,** Department of Physical and Analytical Chemistry, Faculty of Chemistry, University of Oviedo, C/Julían Clavería, no. 8 33006 Oviedo, Spain **Tel:** +34 85 10 34 74. **Fax:** +34 85 10 31 25
5–10	**OPTCON '95**	San Jose, USA	**Meetings Department,** Optical Society of America, 2010 Massachusetts Avenue, NW, Washington, DC 20036-1023, USA **Tel:** +1 202 223 9034. **Fax:** +1 202 416 6100
8–9	**Biological Applications of Inorganic Mass Spectrometry**	Norwich, UK	**Institute of Food Research,** Norwich Laboratory, Norwich Research Park, Colney Lane, Norwich, UK NR4 7UA
14–15	**International Conference for Chemical Information Users**	Manchester, UK	**Dr. M. P. Coward,** Chemistry Department, UMIST, P.O. Box 88, Manchester, UK M60 1QD **Tel:** +44 (0)161 200 4491. **Fax:** +44 (0)161 228 1250

December

Date	Conference	Location	Contact
17–22	**International Symposium on Environmental Biomonitoring and Specimen Banking**	Hawaii, USA	**K. S. Subramanian,** Environmental Health Directorate, Health Canada, Tunney's Pasture, Ottawa, Ontario, Canada K1A OL2 **Tel:** +1 613 957 1874. **Fax:** +1 613 941 4545
20–21	**2nd LC/MS Symposium**	Cambridge, UK	**Dr. J. Oxford,** Glaxo Research and Development, Park Road, Ware, Hertfordshire, UK SG12 0DJ

Date	Conference	Location	Contact

1996
January

8–13	**1996 Winter Conference on Plasma Spectrometry**	Florida, USA	**R. Barnes,** Department of Chemistry, Lederle GRC Tower, University of Massachusettes, P.O. Box 34510, Amherst, MA 01003-4510, USA **Tel:** +1 413 545 2294. **Fax:** +1 413 545 4490
21–25	**VIth Latin American Congress on Chromatography**	Caracas, Venezuela	**Irene Romero,** Interep SA, P.O. Box 76343, Caracas 1070-A, Venezuela

February

6–9	**Fourth International Symposium on Hyphenated Techniques in Chromatography (HTC 4); Hyphenated Chromatographic Analysers**	Bruges, Belgium	**Dr. R. Smits,** Royal Flemish Chemical Society (KVCV), Working Party on Chromatography, BASF Antwerpen N.V., Central Laboratory, Haven 725, Scheldelaan 600, B-2040 Antwerp, Belgium **Tel:** +32 3 561 2831. **Fax:** +32 3 561 3250

March

17–21	**47th Pittsburgh Conference on Analytical Chemistry and Applied Spectroscopy**	Atlanta, USA	**The Pittsburgh Conference,** 300 Penn Center Boulevard, Suite 332, Pittsburgh, PA 15235-5503 USA **Tel:** +1 412 825 3220. **Fax:** +1 412 825 3224
31–4/4	**7th International Symposium on Supercritical Fluid Chromatography and Extraction**	Indianapolis, USA	**Janet Cunningham,** Barr Enterprises, 10120 Kelly Road, P.O. Box 279, Walkersville, MD 21793 USA **Tel:** +1 301 898 3772. **Fax:** +1 301 898 5598

April

9–12	**26th International Symposium on Environmental Analytical Chemistry**	Vienna, Austria	**Professor Dr. M. Grasserbauer,** Institute for Analytical Chemistry, Vienna University of Technology, Getreidemarkt 9/151, A-1060 Wien, Austria **Fax:** +43 1 5867813
23–26	**Analytica Conference '96**	München, Germany	**Congress Center,** Messegelände, D-80325 München, Germany **Tel:** +49 89 5107 159. **Fax:** +49 89 5107 180

May

7–9	**VIIth International Symposium on Luminescence Spectrometry in Biomedical Analysis—Detection Techniques and Applications in Chromatography and Capillary Electrophoresis**	Monte-Carlo, Monaco	**Professor Willy R. G. Baeyens,** University of Ghent, Pharmaceutical Institute, Department of Pharmaceutical Analysis, Harelbekestraat 72, B-9000 Ghent, Belgium **Tel:** +32 9 221 8951. **Fax:** +32 9 221 4175
20–24	**18th International Symposium on Capillary Chromatography**	Riva del Garda, Italy	**Professor D. P. Sandra,** I.O.P.M.S., Kennedypark 20, B-8500 Kortrijk, Belgium **Tel:** +32 56 204960. **Fax:** +32 56 204859
23–25	**XIIIth National Conference on Analytical Chemistry**	Craiova, Romania	**Romanian Society of Analytical Chemistry,** 13 Boulevard Republicii, Sector 3, 70346 Bucharest, Romania **Tel:** +40 1 631 00 60. **Fax:** +40 1 631 00 60

June

16–21	**HPLC '96: 20th International Symposium on High Performance Liquid Chromatography**	San Francisco, USA	**Mrs. Janet Cunningham,** Barr Enterprises, P.O. Box 279, Walkersville, MD 21793, USA **Tel:** +1 301 898 3772. **Fax:** +1 301 898 5596

July

8–12	**XVI International Congress of Clinical Chemistry**	London, UK	**Mrs. Pat Nielsen,** XVIth International Congress of Clinical Chemistry, P.O. Box 227, Buckingham, UK MK18 5PN **Fax:** +44 (0)1280 6487
17–19	**8th Biennial National Atomic Spectroscopy Symposium (BNASS)**	Norwich, UK	**Dr. S. J. Haswell,** School of Chemistry, University of Hull, Hull, UK HU6 7RX **Tel:** +44 (0)1482 465469. **Fax:** +44 (0)1482 466410

Courses

Date	Conference	Location	Contact
1995 **May**			
10	**Education and Training of Chromatographers**	London, UK	**Dr. D. Simpson,** Analysis for Industry, Factories 2/3, Bosworth House, High Street, Thorpe-le-Soken, Essex, UK CO16 0EA **Tel:** +44 (0)1255 861714. **Fax:** +44 (0)1255 662111
17	**Clinical Waste**	Sheffield, UK	**Maria Baldham,** The Division of Adult Continuing Education, The University of Sheffield, 196–198 West Street, Sheffield, UK S1 4ET **Tel:** +44 (0)114 282 5391. **Fax:** +44 (0)114 276 8653
18	**Meat Authenticity: Introduction to Immunoassay Test Kits**	Campden, UK	**Training Department,** Campden Food and Drink Research Association, Chipping Campden, Gloucester, UK GL55 6LD **Tel:** +44 (0)1386 840319. **Fax:** +44 (0)1386 841306
21	**Techniques for Polymer Analysis and Characterization**	Sanibel Island, USA	**Dr. Petr Munk,** Department of Chemistry, University of Texas at Austin, Austin, Texas 78712, USA **Tel:** +1 512 471 4179. **Fax:** +1 512 471 8696
22–25	**Modern Practice of Gas Chromatography**	Pensylvania, USA	**Sally Stafford,** Hewlett-Packard, Little Falls Site, 2850 Centerville Road, Wilmington, DE 19808-1610, USA **Tel:** +1 302 633 8444
30–1/6	**Sixteenth Annual Introductory HPLC Short Course**	Pensylvania, USA	**Bill Champion,** DuPont Merck Pharmaceutical Company, PRF Building, Chambers Works, Deepwater, NJ 08023, USA **Tel:** +1 609 540 4826
June			
5–7	**Advanced HPLC Short Course**	Pensylvania, USA	**Jim Alexander,** Rohm and Haas Laboratories, 727 Norristown Road, Spring House, PA 19477, USA **Tel:** +1 610 619 5226
7–12	**4th Annual Course on Practical Methods of Digestion for Trace Analysis**	Amherst, USA	**Nancy Teranto,** Questron Corporation, 4044 Quakerbridge Road, Mercerville, NJ 08619, USA **Tel:** +1 609 587 6898. **Fax:** +1 609 587 0513
6–7	**Industrial Waste Water Part I**	Sheffield, UK	**Maria Baldham,** The Division of Adult Continuing Education, The University of Sheffield, 196–198 West Street, Sheffield, UK S1 4ET **Tel:** +44 (0)114 282 5391. **Fax:** +44 (0)114 270 8653
6–8	**5th Annual Flow Injection Atomic Spectrometry Short Course**	Amherst, USA	**J. Tyson,** Department of Chemistry, LGRC Tower, University of Massachusetts, Box 34510, Amherst, MA 01003-4510 USA **Tel:** +1 413 545 0195. **Fax:** +1 413 545 4846
8	**DSC Calibration—Temperature, Enthalpy, Heat Capacity Short Course**	Leeds, UK	**Professor Edward Charsley,** Head of the Thermal Analysis Consultancy Service, Leeds Metropolitan University, Calverley Street, Leeds LS1 3HE **Tel:** +44 (0)113 283 3121/3122. **Fax:** +44 (0)113 283 3120
16–20	**Capillary Electrophoresis, Routine Method for the Quality Control of Drugs: Practical Approach**	Montpellier, France	**Professor H. Fabre,** Laboratory of Analytical Chemistry, Faculty of Pharmacy, 15 Avenue Charles Flahault 34060 Montpellier, France **Tel:** +33 67 54 45 20. **Fax:** +33 67 52 89 15
26–30	**Radioisotope Techniques Short Course**	Loughborough, UK	**Dr. P. Warwick,** Department of Chemistry, Loughborough University of Technology, Loughborough, Leicestershire, UK LE11 3TU **Tel:** +44 (0)1509 222585

Conference Report

Geoanalysis 94: An International Symposium on the Analysis of Geological and Environmental Materials*

Geoanalysis 94 attracted more than 120 delegates from 25 countries including the USA, Canada, Australia, Russia, Sweden and the UK. The conference allowed for almost 100 oral and poster presentations embracing a wide field of analytical research.

Although the conference officially opened on Monday, September 19th, the Conference Chairman, Doug Miles (BGS), gave a welcoming address during Sunday evening's drinks reception, provided courtesy of Varian Ltd.

Monday's program was dedicated to the usage, production and development of reference materials. Dr. K. Govindaraju (Geostandards, CRPG), the first invited speaker, presented a lecture illustrating the features and attributes of the GeoStan series of databases. GeoStan allows easy computer access to a reference material database compiled from information collected by an international working group. The database represents over 900 pages of printed text and tables, making information on available geostandards easily accessible *via* computer. This lecture was followed by an invited presentation from Jean Kane (NIST) who highlighted the growing impact of ICP-MS in certifying geochemical reference materials.

The remainder of Monday morning concentrated on the preparation of natural and synthetic reference materials for laboratory use. A particularly interesting lecture was given by Dr. David Cohen from the University of New South Wales, Australia. Dr. Cohen reported on the development of customized synthetic standards with the aim of reducing possible inhomogeneities that could potentially occur in natural geochemical reference materials.

Following a buffet lunch, the afternoon speakers emphasized the need for international cooperation in quality control. Invited lectures were given by Dr. Michael Thompson

(University of London), and also by Dr. Chris Riddle (Management Board Secretariat, Canada) who presented a Canadian perspective. Further presentations were concerned with laboratory programs to ensure reliability and accuracy of data produced. Professor R. K. O'Nions of the University of Cambridge presented the final plenary lecture of the day on 'High Resolution SIMS Instrumentation in the Earth Sciences'. A varied poster display was also available for viewing throughout the day.

On Monday evening, an informal drinks gathering was followed by dinner and an opportunity to attend a workshop on a potential Geoanalytical Accreditation Program led by Dr. Riddle. As an alternative, a midnight bar extension, along with the close proximity of Ambleside allowed an enjoyable end to the day.

Tuesday's first plenary lecture was given by Dr. G. Remond of BRGM, Orleans, who discussed the advantages and limitations of layered and ion-implanted specimens as possible reference materials to calibrate analytical instruments. The lecture program was then streamed to accommodate presentations concerning neutron activation analysis and ion and electron probe techniques. The ion and electron probe stream chaired by Drs. Stephen Reeder (BGS) and Richard Hinton (University of Edinburgh) presented academic research as well as highlighting the commercial applicability of such techniques. Dr. Susan Parry (Imperial College Reactor Centre) and Professor Eiliv Steinnes (University of Trondheim) chaired the neutron activation stream, which included a presentation by Peter Bode of Delft University of Technology describing a developed INAA method that allows multi-element analysis of samples as large as 100 cm in length and 15 cm in diameter. Professor Peter Vaganov of St. Petersburg University illustrated the use of INAA in the study of

Conference delegates outside British Nuclear Fuel's reprocessing plant at Sellafield.

The Conference Dinner at Merewood Country House. Clockwise from left: Dr. K. Gorindaraju, Dr. J. M. Richardson, Dr. P. J. Potts, Ms. G. E. Hall, Mr. D. L. Miles, Dr. C. Riddle and Ms. J. M. Cook.

combustion products from power plants in China and Estonia. On an environmental note, Dr. Marina Frontasyeva (Frank Laboratory of Neutron Physics, Russia) highlighted the role of INAA in the study of mosses, which have been used to study changes in the atmospheric deposition of metals around an iron smelter complex in Northern Norway.

In the afternoon, Professor Iain Thornton (University of London) presented a well-received lecture concerning challenges to the analyst in the assessment of contaminated land. The environmental theme was continued throughout the afternoon in the first stream of lectures which focused on the role of geochemical analysis in pollutant studies of soils and waters. Professor Xuejing Xie (IGGE, China) presented a lecture on the analytical requirements for international geochemical mapping, and this was complemented by an open discussion of the subject later in the evening. The parallel session on ICP-MS, chaired by Dr. Kym Jarvis (Imperial College at Silwood Park) and Jenny Cook (BGS), highlighted the excellent sensitivity and accuracy of ICP-MS in the study of minor and trace elements including gold, the PGEs, yttrium, boron and the REEs. Again, a variety of research posters and commercial displays complemented the day's lectures.

Wednesday's plenary lecture, given by Gwendy Hall of the Geological Survey of Canada, gave a comprehensive review of the GSC's research into the analysis of natural background levels of elements where detection limits must be in the range of ppb or ppt. As an example, the research has shown that terbium and other REEs in the lakes of Baie d'Espoir, Newfoundland, clearly delineate the bedrock geology, even at low ppt concentrations. The first stream of lectures on Wednesday morning centred on exploration and waters. Presentations were wide ranging, including Angela Giblin's (CSIRO-DEM, Australia) lecture on the use of high quality groundwater analysis in the detection of concealed ore deposits to a presentation discussing trace metal analysis in oils and source rocks given by S. Olsen of Rogaland Research, Stavanger, Norway. A simultaneous stream on laser ablation ICP-MS included presentations on the use of this technique in the analysis of minerals, biologically derived materials and tree ring profiles.

Wednesday afternoon was devoted to recreational activities and arrangements had been made for 30 delegates to visit British Nuclear Fuel's reprocessing plant at Sellafield. For the remaining delegates, fine sunny weather provided excellent conditions for an organized boat trip on Lake Windermere, or to explore the scenic surroundings. In the evening, the conference dinner was held at the Merewood Country House Hotel, close to the lake, with views of the Cumbrian Mountains. A relaxed sherry reception allowed delegates to socialize before an excellent dinner. A return to the conference centre was made at around midnight where drinks continued to flow well into the early hours, accounting for a few absences at Thursday's breakfast!

The final day of the conference was opened with a plenary lecture by Professor Klaus Heumann of the University of Regensburg, Germany, entitled 'Developments in Thermal Ionization Techniques for Isotope Analysis'. The lecture programme was then split to allow streams on isotope geochemistry and X-ray fluorescence. The isotope geochemistry stream was varied and included presentations highlighting the latest isotopic analytical developments and their applications. Similarly, the XRF stream presented a broad range of research and applications. Lecture topics included the analysis of water treatment plant sludges, given by Margaret West of Sheffield Hallam University, and XRF analysis of environmental Pb by Dr. Jacques Renault of the New Mexico Bureau of Mines and Mineral Resources.

The closing afternoon was dedicated to innovations in analytical developments, whilst the poster programme centred on exploration and geochemical techniques. The conference was officialy closed after these presentations although the programme continued into Friday with a Lake District field trip and a workshop on geological reference materials.

Geoanalysis 94 brought together a wide range of scientists from national geological surveys, research institutes, commercial operators and universities. The organising committee are to be praised in succeeding in making Geoanalysis 94 a truly international conference.

Robert Adkins
Department of Geology
Royal Holloway, University of London

Future Issues will Include—

Modified Method for the Analysis of Anionic Surfactants as Methylene Blue Active Substances—**Steven K. Dentel, Srinivasarao Chitikela and Herbert E. Allen**

Simultaneous Determination of Organic Acids, Inorganic Anions and Cations in Beverages by Ion Chromatography With a Mixed-bed Stationary Phase of Anion-exchanger and Cation-exchanger—**Ming-Yu Ding, Yoshihito Suzuki and Hitoshi Koizumi**

Continuous and Flow-Injection Potentiometry of Complex-Bonded Metal Ions by the Standard Addition Method—**Ivelin Rizov and Liliana Ilcheva**

Reversed-phase High-performacne Liquid Chromatography Separation of Titanium, Vanadium, Niobium and Tantalum Ternary Complexes with Hydrogen Peroxide and 2-(5-Bromo-2-pyriylazo)-5-diethylaminophenol. Determination of Titanium, Vanadium and Tantalum in Real Samples—**Slawomir Oswaldowski**

Photoluminescence of Pyrenebutyric acid Incorporated Into Silicone Film as a Structural Probe and its Applciation for Luminescent Oxygen Sensor—**Masao Kaneko and Toru Ishiji**

Improved Detection Limits for Transient Signal Analysis of Fluid Inclusions by Inductively Coupled Plasma Atomic Emission Spectrometry Using Correlated Background Correction—**M. H. Ramsey, Barry J. Coles, Sarah Gleeson and Jamie J. Wilkinson**

Measurement of Boron Isotope ratios in Groundwater Studies—**N. C. Porteous, J. N. Walsh and Kym E. Jarvis**

Flow Injection Based Renewable Fibre Optic Sensor Principle and Validation on Colorimetry of Chromium(VI)—**Jaromir Růžička and Oleg Egorov**

Prediction of Some Physico-Chemical Parameters in Red Wines From Ultraviolet-visible Spectrum Using a Partial Least-Squares Model in Latent Variables—**Carmen Garcia-Jares and Bernard Medina**

Thermal Lens Spectrometry—**R. D. Snook and R. D. Lowe**

Estimation of Uncertainty in Multivariate Vibrational Spectroscopy—**S. J. Haswell, Allison J. Hardy, Wolfhard Wegscheider and Perry A. Hailey**

Using Instrumental Techniques to Increase the Accuracy of Classical Analyses. Part 1. The Gravimetric Determination of Sulfate—**Thomas W. Vetter, Kenneth W. Pratt, G. C. Turk, Charles M. Beck and Therese A. Butler**

Determination of Platinum in Human Blood by Using Inductively Coupled Plasma Atomic Emission Spectrometry With Ultrasonic Nebulizer—**Vito Di Noto, Dan Ni, Lisa Dalla Via, Fabio Scomazzon, Maria Viviani, Francesca Bortolozzo and Maurizo Vidali**

Determination of Iodine Concentrations in Human Milk, Cow's Milk and Infant Formula—**I. G. Gokmen and G. Dagli**

Prototype, Solid-phase, Glucose Biosensor—**Markas A. T. Gilmartin, John P. Hart and David T. Patton**

Determination of Tributyltin and Triphenyltin Compounds in Hair Using Hydrolysis Technique and Gas Chromatography With Flame Photometric Detection—**Makoto Nagase, Hiroyuki Kondo and Kiyoshi Hasebe**

Quantatitive Analysis of 2,6-Ditertiarybutyl-4-methylphenol (Butylated-Hydroxytoluene, BHT) Antioxidant in a Solvent-formulated Liquid Polychloroprene Adhesive and in a Cured Polychloroprene Adhesive Films—**Robert A. Franich, Hank W. Kroese and Gerry Lane**

Complexometric Determination of Thallium(III) Using Sodium Sulfite as a Selective Releasing Agent—**B. Narayana, C. H. Raghavan Nambiar, B. Uralidhara Rao and Biju Mathew**

Design and Characterization of Sodium-Selective Optode Membranes Based on Lipophilic Tetraester of Calix[4]arene—**Wing Hong Chan, Albert W. M. Lee, Ching Man Lee, Kei Wang Yau and Kemin Wang**

Penzothiazole Derivatives as Substrates for Alkaline Phosphatase Assay with Fluorescence and Chemiluminescence Detection—**Kazumi Sasamoto, Gang Deng, Tamano Ushijima, Yosuke Ohkura and Keiyu Ueno**

Analysis of Pharmaceutical Preparations Containing Catecholamines by Micellar Liquid Chromatography with Spectrophotometric Detection—**R. M. Villanueva Camanas, J. M. Sanchis Mallols, J. R. Torres Lapasio and G. Ramis-Ramos**

Determination of the Concentrations of the Steroids Estradiol, Progesterone and Testosterone in Bovine Sera: Comparison of Commercial DELFIA Kits with Conventional Radio- and Enzyme-Immunoassays—**C. T. Elliott, Kathryn S. Francis, Hugh D. Shortt and William J. McCaughey**

Spectrophotometric Determination of Anionic Surfactants in Seawater Based on Ion-pair Extraction with Bis[2-(5-trifluoromethyl-2-pyridylazo)-5-diethylaminophenolato] Cobalt(III) as Counter Ion—**Issei Kasahara, Kanae Hashimoto, Tomoko Kawabe, Akiko Kunita, Keiji Magawa, Noriko Hatta, Shigeru Taguchi and Katsumi Goto**

Utilization of Thermal Decomposition of Immobilized Compounds for the Generation of Gaseous Standard Mixtures Used in the Calibration of Gas Analysers—**Jacek Namiesnik, Piotr Komeczka, Andrej Przyjazny, Elzbieta Luboch and Jan F. Biernat**

Edible Fats and Oils Reference Materials for Sterol Analysis With Particular Attention to Cholesterol. Part 2. Certification of Sterols Mass Fraction—**G. Lognay, John Pearse, W. Dennis Pocklington, A. Boenke, Barbel Schurer and Peter J. Wagstaffe**

Technical Abbreviations and Acronyms

The presence of an abbreviation or acronym in this list should NOT be read as a recommendation for its use. However those defined here, need not be defined in the text of your manuscript.

AAS	atomic absorption spectrometry	LOQ	limit of quantification
ac	alternating current	mp	melting point
A/D	analogue-to-digital	MRL	maximum residue limit
ADC	analogue-to-digital converter	mRNA	messenger ribonucleic acid
ANOVA	analysis of variance	MS	mass spectrometry
AOAC	Association of Official Analytical Chemists	NIR	near-infrared
		NMR	nuclear magnetic resonance
ASTM	American Society for Testing and Materials	NIST	National Institute of Standards and Technology
bp	boiling point	od	outer diameter
BSA	bovine serum albumin	OES	optical emission spectrometry
BSI	British Standards Institution	PBS	phosphate buffered saline
CEN	European Committee for Standardization	PCB	polychlorinated biphenyl
		PAH	polycyclic aromatic hydrocarbon
cpm	counts per minute	PGE	platinum group element
CMOS	complementary metal oxide silicon	PIXE	particle/proton-induced X-ray emission
c.m.c.	critical micellization concentration		
CRM	certified reference material	ppt	parts per trillion (10^{12}; pg g^{-1})
CVAAS	cold vapour atomic absorption spectrometry	ppb	parts per billion (10^9; ng g^{-1})
		ppm	parts per million (10^6; µg g^{-1})
c.w.	continuous wave	PTFE	poly(tetrafluoroethylene)
CZE	capillary zone electrophoresis	PVC	poly(vinyl chloride)
dc	direct current	PDVB	poly(divinyl benzene)
dpm	disintegrations per minute	QC	quality control
DRIFT	diffuse reflectance infrared Fourier transform spectroscopy	QA	quality assurance
		REE	rare earth element
DELFIA	dissociation enhanced lanthanide fluorescence immunoassay	rf	radiofrequency
		RIMS	resonance-ionization mass spectrometry
DNA	deoxyribose nucleic acid		
EDTA	ethylenediaminetetraacetic acid	rms	root mean square
ELISA	enzyme linked immunosorbent assay	rpm	revolutions per minute
		RNA	ribonucleic acid
emf	electromotive force	SCE	saturated calomel (reference) electrode
ETAAS	electrothermal atomic absorption spectrometry		
		SE	standard error
EXAFS	extended X-ray absorption fine structure spectroscopy	SEM	scanning/surface (reflection) electron microscopy
EPA	Environmental Protection Agency	SIMS	secondary-ion mass spectrometry
FAAS	flame atomic absorption spectrometry	SIMCA	soft independent modelling of class analogy, statistical isolinear multicategory analysis
FAB	fast atom bombardment		
FAO-WHO	Food and Agriculture Organization, World Health Organization	SRM	Standard Reference Material
		STM	scanning tunnelling (electron) microscopy
FIR	far-infrared		
FT	Fourier transform	STP	standard temperature and pressure
FPLC	fast protein liquid chromatography	TIMS	thermal ionization mass spectrometry
FPD	flame photometric detector		
GC	gas chromatography	TLC	thin-layer chromatography
GLC	gas–liquid chromatography	TOF	time-of-flight
HGAAS	hydride generation atomic absorption spectroscopy	TGA	thermogravimetric analysis
		TMS	trimethylsilane
HPLC	high-performance liquid chromatography	tris	2-amino-2-(hydroxymethyl)-propane-1,3-diol
ICP	inductively coupled plasma	TRIS	tris(hydroxymethyl)methylamine
id	internal diameter	UV	ultraviolet
INAA	instrumental neutron activation analysis	UV/VIS	ultraviolet–visible
		VDU	visual display unit
IR	infrared	XRD	X-ray diffraction
ISFET	ion-selective field effect transistor	XRF	X-ray fluorescence
iv	intravenous	YAG	yttrium aluminium garnet
im	intramuscular		
IGFET	insulated gate field effect transistor	***Commonly Used Symbols***	
		M	molecular mass
ISE	ion-selective electrode	M_r	relative molecular mass
LC	liquid chromatography	r	correlation coefficient
LED	light emitting diode	s	standard deviation
LOD	limit of determination	u	atomic mass

The Analyst

The analytical journal of The Royal Society of Chemistry

CONTENTS